EMERGING INFECTIOUS DISEASES®

SARS-CoV-2 and Influenza Virus Infections

July 2022

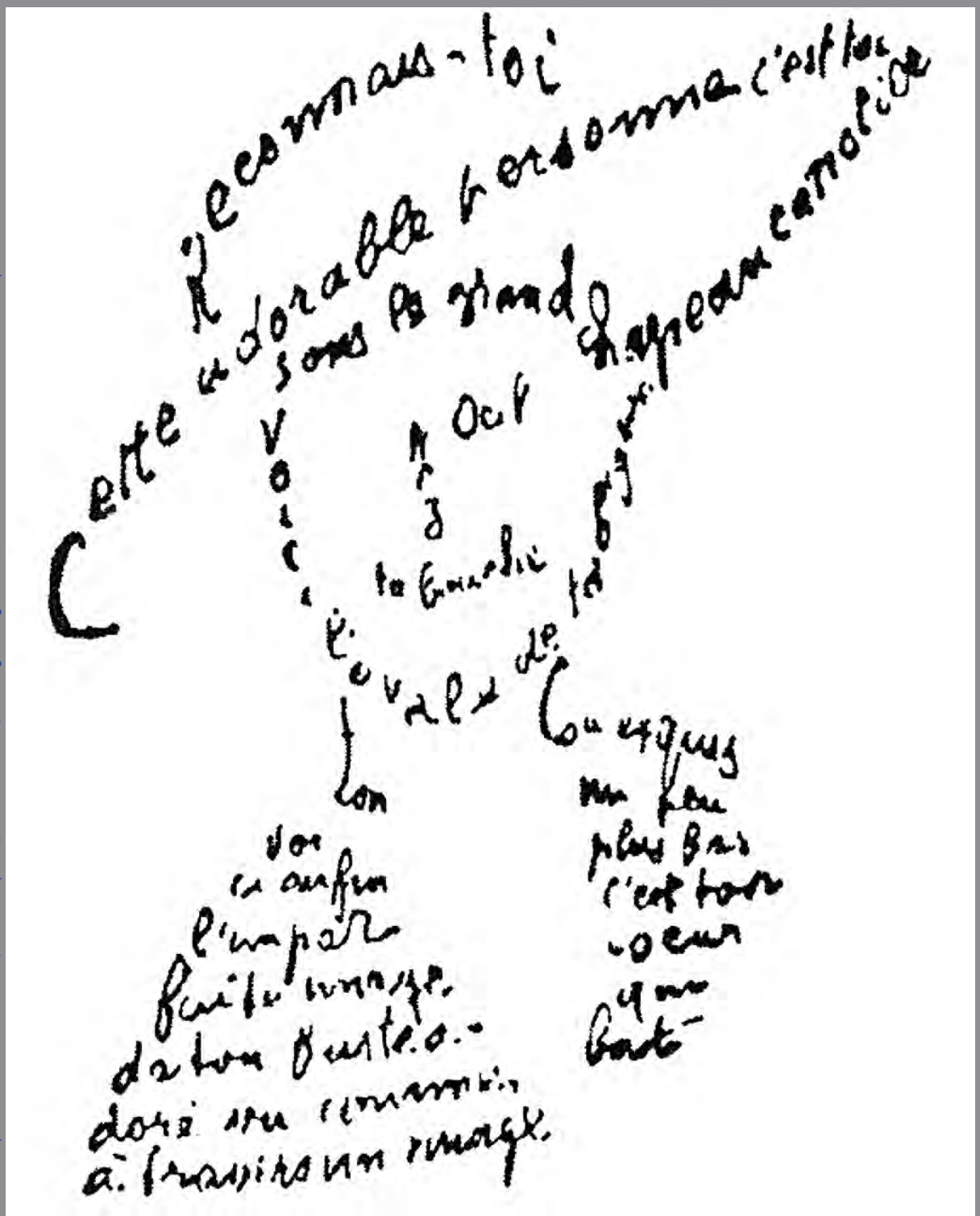

Guillaume Apollinaire (1880–1918), *Calligram of Guillaume Apollinaire*, entitled *Poème du 9 Février 1915* (Poem of February 9, 1915). Printed in Poèmes de la Paix et de la Guerre, 1913–1916 (Poems of Peace and about War, 1913–1916). Paris, Mercure de France, 1918.Digital image available from the Online Collection of Duke University Libraries.

EMERGING INFECTIOUS DISEASES®

Emerging Infectious Diseases is published monthly by the Centers for Disease Control and Prevention, 1600 Clifton Rd NE, Mailstop H16-2, Atlanta, GA 30329-4027, USA. Telephone 404-639-1960; email, eideditor@cdc.gov

EMERGING INFECTIOUS DISEASES®

SARS-CoV-2 and Influenza Virus Infections **July 2022**

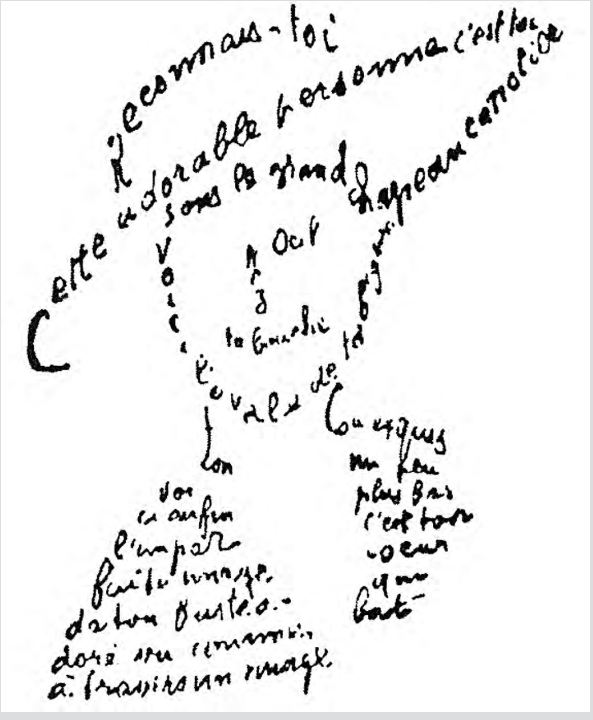

On the Cover

Guillaume Apollinaire (1880–1918), *Calligram of Guillaume Apollinaire*, entitled *Poème du 9 Février 1915* (Poem of February 9, 1915). Printed in Poèmes de la Paix et de la Guerre, 1913-1916 (Poems of Peace and about War, 1913–1916). Paris, Mercure de France, 1918. Digital image available from the Online Collection of Duke University Libraries.

About the Cover p. 1537

Synopses

Medscape EDUCATION ACTIVITY

Research

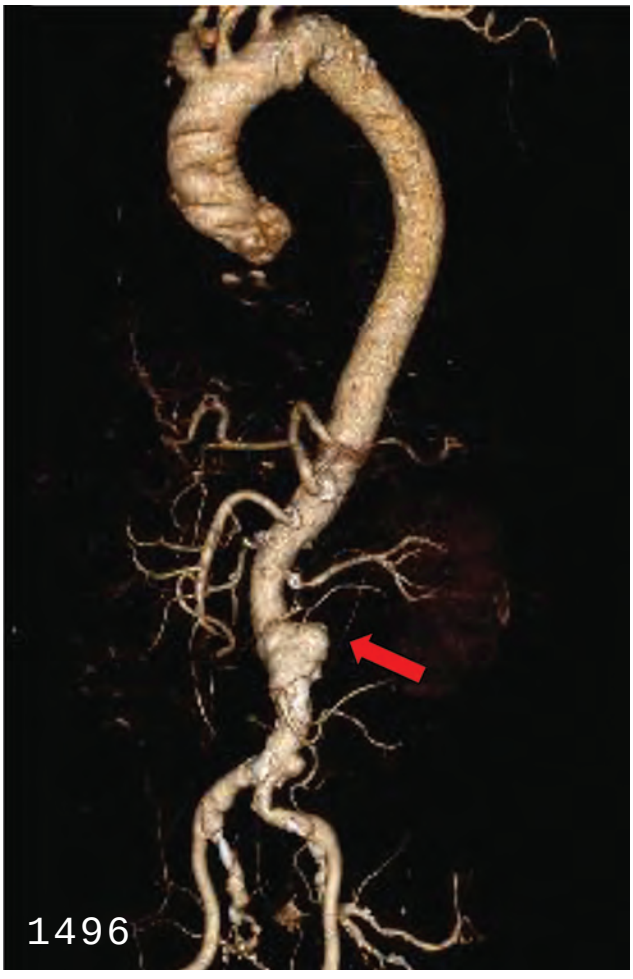

Dispatches

EMERGING INFECTIOUS DISEASES®
July 2022

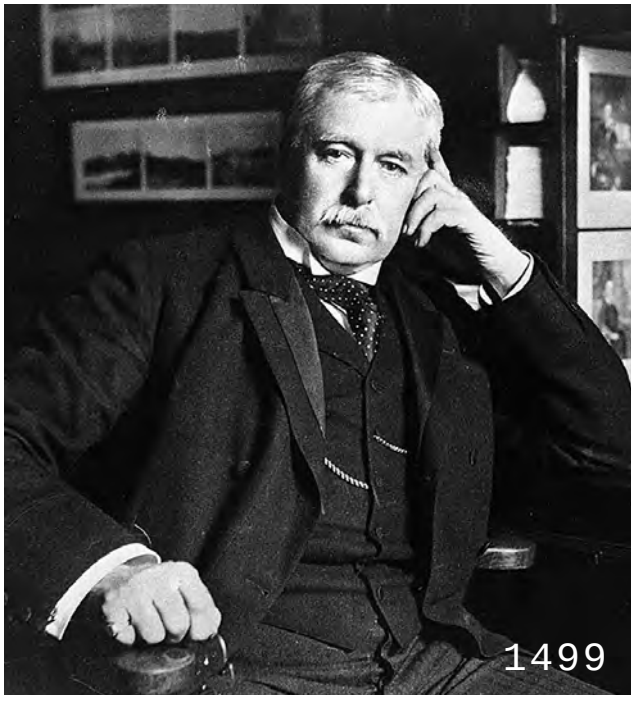

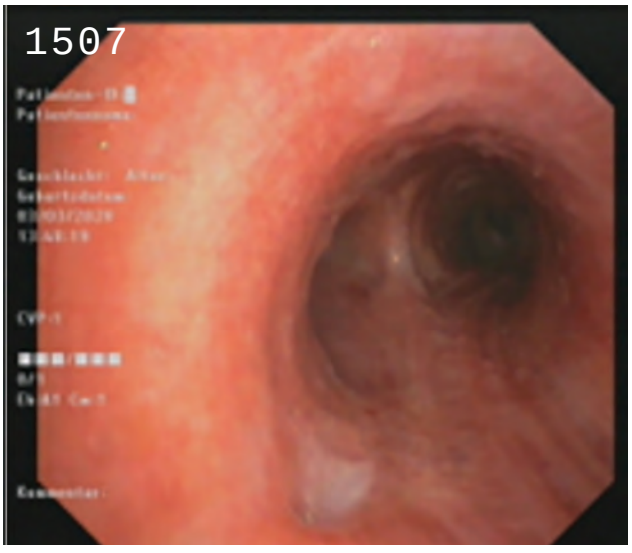

Photo Quiz

Another Dimension

Research Letters

EMERGING INFECTIOUS DISEASES®
July 2022

About the Cover

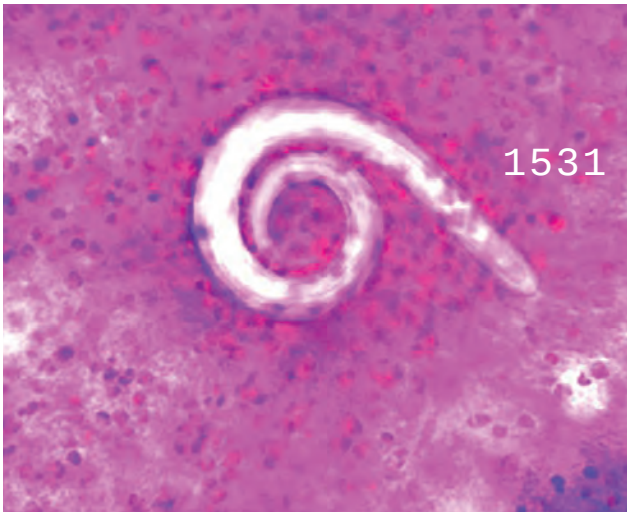

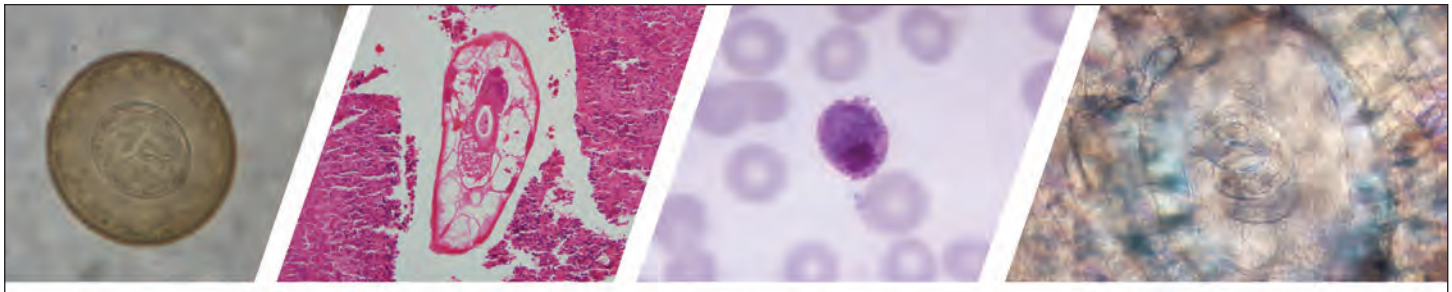

DPDx

Diagnostic Assistance and Training in Laboratory Identification of Parasites

A free service of CDC available to laboratorians, pathologists, and other health professionals in the United States and abroad

- Diagnosis from photographs of worms, histological sections, fecal, blood, and other specimen types
- Expert diagnostic review
- Formal diagnostic laboratory report
- Submission of samples via secure file share

Visit the DPDx website for information on laboratory diagnosis, geographic distribution, clinical features, parasite life cycles, and training via Monthly Case Studies of parasitic diseases.

www.cdc.gov/dpdx
dpdx@cdc.gov

U.S. Department of Health and Human Services
Centers for Disease Control and Prevention

CS272346-DE

Updated Estimates and Mapping for Prevalence of Chagas Disease among Adults, United States

Amanda Irish, Jeffrey D. Whitman, Eva H. Clark, Rachel Marcus, Caryn Bern

Medscape ACTIVITY EDUCATION

In support of improving patient care, this activity has been planned and implemented by Medscape, LLC and Emerging Infectious Diseases. Medscape, LLC is jointly accredited by the Accreditation Council for Continuing Medical Education (ACCME), the Accreditation Council for Pharmacy Education (ACPE), and the American Nurses Credentialing Center (ANCC), to provide continuing education for the healthcare team.

Medscape, LLC designates this Journal-based CME activity for a maximum of 1.00 ***AMA PRA Category 1 Credit(s)™***. Physicians should claim only the credit commensurate with the extent of their participation in the activity.

Successful completion of this CME activity, which includes participation in the evaluation component, enables the participant to earn up to 1.0 MOC points in the American Board of Internal Medicine's (ABIM) Maintenance of Certification (MOC) program. Participants will earn MOC points equivalent to the amount of CME credits claimed for the activity. It is the CME activity provider's responsibility to submit participant completion information to ACCME for the purpose of granting ABIM MOC credit.

All other clinicians completing this activity will be issued a certificate of participation. To participate in this journal CME activity: (1) review the learning objectives and author disclosures; (2) study the education content; (3) take the post-test with a 75% minimum passing score and complete the evaluation at http://www.medscape.org/journal/eid; and (4) view/print certificate. For CME questions, see page 1541.

Release date: June 17, 2022; Expiration date: June 17, 2023

Learning Objectives

Upon completion of this activity, participants will be able to:

- Evaluate the prognosis of Chagas disease
- Analyze the epidemiology of Chagas disease in the United States
- Distinguish US metropolitan areas with the highest rates of Chagas disease
- Analyze the prevalence of Chagas disease based on country of origin in Latin America.

CME Editor

Dana C. Dolan, BS, Technical Writer/Editor, Emerging Infectious Diseases. *Disclosure: Dana C. Dolan, BS, has disclosed no relevant financial relationships.*

CME Author

Charles P. Vega, MD, Health Sciences Clinical Professor of Family Medicine, University of California, Irvine School of Medicine, Irvine, California. *Disclosure: Charles P. Vega, MD, has disclosed the following relevant financial relationships: served as an advisor or consultant for GlaxoSmithKline; Johnson & Johnson Pharmaceutical Research & Development, L.L.C.*

Authors

Amanda Irish, DVM; Jeffrey D. Whitman, MD; Eva H. Clark, MD; Rachel Marcus, MD; and ***Caryn Bern, MD.***

Author affiliations: University of California–San Francisco, San Francisco, California, USA (A. Irish, J.D. Whitman, C. Bern); Baylor College of Medicine, Houston, Texas, USA (E.H. Clark); Medstar Union Memorial Hospital and Latin American Society of Chagas, Washington, DC, USA (R. Marcus)

DOI: https://doi.org/10.3201/eid2807.212221

We combined American Community Survey data with age-specific *Trypanosoma cruzi* prevalence derived from US surveys and World Health Organization reports to yield estimates of Chagas disease in the United States, which we mapped at the local level. In addition, we used blood donor data to estimate the relative prevalence of autochthonous *T. cruzi* infection. Our estimates indicate that 288,000 infected persons, including 57,000 Chagas cardiomyopathy patients and 43,000 infected reproductive-age women, currently live in the United States; 22–108 congenital infections occur annually. We estimated ≈10,000 prevalent cases of locally acquired *T. cruzi* infection. Mapping shows marked geographic heterogeneity of *T. cruzi* prevalence and illness. Reliable demographic and geographic data are key to guiding prevention and management of Chagas disease. Population-based surveys in high prevalence areas could improve the evidence base for future estimates. Knowledge of the demographics and geographic distribution of affected persons may aid practitioners in recognizing Chagas disease.

Six million persons are estimated to have Chagas disease in the Americas; 20%–30% of those cases will progress to cardiac or gastrointestinal disease (*1*). Early treatment of infection with the causative parasite, *Trypanosoma cruzi*, provides the best chance to decrease progression risk; cure rates are ≥60% in those treated as children (*2*,*3*). Cure rates among adults are unclear; the accepted test of cure is reversion to negative serologic test results, which requires years to decades, and the time to negative serologic results is inversely proportional to the duration of infection (*4*). Because the date of *T. cruzi* infection is nearly always unknown, age is commonly used as a proxy for duration. Infected persons are typically asymptomatic for decades. In those with established Chagas cardiomyopathy, antiparasitic treatment is unlikely to alter heart disease progression (*5*). Thus, early, active screening during the asymptomatic period is essential to achieve timely diagnosis and effective treatment. Since the establishment of regional control programs in the 1990s, many Latin America countries have mounted community- and facility-based programs, most commonly focused on screening of children and pregnant women (*6*,*7*). No such large-scale programs exist in the United States.

Enzootic transmission by local triatomine species occurs across the southern United States from coast to coast; Lynn et al. summarized 76 suspected or confirmed autochthonous human *T. cruzi* infections (*8*). However, locally acquired infections are vastly outnumbered by those acquired by immigrants from Latin America in their countries of origin before arrival in the United States. No nationally representative *T. cruzi* prevalence data exist for the United States; disease burden estimates have been based on reported national prevalence figures from Latin America countries. These estimates suggest that 240,000–350,000 US residents of Latin America origin may have *T. cruzi* infection (*9*). However, infection rates are heterogeneous within countries, so national-level prevalence estimates may not reflect prevalence among US immigrants.

Calls for more widespread screening and diagnostic testing for Chagas disease in the United States are growing (*10*–*12*). Finer-scale geographic data would be of great help in the targeting of such efforts. Local screening of at-risk populations in Los Angeles, California; the District of Columbia; and the Boston, Massachusetts, metropolitan areas provide a more accurate reflection of prevalence in some US populations (*13*–*15*). Using data from the American Community Survey (ACS) (*16*), we developed new age-structured estimates and interactive maps of Chagas disease prevalence at the local level. We present these data to support geographic targeting of screening efforts and setting priorities for healthcare providers and public health outreach to address Chagas disease in the United States.

Methods

Prevalence by Age and Country of Origin

Because *T. cruzi* infection is lifelong in the absence of effective antiparasitic treatment, the prevalence of infection tends to rise as age increases (*17*). Those patterns may also reflect improved vector control for patients who grew up more recently in endemic settings compared with those in older age cohorts (*17*); also, age is used as a determinant for treatment recommendations (*1*). Together, these issues make age-structured estimates crucial to public health efforts. Past estimates have relied on aggregate prevalence figures derived from data provided by member countries and published by the World Health Organization (*18*). For our estimates, we used *T. cruzi* seroprevalence data from US populations to the greatest extent possible (*13*–*15*). Data are available for immigrants from the most frequent Chagas disease–endemic countries of origin: Mexico, El Salvador, Guatemala, Honduras, and Colombia. In addition, data are available from a metropolitan area with a high number of immigrants from Bolivia, a group that contributes disproportionately to the Chagas disease burden because of very high prevalence in some regions of Bolivia (*13*). Data for

children <18 years of age are extremely sparse. One of the screening studies that underpin our assumptions included 225 children, of whom none were infected (*14*). Those data were insufficient to obtain a reliable estimate for children; for that reason, our estimates are for adults only.

We used the age-specific pattern for El Salvador in US survey data to model prevalence patterns for immigrants from other countries of origin. Although more immigrants to the United States are from Mexico than El Salvador, *T. cruzi* prevalence is substantially higher among those from El Salvador (*13*,*14*,*19*,*20*); for this reason, the patterns were clearer and the age-stratified estimates more stable for immigrants from El Salvador. The general finding of prevalence increasing with age holds true in data from immigrants from Latin America in the United States (*13*–*15*), as well as in surveys from urban and rural areas of Latin America (*21*–*23*). We then calculated the ratio of the overall prevalence in persons from a given country to the prevalence for immigrants from El Salvador. We multiplied this country-level correction factor by the El Salvador estimates to yield estimated age-specific prevalence for immigrants from each country (Appendix Table 1, https://wwwnc.cdc.gov/EID/article/28/7/21-2221-App1.pdf). For Mexico, Guatemala, Honduras, Colombia and Bolivia, we derived the correction factor from the mean of estimated prevalence from US surveys plus the WHO estimate; for all other countries of origin, we used WHO estimates (*18*).

Estimates of Foreign-Born Population by Age Group and Public Use Micro-Area

The ACS is an annual survey conducted to supplement the decennial census (*16*). We used the 5-year data, based on a 5% sample of the US population, because they provide the most statistically reliable estimates, a particular concern for this study because we calculated estimates for small population subgroups at the public use micro-area (PUMA) level for mapping. PUMAs partition states into areas containing ≥100,000 residents and are the smallest geographic area for which complete microdata are available. Because not all counties can be characterized using PUMA data, we could not map at the county level. Estimates are interpreted as period estimates (e.g., the Chagas disease prevalence in 2014–2018).

We extracted relevant microdata for 2014–2018 from IPUMS-USA, which collects and harmonizes data from the census and ACS (Appendix 1). Using these data, we estimated the overall adult population and population of adult Latin America–born US residents by country of origin and age group (Appendix Table 2).

Estimates of the Clinical Burden of Chagas Disease in the United States

We used the infection prevalence and population figures to calculate the prevalence of Chagas disease at the PUMA level for mapping and national level for summary estimates. We produced estimates of the number of patients with Chagas cardiomyopathy in the United States by applying age-specific cardiomyopathy prevalence rates among *T. cruzi*–infected persons in population-based studies from disease-endemic countries to our US infection estimates by age group (*24*–*26*).

We estimated the risk for congenital transmission in the United States using age-specific infection prevalence and birth rate statistics. To estimate age-specific birth rates among foreign-born women from Latin America, we started with the reported number of live births per 1,000 Hispanic women by age group in 2017 (*27*). That figure includes women of Hispanic origin born in the US as well as women born in Latin America. We therefore multiplied by a correction factor of 1.22 to adjust for the higher birth rate among US resident women born in Latin America (82.3) compared with all Hispanic women (67.6) (*27*,*28*). We then applied a range of vertical transmission rates of 1%–5% to estimate a likely range for the number of congenitally infected infants born in 2017. In a recent meta-analysis, the estimated vertical transmission rate for *T. cruzi*–infected women in nonendemic countries was 2.7%, falling within the range we used (*29*). However, most of the data in the meta-analysis came from immigrants from Bolivia in Spain. Data for women from Mexico and Central America are extremely sparse, and we felt the uncertainty expressed by the range was more appropriate than a single point estimate.

Finally, we calculated the relative number of locally acquired autochthonous *T. cruzi* infections in the United States, based on estimates that 5.5%–7.5% of blood donor infections were locally acquired (*30*). We corrected for underrepresentation of Hispanic populations in donor data (*31*).

Statistical Analysis and Mapping

We performed analyses in R version 4.0.4 (https://www.r-project.org). We obtained point estimates and 95% CIs using person-level replicate weights. We generated interactive, web-based maps to display estimates for the total number of infected adults and the prevalence of Chagas disease in the total

population and in the Latin America–born population at the PUMA level (Appendix 1).

Results

We estimated that 287,711 adult Latin America–born US residents were living with Chagas disease during the period 2014–2018 (Table 1). Of those, 68% (196,907) were ≥50 years of age; case numbers were low in younger age groups. The marked age dependence of both *T. cruzi* infection prevalence and Chagas cardiomyopathy indicates that >85% of the estimated 57,000 Chagas cardiomyopathy cases occur in those ≥50 years of age (Table 2). Because prevalence among women of childbearing age is relatively low, we estimate relatively few congenital infections (Table 3). On the basis of blood donor data, we estimated as many as 10,000 locally acquired *T. cruzi* infections in the United States (Appendix Table 3).

The PUMA-level maps illustrate the marked geographic heterogeneity of estimated *T. cruzi* infection prevalence and the burden of Chagas disease in the United States (https://amandairish.github.io/chagas_maps). Foci of high disease burden vary substantially in demography, geography and healthcare access, as we saw in the Houston, Texas, metropolitan area (Appendix 2, https://wwwnc.cdc.gov/EID/article/28/7/21-2221-App2.pdf); in southern California (Appendix 3, https://wwwnc.cdc.gov/EID/article/28/7/21-2221-App3.pdf); and in the Washington, DC, metropolitan area (Appendix 4, https://wwwnc.cdc.gov/EID/article/28/7/21-2221-App4.pdf). The metropolitan areas with the highest number of estimated Chagas disease cases reflect major population centers, whereas areas with the highest percentage of infected residents include midsized cities in states with a high proportion of Latin America–born residents (Table 4).

Discussion

To address Chagas disease in the United States, public health practitioners and healthcare providers need to know where and among whom to target their efforts. Our updated estimates define the demographics and provide a detailed geography of Chagas disease. In data from both the United States (*13*–*15*) and Chagas disease–endemic countries (*21*–*23*), the infection prevalence increases with increasing age. The use of prevalence and age structure assumptions based on data from several US populations of interest make these new estimates a more accurate reflection of *T. cruzi* infection and illness than previous calculations (*9*,*32*). By mapping the resulting data at the most local level possible, we have constructed interactive maps that enable providers to assess risk in their catchment area (*16*). Such maps could be developed to target screening efforts for other conditions for which migrants bear a disproportionate risk (*33*).

These new estimates add nuance to the already complex landscape of efforts to address Chagas disease (*1*,*34*). Our updated estimate of ≈288,000 *T. cruzi*–infected US residents is consistent with earlier figures of ≈240,000 to ≈350,000 (*9*,*32*). However, our new age-structured estimates indicate that two thirds of persons with Chagas disease in the United States are ≥50 years of age. This finding substantially increases the estimate of patients with Chagas cardiomyopathy

Table 1. Estimates of the number of Latin America–born adults with Chagas disease in the United States

Birth country	*Trypanosoma cruzi* infection prevalence, %	Estimated no. infected adults by age group			
		All ages	18–34	35–49	≥50
Argentina	3.64	14,463	600	2,592	11,271
Belize	0.33	344	15	53	276
Bolivia	18.3	27,335	1,650	5,262	20,423
Brazil	0.61	3,865	379	1,049	2,437
Chile	0.70	1,560	69	226	1,265
Colombia	0.51	7,840	398	1,260	6,182
Costa Rica	0.17	289	18	55	216
Ecuador	1.38	11,200	719	2,316	8,165
El Salvador	1.90	41,788	3,287	11,260	27,241
Guatemala	1.13	14,143	1,846	4,109	8,188
Guyana, French Guiana, Suriname	0.84	5,171	183	746	4,242
Honduras	0.65	5,208	671	1,606	2,931
Mexico	0.73	141,554	10,730	36,413	94,411
Nicaragua	0.52	2,773	131	528	2,114
Panama	0.52	1,810	64	233	1,513
Paraguay	2.13	679	75	134	470
Peru	0.44	4,125	192	728	3,205
Uruguay	0.24	234	11	39	184
Venezuela	0.71	3,330	315	842	2,173
All Latin America countries	1.64	287,711	21,353	69,451	196,907

(57,000 in our estimates vs. 30,000–45,000 in the 2009 estimates) and decreases the projected number of annual congenital *T. cruzi* infections (22–108 in our data vs. 63–315 in 2009 data) (*32*).

Antitrypanosomal treatment recommendations are strongest for younger age groups, based on the more robust data for benefit among children than adults (*35*,*36*). In the United States, as in Latin America, at-risk women of reproductive age should be screened for Chagas disease, to offer them treatment and detect infected infants early in life (*36*,*37*). Treatment of women before pregnancy is associated with an estimated 95% decrease in risk for subsequent congenital transmission (*4*,*38*). We were unable to make a disease burden estimate for children <18 years of age; 1 of the 3 US studies used to underpin the estimates included children, none of whom was infected (*14*). Children in the United States are also at risk if they were born to women with Chagas disease; hundreds of US-born children <18 are probably living with undetected *T. cruzi* infection acquired at birth. Maternal birthplace is, therefore, a crucial piece of information to assess risk among US-born persons with roots in Latin America.

Persons with Chagas cardiomyopathy also benefit from accurate and timely diagnosis. Clinical trial data have failed to show substantial effects of antitrypanosomal therapy on progression of established Chagas cardiomyopathy, reinforcing the urgency to institute active screening to detect infections before cardiac damage occurs (*5*,*39*). Nevertheless, good cardiac management substantially improves survival and quality of life, and the United States has the resources to appropriately evaluate and manage every infected patient (*40*). Patients who receive cardiac transplants for end-stage Chagas cardiomyopathy have a survival rate equivalent to or better than that of patients who receive transplants for other etiologies, as long as the infection is recognized and the patient actively monitored for reactivation (*41*–*43*). Pretransplant diagnosis of *T. cruzi* infection is crucial to ensure good outcomes (*41*).

Table 2. Estimated Latin America–born persons with Chagas cardiomyopathy in the United States

Age, y	No. infected	No. (%) with Chagas cardiomyopathy
18–34	21,353	854 (4)
35–49	69,451	6,945 (10)
≥50	196,907	49,227(25)
All ages	287,711	57,027 (19.8)

Our estimates improve on previous efforts (*9*,*32*) but suffer from some of the same limitations in the empirical data underpinning their assumptions. US data were available from 3 metropolitan areas (*13*–*15*), and data for children were extremely sparse. The US data were based on clinical screening and community convenience samples, not population-based sampling. The results may be affected by differences in access to care, catchment areas, and awareness among participants. ACS datasets lack the data needed to make estimates for some counties, including several of those comprising the highest-burden PUMAs. Thus, we were unable to show a county-level map, which might have been useful for public health targeting. We have no direct data for the incidence of congenital *T. cruzi* transmission in the United States. Only 2 congenital infections have been reported, both with moderately severe manifestations (*44*,*45*). In the absence of screening, most infected infants with minimal or no symptoms were undoubtedly missed. Because of the indirect calculation method, and because foreign-born donors may have been less likely than US-born donors to participate in the donor follow-up study (*30*), our estimate for locally acquired Chagas disease provides an indication of the relative order of magnitude of this problem and may represent an overestimate.

Effectively addressing Chagas disease is complicated by the heterogeneity of healthcare systems in the United States. States play a major role in determining services for the indigent, uninsured, and undocumented persons who are at highest risk for Chagas disease, so there is no universal pathway for these persons to receive affordable healthcare (*46*). Nevertheless, most states have programs to cover

Table 3. Estimated annual births to *Trypanosoma cruzi*–infected women and congenital infections, United States

Maternal age, y	No. women infected	Live births/ 1,000 women*	No. births to infected women	No. infected infants/y	
				Lower limit, 1%	Upper limit, 5%
18–19	683	64.3	44	0	2
20–24	2,134	114.4	244	2	12
25–29	3,051	136.4	416	4	21
30–34	3,933	117.6	463	5	23
35–39	11,553	66.6	770	8	38
40–44	11,573	17.7	205	2	10
45–49	10,356	1.2	13	0	1
All ages	43,283		2,154	22	108

*Age-specific birth rates for all Hispanic women in 2017 multiplied by 1.22 to correct for higher birth rates among foreign-born Hispanic women (see Methods).

Table 4. US metropolitan areas with the highest estimated prevalence of Chagas disease

Location	*Trypanosoma cruzi*–infected adults	Prevalence in total adult population, %	Prevalence in Latin America–born adult population, %
Top 10 in total number of *T. cruzi*–infected adults			
Los Angeles-Long Beach-Anaheim, CA	44,768	0.43	1.97
New York-Newark-Jersey City, NY-NJ-PA	28,304	0.18	1.89
Washington-Arlington-Alexandria, DC-VA-MD-WV	17,745	0.38	3.85
Miami-Fort Lauderdale-West Palm Beach, FL	15,586	0.32	1.93
Houston-The Woodlands-Sugar Land, TX	14,175	0.29	1.60
Riverside-San Bernardino-Ontario, CA	11,070	0.33	1.71
Chicago-Naperville-Elgin, IL-IN-WI	10,931	0.15	1.51
Dallas-Fort Worth-Arlington, TX	9,887	0.19	1.37
San Francisco-Oakland-Hayward, CA	6,898	0.18	1.76
San Diego-Carlsbad, CA	5,730	0.22	1.54
Top 10 in overall *T. cruzi* prevalence			
El Centro, CA	956	0.74	1.76
Laredo, TX	1,025	0.57	1.49
McAllen-Edinburg-Mission, TX	3,193	0.56	1.49
El Paso, TX	3,387	0.56	1.77
Brownsville-Harlingen, TX	1,564	0.54	1.66
Yuma, AZ	738	0.48	1.56
Los Angeles-Long Beach-Anaheim, CA	44,768	0.43	1.97
Salinas, CA	1,503	0.41	1.35
Merced, CA	756	0.40	1.46
Washington-Arlington-Alexandria, DC-VA-MD-WV	17,745	0.38	3.85

uninsured pregnant women, infants, and young children. Thus, prenatal testing and evaluation of newborns and older children of infected women constitute high-priority, cost-effective aspects of Chagas disease control that should be within our immediate reach (*11*,*12*). Managing the chronic sequelae of Chagas disease is complex and costly, and access to such care for uninsured patients varies widely from state to state. Federally qualified health centers may lack the capacity to provide access to specialty services such as infectious diseases, cardiology, and gastroenterology (*47*). Strategies to enhance awareness among relevant providers, including primary care physicians, obstetricians, cardiologists and gastroenterologists, are urgently needed. Targeting locations with the highest Chagas disease burden will improve screening, management and health care access (*48*).

Early treatment has the potential to prevent congenital transmission and decrease the future burden of cardiomyopathy and other chronic sequelae of Chagas disease. Screening of asymptomatic persons at epidemiologic risk will be essential to achieve these goals (*12*). Population-based surveys in high-prevalence areas could identify those eligible for treatment, and at the same time, greatly improve the evidence base for future estimates. However, such surveys would be much more resource intensive than screening in primary-healthcare settings. Early recognition of Chagas cardiomyopathy is equally necessary to guide accurate medical and surgical management to improve quality of life and survival. Many of those at highest risk for COVID-19 include the target populations identified in our Chagas disease estimates, and the outreach methods and community partnerships crucial to the response to the pandemic provide a potential template for addressing Chagas disease (*49*).

Acknowledgments

We thank Yagahira Castro-Sesquen, Jennifer Manne-Goehler, and Julia Koehler for sharing age- and country-specific prevalence figures from their screening studies.

C.B. receives royalties for UpToDate topics related to Chagas disease. E.H.C. was supported by National Institutes of Health NIAID K23AI168583-01.

A.I. conducted the data analysis, generated the maps, drafted part of the manuscript, and reviewed and revised the manuscript. J.D.W. contributed to interpretation of the study findings, drafted part of the manuscript, and reviewed and revised the manuscript. E.H.C. contributed to interpretation of the study findings, drafted part of the manuscript, and reviewed and revised the manuscript. R.M. contributed to interpretation of the study findings, drafted part of the manuscript, and reviewed and revised the manuscript. C.B. conceptualized and designed the study, assisted with data analysis, contributed to interpretation of the study findings, drafted part of the manuscript, and reviewed and revised the manuscript. All authors approved the final manuscript as submitted and agree to be accountable for all aspects of the work.

About the Author

Dr. Irish, a veterinarian by training, is a PhD candidate in epidemiology and translational science at the University of California—San Francisco. Her primary research interests are infectious disease epidemiology, particularly of zoonoses, as well as spatial and social epidemiology.

References

1. Bern C, Messenger LA, Whitman JD, Maguire JH. Chagas disease in the United States: a public health approach. Clin Microbiol Rev. 2019;33:e00023-19. https://doi.org/10.1128/CMR.00023-19
2. de Andrade AL, Zicker F, de Oliveira RM, Almeida Silva S, Luquetti A, Travassos LR, et al. Randomised trial of efficacy of benznidazole in treatment of early *Trypanosoma cruzi* infection. Lancet. 1996;348:1407–13. https://doi.org/10.1016/S0140-6736(96)04128-1
3. Sosa Estani S, Segura EL, Ruiz AM, Velazquez E, Porcel BM, Yampotis C. Efficacy of chemotherapy with benznidazole in children in the indeterminate phase of Chagas' disease. Am J Trop Med Hyg. 1998;59:526–9. https://doi.org/10.4269/ajtmh.1998.59.526
4. Fabbro DL, Danesi E, Olivera V, Codebó MO, Denner S, Heredia C, et al. Trypanocide treatment of women infected with *Trypanosoma cruzi* and its effect on preventing congenital Chagas. PLoS Negl Trop Dis. 2014;8:e3312. https://doi.org/10.1371/journal.pntd.0003312
5. Morillo CA, Marin-Neto JA, Avezum A, Sosa-Estani S, Rassi A Jr, Rosas F, et al.; BENEFIT Investigators. Randomized trial of benznidazole for chronic Chagas' cardiomyopathy. N Engl J Med. 2015;373:1295–306. https://doi.org/10.1056/NEJMoa1507574
6. Alonso-Vega C, Billot C, Torrico F. Achievements and challenges upon the implementation of a program for national control of congenital Chagas in Bolivia: results 2004–2009. PLoS Negl Trop Dis. 2013;7:e2304. https://doi.org/10.1371/journal.pntd.0002304
7. Yun O, Lima MA, Ellman T, Chambi W, Castillo S, Flevaud L, et al. Feasibility, drug safety, and effectiveness of etiological treatment programs for Chagas disease in Honduras, Guatemala, and Bolivia: 10-year experience of Médecins Sans Frontières. PLoS Negl Trop Dis. 2009;3:e488. https://doi.org/10.1371/journal.pntd.0000488
8. Lynn MK, Bossak BH, Sandifer PA, Watson A, Nolan MS. Contemporary autochthonous human Chagas disease in the USA. Acta Trop. 2020;205:105361. https://doi.org/10.1016/j.actatropica.2020.105361
9. Manne-Goehler J, Umeh CA, Montgomery SP, Wirtz VJ. Estimating the burden of Chagas disease in the United States. PLoS Negl Trop Dis. 2016;10:e0005033. https://doi.org/10.1371/journal.pntd.0005033
10. Montgomery SP, Starr MC, Cantey PT, Edwards MS, Meymandi SK. Neglected parasitic infections in the United States: Chagas disease. Am J Trop Med Hyg. 2014;90:814–8. https://doi.org/10.4269/ajtmh.13-0726
11. Stillwaggon E, Perez-Zetune V, Bialek SR, Montgomery SP. Congenital Chagas disease in the United States: cost savings through maternal screening. Am J Trop Med Hyg. 2018;98:1733–42. https://doi.org/10.4269/ajtmh.17-0818
12. Forsyth CJ, Manne-Goehler J, Bern C, Whitman J, Hochberg NS, Edwards M, et al. Recommendations for screening and diagnosis of Chagas disease in the United States. J Infect Dis. 2021 Oct 8 [Epub ahead of print]. https://doi.org/10.1093/infdis/jiab513
13. Castro-Sesquen YE, Saldaña A, Patino Nava D, Bayangos T, Paulette Evans D, DeToy K, et al. Use of a latent class analysis in the diagnosis of chronic Chagas disease in the Washington Metropolitan area. Clin Infect Dis. 2020 Aug 7 [Epub ahead of print]
14. Manne-Goehler J, Davis J, Perez JH, Collins K, Harakawa H, Hochberg N, et al. The results of a primary care-based screening program for *Trypanosoma cruzi* in East Boston, Massachusetts. IDWeek: Infectious Diseases Society of America; San Francisco, CA, USA: 2018 October 3–7.
15. Meymandi SK, Forsyth CJ, Soverow J, Hernandez S, Sanchez D, Montgomery SP, et al. Prevalence of Chagas disease in the Latin American-born population of Los Angeles. Clin Infect Dis. 2017;64:1182–8. https://doi.org/10.1093/cid/cix064
16. United States Census Bureau. About the American Community Survey (ACS). 2021 Jan 4 [cited 2021 Aug 5]. https://www.census.gov/programs-surveys/acs/about.html
17. Cucunubá ZM, Nouvellet P, Conteh L, Vera MJ, Angulo VM, Dib JC, et al. Modelling historical changes in the force-of-infection of Chagas disease to inform control and elimination programmes: application in Colombia. BMJ Glob Health. 2017;2:e000345. https://doi.org/10.1136/bmjgh-2017-000345
18. World Health Organization. Chagas disease in Latin America: an epidemiological update based on 2010 estimates. Wkly Epidemiol Rec. 2015;90:33–43.
19. Meymandi SK, Hernandez S, Forsyth CJ. A community-based screening program for Chagas disease in the USA. Trends Parasitol. 2017;33:828–31. https://doi.org/10.1016/j.pt.2017.07.003
20. Edwards MS, Rench MA, Todd CW, Czaicki N, Steurer FJ, Bern C, et al. Perinatal screening for Chagas disease in southern Texas. J Pediatric Infect Dis Soc. 2015;4:67–70. https://doi.org/10.1093/jpids/pit056
21. Cedillos R, Francia H, Soundy C, Ascencio G, Valcarcel N. Epidemiological study of *Trypanosoma cruzi* infection in El Salvador, Central America [in Spanish]. Minerva Revista en Línea CIC-UES. 2011;2:35–46.
22. González-Guzmán S, Pichardo-Ávila S, Mimbrera-Rodríguez E, Crescencio-Trujillo JA, Gasca-Leyva ML, Martínez-Hernández F, et al. Seroprevalence of human *Trypanosoma cruzi* infection in the north of Estado de Mexico. Rev Soc Bras Med Trop. 2017;50:839–42. https://doi.org/10.1590/0037-8682-0512-2016
23. Paz-Bailey G, Monroy C, Rodas A, Rosales R, Tabaru R, Davies C, et al. Incidence of *Trypanosoma cruzi* infection in two Guatemalan communities. Trans R Soc Trop Med Hyg. 2002;96:48–52. https://doi.org/10.1016/S0035-9203(02)90236-1
24. Fernandez AB, Nunes MC, Clark EH, Samuels A, Menacho S, Gomez J, et al. Electrocardiographic and echocardiographic abnormalities in Chagas disease: findings in residents of rural Bolivian communities hyperendemic for Chagas disease. Glob Heart. 2015;10:159–66. https://doi.org/10.1016/j.gheart.2015.07.004
25. Maguire JH, Mott KE, Lehman JS, Hoff R, Muniz TM, Guimarães AC, et al. Relationship of electrocardiographic abnormalities and seropositivity to *Trypanosoma cruzi* within a rural community in northeast Brazil. Am Heart J. 1983;105:287–94. https://doi.org/10.1016/0002-8703(83)90529-X
26. Williams-Blangero S, Magalhaes T, Rainwater E, Blangero J, Corrêa-Oliveira R, VandeBerg JL. Electrocardiographic characteristics in a population with high rates of seropositivity for *Trypanosoma cruzi* infection. Am J Trop Med Hyg. 2007;77:495–9. https://doi.org/10.4269/ajtmh.2007.77.495
27. Martin JA, Hamilton BE, Osterman MJK, Driscoll AK, Drake P. Births: final data for 2017. Natl Vital Stat Rep. 2018;67:1–50.

28. Livingston G. Hispanic women no longer account for the majority of immigrant births in the U.S. 2019 [cited 2021 Jul 23]. https://www.pewresearch.org/fact-tank/2019/08/08/hispanic-women-no-longer-account-for-the-majority-of-immigrant-births-in-the-u-s
29. Howard EJ, Xiong X, Carlier Y, Sosa-Estani S, Buekens P. Frequency of the congenital transmission of *Trypanosoma cruzi*: a systematic review and meta-analysis. BJOG. 2014;121:22–33. https://doi.org/10.1111/1471-0528.12396
30. Cantey PT, Stramer SL, Townsend RL, Kamel H, Ofafa K, Todd CW, et al. The United States *Trypanosoma cruzi* Infection Study: evidence for vector-borne transmission of the parasite that causes Chagas disease among United States blood donors. Transfusion. 2012;52:1922–30. https://doi.org/10.1111/j.1537-2995.2012.03581.x
31. Murphy EL, Shaz B, Hillyer CD, Carey P, Custer BS, Hirschler N, et al.; NHLBI Retrovirus Epidemiology in Blood Donors Study-II (REDS-II). Minority and foreign-born representation among US blood donors: demographics and donation frequency for 2006. Transfusion. 2009;49:2221–8. https://doi.org/10.1111/j.1537-2995.2009.02271.x
32. Bern C, Montgomery SP. An estimate of the burden of Chagas disease in the United States. Clin Infect Dis. 2009;49:e52–4. https://doi.org/10.1086/605091
33. Berto CG, Coyle CM, Friedman L, Walker PF. Where was my patient born? The intersection of tropical medicine and migrant health. Curr Opin Infect Dis. 2021;34:447–54. https://doi.org/10.1097/QCO.0000000000000773
34. Montgomery SP, Parise ME, Dotson EM, Bialek SR. What do we know about Chagas disease in the United States? Am J Trop Med Hyg. 2016;95:1225–7. https://doi.org/10.4269/ajtmh.16-0213
35. Bern C, Montgomery SP, Herwaldt BL, Rassi A Jr, Marin-Neto JA, Dantas RO, et al. Evaluation and treatment of chagas disease in the United States: a systematic review. JAMA. 2007;298:2171–81. https://doi.org/10.1001/jama.298.18.2171
36. Dias JC, Ramos AN, Jr., Gontijo ED, Luquetti A, Shikanai-Yasuda MA, Coura JR, et al. 2nd Brazilian consensus on Chagas Disease, 2015. Rev Soc Bras Med Trop. 2016;49(Suppl 1):3–60. https://doi.org/10.1590/0037-8682-0505-2016
37. Edwards MS, Stimpert KK, Bialek SR, Montgomery SP. Evaluation and management of congenital Chagas disease in the United States. J Pediatric Infect Dis Soc. 2019;8:461–9. https://doi.org/10.1093/jpids/piz018
38. Álvarez MG, Vigliano C, Lococo B, Bertocchi G, Viotti R. Prevention of congenital Chagas disease by Benznidazole treatment in reproductive-age women. An observational study. Acta Trop. 2017;174:149–52. https://doi.org/10.1016/j.actatropica.2017.07.004
39. Maguire JH. Treatment of Chagas' disease—time is running out. N Engl J Med. 2015;373:1369–70. https://doi.org/10.1056/NEJMe1510170
40. Nunes MCP, Beaton A, Acquatella H, Bern C, Bolger AF, Echeverría LE, et al.; American Heart Association Rheumatic Fever, Endocarditis and Kawasaki Disease Committee of the Council on Cardiovascular Disease in the Young; Council on Cardiovascular and Stroke Nursing; and Stroke Council. Chagas cardiomyopathy: an update of current clinical knowledge and management: a scientific statement from the American Heart Association. Circulation. 2018;138:e169–209. https://doi.org/10.1161/CIR.0000000000000599
41. Gray EB, La Hoz RM, Green JS, Vikram HR, Benedict T, Rivera H, et al. Reactivation of Chagas disease among heart transplant recipients in the United States, 2012–2016. Transpl Infect Dis. 2018;20:e12996. https://doi.org/10.1111/tid.12996
42. Kransdorf EP, Zakowski PC, Kobashigawa JA. Chagas disease in solid organ and heart transplantation. Curr Opin Infect Dis. 2014;27:418–24. https://doi.org/10.1097/QCO.0000000000000088
43. Bocchi EA, Fiorelli A; First Guidelines Group for Heart Transplantation of the Brazilian Society of Cardiology. The paradox of survival results after heart transplantation for cardiomyopathy caused by *Trypanosoma cruzi.* Ann Thorac Surg. 2001;71:1833–8. https://doi.org/10.1016/S0003-4975(01)02587-5
44. Alarcón A, Morgan M, Montgomery SP, Scavo L, Wong EC, Hahn A, et al. Diagnosis and treatment of congenital Chagas disease in a premature infant. J Pediatric Infect Dis Soc. 2016;5:e28–31. https://doi.org/10.1093/jpids/piw043
45. Centers for Disease Control and Prevention (CDC). Congenital transmission of Chagas disease—Virginia, 2010. MMWR Morb Mortal Wkly Rep. 2012;61:477–9.
46. Forsyth C, Meymandi S, Moss I, Cone J, Cohen R, Batista C. Proposed multidimensional framework for understanding Chagas disease healthcare barriers in the United States. PLoS Negl Trop Dis. 2019;13:e0007447. https://doi.org/10.1371/journal.pntd.0007447
47. Manne-Goehler J, Reich MR, Wirtz VJ. Access to care for Chagas disease in the United States: a health systems analysis. Am J Trop Med Hyg. 2015;93:108–13. https://doi.org/10.4269/ajtmh.14-0826
48. Stimpert KK, Montgomery SP. Physician awareness of Chagas disease, USA. Emerg Infect Dis. 2010;16:871–2. https://doi.org/10.3201/eid1605.091440
49. Chamie G, Marquez C, Crawford E, Peng J, Petersen M, Schwab D, et al.; CLIAhub Consortium. Community transmission of severe acute respiratory syndrome coronavirus 2 disproportionately affects the Latinx population during shelter-in-place in San Francisco. Clin Infect Dis. 2021;73(Suppl 2):S127–35. https://doi.org/10.1093/cid/ciaa1234

Address for correspondence: Caryn Bern, Department of Epidemiology and Biostatistics, School of Medicine, University of California San Francisco, 550 16th St, San Francisco, CA 94158, USA; email: Caryn.Bern2@ucsf.edu

Vaccine Effectiveness during Outbreak of COVID-19 Alpha (B.1.1.7) Variant in Men's Correctional Facility, United States

Rachel A. Silverman,[1] Alessandro Ceci,[1] Alasdair Cohen, Meagan Helmick, Erica Short, Paige Bordwine, Michael J. Friedlander, Carla V. Finkielstein

In April 2021, a COVID-19 outbreak occurred at a correctional facility in rural Virginia, USA. Eighty-four infections were identified among 854 incarcerated persons by facilitywide testing with reverse transcription quantitative PCR (qRT-PCR). We used whole-genome sequencing to link all infections to 2 employees infected with the B.1.1.7α (UK) variant. The relative risk comparing unvaccinated to fully vaccinated persons (mRNA-1273 [Moderna, https://www.modernatx.com]) was 7.8 (95% CI 4.8–12.7), corresponding to a vaccine effectiveness of 87.1% (95% CI 79.0%–92.1%). Average qRT-PCR cycle threshold values were lower, suggesting higher viral loads, among unvaccinated infected than vaccinated cases for the nucleocapsid, envelope, and spike genes. Vaccination was highly effective at preventing SARS-CoV-2 infection in this high-risk setting. This approach can be applied to similar settings to estimate vaccine effectiveness as variants emerge to guide public health strategies during the ongoing pandemic.

Incarcerated populations are especially vulnerable to communicable disease spread, including SARS-CoV-2, the virus responsible for COVID-19 (*1*–*3*). Outbreaks in correctional facilities have been linked to outbreaks and disease spread in the wider community (*4*,*5*). Although incarcerated persons and correctional staff were recommended as a priority group to receive vaccination (*6*), reported willingness among employees and incarcerated persons to receive COVID-19 vaccines was lower than among the general population (*7*). Thus, outbreaks in prisons present a valuable opportunity to assess vaccine effectiveness in a real-world, high-risk environment.

Outbreak and Conditions

On April 7, 2021, a COVID-19 outbreak in a men's correctional facility in southwest Virginia was reported to the local branch of the Virginia Health Department (VDH) (Figure 1). Before this outbreak, this facility reported 46 employees and 2 residents (persons who were incarcerated) tested positive for SARS-CoV-2 during June 28, 2020–March 20, 2021, as well as 3 additional positive tests among employees during March 21–April 3, 2021. VDH was notified of 15 residents testing positive by rapid antigen test (BinaxNOW; Abbott, https://www.abbott.com), on April 7, followed by 4 more cases confirmed April 8–9, for a total of 19 positive antigen test results among 46 total residents who were tested because of symptoms or contact with a symptomatic or positive person (Figure 1).

On April 13 and April 27, 2021, employees and residents of the correctional facility were offered (with the option to decline) a quantitative reverse transcription PCR (qRT-PCR)–based test for SARS-CoV-2 using nasopharyngeal specimens as part of the VDH outbreak response. We conducted whole-genome sequencing and single-amplicon analyses on all positive samples to identify the source of the outbreak and the virus variants. At the time of the outbreak, the facility housed 865 residents (within the facility's capacity) and had 300 employees. COVID-19 vaccines had been offered to both employees and residents, who were eligible as a priority population in early 2021. Health department officials stated that a total of 668

Author affiliations: Virginia Tech, Blacksburg, Virginia, USA (R.A. Silverman, A. Cohen, M.J. Friedlander, C.V. Finkielstein); Fralin Biomedical Research Institute, Roanoke, Virginia, USA (A. Ceci, M.J. Friedlander, C.V. Finkielstein); Virginia Department of Health, Richmond, Virginia, USA (M. Helmick, E. Short, P. Bordwine).

DOI: https://doi.org/10.3201/eid2807.220091

[1]These authors contributed equally to this article.

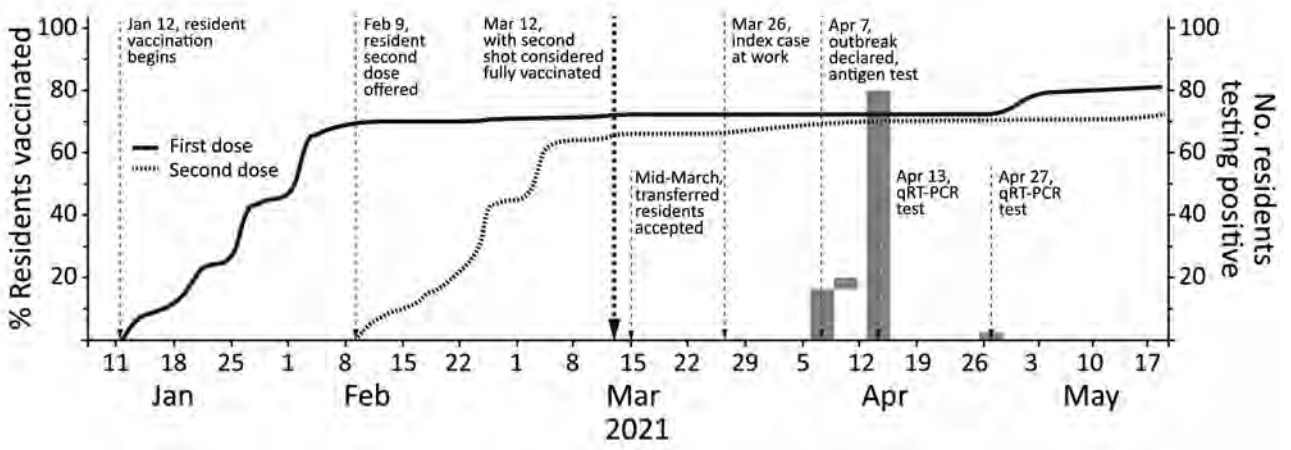

Figure 1. Timeline of SARS-CoV-2 vaccination rollout for incarcerated persons at a correctional facility in rural southwest Virginia included in analysis of vaccine effectiveness during a facility outbreak, April 2021.

residents (77.2%) and 116 employees (38.7%) were fully vaccinated at the time of the outbreak. All vaccinated residents had received the Moderna vaccine (mRNA-1273). All cases associated with the outbreak were identified within 5 months of the initial vaccination rollout for residents and less than 3 months after their first opportunity to be fully vaccinated.

Mitigation measures for employees have been in place at this facility since April 2020 and include the use of mandatory face coverings and screening for symptoms 3 separate times before accessing residential areas. Employees were required to wear N95 masks when working with a positive resident, N95 or surgical masks when working with residents placed in quarantine, and cloth masks when working with persons with no known exposures or cases. Mitigation measures in place for the residents include daily medical screening, zone separations (e.g., quarantine and isolation units), cloth face coverings, limited transfers between housing units, discontinued cafeteria-style meals, and increased cleaning in living quarters. Routine surveillance testing was not conducted before this outbreak; however, once a case was identified, all employee close contacts were excluded from work and required to test negative before returning. Residents in close contact were moved to a yellow zone (e.g., quarantine precautions) with increased screening; they were tested if symptoms developed and before they returned to the green zone (e.g., general precautions). In accordance with VDH recommendations, facilitywide qRT-PCR testing was conducted in November 2020 (2 residents tested positive with no subsequent transmission) and in February 2021 (0 residents tested positive).

In the April 2021 outbreak, the initial patient, a resident, was tested because he reported symptoms during the daily screening; the result was positive. Everyone in that housing unit was then tested, and additional positives were identified. In the next week, additional symptomatic residents in that unit were tested and were positive. At the time of the outbreak, all vaccinated residents had received Moderna vaccines (mRNA-1273; https://www.modernatx.com). Vaccinated employees may have received either Moderna or Pfizer-BioNTech (BNT162b2; https://www.pfizer.com). The use of N95 masks was recommended in all units with positive cases or exposures during the April 2021 outbreak once it was identified.

The VDH April 2021 outbreak response included a site visit from an infection preventionist. VDH epidemiology staff identified multiple failures contributing to the outbreak, including improper mask use by some employees and a screening failure of a mildly symptomatic employee. VDH determined that 2 unvaccinated employees had come to work while infectious; their samples were collected on March 28 and March 31, and both tested positive for SARS-CoV-2. Sequence analyses identified mutations confirming that all cases resulted from these 2 employees. The VDH investigation established that the earliest day the index-case employee worked while infectious was March 26.

Methods

We linked vaccine, demographic, and laboratory information using deidentified, automatically generated, unique identifiers that were verified by VDH staff with access to identifiable information. We excluded persons from participating if information was incomplete or if staff were unable to verifiably link subject information to their laboratory results in the

data. Available demographic information was age, sex, and race.

We defined being fully vaccinated as having received a second vaccination by March 12, which was ≥14 days before the initial infectious employee returned to work on March 26 following out-of-state travel. We defined being partially vaccinated as having received 1 dose by March 12. We defined unvaccinated as receiving the vaccine on or after March 13 or not having received a vaccine at the time of this analysis. We defined SARS-CoV-2 infection as testing positive by qRT-PCR (*8*) or the rapid BinaxNOW antigen test.

Our qRT-PCR test received Emergency Use Authorization status from the FDA. The test's technical development, as well as the assays that determine its specificity, sensitivity, and validation, have been described previously (*8*). Of note, specimens collected for analysis are transported in a specially formulated transport media containing chaotropic agents and stabilizers that ensure the quality of the sample is maintained for up to 10 days, even in the absence of a cold chain (*8*). The quantitative aspect of the assay helps determine the viral load of the sample: each plate includes dilution standard curves with known number of copies for each nucleocapsid protein (*N*) and ribonuclease P/MRP subunit P30 (*RPP30*) gene (range 5–500,000 copies/reaction for each gene) for which a specific cycle threshold (Ct) is generated and clinical results are extrapolated to estimate viral copies. Each person's sample had 2 replicates qRT-PCR Ct values generated for each gene (*N*, envelope [E], spike [*S*], and housekeeping *RPP30*) (*8*). We used the mean Ct of each gene to generate the raw Ct value for comparison to the reference curve. In rare instances, a single value was used if one of the replicates did not amplify for a gene after a 45-cycle amplification limit; out of 92 cases, we did this for *N* gene for 3 cases, for 4 cases for *E* gene, and for 3 cases for *S* gene. We normalized Ct values by multiplying raw Cts by a correction factor defined as the ratio of the sample's mean Ct value for *RPP30* over the mean *RPP30* for all samples in the plate (*9*).

We obtained genome data on all qRT-PCR positive samples using next-generation sequencing and amplicon sequencing approaches. In brief, we sequenced genomic libraries on a MiSeq system (Illumina, https://www.illumina.com) and aligned FASTQ reads to the Wuhan-Hu-1 sequence (GenBank accession no. NC_045512.2). In all cases, Illumina coverage of the consensus sequence was >99.4% of the reference genome. For single-amplicon sequencing, we performed targeted amplification using 13 sets of primers designed in-house for SARS-CoV-2 (*10*). We confirmed mutations by Sanger sequencing.

We limited statistical analyses to the residential population. We excluded data for employees whose demographic data were unavailable or whose tests were conducted outside the correctional facility. First, we assessed disparities in vaccination status across age and race at the time of the outbreak. Second, we estimated the relative risk (RR) of a SARS-CoV-2 infection regardless of symptoms when comparing unvaccinated to vaccinated residents using Poisson regression with robust variance estimates, with and without adjustment for age and race. We calculated vaccine effectiveness (VE) using the estimated RR from these models in which the numerator is the risk among unvaccinated and the denominator is the risk among vaccinated (VE = 1 – 1/RR). Third, we investigated differences in infection risk by age and race, stratifying this by vaccine status in Poisson regression with robust variance estimates. Last, we compared normalized Ct values between vaccinated and unvaccinated cases, with and without adjustment for age and race, using linear regression with robust variance estimates.

Results

Test results from qRT-PCR were available for 854 (98.7%) of the 865 male residents at the facility at the time of the outbreak; 14 (1.6%) results were reported to be indeterminate (*7*). The timeline for testing was as follows: 823 residents were tested on April 13; of those, 732 were retested on April 27, and another 31 were tested on that date for the first time. Of the 19 residents who rapid-tested positive during April 7–9, a total of 17 were tested by qRT-PCR on April 13, and 16 yielded positive results. Although no deaths were reported as a result of this outbreak, an unvaccinated 64-year-old White male resident was hospitalized. Sequence analysis found that all qRT-PCR positive cases were linked to 1 of 2 index cases (employees); 96.2% of samples were identified as the B.1.1.7α (UK) variant of SARS-CoV-2. Of those, 3.8% did not pass the quality control metrics required to assign a variant.

Among the 854 residents with test results (35.8% White, 63.7% African American; mean age 40.4 years, range 18.8–86.0 years), 566 (66.3%) were considered fully vaccinated (76.1% White and 60.7% African American; mean age 42.4 years), 49 (5.7%) were partially vaccinated, and 239 (28.0%) were unvaccinated (mean age 35.4 years) by March 26. For both unvaccinated and vaccinated residents, the mean age was higher among positive cases compared with negative cases (38.5 vs. 34.3 years for unvaccinated; 43.2 vs.

42.3 years for fully vaccinated). Indeterminate qRT-PCR results were reported for 9 (1.6%) fully vaccinated and 5 (2.1%) unvaccinated residents and were excluded from the analyses. For those considered fully vaccinated, the median time from the second shot to March 28 was 33 days (26–46 days) for cases and 32 days (17–47 days) for noncases.

Among the 840 with definitive qRT-PCR test results, 19/557 (3.4%) fully vaccinated, 3/49 (6.1%) partially vaccinated, and 62/234 (26.5%) unvaccinated residents tested positive for SARS-CoV-2 infection (Figure 1). Partially vaccinated residents were excluded from subsequent analysis because of the small number. In unadjusted Poisson regression, unvaccinated residents were 7.8 (95% CI 4.8–12.7; p<0.001) times more likely to test positive during the April outbreak than were fully vaccinated residents (Table). This result corresponds to an unadjusted vaccine effectiveness VE of 87.1% (95% CI 79.0%–92.1%). Adjusting for age and race, unvaccinated residents were 8.8 (95% CI 5.2–14.9) times more likely to test positive compared with fully vaccinated residents, corresponding to an adjusted VE of 88.7% (95% CI 80.9%–93.3%; p<0.001).

When we adjusted for vaccine status, age, and race, older age was more statistically significant with testing positive (a 1-year increase in age RR 1.03, 95% CI 1.01–1.05; p = 0.005), and race was not statistically significant with testing positive (African American vs. White RR 1.51, 95% CI 0.91–2.49; p = 0.109). When we stratified by vaccine status and adjusted by race, age was associated only with testing positive among unvaccinated persons (RR 1.04, 95% CI 1.01–1.06; p = 0.001); we observed no association between testing positive and age among vaccinated residents (RR 1.01, 95% CI 0.97–1.05; p = 0.715).

Among the infected, the unvaccinated showed lower raw and normalized Ct values compared to the vaccinated, indicating a higher viral load among the unvaccinated for all 3 genes (*N, E,* and *S*) (Figure 2). Normalized Ct values were statistically significantly lower among the unvaccinated compared with the vaccinated when we adjusted for age and race in linear regression for all 3 genes: for *N*, Ct value difference = 4.06 (95% CI 0.69–7.42; p = 0.019); for *E*, Ct value difference = 4.22 (95% CI 1.00–7.44; p = 0.011); for *S*, Ct value difference 3.90 (95% CI 0.49–7.32; p = 0.026).

Discussion

This study shows that the Moderna vaccine for COVID-19 is highly effective at preventing SARS-CoV-2 infection among high-risk incarcerated persons, reducing infections by 87% when comparing vaccinated to unvaccinated persons. Although we observed some breakthrough cases, severe COVID-19 was uncommon (1 hospitalization) during this outbreak, and VE remained high and in agreement with reports in other settings in which the B.1.1.7α (UK) variant was prevalent (*11*). Results showed that younger age and Black or African American race were associated with lower vaccine uptake compared to older and non-Hispanic White populations; these differences were observed in the general US population as well (*12*).

Of note, and largely because of the rapid public health response to this outbreak, some case information was not collected; thus, this study has several limitations. First, we did not collect information on comorbidities, symptoms, stage of infection at the time of the test, prior infection and potential associated immunity, and ethnicity. Second, there was no information on contact patterns and corresponding risk for exposure. Third, 14 qRT-PCR results were indeterminate and excluded from the analysis. Fourth, some cases early in the outbreak (during March 28–April 13) could have been missed and misclassified

Table. Relative risk of SARS-CoV-2 infection among incarcerated persons during an outbreak at a men's correctional facility in rural Virginia, April 2021*

	Unadjusted		Adjusted	
Characteristic	No. persons	RR (95% CI)	No. persons	RR (95% CI)
Combined				
Unvaccinated *vs*. fully vaccinated	791	7.77 (4.75–12.69)†	787	8.82 (5.23–14.90)†
Age, 1 y increase	791	0.99 (0.98–1.01)	787	1.03 (1.01–1.05)‡
Race. Black *vs.* White	787	1.96 (1.19–3.258)‡	787	1.51 (0.91–2.49)
Stratified by vaccine status				
Fully vaccinated				
Age, 1 y increase	557	1.01 (0.97–1.05)	554	1.01 (0.97–1.05)
Race, Black vs. White	554	1.21 (0.48–3.02)	554	1.24 (0.49–3.14)
Unvaccinated				
Age, 1 y increase	234	1.03 (1.01–1.05)‡	233	1.04 (1.01–1.06)‡
Race, Black vs. White	233	1.40 (0.79–2.49)	233	1.70 (0.92–3.14)

*Relative risk calculated using Poisson regression. RR, relative risk.
†p<0.001.
‡p<0.01.

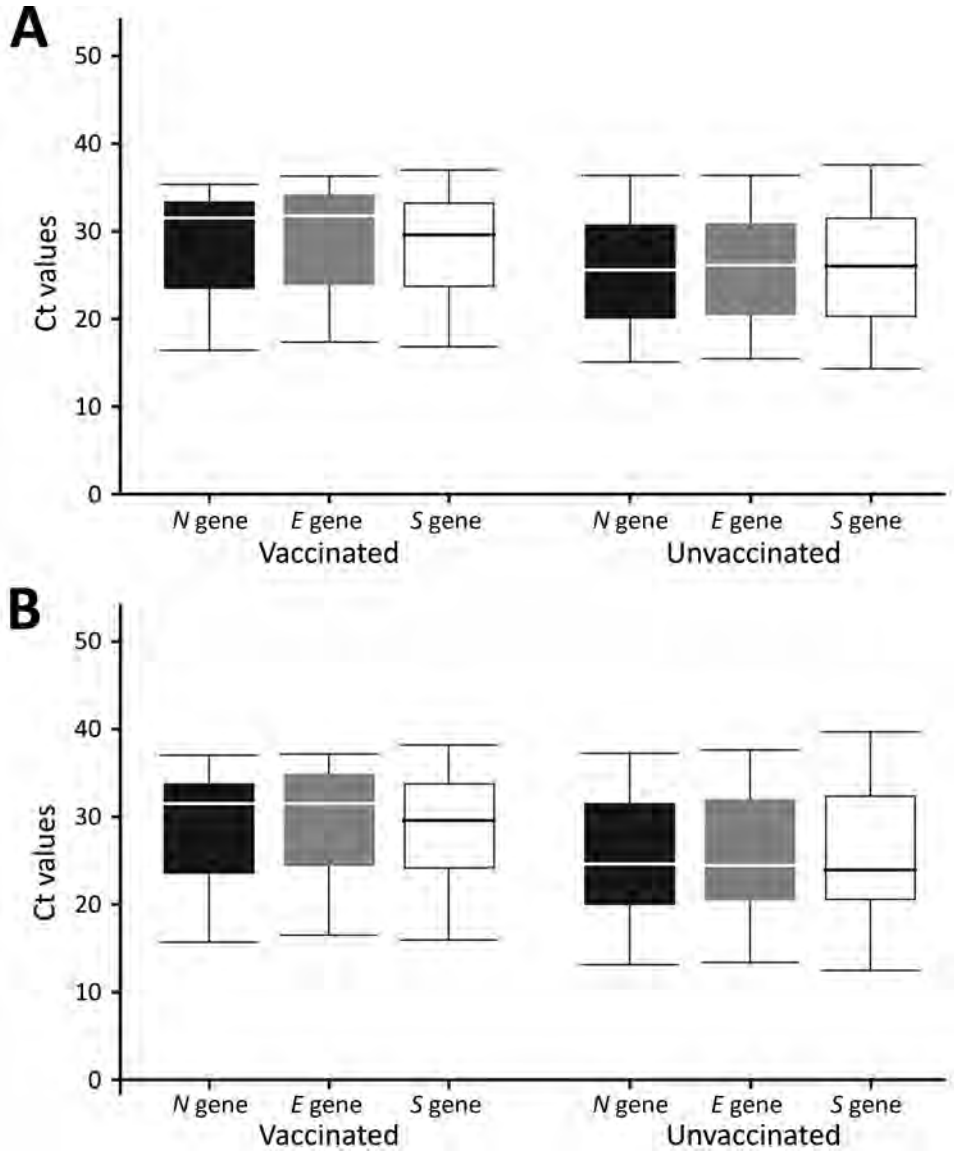

Figure 2. Raw (A) and normalized (B) Ct values for SARS-CoV-2 *N*, *E*, and *S* genes in samples collected from fully vaccinated and unvaccinated infected incarcerated persons during a facility outbreak, April 2021. The midline of the boxes represent the medians of the observations, the bottoms represents the first quartile, and the tops represent the third quartile; whiskers represent the minimum and maximum observations. In unadjusted linear regression comparing fully vaccinated to unvaccinated infected persons, only the E gene had statistically significantly different raw Ct values ($p<0.05$). All 3 genes had statistically significantly different normalized Ct values. Ct, cycle threshold; E, envelope; N, nucleocapsid; S, spike.

as negative based on the initial qRT-PCR testing on April 13. However, we expect any such misclassification to be nondifferential with respect to vaccination status, resulting in an attenuation toward the null, and our results would be an underestimation of the true vaccine effectiveness. Finally, information regarding why some persons chose not to receive the vaccine or were not tested by qRT-PCR on either April 13 or April 27 was unavailable, which could bias the estimates of vaccine effectiveness if patients not being vaccinated or tested correlated with prior infection (and associated immunity). Fortunately, almost all residents (99%) were qRT-PCR tested on April 13, April 27, or both, and information was verified whenever possible. Therefore, any missing data or residual errors likely have minimal effect on estimates. Of note, most residents in the study had been housed long-term in this facility because no transfers into the facility occurred until mid-March 2021 and no prior COVID-19 outbreaks among residents were reported before April 2021. Thus, immunity from prior infections is likely negligible.

Methods from this study can be applied to similar settings. As new variants emerge and immunity may decrease (*13*), continued VE monitoring is needed to ensure public health strategies are well-informed and effective, especially in high-risk settings such as correctional facilities (*14*). High vaccination coverage among incarcerated persons, correctional facility staff, and the general population is critical to alleviate the challenges of the ongoing pandemic. In addition, sentinel or universal testing in correctional facilities

may be necessary to prevent outbreaks (*15*), along with maintained compliance of other mitigation measures, such as masking and screening, proper ventilation, and vaccination boosters.

This project was supported by a Go Virginia Economic Resilience and Recovery Grant (20-GOVA-ERR-02A and 20-GOVA-ERR-02D), the Department of General Services of the Commonwealth of Virginia (DGS-201020-UVT), and funds from Virginia Tech, the Fralin Biomedical Research Institute at Virginia Tech Carilion, and the Fralin Life Sciences Institute.

About the Author

Dr. Silverman is a research scientist in epidemiology at the Center for Public Health Practice and Research in the Department of Population Sciences at Virginia Polytechnic Institute and State University, Blacksburg, Virginia. Her primary research interests focus on infectious disease epidemiology. Mr. Ceci is a senior staff scientist at the Molecular Diagnostics Laboratory, Fralin Biomedical Research Institute, Roanoke, Virginia.

References

1. Jiménez MC, Cowger TL, Simon LE, Behn M, Cassarino N, Bassett MT. Epidemiology of COVID-19 among incarcerated individuals and staff in Massachusetts jails and prisons. JAMA Netw Open. 2020;3:e2018851. https://doi.org/10.1001/jamanetworkopen.2020.18851
2. Hawks L, Woolhandler S, McCormick D. COVID-19 in prisons and jails in the United States. JAMA Intern Med. 2020;180:1041–2. https://doi.org/10.1001/jamainternmed.2020.1856
3. Hershow RB, Segaloff HE, Shockey AC, Florek KR, Murphy SK, DuBose W, et al. Rapid spread of SARS-CoV-2 in a state prison after introduction by newly transferred incarcerated persons—Wisconsin, August 14–October 22, 2020. MMWR Morb Mortal Wkly Rep. 2021;70:478–82. https://doi.org/10.15585/mmwr.mm7013a4
4. Lewis NM, Salmanson AP, Price A, Risk I, Guymon C, Wisner M, et al. Community-associated outbreak of COVID-19 in a correctional facility—Utah, September 2020–January 2021. MMWR Morb Mortal Wkly Rep. 2021;70:467–72. https://doi.org/10.15585/mmwr.mm7013a2
5. Sims KM, Foltz J, Skidmore ME. Prisons and COVID-19 spread in the United States. Am J Public Health. 2021;111:1534–41. https://doi.org/10.2105/AJPH.2021.306352
6. Strodel R, Dayton L, Garrison-Desany HM, Eber G, Beyrer C, Arscott J, et al. COVID-19 vaccine prioritization of incarcerated people relative to other vulnerable groups: An analysis of state plans. PLoS One. 2021;16:e0253208. https://doi.org/10.1371/journal.pone.0253208
7. Stern MF, Piasecki AM, Strick LB, Rajeshwar P, Tyagi E, Dolovich S, et al. Willingness to receive a COVID-19 vaccination among incarcerated or detained persons in correctional and detention facilities—four states, September–December 2020. MMWR Morb Mortal Wkly Rep. 2021;70:473–7. https://doi.org/10.15585/mmwr.mm7013a3
8. Ceci A, Muñoz-Ballester C, Tegge AN, Brown KL, Umans RA, Michel FM, et al. Development and implementation of a scalable and versatile test for COVID-19 diagnostics in rural communities. Nat Commun. 2021;12:4400. https://doi.org/10.1038/s41467-021-24552-4
9. Bouscambert Duchamp M, Casalegno JS, Gillet Y, Frobert E, Bernard E, Escuret V, et al. Pandemic A(H1N1)2009 influenza virus detection by real time RT-PCR: is viral quantification useful? Clin Microbiol Infect. 2010;16:317–21. https://doi.org/10.1111/j.1469-0691.2010.03169.x
10. Quick J, Grubaugh ND, Pullan ST, Claro IM, Smith AD, Gangavarapu K, et al. Multiplex PCR method for MinION and Illumina sequencing of Zika and other virus genomes directly from clinical samples. Nat Protoc. 2017;12:1261–76. https://doi.org/10.1038/nprot.2017.066
11. Charmet T, Schaeffer L, Grant R, Galmiche S, Chény O, Von Platen C, et al. Impact of original, B.1.1.7, and B.1.351/P.1 SARS-CoV-2 lineages on vaccine effectiveness of two doses of COVID-19 mRNA vaccines: results from a nationwide case–control study in France. Lancet Reg Health Eur. 2021;8:100171. https://doi.org/10.1016/j.lanepe.2021.100171
12. Nguyen KH, Srivastav A, Razzaghi H, Williams W, Lindley MC, Jorgensen C, et al. COVID-19 vaccination intent, perceptions, and reasons for not vaccinating among groups prioritized for early vaccination—United States, September and December 2020. MMWR Morb Mortal Wkly Rep. 2021;70:217–22. https://doi.org/10.15585/mmwr.mm7006e3
13. Collie S, Champion J, Moultrie H, Bekker LG, Gray G. Effectiveness of BNT162b2 vaccine against Omicron variant in South Africa. N Engl J Med. 2022;386:494–6
14. Hagan LM, McCormick DW, Lee C, Sleweon S, Nicolae L, Dixon T, et al. Outbreak of SARS-CoV-2 B.1.617.2 (Delta) variant infections among incarcerated persons in a federal prison—Texas, July–August 2021. MMWR Morb Mortal Wkly Rep. 2021;70:1349–54. https://doi.org/10.15585/mmwr.mm7038e3
15. Hagan LM, Williams SP, Spaulding AC, Toblin RL, Figlenski J, Ocampo J, et al. Mass testing for SARS-CoV-2 in 16 prisons and jails—six jurisdictions, United States, April–May 2020. MMWR Morb Mortal Wkly Rep. 2020;69:1139–43. https://doi.org/10.15585/mmwr.mm6933a3

Address for correspondence: Carla V. Finkielstein, Fralin Biomedical Research Institute at VTC, 2 Riverside Cir, Roanoke, VA 24016, USA; email: finkielc@vt.edu

Enterovirus D68 in Hospitalized Children, Barcelona, Spain, 2014–2021

Cristina Andrés,[1] Jorgina Vila,[1] Anna Creus-Costa, Maria Piñana, Alejandra González-Sánchez, Juliana Esperalba, Maria Gema Codina, Carla Castillo, Maria Carmen Martín, Francisco Fuentes, Susana Rubio, Karen García-Comuñas, Rodrigo Vásquez-Mercado, Narcís Saubi, Carlos Rodrigo, Tomàs Pumarola, Andrés Antón

To determine molecular epidemiology and clinical features of enterovirus D68 (EV-D68) infections, we reviewed EV-D68–associated respiratory cases at a hospital in Barcelona, Spain, during 2014–2021. Respiratory samples were collected from hospitalized patients or outpatients with symptoms of acute respiratory tract infection or suggestive of enterovirus infection. Enterovirus detection was performed by real-time multiplex reverse transcription PCR and characterization by phylogenetic analysis of the partial viral protein 1 coding region sequences. From 184 patients with EV-D68 infection, circulating subclades were B3 (80%), D1 (17%), B2 (1%), and A (<1%); clade proportions shifted over time. EV-D68 was detected mostly in children (86%) and biennially (2016, 2018, 2021). In patients <16 years of age, the most common sign/symptom was lower respiratory tract infection, for which 11.8% required pediatric intensive care unit admission and 2.3% required invasive mechanical ventilation; neurologic complications developed in 1. The potential neurotropism indicates that enterovirus surveillance should be mandatory.

In 1962, enterovirus D68 (EV-D68) was first isolated from the oropharynx of children in California, USA, who were hospitalized for lower respiratory tract infection (LRTI) (*1*). Although infections can occur at any age, children are the most susceptible to enterovirus infections (*2*). In temperate countries, enterovirus circulation usually follows a seasonal pattern, peaking in late summer and early autumn, but a second peak can also be detected during spring (*3*).

Until 2007, EV-D68 was rarely implicated in severe diseases and was poorly detected, associated only with small outbreaks in the United States and the Netherlands (*4*,*5*). However, in 2014, EV-D68 gained attention because of a large outbreak in the United States that was associated with severe respiratory illness and, in some cases, with neurologic complications, such as acute flaccid paralysis (AFP) (*6*). In Europe, circulation of EV-D68 was low and mild, but circulation increased in the following years, especially in 2021, after preventive measures for SARS-CoV-2 were eased (*7*). We reviewed EV-D68–associated respiratory cases, particularly in children, diagnosed at a tertiary-care university hospital in Barcelona (Catalonia, Spain) during 2014–2021. Institutional review board approval (PR(AG)173/2017) was obtained from the HUVH Clinical Research Ethics Committee.

Materials and Methods

Patients and Samples

During October 2014–November 2021, upper and lower respiratory tract specimens were collected by hospital staff and sent to the Respiratory Viruses Unit of the Vall d'Hebron University Hospital laboratory for confirmation of respiratory viruses. Samples were taken according to clinical criteria from patients with suspected acute respiratory tract infection or enterovirus infection who were hospitalized or sought care at the emergency department. In addition,

Author affiliations: Hospital Universitari Vall d'Hebron, Vall d'Hebron Research Institute, Barcelona, Spain (C. Andrés, J. Vila, A. Creus-Costa, M. Piñana, A. González-Sánchez, J. Esperalba, M.G. Codina, C. Castillo, M. Carmen Martín, F. Fuentes, S. Rubio, K. García-Comuñas, R. Vásquez-Mercado, N. Saubi, C. Rodrigo, T. Pumarola, A. Antón); CIBER de Enfermedades Infecciosas, Instituto de SaludCarlos III, Madrid, Spain (C. Andrés, M. Piñana, A. González-Sánchez, J. Esperalba, M.G. Codina, N. Saubi, T. Pumarola, A. Antón); Hospital Universitari Germans Trias i Pujol, Barcelona (C. Rodrigo)

DOI: https://doi.org/10.3201/eid2807.220264

[1]These authors contributed equally to this article.

since September 2021, respiratory samples for SARS-CoV-2 screening were further tested for other respiratory viruses. We retrospectively collected patient demographic features (sex and age) for all laboratory-confirmed cases of enterovirus infection and collected clinical data only for patients <16 years of age (pediatric population).

Regarding the clinical definitions used, upper respiratory tract infections (URTIs) were infections from the nose to the larynx; LRTIs were recurrent wheezing, asthma, bronchiolitis, and pneumonia. To ensure that the length of hospital stay or respiratory support were associated only with EV-D68, we studied LRTI severity in patients requiring admission because of respiratory tract infection. Respiratory support was divided into 5 groups: none, oxygen through nasal cannula, high-flow nasal cannula, noninvasive mechanical ventilation, and invasive mechanical ventilation. EV-D68–associated AFP was defined as myelitis causing sudden onset of paralysis with T2 hyperintensity in medulla gray matter with dorsal brain stem variably affected on magnetic resonance images and EV-D68 detected in respiratory specimens.

Enterovirus Detection and Characterization

We performed enterovirus detection by using specific real-time multiplex reverse transcription, as previously described (*8*). The characterization of enterovirus was performed by the phylogenetic analyses of the partial viral protein 1 (VP1) coding-region according to the protocol recommended by the World Health Organization, with minor modifications (*8*).

Statistical Analyses

We performed statistical analysis by using SPSS version 22 (SPSS Inc., https://www.ibm.com). To assess associations between categorical variables, we performed χ^2 testing and calculated Z scores. We considered $p<0.05$ to be significant.

Results

Over the 7 years of the study, 67,798 respiratory specimens (39,183 patients) were received for laboratory confirmation of respiratory viruses. A total of 1,423 (2%) samples from 1,313 (3%) patients were laboratory confirmed as containing enterovirus. Phylogenetic analysis of the partial VP1 coding region revealed that 187 (13%) of the 1,423 strains from 184 (14%) of the 1,313 patients were EV-D68 (147 subclade B3, 80%; 32 newly emerged subclade D1, 17%; 2 subclade B2, 1%; and 1 subclade A, <1%) (Appendix Figure 2, https://wwwnc.cdc.gov/EID/article/28/7/22-0264-App1.pdf). EV-D68 was detected mostly in pediatric populations (158/184; 86%) (median age 3 years; interquartile range 1.73–6 years; age range 8 months to 77 years), especially in patients <5 years of age (117/158; 74%). The distribution of EV-D68 infections (Appendix Figure 1) was like that of other enteroviruses; circulation peaked in autumn and spring, especially during 2016, 2018, and 2021; fewer cases were reported in 2015, 2017, 2019; and no cases were reported in 2020. Circulation of strains belonging to the several subclades shifted throughout the study period; B3 predominated until 2017, and B3 and D1 co-circulated until 2021, when B3 was predominant (Table 1; Appendix Figure 1). Moreover, the distribution of these clades among the studied population differed ($p<0.00001$) (Appendix Table). B3 was detected mostly among the pediatric population (<16 years of age, 95% of cases), whereas subclade D1 was detected equally in pediatric and adult (≥16 years) populations (17/32 [53%] vs. 15/32 [47%]; $p<0.00001$).

Among the 158 children with EV-D68, 76 (48%) were hospitalized and 82 (52%) were seen as outpatients (Table 2). Until 2021, a total of 12/82 (15%) patients were outpatients, compared with 70/82 (85%) during 2021.

With regard to clinical signs and symptoms, most common were LRTI (101/158; 64%), followed by URTI (37/158; 23%). A total of 9/158 (6%) pediatric

Table 1. Distribution of enterovirus D68 subclades, by year, for all patients and hospitalized children, Barcelona, Spain, 2014–2021*

	Year								
Clade	2014	2015	2016	2017	2018	2019	2020	2021	Total
All									
A	1								1
B2		1	1						2
B3		6	26		24			91	147
D1	4			3	20	2		3	32
Hospitalized children									
A									
B2		1	1						2
B3		6	21		17			20	64
D1	3			1	5				9
Total	5	7	27	3	44	2		94	

*Blank cells indicate zero.

Table 2. Demographic and clinical characteristics of patients in study of enterovirus-D68 in hospitalized children, Barcelona, Spain, 2014–2021*

Characteristic	Hospitalized, no. (%)†	Outpatient, no. (%)
Sex		
M	44 (57.9)	47/82 (57.3)
F	56 (42.1)	35 (42.7)
Age, y		
<2	24 (31.6)	24 (29.3)
2–4	34 (44.7)	34 (41.4)
≥5	18 (23.7)	24 (29.3)
Signs/symptoms‡		
LRTI	56 (73.6)	45 (54.9)
>24 mo	40 (71.4)	36 (80.0)
≤24 mo	16 (28.6)	9 (20.0)
URTI	10 (13.2)	27 (32.9)
Other	10 (13.2)	10 (12.2)
Treatment for LRTI		
Chronic respiratory comorbidities	28/56 (50)	20/45 (44.4)
Asthma-directed therapies		
β2 agonists	52/56 (92.9)	43/45 (95.6)
Systemic corticosteroids	51/56 (91.1)	34/45 (75.6)
Hospitalization for LRTI		
Hospital length of stay, d§	3 (1–5)	NA
Respiratory support§	44 (78.6)	NA
Maximum respiratory support required¶		
Conventional oxygen	23 (52.3)	NA
HFNC	13 (29.5)	NA
NIMV	6 (13.6)	NA
IMV	1 (2.3)	NA
ECMO	1 (2.3)	NA
Duration of respiratory support§¶#	3 (1–4)	
PICU admission	9 (11.8)	NA
PICU length of stay, d§	4 (2–9)	NA

*Units of measure are no. (%) unless otherwise indicated. ECMO, extracorporeal membrane oxygenation; HFNC, high-flow nasal cannula; IMV, invasive mechanical ventilation; LRTI, lower respiratory tract infection; NA, not applicable; NIMV, noninvasive mechanical ventilation; PICU, pediatric intensive care unit; URTI, upper respiratory tract infection.
†Percentages are calculated vertically, according to the total cases.
‡The main symptom at time of hospital admission or consultation.
§For continuous variables, means and interquartile ranges are indicated.
¶Three patients received home mechanical ventilation and required increased respiratory support during hospitalization.
#Excludes the 3 patients with home mechanical ventilation and the patient who received ECMO.

patients had fever as the only sign, 6/158 (4%) had gastroenteritis, and 1 (1%) had myelitis and AFP (a 2-year-old girl with no underlying diseases but not fully recovered with quadriplegia and respiratory failure requiring home tracheotomy mechanical ventilation and feeding through gastrostomy). The remaining (4/158; 2.5%) patients were asymptomatic.

Discussion

Interest in EV-D68 was limited until the large outbreak that occurred in the United States in 2014 (*6*,*9*). Although EV-D68 circulation had been previously described, that large outbreak affecting mainly children was associated not only with severe respiratory disease but also with neurologic complications in some cases. Furthermore, the circulating EV-D68 strains belonged to previously circulating lineages, and therefore, there was no clear evidence of a new virus strain associated with increased severity (*6*,*9*). Nevertheless, during the same period, further studies began not only in the United States but also in Europe to monitor EV-D68 circulation (*10*). Results revealed a low level of EV-D68 detection and milder clinical manifestations in Europe compared with those in the United States (*10*). Similarly, the EV-D68 circulation in Barcelona was low during that period (*8*). However, in the following seasons, the trend increased, particularly during 2016 and 2018, as reported in other regions of Spain (*11*) and Europe (*12*,*13*), especially the upsurge observed during the 2021–22 season (*7*). According to those data, EV-D68 seems to follow a biennial circulation pattern as recently defined (*14*,*15*), which was displaced during 2020 because of the COVID-19 pandemic, but higher numbers of cases were detected during 2021 (*7*).

Four distinct clades of EV-D68 (A–D) have been described (*16*) in addition to subclades A, B1, B2, and B3 (*10*,*17*). Clades cocirculated variably; B3 predominated during the studied seasons, which is in concordance with other reports (*10*,*18*). Moreover, in our study, viruses belonging to the new emerging subclade D1 within clade D, were mainly

detected during 2018, and cocirculation with subclade B3 was equal until 2018, as recently reported around Europe (France and Italy) (*12*,*19*). Furthermore, subclade D1 was observed similarly among pediatric and adult populations, compared with B3, which was mostly detected in children. This age effect depending on clade, in concordance with our results, has been reported in other studies (*19*,*20*). Of note, a recent study reported changes in the VP1 region of D1 associated with lower cross-protection in adults (*21*).

The most common clinical features of EV-D68 infection in children in this study were respiratory, and AFP developed in only 1 patient. EV-D68 has been mostly associated with LRTI in children >2 years of age, 50%–70% of whom previously had asthma or recurrent wheezing and 20% of whom had no comorbidities, as described in our study. In addition, most cases from our study were mild; few patients were admitted to intensive care units (ICUs). However, during the US outbreak in 2014, respiratory signs/symptoms reported for hospitalized patients were more severe: 59% of patients required ICU admission, 23% noninvasive mechanical ventilation, and 8% invasive mechanical ventilation; therefore, previous asthma or reactive airway disease might increase the risk for ICU admission and the need for ventilatory support (*22*). Despite changes in the virologic properties of circulating viruses, the clinical features remained similar to those reported in 2014 in Europe, in contrast to the United States and Canada. In addition, during the US outbreak, AFP cases associated with EV-D68 infection (subclade B3), in which this virus was the only pathogen isolated, increased (*6*,*9*). Although enteroviruses are known to be neurotropic, we detected only 1 case of AFP associated with EV-D68 subclade B3 infection.

The potential neurotropism of EV-D68 and other enteroviruses suggests that surveillance should be mandatory, which is one of the aims of the European Non-Polio Enterovirus Network (https://www.escv.eu/enpen). The year-round circulation of EV-D68 should help with close monitoring of this enterovirus, as well as prompt response to the potential occurrence of outbreaks and related clinical burden.

This study was supported by the Spanish Ministry of Economy and Competitiveness, Instituto de Salud Carlos III, cofinanced by the European Development Regional Fund "A way to achieve Europe," Spanish Network for Research in Infectious Diseases (REIPI RD16/0016/0003).

About the Author

Dr. Andrés is a postdoctoral researcher at the Respiratory Viruses Unit in the Microbiology Department of Hospital Univeristari Vall d'Hebron. Her research interests are the epidemiology and molecular characterization based on whole-genome sequencing of viruses, especially influenza viruses, enteroviruses, rhinoviruses, and coronaviruses.

References

1. Schieble JH, Fox VL, Lennette EH. A probable new human picornavirus associated with respiratory diseases. Am J Epidemiol. 1967;85:297–310. https://doi.org/10.1093/oxfordjournals.aje.a120693
2. Khetsuriani N, Lamonte-Fowlkes A, Oberst S, Pallansch MA; Centers for Disease Control and Prevention. Enterovirus surveillance—United States, 1970–2005. MMWR Surveill Summ. 2006;55:1–20.
3. European Centre for Disease Prevention and Control. Rapid risk assessment—outbreak of enterovirus A71 with severe neurological symptoms among children in Catalonia, Spain [cited 2021 Jun 15]. https://www.ecdc.europa.eu/sites/default/files/media/en/publications/Publications/07-06-2016-RRA-Enterovirus%2071-Spain.pdf
4. Meijer A, van der Sanden S, Snijders BE, Jaramillo-Gutierrez G, Bont L, van der Ent CK, et al. Emergence and epidemic occurrence of enterovirus 68 respiratory infections in The Netherlands in 2010. Virology. 2012;423:49–57. https://doi.org/10.1016/j.virol.2011.11.021
5. Rahamat-Langendoen J, Riezebos-Brilman A, Borger R, van der Heide R, Brandenburg A, Schölvinck E, et al. Upsurge of human enterovirus 68 infections in patients with severe respiratory tract infections. J Clin Virol. 2011;52:103–6. https://doi.org/10.1016/j.jcv.2011.06.019
6. Midgley CM, Jackson MA, Selvarangan R, Turabelidze G, Obringer E, Johnson D, et al. Severe respiratory illness associated with enterovirus D68–Missouri and Illinois, 2014. MMWR Morb Mortal Wkly Rep. 2014;63:798–9.
7. Benschop KS, Albert J, Anton A, Andrés C, Aranzamendi M, Armannsdóttir B, et al. Re-emergence of enterovirus D68 in Europe after easing the COVID-19 lockdown, September 2021. Euro Surveill. 2021;26. https://doi.org/10.2807/1560-7917.ES.2021.26.45.2100998
8. Andrés C, Vila J, Gimferrer L, Piñana M, Esperalba J, Codina MG, et al. Surveillance of enteroviruses from paediatric patients attended at a tertiary hospital in Catalonia from 2014 to 2017. J Clin Virol. 2019;110:29–35. https://doi.org/10.1016/j.jcv.2018.11.004
9. Midgley CM, Watson JT, Nix WA, Curns AT, Rogers SL, Brown BA, et al.; EV-D68 Working Group. Severe respiratory illness associated with a nationwide outbreak of enterovirus D68 in the USA (2014): a descriptive epidemiological investigation. Lancet Respir Med. 2015;3:879–87. https://doi.org/10.1016/S2213-2600(15)00335-5
10. Poelman R, Schuffenecker I, Van Leer-Buter C, Josset L, Niesters HG, Lina B; ESCV-ECDC EV-D68 Study Group. European surveillance for enterovirus D68 during the emerging North-American outbreak in 2014. J Clin Virol. 2015;71:1–9. https://doi.org/10.1016/j.jcv.2015.07.296
11. Cabrerizo M, García-Iñiguez JP, Munell F, Amado A, Madurga-Revilla P, Rodrigo C, et al. First cases of severe flaccid paralysis associated with enterovirus D68 infection in Spain, 2015–2016. Pediatr Infect Dis J. 2017;36:1214–6. https://doi.org/10.1097/INF.0000000000001668

12. Pellegrinelli L, Giardina F, Lunghi G, Uceda Renteria SC, Greco L, Fratini A, et al. Emergence of divergent enterovirus (EV) D68 sub-clade D1 strains, northern Italy, September to October 2018. Euro Surveill. 2019;24. https://doi.org/10.2807/1560-7917.ES.2018.24.7.1900090
13. Cottrell S, Moore C, Perry M, Hilvers E, Williams C, Shankar AG. Prospective enterovirus D68 (EV-D68) surveillance from September 2015 to November 2018 indicates a current wave of activity in Wales. Euro Surveill. 2018;23. https://doi.org/10.2807/1560-7917.ES.2018.23.46.1800578
14. Kramer R, Sabatier M, Wirth T, Pichon M, Lina B, Schuffenecker I, et al. Molecular diversity and biennial circulation of enterovirus D68: a systematic screening study in Lyon, France, 2010 to 2016. Euro Surveill. 2018;23. https://doi.org/10.2807/1560-7917.ES.2018.23.37.1700711
15. Messacar K, Pretty K, Reno S, Dominguez SR. Continued biennial circulation of enterovirus D68 in Colorado. J Clin Virol. 2019;113:24–6. https://doi.org/10.1016/j.jcv.2019.01.008
16. Tokarz R, Firth C, Madhi SA, Howie SRC, Wu W, Sall AA, et al. Worldwide emergence of multiple clades of enterovirus 68. J Gen Virol. 2012;93:1952–8. https://doi.org/10.1099/vir.0.043935-0
17. Gong YN, Yang SL, Shih SR, Huang YC, Chang PY, Huang CG, et al. Molecular evolution and the global reemergence of enterovirus D68 by genome-wide analysis. Medicine (Baltimore). 2016;95:e4416. https://doi.org/10.1097/MD.0000000000004416
18. Knoester M, Helfferich J, Poelman R, Van Leer-Buter C, Brouwer OF, Niesters HGM; 2016 EV-D68 AFM Working Group. Twenty-nine cases of enterovirus-D68-associated acute flaccid myelitis in Europe 2016: a case series and epidemiologic overview. Pediatr Infect Dis J. 2019;38:16–21. https://doi.org/10.1097/INF.0000000000002188
19. Bal A, Sabatier M, Wirth T, Coste-Burel M, Lazrek M, Stefic K, et al. Emergence of enterovirus D68 clade D1, France, August to November 2018. Euro Surveill. 2019;24. https://doi.org/10.2807/1560-7917.ES.2019.24.3.1800699
20. Schuffenecker I, Mirand A, Josset L, Henquell C, Hecquet D, Pilorgé L, et al. Epidemiological and clinical characteristics of patients infected with enterovirus D68, France, July to December 2014. Euro Surveill. 2016;21. https://doi.org/10.2807/1560-7917.ES.2016.21.19.30226
21. Duval M, Mirand A, Lesens O, Bay JO, Caillaud D, Gallot D, et al. Retrospective study of the upsurge of enterovirus D68 clade D1 among adults (2014–2018). Viruses. 2021;13:1607. https://doi.org/10.3390/v13081607
22. Greninger AL, Naccache SN, Messacar K, Clayton A, Yu G, Somasekar S, et al. A novel outbreak enterovirus D68 strain associated with acute flaccid myelitis cases in the USA (2012–14): a retrospective cohort study. Lancet Infect Dis. 2015;15:671–82. https://doi.org/10.1016/S1473-3099(15)70093-9

Address for correspondence: Tomàs Pumarola, Respiratory Viruses Unit, Virology Section, Microbiology Department, Hospital Universitari Vall d'Hebron, Vall d'Hebron Research Institute, Universitat Autònoma de Barcelona, Passeig Vall d'Hebron 119-129, 08035 Barcelona, Spain; email: virusrespiratoris@vhebron.net

Epidemiologic, Clinical, and Genetic Characteristics of Human Infections with Influenza A(H5N6) Viruses, China

Wenfei Zhu,[1] Xiyan Li,[1] Jie Dong,[1] Hong Bo, Jia Liu, Jiaying Yang, Ye Zhang, Hejiang Wei, Weijuan Huang, Xiang Zhao, Tao Chen, Jing Yang, Zi Li, Xiaoxu Zeng, Chao Li, Jing Tang, Li Xin, Rongbao Gao, Liqi Liu, Min Tan, Yuelong Shu, Lei Yang, Dayan Wang

The recent rise in the frequency of influenza A(H5N6) infections in China has raised serious concerns about whether the risk for human infection has increased. We surveyed epidemiologic, clinical, and genetic data of human infections with A(H5N6) viruses. Severe disease occurred in 93.8% of cases, and the fatality rate was 55.4%. Median patient age was 51 years. Most H5N6 hemagglutinin (HA) genes in human isolates in 2021 originated from subclade 2.3.4.4b; we estimated the time to most recent common ancestor as June 16, 2020. A total of 13 genotypes with HA genes from multiple subclades in clade 2.3.4.4 were identified in human isolates. Of note, 4 new genotypes detected in 2021 were the major causes of increased H5N6 virus infections. Mammalian-adapted mutations were found in HA and internal genes. Although we found no evidence of human-to-human transmission, continuous evolution of H5N6 viruses may increase the risk for human infections.

Various subtypes of avian influenza viruses (AIVs) circulate globally in wild birds. Domestic poultry are also susceptible to these viruses and, occasionally, AIVs have become able to cross the species barrier to infect humans (*1*–*4*). In China, situations in which human infections with AIVs have occurred can be complicated; many subtypes of AIVs have been reported, including influenza A(H5N1), A(H5N6), A(H7N4), A(H7N9), A(H9N2), A(H10N8), and A(H10N3) (*4*,*5*). Highly pathogenic avian influenza (HPAI) A(H5) viruses have continually caused worldwide outbreaks in both wild birds and poultry, with some spillover to humans, most notably 863 HPAI A(H5N1) cases, 456 of which were fatal (*6*).

In April 2014, the first human infection with HPAI A(H5N6) virus was reported in Sichuan Province, China (*1*). Since then, human cases have been continuously documented in China. By the end of 2021, 66 cases had been documented globally, 36 of which were fatal. Of those, 65 cases were in China, and the remaining case was reported in Laos.

Since its emergence in Guangdong Province in 1996, HPAI H5 type viruses became endemic in birds in China and other regions and developed into distinct clades (*7*). The clade 2.3.4.4 H5 viruses were first reported in migratory birds in eastern China in 2013, followed by outbreaks in both wild and domestic birds in South Korea at the beginning of 2014. Thereafter, clade 2.3.4.4 H5 viruses spread westward and eastward from Asia to other

Author affiliations: National Institute for Viral Disease Control and Prevention, Chinese Center for Disease Control and Prevention, Beijing, China (W. Zhu, X. Li, J. Dong, H. Bo, J. Liu, Jiaying Yang, Y. Zhang, H. Wei, W. Huang, X. Zhao, T. Chen, Jing Yang, Z. Li, X. Zeng, J. Tang, L. Xin, R. Gao, L. Liu, M. Tan, Y. Shu, L. Yang, D. Wang); Chinese Center for Disease Control and Prevention, Beijing (C. Li); World Health Organization Collaborating Centre for Reference and Research on Influenza, Beijing (W. Zhu, X. Li, J. Dong, H. Bo, J. Liu, Jiaying Yang, Y. Zhang, H. Wei, W. Huang, X. Zhao, T. Chen, Jing Yang, Z. Li, X. Zeng, J. Tang, L. Xin, R. Gao, L. Liu, M. Tan, Y. Shu, L. Yang, D. Wang); Key Laboratory for Medical Virology, National Health and Family Planning Commission, Beijing (W. Zhu, X. Li, J. Dong, H. Bo, J. Liu, Jiaying Yang, Y. Zhang, H. Wei, W. Huang, X. Zhao, T. Chen, Jing Yang, Z. Li, X. Zeng, J. Tang, L. Xin, R. Gao, L. Liu, M. Tan, Y. Shu, L. Yang, D. Wang); Sun Yat-sen University, Guangzhou, China (Jiaying Yang, Y. Shu)

DOI: https://doi.org/10.3201/eid2807.212482

[1]These authors contributed equally to this article.

continents, accompanied by multiple reassortment events between clade 2.3.4.4 H5 viruses and other AIVs circulating in wild and domestic birds (*8*,*9*). Clade 2.3.4.4 H5N6 AIV has been mainly endemic among birds in China and southeast Asia since 2013 (*10*–*12*), gradually replacing H5N1 as a dominant AIV subtype in poultry across southern China (*13*). Similar to H7N9 AIV, reassortments among H5N6 and H9N2 AIVs occurred dynamically (*14*–*16*). Furthermore, many other subtypes of AIVs were documented to donate their internal genes to H5N6, including AIVs from wild birds (*11*,*17*,*18*). Thus, H5N6 genotypes diversified both in poultry and humans (*11*,*16*–*18*).

Genetic and biologic characteristics indicated that H5N6 viruses were highly pathogenic in chickens (*19*–*21*). Studies have shown that some H5N6 viruses of clade 2.3.4.4 possessed the ability to bind both avian-origin and human-origin sialic acid receptors and had the ability to attach to human tracheal epithelial and alveolar tissues (*22*). Although H5N6 viruses were not as pathogenic in mice and ferrets as their parental clade 2.3.4 H5N1 viruses, they exhibited greater transmissibility than H5N1 viruses in a ferret model (*22*,*23*). Thus, clade 2.3.4.4 H5N6 viruses demonstrated higher potential to transmit among humans.

During the COVID-19 pandemic, seasonal influenza infections notably decreased worldwide compared with previous flu seasons (*24*). However, human infections with zoonotic influenza viruses do not appear to have decreased. Of note, a recent rise in the frequency of H5N6 cases was observed (*25*). For the purposes of preparing for future possible pandemics, investigating the epidemiologic, clinical, and genetic characteristics of H5N6 AIVs that infect humans is critical.

Methods

Study Cases

In China, all laboratory-confirmed influenza A(H5N6) cases are reported through a national surveillance system. Patients with respiratory tract specimens that test positive for H5 and N6 by real-time reverse transcription PCR are confirmed as H5N6 infections. Demographic, epidemiologic, and basic clinical data on influenza A(H5N6) cases are collected on standardized forms. We included information regarding age; sex; place of residence; symptoms at illness onset; comorbidities associated with increased risk for influenza complications; dates of illness onset, hospital admission, death or discharge, and clinical treatments; and potential exposures to domestic or retail animals and visits to live poultry markets in our analysis.

Ethics

The National Health Commission of the People's Republic of China determined that the collection of data on each H5N6 case was part of a continuing public health investigation of an emerging outbreak. Thus, the ethics approval was exempt from official review by our institutional review board.

Virus Isolation

We used original samples from human cases for H5/N6 subtyping by real-time reverse transcription PCR (*26*). We selected positive samples for virus isolation. We conducted the isolation of H5N6 viruses in a BioSafety Level 3 laboratory by inoculating 0.2 mL of original sample into 9- to 11-day specific pathogen–free embryonated chicken eggs. After samples incubated for 36–48 hours at 37°C, we harvested allantoic fluids.

RNA Extraction and Genome Sequencing

We extracted RNA from the original samples and isolated viruses by using the QIAamp viral RNA mini kit (QIAGEN, https://www.qiagen.com) and performed sequencing as follows. As previously described (*27*), we subjected extracted RNA to reverse transcription and amplification. We then implemented whole-genome sequencing of FluA on the MiSeq or Miniseq high-throughput sequencing platform (Illumina, https://www.illumina.com) (*28*). We predominately conducted data analysis and genome sequence acquisition by using a pipeline established in our laboratory. We trimmed low-quality reads, sampled the filtered reads, and de novo assembled using Velvet version 1.2.10 (https://guix.gnu.org/en/packages/velvet-1.2.10) and Newbler Assembler version 2.5. We blasted contigs against a database generated by CD-HIT that clusters all FluA sequences collected from the GISAID EpiFlu database (http://www.gisaid.org) and National Center for Biotechnology Information (NCBI) Influenza Virus Database. We selected sequences with the highest similarity as references and used bowtie2 version 2.1.0 (https://sourceforge.net/projects/bowtie-bio/files/bowtie2/2.1.0) for read mapping. We obtained FluA genome sequences by extracting the consensus sequences from the mapping results, with a coverage depth of at least 30× at each site on the 8 segments. We submitted the genome sequences of influenza A(H5N6) viruses determined in this study to

GISAID (Appendix Table 1, https://wwwnc.cdc.gov/EID/article/28/7/21-2482-App1.pdf).

Sequence Alignment and Phylogenetic Analysis

We collected all H5N6 human isolate sequences, including sequences from GISAID, and downloaded the top 100 sequences of avian viruses with high similarity to each representative sequence through BLAST (https://blast.ncbi.nlm.nih.gov/Blast.cgi) from GISAID. We used CD-HIT to reduce the sequence redundancy of phylogenetic analysis and performed sequence alignments by using MAFFT software version 6.857b (https://mafft.cbrc.jp/alignment/software). We constructed a maximum-likelihood phylogenetic tree for the nucleotide sequences of each gene of selected influenza viruses under the GTRGAMMAR model with 1,000 bootstrap replicates, using RAxML (*29*). To estimate the time to most recent common ancestor (tMRCA) of hemagglutinin (HA) and neuraminidase (NA) genes of the H5N6 virus, we selected nonredundant subdatasets to run time-measured Bayesian Markov chain Monte Carlo analysis by BEAST v1.10.4 (*30*). We used the SRD06 substitution model (*31*) and the uncorrelated relaxed molecular clock model and set the Bayesian skygrid coalescent as the tree prior. We ran the Bayesian Markov chain Monte Carlo for up to 1×10^8 steps, with samples for each 10,000 steps to achieve convergence. We used tracer version 1.6 (https://bioweb.pasteur.fr/packages/pack@Tracer@v1.6) to examine effective sample size values >200.

Statistical Analysis

We summarized continuous variables as either means ± SD or medians with interquartile ranges (IQRs). For categorical variables, we calculated the percentages of patients in each category. We used parametric tests to analyze normally distributed variables and nonparametric tests to analyze non–normally distributed variables. We used an unpaired Student *t* test, Wilcoxon rank-sum test, χ^2 test, or Fisher exact test, as appropriate, to compare the epidemiologic and clinical characteristics of subgroups of patients who were infected with influenza A(H5N6) virus before or during 2021. We calculated 95% CIs for the means of normally distributed data and the risk estimates by using the binomial distribution. We considered a p value of <0.05 statistically significant. We performed all analyses in SAS version 9.4 (SAS Institute, Inc., https://www.sas.com).

Results

Epidemiologic Findings

During April 21, 2014–December 31, 2021, a total of 65 cases of human influenza A(H5N6) infection were reported in China; illness onset dates occurred during April 13, 2014–December 31, 2021. The case-fatality rate (CFR) was 55.4% (36/65). Most cases were reported through pneumonia surveillance and were identified by Chinese National Influenza Surveillance Network laboratories; however, 15 cases in 2020 and 2021 were first identified through third-party sequencing agencies and reported to Chinese National Influenza Surveillance Network laboratories for confirmation.

The number of human cases of H5N6 infection reported for each year from 2014 to 2021 was 2 for 2014, 6 for 2015, 9 for 2016, 2 for 2017, 4 for 2018, 1 for 2019, 5 for 2020, and 36 for 2021 (Figure 1). These cases were distributed across 14 provinces in China; most (64/65) cases were detected in southern China (Figure 2). The H5N6 cases were predominantly in adults; median patient age was 51 (IQR 36–57) years (Table 1). More than half (45/65, 69.2%) of H5N6 cases occurred in persons 18–59 years of age. Men accounted for 50.8% (33/65) of H5N6 infections (Table 1).

Poultry exposure is the main risk factor for human infection with AIVs. Nearly half (31/65) of the H5N6 cases occurred in residents of rural areas, where birds were raised. Among the 65 cases, information regarding history of poultry exposure was available for 61 (93.8%) persons; the most common exposures were visiting a live poultry market (38, 62.3%) and exposure to backyard poultry (28, 45.9%). Two cases reported in August 2021 were in a husband and wife, both of whom reported poultry exposure. All close

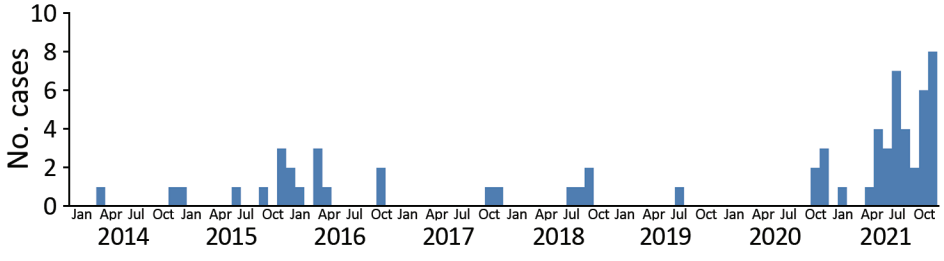

Figure 1. Temporal distribution of 65 human infections with influenza A(H5N6) virus, by month, China, April 21, 2014–December 31, 2021.

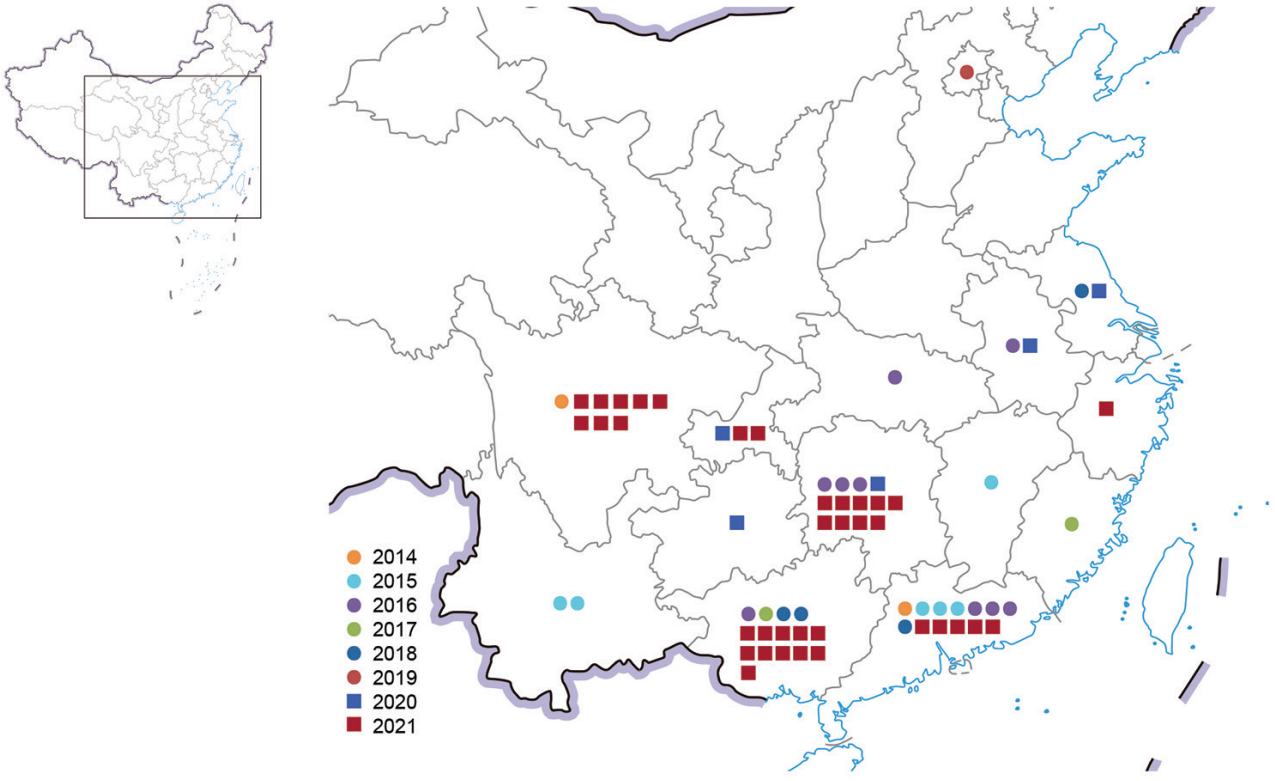

Figure 2. Spatial distribution of 65 human infections with influenza A(H5N6) virus, China, by year, April 21, 2014–December 31, 2021.

contacts were investigated, and no influenza-like illness symptoms were observed for any household contacts. However, human-to-human transmission cannot be ruled out for the infections in the husband and wife.

Clinical Findings

Of the 65 case-patients, 31 reported comorbidities (Table 1), 24 were otherwise healthy, and 10 did not report information on other health conditions. The prevalence of coronary heart disease and cancer in influenza H5N6 case-patients was higher than in the general population in China (Appendix Table 2).

The most commonly reported symptoms at onset of illness were fever (73.4%) and cough (59.4%) (Table 2), indicating that H5N6 infection is difficult to distinguish from other respiratory illnesses, including seasonal influenza viruses, in terms of early symptoms. The median onset-to-admission interval was 4 days (IQR 2–6 days), and the median onset-to-laboratory confirmation delay was 9 days (IQR 7–12 days).

Antiviral treatments targeting NA were given to 60% of patients. However, the median time from illness onset to antiviral treatment was 5 days (IQR 3–9 days) (Figure 3). For patients in whom time from illness onset to initiation of antiviral treatment was ≤5 days, CFR was 38.1% (8/21), lower than in patients for whom that interval was >5 days (66.7% [12/18]). For case-patients who received no antiviral treatment, CFR was 65.2% (15/23). Although not statistically significant ($p = 0.13$), differences did exist in the CFR value among these groups, indicating that early initiation of antiviral treatments could increase the survival rate of H5N6 patients.

Severe disease occurred in 93.8% of cases, and complications developed in 86.2% of patients (Table 1). A total of 51 case-patients required admission to the intensive care unit for treatment; 41 persons underwent mechanical ventilation, and 14 persons required extracorporeal membrane oxygenation (Table 1). We estimated that the hospitalization fatality risks were 59.0% (95% CI 46.7%–71.4%). No significant difference was observed in terms of mean age between fatal cases (45.2 ± 19.9 years) and survivors (45.1 ± 20.2 years).

Comparative Epidemiology of H5N6 Infections

To identify any possible changes to risk for H5N6 infection before and during 2021 in China, we comparatively analyzed epidemiologic and clinical characteristics of human infections. We observed no significant difference in fatality rate, sex distribution, or the

course of disease (Table 3; Appendix Figure 1). However, differences between the seasonal distributions of H5N6 infections were evident (Figure 1). In previous years, few cases were reported during June–September, but an increase in H5N6 infections occurred during summer 2021. In addition, we observed a marked difference in case-patients' geographic location in 2021 (Table 3). Approximately 34.5% of H5N6 case-patients before 2021 lived in rural areas; during 2021, ≈58.3% of case-patients lived in rural areas ($p<0.05$). Furthermore, the average age of patients who were infected with or died of H5N6 viruses was much lower before 2021 than during 2021. The median age of those infected with H5N6 viruses was 40 years (IQR 25–50 years) before 2021 versus 54 years (IQR 49.5–60.5 years) during 2021 ($p<0.001$) (Table 3). The mean age of persons who died of H5N6 infection was 37.7 years (95% CI 27.9–47.4, SD 19.6 years) before 2021 versus 52.8 years (95% CI 44.0–61.6,; SD 17.7 years) during 2021 ($p<0.05$). Of note, third-party sequencing agencies started to play a role in diagnosing H5N6 viruses after the COVID-19 pandemic began. More than one third of cases in 2021 were first detected by hospitals sending samples from patients with pneumonia to third-party agencies.

Table 1. Characteristics of 65 laboratory-confirmed cases of human infection with avian influenza A(H5N6) virus, China*

Characteristic	No. case-patients
Median age (IQR)	51 (36–57)
Age group, y	
0–17	8 (12.3)
18–59	45 (69.2)
≥60	12 (18.5)
Sex	
M	33 (50.8)
F	32 (49.2)
Residence	
Urban	34 (52.3)
Rural	31 (47.7)
Fatalities (CFR)	36 (55.4)
Poultry exposure	
Any exposure to poultry	61 (93.8)
Visited live poultry market	38 (62.3)
Exposure to backyard poultry	28 (45.9)
Exposure to sick or dead poultry	23 (37.7)
Processed poultry	28 (45.9)
A(H5) positive in related bird or avian-related environment	55 (90.2)
Comorbidities†	31 (47.7)
Disease severity	
Mild	4 (6.2)
Severe‡	61 (93.8)
Treatment	
Oseltamivir	39 (60.0)
Mechanical ventilation	41 (63.1)
ECMO	14 (21.5)
Admission to ICU	51 (78.5)
Complications§	
Yes	56 (86.2)
No	7 (10.8)
Unknown	2 (3.1)

*Values are no. (%) except as indicated. CFR, case-fatality rate; ECMO, extracorporeal membrane oxygenation; ICU, intensive care unit; IQR, interquartile range.
†Only comorbidities associated with a high risk for influenza complications (*32*,*33*) were counted here, including chronic respiratory disease, asthma, chronic cardiovascular disease, diabetes, chronic liver disease, chronic kidney disease, immunosuppressed status, and neuromuscular disorders.
‡Severe symptoms were defined according to the Diagnosis and Treatment Plan for Influenza issued by the National Health Commission of the People's Republic of China (http://www.gov.cn/zhengce/zhengceku/2020-11/05/5557639/files/74899af960ff4f228e280d08b60d2af1.pdf).
§Complications included secondary bacterial pneumonia, bronchitis, exacerbations of underlying respiratory conditions, laryngotracheobronchitis; and other less common complications may occur (*33*).

Table 2. List of symptoms at illness onset of 64 laboratory-confirmed cases of human infection with avian influenza A(H5N6) virus, China*

Symptoms at illness onset	No. (%)
Fever (≥38°C)	47 (73.4)
Cough	38 (59.4)
Sputum	15 (23.4)
Fatigue	15 (23.4)
Dizziness	14 (21.9)
Chills	14 (21.9)
Headache	13 (20.3)
Shortness of breath	9 (14.1)
Muscle soreness	7 (10.9)
Sore throat	6 (12.2)
Nasal congestion	6 (9.4)
Coryza	5 (7.8)
Vomiting	4 (6.3)
Chest pain	2 (3.1)

*Information for 1 case was not available.

Evolutionary Relationships of HA and NA Genes of H5N6 Viruses Isolated from Humans

To elucidate the evolutionary pattern of divergence, we analyzed the genetic relationships of the HA and NA genes of 42 human H5N6 viruses with other clade 2.3.4.4 H5N6 genomes available in public databases. According to World Health Organization (WHO) nomenclature of HA genes in clade 2.3.4.4, HPAI H5N6 viruses can be divided into 8 subclades, a–h (Figure 4). All human isolates of H5N6 viruses clustered with vaccine strains recommended by the WHO. The first human virus isolated in 2014, A/Sichuan/26221/2014(H5N6), belonged to subclade 2.3.4.4a; 5 viruses isolated in 2015 were grouped into subclade 2.3.4.4d; and viruses isolated in 2016 belonged to subclade 2.3.4.4g. Subclade 2.3.4.4h viruses were isolated from 2015 through 2021. Of note, most H5N6 human viruses in 2021 (18/20) grouped into genetic subclade 2.3.4.4b. The median tMRCA among the HA genes of clade 2.3.4.4b H5N6 human viruses in 2021 was estimated to be June 16, 2020 (95% highest posterior density March 29, 2020–August 23, 2020).

Phylogenetic analysis of the N6 genes revealed 2 subclades (Figure 5). Almost all viruses

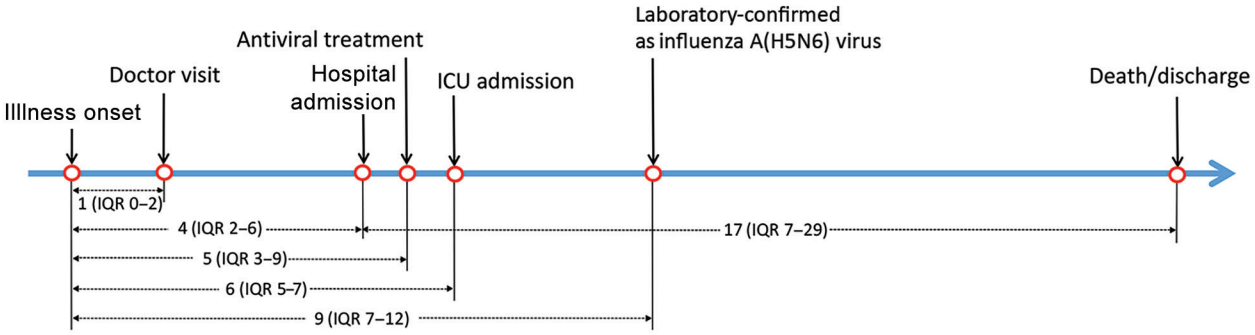

Figure 3. Disease courses of human infections with influenza A (H5N6) virus, China, April 21, 2014–December 31, 2021. Intervals are given as median (IQR) days. ICU, intensive care unit; IQR, interquartile range.

fell into the subgroup with an 11-residue deletion at position 59–69 in the NA stalk. Only 1 virus, A/Sichuan/26221/2014(H5N6), had full-length NA protein. The tMRCA among the N6 genes of clade 2.3.4.4b H5N6 human viruses from 2021 was estimated to be January 19, 2015 (95% highest posterior density June 16, 2014–June 17, 2015). These results indicated that clade 2.3.4.4b H5N6 viruses were generated by multiple reassortment events.

Classification and Temporal Distribution of H5N6 Genotypes Isolated from Humans

The phylogenetic analysis exhibited dynamic donation of the 8 gene segments to H5N6 viruses, including those from the Eurasian gene pool, H9N2 AIVs, and so on (Appendix Figure 2). Each gene of the human isolates showed a highly homologous sequence origin from poultry viruses, wild bird viruses, or both. On the basis of different clade combinations

Table 3. Comparison of characteristics of laboratory-confirmed cases of human infection with avian influenza A(H5N6) virus before and during 2021, China*

Characteristic	No. case-patients before 2021, n = 29	No. case-patients during 2021, n = 36	p value
Sex			
M	12 (41.4)	21 (58.3)	0.17
F	17 (58.6)	15 (41.7)	
Median age, y (IQR)	40 (25-50)	54 (49.5–60.5)	<0.001
Age group, y			<0.05
0–15	6 (20.7)	2 (5.6)	
16–59	21 (72.4)	24 (66.7)	
≥60	2 (6.9)	10 (27.8)	
Rural residence	10 (34.5)	21 (58.3)	0.06
Fatality	18 (62.1)	18 (53.0)	0.47
Poultry exposure ≤10 d before illness onset			
Any exposure to poultry	25 (86.2)	36 (100.0)	<0.05
Visited live poultry market	18 (78.3)	20 (58.8)	0.13
Exposure to backyard poultry	8 (34.8)	20 (58.8)	0.07
Exposure to sick or dead poultry	7 (30.4)	16 (45.7)	0.24
Processed poultry: slaughtered, cleaned, depilated, cooked	11 (50.0)	17 (51.5)	0.91
Comorbidities†			
Any‡	11 (44.0)	20 (66.7)	0.09
Hypertension	3 (12.0)	11 (36.7)	<0.05
Diabetes	2 (8.0)	2 (6.7)	1.00
Coronary heart disease	3 (12.0)	5 (16.7)	0.72
Cancer	4 (16.0)	2 (6.7)	0.39
Chronic renal disease	0 (0.0)	4 (13.3)	0.12
Median time from illness onset to hospital admission, d (IQR)	5 (2.0–6.0)	4 (2.5–6.0)	0.61
Median time from illness onset to laboratory confirmation, d (IQR)	9 (7.0–12.0)	8.5 (7.0-12.0)	0.90
Median time from illness onset to oseltamivir treatment, d (IQR)	5 (3.0–9.0)	6 (2.0-8.0)	0.94
Median time from illness onset to ICU admission, d (IQR)	6 (5.0–7.0)	6 (4.5-8.0)	0.60
Median time from hospital admission to death, d (IQR)	16 (3.0–24.0)	12 (8.0–26.0)	0.50
Mean time from hospital admission to discharge, d (SD)	26.0 ± 19.0	30.7 ± 19.3	0.68

*Values are no. (%) except as indicated. IQR, interquartile range.
†Only underlying diseases associated with a high risk for influenza complications (***32***) were counted here, including chronic respiratory disease, asthma, chronic cardiovascular disease, diabetes, chronic liver disease, chronic kidney disease, immunosuppressed status, and neuromuscular disorders.
‡Ten cases for which existence of comorbidities was unknown were excluded.

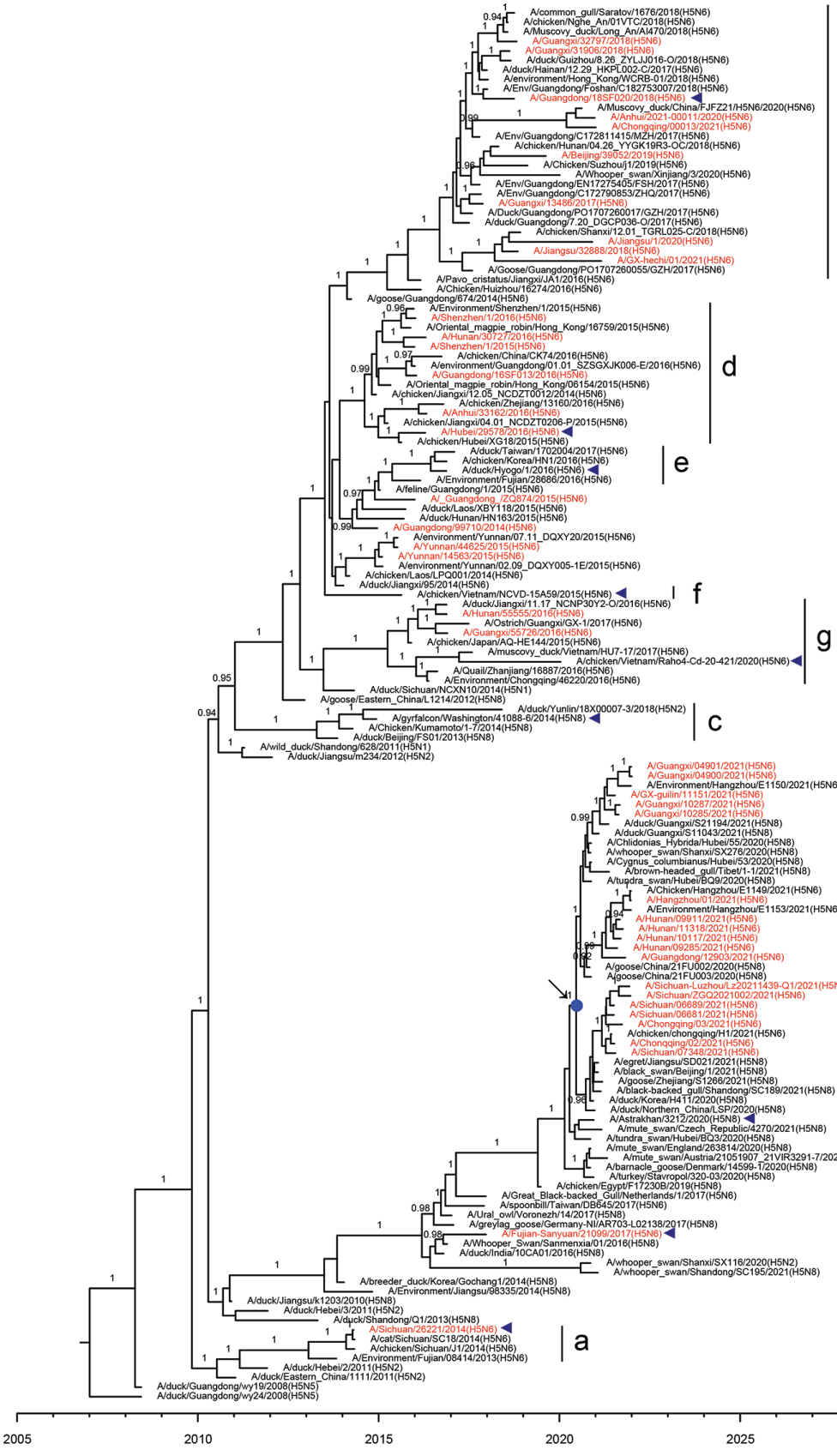

Figure 4. Maximum clade credibility trees of hemagglutinin gene of influenza A(H5N6) viruses, China. Red indicates human-origin H5N6 viruses; blue triangles indicate H5Ny vaccine strains recommended by the World Health Organization; blue dot indicates the most recent common ancestry of clade 2.3.4.4b A(H5N6) human viruses in 2021. Posterior probabilities ≥0.9 are labeled on the branches.

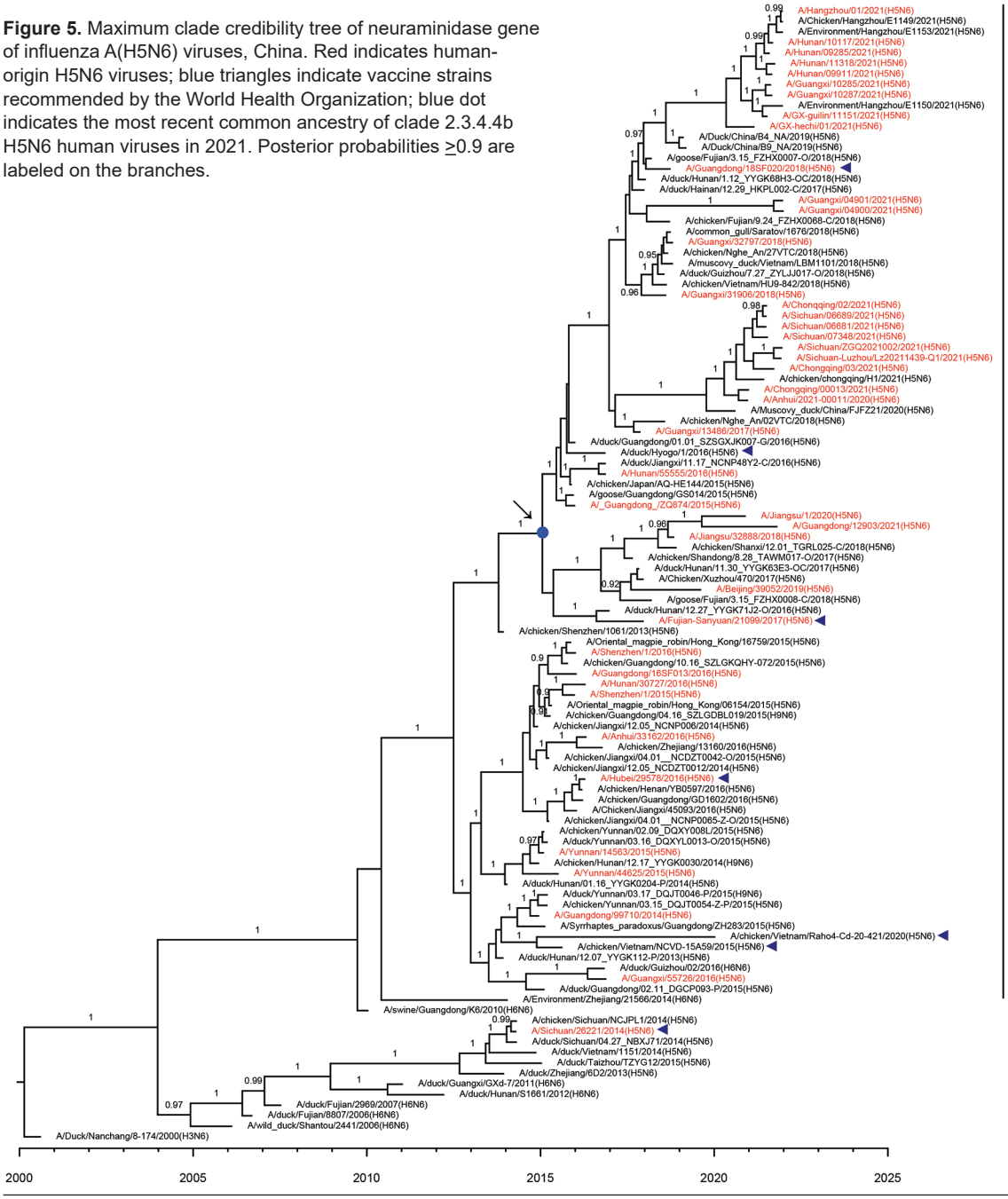

Figure 5. Maximum clade credibility tree of neuraminidase gene of influenza A(H5N6) viruses, China. Red indicates human-origin H5N6 viruses; blue triangles indicate vaccine strains recommended by the World Health Organization; blue dot indicates the most recent common ancestry of clade 2.3.4.4b H5N6 human viruses in 2021. Posterior probabilities ≥0.9 are labeled on the branches.

of 6 internal genes, we identified a total of 13 H5N6 genotypes, termed 2014A, 2014B, 2015A, 2015B, 2016A, 2016B, 2017A, 2018A, 2020A, 2021A, 2021B, 2021C, and 2021D (Figure 6). Several of these genotypes (e.g., 2014A and 2014B) were only identified in 1 case. In contrast, genotype 2015A was first detected in 2015 but continuously caused human infections during 2017–2021. Genotype 2015B contained a set of internal genes derived from H9N2 viruses in poultry and infected at least 8 persons during 2015–2016. However, no cases infected with this genotype were detected in the years after. Genotype 2020A emerged in 2020 and had 6 internal genes originating from the Eurasian gene pool and clade 2.3.2.1c H5N1 viruses. In 2021, a total of 4 new genotypes (2021A, 2021B, 2021C, and 2021D) acquiring genes from clade 2.3.4.4b H5N8 viruses, H5N1 viruses, and the Eurasian gene pool were identified. Five human isolates from Sichuan and Chongqing provinces belonged to genotype 2021A,

and 9 human isolates from Hunan, Guangxi, and Zhejiang provinces were classified into genotype 2021B. Genotype 2021C and 2021D contained 1 virus each. Partial sequences were obtained from another 3 human viruses detected in 2021; their available sequences were closely related to those of the new genotype viruses. These findings might indicate the cross-species advantages of these newly emerged H5N6 genotypes to infect humans.

Key Amino Acid Mutations Occurring in H5N6 Viruses Isolated from Humans

We analyzed molecular substitutions associated with increased virulence and transmissibility in mammals and reduced susceptibility to antiviral drugs. All H5N6 human viruses obtained a 5–amino acid insertion in the HA cleavage site, except for A/Anhui/33162/2016(H5N6), which had 1 more amino acid insertion. Substitution Q226L (H3 numbering)

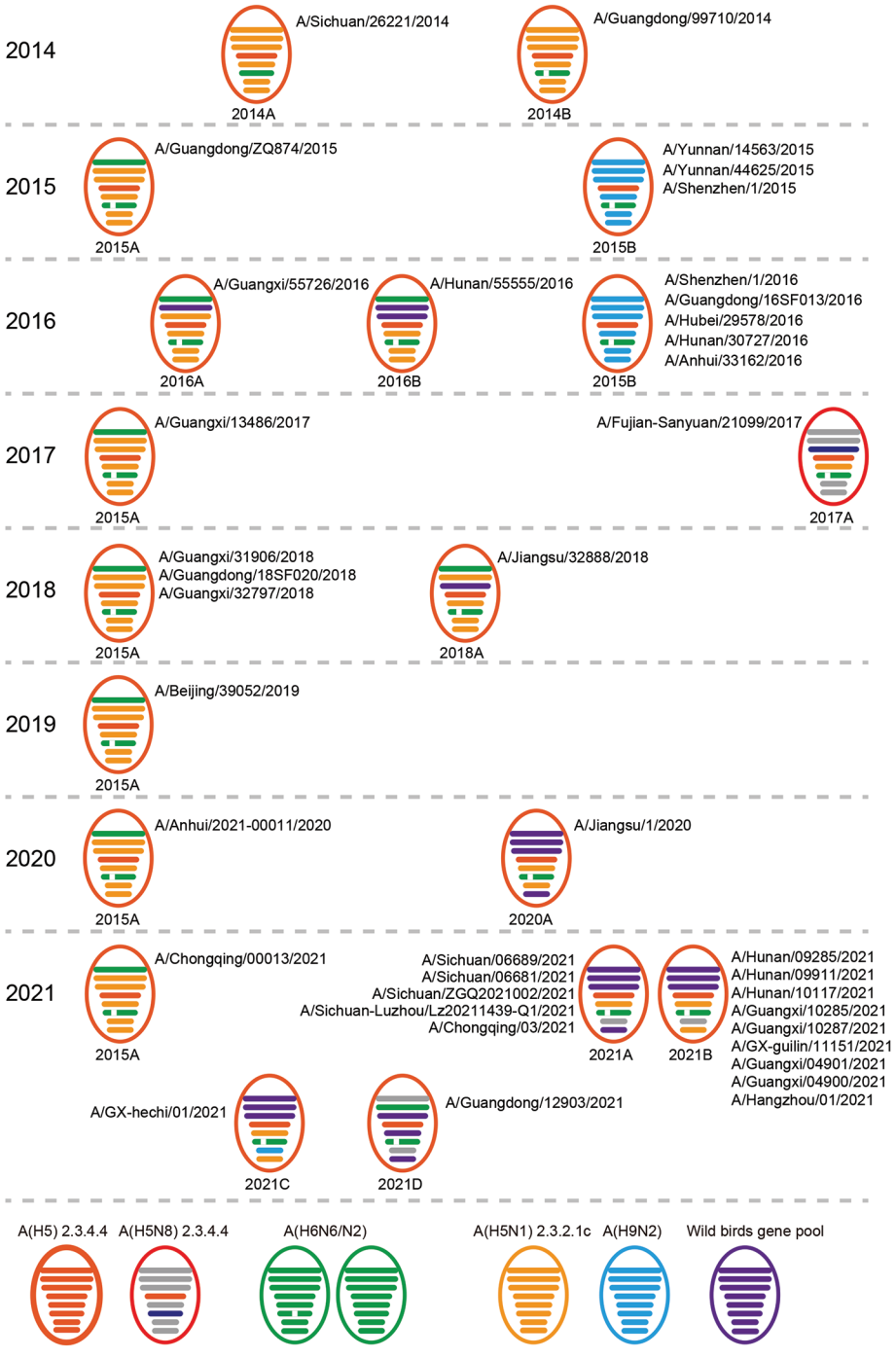

Figure 6. Diversity and prevalence of influenza A(H5N6) viruses isolated from humans, China. Circles represent the corresponding virus genotypes and their times of isolation. Gene segments are ordered as polymerase basic 2, polymerase basic 1, polymerase acidic, hemagglutinin, nucleoprotein, neuraminidase, matrix, and nonstructural from top to bottom within circles. A total of 13 genotypes are listed; the genotype name is shown under each circle. Names of each human H5N6 virus are listed besides the genotype to which they belong. To illustrate the history of reassortant events, segments in descendant viruses are colored according to their corresponding source viruses on the bottom line.

in HA protein, which had previously been reportedly associated with a switch in receptor specificity from avian-type (α2–3Gal) to human-type (α2–6Gal) (*34*–*36*), was detected from 2 viruses, A/Sichuan-Luzhou/LZ 20211439-Q1/2021 (H5N6) and A/Hunan/09285/2021(H5N6). Substitution S227R in HA protein, which could also alter receptor specificity (*37*), was detected in 32 human viruses. Another

Table 4. Mammalian adaptation–related molecular markers of the human and nonhuman A(H5N6) viruses, China

Protein	Biologic effect	Mutations	Amino acids	Human viruses	Nonhuman viruses
HA*	Altered receptor specificity	T192I	T	22	1,238
			A	2	24
			I	18	36
			K	0	2
	Altered receptor specificity	Q226L	Q	39	1,302
			L	2	0
			Q\R	1	0
	Altered receptor specificity	S227N/R	S	6	136
			G	3	31
			H	1	2
			H/R	2	0
			Q	0	92
			R	30	1,036
			C	0	4
	Altered receptor specificity	G228S	G	42	1,302
NA†	Reduced susceptibility to neuraminidase inhibitors	E119V/A/D	E	41	1,253
			D	1	34
			G	0	1
M2	Reduced susceptibility to amantadine	V27A	V	41	1,154
			A	1	20
			G	0	9
			I	0	15
	Reduced susceptibility to amantadine	A30V/T/S	A	41	1,197
			A/T	1	0
			S	0	1
	Reduced susceptibility to amantadine	S31N/G	S	33	994
			N	9	204
PA	Reduced susceptibility to endonuclease inhibitors	I38M/T/S/L	I	39	1,181
			L	0	1
			M	0	1
			V	1	1
PB2	Increased virulence in mammalian models	Q591K	Q	40	1,194
			K	1	0
	Increased virulence in mammalian models	E627K	E	28	1,180
			K	12	3
			E/V	1	1
			V	0	9
	Increased virulence in mammalian models	D701N	D	36	1,193
			D/N	1	0
			N	4	0
NS1	Altered virulence in mice	D92E	D	18	185
			E	24	1,011
			G	0	1
	Altered virulence in mice	L103F	L	8	165
			F	26	1,020
			S	0	11
			V	7	1
			Y	1	0
	Altered virulence in mice	I106M	I	8	166
			K	0	4
			M	34	1,027
M1	Altered virulence in mice	N30D	D	42	1,200
	Impacts growth and transmission in the guinea pig	P41A	A	42	1,199
			S	0	1
	Altered virulence in mice	T139A	T	40	1,113
			A	2	58
			P	0	29
	Altered virulence in mice	T215A	A	42	1,200

*H3 numbering system was used.
†N2 numbering system was used.

receptor-changing substitution, T192I (*38*), was newly detected in clade 2.3.4.4b viruses from 2021 cases (Table 4; Appendix Table 3).

Several mammalian-adapted mutations have occurred in PB2 protein of H5N6 viruses (Appendix Table 3). The substitutions E627K and D701N in PB2 protein, which were associated with increased polymerase activities or enhanced virulence in mice, occurred in 12/42 (E627K) and 5/42 (D701N) human viruses. A high proportion of these substitutions were observed in genotype 2015B viruses; 6/8 viruses acquired the E627K substitution and 1/8 viruses acquired the D701N substitution. These phenomena were frequently observed when an AIV transmitted to a mammalian host (*39*–*42*). These findings further confirmed that the infection source of H5N6 cases was poultry populations.

All genotype H5N6 viruses had 31S in M2 protein, except for genotype 2015B viruses. The genotype 2015B viruses contained 8 viruses, and exclusively had 31N in M2 protein, indicating their reduced susceptibility to amantadine (*43*). Mutations associated with drug resistance in the NA protein (E119D) only occurred in 1 human virus A/Anhui/33162/2016(H5N6). Mutation of I38V in PA, which might affect susceptibility to endonuclease inhibitors, was found in A/Jiangsu/32888/2018(H5N6). In addition, residues in the M1 and NS1 proteins of several H5N6 viruses showed changes that might alter virulence in mice (Appendix Table 3).

Discussion

Among AIVs, viruses of subtypes H5 and H7 have been of particular concern because of their high rates of death. The hospitalization fatality risk for H5N6 infections (59.0%) was slightly lower than that for H5N1 infections (70.0%) but higher than that for H7N9 (35.0%) (*44*). In addition, the median age of patients with H5N6 virus (51 years) was older than the median age for patients with H5N1 virus (26 years) but younger than the age for patients with H7N9 virus (62 years) (*44*).

On the basis of epidemiologic investigations, 93.8% of influenza H5N6 case-patients were confirmed to have poultry exposure history. The contamination of live poultry markets and backyard birds, as well as the practice of processing poultry without personal protection, could be ongoing exposure sources for influenza A(H5N6) virus. While H5N6 viruses continue to circulate in poultry, human infections will undoubtedly continue.

WHO has recommended early antiviral therapy, ideally within 48 hours of symptom onset, for suspected or confirmed influenza patients (*45*). Our study found that early initiation of antiviral treatments could reduce the fatality rate in H5N6 patients to some extent. However, symptoms at the onset of influenza H5N6 infections were clinically similar to those of other respiratory pathogen infections. Thus, increased sensitivity of diagnostic systems is needed to improve case identification and initiate timely antiviral treatment.

During the COVID-19 pandemic, diagnostic capacity for respiratory illnesses among human health systems in China, including hospitals, Centers for Disease Control and Prevention at different levels, and third-party agencies, was increased. In our study, clinical samples from 15 H5N6 cases during the COVID-19 pandemic (2 in 2020 and 13 in 2021) were first identified by third party agencies. This additional diagnostic capacity contributed to the detection of H5N6 cases reported in 2021.

Genetic analysis in our study detected at least 13 types of reassortant H5N6 viruses in infected humans in China (Figure 6). Origins of internal genes were dramatically diversified, indicating the advanced genetic compatibility of H5N6 viruses with other AIVs. In 2021, a total of 4 new H5N6 genotype viruses emerged and accounted for almost all of the H5N6 human viruses based on the available full genome. Of note, different from previously isolated viruses, the HA gene of almost all H5N6 human viruses in 2021 belonged to genetic clade 2.3.4.4b and was closely related to that of the first H5N8 isolate, which caused infection in a patient in Russia (*46*). Additional mammal-adapted mutations, including Q226L and T192I in the HA protein, which could increase the viral affinity for human cells, were also detected (Appendix Table 3), indicating the viral adaptation process from birds to humans.

In summary, although we observed a rise in the number of influenza A(H5N6) infections in 2021, the disease course and CFR were comparable to previously detected H5N6 cases. Antiviral drugs remain effective if used early. However, new genotype viruses and mammal-adapted substitutions emerged. Moreover, reports from OFFLU (https://www.offlu.org) and WHO have documented that clade 2.3.4.4h and 2.3.4.4b H5N6 viruses and clade 2.3.4.4b H5N8 viruses have been detected in poultry and wild birds in China. Considering the continuous viral circulation in birds and incidence of human infection, more H5N6 variants and genotypes with further advantages in humans might emerge. Increased attention to such emerging viruses is vital for public health and pandemic preparedness.

Acknowledgments

We thank the Chinese National Influenza Surveillance Network and the authors and laboratories for sharing the influenza A(H5N6) sequences in GISAID's EpiFlu Database. We thank the following provincial Centers for Disease Control and Prevention for their data sharing on H5N6 cases: Anhui, Beijing, Chongqing, Fujian, Guangdong, Guangxi, Guizhou, Hubei, Hunan, Jiangsu, Jiangxi, Sichuan, Yunnan, and Zhejiang.

This study was supported by the National Nature Science Foundation of China (81961128002, 81971941, and 31970643). The funding bodies had no role in study design, data collection and analysis, preparation of the manuscript, or the decision to publish.

About the Author

Dr. Zhu works in the Chinese National Influenza Center, National Institute for Viral Disease Control and Prevention, China Center for Disease Control and Prevention. Her research interests include evolutionary analysis and pathogenicity mechanism of influenza viruses.

References

1. Pan M, Gao R, Lv Q, Huang S, Zhou Z, Yang L, et al. Human infection with a novel, highly pathogenic avian influenza A (H5N6) virus: Virological and clinical findings. J Infect. 2016;72:52–9. https://doi.org/10.1016/j.jinf.2015.06.009
2. Chen H, Yuan H, Gao R, Zhang J, Wang D, Xiong Y, et al. Clinical and epidemiological characteristics of a fatal case of avian influenza A H10N8 virus infection: a descriptive study. Lancet. 2014;383:714–21. https://doi.org/10.1016/S0140-6736(14)60111-2
3. Gao R, Cao B, Hu Y, Feng Z, Wang D, Hu W, et al. Human infection with a novel avian-origin influenza A (H7N9) virus. N Engl J Med. 2013;368:1888–97. https://doi.org/10.1056/NEJMoa1304459
4. Wang D, Zhu W, Yang L, Shu Y. The epidemiology, virology, and pathogenicity of human infections with avian influenza viruses. Cold Spring Harb Perspect Med. 2021;11:a038620. https://doi.org/10.1101/cshperspect.a038620
5. Yang L, Zhao X, Li X, Bo H, Li D, Liu J, et al. Case report for human infection with a highly pathogenic avian influenza A(H5N6) virus in Beijing, China 2019. Biosafety and Health. 2020;2:49–52. https://doi.org/10.1016/j.bsheal.2020.02.003
6. World Health Organization. Cumulative number of confirmed human cases for avian influenza A(H5N1) reported to WHO, 2003–2021, 1 October 2021 [cited 2021 Nov 19]. https://www.who.int/publications/m/item/cumulative-number-of-confirmed-human-cases-for-avian-influenza-a(h5n1)-reported-to-who-2003-2021-1-october-2021
7. Li KS, Guan Y, Wang J, Smith GJ, Xu KM, Duan L, et al. Genesis of a highly pathogenic and potentially pandemic H5N1 influenza virus in eastern Asia. Nature. 2004;430:209–13. https://doi.org/10.1038/nature02746
8. Jeong J, Kang HM, Lee EK, Song BM, Kwon YK, Kim HR, et al. Highly pathogenic avian influenza virus (H5N8) in domestic poultry and its relationship with migratory birds in South Korea during 2014. Vet Microbiol. 2014;173:249–57. https://doi.org/10.1016/j.vetmic.2014.08.002
9. Lee DH, Torchetti MK, Winker K, Ip HS, Song CS, Swayne DE. Intercontinental spread of Asian-origin H5N8 to North America through Beringia by migratory birds. J Virol. 2015;89:6521–4. https://doi.org/10.1128/JVI.00728-15
10. Butler J, Stewart CR, Layton DS, Phommachanh P, Harper J, Payne J, et al. Novel reassortant H5N6 influenza A virus from the Lao People's Democratic Republic is highly pathogenic in chickens. PLoS One. 2016;11:e0162375. https://doi.org/10.1371/journal.pone.0162375
11. Yang L, Zhu W, Li X, Bo H, Zhang Y, Zou S, et al. Genesis and dissemination of highly pathogenic H5N6 avian influenza viruses. J Virol. 2017;91:e02199–16. https://doi.org/10.1128/JVI.02199-16
12. Chu DH, Okamatsu M, Matsuno K, Hiono T, Ogasawara K, Nguyen LT, et al. Genetic and antigenic characterization of H5, H6 and H9 avian influenza viruses circulating in live bird markets with intervention in the center part of Vietnam. Vet Microbiol. 2016;192:194–203. https://doi.org/10.1016/j.vetmic.2016.07.016
13. Bi Y, Chen Q, Wang Q, Chen J, Jin T, Wong G, et al. Genesis, evolution and prevalence of H5N6 avian influenza viruses in China. Cell Host Microbe. 2016;20:810–21. https://doi.org/10.1016/j.chom.2016.10.022
14. Xu W, Li X, Bai T, Zhao X, Zhao X, Zhang Y, et al. A fatal case of infection with a further reassortant, highly pathogenic avian influenza (HPAI) H5N6 virus in Yunnan, China. Infect Genet Evol. 2016;40:63–6. https://doi.org/10.1016/j.meegid.2016.02.020
15. Yang L, Zhu W, Li X, Bo H, Zhang Y, Zou S, et al. Genesis and dissemination of highly pathogenic H5N6 avian influenza viruses. J Virol. 2017;91:e02199-16. https://doi.org/10.1128/JVI.02199-16
16. Cui Y, Li Y, Li M, Zhao L, Wang D, Tian J, et al. Evolution and extensive reassortment of H5 influenza viruses isolated from wild birds in China over the past decade. Emerg Microbes Infect. 2020;9:1793–803. https://doi.org/10.1080/22221751.2020.1797542
17. Zhang Y, Chen M, Huang Y, Zhu W, Yang L, Gao L, et al. Human infections with novel reassortant H5N6 avian influenza viruses in China. Emerg Microbes Infect. 2017;6:e50. https://doi.org/10.1038/emi.2017.38
18. Sun W, Li J, Hu J, Jiang D, Xing C, Zhan T, et al. Genetic analysis and biological characteristics of different internal gene origin H5N6 reassortment avian influenza virus in China in 2016. Vet Microbiol. 2018;219:200–11. https://doi.org/10.1016/j.vetmic.2018.04.023
19. Chen Z, Wang Z, Zhao X, Guan Y, Xue Q, Li J, et al. Pathogenicity of different H5N6 highly pathogenic avian influenza virus strains and host immune responses in chickens. Vet Microbiol. 2020;246:108745. https://doi.org/10.1016/j.vetmic.2020.108745
20. Sun H, Pu J, Hu J, Liu L, Xu G, Gao GF, et al. Characterization of clade 2.3.4.4 highly pathogenic H5 avian influenza viruses in ducks and chickens. Vet Microbiol. 2016;182:116–22. https://doi.org/10.1016/j.vetmic.2015.11.001
21. Li Y, Li M, Li Y, Tian J, Bai X, Yang C, et al. Outbreaks of highly pathogenic avian influenza (H5N6) virus subclade 2.3.4.4h in Swans, Xinjiang, Western China, 2020. Emerg Infect Dis. 2020;26:2956–60. https://doi.org/10.3201/eid2612.201201
22. Sun H, Pu J, Wei Y, Sun Y, Hu J, Liu L, et al. Highly pathogenic avian influenza H5N6 Viruses exhibit enhanced affinity for human type sialic acid receptor and in-contact

transmission in model ferrets. J Virol. 2016;90:6235–43. https://doi.org/10.1128/JVI.00127-16
23. Bi Y, Liu H, Xiong C, Di Liu, Shi W, Li M, et al. Novel avian influenza A (H5N6) viruses isolated in migratory waterfowl before the first human case reported in China, 2014. Sci Rep. 2016;6:29888. https://doi.org/10.1038/srep29888
24. Koutsakos M, Wheatley AK, Laurie K, Kent SJ, Rockman S. Influenza lineage extinction during the COVID-19 pandemic? Nat Rev Microbiol. 2021;19:741–2. https://doi.org/10.1038/s41579-021-00642-4
25. World Health Organization. Assessment of risk associated with highly pathogenic avian influenza A(H5N6) virus [cited 2021 Nov 19]. https://cdn.who.int/media/docs/default-source/influenza/avian-and-other-zoonotic-influenza/a(h5n6)-risk-assessment.pdf
26. Yu L, Wang Z, Chen Y, Ding W, Jia H, Chan JF, et al. Clinical, virological, and histopathological manifestations of fatal human infections by avian influenza A(H7N9) virus. Clin Infect Dis. 2013;57:1449–57. https://doi.org/10.1093/cid/cit541
27. Zhou B, Donnelly ME, Scholes DT, St George K, Hatta M, Kawaoka Y, et al. Single-reaction genomic amplification accelerates sequencing and vaccine production for classical and Swine origin human influenza a viruses. J Virol. 2009;83:10309–13. https://doi.org/10.1128/JVI.01109-09
28. McGinnis J, Laplante J, Shudt M, George KS. Next generation sequencing for whole genome analysis and surveillance of influenza A viruses [Erratum in: J Clin Virol. 2017;93:65]. J Clin Virol. 2016;79:44–50. https://doi.org/10.1016/j.jcv.2016.03.005
29. Stamatakis A. RAxML version 8: a tool for phylogenetic analysis and post-analysis of large phylogenies. Bioinformatics. 2014;30:1312–3. https://doi.org/10.1093/bioinformatics/btu033
30. Drummond AJ, Rambaut A. BEAST: Bayesian evolutionary analysis by sampling trees. BMC Evol Biol. 2007;7:214. https://doi.org/10.1186/1471-2148-7-214
31. Drummond AJ, Rambaut A, Shapiro B, Pybus OG. Bayesian coalescent inference of past population dynamics from molecular sequences. Mol Biol Evol. 2005;22:1185–92. https://doi.org/10.1093/molbev/msi103
32. Fiore AE, Shay DK, Broder K, Iskander JK, Uyeki TM, Mootrey G, et al. Prevention and control of influenza: recommendations of the Advisory Committee on Immunization Practices (ACIP), 2008. MMWR Recomm Rep. 2008;57:1–60.
33. Hall E. Influenza. In: Epidemiology and prevention of vaccine-preventable diseases, 14th edition. 2021 [cited 2022 Apr 21]. https://www.cdc.gov/vaccines/pubs/pinkbook/flu.html#impact
34. Shi Y, Zhang W, Wang F, Qi J, Wu Y, Song H, et al. Structures and receptor binding of hemagglutinins from human-infecting H7N9 influenza viruses. Science. 2013;342:243–7. https://doi.org/10.1126/science.1242917
35. Xu R, de Vries RP, Zhu X, Nycholat CM, McBride R, Yu W, et al. Preferential recognition of avian-like receptors in human influenza A H7N9 viruses. Science. 2013;342:1230–5. https://doi.org/10.1126/science.1243761
36. Ramos I, Krammer F, Hai R, Aguilera D, Bernal-Rubio D, Steel J, et al. H7N9 influenza viruses interact preferentially with α2,3-linked sialic acids and bind weakly to α2,6-linked sialic acids. J Gen Virol. 2013;94:2417–23. https://doi.org/10.1099/vir.0.056184-0
37. Guo H, de Vries E, McBride R, Dekkers J, Peng W, Bouwman KM, et al. Highly pathogenic influenza A(H5Nx) viruses with altered H5 receptor-binding specificity. Emerg Infect Dis. 2017;23:220–31. https://doi.org/10.3201/eid2302.161072
38. Yang ZY, Wei CJ, Kong WP, Wu L, Xu L, Smith DF, et al. Immunization by avian H5 influenza hemagglutinin mutants with altered receptor binding specificity. Science. 2007;317:825–8. https://doi.org/10.1126/science.1135165
39. Steel J, Lowen AC, Mubareka S, Palese P. Transmission of influenza virus in a mammalian host is increased by PB2 amino acids 627K or 627E/701N. PLoS Pathog. 2009;5:e1000252. https://doi.org/10.1371/journal.ppat.1000252
40. Li Z, Chen H, Jiao P, Deng G, Tian G, Li Y, et al. Molecular basis of replication of duck H5N1 influenza viruses in a mammalian mouse model. J Virol. 2005;79:12058–64. https://doi.org/10.1128/JVI.79.18.12058-12064.2005
41. Subbarao EK, London W, Murphy BR. A single amino acid in the PB2 gene of influenza A virus is a determinant of host range. J Virol. 1993;67:1761–4. https://doi.org/10.1128/jvi.67.4.1761-1764.1993
42. Gabriel G, Dauber B, Wolff T, Planz O, Klenk HD, Stech J. The viral polymerase mediates adaptation of an avian influenza virus to a mammalian host. Proc Natl Acad Sci U S A. 2005;102:18590–5. https://doi.org/10.1073/pnas.0507415102
43. Lan Y, Zhang Y, Dong L, Wang D, Huang W, Xin L, et al. A comprehensive surveillance of adamantane resistance among human influenza A virus isolated from mainland China between 1956 and 2009. Antivir Ther. 2010;15:853–9. https://doi.org/10.3851/IMP1656
44. Cowling BJ, Jin L, Lau EH, Liao Q, Wu P, Jiang H, et al. Comparative epidemiology of human infections with avian influenza A H7N9 and H5N1 viruses in China: a population-based study of laboratory-confirmed cases. Lancet. 2013;382:129–37. https://doi.org/10.1016/S0140-6736(13)61171-X
45. Fiore AE, Fry A, Shay D, Gubareva L, Bresee JS, Uyeki TM, et al. Antiviral agents for the treatment and chemoprophylaxis of influenza—recommendations of the Advisory Committee on Immunization Practices (ACIP). MMWR Recomm Rep. 2011;60:1–24.
46. Pyankova OG, Susloparov IM, Moiseeva AA, Kolosova NP, Onkhonova GS, Danilenko AV, et al. Isolation of clade 2.3.4.4b A(H5N8), a highly pathogenic avian influenza virus, from a worker during an outbreak on a poultry farm, Russia, December 2020. Euro Surveill. 2021;26. https://doi.org/10.2807/1560-7917.ES.2021.26.24.2100439

Address for correspondence: Lei Yang or Dayan Wang, National Institute for Viral Disease Control and Prevention, China CDC, 155 Changbai Rd, Changping District, Beijing, 102206, China; email: yanglei@ivdc.chinacdc.cn or wangdayan@ivdc.chinacdc.cn

Measuring Basic Reproduction Number to Assess Effects of Nonpharmaceutical Interventions on Nosocomial SARS-CoV-2 Transmission

George Shirreff, Jean-Ralph Zahar, Simon Cauchemez, Laura Temime,[1] Lulla Opatowski,[1]
EMEA-MESuRS Working Group on the Nosocomial Modelling of SARS-CoV-2[2]

Outbreaks of SARS-CoV-2 infection frequently occur in hospitals. Preventing nosocomial infection requires insight into hospital transmission. However, estimates of the basic reproduction number (R_0) in care facilities are lacking. Analyzing a closely monitored SARS-CoV-2 outbreak in a hospital in early 2020, we estimated the patient-to-patient transmission rate and R_0. We developed a model for SARS-CoV-2 nosocomial transmission that accounts for stochastic effects and undetected infections and fit it to patient test results. The model formalizes changes in testing capacity over time, and accounts for evolving PCR sensitivity at different stages of infection. R_0 estimates varied considerably across wards, ranging from 3 to 15 in different wards. During the outbreak, the hospital introduced a contact precautions policy. Our results strongly support a reduction in the hospital-level R_0 after this policy was implemented, from 8.7 to 1.3, corresponding to a policy efficacy of 85% and demonstrating the effectiveness of nonpharmaceutical interventions.

Despite sweeping control measures, SARS-CoV-2 continues to pose a major threat to older persons and persons with comorbidities, both of whom can have poorer clinical outcomes (*1*,*2*). Thus, hospitals and long-term care facilities (LTCFs) must be particularly vigilant to prevent the spread of SARS-CoV-2 infection among their patients. Nosocomial spread has been an issue since the pandemic began in 2020, and many outbreaks have occurred in hospitals and healthcare facilities, often with high attack and mortality rates (*3*).

To control nosocomial spread, healthcare facilities have progressively implemented preventive measures, such as generalized masking, testing campaigns among patients and staff, isolation, visitor restrictions (*3*), and more recently vaccination (*4*). However, the risk for viral transmission among hospital patients and staff and the effectiveness of control measures remain unclear, and outbreaks still occur (*3*,*5*,*6*).

The basic reproduction number (R_0) refers to the number of secondary infections caused by a single index infection in an otherwise susceptible population. R_0 has been widely used as an indicator of SARS-CoV-2 epidemic risk and has also proved valuable for evaluating testing strategies and other preventive measures within healthcare settings (*7*,*8*). R_0 likely varies between types of healthcare facilities and differs considerably from estimates in the general community (*9*). However, estimating R_0 in healthcare settings is more challenging than estimating R_0 in the community. The populations in institutions are small and epidemics are highly stochastic. More data usually are available from hospitals or wards that have more cases. Healthcare facilities rarely test patients randomly or at multiple times during their hospitalizations. Most available data from hospital outbreaks consist of distributions of positive tests over time in a context of evolving testing policy and capacity.

Author affiliations: Institut Pasteur, Université Paris Cité, Paris, France (G. Shirreff, S. Cauchemez, L. Opatowski); Conservatoire National des Arts et Métiers, Paris (G. Shirreff, L. Temime); University of Versailles Saint-Quentin-en-Yvelines, Montigny-le-Bretonneux, France (G. Shirreff, L. Opatowski); Assistance Publique–Hôpitaux de Paris, Bobigny, France (J.-R. Zahar); PACRI Unit, Paris (L. Temime)

DOI: https://doi.org/10.3201/eid2807.212339

[1]These authors were co-principal investigators.

[2]Members of the workgroup are listed at the end of this article.

At the beginning of the pandemic, most countries had no standard strategy or recommendation on how surveillance should be carried out and tests distributed. Testing was mostly conducted on symptomatic patients, and surveillance consisted of possible contact tracing around detected cases. However, unreported asymptomatic cases could represent a substantial fraction of transmissions, and little data on the testing policy are available to estimate how many cases fell through the gaps.

Here, we propose a new framework to analyze detailed hospital test data by using a stochastic transmission model explicitly accounting for testing policy. We estimated R_0 in the context of a large SARS-CoV-2 outbreak in a LTCF. The outbreak had a high initial R_0, and we reconstructed the unobserved epidemic to assess effectiveness of nonpharmaceutical interventions.

Methods

Hospital and Patient Information

Available data came from a LTCF in Paris, France. The hospital has 3 buildings (A, B, and C), each of which has 4 floors (0–3) that we considered as separate wards. The results of all valid PCR tests were available for each patient identification number during March 1–April 30, 2020 (61 days). Patient information also included the ward to which they were admitted or transferred, admission and discharge dates, and any symptoms they had at first positive test. All dates we provide are relative to the date of the first positive sample in the facility. We censored the data from day 51 onward because the hospital began to change the containment policy after that point. We excluded 23 patients from any ward-level analysis because the ward in which they were tested was unknown (Appendix, https://wwwnc.cdc.gov/EID/article/28/7/21-2339-App1.pdf). We only used anonymized, aggregated patient data and did not collect additional patient data beyond those for clinical use. The Comité Local d'Ethique pour la Recherche Clinique des HUPSSD Avicenne-Jean Verdier-René Muret approved the study as protocol no. CLEA-2021-190.

Laboratory Testing

The LTCF collected all nasopharyngeal swab samples from patients. Reasons for testing included having symptoms characteristic of SARS-CoV-2, having had contact with a positive case, or patient transfer between wards or into or out of the hospital (Appendix).

Model Description

We modeled the spread of infection within the LTCF population by using a modified stochastic susceptible-exposed-infected-recovered model (Figure 1; Appendix, Appendix Table 1). We defined the force of infection at a given time, $\lambda(t)$, as the per-capita rate at which susceptible persons become infected, which we determined by the transmission rate, β, and the proportion of infectious patients at that time (Appendix). On the date the epidemic began (t_{init}), we considered a specific number (E_{init}) of persons infected. We assumed persons in infectious incubation had reduced infectiousness by a factor of ε, compared with symptomatic infected persons. Similarly, we assumed asymptomatic infectious persons had lower infectiousness by a factor of κ_1.

To fully determine transmission over the outbreak period, we compared 2 distinct models. In the primary model, we assumed a single transmission rate, β, throughout the study period. However, based on knowledge of changing practices within the hospital, we defined a more complex, 2-phase model in which each phase had its own transmission rate, β_1 and β_2, and was delimited by an inflection date, $t_{inflect}$. Potential values for $t_{inflect}$ ranged from day 1, which was the date of the first positive sample, through day 16, which was >1 week after the facility introduced contact precautions and France implemented a generalized lockdown.

We directly computed R_0 for each stage of infection from the transmission rate, duration of each infectious stage, and the probability infected persons would become symptomatic (Appendix). For the 2-phase model, we computed the average R_0 by weighting each phase by its duration (Appendix).

Observation Model

Because of asymptomatic infections, imperfect test sensitivity, and irregular availability of tests, the facility could not identify all infected patients. To account for the imperfect reporting, we added an observation model to the transmission model (Appendix, Appendix Figure 1). The observation model assumes all persons are initially untested, but upon testing, the model moves them to an equivalent tested state. Any patient can be retested in the model, but retesting occurs at a reduced relative rate, ϕ, estimated directly from the number of tests and retests in the available data (Appendix). When a person in the model develops symptoms, they lose their tested status and rejoin the untested compartment, I_s (Figure 1), enabling the model to account for increased testing when symptoms appear in a patient.

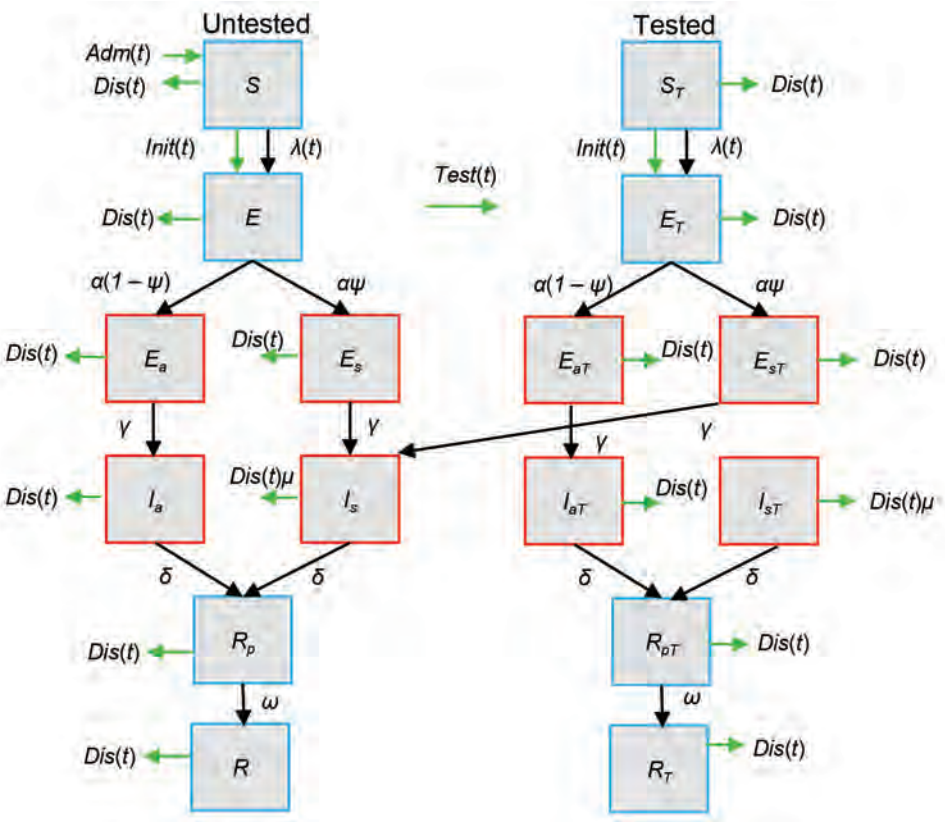

Figure 1. Compartmental susceptible-exposed-infectious-recovered model used to estimate nosocomial SARS-CoV-2 transmission rates on the basis of data for a long-term care facility in France. Red boxes indicate SARS-CoV-2 infectious compartments and blue boxes indicate noninfectious compartments. The left side shows the trajectory of untested persons, the right side shows tested persons. If untested persons are tested at any point in state *X*, they will enter the equivalent tested compartment (X_T, right panel), which is epidemiologically identical except for the testing rate. Patients in the susceptible state (*S*) can become infected by contact with infectious patients. When infected, patients move to the noninfectious incubation (*E*) compartment, after which they can either enter an asymptomatic or a symptomatic pathway of infectiousness. Each pathway has an infectious incubation period (E_a, E_s) before asymptomatic (I_a) or symptomatic (I_s) infection begins. After full infection, patients recover into a noninfectious state (R_p) where they are still likely to test positive before full recovery (*R*) when the probability of testing positive diminishes to (1 – test specificity). Green arrows refer to processes, initiation (*Init*), admission (*Adm*), discharge (*Dis*), and testing (*Test*), that occur a specified number of times on a given day according to model inputs. Black arrows indicate processes that are natural for infection and are entirely stochastic (Appendix Methods, Figure 1). *E*, exposed; E_a, asymptomatic exposed; E_{aT}, asymptomatic exposed and tested; E_s, symptomatic exposed; E_{sT}, symptomatic exposed and tested; E_T, exposed and tested; *I*, infectious; I_a, asymptomatic infectious; I_{aT}, asymptomatic infectious and tested; I_s, symptomatic infectious; I_{sT}, symptomatic infectious and tested; I_T, infectious and tested; *R*, recovered; R_p, recovered to noninfectious state; R_{pT}, recovered to noninfectious state and tested; R_T, recovered and tested; *S*, susceptible; *t*, time; α, rate of progression from noninfectious incubation; ψ, proportion of patients entering symptomatic pathway; λ(t), force of infection at time t; α, rate of progression from infectious incubation; δ, rate of progression from symptomatic infection; μ, relative rate of discharge for symptomatic patients relative to any nonsymptomatic patient; ω, rate at which viral shedding ceases during recovery.

However, testing does not change the rates of infectiousness or disease progression.

We used hospital data on the number of admissions, discharges, and tests per day as inputs (Appendix, Appendix Figure 2). The model considers admitted patients are in a susceptible untested state and are discharged at random from any state with a relative rate, μ, for symptomatic patients. For any day that tests are performed, the model prioritizes patients who have not been tested since becoming symptomatic and conducts any remaining tests at random on the rest of the population (Appendix, Appendix Figure 1). We used the sensitivity and specificity of the PCR test at the stage of infection to determine whether patients test positive or negative for SARS-CoV-2.

Statistical Inference

We calculated the likelihood by comparing the observed numbers of positive and negative cases on each day with the expected numbers generated by the internal model state via the observation process, assuming a binomial distribution (Appendix). We used iterative filtering in the pomp package (*10*) in R (R Foundation for Statistical Computing, https://www.r-project.org) to estimate parameters. In addition to estimating transmission rates, β, or β_1 and β_2, we also estimated the virus introduction time, t_{init}, and fixed the initial number of infections, E_{init}, to 1. For each analysis comprising the same model, dataset, and fixed parameter values, we used profile likelihood to calculate 95% CI for the estimated parameters (Appendix). We

compared models by calculating the Akaike information criterion (AIC).

Model Inference Validation

As a preliminary step, we tested the model and inference methodology on synthetic data. We used this test to ensure that known simulated transmission rates (β, or β_1 and β_2) and t_{init} could be recovered by statistical inference (Appendix).

Hospital- and Ward-Level Analyses

We first analyzed data at the hospital level, assuming homogeneous mixing across all buildings and wards. We then analyzed the data and estimated parameters for each ward separately. After parameter estimation, we conducted simulations of the visible and undetected parts of the epidemic at both the hospital and ward levels (Appendix).

Sensitivity Analysis and Time-Varying Reproduction Number

We conducted a sensitivity analysis to identify parameters with variations that most affected our estimated parameters. We perturbed the input parameters, using the lower and upper bound of the CI reported in the literature, and replicated the analysis. For comparison, we used incident cases to calculate the time-varying reproduction number (R_t) across the entire hospital by using the EpiEstim package (https://CRAN.R-project.org/package=EpiEstim) (Appendix).

Results

A total of 459 patients were in the hospital during the study period. PCR testing began on day −6; we consider day 1 as the first positive sample was collected. By the end of day 50, 152/312 patients sampled tested positive (Figure 2, panels A, B). The secondary attack

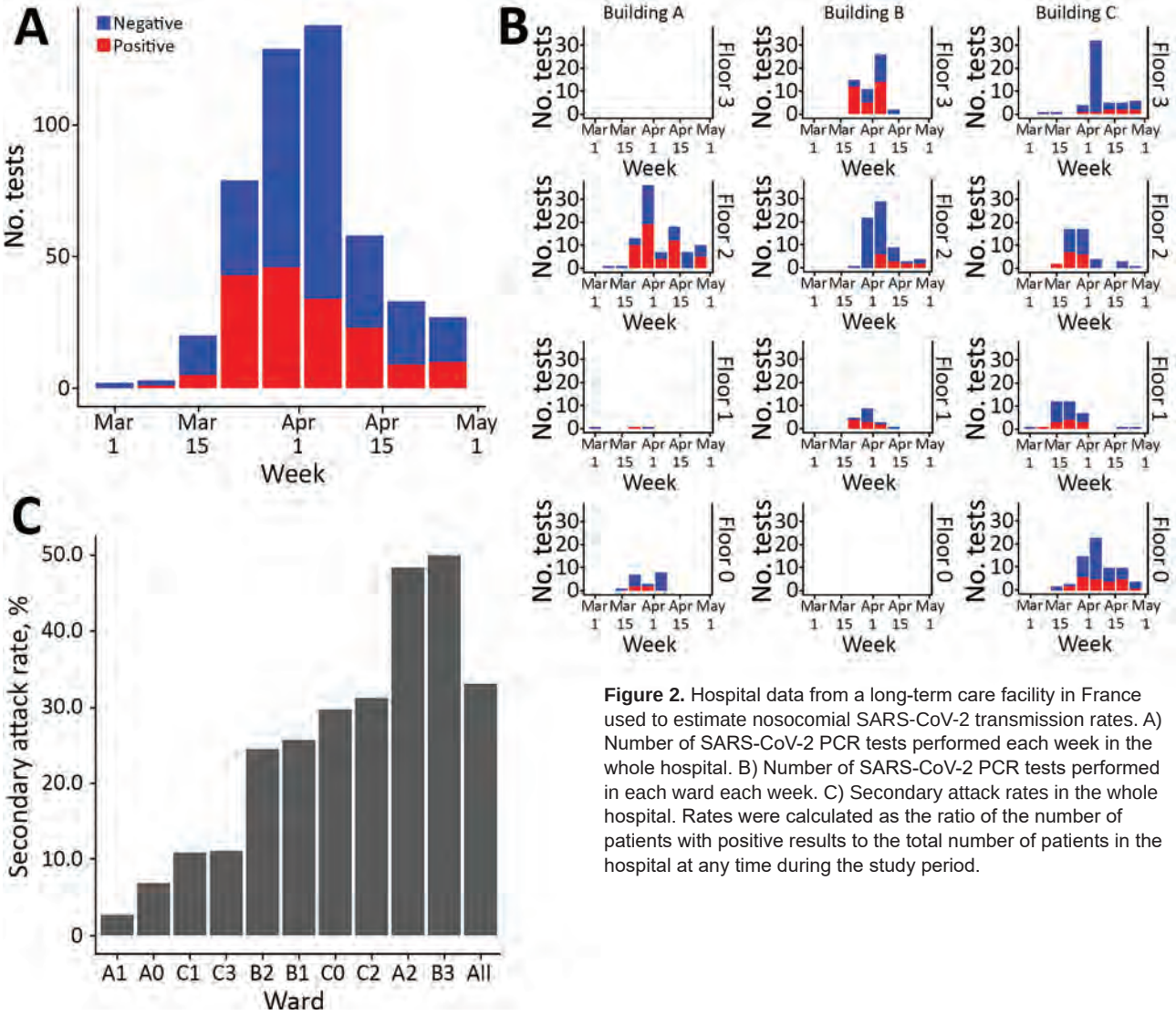

Figure 2. Hospital data from a long-term care facility in France used to estimate nosocomial SARS-CoV-2 transmission rates. A) Number of SARS-CoV-2 PCR tests performed each week in the whole hospital. B) Number of SARS-CoV-2 PCR tests performed in each ward each week. C) Secondary attack rates in the whole hospital. Rates were calculated as the ratio of the number of patients with positive results to the total number of patients in the hospital at any time during the study period.

rate differed substantially between wards (Figure 2, panel C), ranging from 3% to 50%, and the overall secondary attack rate was 33%.

Model Inference Validation Results

The results of the validation of parameter inference on synthetic data suggest that sufficient power was available at the hospital level to recover parameters with relatively good accuracy (Appendix, Appendix Figures 4, 5). However, power was not always sufficient at the ward level, and we restricted our subsequent analysis of wards to only those where the recovered estimates did not deviate excessively in the estimates of β (Appendix Figures 6,7).

Whole-Hospital Analysis

We calculated estimations of transmission rates at the whole hospital level (Table 1; Appendix). In the 2-phase model, using day 12 as $t_{inflect}$ gave the best model fit (Appendix Table 4), which is 6 days after the facility officially introduced an obligatory mask-wearing policy and cancellation of all group activities between patients. This model proved a better fit to the data than the 1-phase model, as measured by the AIC (Table 1). Simulated curves from the observed epidemic produced by the models show that the 2-phase model captured the early peak in cases better than the 1-phase model (Figure 3, panels A, B).

In the 2-phase model where $t_{inflect} = 12$, we observed a notable difference between the transmission rates estimated before and after $t_{inflect}$, which we assume to be attributable to the new contact precautions. The transmission rate fell from 1.3 (95% CI 0.8–2.4) to 0.19 (95% CI 0.10–0.30) infections/patient/day in symptomatic infection, corresponding to a drop in R_0 from 8.7 (95% CI 5.1–16.3) to 1.3 (95% CI 0.7–2.0). This result translates to an 85% (95% CI 66%–94%) decrease of the transmission risk after generalized implementation of contact precautions. Although the value of $t_{inflect}$ had a substantial effect on the absolute values of the transmission rates, the size of the decrease in transmission rate was relatively stable, ranging from 81%–89% (Appendix Table 4). At peak prevalence of infectious patients, we estimated the proportion of undetected infections at 60%, and overall, ≈25% of cases were undetected over the entire study period (Figure 4, panel A).

Ward-Level Analysis

We calculated estimates and corresponding fits for each individual ward for which the 1-phase model could be validated (Table 2; Figure 3, panel B). We reconstructed the undetected parts of the epidemic (Figure 4, panel B). We also conducted ward-level analysis using the 2-phase model but this did not improve the fit (Appendix, Appendix Table 5).

Point estimates for β ranged from 0.42 to 2.13 across the studied wards. We were only able to calculate an upper bound for the transmission rate in 1 ward, C3; the resulting range estimate of 0.42 (0.11–1.30) infections/patient/day corresponds to an R_0 of 2.87 (0.75–8.84). However, we could estimate a lower bound for each ward; the highest value, 0.51 infections/patient/day in ward A2, corresponds to a minimum R_0 of 3.47.

Sensitivity Analysis Results

For most parameters, perturbing had relatively minor effects on the estimated transmission rates for the 2 phases, or on t_{init} (Appendix, Appendix Figure 8). The transmission rate in the second phase, β_2, was the most sensitive, and most markedly sensitive to the duration of symptomatic infection ($1/\delta$).

R_t Results

We calculated R_t estimates by using EpiEstim (Appendix, Appendix Figure 9). The value was initially 10, then fell to <3, before a second peak.

Discussion

We developed a specific framework to analyze SARS-CoV-2 data from a hospital outbreak using a transmission model of patient-to-patient infection. We estimated transmission rates from a LTCF during March–April 2020, across the entire hospital and in individual wards. We assessed 1 or 2

Table 1. Best estimates and ranges for parameters from 2 models applied to hospital data from a long-term care facility in France to estimate nosocomial transmission rates of SARS-CoV-2*

	Model	
Parameter	1-phase	2-phase†
β	0.38 (0.30–0.60)	NA
β_1	NA	1.28 (0.76–2.40)
β_2	NA	0.19 (0.10–0.30)
R_0	2.6 (2.0–4.1)	NA
R_0 before	NA	8.72 (5.14–16.32)
R_0 after	NA	1.33 (0.68–2.04)
R_0 combined	NA	5.72 (3.62–8.70)
Intervention efficacy‡	NA	0.85 (0.66–0.94)
t_{init}	−22 (−39 to −4)	−4 (−25 to −1)
AIC	657.33	628.85

*The value of E_{init} was fixed at day 1 and the value of $t_{inflect}$ at day 12. The R_0 values were calculated by using equations 4 and 5 (Appendix). AIC, Akaike information criterion; NA, not applicable; R_0, basic reproduction number; β, current transmission rate per day; β_1, transmission rate per day before inflection date; β_2, transmission rate per day after inflection date; E_{init}, number of initial infections at date t_{init}; R_0, basic reproduction number; t_{init}, date on which the initial infection occurs.
†R_0 was calculated before and after inflection date in the 2-phase model.
‡The intervention efficacy was calculated as $1 - \beta_2/\beta_1$. Days for t_{init} are relative to the first positive sample on day 1.

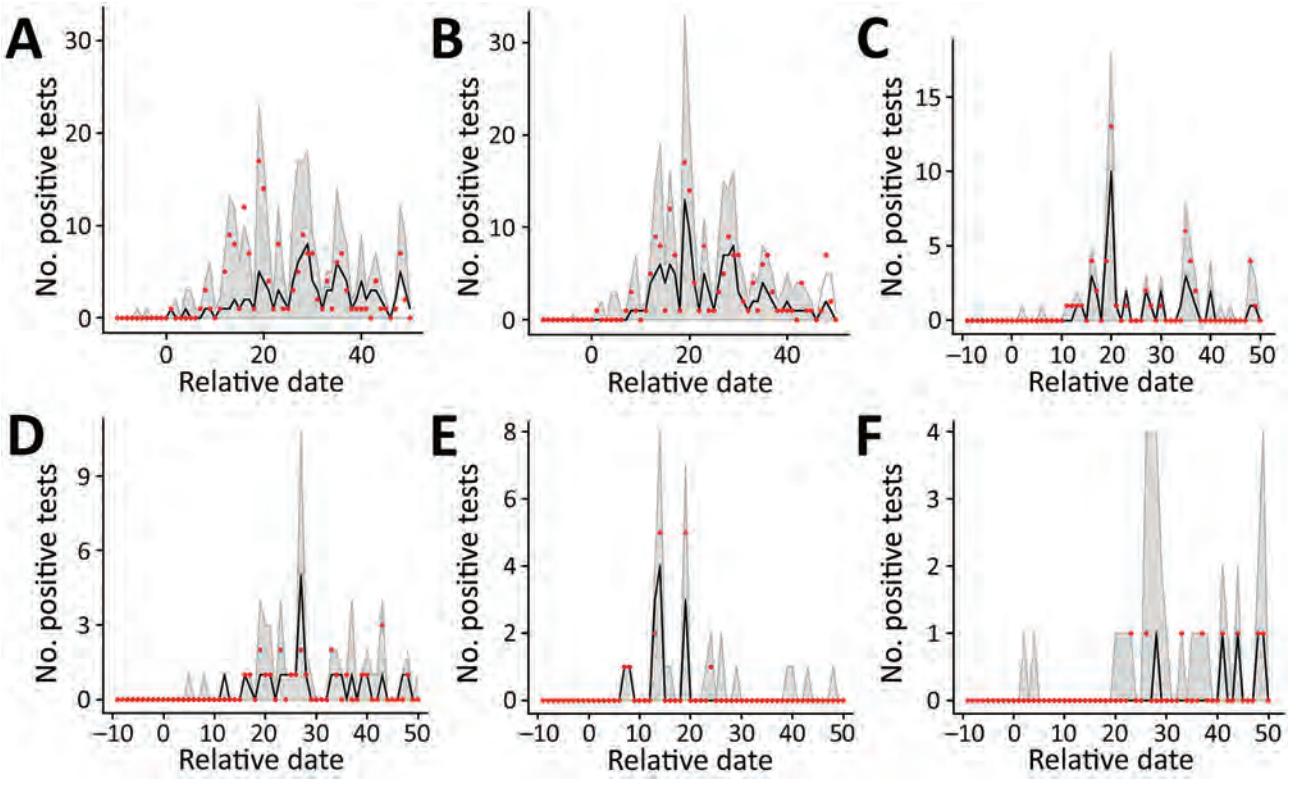

Figure 3. Results of simulated epidemics in a model of nosocomial SARS-CoV-2 transmission using estimated parameters determined on the basis of data from a long-term care facility in France. A) 1-phase model for the whole hospital. B) 2-phase model for the whole hospital. C–F) 1-phase model for individual wards: A2 (C), C0 (D), C2 (E), and C3 (F). Red dots show the observed number of positive tests in the data, black dashed lines indicate the median across that date for all simulations, and gray shading indicates the 95% CI range of the simulated values. Input parameter sets were included if their likelihood fell within the 95% CI relative to the maximum likelihood for 1- and 2-phase models for the whole hospital and individual wards. Estimated parameters are from Tables 1, 2. Extinct epidemics (i.e., those having <3 cumulative cases) were excluded from the distribution.

phases of transmission delimited by a specific change date ($t_{inflect}$) corresponding to implementation of contact precautions, including obligatory mask-wearing for patients and staff, and the cessation of group activities.

We found that the 2-phase model was better supported by the data aggregated across the entire hospital than a model with a single transmission rate, and the 2-phase model better captured the early peak in cases. Model validation suggested sufficient power to estimate transmission rates in 2 phases. The early phase rate (1.3 transmissions/patient/day) corresponded to an early R_0 of 8.7 and the late phase rate (0.19 transmissions/patient/day) corresponded to a late R_0 of 1.3. This change in transmission rate can largely be explained by the initial absence of preventive measures after the policy recommendation on day 6 and its gradual implementation over the next week. Under this assumption, the measures introduced were 85% (95% CI 66%–94%) effective at reducing transmission. The high estimates in the first phase suggest an explosive outbreak or superspreading event, which is consistent with the high secondary attack rate (33%). The estimates in the second phase, after the updated policy, might be more representative of current transmission rates in hospitals, which can provide and encourage the use of personal protective equipment.

Little research is available for the effect of contact precautions against SARS-CoV-2 transmission in healthcare settings. A meta-analysis of the effect of mask use against nosocomial transmission of coronaviruses found 67% protective efficacy of facemasks and 96% efficacy of N95 respirators (*11*), but the 1 study involving SARS-CoV-2 only examined a protective effect for healthcare workers (HCWs), which was unquantifiable because no infections were reported in the masked group (*12*). Several modeling studies have quantified the level of mask wearing that would prevent epidemic spread of SARS-CoV-2 in the community (*13*–*15*; D. Kai et al., unpub. data, http://arxiv.org/abs/2004.13553), but studies of interventions

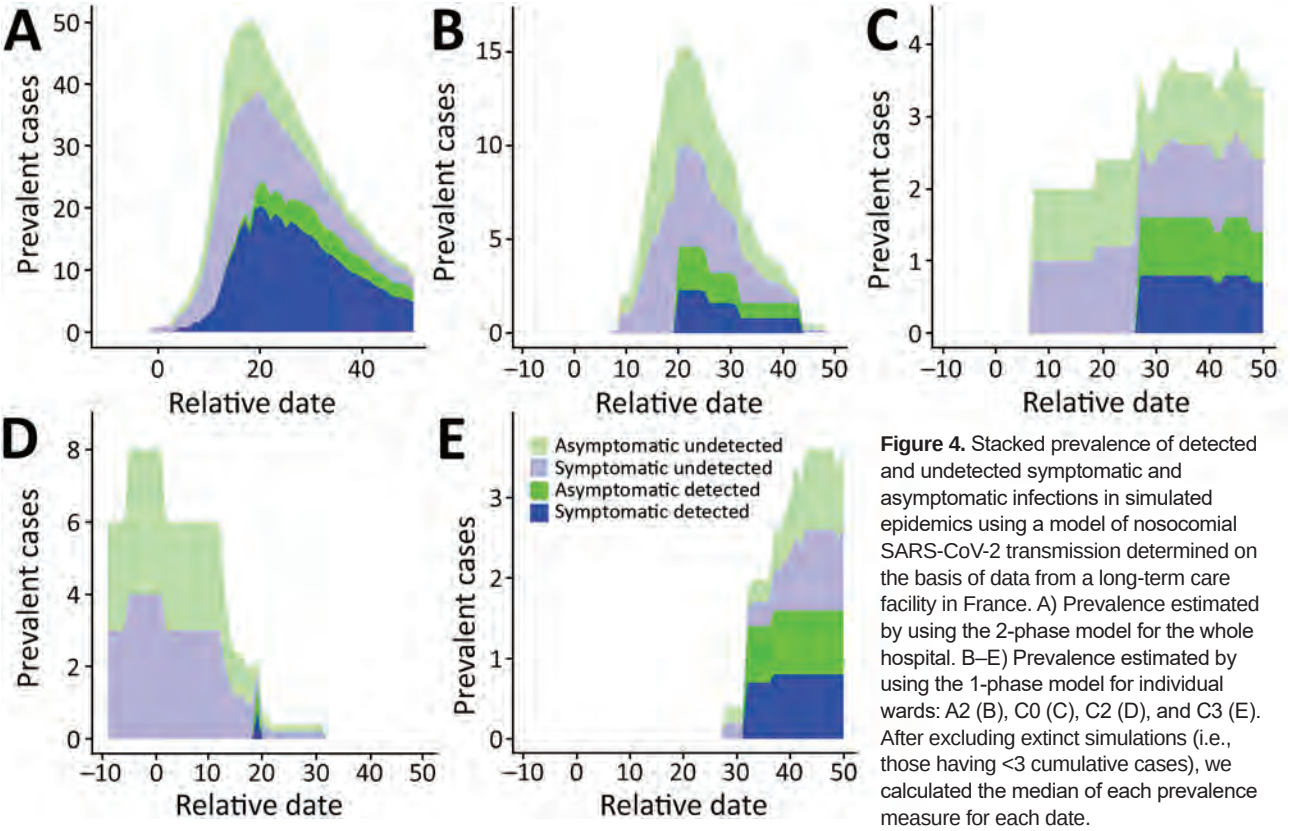

Figure 4. Stacked prevalence of detected and undetected symptomatic and asymptomatic infections in simulated epidemics using a model of nosocomial SARS-CoV-2 transmission determined on the basis of data from a long-term care facility in France. A) Prevalence estimated by using the 2-phase model for the whole hospital. B–E) Prevalence estimated by using the 1-phase model for individual wards: A2 (B), C0 (C), C2 (D), and C3 (E). After excluding extinct simulations (i.e., those having <3 cumulative cases), we calculated the median of each prevalence measure for each date.

for prevention of patient-to-patient transmission in healthcare environments are lacking.

Few other studies have published estimates of R_0 in healthcare settings. By analyzing the initial exponential growth phase of a hospital epidemic, one study computed an expedient estimate of R_0 for patients (1.13) and hospital staff (1.21) (*16*), but that study did not account for asymptomatic infections and did not provide a range for the R_0 estimates (*17*). In another study, the authors estimated an R_0 of 1.021 (95% CI 1.018–1.024) across 12 nursing homes based on a single introduction per floor of each institution and a secondary attack rate of 4.1% among 930 residents (B. Reyné et al., unpub. data, https://doi.org/10.1101/2020.11.27.20239913). The heterogeneity of transmission between different wards was also demonstrated in a previous review and meta-analysis in which the authors calculated an average observed reproduction number of 1.18 across 4 different healthcare settings (*18*), but showed much heterogeneity between settings; 1 was 4.5, and 3 were <0.25. A fourth study analyzed several hospitals in Canada by using incident cases and estimated an R_0 of 2.51, which ranged from 0.56 to 9.17 in individual facilities (*19*). However, the authors of that study did not model asymptomatic infection or account for negative test results or the outcomes of testing at different infectious stages (*19*).

To assess how estimates vary when looking at smaller subpopulations, we separately fit a 1-phase model to data from each ward. Using this method, we

Table 2. Characteristics and parameter estimates in hospital wards in a long-term care facility in France used to estimate nosocomial transmission rates of SARS-CoV-2*

Ward	No. beds	Total no. patients	Day of first positive case	No. cases	β	R_0†	t_{init}
A2	48	62	11	30	1.29 (0.51–NE)	8.76 (3.47–NE)	2 (−14 to 29)
C0	37	74	16	22	0.56 (0.22–NE)	3.79 (1.50–NE)	4 (−39 to 9)
C2	37	48	7	15	2.13 (0.29–NE)	14.46 (1.97–NE)	−8 (−39 to –14)
C3	37	63	24	7	0.42 (0.11–1.30)	2.87 (0.75–8.84)	19 (−9 to 21)

*Estimates and 95% CI for β, R_0, and t_{init} are from the fitting the 1-phase model to data from each ward (E_{init} = 1). In many instances, the upper bound of the 95% CI for β, and in the most likely value of β for some wards, could not be estimated due to a flat likelihood surface, in which case the value is given as NE. NE, not estimated; β, current transmission rate per day; E_{init}, number of initial infections at date t_{init}; R_0, basic reproduction number; t_{init}, date on which the initial infection occurs.
†The R_0 values were calculated using equation 4 (Appendix).

could not always estimate upper bounds of the transmission rates, probably because of strong stochasticity and scarcity of observed cases, an inherent feature of SARS-CoV-2 in which a large proportion of infected persons remain asymptomatic. However, our validation analyses suggested that point estimates for transmission rates across the wards could be consistently estimated. Applied to our dataset, estimated transmission rates ranged from 0.4 to 2.1, corresponding to an R_0 of 2.9–14.5. This heterogeneity might have been driven by differences in the timing of and compliance with preventive measures or by differences in contact patterns between staff and patients.

Calibrating models to real hospital outbreaks and estimating transmission rates provides more realistic transmission models to evaluate scenarios with alternative surveillance or control measures. We estimated the response to introducing barrier interventions at the beginning of the COVID-19 pandemic, when population immunity was minimal. Investigating alternative scenarios involving contemporary levels of population immunity or other viral variants could be easily achieved by updating the model parameters, such as the initial level of immunity or transmission rates. Updating parameters would enable prediction of the probability and size of hospital outbreaks and evaluation of testing strategies to prevent spread. As mentioned, a major challenge in analyzing outbreaks in hospitals or other small, closed environments lies in the consideration of imperfect testing practice, which we addressed through the observation model. First, a substantial proportion of infectious persons were not symptomatic; therefore, they were less likely to be tested, and we accounted for this difference in the model testing policy. Second, PCR test sensitivity is imperfect and depends on the time from infection, which is we also reflected in our evolving test sensitivity for different stages of infection. Finally, testing procedures were not regular and might have been affected by many factors not directly related to the epidemiologic situation, such as the day of the week, the available testing capacity, or changing strategies at the local scale. We addressed irregular testing procedures by using the number of tests per day directly described in the data rather than determining the number of tests performed from the number of infected persons. The model also tracked testing status to include realistic probabilities for testing and retesting of patients.

We compared our results with R_t from the commonly used EpiEstim package, which demonstrated the additional value of our approach. Ignoring negative tests and the complexity of testing policies, this simpler approach captured the high initial R_0 and subsequent fall but also showed a second peak that likely resulted from increased testing rather than an actual increase in transmission rate.

Our analysis has several limitations resulting from simplifying assumptions. First, we did not account for the possibility of imported infections other than the index case or cases; instead, we assumed that the force of infection from other patients would substantially outweigh that from the community. Second, because we had no data on infectious status for HCWs during the study period, we focused on patients and did not explicitly model acquisition by nor transmission from HCWs, although HCWs were implicitly considered potential vectors of patient-to-patient transmission. Rates of transmission from infectious patients to HCWs are relatively low (*20*,*21*), as are transmission rates from HCWs to patients (*22*), although these rates might have been higher in the early stages of the pandemic, considering low levels of hand hygiene (*23*). Ignoring the contribution of HCWs to new infections in the analysis suggests that we might have overestimated the transmission risk from infectious patients, but our estimates can still be interpreted as valid measures of the nosocomial risk to patients. Third, the model relies on parameters taken from the literature, which may be inaccurate. However, we conducted a sensitivity analysis to measure the sensitivity of transmission rates to appropriate variation in these parameters, and our main results remained unaffected. Finally, we note that the decision to analyze data from this hospital is partly due to the size of the outbreak, implying a selection bias toward a higher transmission rate than would be typical across all hospitals. However, >44,000 nosocomial infections were reported in France by February 14, 2021 (*24*), most of which consisted of clusters of cases; thus, our results can be interpreted as plausible for a hospital at risk for an outbreak. In addition, the model framework we propose is suitable for estimating transmission rates in any healthcare environment, and we provide some guidance for adaptation (Appendix).

In conclusion, the novel dynamic modeling framework we propose realistically simulates evolving testing policies and could easily be used on similar nosocomial COVID-19 datasets. The model also could be adapted for specific epidemiologic features, such as patient isolation. Overall, our results underline both the substantial potential effect of protective interventions introduced in healthcare settings and the considerable heterogeneity in transmission rates between hospital wards.

Additional members of EMEA-MESuRS Working Group on the Nosocomial Modelling of SARS-CoV-2: Sophie Chervet, Audrey Duval, Kévin Jean, Sofía Jijón, Ajmal Oodally, David R.M. Smith, and Cynthia Tamandjou.

Acknowledgments

We thank Sandrine Jacques for data collation, Niels Hendrickx for discussion of the results, and Matthieu Domenech de Cellès for advice on the statistical inference.

This work was supported directly by internal resources from the French National Institute for Health and Medical Research, the Institut Pasteur, the Conservatoire National des Arts et Métiers, and the University of Versailles-Saint-Quentin-en-Yvelines/University of Paris-Saclay. This study received funding through the MODCOV project from the Fondation de France (grant no. 106059) as part of the alliance framework "Tous unis contre le virus," the Université Paris-Saclay (no. AAP Covid-19 2020) and the French government through its National Research Agency (project no. SPHINX-17-CE36-0008-01).

G.S. constructed the model, conducted the analysis, and produced the draft and graphics. J.R.Z. produced the data and provided the medical perspective to inform model assumptions. S.C. made substantial contributions to the interpretation of results. L.T. and L.O. conceived the study, had regular input on analysis and interpretation, and contributed to the writing. All authors read, provided comments on, and approved the final manuscript.

About the Author

Dr. Shirreff is a postdoctoral researcher in nosocomial infectious disease at Conservatoire Nationale des Arts et Métiers, University of Versailles, and Institut Pasteur, Paris, France. His research focuses on understanding infectious disease transmission using mathematical models and modern tools for data capture.

References

1. Guan WJ, Liang WH, Zhao Y, Liang HR, Chen ZS, Li YM, et al.; China Medical Treatment Expert Group for COVID-19. Comorbidity and its impact on 1590 patients with COVID-19 in China: a nationwide analysis. Eur Respir J. 2020;55:2000547. https://doi.org/10.1183/13993003.00547-2020
2. Wu C, Chen X, Cai Y, Xia J, Zhou X, Xu S, et al. Risk factors associated with acute respiratory distress syndrome and death in patients with coronavirus disease 2019 pneumonia in Wuhan, China. JAMA Intern Med. 2020;180:934–43. https://doi.org/10.1001/jamainternmed.2020.0994
3. Abbas M, Robalo Nunes T, Martischang R, Zingg W, Iten A, Pittet D, et al. Nosocomial transmission and outbreaks of coronavirus disease 2019: the need to protect both patients and healthcare workers. Antimicrob Resist Infect Control. 2021;10:7. https://doi.org/10.1186/s13756-020-00875-7
4. Hall VJ, Foulkes S, Saei A, Andrews N, Oguti B, Charlett A, et al.; SIREN Study Group. COVID-19 vaccine coverage in health-care workers in England and effectiveness of BNT162b2 mRNA vaccine against infection (SIREN): a prospective, multicentre, cohort study. Lancet. 2021;397:1725–35. https://doi.org/10.1016/S0140-6736(21)00790-X
5. Cheng VC–C, Fung KS-C, Siu GK-H, Wong S-C, Cheng LS-K, Wong M-S, et al. Nosocomial outbreak of COVID-19 by possible airborne transmission leading to a superspreading event. Clin Infect Dis. 2021;73:e1356–64. https://doi.org/10.1093/cid/ciab313
6. Du Q, Zhang D, Hu W, Li X, Xia Q, Wen T, et al. Nosocomial infection of COVID-19: A new challenge for healthcare professionals. Int J Mol Med. 2021;47:31. https://doi.org/10.3892/ijmm.2021.4864
7. Anderson RM, Heesterbeek H, Klinkenberg D, Hollingsworth TD. How will country-based mitigation measures influence the course of the COVID-19 epidemic? Lancet. 2020;395:931–4. https://doi.org/10.1016/S0140-6736(20)30567-5
8. Smith DRM, Duval A, Pouwels KB, Guillemot D, Fernandes J, Huynh B-T, et al.; AP-HP/Universities/Inserm COVID-19 research collaboration. Optimizing COVID-19 surveillance in long-term care facilities: a modelling study. BMC Med. 2020;18:386. https://doi.org/10.1186/s12916-020-01866-6
9. Temime L, Gustin M-P, Duval A, Buetti N, Crépey P, Guillemot D, et al. A conceptual discussion about the basic reproductive number of severe acute respiratory syndrome coronavirus 2 in healthcare settings. Clin Infect Dis. 2020;72:141–3. https://doi.org/10.1093/cid/ciaa682
10. King AA, Nguyen D, Ionides EL. Statistical inference for partially observed Markov processes via the R package pomp. J Stat Softw. 2016;69:1–43. https://doi.org/10.18637/jss.v069.i12
11. Chu DK, Akl EA, Duda S, Solo K, Yaacoub S, Schünemann HJ, et al.; COVID-19 Systematic Urgent Review Group Effort (SURGE) study authors. Physical distancing, face masks, and eye protection to prevent person-to-person transmission of SARS-CoV-2 and COVID-19: a systematic review and meta-analysis. Lancet. 2020;395:1973–87. https://doi.org/10.1016/S0140-6736(20)31142-9
12. Wang X, Pan Z, Cheng Z. Association between 2019-nCoV transmission and N95 respirator use. J Hosp Infect. 2020;105:104–5. https://doi.org/10.1016/j.jhin.2020.02.021
13. Tian L, Li X, Qi F, Tang Q-Y, Tang V, Liu J, et al. Harnessing peak transmission around symptom onset for non-pharmaceutical intervention and containment of the COVID-19 pandemic. Nat Commun. 2021;12:1147. https://doi.org/10.1038/s41467-021-21385-z
14. Stutt ROJH, Retkute R, Bradley M, Gilligan CA, Colvin J. A modelling framework to assess the likely effectiveness of facemasks in combination with 'lock-down' in managing the COVID-19 pandemic. Proc R Soc Math Phys Eng Sci. 2020;476:20200376. https://doi.org/10.1098/rspa.2020.0376
15. Fisman DN, Greer AL, Tuite AR. Bidirectional impact of imperfect mask use on reproduction number of COVID-19: a next generation matrix approach. Infect Dis Model. 2020;5:405–8. https://doi.org/10.1016/j.idm.2020.06.004
16. Tang JW, Young S, May S, Bird P, Bron J, Mohamedanif T, et al. Comparing hospitalised, community and staff COVID-19 infection rates during the early phase of the

evolving COVID-19 epidemic. J Infect. 2020;81:647–79. https://doi.org/10.1016/j.jinf.2020.05.029
17. Accorsi E, Qiu X, Rumpler E, Kennedy-Shaffer L, Kahn R, Joshi K, et al. How to detect and reduce potential sources of biases in studies of SARS-CoV-2 and COVID-19. Eur J Epidemiol. 2021;36:179–96. https://doi.org/10.1007/s10654-021-00727-7
18. Thompson HA, Mousa A, Dighe A, Fu H, Arnedo-Pena A, Barrett P, et al. Severe acute respiratory syndrome coronavirus 2 (SARS-CoV-2) setting-specific transmission rates: a systematic review and meta-analysis. Clin Infect Dis. 2021;73:e754–64. https://doi.org/10.1093/cid/ciab100
19. Stockdale JE, Anderson SC, Edwards AM, Iyaniwura SA, Mulberry N, Otterstatter MC, et al. Quantifying transmissibility of SARS-CoV-2 and impact of intervention within long-term healthcare facilities. R Soc Open Sci. 2022;9:211710. https://doi.org/10.1098/rsos.211710
20. Basso T, Nordbø SA, Sundqvist E, Martinsen TC, Witsø E, Wik TS. Transmission of infection from non-isolated patients with COVID-19 to healthcare workers. J Hosp Infect. 2020;106:639–42. https://doi.org/10.1016/j.jhin.2020.08.015
21. Tong X, Ning M, Huang R, Jia B, Yan X, Xiong Y, et al. Surveillance of SARS-CoV-2 infection among frontline health care workers in Wuhan during COVID-19 outbreak. Immun Inflamm Dis. 2020;8:840–3. https://doi.org/10.1002/iid3.340
22. Baker MA, Fiumara K, Rhee C, Williams SA, Tucker R, Wickner P, et al. Low risk of coronavirus disease (COVID-19) among patients exposed to infected healthcare workers. Clin Infect Dis. 2021;73:e1878–80. https://doi.org/10.1093/cid/ciaa1269
23. Huang F, Armando M, Dufau S, Florea O, Brouqui P, Boudjema S. COVID-19 outbreak and healthcare worker behavioural change toward hand hygiene practices. J Hosp Infect. 2021;111:27–34. https://doi.org/10.1016/j.jhin.2021.03.004
24. Public Health France. COVID-19 epidemiologic update for February 18, 2021 [in French] [cited 2021 Jul 12]. https://www.santepubliquefrance.fr/maladies-et-traumatismes/maladies-et-infections-respiratoires/infection-a-coronavirus/documents/bulletin-national/covid-19-point-epidemiologique-du-18-fevrier-2021

Address for correspondence: George Shirreff, Institut Pasteur, National des Arts et Métiers, 25–28 rue Dr. Roux, Paris 75015, France; email: george.shirreff@pasteur.fr

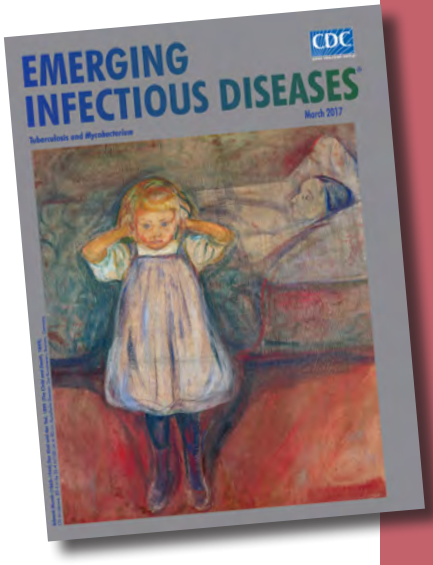

Originally published in March 2017

etymologia revisited

Mycobacterium chimaera

[mi'ko-bak-tēr'e-əm ki-mēr'ə]

Formerly an unnamed *Mycobacterium* sequevar within the *M. avium–M. intracellulare–M. scrofulaceum* group (MAIS), *M. chimaera* is an emerging opportunistic pathogen that can cause infections of heart valve prostheses, vascular grafts, and disseminated infections after open-heart surgery. Heater–cooler units used to regulate blood temperature during cardiopulmonary bypass have been implicated, although most isolates are respiratory. In 2004, Tortoli et al. proposed the name M. chimaera for strains that a reverse hybridization–based line probe assay suggested belonged to MAIS but were different from *M. avium*, *M. intracellulare*, or *M. scrofulaceum*. The new species name comes from the chimera, a mythological being made up of parts of 3 different animals.

Sources:

1. Schreiber PW, Kuster SP, Hasse B, Bayard C, Rüegg C, Kohler P, et al. Reemergence of *Mycobacterium chimaera* in heater–cooler units despite intensified cleaning and disinfection protocol. Emerg Infect Dis. 2016;22:1830–3.
2. Struelens MJ, Plachouras D. *Mycobacterium chimaer*a infections associated with heater-cooler units (HCU): closing another loophole in patient safety. Euro Surveill. 2016;21:1–3.
3. Tortoli E, Rindi L, Garcia MJ, Chiaradonna P, Dei R, Garzelli C, et al. Proposal to elevate the genetic variant MAC-A, included in the *Mycobacterium avium* complex, to species rank as *Mycobacterium chimaera* sp. nov. Int J Syst Evol Microbiol. 2004;54:1277–85.

https://wwwnc.cdc.gov/eid/article/23/3/et-2303_article

Analyzing and Modeling the Spread of SARS-CoV-2 Omicron Lineages BA.1 and BA.2, France, September 2021–February 2022

Mircea T. Sofonea, Bénédicte Roquebert, Vincent Foulongne, David Morquin, Laura Verdurme, Sabine Trombert-Paolantoni, Mathilde Roussel, Jean-Christophe Bonetti, Judith Zerah, Stéphanie Haim-Boukobza, Samuel Alizon

We analyzed 324,734 SARS-CoV-2 variant screening tests from France enriched with 16,973 whole-genome sequences sampled during September 1, 2021–February 28, 2022. Results showed the estimated growth advantage of the Omicron variant over the Delta variant to be 105% (95% CI 96%–114%) and that of the BA.2 lineage over the BA.1 lineage to be 49% (95% CI 44%–52%). Quantitative PCR cycle threshold values were consistent with an increased ability of Omicron to generate breakthrough infections. Epidemiologic modeling shows that, in spite of its decreased virulence, the Omicron variant can generate important critical COVID-19 activity in hospitals in France. The magnitude of the BA.2 wave in hospitals depends on the level of relaxing of control measures but remains lower than that of BA.1 in median scenarios.

The Omicron SARS-CoV-2 variant of concern (Pango lineage B.1.1.529, GISAID clade GR/484A) was detected in South Africa on November 26, 2021 (*1*). Rapid analyses demonstrated its increased transmissibility (C.A.B. Pearson et al., unpub. data, https://doi.org/10.1101/2021.12.19.21268038), high immune evasion potential (*2*,*3*), and low virulence (*4*–*6*) compared with the Delta variant. Furthermore, the biology of the virus appears to be different, having the potential to enter human cells through endocytosis and a pronounced tropism for the upper respiratory tract (*7*–*9*; T.P. Peacock et al., unpub. data, https://doi.org/10.1101/2021.12.31.474653; B.J. Willett et al., unpub. data, https://doi.org/10.1101/2022.01.03.21268111). After South Africa, the Omicron variant caused epidemic waves in many countries, including the United Kingdom (*10*), Denmark (*11*), and countries of North America (*12*).

The first Omicron lineage to dominate was BA.1 (B.1.1.529.1, Nextstrain clade 21K). However, in some countries, such as Denmark, its sister lineage BA.2 (former B.1.1.529.2, Nextstrain clade 21L) rapidly became dominant. BA.1 and BA.2 are highly divergent lineages (A.Z. Mykytyn et al., unpub. data, https://doi.org/10.1101/2022.02.23.481644), but their virulence and biology appear to be similar and the cross-immunity strong (M. Stegger et al., unpub. data, https://doi.org/10.1101/2022.02.19.22271112). Early reports suggest that BA.2 has a growth advantage over BA.1 (F.P. Lyngse et al., unpub. data, https://doi.org/10.1101/2022.01.28.22270044), possibly from a shorter generation time (i.e., average delay between consecutive infections in a transmission chain) (*10*).

Since January 2021, all the positive samples in France have been screened with variant-specific quantitative PCR (qPCR) assays targeting specific mutations (*13*). This close monitoring of the epidemic has low specificity, and the mutations targeted need to be updated to match the circulating variants, which is also why the monitoring is complemented by the whole-genome sequencing (WGS) of a subset of the samples.

We analyzed 324,734 variant-specific screening tests performed during September 1, 2021–February 28, 2022, in all 13 regions of mainland France. To understand lineage circulation, we generated SARS-CoV-2 whole-genome sequences for 16,973 of

Author affiliations: Université de Montpellier, Montpellier, France (M.T. Sofonea); Laboratoire Cerba, Saint Ouen L'Aumône, France (B. Roquebert, L. Verdurme, S. Trombert-Paolantoni, M. Roussel, S. Haim-Boukobza); Centre Hospitalier Universitaire de Montpellier, Montpellier (V. Foulongne, D. Morquin); Laboratoire Cerballiance Paris et Île-de-France Est, Paris, France (J.-C. Bonetti, J. Zerah); Centre National de la Recherche Scientifique, Paris (S. Alizon)

DOI: https://doi.org/10.3201/eid2807.220033

Table 1. Main characteristics of SARS-CoV-2 variant-specific screening tests (N = 131,478), France, September 1–December 18, 2021*

Characteristic	Value
Age of patient, y, median (95% CI)	36 (6–74)
Assay	
TIB Molbiol	4,887 (3.7)
PerkinElmer	33,037 (25.1)
ID Solutions (Evolution)	93,554 (71.2)
Context	
General population	127,337 (96.9)
Hospital	4,141 (3.1)
Region	
Ile-de-France	51,407 (39.1)
Hauts-de-France	16,938 (12.9)
Normandie	11,996 (9.1)
Nouvelle-Aquitaine	8,516 (6.5)
Provence-Alpes-Côte d'Azur	7,549 (5.7)
Occitanie	7,143 (5.4)
Corse	5,528 (4.2)
Bourgogne-Franche-Comté	5,155 (3.9)
Grand Est	5,136 (3.9)
Centre-Val de Loire	4,811 (3.7)
Bretagne	3,455 (2.6)
Other	1,296 (0.9)
Outcome	
A0B0C1	101,970 (77.6)
A0B0C0	6,969 (5.3)
A0B1C1	899 (0.68)
A1B0C1	37 (<0.1)
A1B0C0	15 (<0.1)
Other	21,588 (16.4)

*Values are no. (%) patients except as indicated.

these samples (5.2%) over the same period. We analyzed the cycle threshold (Ct) values of the qPCR to gain further insights into the biology and epidemiology of the infections. Finally, we used these results to explore prospective scenarios regarding the dynamics of critical care unit (CCU) occupancy in France in 2022. This study was approved by the Institutional Review Board of the Centre Hospitalier Universitaire of Montpellier and is registered at ClinicalTrials.gov (identifier no. NCT04738331).

Table 2. Results of ID Solution Revolution SARS-CoV-2 variant-specific screening tests (N = 193,256), France, December 18, 2021–February 28, 2022*

Characteristic	Value
Age of patient, y, median (95% CI)	36 (6–74)
Context	
General population	187,292 (96.9)
Hospital	5,964 (3.1)
Region	
Ile-de-France	40,185 (20.8)
Hauts-de-France	26,382 (13.7)
Normandie	31,205 (16.2)
Nouvelle-Aquitaine	13,236 (6.9)
Provence-Alpes-Côte d'Azur	31,299 (16.2)
Occitanie	9,034 (4.7)
Corse	8,031 (4.2)
Bourgogne-Franche-Comté	4,366 (2.3)
Grand Est	6,865 (3.6)
Centre-Val de Loire	10,412 (5.4)
Bretagne	9,405 (4.9)
Other	2,836 (1.5)
Outcome	
A0B9C1D0	12,955 (6.7)
A0B9C0D1	154,134 (79.8)
A0B9C1D1	173 (0.1)
A1B9C0D0	4,762 (2.5)
Other	21,232 (10.9)

*Values are no. (%) patients except as indicated.

Methods

Cohort Description

The variant screening tests were performed by Cerba Laboratory (Saint Ouen L'Aumône, France) on samples that originated from partner centers in mainland France and tested positive for SARS-CoV-2 with a generic qPCR assay. Most of the samples originated from the general population (Tables 1, 2). We did not have access to additional details about patient symptoms; however, according to an earlier study on a similar cohort, nearly all the samples originated from nasopharyngeal swab specimens, and the proportion of symptomatic and asymptomatic individuals were comparable among the positive tests (*14*). To limit epidemiologic biases, we removed persons >80 years or <5 years of age from the dataset.

Variant-Specific Screening Tests

We first analyzed 131,478 screening tests performed during September 1–December 18, 2021. The assays used over this first period were ID SARS-CoV-2/VOC Evolution Pentaplex (ID Solutions, https://www.id-solutions.fr) (93,554 tests), VariantDetect (PerkinElmer, https://www.perkinelmer.com) (33,037 tests), and VirSNiP (TIB Molbiol, https://www.tib-molbiol.de) (4,887 tests). These tests targeted 3 mutations in the SARS-CoV-2 spike protein: E484K (mutation A), E484Q (mutation B), and L452R (mutation C). Denoting the absence of a mutation by a 0 and its presence by 1, A0B0C1 mostly corresponds to infections caused by the Delta variant, A0B0C0 to the Alpha or Omicron variant or an ancestral lineage, A0B1C1 to Kappa or Kappa-like variants, A1B0C0 to the Beta or the Gamma variant, and A1B0C1 to a Delta variant with an E484K mutation.

Because of the shift in variant frequencies, new screening assays were implemented in late 2021. We analyzed 193,256 tests performed during December 6, 2021–February 28, 2022, all using the assay ID SARS-CoV-2/VOC Revolution Pentaplex (ID Solutions). This assay still targeted mutations A and mutation C but also targeted S:K417N (mutation D). Denoting nontested mutations with a 9, then A0B9C1D0 most likely indicates infections caused by the Delta variant, A0B9C0D1 by the Omicron

variant, A1B9C0D0 by the Gamma variant, A1B9C0D1 by the Beta variant, and A0B9C0D0 by the Alpha variant or the B.1.640 lineage. Finally, A0B9C1D1 can either indicate an infection by Delta with a 417N mutation, Omicron with a 452R mutation, or a Delta–Omicron co-infection.

For the ID Solutions Pentaplex tests, we analyzed 4 Ct values. Three of these values correspond to primers targeting the mutations of interest: S:417N, S:452R, or S:484K, the last to a primer targeting the nucleoprotein gene, which was used as a control.

Whole-Genome Sequencing

Next-generation sequencing (NGS) was performed by Cerba Laboratory for 16,973 samples with a Ct <30 using the CovidSeq amplicon-based NGS assay according to supplier recommendations (Illumina, https://www.illumina.com) and after a Janus/Chemagic RNA extraction (Perkin Elmer) from the nasopharyngeal swab. All sequences obtained were submitted to the EMERGEN Consortium Database (Santé Publique France, https://www.santepubliquefrance.fr/dossiers/coronavirus-covid-19/consortium-emergen) and GISAID (https://www.gisaid.org).

Statistical Analyses

Multinomial log-Linear Model

We performed a multinomial log-linear model with the formula variant = $\beta_0 + \beta_1$ age + β_2 assay + β_3 location_sampling + β_4 date:region + ε, where the β_i are the model parameters, ε the residuals, and the variable age is the individual age (treated as an integer and centered and scaled), location_sampling is a binary variable indicating whether the sample was collected in a hospital or in the general population, assay is the qPCR assay used, date is the sampling date (treated as an integer and centered and scaled), and region is the administrative region of residency in France. We included interactions between region and sampling date to detect temporal trends.

To make results easier to interpret, we computed relative risk ratios (RRRs). These ratios reflect, for a given variable, the risk for belonging to 1 of the outcomes (variant detection in this study) compared with the control group.

Growth Advantage Calculation

We computed growth advantages by using earlier methods based on Malthusian population growth rates (*15*–*18*). If we denote by $p(t)$ the frequency of an allele of interest (e.g., A0B0C0 test results) in the population (e.g., A0B0C0 and A0B0C1 test result), then the selection coefficient corresponds to the following rate:

$$s = \frac{d}{dt}\log\left(\frac{p(t)}{1-p(t)}\right).$$

This value is the inverse of a duration, and comparing it to earlier estimates requires a scaling for the generation time, the mean of which, T, is approximated by the mean serial interval (*19*). Overall, the growth advantage of a variant (e.g., A0B0C0) over another (e.g., A0B0C1) scaled for 1 infection generation is denoted as s_T and given by the formula $s_T = s \times T$. We estimated s_T by using the fitted values from a generalized linear model with a logit link to control for the covariates listed.

We used 21-day windows to estimate growth advantage, which corresponds to >4 generations of infection given the average generation time used. This number was chosen to be able to detect potential signals, while still obtaining a good temporal resolution of the estimated.

Ct Values Linear Modeling

We used a linear model with the following formula: Ct = $\gamma_0 + \gamma_1$ age + γ_2 variant + γ_3 location_sampling + γ_4 date × region + ε, where the γ_i indicate the model parameters, ε the residuals, and the covariates are the same as in the multinomial model. The variant was determined either by reverse transcription qPCR or WGS. The sampling date was included in the model because growing epidemics can be associated with lower Ct values than declining epidemics (*14*,*20*).

Using a likelihood ratio test, we showed that the presence of the variant covariate does improve the model. We assessed covariate significance by using an analysis of variance (ANOVA) with a type II error using the ANOVA function from the companion to applied regression package in R (R Project for Statistical Computing, https://www.r-project.org). We computed estimated marginal means for the Ct values associated with the screening tests results by using the emmeans function from the eponym R package. We plotted the fitted values from the linear model by using the predict function in R. The statistical methods are further described (Appendix 1, https://wwwnc.cdc.gov/EID/article/28/7/22-0033-App1.pdf), and raw data and R scripts are available online (https://doi.org/10.5281/zenodo.6536220).

Epidemiologic Modeling

We used the previously developed framework Covidsim, which accurately captures the national CCU admissions for SARS-CoV-2 in France and the associated

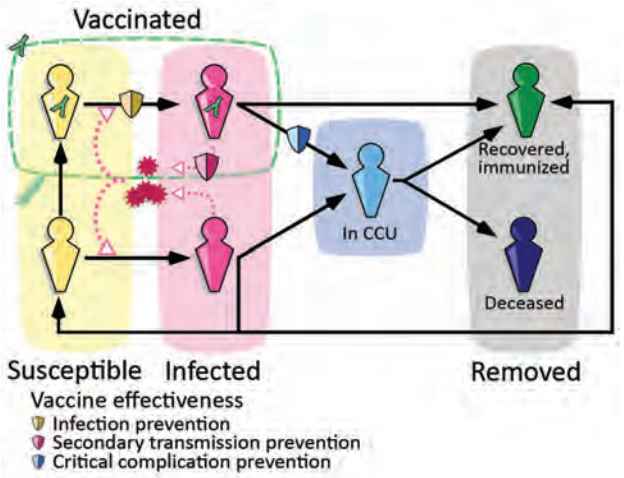

Figure 1. Epidemiologic modeling of the SARS-CoV-2 Omicron BA.2 wave dynamics, France. Simplified flowchart of the Covidsim framework. Persons can move between several compartments in the general population (in yellow or pink depending on the infection status), in CCUs in blue and removed from the system, either because of their immunity to BA.2 or of death (in gray). Part of the general population is vaccinated (green dashed line), which affects epidemiologic dynamics in 3 ways (illustrated with the shields), namely reduced infectivity, reduced virulence, and reduced risk for infection. CCU, critical care unit.

mortality incidence time series (*21*). The underlying model is deterministic, is structured in discrete time, and uses CCU incidence and prevalence data, as well as mortality data, to estimate parameters of interest (Figure 1, Appendix 1). A retrospective analysis showed its ability to provide robust projections up to 5 weeks ahead (*22*).

In the model, the number of vaccinated persons followed the national campaign in France (Système d'Information VAccin Covid data) and the number of persons with postinfectious immunity results from the model's reconstruction of the epidemic. The protection against infection and severe illness depends on the type of immunity (vaccine [*23*] or postinfectious [*24*]) and the variant. These values, like others, were informed from literature data, technical reports, and preliminary work.

Having a mechanistic model enables us to explore prospective scenarios for CCU activity. We did so by formulating assumptions regarding the intensity of future control measures and incorporating our estimates of growth advantage and relative frequency of the variants into the model.

In this study, the temporal reproduction number (Rt) corresponds to the average number of secondary infections caused by an infected person at date t and is estimated by using national hospital admission data (https://www.data.gouv.fr/fr/datasets/donnees-hospitalieres-relatives-a-lepidemie-de-covid-19) and the EpiEstim method (*25*). We shifted the dates in the incidence time series to compute Rt, setting the median time between infection and CCU admission to 14 days (*21*,*26*).

Results

A0B0C0 Emergence

We first analyzed variant-specific screening tests collected during September 1–December 18, 2021 (Figure 2, panel A). Most of these tests originated from the general population (96.6%) and showed coverage differences between regions of France (Table 1). The most common assay used (71%) was that from ID

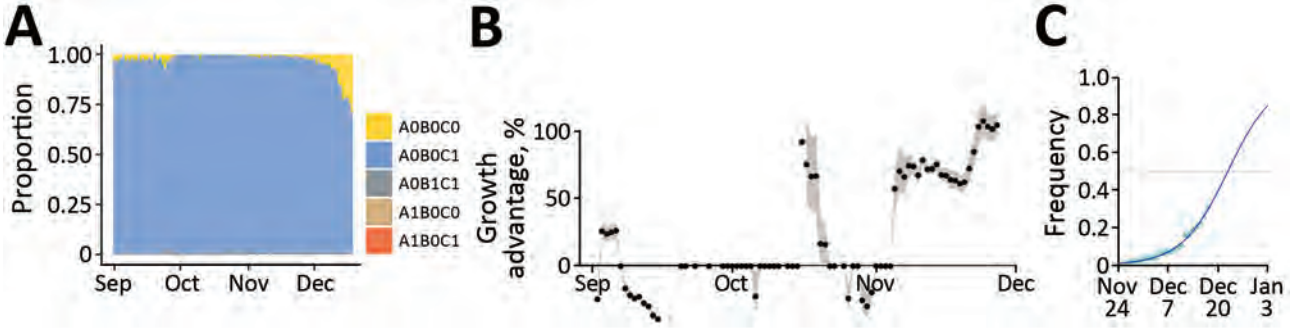

Figure 2. Monitoring and quantifying variant spread in using SARS-CoV-2 variant-specific screening tests (N = 103,757), France, October 1–December 18, 2021. A) Raw proportion of the test outcomes. B) Growth advantage of A0B0C0 tests over A0B0C1 in France. Points indicate the median growth advantage estimated on a 21-day sliding window; the gray shading indicates 95% CI. C) Estimated frequency and growth advantage of A0B0C0 relative to the sum of A0B0C0 and A0B0C1 tests in France, corresponding to the last point of panel A. Triangles show the fitted values from the model, the line the model output, and the gray shading the 95% CI. Raw occurrence data from panel A is stratified by region in Appendix 1 Figure 1 (https://wwwnc.cdc.gov/EID/article/28/7/22-0033-App1.pdf). Test designations indicate the absence of a mutation by a 0 and its presence by 1; the mutations are S:484K (A), S:E484Q (B), and S:452R (C); A0B0C1 mostly corresponds to Delta variant, A0B0C0 to Alpha or Omicron variant or an ancestral lineage, A0B1C1 to Kappa or Kappa-like variants, A1B0C0 to Beta or the Gamma variant, and A1B0C1 to a Delta variant with an E484K mutation.

Solutions (Evolution). The raw number of tests performed follows the incidence curve of the epidemic (Appendix 1 Figure 1).

Focusing on the tests performed during October 25–December 18, 2021 (i.e., when the epidemic was increasing), we used a multinomial regression model to identify covariates associated with the test outcome (Table 3). A0B0C0 infections (consistent with Omicron) were found in younger persons than were A0B0C1 infections (consistent with Delta); RRR was 0.85 (95% CI 0.83–0.88) per age unit (equal to 56 years in this study). We also detected strong temporal increases in most of the regions of France that had RRR >10 per day. In some regions, we detected a temporal increase of A0B1C1 tests, consistent with the Kappa variant. Finally, in our dataset, the (rare) A1B0C1 tests only showed a slight temporal increase in 2 regions (Bretagne and Hauts-de-France).

We then estimated growth advantages of A0B0C0 over A0B0C1 infections during 21-day time windows. The advantage was adjusted for covariates and assumed to be constant over each window. In September 2021, A0B0C0 infections were spreading less rapidly than A0B0C1 (Figure 2, panel B). This finding is consistent with the rapid increase of the Delta variant at the time (*18*). The pattern shifted at the end of November, with a 50% growth advantage of A0B0C0 infections, which increased to 105% (95% CI 96.1%–114%) in the last time window. According to this model, A0B0C0 infections became more frequent than A0B0C1 infections during the week of December 20 (Figure 2, panel C), with strong variations across regions (Appendix 1 Figure 1).

The A0B9C0D1/Omicron Wave

The new screening test targeting the K417N mutation enabled us to better document the spread of the Omicron variant (Table 2). In December 2021, the A0B0C0 wave was mainly caused by viruses bearing the K417N mutation (Figure 3, panel A). Furthermore, the proportion of A0B0C0 tests not attributable to Omicron decreased toward the end of the year. Finally, we also noted potential co-infections of Omicron and Delta in December.

We then estimated the growth advantage of A0B9C0D1 over A0B9C1D0 during December 6, 2021–February 28, 2022 (Figure 3, panel B). The resulting estimate (96.5% [95% CI 87.9%–105%]) is very consistent with the results obtained using a less-specific test on the early stages of the wave.

We observed a shift between the Omicron waves in the different regions of France (Figure 4). For instance, in the South-East area, Delta was still dominant during week 51 of 2021. As expected, we also saw that tests consistent with co-infections of Omicron and Delta were more frequent in regions where the 2 variants were cocirculating in substantial

Table 3. Relative risk ratios of covariates associated with SARS-CoV-2 variant-specific screening tests (N = 103,757), France, October 1–December 18, 2021*

Covariate	Relative risk ratio (95% CI)				
	A0B0C0	A0B1C1	A1B0C0	A1B0C1	Other
Intercept	0 (0.00–0.01)	0.01 (0–01)	NS (0–0)	NS (0–0)	0.18 (0.17–0.18)
Age, scaled†	0.85 (0.83–0.88)	1.08 (1.0–1.2)	NS (0.7–2.4)	NS (0.5–1)	0.82 (0.8–0.83)
Context					
General population	Referent	Referent	Referent	Referent	Referent
Hospital	NS (0.82–1.1)	0.37 (0.2–0.69)	NS —	NS —	0.88 (0.79–0.99)
Assay					
ID Solutions	Referent	Referent	Referent	Referent	Referent
PerkinElmer	2.0 (1.8–2.1)	0.46 (0.38–0.56)	NS (0–3.8)	NS (0.1–1.1)	0.82 (078–0.85)
TIB Molbiol	2.1 (1.6–2.6)	10.9 (9–13)	NS (0.9–23)	8.3 (3.1–22)	1.94 (1.8–2.1)
Date and region					
Ile-de-France	87.0 (75–100)	4.4 (3.4–5.7)	NS (0–7.5)	NS (0.3–6.5)	1.7 (1.6–1.8)
Bourgogne-Franche-Comté	10.5 (7.8–14)	8.3 (5.6–12)	NS (no values)	NS (0–49)	0.63 (0.53–0.74)
Bretagne	37.6 (28–51)	NS (0.91–5.4)	NS (no values)	21.6 (2–200)	1.3 (1.1–1.6)
Centre-Val de Loire	46.1 (37–57)	NA (0.8–3.5)	NS (0–370)	NS (0–98)	NS (0–0)
Corse	86.4 (71–100)	0.2 (0.05–0.5)	NS (0–310)	NS (0–56)	1.9 (1.7–2.2)
Grand Est	22.2 (18–28)	3.7 (2.3–5.8)	NS (0.5–80)	NS (0–100)	0.49 (0.42–0.58)
Hauts-de-France	44.8 (38–53)	NS (0.4–1.2)	NS (0–10)	18.0 (5.5–58)	1.17 (1.10–1.30)
Normandie	38.2 (32–46)	2.2 (1.4–3.4)	NS (0–23)	NS (0–15)	0.77 (0.69–0.86)
Nouvelle-Aquitaine	17.6 (14–22)	2.7 (1.7–4.4)	NS (0–51)	NS (0–16)	0.43 (0.37–0.50)
Occitanie	19.8 (16–25)	7.7 (5.3–11)	NS (0–95)	NS (0–31)	NS (0.82–1.1)
Provence-Alpes-Côte d'Azur	19.5 (16–25)	NS (0.6–2.2)	NS (0–320)	NS (0–67)	0.62 (0.54–0.71)
Other	37.6 (26–54)	NS (0.6–6.7)	NS (no values)	NS (no values)	NS (0.63–1.10)

*Model only analyzes tests performed after October 25, 2021; tests performed before that date are described in Appendix 1 Table 1 (https://wwwnc.cdc.gov/EID/article/28/7/22-0033-App1.pdf). NS, not significant.
†Age variable is centered and scaled (1 scaled unit corresponds to 56 years).

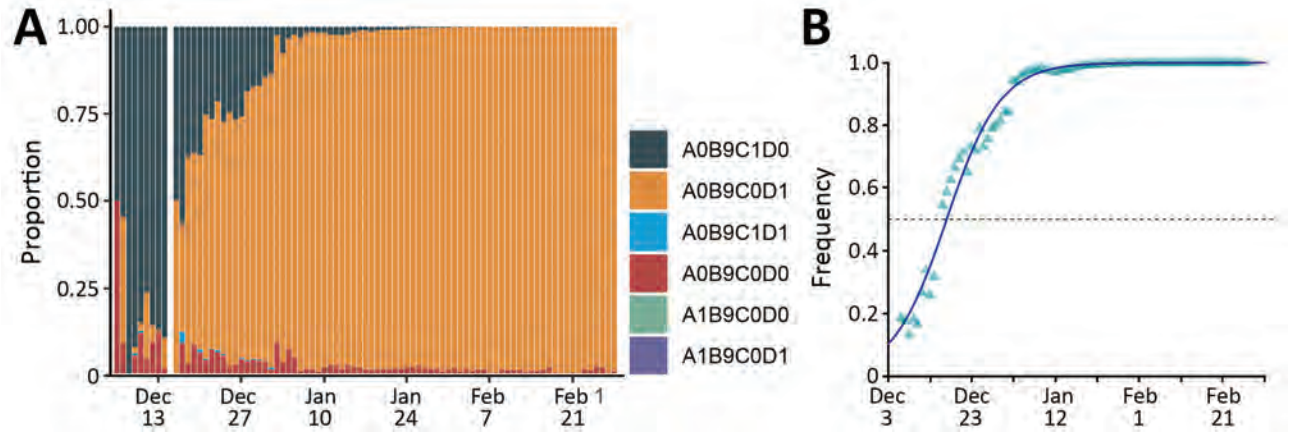

Figure 3. Monitoring and quantifying variant spread using ID Solutions Revolution tests (N = 193,256), France, December 6, 2021–February 28, 2022. A) Raw proportion of the test outcomes. B) Estimated frequency of A0B9C0D1 relative to the sum of A0B9C0D1 and A0B9C1D0 tests in France. Raw occurrence data from panel A is stratified by region in Appendix 1 Figure 2 (https://wwwnc.cdc.gov/EID/article/28/7/22-0033-App1.pdf). Test designations indicate the absence of a mutation by a 0 and its presence by 1 (9 means the mutation was not tested); mutations are the same as in Figure 2 and D is S:417N; A0B9C0D1 mostly corresponds to Omicron variant, A0B9C1D0 to Delta variant and A0B9C1D1 to Omicron-Delta coinfection.

frequencies. This shift in different regions can explain the second increase in growth advantage of A0B0C0 tests observed in November (Figure 2, panel C).

Sequencing Reveals a Shift from BA.1 to BA.2

Because variant screening tests only target 3 mutations, we analyzed whole-genome sequences of ≈5% of the positive samples (Figure 5, panel A). This analysis revealed that before October 2021, A0B0C0 tests mostly originated from Delta variant infections, whereas in November they originated from rare lineages or from the 20C lineage. A more precise analysis shows that these mostly correspond to the B.1.640 lineage. Beginning near the end of November, half of these tests were associated with the Omicron variant; this percentage increased to >80% during December.

Beginning in the second week of January 2022, some of the screening outcomes consistent with Omicron (A0B9C0D1) were associated with the BA.2 variant (Figure 5, panel B). This proportion increased over the next several weeks. Using the sequencing data, we estimated a growth advantage of BA.2 over the BA.1 Omicron lineage of 48.9% (95% CI 44.2%–53.6%). BA.2 accounted for most variants at the end of February, meaning that the Omicron variant BA.1 lineage only dominated the epidemic in France for <3 months (Figure 5, panel B).

Ct Differences

For the tests performed during December 16, 2021–February 28, 2022, we used a linear model to explore differences in Ct values between variants. All the covariates were significant according to ANOVA with a type II error (Appendix 1 Table 1). Ct values tended to decrease with age or to be lower in samples from hospitals (Appendix 1 Table 2), which is consistent with earlier results (*14*). Furthermore, A0B9C0D1 tests exhibited significantly higher Ct values than

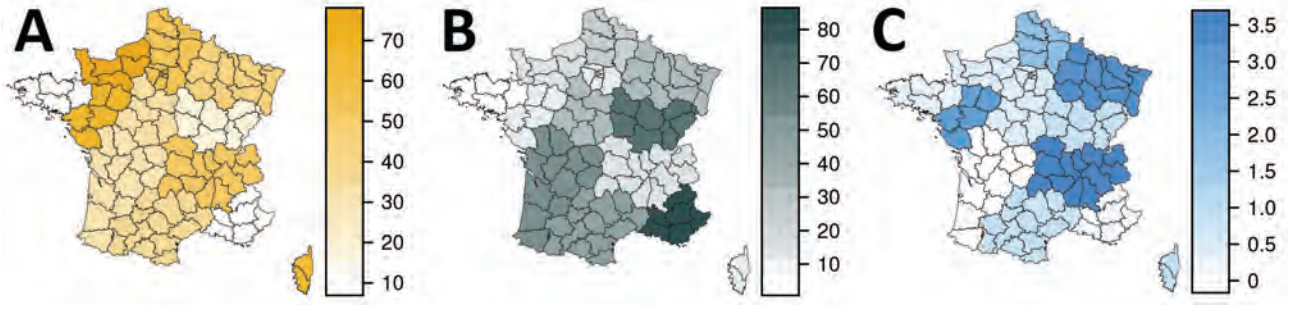

Figure 4. Frequency of A0B9C0D1 (A), A0B9C1D0 (B), and A0B9C1D1 (C) SARS-CoV-2 variant test results in mainland regions of France during week 51 of 2021. The colors show the prevalences (in percentages), which are corrected for covariates (age and sampling context). Includes 7,166 tests of the tests shown in Figure 3 but performed December 20–26, 2021. Test designation is the same as in Figure 3.

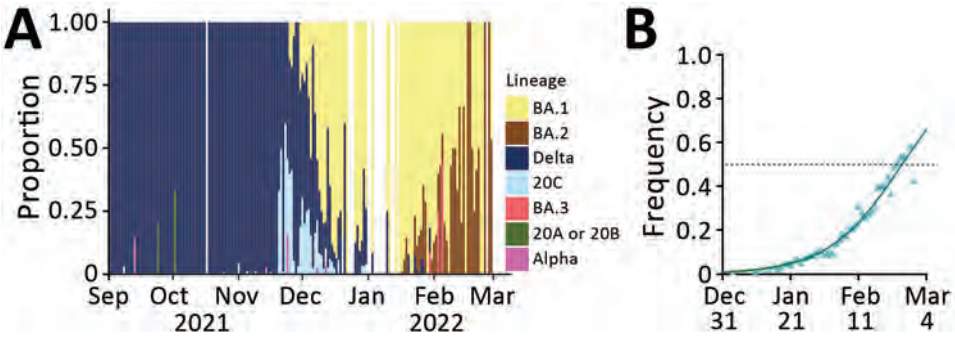

Figure 5. Monitoring and quantifying SARS-CoV-2 variant spread using whole-genome sequencing, France. A) Raw proportion of SARS-CoV-2 lineages inferred from whole-genome sequences of 16,973 samples. B) Estimated proportion and growth advantage of the BA.2 variant with respect to the BA.1 variant. Raw occurrence data from panel A is stratified by region in Appendix 1 Figure 3 (https://wwwnc.cdc.gov/EID/article/28/7/22-0033-App1.pdf).

A0B9C1D0; fitted median values were 22.1 versus 21.4 (Figure 6, panel A). This result suggests lower amounts of genetic material in the samples.

To further investigate these patterns, we analyzed the Ct values of the mutations targeted by the assay. We found that the Ct for the 417N mutation was higher in single infections (A0B9C0D1) than in co-infections (A0B9C1D1) (Figure 6, panel B). This finding is consistent with the greater ability of Omicron compared with Delta to infect immunized hosts, assuming that such breakthrough infections have a lower virus load (*27*,*28*).

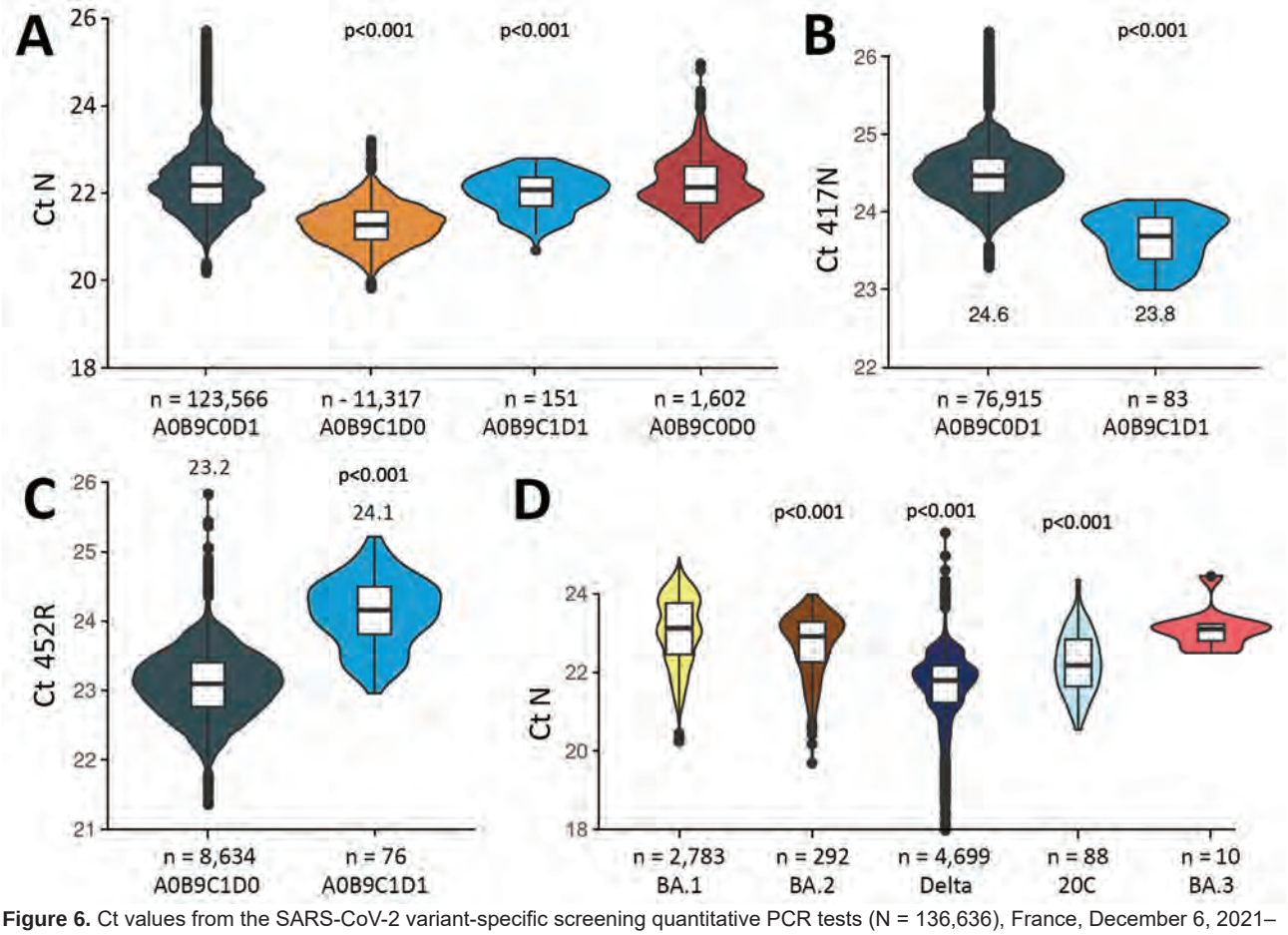

Figure 6. Ct values from the SARS-CoV-2 variant-specific screening quantitative PCR tests (N = 136,636), France, December 6, 2021–February 28, 2022. Ct values refer to the control (nucleoprotein) gene (A and D), 417N mutation (B), and 452R mutation (C). Values are shown as a function of the test outcome (A, B, and C) or the virus lineage (D). P values derived from a t-test where the reference variable is either A0B9C0D1 or BA.1. Boxes within violin plots show the median (horizontal line within box), 50% (box tops and bottoms), and 95% CIs (error bars). Tests were the same as in Figure 3, but only screening tests with Ct <28 were included to ensure robust screening results. Ct, cycle threshold; N, nucleoprotein gene.

For the 452R mutation, we found the opposite pattern (Figure 6, panel C).

Finally, we analyzed the Ct values of the control gene as a function of the virus lineage inferred from the NGS data (Figure 6, panel D). BA.1 samples had higher Ct values than did Delta samples. Furthermore, BA.2 samples had lower Ct values than did BA.1 samples.

Modeling Scenarios

On December 22, 2021, we incorporated the inferred growth advantage of Omicron/BA.1 over Delta into Covidsim (*21*) to explore an optimistic and a pessimistic scenario running through mid-March 2022. These scenarios differed in terms of the assumptions made regarding the reduction of Omicron virulence compared with Delta (3-fold vs. 2-fold) and vaccine protection against infection (75% vs. 40%) and severe illness (95% vs. 80%). Even though our assumption that the epidemic was under control at the end of 2021 was too optimistic, both the optimistic and the pessimistic scenarios showed that CCU activity was likely to remain high over January and February 2022, which proved to be accurate (Appendix 1, Appendix 1 Figure 4).

Given our estimations of the frequency of the Omicron/BA.2 sublineage in the population and its growth advantage over BA.1, we can predict the temporal increase of the epidemic Rt. We compared this predicted Rt with that calculated for the period March 1–10, 2022, using national hospital admission data, and found that from March 3 the ratio between the 2 was greater than unity (Figure 7, panel A). This result suggests that the epidemic growth cannot solely be explained by variant replacement and involves other drivers (e.g., the end of the holiday periods in some regions starting February 21, 2022).

Finally, on March 17, 2022, by using consolidated estimates of relative virulence (*6*) and vaccine effectiveness (*23*) for Omicron variants, we explored 2 prospective scenarios for nationwide COVID-19 CCU activity depending on the intensity of the relaxation of the control over the epidemic: Rt at the peak as 1.1 or 1.6 (Figure 7, panel B). We found that a new hospital peak was possible in the more pessimistic case, but its height remained below half of the peak experienced during the first Omicron wave in January.

Discussion

Variant-specific qPCR represents a flexible and cost-efficient surveillance method to obtain timely descriptions of SARS-CoV-2 epidemics. Thanks to a dense follow-up, we estimated that the Omicron variant spread in France with a 2-fold growth advantage over Delta (i.e., higher than that recorded for the Delta variant vs. the Alpha variant in June 2021) (*18*). This finding is consistent with estimates from South Africa (C.A.B. Pearson et al., unpub. data) and the United Kingdom (S. Abbott, et al., unpub. data, https://doi.org/10.1101/2022.01.08.22268920). Some estimates from Denmark suggest even higher advantages but using a different method (relying on reproduction numbers and not growth rates) and GISAID genomic data, which means a lower coverage and potentially strong reporting delays (*29*).

Thanks to the WGS of 5% of the samples, we were able to confirm the nature of the variants spreading and to detect a replacement of the BA.1 Omicron lineage by the BA.2 with a growth advantage of ≈50% (the precise value depends on the serial interval used [19]). This finding is consistent with the qualitative trends reported from South Africa (*30*) and the United

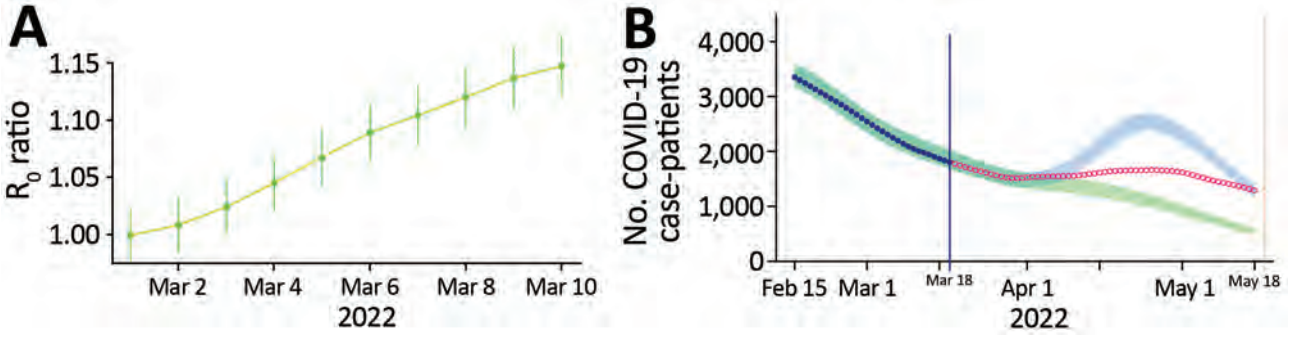

Figure 7. Analyzing and modeling the SARS-CoV-2 Omicron BA.2 epidemic wave in France. A) Ratio between the predicted and observed reproduction number (R0) based on BA.2 frequency and growth advantage. B) National critical care bed occupancy in 2 scenarios depending on baseline transmission increase. CIs are calculated from that of the frequency and growth advantage of BA.2 (Figure 5, panel B). The vertical blue line indicates the day the model was performed, the dark blue dots the data, and the shaded areas the 95% range of the model simulations. The 2 scenarios differ according to the capping of the increase of the baseline transmission rate, mimicking either a limited (green) or a strong (blue) easing preventive measures in March 2022 in France. Red open circles indicate data collected after the scenarios were modeled (i.e., not used in the inference or the modeling). The vertical yellow line indicated the last day the data were collected for the figure. Appendix 1 (https://wwwnc.cdc.gov/EID/article/28/7/22-0033-App1.pdf) further details model.

Kingdom (*10*) and from household data in Denmark (F.P. Lyngse et al., unpub. data). Note that these estimates tend to rely on the spike gene target failure, which is observed in a ThermoFisher assay for Omicron/BA.1 but not for Delta and not for BA.2. In our study, using variant-specific screening tests designed to target 3 specific mutations conferred a greater specificity of the results.

By analyzing qPCR Ct values, we found that samples from BA.1/Omicron infections had significantly higher Ct values than those from Delta infections. Although care must be taken when analyzing Ct values, especially for coronaviruses (*31*), this finding suggests a lower amount of virus genetic material in the samples. This result is intriguing given the large growth advantage of Omicron over Delta. A possible interpretation is that the Omicron variant is more prone to infecting immunized hosts (*2*,*3*) and, in vaccinated hosts, such breakthrough infections have been reported to have lower virus load than infections of nonvaccinated hosts (*27*,*28*).

We did not have access to the vaccination status of the persons from whom samples were taken. However, a potential overrepresentation of immunized hosts among Omicron infections is consistent with the lower values for the Ct associated with the 417N mutation in Delta–Omicron co-infections compared with Omicron monoinfections. Because Delta is less prone to immune evasion than Omicron, we expect the proportion of immunized hosts to be low in co-infections.

A limitation of our approach is that we cannot readily identify the origin of the growth advantage of BA.2 with respect to BA.1. This advantage could be caused by a shorter generation time for BA.2 infections (*10*), which is consistent with our finding that BA.2 samples have lower Ct values than those for BA.1 samples. Furthermore, although we do control for the sampling date as a covariate, this difference could reflect the epidemic trend given that Ct values are expected to be lower in expanding epidemics (*14*,*20*).

Our study highlights both the strengths and weaknesses of variant-specific screening assays (also sometimes called allele-specific reverse transcription qPCR). The advantage is that these assays enable rapid detection of variant replacement (we could detect a signal in the A0B0C0 tests in early December, at a time when the Omicron frequency <5%). However, the information about the circulating lineage is limited and, for example, the onset of the BA.2 wave in France could only be detected by using sequencing data. Furthermore, test interpretations vary with time. Before September 2020, some A0B0C0 tests were caused by the Alpha variant and by the Delta variant with a low Ct. In late October, before being associated with Omicron infections, most of these tests were probably attributable to lineage B.1.640, first detected in the Democratic Republic of the Congo (*32*). Temporal variations (Figure 2, panel B) may also originate from spatial heterogeneity; growth advantages are calculated for large administrative units, and variant epidemics can be at different stages in different regions. Finally, delays in data reporting can matter in the initial stages of variant epidemics.

Beyond nowcasting (near–real-time estimating) variant replacement rates, epidemiologic models represent a powerful tool to explore prospective scenarios. By combining our estimates of growth advantage with literature data, especially on vaccine protection, we showed that the decrease in Omicron virulence (*6*) was not sufficient to allow for a steep decrease in critical COVID-19 activity in hospitals in France >1 month before the reported incidence peak, hence helping CCU to anticipate the number of beds necessary and plan for the return to regular activity for the other hospital sectors.

Acknowledgments

The authors thank the Experimental and Theoretical Evolution team from Maladies Infectieuses et Vecteurs: Écologie, Génétique, Évolution et Contrôle, University of Montpellier, for discussion, as well as the EMERGEN consortium (complete member list in Appendix 2, https://wwwnc.cdc.gov/EID/article/28/7/22-0033-App2.xlsx).

This project was supported by the Occitanie Region and the Agence Nationale de la Recherche through a grant to the PhyEpi Project and by Agence Nationale de la Recherche Maladies Infectieuses Émergentes to the MODVAR project (grant no. ANRS0151).

About the Author

Dr. Sofonea is associate professor at University of Montpellier and heads the Experimental and Theoretical Evolution team. His research interests include epidemiology, stochastic modelling, spatial data analysis, and public health.

References

1. Viana R, Moyo S, Amoako DG, Tegally H, Scheepers C, Althaus CL, et al. Rapid epidemic expansion of the SARS-CoV-2 Omicron variant in southern Africa. Nature. 2022;603:679–86. https://doi.org/10.1038/s41586-022-04411-y
2. Planas D, Saunders N, Maes P, Guivel-Benhassine F, Planchais C, Buchrieser J, et al. Considerable escape of

SARS-CoV-2 Omicron to antibody neutralization. Nature. 2022;602:671–5. https://doi.org/10.1038/s41586-021-04389-z
3. Takashita E, Kinoshita N, Yamayoshi S, Sakai-Tagawa Y, Fujisaki S, Ito M, et al. Efficacy of antibodies and antiviral drugs against Covid-19 Omicron variant. N Engl J Med. 2022;386:995–8. https://doi.org/10.1056/NEJMc2119407
4. WHO Collaborating Centre for Infectious Disease Modelling, MRC Centre for Global Infectious Disease Analysis, Jameel Institute, Imperial College London. Report 50: hospitalisation risk for Omicron cases in England. 2021 Dec 21 [cited 2022 May 6]. http://www.imperial.ac.uk/medicine/departments/school-public-health/infectious-disease-epidemiology/mrc-global-infectious-disease-analysis/covid-19/report-50-severity-omicron
5. Maslo C, Friedland R, Toubkin M, Laubscher A, Akaloo T, Kama B. Characteristics and outcomes of hospitalized patients in South Africa during the COVID-19 Omicron wave compared with previous waves. JAMA. 2022;327:583–4. https://doi.org/10.1001/jama.2021.24868
6. Nyberg T, Ferguson NM, Nash SG, Webster HH, Flaxman S, Andrews N, et al.; COVID-19 Genomics UK (COG-UK) consortium. Comparative analysis of the risks of hospitalisation and death associated with SARS-CoV-2 omicron (B.1.1.529) and delta (B.1.617.2) variants in England: a cohort study. Lancet. 2022;399:1303–12. https://doi.org/10.1016/S0140-6736(22)00462-7
7. Meng B, Abdullahi A, Ferreira IATM, Goonawardane N, Saito A, Kimura I, et al.; CITIID-NIHR BioResource COVID-19 Collaboration; Genotype to Phenotype Japan (G2P-Japan) Consortium; Ecuador-COVID19 Consortium. Altered TMPRSS2 usage by SARS-CoV-2 Omicron impacts infectivity and fusogenicity. Nature. 2022;603:706–14. https://doi.org/10.1038/s41586-022-04474-x
8. Hui KPY, Ho JCW, Cheung MC, Ng KC, Ching RHH, Lai KL, et al. SARS-CoV-2 Omicron variant replication in human bronchus and lung ex vivo. Nature. 2022;603:715–20. https://doi.org/10.1038/s41586-022-04479-6
9. Suzuki R, Yamasoba D, Kimura I, Wang L, Kishimoto M, Ito J, et al.; Genotype to Phenotype Japan (G2P-Japan) Consortium. Attenuated fusogenicity and pathogenicity of SARS-CoV-2 Omicron variant. Nature. 2022;603:700–5. https://doi.org/10.1038/s41586-022-04462-1
10. UK Health Security Agency. SARS-CoV-2 variants of concern and variants under investigation in Technical briefing 36. 2022 Feb 11 [cited 2022 May 6]. https://assets.publishing.service.gov.uk/government/uploads/system/uploads/attachment_data/file/1056487/Technical-Briefing-36-22.02.22.pdf
11. Espenhain L, Funk T, Overvad M, Edslev SM, Fonager J, Ingham AC, et al. Epidemiological characterisation of the first 785 SARS-CoV-2 Omicron variant cases in Denmark, December 2021. Euro Surveill. 2021;26:2101146. https://doi.org/10.2807/1560-7917.ES.2021.26.50.2101146
12. Ritchie H, Rodés-Guirao L, Appel C, Giattino C, Ortiz-Ospina E, Hasell J, et al. Coronavirus pandemic (COVID-19). Our World in Data. 2020 [cited 2022 May 6]. https://ourworldindata.org/coronavirus
13. Haim-Boukobza S, Roquebert B, Trombert-Paolantoni S, Lecorche E, Verdurme L, Foulongne V, et al. Detecting rapid spread of SARS-CoV-2 variants, France, January 26–February 16, 2021. Emerg Infect Dis. 2021;27:1496–9. https://doi.org/10.3201/eid2705.210397
14. Alizon S, Selinger C, Sofonea MT, Haim-Boukobza S, Giannoli JM, Ninove L, et al.; SFM COVID-19 study group. Epidemiological and clinical insights from SARS-CoV-2 RT-PCR crossing threshold values, France, January to November 2020. Euro Surveill. 2022;27:2100406. https://doi.org/10.2807/1560-7917.ES.2022.27.6.2100406
15. Chevin LM. On measuring selection in experimental evolution. Biol Lett. 2011;7:210–3. https://doi.org/10.1098/rsbl.2010.0580
16. Davies NG, Abbott S, Barnard RC, Jarvis CI, Kucharski AJ, Munday JD, et al.; CMMID COVID-19 Working Group; COVID-19 Genomics UK (COG-UK) Consortium. Estimated transmissibility and impact of SARS-CoV-2 lineage B.1.1.7 in England. Science. 2021;372:eabg3055. https://doi.org/10.1126/science.abg3055
17. Volz E, Mishra S, Chand M, Barrett JC, Johnson R, Geidelberg L, et al.; COVID-19 Genomics UK (COG-UK) consortium. Assessing transmissibility of SARS-CoV-2 lineage B.1.1.7 in England. Nature. 2021;593:266–9. https://doi.org/10.1038/s41586-021-03470-x
18. Alizon S, Haim-Boukobza S, Foulongne V, Verdurme L, Trombert-Paolantoni S, Lecorche E, et al. Rapid spread of the SARS-CoV-2 Delta variant in some French regions, June 2021. Euro Surveill. 2021;26:2100573. https://doi.org/10.2807/1560-7917.ES.2021.26.28.2100573
19. Nishiura H, Linton NM, Akhmetzhanov AR. Serial interval of novel coronavirus (COVID-19) infections. Int J Infect Dis. 2020;93:284–6. https://doi.org/10.1016/j.ijid.2020.02.060
20. Hay JA, Kennedy-Shaffer L, Kanjilal S, Lennon NJ, Gabriel SB, Lipsitch M, et al. Estimating epidemiologic dynamics from cross-sectional viral load distributions. Science. 2021;373:eabh0635. https://doi.org/10.1126/science.abh0635
21. Sofonea MT, Reyné B, Elie B, Djidjou-Demasse R, Selinger C, Michalakis Y, et al. Memory is key in capturing COVID-19 epidemiological dynamics. Epidemics. 2021;35:100459. https://doi.org/10.1016/j.epidem.2021.100459
22. Sofonea MT, Alizon S. Anticipating COVID-19 intensive care unit capacity strain: a look back at epidemiological projections in France. Anaesth Crit Care Pain Med. 2021;40:100943. https://doi.org/10.1016/j.accpm.2021.100943
23. UK Health Security Agency. COVID-19 vaccine surveillance report, week 10. 2022 Mar 10 [cited 2022 May 6]. https://assets.publishing.service.gov.uk/government/uploads/system/uploads/attachment_data/file/1060787/Vaccine_surveillance_report_-_week_10.pdf
24. Hall VJ, Foulkes S, Charlett A, Atti A, Monk EJM, Simmons R, et al.; SIREN Study Group. SARS-CoV-2 infection rates of antibody-positive compared with antibody-negative health-care workers in England: a large, multicentre, prospective cohort study (SIREN). Lancet. 2021;397:1459–69. https://doi.org/10.1016/S0140-6736(21)00675-9
25. Cori A, Ferguson NM, Fraser C, Cauchemez S. A new framework and software to estimate time-varying reproduction numbers during epidemics. Am J Epidemiol. 2013;178:1505–12. https://doi.org/10.1093/aje/kwt133
26. Salje H, Tran Kiem C, Lefrancq N, Courtejoie N, Bosetti P, Paireau J, et al. Estimating the burden of SARS-CoV-2 in France. Science. 2020;369:208–11. https://doi.org/10.1126/science.abc3517
27. Blanquart F, Abad C, Ambroise J, Bernard M, Cosentino G, Giannoli JM, et al. Characterisation of vaccine breakthrough infections of SARS-CoV-2 Delta and Alpha variants and within-host viral load dynamics in the community, France, June to July 2021. Euro Surveill. 2021;26:2100824. https://doi.org/10.2807/1560-7917.ES.2021.26.37.2100824
28. Puhach O, Adea K, Hulo N, Sattonnet P, Genecand C, Iten A, et al. Infectious viral load in unvaccinated and vaccinated individuals infected with ancestral, Delta

or Omicron SARS-CoV-2. Nat Med. 2022 Apr 8 [Epub ahead of print]. https://doi.org/10.1038/s41591-022-01816-0
29. Ito K, Piantham C, Nishiura H. Relative instantaneous reproduction number of Omicron SARS-CoV-2 variant with respect to the Delta variant in Denmark. J Med Virol. 2022;94:2265–8. https://doi.org/10.1002/jmv.27560
30. Wolter N, Jassat W, Walaza S, Welch R, Moultrie H, Groome M, et al. Early assessment of the clinical severity of the SARS-CoV-2 omicron variant in South Africa: a data linkage study. Lancet. 2022;399:437–46. https://doi.org/10.1016/S0140-6736(22)00017-4
31. Michalakis Y, Sofonea MT, Alizon S, Bravo IG. SARS-CoV-2 viral RNA levels are not 'viral load'. Trends Microbiol. 2021;29:970–2. https://doi.org/10.1016/j.tim.2021.08.008
32. Mastrovito B, Naimi C, Kouam L, Naudot X, Fournier L, Spaccaferri G, et al. Investigation of outbreak cases infected with the SARS-CoV-2 B.1.640 variant in a fully vaccinated elderly population, Normandy, France, November to December 2021. Euro Surveill. 2022;27:2200078. https://doi.org/10.2807/1560-7917.ES.2022.27.6.2200078

Address for correspondence: Samuel Alizon, Center for Interdisciplinary Research in Biology, Collège de France, 11 place Marcelin Berthelot, 75005 Paris, France; email: samuel.alizon@cnrs.fr

Effect of Returning University Students on COVID-19 Infections in England, 2020

David Leeman, Joe Flannagan, Dimple Chudasama, Kyle Dack, Charlotte Anderson, Gavin Dabrera, Theresa Lamagni

Each September in England, ≈1 million students relocate to study at universities. To determine COVID-19 cases and outbreaks among university students after their return to university during the COVID pandemic in September 2020, we identified students with COVID-19 (student case-patients) by reviewing contact tracing records identifying attendance at university and residence in student accommodations identified by matching case-patients' residential addresses with national property databases. We determined COVID-19 rates in towns/cities with and without a university campus. We identified 53,430 student case-patients during September 1–December 31, 2020, which accounted for 2.7% of all cases during this period. Student case-patients increased rapidly after the start of the term, driven initially by cases and outbreaks in student accommodations. Case rates among students 18–23 years of age doubled at the start of term in towns with universities. Our findings highlight the need for face-to-face and control measures to reduce virus transmission.

COVID-19 cases in England first peaked in April 2020, after national lockdown measures were introduced on March 26, 2020; cases decreased in June 2020 and remained relatively low throughout the summer. Starting at the end of August, cases increased, especially during October and November (*1*). Because September is the beginning of the academic year in the United Kingdom, this growth coincided with the annual mass migration of university students across the country.

Approximately 2.5 million students study at higher education institutions in the United Kingdom (*2*), accounting for ≈3% of the UK population; 2 million study at universities in England. In the 2019–20 academic year, ≈1.1 million full-time students lived in accommodations other than their normal residence (their own or their parents'/guardians') (*3*). Concerns were raised over the return of university students for face-to-face learning in the 2020 autumn term. Some institutions decided to keep learning online, but overall, the government advised universities to encourage in-person return. Immediately after the start of the term, COVID-19 outbreaks associated with universities were identified and received substantial media attention. On October 12, the government stated that 9,000 COVID-19 cases had been identified among students in the previous week and that 1 university (Nottingham) accounted for 1,510 of these cases (*4*).

Several projects have been undertaken to learn more about transmission of SARS-CoV-2 within educational establishments (*5*) and infection rates among the school-age population (*6*). We used national testing and contact tracing data linked to property classifications to describe SARS-CoV-2 infections among those reporting attendance at a university and those living in student accommodations.

The UK Health Security Agency has legal permission, provided by Regulation 3 of The Health Service (Control of Patient Information) Regulations 2002, to process patient confidential information for national surveillance of communicable diseases. Thus, individual patient consent was not required.

Methods

Data Collection

We extracted cases from the second-generation surveillance system (*7*). All test-positive cases of COVID-19 are notifiable through reporting to the second-generation surveillance system, including positive results from lateral flow devices. During the study period, routine testing of asymptomatic persons was not yet available, so reported case-patients were predominately symptomatic. Mass testing for asymptomatic students was introduced at the end of November 2020, when students were asked to complete testing before returning home (*8*). Routine

Author affiliation: UK Health Security Agency, London, UK

DOI: https://doi.org/10.3201/eid2807.212332

testing for asymptomatic students was not introduced until the spring term of 2021 (*9*).

As part of routine contact tracing, to identify presymptomatic contacts and potential sources of infection, persons with positive test results were asked about their events and activities of the 7 days before symptom onset (or test date), including whether they had attended an education setting, up to the time of contact tracing. To identify all case-patients reporting attendance at a university, those with positive test results were linked to exposure data in National Health Service (NHS) Test and Trace (https://www.gov.uk/guidance/nhs-test-and-trace-how-it-works). On October 23, 2020, the standard questions changed to further differentiate between attending or working at a university.

Data Linkage and Assignment

Case-patient and contact tracing data were linked by the specimen number of the positive test. Case-patients that did not link by specimen number were linked by NHS number and date of birth.

We identified accommodation type by matching case-patients' full addresses to the reference database Ordnance Survey Address Base Premium (*10*). This database provided each address with a unique property reference number (UPRN); a basic land and property unit (BLPU) class; and where available, a parent UPRN enabling us to map case-patients against a specific residential location. Parent UPRNs exist for properties that may have multiple subproperties within (e.g., a block of flats for which the parent UPRN identifies the entire block and individual UPRNs are assigned to the individual flats).

To determine whether student case-patients affected case rates among the wider population, we compared age-specific case rates between university and nonuniversity towns throughout the autumn term by using Office for National Statistics (ONS) 2019 midyear population estimates by age (*11*). ONS midyear estimates use census data to provide official population estimates and count students at their term-time addresses (*12*). Towns and cities were identified by using the ONS major towns and cities dataset, which includes towns or cities with a resident or workday population of ≥75,000 (*13*). Cases were matched to these municipalities by the lower superoutput area associated with their postal code of residence. We matched universities to towns by using the registered address as recorded against their learning provider reference number (*14*). We manually reviewed remaining towns to check for satellite campuses or other higher education institutions (some higher education institutions are not registered providers and have their qualifications granted by another institution and therefore have no learning provider reference number). We excluded from analysis towns with only satellite campuses.

We identified towns with no university and >60 minutes travel by public transport (based on Google Maps journey planner) from the nearest university campus and matched them to a university town according to region and population density within 20%. Because we found multiple matches, with either nonuniversity towns matching to multiple university towns or vice versa, we created a loop by randomly selecting matched towns until each pair was unique with no duplicated towns.

Definitions

We defined case-patients as all persons with positive test results reported to the second-generation surveillance system with an earliest reported specimen date of September 1–December 31, 2020. Student accommodation was defined as 1 of the following: properties with a BLPU classification of higher education or university; properties with a classification of college, in which all case-patients were ≥18 years of age; properties with a classification of residential education, for which the address included any of the terms university, hall of residence, halls of residence, student accommodation; properties with a classification of residential education and for which ≥90% of case-patients were ≥18 years of age; properties classified as parent shell or property shell, for which the address included any of the terms university, student, hall of residence, halls of residence; or properties with a classification of college, other educational establishment, residential education, parent shell, or property shell, from which >5 case-patients reported attendance at university to contact tracers. Students were defined as case-patients if they either resided in student accommodation premises as defined above or reported attendance at a university to NHS Test and Trace. Outbreaks were defined as ≥2 cases at the same residence (determined by UPRN), within a recurring 14-day period. Properties could have multiple outbreaks recorded if further cases were identified >14 days past a previous outbreak. University towns were defined as any town or city in England meeting the ONS definition of major towns and cities with a higher education campus. Nonuniversity towns were defined as any town or city in England meeting the ONS definition of major towns and cities with no higher education campus and requiring >60 minutes travel from the nearest campus by public transport.

Analysis

We described case-patients according to demographics and accommodation type by collapsing BLPU classifications into 4 main groups: residential accommodation (i.e., houses or flats/apartments), student accommodations (as defined previously), registered houses of multiple occupancy (HMO), and other. We described outbreaks involving students according to size, duration of time between the first and last case, and property type. We compared these outbreaks with outbreaks involving no identified students. We compared university and nonuniversity towns by calculating and plotting rates for the total population, for the population 18–23 years of age, and the total population minus those 18–23 years of age.

Results

Classification of Student Case-Patients and Student Accommodations

During September 1–December 31, 2020, a total of 1,999,180 cases of COVID-19 were reported in England. Contact tracing with NHS Test and Trace was completed for 1,648,220 (82.4%), among which attendance at a university was reported by 39,032 (2.4%). Among all 1,999,180 case-patients, 19,901 (1%) resided in a property classified as student accommodation (1,820 UPRNs met the definition of student accommodation; Appendix Figure 1, https://wwwnc.cdc.gov/EID/article/28/7/21-2332-App1.pdf). A total of 53,430 (2.7%) case-patients met the definition of student on the basis of residence or information relayed to contact tracers; these students are hereafter referred to as student case-patients.

Most (33,529 [85.9%]) case-patients who reported university attendance to contact tracers did not live in student accommodations. This percentage decreased to 73% (4,844) of 6,632 students 18 years of age who attended university. For all case-patients living in student accommodations, the median age was 19 (interquartile range [IQR] 18–20]) years, which was slightly younger than the age of student case-patients living in other types of accommodation (median age 20 [IQR 19–22]) years. This age profile reflects the common nature of student accommodations being used by first-year students who then move on to privately rented accommodations.

Description of Student Case-Patients

The median age for student case-patients was 20 (IQR 19–22) years, 17 years younger than the median age for all case-patients. A slightly higher proportion of student case-patients than of case-patients were female (57.1% vs. 53.2%) (Table 1). Case numbers among students and the proportion of all cases they represented increased rapidly during the start of the university term from 0.7% (117/17,508) in the first week of September to 7.8% (6,709/85,929) in the first week of October. At the beginning of the term, ≈60%–70% of student case-patients resided in student accommodations, and although the number of student case-patients remained high until mid-November, the proportion in student accommodations had dropped to 20%–30%. When we considered only case-patients who reported attendance at a university, the trend differed with a smaller increase in cases at the start of the term and a lower proportion residing in student accommodations (Figure 1). The peak of infections for all student case-patients was reached quickly after the start of term in the first week of October but peaked around 2 weeks later among those specifically reporting attendance at a university.

We found a similar, but more pronounced, trend among the student-age population (18–23 years of age). Case numbers and rates increased substantially among this population from 11 cases/100,000 persons in this age range in England on September 1, 2020, to 99 cases/100,000 persons on October 1, 2020. Comparatively, the rate among the rest of the population increased from 3 to 13 cases/100,000 persons in the same period. By the end of September 2020, case-patients 18–23 years of age accounted for ≈30% of all cases in England, reaching a daily high of 44.1% (3,842/8,718) on September 29, 2020.

Accommodation Types and Residential Outbreaks

Student case-patients were geographically dispersed across England, concentrated around major urban areas (Figure 2). When counted by upper tier local authority boundary, the highest number of student case-patients was in Nottingham (n = 3,021), >1,000 more than the second highest, who were in Sheffield (n = 1,976). Other areas with >1,500 case-patients were Manchester (n = 1,912), Bristol (n= 1,710), Leeds (n = 1,681), and Birmingham (n = 1,544). Most of the 53,450 student case-patients lived either in student accommodations (19,901 [37.2%]) or private residential properties such as houses or flats (27,128 [50.8%]). A smaller proportion (3%, n = 1.617) lived in HMOs, but this proportion was 6 times larger than that of all case-patients who lived in HMOs; 16.4% (1,617/9,838) of all case-patients who resided in HMOs were identified as students. The highest proportions of student case-patients living in student accommodations were in Nottingham (76.7%, n = 2,316/3,021), Sheffield (75.6%, n = 1,494/1,976), York (73.2%, n = 517/706), Coventry (71.2%, n = 679/954), and Newcastle (70.3%, n = 937/1,333). Nottingham had the

highest number of case-patients living in student accommodations (n = 2,316).

Nearly half of all case-patients (48.3%, n = 964,902) were identified as being involved in 1 of 371,937 residential outbreaks. Just under 4% of these outbreaks included ≥1 student (3.6%, 13,572/371,937). Outbreaks that included ≥1 student had a median number of 3 (IQR 2–4) cases/outbreak, which was slightly more than that of all other outbreaks (median 2, IQR 2–3 cases) (Table 2). Outbreaks within student accommodations lasted a median of 6 (IQR 2–13) days, compared with 2 (IQR 0–5) days for all other residential settings.

The number of residential outbreaks involving students after the start of the term increased immediately. This increase was largely driven by outbreaks within student accommodations; at the start of the term; ≈70% of outbreaks were in student accommodations. The initial increase was followed by 2 larger peaks, mainly in other residential settings (Figure 3). Those 2 peaks followed the trend for all residential outbreaks during this period; the number of outbreaks decreased after the introduction of national restrictions in November.

Overall, the proportion of outbreaks involving students increased from 0.7% (18/2,440) in the first week of September 2020 to 7.3% (519/7,149) in the final week of September 2020. This proportion decreased and remained at 3%–5% until the end of December, when it returned to 1%.

Comparison between Towns

We identified 20 towns (10 with universities and 10 without) for comparing COVID-19 incidence rates during the commencement of the autumn term (Appendix Table 1, https://wwwnc.cdc.gov/EID/article/28/7/21-2332-App1.pdf). Rates in university

Table 1. Characteristics of COVID-19 case-patients, by university classification, England, September 1–December 31, 2020*

Characteristic	No. (%) students			
	Attending university, n = 39,032†	Residing in student accommodation, n = 19,901‡	Total student case-patients, n = 53,430§	Total case-patients, n = 1,999,180¶
Sex				
F	22,517 (57.7)	11,109 (55.8)	30,526 (57.1)	1,063,624 (53.2)
M	15,833 (40.6)	8,555 (43.0)	22,042 (41.3)	918,902 (46.0)
Unknown	682 (1.7)	237 (1.2)	862 (1.6)	16,654 (0.8)
Ethnicity				
Asian/Asian British	6,479 (16.6)	1,847 (9.3)	7,775 (14.6)	285,562 (14.3)
Black/Black British	2,060 (5.3)	758 (3.8)	2,566 (4.8)	78,529 (3.9)
Mixed	1,519 (3.9)	800 (4.0)	2,085 (3.9)	45,762 (2.3)
Other	991 (2.5)	329 (1.7)	1,207 (2.3)	37,166 (1.9)
Unknown	1,744 (4.5)	1,357 (6.8)	2,790 (5.2)	75,857 (3.8)
White	26,239 (67.2)	14,810 (74.4)	37,007 (69.3)	1,476,304 (73.8)
Region				
East Midlands	4,487 (11.5)	3,884 (19.5)	7,292 (13.6)	166,352 (8.3)
East of England	3,160 (8.1)	1,184 (5.9)	3,854 (7.2)	199,341 (10.0)
London	7,136 (18.3)	1,419 (7.1)	8,056 (15.1)	378,483 (18.9)
North East	1,843 (4.7)	1,808 (9.1)	3,411 (6.4)	109,891 (5.5)
North West	4,211 (10.8)	2,395 (12.0)	6,265 (11.7)	326,296 (16.3)
South East	5,694 (14.6)	1,788 (9.0)	6,794 (12.7)	261,810 (13.1)
South West	4,394 (11.3)	2,801 (14.1)	6,194 (11.6)	107,119 (5.4)
West Midlands	3,836 (9.8)	1,535 (7.7)	4,833 (9.0)	208,755 (10.4)
Yorkshire and Humber	3,806 (9.8)	3,067 (15.4)	6,251 (11.7)	224,888 (11.2)
Unknown	465 (1.2)	20 (0.1)	480 (0.9)	16,245 (0.8)
Accommodation type				
Student accommodation	5,503 (14.1)	19,901 (100)	19,901 (37.2)	19,901 (1.0)
Detached house	6,446 (16.5)		6,446 (12.1)	341,391 (17.1)
Semidetached house	7,142 (18.3)	0	7,142 (13.4)	552,024 (27.6)
Terraced house	9,347 (23.9)	0	9,347 (17.5)	589,178 (29.5)
Flat	4,193 (10.7)	0	4,193 (7.8)	246,493 (12.3)
HMO	1,617 (4.1)	0	1,617 (3.0)	9,838 (0.5)
Property shell	70 (1.8)	0	700 (1.3)	18,554 (0.9)
Other	4,08 (10.5)	0	4,084 (7.6)	221,801 (11.1)
Deaths#	15 0	14 (0.1)	28 (0.1)	53,648 (2.7)
Cases in outbreak	17,553 (45.0)	14,375 (72.2)	27,90 (52.2)	964,902 (48.3)

*HMO, houses of multiple occupancy.
†Median age 20 y.
‡Median age 19 y.
§Median age 20 y. Because data for case-patients can appear in both the attending university and student accommodation columns, the total is less than the sum of these 2 columns.
¶Median age 37 y.
#Deaths recorded within 28 d of first positive test result.

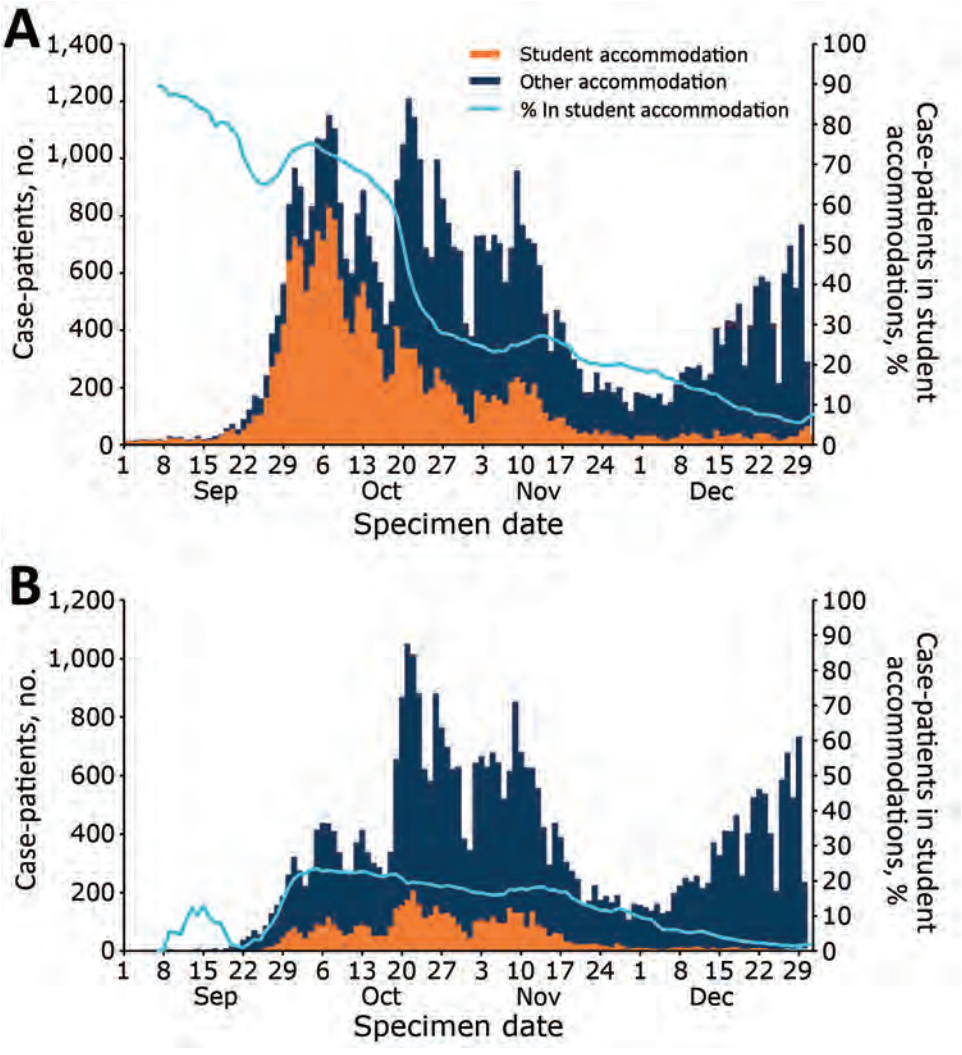

Figure 1. Student COVID-19 case-patients, by specimen date and accommodation type, England, September 1–December 31, 2020.

towns showed a clear uptick at the start of the term (week 39), and rates in nonuniversity towns increased with a more gradual slope. When split by age, this increase in rates among university towns was clearly being driven by those 18–23 years of age, for whom rates were double those seen in nonuniversity towns (Figure 4). However, as the rate increase in university towns slowed, the overall rate in nonuniversity towns caught up by week 46.

A second period of national restrictions was introduced on November 5; COVID-19 incidence rates decreased in the following weeks. The reduction was more pronounced in university towns; overall rates decreased only modestly in nonuniversity towns. The restrictions ended on December 2, after which rates in nonuniversity towns increased faster than in university towns. Furthermore, rates among persons 18–23 years of age in university towns were much closer to the overall rates, whereas in nonuniversity towns, rates remained higher. By week 51, the cumulative rate in nonuniversity towns had overtaken that of university towns; the following week, the cumulative rate in persons 18–23 years of age in nonuniversity towns also overtook that of rates for university towns (Appendix Figure 2).

Discussion

Our novel approach for classifying COVID-19 case-patients as students on the basis of address classifications and contact tracing data showed a large increase in student case-patients immediately after the start of term. The increase was initially driven by students residing in student accommodations, followed by students living in other types of accommodations. Although case-patients in student accommodations initially peaked at the start of term, followed by some peaking at much lower levels, student case-patients in other types of accommodations peaked at high levels multiple times during the term. We hypothesize that this difference

Table 2. Characteristics of residence types involved with COVID-19 outbreaks, England, September 1–December 31, 2020*

Property type	No. clusters	Clusters including a student, no.	Clusters including a student, %	Outbreaks containing students			
				Median cluster size, no. cases	Cluster size range (IQR)	Med cluster duration d	Cluster duration range (IQR)
Detached	74,580	2,189	2.9	3	2–12 (2–4)	3	0–25 (1–5)
Semidetached	116,554	3,008	2.6	3	2–14 (2–4)	3	0–31 (1–6)
Terraced	119,327	3,967	3.3	3	2–9 (2–4)	3	0–25 (1–5)
Flat	40,509	1,440	3.6	2	2–15 (2–3)	2	0–31 (0–5)
HMO	1,402	423	30.2	2	2–20 (2–3)	2	0–26 (0–5)
Property shell, not defined	2,683	207	7.7	2	2–28 (2–3)	3	0–37 (1–7)
Student accommodation	1,917	1,917	100	3	2–229 (2–5)	6	0–75 (2–13)
Other	14,965	421	2.8	3	2–114 (2–4)	3	0–58 (1–7)
Total	371937	13,572	3.6	3	2–229 (2–4)	3	0–75 (1–6)

*HMO, houses of multiple occupancy; IQR, interquartile range.

most likely resulted from the combination of stricter enforcement of control measures in university accommodations, where student self-isolation was enforced by campus security (*15*), and the smaller proportion of students living in student accommodations (*16*) resulting in fewer susceptible students after the initial peak.

Increased rates of COVID-19 cases spilled over into the broader student-age population; rates among persons 18–23 years of age in university towns were double that in nonuniversity towns. Rates were substantially affected by the start of national restrictions, after which rates were consistently higher in nonuniversity towns than in university towns. The combination of enforced control measures in student accommodations and national restrictions seems to have had a greater effect

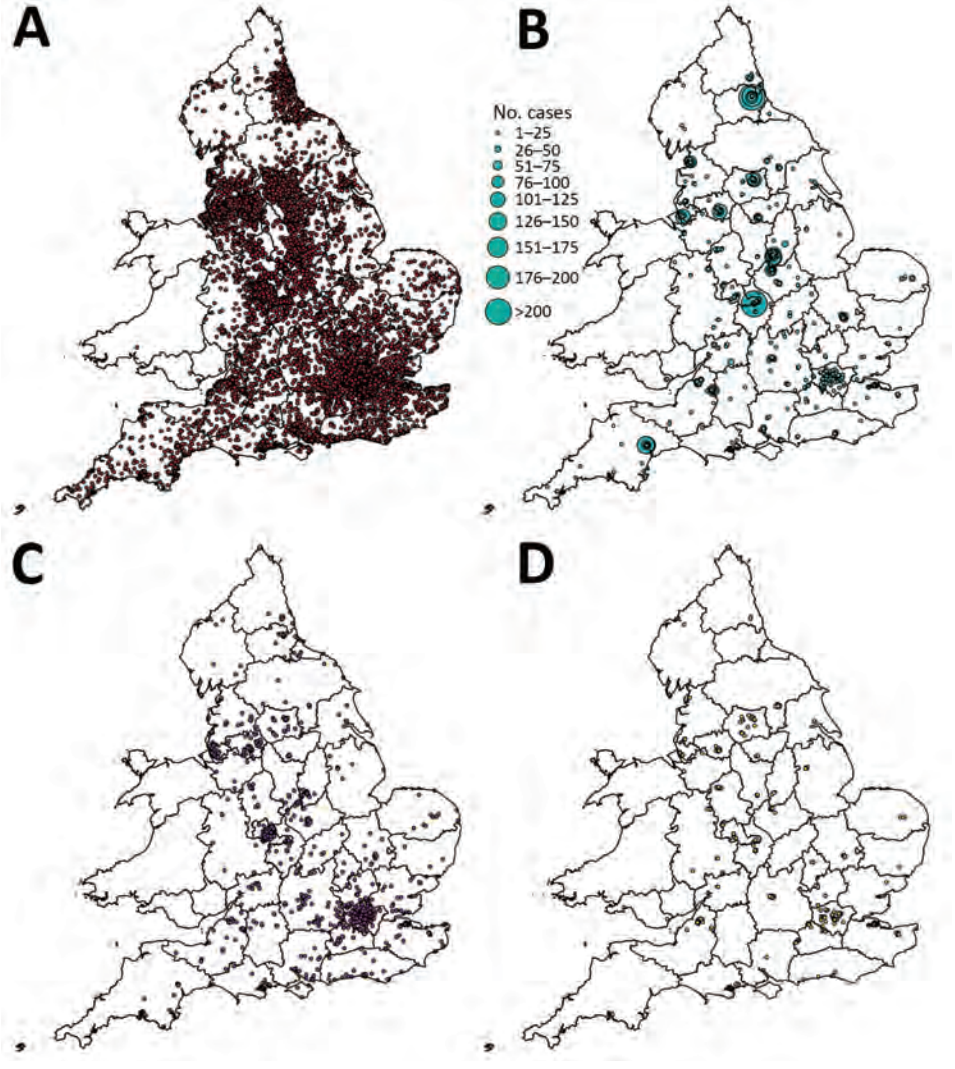

Figure 2. COVID-19 student case-patients, by location and property type, England, September 1–December 31, 2020. A) Private residences; B) student accommodations, showing rates of student cases; C) other accommodation type; D) houses of multiple occupancy.

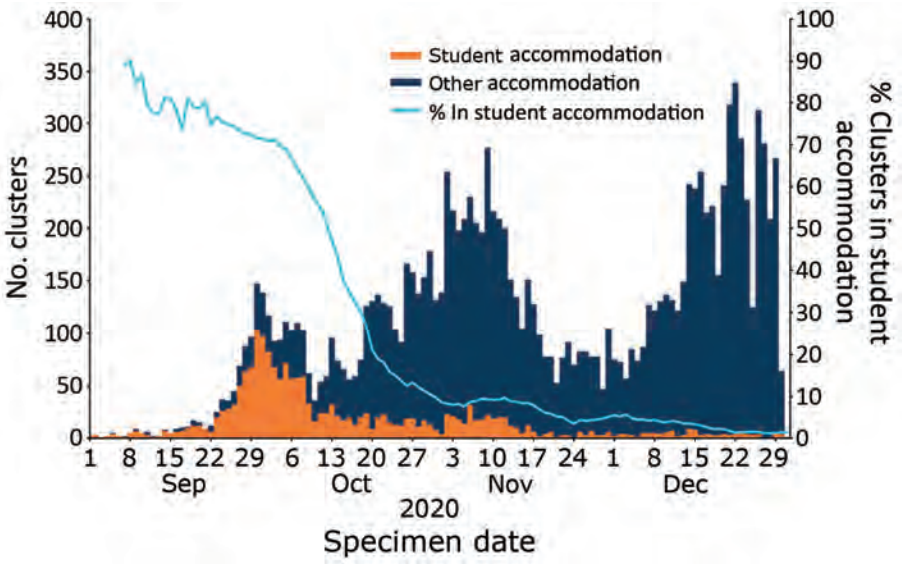

Figure 3. COVID-19 residential clusters involving ≥1 student, by specimen date of first case and accommodation type, England, September 1–December 31, 2020.

in university towns, but without those measures, high rates of transmission among the student-age population would probably have been sustained.

Other studies have similarly shown high case numbers and outbreaks among students and within student accommodations in the United Kingdom (*5*,*17*) and the United States (*18*,*19*), particularly when students return to campus and student accommodations. Less is known about the effect on the wider community around a campus (*20*; C.R.K. Arnold et al., unpub. data, https://www.medrxiv.org/content/10.1101/2021.02.17.21251942v5). Our study shows a deviation of rates at the start of term between university and nonuniversity towns. The effect on wider communities was limited, but rates among persons 18–23 years of age increased 2-fold more in towns with a university campus than in towns without. However, a recent study that used genomic data on university and nonuniversity cases associated with Cambridge University in Cambridge, UK, found limited evidence of transmission across the student and local populations (*21*).

Although routinely monitored severe outcomes, including hospitalizations and deaths, are less common among young adults, COVID-19 infections have substantial direct and indirect effects on young adults. Hospitalizations and deaths do occur among persons in this age group (*22*), and young adults who are hospitalized experience a range of adverse outcomes (*23*). COVID-19 has significantly negatively affected the mental health of young persons, particularly in relation to lockdowns and long periods of self-isolation (*24*). The common use of online teaching added to feelings

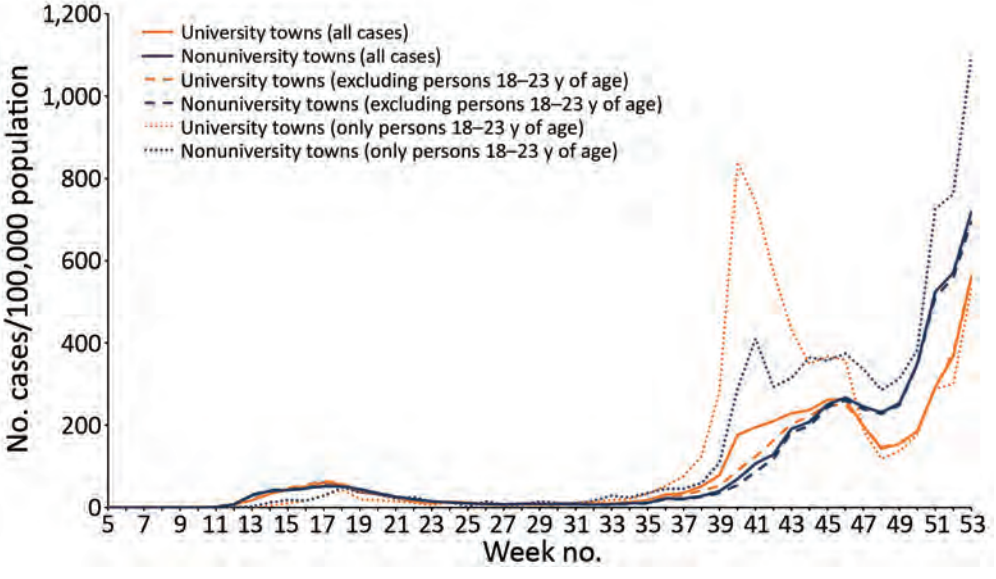

Figure 4. COVID-19 rates (cases/100,000 population) in selected university and nonuniversity towns, England, 2020.

of isolation and loneliness; >50% of students reported dissatisfaction with their social experiences during the autumn term (*5*). The full effect on student achievements and well-being as a result of these disruptions is unlikely to be fully appreciated for some time.

Information about transmission among this population remains limited, but the concentration of cases initially in student accommodations and the shared living arrangements reflect known transmission dynamics of SARS-CoV-2; household transmission is a significant source of infection (*25*). Less well known is the role of face-to-face teaching and in-person lectures with regard to virus transmission between households. The beginning of a term in UK universities is known as fresher's week, when new students arrive in university towns a week before the start of teaching to meet other students and participate in a variety of organized and spontaneous social activities. This mixing of a large, susceptible population from across the country in crowded, enclosed spaces is likely to result in increased cases and poses the potential for more large outbreaks and disruption to teaching across higher-education providers. The 2021–22 academic year differed from the previous academic year in terms of testing and the introduction of COVID-19 vaccinations. By the start of the 2021–22 term, <50% of persons 18–24 years of age had received both vaccine doses (*26*), and case levels remained high throughout the summer and autumn across the entire population, particularly among children and young adults. However, the removal of restrictions and the emergence of the Omicron variant have made ascertaining the effects of student migration on transmission even more challenging.

Ordnance Survey data (https://www.ordnancesurvey.co.uk) to enrich COVID-19 data in England have been used to monitor cases and outbreaks in households (*27*) and within specific properties, including care homes and prisons. Although bespoke student accommodation is a regular feature of universities within England, these premises are not uniformly categorized or recorded; thus, we created a method for categorizing them. Specificity of the definitions used will have led to underestimation of case-patients residing in student accommodations.

By combining data from NHS Test and Trace, we were able to identify a sizable proportion of case-patients that we can confidently define as students. However, an unknown proportion of student case-patients either did not engage with contact tracers or did engage but had not physically attended their campus in the prior 7 days and thus not have been identified as student case-patients. Although using both data sources instead of either source independently enabled us to classify more student case-patients, using both sources favors detection of student case-patients in student accommodations because they can be identified by either method, whereas case-patients in other residential settings can be identified only by contact tracing data. As a result, we have probably overestimated the proportion of case-patients residing in student accommodations; however, because 33,529 student case-patients were identified in other types of accommodation, the effect of overestimation here is probably small.

The comparison between university and nonuniversity towns is limited by the potential for systematic differences between towns that have a university and those that do not. Socioeconomic deprivation and other demographics that affect COVID-19 rates (*28*) have not been accounted for when comparing these towns because of the limited number of nonuniversity towns in England. Therefore, despite a clear difference, we cannot state how much of the observed difference in rates results from the presence or absence of a university within these towns.

Our findings suggest that the annual mass migration of students and housing of large numbers in student accommodations is linked to large increases in SARS-CoV-2 transmission among this population, potentially contributing to large increases in cases in the wider population surrounding a campus. The desire for face-to-face teaching requires this migration because of the preponderance of students in England who study away from home. We therefore recommend further assessment of policy decisions advocating universities' return to face-to-face teaching to ensure that the risks associated with a large increase in case numbers and outbreaks in this population are balanced against the risks associated with remote and online teaching.

Acknowledgments

This work uses data-enrichment processes developed by the COVID-19 Epidemiology Cell and Geographic Information Systems (GIS) team in The UK Health Security Agency. We thank the GIS team for facilitating residential property classification of cases. Data supplied by NHS Test and Trace enabled identification of student case-patients and was possible thanks to the work of contact tracers and health protection teams.

About the Author

Mr. Leeman is a fellow in the UK field epidemiology training program and a specialist registrar in public health, working in the UK Health Security Agency. His research interests include infectious disease epidemiology and outbreak investigations.

References

1. UK Government. Coronavirus (COVID-19) in the UK [cited 2021 Jan 18]. https://coronavirus.data.gov.uk
2. Universities UK. Higher education in numbers [cited 2021 Jan 18]. https://www.universitiesuk.ac.uk/what-we-do/policy-and-research/publications/higher-education-facts-and-figures-2021
3. Higher Education Statistics Agency. Where do HE students study? [cited 2021 Sept 14]. https://www.hesa.ac.uk/data-and-analysis/students/where-study
4. Times Higher Education. COVID-19: UK confirms 9,000 student cases in past week [cited 2021 Jan 18]. https://www.timeshighereducation.com/news/covid-19-uk-confirms-9000-student-cases-past-week
5. Office for National Statistics. How has coronavirus (COVID-19) spread among students in England? [cited 2021 Jan 19]. https://www.ons.gov.uk/peoplepopulationandcommunity/educationandchildcare/articles/howhascoronaviruscovid19spreadamongstudentsinengland/2020-12-21
6. Mensah AA, Sinnathamby M, Zaidi A, Coughlan L, Simmons R, Ismail SA, et al. SARS-CoV-2 infections in children following the full re-opening of schools and the impact of national lockdown: prospective, national observational cohort surveillance, July–December 2020, England. J Infect. 2021;82:67–74. https://doi.org/10.1016/j.jinf.2021.02.022
7. Clare T, Twohig KA, O'Connell A-M, Dabrera G. Timeliness and completeness of laboratory-based surveillance of COVID-19 cases in England. Public Health. 2021;194:163–6. https://doi.org/10.1016/j.puhe.2021.03.012
8. HM Government. COVID-19 winter plan [cited 2021 Oct 3]. https://assets.publishing.service.gov.uk/government/uploads/system/uploads/attachment_data/file/937529/COVID-19_Winter_Plan.pdf
9. Gov.uk. All students offered testing on return to university [cited 2021 Oct 3]. https://www.gov.uk/government/news/all-students-offered-testing-on-return-to-university
10. Chudasama DY, Milbourn H, Nsonwu O, Senyah F, Florence I, Cook B, et al. Penetration and impact of COVID-19 in long term care facilities in England: population surveillance study. Int J Epidemiol. 2021;Sep 1:dyab176.
11 Office for National Statistics. Lower layer Super Output Area population estimates (supporting information) [cited 2021 May 29]. https://www.ons.gov.uk/peoplepopulationandcommunity/populationandmigration/populationestimates/datasets/lowersuperoutputareamidyearpopulationestimates
12. Office for National Statistics. Mid-year population estimates quality and methodology information [cited 2022 Mar 31]. https://www.ons.gov.uk/peoplepopulationandcommunity/populationandmigration/populationestimates/methodologies/midyearpopulationestimatesqmi
13. Office for National Statistics. Lower layer Super Output Area (2011) to major towns and cities (December 2015) lookup for England and Wales [cited 2021 Jun 29]. https://geoportal.statistics.gov.uk/datasets/dc0b24da0880417abc979c705bce3fde_0/explore
14. Data.ac.uk. UK learning providers [cited 2021 Jun 29]. http://learning-provider.data.ac.uk
15. COVID outbreak: Manchester Metropolitan University students in lockdown. BBC News [cited 2022 Mar 23]. https://www.bbc.co.uk/news/uk-england-manchester-54289648
16. Office for Students. Coronavirus briefing note: student accommodation [cited 2022 Mar 23]. https://www.officeforstudents.org.uk/publications/coronavirus-briefing-note-student-accommodation
17. Vusirikala A, Whitaker H, Jones S, Tessier E, Borrow R, Linley E, et al. Seroprevalence of SARS-CoV-2 antibodies in university students: cross-sectional study, December 2020, England. J Infect. 2021;83:104–11. https://doi.org/10.1016/j.jinf.2021.04.028
18. Doyle K, Teran RA, Reefhuis J, Kerins JL, Qiu X, Green SJ, et al. Multiple variants of SARS-CoV-2 in a university outbreak after spring break—Chicago, Illinois, March–May 2021. MMWR Morb Mortal Wkly Rep. 2021;70:1195–200. https://doi.org/10.15585/mmwr.mm7035a3
19. Wilson E, Donovan CV, Campbell M, Chai T, Pittman K, Seña AC, et al. Multiple COVID-19 clusters on a university campus—North Carolina, August 2020. MMWR Morb Mortal Wkly Rep. 2020;69:1416–8. https://doi.org/10.15585/mmwr.mm6939e3
20. Cipriano LE, Haddara WMR, Zaric GS, Enns EA. Impact of university re-opening on total community COVID-19 burden. PLoS One. 2021;16:e0255782. https://doi.org/10.1371/journal.pone.0255782
21. Aggarwal D, Warne B, Jahun AS, Hamilton WL, Fieldman T, du Plessis L, et al.; Cambridge Covid-19 Testing Centre; University of Cambridge Asymptomatic COVID-19 Screening Programme Consortium; COVID-19 Genomics UK (COG-UK) Consortium. Genomic epidemiology of SARS-CoV-2 in a UK university identifies dynamics of transmission. Nat Commun. 2022;13:751. https://doi.org/10.1038/s41467-021-27942-w
22. Office for National Statistics. Coronavirus (COVID-19) latest insights: deaths [cited 2021 Oct 3]. https://www.ons.gov.uk/peoplepopulationandcommunity/healthandsocialcare/conditionsanddiseases/articles/coronaviruscovid19latestinsights/deaths#deaths-by-age
23. Cunningham JW, Vaduganathan M, Claggett BL, Jering KS, Bhatt AS, Rosenthal N, et al. Clinical outcomes in young US adults hospitalized with COVID-19. JAMA Intern Med. 2020;181:379–81. https://doi.org/10.1001/jamainternmed.2020.5313
24. The Health Foundation. Generation COVID-19 [cited 2021 Oct 3]. https://www.health.org.uk/publications/long-reads/generation-covid-19
25. Madewell ZJ, Yang Y, Longini IM Jr, Halloran ME, Dean NE. Household transmission of SARS-CoV-2 a systematic review and meta-analysis. JAMA Netw Open. 2020;3:e2031756. https://doi.org/10.1001/jamanetworkopen.2020.31756
26. Public Health England. COVID-19 vaccine surveillance report week 36 [cited 2021 Sep 14]. https://assets.publishing.service.gov.uk/government/uploads/system/uploads/attachment_data/file/1016465/Vaccine_surveillance_report_-_week_36.pdf
27. Chudasama DY, Flannagan J, Collin SM, Charlett A, Twohig KA, Lamagni T, et al. Household clustering of SARS-CoV-2 variant of concern B.1.1.7 (VOC-202012-01) in England. J Infect. 2021;83:e26–8. https://doi.org/10.1016/j.jinf.2021.04.029
28. Public Health England. Disparities in the risk and outcomes of COVID-19 [cited 2021 Oct 4]. https://assets.publishing.service.gov.uk/government/uploads/system/uploads/attachment_data/file/908434/Disparities_in_the_risk_and_outcomes_of_COVID_August_2020_update.pdf

Address for correspondence: David Leeman, COVID-19 Epidemiology Cell, UK Health Security Agency, 61 Colindale Ave, London, NW9 5EQ, UK; email: david.leeman@phe.gov.uk

Self-Reported and Physiologic Reactions to Third BNT162b2 mRNA COVID-19 (Booster) Vaccine Dose

Merav Mofaz, Matan Yechezkel, Grace Guan, Margaret L. Brandeau, Tal Patalon, Sivan Gazit, Dan Yamin,[1] Erez Shmueli[1]

Despite extensive technological advances in recent years, objective and continuous assessment of physiologic measures after vaccination is rarely performed. We conducted a prospective observational study to evaluate short-term self-reported and physiologic reactions to the booster BNT162b2 mRNA (Pfizer-BioNTech, https://www.pfizer.com) vaccine dose. A total of 1,609 participants were equipped with smartwatches and completed daily questionnaires through a dedicated mobile application. The extent of systemic reactions reported after the booster dose was similar to that of the second dose and considerably greater than that of the first dose. Analyses of objective heart rate and heart rate variability measures recorded by smartwatches further supported this finding. Subjective and objective reactions after the booster dose were more apparent in younger participants and in participants who did not have underlying medical conditions. Our findings further support the safety of the booster dose from subjective and objective perspectives and underscore the need for integrating wearables in clinical trials.

The severe acute respiratory syndrome coronavirus 2 Delta variant (also termed variant B.1.617.2) was discovered in October 2020 in India and was designated as a variant of concern by the World Health Organization in May 2021 (*1*–*3*). Since its discovery, it has spread worldwide and has rapidly become the most dominant variant in many countries (*4*–*7*). Although the BNT162b2 COVID-19 vaccine (Pfizer-BioNTech, https://www.pfizer.com) is highly effective against the Alpha variant (*8*), recent studies show that the effectiveness of the Pfizer-BioNTech vaccines is notably lower against the Delta variant: 88% compared with 93.7% against the Alpha variant (*9*–*12*). Moreover, recent evidence shows that fully vaccinated persons infected with the virus can easily transmit it because their peak viral burden is similar to that observed for unvaccinated persons (*7*,*10*). In Israel, the Delta variant has accelerated coronavirus disease (COVID-19) infection and hospitalization; numbers doubled every 10 days during July 1–August 9, 2021 (*7*,*13*), despite the high coverage of the BNT162b2 vaccine in Israel during this period, which was >75% coverage with 2 Pfizer doses in the eligible population (persons ≥12 years of age) (*13*).

The rapid increase in hospitalizations associated with the Delta-driven COVID-19 resurgence and the imminent risk for hospital overcrowding led the Israeli government to initialize on July 30, 2021, an unparalleled, proactive, national third (booster) vaccine shot campaign, offering the BNT162b2 mRNA COVID-19 vaccine to persons >60 years of age. On August 13, 2021, the booster campaign was expanded to include persons >50 years of age and reached 63% third-dose coverage among the eligible population within only 26 days (*7*,*14*–*16*). Two weeks later, on August 29, 2021, the campaign was expanded to include all persons ≥16 years of age, requiring only that 5 months had passed since the receipt of the second dose. This effort reached 40% third-dose coverage among the eligible population <50 years of age within 16 days (*13*,*17*).

Limited information is available on the safety of a BNT162b2 third dose (*18*,*19*). Such a booster vaccine has yet to be authorized by the US Food and Drug Administration (FDA) for the general population (*20*). Although recent evidence shows that a third BNT162b2 dose for immunocompromised persons

Author affiliations: Tel Aviv University, Tel Aviv, Israel (M. Mofaz, M. Yechezkel, D. Yamin, E. Shmueli); Stanford University, Stanford, California, USA (G. Guan, M.L. Brandeau); Maccabi Healthcare Services, Tel Aviv (T. Patalon, S. Gazit); Massachusetts nstitute of Technology Media Laboratory, Cambridge Massachusetts, USA (E. Shmueli)

DOI: https://doi.org/10.3201/eid2807.212330

[1]These authors contributed equally to this article.

has a favorable safety profile (*19*,*21*), the safety of a third (booster) dose in the general population has not yet been fully established.

Clinical trial guidelines for assessing the safety of vaccines, including the FDA criteria (*22*), are primarily based on subjective, self-reported questionnaires. Despite the extensive advances in recent years, objective, continuous assessment of physiologic measures postvaccination is rarely performed. Two recent pioneering studies demonstrated the use of wearable devices to monitor short-term physiologic changes after the first and second doses of the BNT162b2 mRNA vaccine. The first study (*23*) used a chest-patch sensor to monitor changes in 13 different cardiovascular and hemodynamic vitals in a cohort of 160 persons up to 3 days postvaccination. The second study (*24*) used a consumer-grade smartwatch to evaluate changes in heart rate variability (HRV), resting heart rate, and respiration rate in a cohort of 19 persons. Both studies found major changes in several physiologic measures in the first days after vaccination.

We evaluated the short-term effects of a third BNT162b2 mRNA COVID-19 vaccine dose on self-reported and physiologic indicators on a relatively large sample. Specifically, we tested 2,912 participants; of these persons, 1,609 participants received ≥1 doses of the BNT162b2 vaccine after entering the study. Participants were equipped with Garmin (https://www.garmin.com) Vivosmart 4 smart fitness trackers and completed daily questionnaires by using a dedicated mobile application for 37 days, starting 7 days before vaccination. The mobile application collected daily self-reported questionnaires on local and systemic reactions, as well as various well-being indicators. The smartwatch continuously monitored several physiologic measures, including heart rate, HRV, and blood oxygen saturation level (SpO_2). Our analysis of comprehensive data for each participant examined the safety of a third (booster) vaccine dose from a subjective perspective (self-reported questionnaire) and an objective perspective (smartwatch data).

Materials and Methods

Study Design and Participants

The 2,912 participants (≥18 years of age) in our study were recruited during November 1, 2020–September 15, 2021. The 1,609 participants who reported receipt of ≥1 of the 3 BNT162b2 mRNA COVID-19 vaccine shots after joining the study served as the base dataset for our analysis. All participants received the BNT162b2 mRNA vaccine. Specifically, of the 1,609 participants, during the study, 223 received their first dose, 351 their second dose, and 1,344 their third dose. Among these participants, 111 received both the second and third doses, 85 received both the first and third doses, and 80 received all 3 doses.

We used a professional survey company to recruit participants and ensure they followed through with the study requirements. Participant recruitment was performed by using advertisements on social media and word-of-mouth. Each participant provided informed consent by signing a form after receiving a comprehensive explanation on the study. Participants then completed a 1-time enrollment questionnaire, were equipped with Garmin Vivosmart 4 smartwatches, and installed 2 applications on their mobile phones: the PerMed application (*25*), which collected daily self-reported questionnaires, and an application that passively recorded the smartwatch data. Participants were asked to wear their smartwatches as much as possible. The survey company ensured that participants' questionnaires were completed daily, that their smartwatches were charged and properly worn, and that any technical problems with the mobile applications or smartwatch were resolved. Participants were monitored through the mobile application and smartwatches for 37 days, starting 7 days before vaccination.

We implemented several preventive measures to minimize attrition and churn (attrition rate) of participants and consequently improve the quality, continuity, and reliability of the collected data. First, each day, if by 7:00 PM participants had not yet completed the daily questionnaire, they received a reminder notification through the PerMed application. During the peak periods of COVID-19 vaccination in Israel, we increased the frequency of the reminders and adjusted their content. Second, we developed a dedicated dashboard that enabled the survey company to identify participants who continually neglected to complete the daily questionnaires or did not wear their smartwatch for a long period of time; these participants were contacted by the survey company (either by text messages or telephone calls) and were encouraged to better adhere to the study protocol. Third, to strengthen participants' engagement, a weekly personalized summary report was generated for each participant and was available inside the PerMed application. Similarly, we sent a monthly newsletter that contained recent findings from the study and useful tips regarding the smartwatch's capabilities to the participants.

PerMed Mobile Application

Participants used the PerMed mobile application (*25*) to fill out daily questionnaires. The questionnaire enabled participants to report various well-being indicators, including mood level (on a scale of 1 [awful] to 5 [excellent]), stress level (on a scale of 1 [very low] to 5 [very high]), sport activity duration (in minutes), and sleep quality (on a scale of 1 [awful] to 5 [excellent]). The questionnaire also collected data on clinical symptoms consistent with the local and systemic reactions observed in the BNT162b2 mRNA COVID-19 clinical trial (*26*), with an option to add other symptoms as free text (Appendix, https://wwwnc.cdc.gov/EID/article/28/7/21-2330-App1.pdf).

Smartwatch

Participants were equipped with Garmin Vivosmart 4 smart fitness trackers. Among other features, the smartwatch provides all-day heart rate and HRV and overnight SpO_2 tracking capabilities (*27*).

The optical wrist heart rate monitor of the smartwatch is designed to continuously monitor heart rate. The frequency at which heart rate is measured varies and might depend on the level of activity of the user: when the user starts an activity, the optical heart rate monitor's measurement frequency increases.

Because HRV is not easily accessible through Garmin's application programming interface, we use Garmin's stress level instead, which is calculated on the basis of HRV. Specifically, the device uses heart rate data to determine the interval between each heartbeat. The variable length of time between each heartbeat is regulated by the body's autonomic nervous system. Less variability between beats correlates with higher stress levels, whereas an increase in variability indicates less stress (*28*). A similar relationship between HRV and stress was also seen by Kim et al. (*29*) and Pereira et al. (*30*).

The pulse oximetry monitor of the smartwatch uses a combination of red and infrared lights with sensors on the back of the device to estimate the percentage of oxygenated blood (peripheral SpO_2%). This monitor is activated each day at a fixed time for 4 hours (the default is 2:00–6:00 AM). When we examined data collected in our study, we identified a heart rate sample approximately every 15 seconds, an HRV sample every 180 seconds, and an SpO_2 sample every 60 seconds.

Although the Garmin smartwatch provides state-of-the-art wrist monitoring, it is not a medical-grade device. Some readings might be inaccurate under certain circumstances, depending on factors such as the fit of the device and the type and intensity of the activity undertaken by a participant (*31*–*33*).

Statistical Analysis

We preprocessed questionnaire data by manually categorizing any self-reported symptom entered as free text. In addition, if participants completed the questionnaire >1 time in 1 day, we used the last entry from that day for the analysis. We preprocessed smartwatch data as follows. We computed the mean value of each hour of data. We then performed linear interpolation to impute missing hourly means and smoothed the data by calculating the 5-hour moving average.

For each participant, we defined the 7-day period before vaccination as the baseline period. We noted any clinical symptoms from the last questionnaire completed during the baseline period. Next, we calculated the percentage of participants who reported new systemic reactions in the 48 hours after vaccination. For each reaction, we used a β distribution to determine a 90% CI. To determine the statistical significance of differences between the first and third doses and between the second and third doses as reflected by the extent of reported reactions, we used a test for comparing proportions of 2 partially overlapping samples with unequal variance (*34*).

We also calculated the mean difference in well-being indicators between the postvaccination and baseline periods. Specifically, for each indicator, for each of the 3 days postvaccination and for each participant, we calculated the difference between that indicator's value and its corresponding value in the baseline period. We then calculated the mean value over all participants and the associated 90% CI.

To compare the changes in smartwatch physiologic indicators over the 7 days (168 hours) postvaccination with those of the baseline period, we performed the following steps. First, for each participant and each hour during the 7 days postvaccination, we calculated the difference between that hour's indicator value and that of the corresponding hour in the baseline period (keeping the same day of the week and same hour during the day). Then, we aggregated each hour's differences over all participants to calculate a mean difference and associated 90% CI, which is analogous to a 1-sided t-test a with significance level of 0.05. To determine the statistical significance of differences between the first and third doses and between the second and third doses as reflected by changes in smartwatch indicators during the 48 hours postvaccination, we used a test for comparing means of 2 partially overlapping samples with unequal variance (*35*).

We repeated our analyses for the third dose stratified by age groups (<50, 50–64, and ≥65 of age), sex, and underlying medical condition (present

versus not present) from a specified list (Table). To determine the statistical significance of differences between the groups in these analyses, we used a t-test for comparing the means of 2 independent samples with unequal variance.

Ethics Approval

Before participating in the study, all persons were advised, both orally and in writing, as to the nature of the study and provided written informed consent. The study was approved by the Maccabi Health Services Helsinki Institutional Review Board (protocol no. 0122–20-MHS).

Results

Of the 1,609 participants who received ≥1 dose of the BNT162b2 vaccine after joining the study, 854 (53.08%) were women and 755 (46.92%) men. Their ages were 18–88 years; median age was 52 years (Table). A total of 1,258 (78.19%) participants had a body mass index <30 kg/m^2, and 412 (25.61%) had ≥1 specific underlying medical condition (Table). The distributions of age and sex and underlying medical conditions were relatively invariable across the recipients of the first, second, and third doses (Table).

Our examination of self-reported reactions showed that the extent of systemic reactions reported after the third vaccine dose was similar to those reported after the second dose (p = 0.76) and considerably greater than those observed after the first dose (p<0.001) (Figure 1). Specifically, 60.4% (90% CI 57.9%–62.9%) of the participants did not report any new symptoms after receiving the third dose compared with 86.5% (90% CI 81.9%–91.0%) after the first dose and 63.6% (90% CI 59.1%–67.8%) after the second dose. Moreover, the most frequently reported types of reactions (fatigue, headache, muscle pain, fever, and chills) were similar after the second and third doses. These reactions decreased in nearly all participants within 3 days (Appendix Figure 8). These trends are consistent with those reported for the first and second dose BNT162b2 mRNA vaccine clinical trial (*26*).

For the self-reported well-being indicators (Figure 2), we found that during the first 2 days after the third vaccine dose, participants showed a major reduction in mood level (Figure 2, panel A), sport duration (Figure 2, panel C), and sleep quality (Figure 2, panel D) and a large increase in stress level (Figure 2, panel B) compared with baseline levels. These changes decreased on the third day postvaccination. A similar trend was observed after the second vaccine dose, except for the reported stress level, which remained below the baseline level during the second and third days postvaccination.

We observed similar trends when analyzing objective and continuous physiologic measurements collected by the smartwatch (Figure 3, https://wwwnc.cdc.gov/EID/article/28/7/21-2330-F3.htm; Appendix Figure 1). Specifically, we identified a considerable

Table. Characteristics of participants in study of self-reported and physiologic reactions to third BNT162b2 mRNA coronavirus disease (booster) vaccine dose*

Characteristic	All participants, n = 1,609	First dose, n = 223	Second dose, n = 351	Third dose, n = 1,344
Sex				
M	755 (46.92)	101 (45.29)	160 (45.58)	639 (47.54)
F	854 (53.08)	122 (54.71)	191 (54.42)	705 (52.46)
Age group, y				
18–29	226 (14.23)	14 (6.28)	39 (11.11)	189 (14.06)
30–39	272 (16.90)	11 (4.93)	53 (15.10)	219 (16.29)
40–49	177 (11.00)	15 (6.73)	42 (11.97)	138 (10.27)
50–59	420 (26.10)	64 (28.70)	87 (24.79)	375 (27.90)
60–69	358 (22.25)	70 (31.39)	75 (21.37)	308 (22.92)
≥70	153 (9.51)	49 (21.97)	55 (15.67)	8.56 (115)
Body mass index, kg/m^2				
<30.0	1,258 (78.19)	175 (78.48)	280 (79.77)	77.68 (1,044)
≥30.0	330 (20.51)	41 (18.39)	60 (17.09)	288 (21.43)
Unspecified	21 (1.31)	7 (3.14)	11 (3.13)	12 (0.89)
Underlying medical condition				
Hypertension	228 (14.17)	20.63 (46)	15.95 (56)	14.43 (194)
Diabetes	139 (8.64)	13.00 (29)	7.98 (28)	8.41 (113)
Heart disease	77 (4.79)	7.17 (16)	4.56 (16)	4.99 (67)
Chronic lung disease	81 (5.03)	4.93 (11)	3.70 (13)	5.21 (70)
Immune suppression	13 (0.81)	1.35 (3)	0.85 (3)	0.89 (12)
Cancer	10 (0.62)	0.45 (1)	0.57 (2)	0.67 (9)
Renal failure	8 (0.50)	1.79 (4)	1.42 (5)	0.45 (6)
None of the above	1,180 (73.34)	64.57 (144)	72.08 (253)	73.21 (984)
Unspecified	17 (1.06)	1.35 (3)	2.85 (10)	0.52 (7)

*Values are no. (%). BNT162b2 vaccine, Pfizer-BioNTech (https://www.pfizer.com).

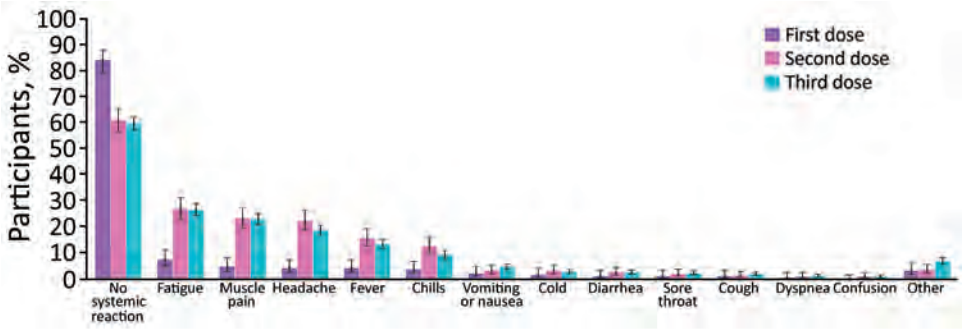

Figure 1. Reactions reported by participants through a mobile application for self-reported and physiologic reactions to BNT162b2 (Pfizer, https://www.pfizer.com) mRNA coronavirus disease vaccine doses. Error bars indicate 90% CIs.

increase in heart rate (Figure 3, panels A–C) and the HRV-based stress indicators (Figure 3, panels D–F) during the first 48 hours after administration of the third dose. Measurements returned to baseline levels within 72 hours. In contrast, our analysis of SpO_2 suggests no apparent changes after vaccination compared with baseline levels (Figure 3, panels G–I), a result that is consistent with the results of Gepner et al. (*23*). The trends observed for the objective heart rate and HRV indicators were consistent with those of the subjective indicators: similar changes after the second and third doses (heart rate p = 0.86, HRV p = 0.54), and greater changes after the third dose than the first dose (heart rate p = 0.004, HRV p<0.001).

We also stratified our analyses of well-being and smartwatch physiologic indicators after the third vaccination by age group, sex, and a previous underlying medical condition (Figure 4; Appendix Figures 2–7). For all stratifications, trends were similar to those observed in the general population. We found considerable changes in the 2 days after vaccine administration that decreased almost entirely after 3 days. We also found that participants ≥65 years of age reported fewer reactions (p<0.001) than did participants 50–65 years of age, who in turn reported even fewer reactions (p = 0.007) than did participants <50 years of age (Figure 4, panel A). In terms of the objective physiologic measures, participants ≥65 years of age showed milder changes in HRV than did participants 50–65 years of age (p = 0.075) and milder changes in heart rate (p = 0.02) than did participants <50 years of age (Figure 4, panel B).

Male participants reported fewer reactions (p<0.001) but did not show milder physiologic changes (heart rate p = 0.37, HRV p = 0.59) than female participants. Participants who had an underlying medical condition reported fewer reactions (p<0.001) and showed milder physiologic changes (heart rate p = 0.042, HRV p = 0.16), compared with participants who did not have an underlying medical condition. Of 9 participants who reported dyspnea, 4 (0.96% of their age group) were <50 years of age, 4 (0.93% of their age group) were 50–64 years of age, and 1 (0.65% of her age group) was ≥65 years of age. One participant

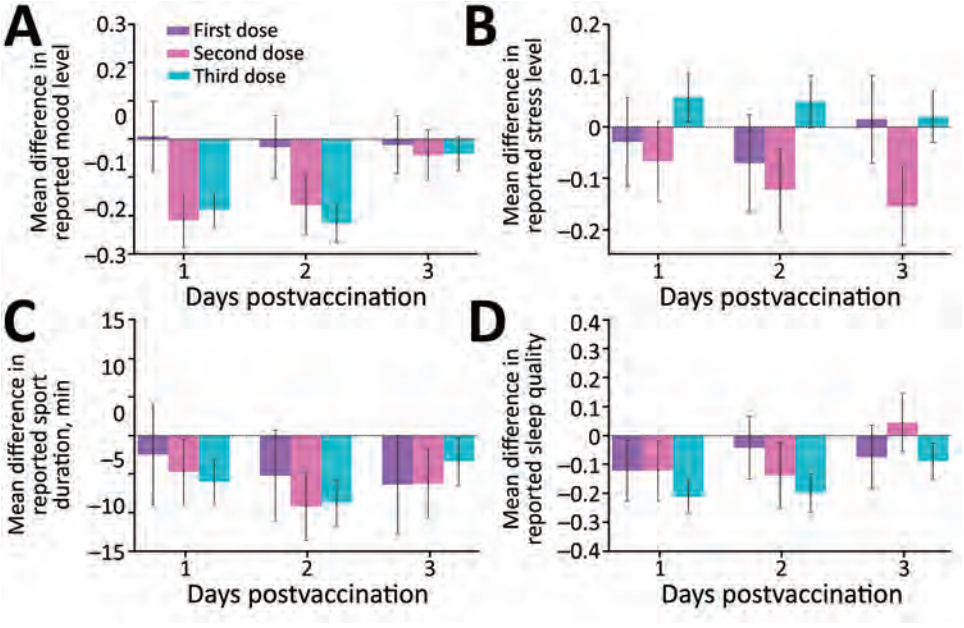

Figure 2. Changes in subjective well-being indicators reported by participants through a mobile application for self-reported and physiologic reactions to BNT162b2 (Pfizer, https://www.pfizer.com) mRNA coronavirus disease vaccine doses. Mean difference compared with baseline levels are shown for the well-being indicators of mood level (A), stress level (B), sport duration (C), and sleep quality (D). Mood level, stress level, and sleep quality were reported on a 1–5 Likert scale. Sport duration was measured in minutes. Error bars indicate 90% CIs. Horizontal dashed lines indicate no change compared with baseline levels.

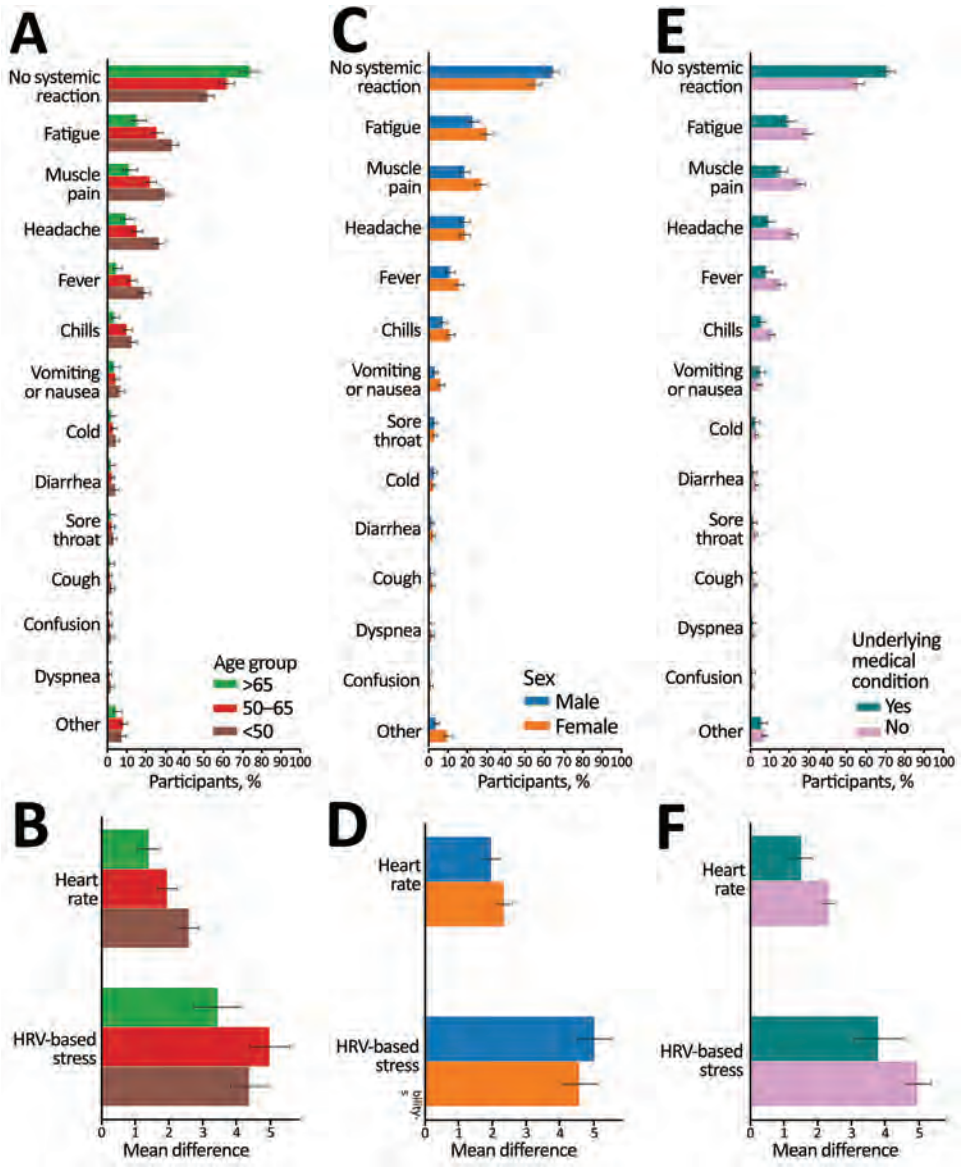

Figure 4. Self-reported and objective reactions following the third vaccine dose, stratified by age, sex, and underlying medical condition for self-reported and physiologic reactions to third BNT162b2 (Pfizer, https://www.pfizer.com) mRNA coronavirus disease vaccine doses. Reactions reported by participants through the mobile application (A, C, E) and objective heart rate and heart rate variability measured through a smartwatch (B, D, F) are shown, stratified by age (A, B), sex (C, D), and underlying medical condition (E, F). Bars indicate percentage of participants with a reported or recorded reaction; error bars indicate 90% CIs.

<50 years of age reported chest pain after vaccination. None of these participants had an underlying medical condition. These reactions (i.e., dyspnea and chest pain) disappeared 2–4 days after vaccination.

Discussion

Our key findings suggest that local and systemic reactions reported after the third (booster) vaccine dose administration are similar to those reported after the second dose and considerably greater than those observed after the first dose. Our analyses of self-reported well-being indicators and objective smartwatch physiologic indicators underscore these results. Furthermore, within 3 days from vaccination with the third dose, all measures returned to their baseline levels in all participants. We identified differences in subpopulations on the basis of sex, age, and underlying medical conditions after administration of the third vaccine dose. It has been suggested that reactions caused by the COVID-19 vaccine are a byproduct of a short burst of interferon type I generation concomitant with induction of an effective immune response (*36*). Interferon type I generation is substantially stronger in women than in men and stronger in younger and healthier persons than in older and less healthy persons. We found that participants <65 years of age, female participants, and participants without an underlying medical condition showed greater reactions in self-reported local and systemic reactions and well-being indicators, as well as in objective physiologic measurements recorded by the smartwatch. Our results are also consistent with the

results of a previous study that found similar trends after the first and second doses (*37*).

Clinical trials have not yet used the comprehensive physiologic measures generated by wearable devices, such as smartwatches. Currently, the FDA and European Medicines Agency evaluate the safety of and create guidelines for newly developed vaccines primarily on the basis of subjective, self-reported questionnaires (*22*,*38*). Much of the scientific literature discusses these self-reported side effects of COVID-19 vaccines. However, integrating wearable devices into clinical trials, alongside self-reported questionnaires, can provide more precise and rich data regarding the vaccines' effects on physiologic measures.

Our study's first limitation is that the 1,609 persons who comprised the base dataset of our analyses might not be representative of the vaccinated population in Israel or globally. Nevertheless, the changes observed in self-reported reactions and well-being indicators, as well as objective physiologic indicators recorded by the smartwatches, were statistically significant and consistent with each other. Moreover, the reaction types, frequency, and duration we observed for the first and second doses were similar to those observed in the BNT162b2 mRNA vaccine clinical trials (*26*). In addition, a clear pattern of returning to baseline levels was observed within 72 hours after vaccination in all examined measures. Although the sample size was limited, trends were consistent regardless of age group, sex, and underlying medical conditions.

Second, we did not explicitly control for the effects of the observational trial setting (e.g., participating in a trial, wearing a smartwatch, potential concerns regarding the vaccine). Any effects of the observational trial setting should, in principle, have similar effects on our analysis of each of the 3 vaccine doses. However, because we found no deviations in most measurements from baseline levels in the subset of participants who received their first dose, we believe the changes observed after the second and third doses arise from an actual reaction to the vaccine.

Third, the smartwatches used to obtain physiologic measurements are not medical-grade devices. Nevertheless, recent studies show a considerably accurate heart rate measurement in the previous versions of the smartwatch used in this study (*31*,*32*). In the same context, for some measures, such as SpO_2, the timing of measurement might be different across participants (e.g., if they changed their default settings). In both instances, it is useful to emphasize that our analyses focused on the change in measurements compared with their baseline values, rather than on their absolute values.

Fourth, all participants in our study received the BNT162b2 mRNA vaccine. Although our findings might not be directly generalized to other types of COVID-19 vaccines, we believe that applying our analyses on other vaccines is likely to yield qualitatively similar findings because of the similarities observed between different COVID-19 vaccines (*26*,*39*,*40*).

It would be useful to evaluate the effect of previous COVID-19 infection episodes on the results we obtained. However, although our data set contains some information on COVID-19 infections of participants during the time they spent in the study, it lacks information on infection episodes that occurred before they joined the study, making such analyses an interesting topic for future research.

Our study strengthens the evidence regarding the short-term safety of the booster BNT162b2 vaccine in several ways. First, reports of local and systemic reactions after the third dose were similar to those observed after the second dose, which was shown in clinical trials to be safe (*26*). Second, the considerable changes observed for all indicators during the first 2 days after receiving the third vaccine, including self-reported reactions and well-being indicators, as wells as objective physiologic indicators collected by the smartwatch, returned to their baseline levels. Third, regardless of the observed differences between subpopulations, our analyses indicated a clear pattern of return to baseline levels in all considered subpopulations. Fourth, we observed no change in SpO_2 compared with baseline levels, indicating that major adverse health consequences are less likely.

In conclusion, our study supports the short-term safety of the third BNT162b2 mRNA COVID-19 (booster) vaccine dose and mitigates, in part, concerns regarding its short-term effects. The medical and scientific communities could greatly benefit from the largely unbiased data generated by digital health technologies, such as the wearable devices that we analyzed in this study. Our findings could also be of interest to public health officials and other stakeholders because it is essential that objective measures are given attention in the critical evaluation of clinical trials.

This study was supported by the European Research Council (project 949850) and the Israel Science Foundation (grant 3409/19) within the Israel Precision Medicine Partnership program. M.L.B. and G.G. received support from a Koret Foundation grant for Smart Cities and Digital Living 2030.

Researchers interested in obtaining an aggregated version of the data and statistical code sufficient to reproduce the results reported in this article should contact the corresponding author (Erez Shmueli, shmueli@tau.ac.il)..

D.Y. and E.S. designed the study; M.M., T.P., S.G., and E.S. collected and assembled data; M.M., G.G., M.L.B., D.Y., and E. S. analyzed and interpreted data; M.M., D.Y., and E.S. performed statistical analysis; M.M., M.Y., D.Y., and E.S. wrote a draft of the article; D.Y. and E.S. critically revised the article and obtained funding for the study, and all authors approved the final version of the article.

About the Author

Mrs. Mofaz is a doctoral candidate in the Industrial Engineering Department at Tel Aviv University, Tel Aviv, Israel. Her primary research interests are personalized medicine and early detection of diseases using machine learning tools.

References

1. Kupferschmidt K, Wadman M. Delta variant triggers new phase in the pandemic. Science. 2021;372:1375–6. https://doi.org/10.1126/science.372.6549.1375
2. World Health Organization. Tracking SARS-CoV-2 variants [cited 2022 Apr 13]. https://www.who.int/en/activities/tracking-SARS-CoV-2-variants
3. Mlcochova P, Kemp SA, Dhar MS, Papa G, Meng B, Ferreira IA, et al.; Indian SARS-CoV-2 Genomics Consortium (INSACOG); Genotype to Phenotype Japan (G2P-Japan) Consortium; CITIID-NIHR BioResource COVID-19 Collaboration. SARS-CoV-2 B.1.617.2 Delta variant replication and immune evasion. Nature. 2021;599:114–9. https://doi.org/10.1038/s41586-021-03944-y
4. Centers for Disease Control and Prevention. Delta variant: what we know about the science [cited 2022 Apr 13]. https://stacks.cdc.gov/view/cdc/108671
5. Mahase E. Delta variant: what is happening with transmission, hospital admissions, and restrictions? BMJ. 2021;373:n1513. https://doi.org/10.1136/bmj.n1513
6. World Health Organization. Weekly epidemiological update on COVID-19, August 17, 2021 [cited 2022 Apr 13]. https://www.who.int/publications/m/item/weekly-epidemiological-update-on-covid-19---17-august-2021
7. Wadman M. Israel's grim warning: Delta can overwhelm shots. Science. 2021;373:838–9. https://doi.org/10.1126/science.373.6557.838
8. Munitz A, Yechezkel M, Dickstein Y, Yamin D, Gerlic M. BNT162b2 vaccination effectively prevents the rapid rise of SARS-CoV-2 variant B.1.1.7 in high-risk populations in Israel. Cell Rep Med. 2021;2:100264. https://doi.org/10.1016/j.xcrm.2021.100264
9. Lopez Bernal J, Andrews N, Gower C, Gallagher E, Simmons R, Thelwall S, et al. Effectiveness of COVID-19 vaccines against the B.1.617.2 (Delta) variant. N Engl J Med. 2021;385:585–94. https://doi.org/10.1056/NEJMoa2108891
10. Pouwels KB, Pritchard E, Matthews PC, Stoesser N, Eyre DW, Vihta K-D, et al. Effect of Delta variant on viral burden and vaccine effectiveness against new SARS-CoV-2 infections in the UK. Nat Med. 2021;27:2127–35. https://doi.org/10.1038/s41591-021-01548-7
11. Sheikh A, McMenamin J, Taylor B, Robertson C; Public Health Scotland and the EAVE II Collaborators. SARS-CoV-2 Delta VOC in Scotland: demographics, risk of hospital admission, and vaccine effectiveness. Lancet. 2021;397:2461–2. https://doi.org/10.1016/S0140-6736(21)01358-1
12. Nasreen S, He S, Chung H, Brown KA, Gubbay JB, Buchan SA, et al. Effectiveness of COVID-19 vaccines against variants of concern in Ontario. Nat Microbiol. 2022;7:379–85. https://doi.org/10.1038/s41564-021-01053-0
13. Centers for Disease Control and Prevention. COVID-19 datasets—government data. [cited 2022 Apr 13]. https://data.cdc.gov/browse?q=covid-19
14. Ministry of Health. The Ministry of Health Director General has approved the recommendation to administer a third vaccine dose to 50-year-olds and older and to other population [cited 2022 Apr 13]. https://www.gov.il/en/departments/news/13082021-01
15. Ministry of Health. The Vaccination Advisory Committee presented data and recommended the administration of a third dose to older adults [cited 2022 Apr 13]. https://www.gov.il/en/departments/news/29072021-04
16. Prime Minister's Office. Statement by PM Bennett on third dose of the COVID vaccine to Israeli citizens over the age of 60 [cited 2022 Apr 13]. https://www.gov.il/en/Departments/news/event_press29071
17. Ministry of Health. The vaccination policy and the new green pass that will take effect soon [cited 2022 Apr 13]. https://www.gov.il/en/departments/news/29082021-01
18. Centers for Disease Control and Prevention. Joint statement from HHS public health and medical experts on COVID-19 booster shots. CDC online newsroom [2022 Apr 13]. https://www.cdc.gov/coronavirus/2019-ncov/vaccines/booster-shot.html?s_cid=11709:covid%20vaccine%20booster:sem.ga:p:RG:GM:gen:PTN.Grants:FY22
19. Centers for Disease Control and Prevention. COVID-19 vaccines for people who are moderately to severely immunocompromised [cited 2022 Apr 13]. https://www.cdc.gov/coronavirus/2019-ncov/vaccines/recommendations/immuno.html?s_cid=10483:immunocompromised%20and%20covid%20vaccine:sem.ga:p: :GM:gen:PTN:FY21
20. US Food and Drug Administration. Joint statement from HHS public health and medical experts on COVID-19 booster shots [2022 Apr 13]. https://www.hhs.gov/about/news/2021/08/18/joint-statement-hhs-public-health-and-medical-experts-covid-19-booster-shots.html
21. Kamar N, Abravanel F, Marion O, Couat C, Izopet J, Del Bello A. Three doses of an mRNA Covid-19 vaccine in solid-organ transplant recipients. N Engl J Med. 2021;385:661–2. https://doi.org/10.1056/NEJMc2108861
22. Food and Drug Administration. Development and licensure of vaccines to prevent COVID-19 [cited 2022 Apr 13]. https://www.fda.gov/media/139638/download
23. Gepner Y, Mofaz M, Oved S, Yechezkel M, Constantini K, Goldstein N, et al. Utilizing wearable sensors for continuous and highly-sensitive monitoring of reactions to the BNT162b2 mRNA COVID-19 vaccine. Commun Med. 2022;2:1–8.
24. Hajduczok AG, DiJoseph KM, Bent B, Thorp AK, Mullholand JB, MacKay SA, et al. Physiologic response to the Pfizer-BioNTech COVID-19 vaccine measured using wearable devices: prospective observational study. JMIR Form Res. 2021;5:e28568. https://doi.org/10.2196/28568
25. Oved S, Mofaz M, Lan A, Einat H, Kronfeld-Schor N, Yamin D, et al. Differential effects of COVID-19 lockdowns on well-being: interaction between age, gender and chronotype. J R Soc Interface. 2021;18:20210078. https://doi.org/10.1098/rsif.2021.0078

26. Polack FP, Thomas SJ, Kitchin N, Absalon J, Gurtman A, Lockhart S, et al.; C4591001 Clinical Trial Group. Safety and efficacy of the BNT162b2 mRNA COVID-19 vaccine. N Engl J Med. 2020;383:2603–15. https://doi.org/10.1056/NEJMoa2034577
27. Garmin. VÍVOSMART® 4 owner's manual. 2018 [cited 2022 Apr 13]. https://www8.garmin.com/manuals/webhelp/vivosmart4/EN-US/vivosmart_4_OM_EN-US.pdf
28. Garmin. What is the stress level feature on my Garmin watch? [cited 2022 Apr 13]. https://support.garmin.com
29. Kim H-G, Cheon E-J, Bai D-S, Lee YH, Koo B-H. Stress and heart rate variability: a meta-analysis and review of the literature. Psychiatry Investig. 2018;15:235–45. https://doi.org/10.30773/pi.2017.08.17
30. Pereira T, Almeida PR, Cunha JP, Aguiar A. Heart rate variability metrics for fine-grained stress level assessment. Comput Methods Programs Biomed. 2017;148:71–80. https://doi.org/10.1016/j.cmpb.2017.06.018
31. Reddy RK, Pooni R, Zaharieva DP, Senf B, El Youssef J, Dassau E, et al. Accuracy of wrist-worn activity monitors during common daily physical activities and types of structured exercise: evaluation study. JMIR Mhealth Uhealth. 2018;6:e10338. https://doi.org/10.2196/10338
32. Bent B, Goldstein BA, Kibbe WA, Dunn JP. Investigating sources of inaccuracy in wearable optical heart rate sensors. NPJ Digit Med. 2020;3:18. https://doi.org/10.1038/s41746-020-0226-6
33. Garmin. Accuracy [cited 2022 Apr 13]. https://support.garmin.com/enUS/?faq=aZc8RezeAb9LjCDpJplTY7#:~:text=Garmin%C2%AE%20GPS%20receivers%20are,to%20its%20Satellite%20Information%20Page
34. Derrick B, Dobson-Mckittrick A, Toher D, White P. Test statistics for comparing two proportions with partially overlapping samples. J Appl Quant Methods. 2015;10:1–14.
35. Derrick B, Russ B, Toher D, White P. Test statistics for the comparison of means for two samples that include both paired and independent observations. J Mod Appl Stat Methods. 2017;16:9. https://doi.org/10.22237/jmasm/1493597280
36. Bunders MJ, Altfeld M. Implications of sex differences in i mmunity for SARS-CoV-2 pathogenesis and design of therapeutic interventions. Immunity. 2020;53:487–95. https://doi.org/10.1016/j.immuni.2020.08.003
37. Menni C, Klaser K, May A, Polidori L, Capdevila J, Louca P, et al. Vaccine side-effects and SARS-CoV-2 infection after vaccination in users of the COVID Symptom Study app in the UK: a prospective observational study. Lancet Infect Dis. 2021;21:939–49. https://doi.org/10.1016/S1473-3099(21)00224-3
38. European Medicines Agency. Clinical trials in human medicines [cited 2022 Apr 13]. https://www.ema.europa.eu/en/human-regulatory/research-development/clinical-trials-human-medicines
39. Baden LR, El Sahly HM, Essink B, Kotloff K, Frey S, Novak R, et al.; COVE Study Group. Efficacy and safety of the mRNA-1273 SARS-CoV-2 vaccine. N Engl J Med. 2021;384:403–16. https://doi.org/10.1056/NEJMoa2035389
40. Voysey M, Clemens SA, Madhi SA, Weckx LY, Folegatti PM, Aley PK, et al.; Oxford COVID Vaccine Trial Group. Safety and efficacy of the ChAdOx1 nCoV-19 vaccine (AZD1222) against SARS-CoV-2: an interim analysis of four randomised controlled trials in Brazil, South Africa, and the UK. Lancet. 2021;397:99–111. https://doi.org/10.1016/S0140-6736(20)32661-1

Address for correspondence: Erez Shmueli, Department of Industrial Engineering, Tel Aviv University, 30 Chaim Levanon St, Tel Aviv 6997801, Israel; email: shmueli@tau.ac.il

Nipah Virus Detection at Bat Roosts after Spillover Events, Bangladesh, 2012–2019

Clifton D. McKee,[1] Ausraful Islam,[1] Mohammed Ziaur Rahman, Salah Uddin Khan, Mahmudur Rahman, Syed M. Satter, Ariful Islam, Claude Kwe Yinda, Jonathan H. Epstein, Peter Daszak, Vincent J. Munster, Peter J. Hudson, Raina K. Plowright, Stephen P. Luby, Emily S. Gurley

Knowledge of the dynamics and genetic diversity of Nipah virus circulating in bats and at the human-animal interface is limited by current sampling efforts, which produce few detections of viral RNA. We report a series of investigations at *Pteropus medius* bat roosts identified near the locations of human Nipah cases in Bangladesh during 2012–2019. Pooled bat urine was collected from 23 roosts; 7 roosts (30%) had ≥1 sample in which Nipah RNA was detected from the first visit. In subsequent visits to these 7 roosts, RNA was detected in bat urine up to 52 days after the presumed exposure of the human case-patient, although the probability of detection declined rapidly with time. These results suggest that rapidly deployed investigations of Nipah virus shedding from bat roosts near human cases could increase the success of viral sequencing compared with background surveillance and could enhance understanding of Nipah virus ecology and evolution.

Nipah virus is a paramyxovirus (genus *Henipavirus*) that has caused outbreaks of neurologic and respiratory disease in humans and livestock in Bangladesh, India, Malaysia, Singapore, and the Philippines (*1*–*4*). The primary hosts of henipaviruses are fruit bats (family Pteropodidae) in Africa, Asia, and Oceania (*5*). Although Nipah virus causes no apparent disease in bats (*6*,*7*), the case-fatality rate in humans can be 40%–70% (*2*,*8*,*9*). In addition, Nipah virus has characteristics that enable repeated human outbreaks. Its bat hosts are widespread in South Asia and Southeast Asia, regions with dense human and livestock populations (*10*), which could lead to virus spillover and spread (*11*). Nipah virus can transmit directly from bats when humans consume date palm sap that is contaminated with bat saliva, urine, or feces or can transmit indirectly through spillover to domesticated animals (*12*–*14*).

Since 2001, Bangladesh has experienced multiple Nipah virus outbreaks with confirmed person-to-person transmission, albeit below the threshold necessary for sustained epidemics (*8*); however, the virus transmitted rapidly among pig populations in Malaysia, producing infection rates of 100% on some farms, and spread between farms through shipments of infected animals (*15*,*16*). No commercially available vaccines or therapeutics for Nipah virus exist to prevent or mitigate disease in case of an epidemic, although these interventions are areas of active research (*17*,*18*). Finally, RNA viruses such as Nipah have high mutation rates, which are a predictor of zoonotic potential (*19*). Although documented genetic diversity within Nipah viruses is limited (*20*–*24*), high mutation rates could potentially produce variants with sufficient transmissibility in humans to cause a sustained epidemic (*25*,*26*). Given the wide geographic range and unsampled diversity of Nipah viruses, variants that are more transmissible among

Author affiliations: Bloomberg School of Public Health, Johns Hopkins University, Baltimore, Maryland, USA (C.D. McKee, E.S. Gurley); icddr,b, Dhaka, Bangladesh (Ausraful Islam, M.Z. Rahman, S.U. Khan, M. Rahman, S.M. Satter, E.S. Gurley); Institute of Epidemiology, Disease Control and Research, Dhaka, Bangladesh (M.Z. Rahman); Global Health Development/Eastern Mediterranean Public Health Network, Amman, Jordan (M.Z. Rahman); Deakin University, Geelong, Victoria, Australia (Ariful Islam); EcoHealth Alliance, New York, New York, USA (Ariful Islam, J.H. Epstein, P. Daszak); National Institute of Allergy and Infectious Diseases, National Institutes of Health, Hamilton, Montana, USA (C.K. Yinda, V.J. Munster); Pennsylvania State University, State College, Pennsylvania, USA (P.J. Hudson); Montana State University, Bozeman, Montana, USA (R.K. Plowright); Stanford University, Stanford, California, USA (S.P. Luby)

DOI: https://doi.org/10.3201/eid2807.212614

[1]These first authors contributed equally to this article.

humans might exist and circulate in bats, and each spillover event could be an opportunity for such variants to emerge (*27*).

Genetic and phenotypic diversity among Nipah viruses exists, but the human health implications are unclear. Nipah virus genotypes from Bangladesh and India are genetically distinct from genotypes from Malaysia (*22*–*24*). Although Malaysia genotypes are less diverse than those from Bangladesh and India (*24*), genotypes from Malaysia derive solely from pigs, humans, and bats during the 1998–1999 outbreak, whereas genotypes from Bangladesh and India derive from multiple human outbreaks and surveys of bats since 2004. Another difference is that person-to-person transmission of Nipah virus has rarely been observed in Malaysia (*28*–*30*) but accounted for one third of reported cases in Bangladesh (*8*) and >75% of cases in India (*1*,*9*,*31*). However, person-to-person transmission in Malaysia was not investigated beyond healthcare workers, and <10% of persons with Nipah virus transmit it to another person, usually a family caregiver (*8*,*28*). Some of this variation in transmission mode and severity could reflect differences in exposure, sampling, infrastructure, and culture between countries, but differences between viral strains might explain additional variation. Case-patients in Malaysia were less likely to experience cough, difficulty breathing, or abnormal chest radiography than case-patients in Bangladesh (*29*,*32*,*33*). These differences in transmissibility and pathogenicity between Nipah virus strains from Malaysia and Bangladesh have been observed in some animal experiments, although with conflicting results (*34*–*36*). The reviewed evidence suggests that genetic variation in Nipah virus might produce differences in pathogenicity or transmissibility, so more transmissible strains of Nipah virus could be circulating undetected in bat populations.

Knowledge of Nipah virus diversity is limited to the few virus sequences obtained to date. Available sequences from GenBank and recent studies (*20*,*24*) include only 76 Nipah virus genomes, 51 of which derive from human patients, and 153 nucleocapsid protein genes, 37 of which derive from humans. Previous studies have not been optimized to characterize Nipah virus genotypes circulating in bats.

The Indian flying fox (*Pteropus medius*) is the major reservoir of Nipah virus in Bangladesh and India (*37*,*38*). Longitudinal surveys indicate that exposure to Nipah virus is high (≈40%) in some *P. medius* populations in Bangladesh on the basis of serologic tests, but the prevalence of detectable Nipah virus RNA is low (<5%) at any given time (*37*). In addition, viral loads in collected bat samples are often low (*24*), limiting the success of virus sequencing or isolation necessary for describing viral diversity. Sampling methods that increase the success of detecting Nipah virus in bats and increase yield so that sequencing is possible would be useful for monitoring genetic changes in this virus. In this study, we focused Nipah virus detection to *P. medius* bat roosts near human cases identified in Bangladesh during outbreak investigations during 2012–2019. We aimed to identify whether bat roosts were actively shedding Nipah virus RNA in urine and how long shedding continued after initial detection. In addition, we sought to identify characteristics of bat roosts potentially associated with higher likelihood of testing positive.

Materials and Methods

Nipah Virus Case Investigations

Human case-patients with suspected Nipah virus infection with a history of consuming date palm sap were identified at 3 surveillance hospitals in the Faridpur, Rajshahi, and Rangpur Districts of Bangladesh (*39*). Additional suspected cases in other regions were identified from media reports (*40*). A total of 47 primary cases of Nipah virus representing spillover from bats were identified in 2012–2018; we investigated 17 in this study. Four additional spillover cases were investigated in 2019, but the total number of spillover cases from that year is unclear because of a lack of reporting. Case exposure to Nipah virus was evaluated with ELISA or PCR (*41*). Investigation teams visited the suspected case villages to gather evidence of case clusters and identify the exposure route (*42*). In some cases, teams were deployed before human cases were confirmed by ELISA or PCR.

Teams searched for *P. medius* bat roosts within a 20 km radius of the human case-patient's residence by asking community members about known roost sites and by scouting. Some identified roosts were located on burial grounds or over water and could not be sampled (Appendix 1 Table 1, https://wwwnc.cdc.gov/EID/article/28/7/21-2614-App1.pdf). During 12:00–4:00 AM, teams placed 4–20 polyethylene tarps under each roost, depending on the available area and size of the roost, to collect urine. Tarps were concentrated under branches with denser aggregations of bats. Tarps were ≈6 feet × 4 feet in size before 2019 and 3 feet × 2 feet in 2019; we made this change so that fewer bats contributed to urine pools to improve estimates of prevalence (*43*). During 5:00–6:00 AM, teams returned to the roosts and collected bat urine from the tarps with a sterile

syringe. Urine collected from tarps was either pooled by individual tarp or mixed together from multiple tarps and then divided into aliquots. We found no significant difference in Nipah detection between the 2 strategies (Appendix 1). We tested aliquots for Nipah virus RNA at icddr,b (Dhaka, Bangladesh) or National Institutes of Health (Hamilton, MT, USA) laboratories by using quantitative real-time reverse transcription PCR (qRT-PCR) targeting the nucleoprotein gene (*44*). Roosts with Nipah virus RNA detected in any aliquots at the first sampling event were revisited (3–16 days between sampling events) until all aliquots from a roost tested negative. Attempts to culture Nipah virus from positive samples at National Institutes of Health yielded no virus isolates; viral culture was not attempted at icddr,b because of the absence of BioSafety Level 4 facilities.

Statistical Analysis

For each laboratory-confirmed spillover case of Nipah virus in a human, we recorded the symptom onset date and the coordinates of the case-patient's residence. Teams identified the probable date of patient exposure to Nipah virus by the date of palm sap consumption for some cases; otherwise, the exposure date was assumed to be 7 days before symptom onset on the basis of the mean incubation period of Nipah virus for primary cases linked to spillover (*45*).

We used logistic regression to assess features of the roost sites associated with a roost testing positive for Nipah virus at the first sampling visit. Covariates in the model included the number of days between the first case-patient exposure to date palm sap and roost sampling, the number of bats in the roost, the distance between the case-patient's home and the roost site, and the number of human spillover cases associated with each nearby roost. We then performed model selection to choose important features using Akaike corrected information criterion (*46*).

For all roost sites that tested positive for Nipah virus at first sampling, we recorded the number of tested urine aliquots that were positive for Nipah virus at each visit. Because cycle threshold (Ct) values from qRT-PCR were not reported for all tests, we used the proportion of positive aliquots as a proxy for the intensity of virus shedding in bats, assuming that roosts with higher virus concentrations in urine would produce more positive aliquots. We then analyzed changes in the proportion of positive aliquots across roosts along 2 time axes. We aligned dates to the number of days since the presumed exposure date of the first human spillover Nipah case associated with each roost site. We then aligned roost-sampling dates to the number of days since the start of the calendar year for comparison. We fit binomial linear models to estimate the probability of detecting a Nipah virus–positive aliquot at each roost along each time axis.

To evaluate the utility of sampling bat roosts near human Nipah virus cases as a surveillance approach, we compared the rate of successful Nipah virus detections from this study to data reported by Epstein et al. (*37*). Samples from that study were collected quarterly from a *P. medius* bat roost in Faridpur District during 2007–2012 as part of a longitudinal study; from visits to different roosts throughout Bangladesh during 2006–2011 as part of a cross-sectional spatial analysis; or as part of Nipah virus outbreak investigations in 2009, 2010, and 2012. Urine samples were either collected from individual bats or from underneath roosts. For these comparisons, we considered each roost visit as a discrete sampling event, including repeat visits to the same roost. Ignoring the initial visits to 7 roosts near 5 suspected human cases that were Nipah virus–negative, the 23 roosts in our study were sampled across 47 visits. We made comparisons between studies for the number of sampling visits with positive Nipah detections and the number of positive urine samples (individual or pooled aliquots from roosts) across all sampling visits or during the first visit to each roost. We evaluated comparisons by using a χ^2 test of proportions or Fisher exact test. We considered statistical tests significant if p values were <0.05.

Ethics

All study participants or proxies provided informed consent before participation and personally identifiable information from patients was delinked from the data before use. Written permission was obtained from the Bangladesh Forest Department for sampling the bats, and team members obtained permission from landowners before sampling roosts. Protocols for case investigations and roost sampling were reviewed and approved by the Institutional Review Board at icddr,b.

Results

Teams investigated roosts near homes of 21 suspected human cases of Nipah virus infection during 2012–2019 (Appendix 1 Table 1). The cases were clustered in the central and northwest districts of Bangladesh, close to the 3 surveillance hospitals (Figure 1). Symptom onset for patients occurred in winter (December–February), with the exception of 1 case-patient in Manikganj District whose symptoms began in March

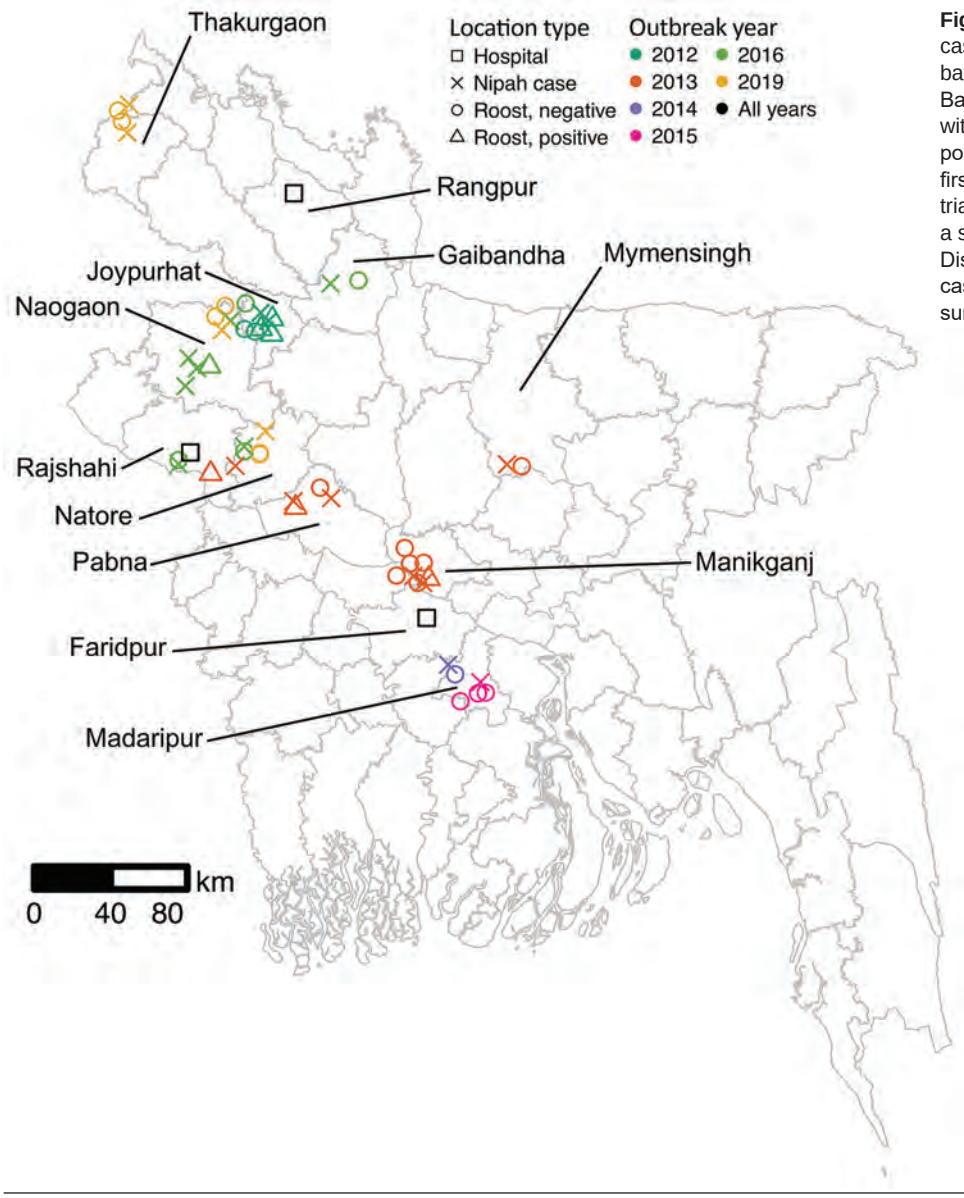

Figure 1. Locations of human Nipah cases (n = 21) and *Pteropus medius* bat roosts (n = 30) investigated in Bangladesh, 2012–2019. Roosts with urine aliquots that tested positive for Nipah virus RNA at the first sampling visit are indicated with triangles. Points have been jittered a small amount to increase visibility. Districts with human Nipah virus cases, identified bat roosts, or Nipah surveillance hospitals are labeled.

2013. No roost investigations were performed in 2017 and 2018 because of funding constraints.

For each case-patient, we identified 1–3 *P. medius* bat roosts within 0–17.9 km of the patient's home (Appendix 2 Table 1, https://wwwnc.cdc.gov/EID/article/28/7/21-2614-App2.xlsx). An additional 5 identified roosts were not sampled because they were located on burial grounds or over water (Appendix 1 Table 1). We sampled a total of 30 roosts. The first sampling visits occurred 17–62 days after the case-patients' exposure to date palm sap, either reported from the case investigation or back-calculated as 7 days before the onset of symptoms (Appendix 2 Table 1). Five of the suspected patients tested negative for Nipah virus by ELISA or PCR, and the 7 roosts identified near the patients' homes yielded no Nipah virus RNA. Because our interest was in whether sampling near human Nipah virus cases would help to identify roosts with active Nipah virus shedding, we excluded suspected but Nipah virus–negative case-patients and associated bat roosts from statistical analyses. Sensitivity analyses that included these samples produced statistically similar results. Testing by qRT-PCR of pooled urine aliquots detected 7/23 (30%) roosts as positive for Nipah virus RNA in ≥1 aliquots at the first sampling visit.

We performed Logistic regression on the presence of Nipah virus RNA in roost urine at the first sampling event on 22 distinct roosts using 4 explanatory variables; 1 roost was omitted because of

missing data on the number of bats. Roosts with positive urine aliquots tended to have more associated human Nipah spillover cases, were sampled sooner after patient exposure, were more distant from patients' homes, and had a smaller number of bats, but none of these variables were significantly associated with roost positivity in univariate or multiple regression analyses (Figure 2; Appendix 1 Table 2), and Akaike corrected information criterion identified the intercept-only model as the best model (Appendix 1 Table 3).

For the 7 roosts where Nipah virus RNA was detected ≥1 time, data were compiled on the number of urine aliquots that tested positive at each repeated sampling visit. Of these 7 roosts, 4 were positive at the first visit only and were revisited only once. The other 3 roosts remained positive at 1–2 additional sampling visits, although the proportion of aliquots that tested positive declined rapidly with the time since exposure of the first associated human case (Figure 3). For the 2 roosts with reported Ct values from qRT-PCR, the proportion of positive aliquots decreased over the repeated sampling visits while Ct values increased, indicating a decline in viral load (Appendix 1 Table 4).

Fitting a binomial model to the PCR data predicted that the probability of detecting at least 1 urine aliquot from under-roost sampling as positive for Nipah virus RNA at the time the associated case-patient was presumably exposed (day 0) was 0.66 (95% CI 0.42–0.84) (Figure 3). This probability declined to 0.02 (95% CI 0.01–0.04) by day 52, when the last positive roost aliquots were detected, and to 0.01 (95% CI 0–0.02) by day 65, when the last roost was sampled. We also fit a binomial model by using the days elapsed since the start of the calendar year (Appendix 1 Figure), but alignment of the virus detections among the roosts was less clustered on that time axis than the days-since-patient-exposure time axis, and the binomial model did not show a significant trend in detection over time.

Roost urine samples from our study and individual urine samples from longitudinally sampled roosts in Epstein et al. (*37*) produced similar proportions of positive sampling visits (comparison A in Table); the detection rate was also similar if only the first visit to each roost in our study was considered (7/23, 30%). In contrast, the proportion of positive aliquots from all sampling visits was significantly higher in our investigations than in the individual urine samples from longitudinal roosts in Epstein et al. (*37*) (comparison B in Table). The detection rate from our study for positive urine aliquots at the first sampling visit

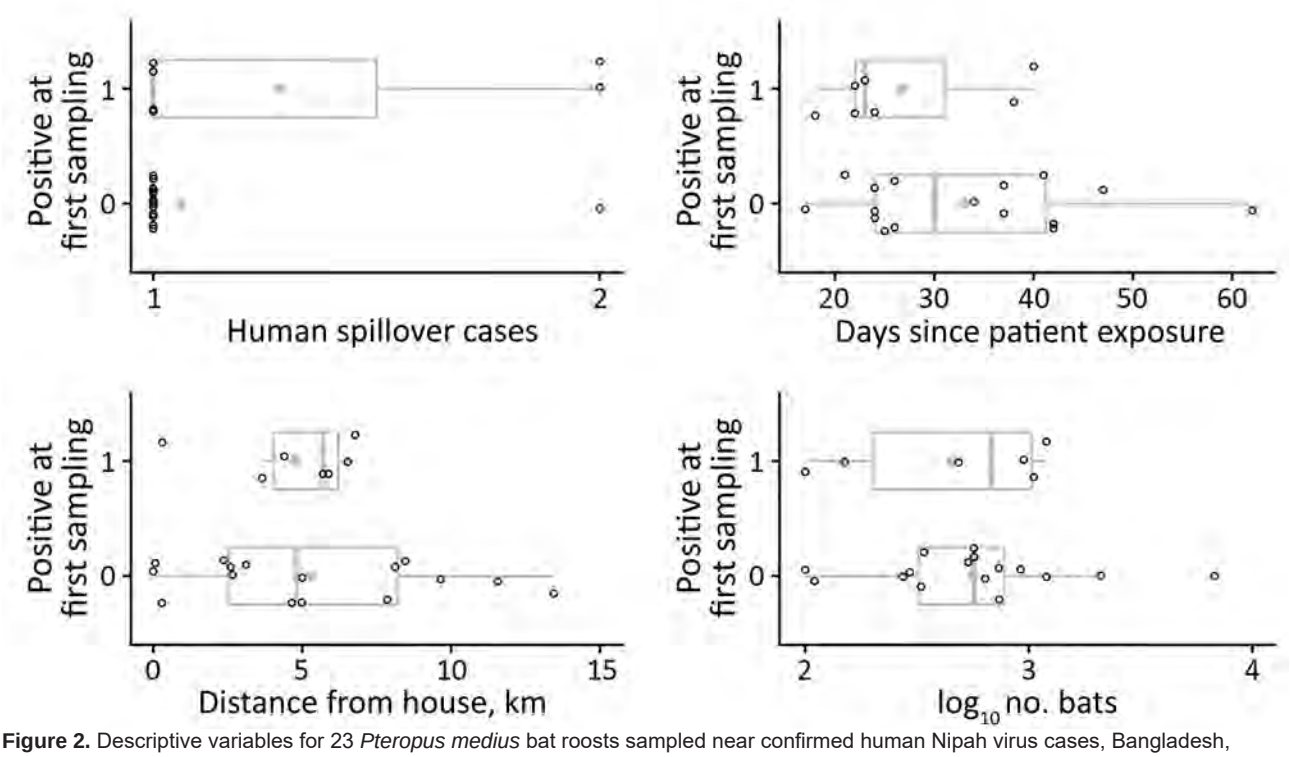

Figure 2. Descriptive variables for 23 *Pteropus medius* bat roosts sampled near confirmed human Nipah virus cases, Bangladesh, 2012–2019. Open circles show the values associated with the first human case associated with each roost; gray circles indicate means for each variable and positivity status (0 or 1). Vertical lines within boxes indicate medians; box left and right edges indicate the 25th and 75th percentiles; error bars indicate ±1.5 times the interquartile range.

was also higher than the detection rate for individual urine samples collected from 8 roosts from a cross-sectional study by Epstein et al. (*37*) (comparison C in Table). The detection rate for positive urine aliquots from our study was substantially higher than the detection rate from similarly pooled urine aliquots from underneath longitudinal and cross-sectional roosts in Epstein et al. (*37*) (comparison D in Table). Last, outbreak investigations of roosts performed by Epstein et al. (*37*) produced a higher detection rate than our own roost investigations (comparison E in Table), although only 4 roosts were visited by Epstein et al. (*37*), and the same roosts were not repeatedly visited as we did in our study.

Discussion

Nipah virus spillover from bats occurs sporadically in Bangladesh, so surveillance that optimizes viral detection in bats is a challenge. In contrast with cross-sectional or longitudinal bat roost surveillance used previously (*37*), the roost sampling in this study was triggered by Nipah virus outbreaks in nearby villages. Our approach identified roosts with active Nipah virus shedding at an equivalent rate to background surveillance (*37*) but had a higher detection rate in roost urine on a per sample basis. These results indicate that investigating roosts near spillover cases is more efficient than cross-sectional or longitudinal surveillance for obtaining samples with detectable viral RNA (Table). Repeated visits to positive roosts also demonstrated that viral RNA was detectable for weeks after the purported exposure date of human cases, although the proportion of positive urine aliquots declined sharply with time. Detections by PCR do not always produce sequences or genomes, so surveillance approaches that increase the number or quality of detections (e.g., higher viral loads) could maximize opportunities to collect samples with

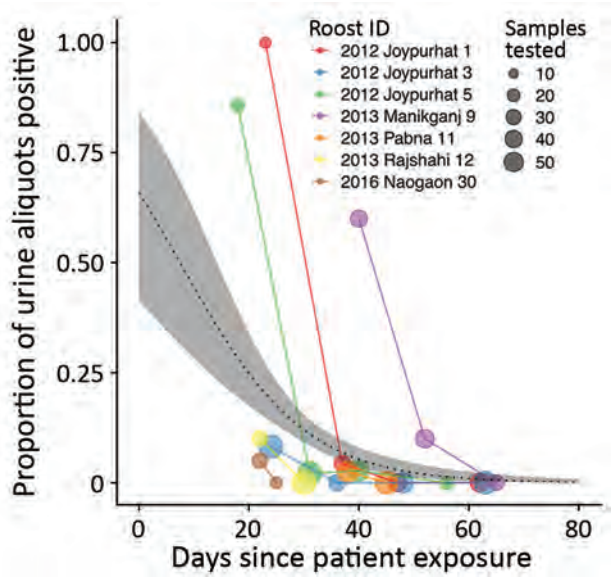

Figure 3. Results of screening of *Pteropus medius* bat roost urine aliquots for Nipah virus RNA, Bangladesh, 2012–2019. For each roost, the proportion of urine aliquots out of the total tested (indicated by the size of the circles) is aligned along a time axis of days since the first associated case-patient was exposed to Nipah virus in date palm sap. Time since patient exposure was either reported during the investigation or back-calculated as 7 days before reported symptom onset.

Table. Nipah virus detection success from study of bat roosts after spillover events, Bangladesh, 2012–2019, compared with results from previous study*

	Data from this study		Data from Epstein et al. (*37*)		
Test ID	Description	No. positive/ no tested (%)	Description	No. positive/ no tested (%)	Statistical test results
A	Positive sampling visits based on pooled roost urine aliquots where ≥1 urine aliquot tested positive†	11/47 (23%)	Positive sampling visits based on individual urine samples from longitudinal roosts where ≥1 individual urine sample tested positive	5/18 (28%)	OR = 0.84,‡ p = 0.76
B	Positive roost urine aliquots from sampled roosts across 47 sampling visits†	51/1,042 (4.9%)	Positive individual urine samples from longitudinal roosts across 18 sampling visits	8/1,671 (0.48%)	χ^2 = 56.8, p<0.001
C	Positive roost urine aliquots from the first visit to 23 sampled roosts†	45/525 (8.6%)	Positive individual urine samples from 8 roosts from a cross-sectional spatial study across districts of Bangladesh	0/555 (0%)	χ^2 = 47.5, p<0.001
D	Positive roost urine aliquots from sampled roosts across 47 sampling visits†	51/1,042 (4.9%)	Positive roost urine aliquots from longitudinal roosts and cross-sectional roosts, excluding samples from outbreak investigations	2/725 (0.28%)	χ^2 = 29.8, p<0.001
E	Positive roost urine aliquots from sampled roosts across 47 sampling visits†	51/1,042 (4.9%)	Positive roost urine aliquots from outbreak investigations, n = 4	19/104 (18.3%)	χ^2 = 27.2, p<0.001

*ID, identification; OR, odds ratio.
†Excludes the 7 roosts associated with 5 human cases that initially tested negative for Nipah virus. Statistical tests that included these samples produced similar results.
‡By Fisher exact test.

sufficient viral RNA for sequencing. These data suggest that rapid investigations to sample urine from bat roosts could increase the probability of detecting and sequencing Nipah virus. Used in combination with longitudinal sampling of roosts and surveillance of human or domesticated animal cases, this method could enhance our understanding of Nipah virus dynamics and genetic diversity in bats.

This study also provides critical information about the timing of Nipah virus shedding in bats in Bangladesh. Longitudinal surveys have shown that Nipah virus shedding from bats is sporadic throughout the year (*37*), so the peaks in viral detection in roost urine from our study likely coincided with shedding events. However, because these shedding events occurred during winter (when date palm sap is harvested for human consumption), bat visits to date palm trees might be more likely to contaminate sap with virus and lead to human infections (*47*). This factor suggests that the intensity of shedding events in bats occurring in winter could help to explain some of the spatiotemporal variation in the number of human spillovers that occur in Bangladesh annually (*42*), although more data on the frequency and timing of shedding events and human sap consumption will be needed to fully understand the dynamics of Nipah virus spillover.

Our findings come with several caveats because of limitations in our sample size and study design. Our analysis of factors associated with a roost testing positive at first sampling was unable to pinpoint significant relationships, likely because of low statistical power. We also did not systematically attempt virus isolation or sequencing in all positive samples, so we cannot estimate the probability of successful isolation or sequencing. However, Nipah virus isolates and sequences have been obtained from some of the roost urine samples included in this study. One of the positive roosts in Joypurhat from 2012 produced 9 nucleocapsid sequences (GenBank accession nos. MT890702–10) (*24*), and the positive roost in Manikganj from 2013 produced 10 virus isolates with full-genome sequences (GenBank accession nos. MK575060–9) (*21*). In fact, of the 39 Nipah virus sequences from bats in Bangladesh, 28 (72%) came from under-roost urine samples and 24 (86%) came from roost investigations near human cases (Appendix 2 Table 2). These patterns suggest that roost urine, especially from roosts near human spillover cases, might contain sufficient Nipah virus for sequencing or culture. Furthermore, in several human case-patients in Joypurhat in 2012 who drank date palm sap, we identified Nipah virus sequences that were genetically similar (>99.6% sequence identity) to sequences from the Joypurhat bat roost (roost 1 in Figure 3), providing additional evidence that connects virus shedding in local bat populations with human cases (Appendix 1). Future investigations could track how viral load in roost urine varies during viral shedding events, which could improve sequencing and isolation success and shed light on the ecologic conditions that lead to Nipah shedding from bats (*48*).

Our case investigations were also limited to the catchment area of 3 surveillance hospitals and the winter seasonality of Nipah virus spillover surveillance. This design systematically misses virus shedding events at bat roosts outside the surveillance area or during seasons when humans are not drinking fresh date palm sap (*13*). The logistical constraints of our surveillance approach cannot capture all Nipah virus genotypes circulating in *P. medius* across Bangladesh, but increasing the number of detections is still crucial, especially given the few Nipah virus isolates currently available (n = 11). Reactive roost investigations could be complemented with additional roost surveys outside of surveillance areas to learn more about Nipah virus transmission and genetic diversity in bat populations across Bangladesh.

This study provides proof of concept that reactive investigations of bat roosts near human Nipah virus cases can complement ongoing surveillance efforts and could increase the likelihood of viral detection and sequencing. Improvements in virus detection would aid in characterizing the genetic diversity of Nipah viruses circulating in bats and identify novel genotypes that might pose pandemic threats. Furthermore, these data provide evidence that viral shedding can continue for weeks after an initial spillover event, posing a hazard for additional contamination. Precise knowledge of when bats are shedding Nipah virus could be used to deploy public health campaigns more efficiently, such as by using barriers to prevent bat access to date palm sap (*49*).

This article was preprinted at https://www.biorxiv.org/content/10.1101/2021.12.29.474445v1.

Acknowledgments

We thank the Bangladesh Forest Department, the Ministry of Environment and Forest for their permission to conduct these investigations. We thank Robert Fischer and Trenton Bushmaker for technical assistance with bat sample screening.

This work was funded by the DARPA PREEMPT program Cooperative Agreement (D18AC00031). Additional funds came from the National Institutes of Health (NIH) grant number 00991, National Academy of Science (NAS) grant

number PGA-2000002048, and the US Agency for International Development (USAID) Emerging Pandemic Threats PREDICT Project Awards GHN-A-00-09-00010-00 and AID-OAA-A-14-00102. C.K.Y. and V.J.M. are supported by the Intramural Research Program of the National Institute of Allergy and Infectious Diseases, National Institutes of Health (1ZIAAI001179-01). R.K.P. was supported by the US National Science Foundation (DEB-1716698) and the USDA National Institute of Food and Agriculture (Hatch project 1015891). J.H.E., Ariful Islam, and P.D. were supported by USAID and NIH NIAID (AI153420). icddr,b acknowledges with gratitude the commitment of NIH, NAS, and DARPA to its research efforts. icddr,b is also grateful to the Governments of Bangladesh, Canada, Sweden, and the United Kingdom for providing core/unrestricted support.

About the Author

Dr. McKee is a postdoctoral fellow in the Department of Epidemiology, John Hopkins Bloomberg School of Public Health. His primary research interests include microbiology, epidemiology, and wildlife disease ecology. Dr. Ausraful Islam is an assistant scientist in the Infectious Diseases Division at icddr,b. His primary research interests include zoonotic disease ecology and epidemiology.

References

1. Chadha MS, Comer JA, Lowe L, Rota PA, Rollin PE, Bellini WJ, et al. Nipah virus-associated encephalitis outbreak, Siliguri, India. Emerg Infect Dis. 2006;12:235–40. https://doi.org/10.3201/eid1202.051247
2. Chua KB, Bellini WJ, Rota PA, Harcourt BH, Tamin A, Lam SK, et al. Nipah virus: a recently emergent deadly paramyxovirus. Science. 2000;288:1432–5. https://doi.org/10.1126/science.288.5470.1432
3. Hsu VP, Hossain MJ, Parashar UD, Ali MM, Ksiazek TG, Kuzmin I, et al. Nipah virus encephalitis reemergence, Bangladesh. Emerg Infect Dis. 2004;10:2082–7. https://doi.org/10.3201/eid1012.040701
4. Ching PKG, de los Reyes VC, Sucaldito MN, Tayag E, Columna-Vingno AB, Malbas FF Jr, et al. Outbreak of henipavirus infection, Philippines, 2014. Emerg Infect Dis. 2015;21:328–31. https://doi.org/10.3201/eid2102.141433
5. Kessler MK, Becker DJ, Peel AJ, Justice NV, Lunn T, Crowley DE, et al. Changing resource landscapes and spillover of henipaviruses. Ann N Y Acad Sci. 2018;1429:78–99. https://doi.org/10.1111/nyas.13910
6. Williamson MM, Hooper PT, Selleck PW, Westbury HA, Slocombe RF. Experimental hendra virus infectionin pregnant guinea-pigs and fruit Bats (*Pteropus poliocephalus*). J Comp Pathol. 2000;122:201–7. https://doi.org/10.1053/jcpa.1999.0364
7. Halpin K, Hyatt AD, Fogarty R, Middleton D, Bingham J, Epstein JH, et al.; Henipavirus Ecology Research Group. Pteropid bats are confirmed as the reservoir hosts of henipaviruses: a comprehensive experimental study of virus transmission. Am J Trop Med Hyg. 2011;85:946–51. https://doi.org/10.4269/ajtmh.2011.10-0567
8. Nikolay B, Salje H, Hossain MJ, Khan AKMD, Sazzad HMS, Rahman M, et al. Transmission of Nipah virus—14 years of investigations in Bangladesh. N Engl J Med. 2019;380:1804–14. https://doi.org/10.1056/NEJMoa1805376
9. Arunkumar G, Chandni R, Mourya DT, Singh SK, Sadanandan R, Sudan P, et al.; Nipah Investigators People and Health Study Group. Outbreak investigation of Nipah virus disease in Kerala, India, 2018. J Infect Dis. 2019;219:1867–78. https://doi.org/10.1093/infdis/jiy612
10. Robinson TP, Wint GRW, Conchedda G, Van Boeckel TP, Ercoli V, Palamara E, et al. Mapping the global distribution of livestock. PLoS One. 2014;9:e96084. https://doi.org/10.1371/journal.pone.0096084
11. Walsh MG, Sawleshwarkar S, Hossain S, Mor SM. Whence the next pandemic? The intersecting global geography of the animal-human interface, poor health systems and air transit centrality reveals conduits for high-impact spillover. One Health. 2020;11:100177. https://doi.org/10.1016/j.onehlt.2020.100177
12. Luby SP, Gurley ES, Hossain MJ. Transmission of human infection with Nipah virus. Clin Infect Dis. 2009;49:1743–8. https://doi.org/10.1086/647951
13. Gurley ES, Hegde ST, Hossain K, Sazzad HMS, Hossain MJ, Rahman M, et al. Convergence of humans, bats, trees, and culture in Nipah virus transmission, Bangladesh. Emerg Infect Dis. 2017;23:1446–53. https://doi.org/10.3201/eid2309.161922
14. Pulliam JRC, Epstein JH, Dushoff J, Rahman SA, Bunning M, Jamaluddin AA, et al.; Henipavirus Ecology Research Group (HERG). Agricultural intensification, priming for persistence and the emergence of Nipah virus: a lethal bat-borne zoonosis. J R Soc Interface. 2012;9:89–101. https://doi.org/10.1098/rsif.2011.0223
15. Mohd Nor MN, Gan CH, Ong BL. Nipah virus infection of pigs in peninsular Malaysia. Rev Sci Tech. 2000;19:160–5. https://doi.org/10.20506/rst.19.1.1202
16. Chua KB. Nipah virus outbreak in Malaysia. J Clin Virol. 2003;26:265–75. https://doi.org/10.1016/S1386-6532(02)00268-8
17. Mehand MS, Al-Shorbaji F, Millett P, Murgue B. The WHO R&D Blueprint: 2018 review of emerging infectious diseases requiring urgent research and development efforts. Antiviral Res. 2018;159:63–7. https://doi.org/10.1016/j.antiviral.2018.09.009
18. Geisbert TW, Bobb K, Borisevich V, Geisbert JB, Agans KN, Cross RW, et al. A single dose investigational subunit vaccine for human use against Nipah virus and Hendra virus. NPJ Vaccines. 2021;6:23. https://doi.org/10.1038/s41541-021-00284-w
19. Olival KJ, Hosseini PR, Zambrana-Torrelio C, Ross N, Bogich TL, Daszak P. Host and viral traits predict zoonotic spillover from mammals [Erratum in: Nature. 2017;548:612]. Nature. 2017;546:646–50. https://doi.org/10.1038/nature22975
20. Whitmer SLM, Lo MK, Sazzad HMS, Zufan S, Gurley ES, Sultana S, et al. Inference of Nipah virus evolution, 1999–2015. Virus Evol. 2021;7:veaa062.
21. Anderson DE, Islam A, Crameri G, Todd S, Islam A, Khan SU, et al. Isolation and full-genome characterization of Nipah viruses from bats, Bangladesh. Emerg Infect Dis. 2019;25:166–70. https://doi.org/10.3201/eid2501.180267
22. Olival KJ, Latinne A, Islam A, Epstein JH, Hersch R, Engstrand RC, et al. Population genetics of fruit bat reservoir informs the dynamics, distribution and diversity of Nipah virus. Mol Ecol. 2020;29:970–85. https://doi.org/10.1111/mec.15288

23. Harcourt BH, Lowe L, Tamin A, Liu X, Bankamp B, Bowden N, et al. Genetic characterization of Nipah virus, Bangladesh, 2004. Emerg Infect Dis. 2005;11:1594–7. https://doi.org/10.3201/eid1110.050513
24. Rahman MZ, Islam MM, Hossain ME, Rahman MM, Islam A, Siddika A, et al. Genetic diversity of Nipah virus in Bangladesh. Int J Infect Dis. 2021;102:144–51. https://doi.org/10.1016/j.ijid.2020.10.041
25. Makeyev EV, Bamford DH. Evolutionary potential of an RNA virus. J Virol. 2004;78:2114–20. https://doi.org/10.1128/JVI.78.4.2114-2120.2004
26. Drake JW, Holland JJ. Mutation rates among RNA viruses. Proc Natl Acad Sci U S A. 1999;96:13910–3. https://doi.org/10.1073/pnas.96.24.13910
27. Luby SP. The pandemic potential of Nipah virus. Antiviral Res. 2013;100:38–43. https://doi.org/10.1016/j.antiviral.2013.07.011
28. Mounts AW, Kaur H, Parashar UD, Ksiazek TG, Cannon D, Arokiasamy JT, et al.; Nipah Virus Nosocomial Study Group. A cohort study of health care workers to assess nosocomial transmissibility of Nipah virus, Malaysia, 1999. J Infect Dis. 2001;183:810–3. https://doi.org/10.1086/318822
29. Goh KJ, Tan CT, Chew NK, Tan PSK, Kamarulzaman A, Sarji SA, et al. Clinical features of Nipah virus encephalitis among pig farmers in Malaysia. N Engl J Med. 2000;342:1229–35. https://doi.org/10.1056/NEJM200004273421701
30. Parashar UD, Sunn LM, Ong F, Mounts AW, Arif MT, Ksiazek TG, et al. Case-control study of risk factors for human infection with a new zoonotic paramyxovirus, Nipah virus, during a 1998–1999 outbreak of severe encephalitis in Malaysia. J Infect Dis. 2000;181:1755–9. https://doi.org/10.1086/315457
31. Arankalle VA, Bandyopadhyay BT, Ramdasi AY, Jadi R, Patil DR, Rahman M, et al. Genomic characterization of Nipah virus, West Bengal, India. Emerg Infect Dis. 2011;17:907–9. https://doi.org/10.3201/eid1705.100968
32. Chong HT, Hossain MJ, Tan CT. Differences in epidemiologic and clinical features of Nipah virus encephalitis between the Malaysian and Bangladesh outbreaks. Neurol Asia. 2008;13:23–6.
33. Hossain MJ, Gurley ES, Montgomery JM, Bell M, Carroll DS, Hsu VP, et al. Clinical presentation of Nipah virus infection in Bangladesh. Clin Infect Dis. 2008;46:977–84. https://doi.org/10.1086/529147
34. Mire CE, Satterfield BA, Geisbert JB, Agans KN, Borisevich V, Yan L, et al. Pathogenic differences between Nipah virus Bangladesh and Malaysia strains in primates: implications for antibody therapy. Sci Rep. 2016;6:30916. https://doi.org/10.1038/srep30916
35. Clayton BA, Middleton D, Bergfeld J, Haining J, Arkinstall R, Wang L, et al. Transmission routes for nipah virus from Malaysia and Bangladesh. Emerg Infect Dis. 2012;18:1983–93. https://doi.org/10.3201/eid1812.120875
36. DeBuysscher BL, de Wit E, Munster VJ, Scott D, Feldmann H, Prescott J. Comparison of the pathogenicity of Nipah virus isolates from Bangladesh and Malaysia in the Syrian hamster. PLoS Negl Trop Dis. 2013;7:e2024. https://doi.org/10.1371/journal.pntd.0002024
37. Epstein JH, Anthony SJ, Islam A, Kilpatrick AM, Ali Khan S, Balkey MD, et al. Nipah virus dynamics in bats and implications for spillover to humans. Proc Natl Acad Sci U S A. 2020;117:29190–201. https://doi.org/10.1073/pnas.2000429117
38. Yadav PD, Shete AM, Kumar GA, Sarkale P, Sahay RR, Radhakrishnan C, et al. Nipah virus sequences from humans and bats during Nipah outbreak, Kerala, India, 2018. Emerg Infect Dis. 2019;25:1003–6. https://doi.org/10.3201/eid2505.181076
39. Naser AM, Hossain MJ, Sazzad HMS, Homaira N, Gurley ES, Podder G, et al. Integrated cluster- and case-based surveillance for detecting stage III zoonotic pathogens: an example of Nipah virus surveillance in Bangladesh. Epidemiol Infect. 2015;143:1922–30. https://doi.org/10.1017/S0950268814002635
40. Ao TT, Rahman M, Haque F, Chakraborty A, Hossain MJ, Haider S, et al. Low-cost national media-based surveillance system for public health events, Bangladesh. Emerg Infect Dis. 2016;22:720–2. https://doi.org/10.3201/eid2204.150330
41. Daniels P, Ksiazek T, Eaton BT. Laboratory diagnosis of Nipah and Hendra virus infections. Microbes Infect. 2001;3:289–95. https://doi.org/10.1016/S1286-4579(01)01382-X
42. Nikolay B, Salje H, Khan AKMD, Sazzad HMS, Satter SM, Rahman M, et al. A framework to monitor changes in transmission and epidemiology of emerging pathogens: lessons from Nipah virus. J Infect Dis. 2020;221(Suppl 4):S363–9. https://doi.org/10.1093/infdis/jiaa074
43. Giles JR, Peel AJ, Wells K, Plowright RK, McCallum H, Restif O. Optimizing noninvasive sampling of a zoonotic bat virus. Ecol Evol. 2021;11:12307–21. https://doi.org/10.1002/ece3.7830
44. Lo MK, Lowe L, Hummel KB, Sazzad HMS, Gurley ES, Hossain MJ, et al. Characterization of Nipah virus from outbreaks in Bangladesh, 2008–2010. Emerg Infect Dis. 2012;18:248–55. https://doi.org/10.3201/eid1802.111492
45. Rahman MA, Hossain MJ, Sultana S, Homaira N, Khan SU, Rahman M, et al. Date palm sap linked to Nipah virus outbreak in Bangladesh, 2008. Vector Borne Zoonotic Dis. 2012;12:65–72. https://doi.org/10.1089/vbz.2011.0656
46. Burnham KP, Anderson DR. Multimodel inference: understanding AIC and BIC in model selection. Sociol Methods Res. 2004;33:261–304. https://doi.org/10.1177/0049124104268644
47. Khan MSU, Hossain J, Gurley ES, Nahar N, Sultana R, Luby SP. Use of infrared camera to understand bats' access to date palm sap: implications for preventing Nipah virus transmission. EcoHealth. 2010;7:517–25. https://doi.org/10.1007/s10393-010-0366-2
48. Plowright RK, Peel AJ, Streicker DG, Gilbert AT, McCallum H, Wood J, et al. Transmission or within-host dynamics driving pulses of zoonotic viruses in reservoir–host populations. PLoS Negl Trop Dis. 2016;10:e0004796. https://doi.org/10.1371/journal.pntd.0004796
49. Khan SU, Gurley ES, Hossain MJ, Nahar N, Sharker MAY, Luby SP. A randomized controlled trial of interventions to impede date palm sap contamination by bats to prevent Nipah virus transmission in Bangladesh. PLoS One. 2012;7:e42689. https://doi.org/10.1371/journal.pone.0042689

Address for correspondence: Clifton D. McKee, Department of Epidemiology, John Hopkins Bloomberg School of Public Health, 615 N Wolfe St, Baltimore, MD 21205, USA; email: cmckee7@jhu.edu

Effect of Agroecosystems on Seroprevalence of St. Louis Encephalitis and West Nile Viruses in Birds, La Pampa, Argentina, 2017–2019

Ana P. Mansilla, Juan M. Grande, Adrián Diaz

In Argentina, the Pampa ecoregion has been almost completely transformed into agroecosystems. To evaluate the environmental (agricultural area, tree coverage, distance to the nearest water body and urban site) and biological (dove, cowbird, and sparrow abundance) effects on free-ranging bird exposure to St. Louis encephalitis virus (SLEV) and West Nile virus (WNV), we used generalized linear mixed models. For 1,019 birds sampled during 2017–2019, neutralizing antibodies were found against SLEV in samples from 60 (5.8%) birds and against WNV for 21 (2.1%). The best variable for explaining SLEV seroprevalence was agricultural area, which had a positive effect; however, for WNV, no model was conclusive. Our results suggest that agroecosystems in the La Pampa ecoregion increase the exposure of avian hosts to SLEV, thus potentially increasing virus activity.

Zoonotic infections, particularly those transmitted from one vertebrate to another by an arthropod vector (vectorborne diseases), have been frequently identified among the most common emerging infectious diseases (*1*). During recent decades, reemergence of many such pathogens (e.g., dengue virus, yellow fever virus, Zika virus, chikungunya virus, Saint Louis encephalitis virus [SLEV], and West Nile virus [WNV]) represents a threat to human health and wildlife conservation (*2*).

SLEV and WNV belong to the family *Flaviviridae*, genus *Flavivirus*. SLEV is endemic to the Americas and has recently re-emerged in the western United States (*3*,*4*), southern Brazil, and central Argentina (*5*). In Argentina, according to ecologic studies, the SLEV transmission network is integrated by *Culex quinquefasciatus*, *Culex interfor*, and *Culex saltanensis* mosquitoes as vectors (*6*) and eared doves (*Zenaida auriculata*) and Picui ground doves (*Columbina picui*) as amplifying urban hosts (*7*). WNV was first detected in the Americas in 1999, causing an encephalitis outbreak among humans and massive mortality events among American crows (*Corvus brachyrhynchos*) (*8*). In 2006 in Argentina, the virus was isolated from sick horses in Buenos Aires and Entre Ríos Provinces (*9*). However, serologic evidence from free-ranging birds indicates previous endemic WNV activity in a large mosaic of resident birds from central and northern Argentina since 2004 (*10*). Vector competence studies have indicated that *Cx. quinquefasciatus* and *Cx. interfor* mosquitoes are able to transmit the local strain of WNV (*11*), whereas host competence studies have identified the Picui ground dove as an amplifier host for WNV (*12*). This finding suggests that ecologic requirements for maintenance could be similar for both viruses.

Land-use changes can affect disease dynamics by modifying the abundance, distribution, behavior, movement, immune response, and community composition of vectors and hosts as well as interactions between vectors and hosts (*13*). In Argentina, the expansion of agriculture into native ecosystems has generated great modifications of the landscape and the biological communities that inhabit these regions. Specifically, because of the aptitude of its soils, the Pampean region, located in the central-eastern part of Argentina, is one of the areas most greatly modified by human activities. This area has almost entirely been converted to large-scale agricultural land, which

Author affiliations: Consejo Nacional de Investigaciones Científicas y Técnicas, Buenos Aires, Argentina (A. P. Mansilla, J. M. Grande, A. Diaz); Universidad Nacional de La Pampa, Santa Rosa, Argentina (A. P. Mansilla, J. M. Grande); and Universidad Nacional de Córdoba, Córdoba, Argentina (A. Diaz)

DOI: https://doi.org/10.3201/eid2807.211485

in turn has generated changes in the abundance of small mammals and birds (*14*). However, some species of rodents and native doves have successfully adapted to these changes and, because of their abundance, are considered agricultural pests (*15*). The large populations of several columbid species, such as eared doves, Picui ground doves, and spot-winged pigeons (*Patagioenas maculosa*), could generate appropriate ecologic conditions for increased SLEV and WNV activity. In this context, our goal was to study the exposure of free-ranging bird communities to SLEV and WNV and to evaluate environmental and biological factors potentially associated with that exposure in agroecosystems in the Pampean region of Argentina.

Bird capture, manipulation, banding, and blood sampling were authorized by the Direction of Natural Resources belonging to the Subsecretary of Agrarian Affairs from the Ministry of Production of La Pampa Province. Birds were handled according to the guidelines for the use of wild birds in research elaborated by the Ornithological Council (https://birdnet.org/wp content/uploads/2017/07/guc3adas-para-la-utilizacion-de-aves-silvestres-en-investigacic3b3n.pdf). Field studies did not involve endangered or protected species.

Methods

Study Area and Sampling Sites

We conducted this study in the northeastern region of La Pampa Province, Argentina, during the period of arbovirus activity (February–April) in 2017–2019. Within the study area, we selected sampling sites for bird captures randomly and included only those with permission from land owners and a minimum distance of 2,000 meters between each other, leading to a total of 12 sampling sites (Figure 1). The study area was formerly part of the Pampean grasslands ecoregion but has been entirely transformed to agriculture. The Pampean grasslands was a vast treeless plain covered by a variety of grasses, such as *Sorghastrum pellitum* and *Elionurus muticus* (*16*). In La Pampa Province, this area is now almost completely transformed, dominated by an agricultural exploitation system based on intensive soybean cultivation via direct sowing methods. Wheat (generally alternated with soybean in the same year), sunflowers, and corn are also cultivated, although to a lesser extent; some plots are seminatural or implanted pastures for cattle (*17*). Toward the center of the province, soybean cultivation is less common and seminatural pastures dominate the landscape, alternating with different crops such as wheat, corn, and sunflowers. This central area also contains some small isolated patches of Caldén (*Prosopis caldenia*) forest in the transition to the Espinal ecoregion (Figure 1). Across the study area, but more markedly in the northeastern region, settlements are surrounded by non-native tree woodlots (sometimes up to 20–30 hectares), which constitute a key element in the presence and abundance of pest birds, such as eared doves (*15*). The climate is dry subhumid; rainfall is distributed throughout the year, but the highest monthly precipitation is in the summer (October–March), increasing in a southwest-to-northeast gradient (*18*).

Bird Collection and Serum Samples

At each site, we operated 7 mist nets for 3 or 4 days during dawn and late afternoon. We banded collected birds with numbered aluminum leg bands displaying the shipping address of the Argentine Museum of Natural Sciences provided by the Aves Argentinas association (https://www.avesargentinas.org.ar). By using a specialized field guide for bird species from Argentina and Uruguay (*19*), we recorded species, age, sex, and regular morphometric measurements for each bird. We collected blood by jugular (most species) or brachial (columbids) venipuncture, with 27-gauge sterile needles, into plastic tubes containing 0.45 mL or 0.9 mL (according to a sample volume of 0.1 mL or 0.2 mL) of minimum essential medium for a serum dilution of ≈1:10. We held tubes at room temperature for 20–30 min for coagulation and then placed them into coolers. At the laboratory, we centrifuged samples at 5,000 × *g* for 15 min for serum separation and then stored them at −20°C. Before releasing the birds, we hydrated those sampled with sugar water. We did not collect blood from birds weighing <10 g.

Serologic Assays and Data Interpretation

We analyzed serum samples to detect neutralizing antibodies by using the plaque-reduction neutralization test. We used low-passage strains of SLEV CbaAr-4005 and WNV E/7229/06. The SLEV CbaAr-4005 strain was isolated from *Cx. quinquefasciatus* mosquitoes collected in Córdoba Province (*20*), and the WNV E/7229/06 strain was isolated from a dead horse in Buenos Aires Province, Argentina (*9*).

We considered all serum samples that neutralized ≥80% of the inoculated plaque-forming units to be positive and subjected samples that were positive for both viruses to titration (*21*). We

prepared 7 serial 2-fold dilutions of serum, resulting in final dilutions of 1:20, 1:40, 1:80, 1:160, 1:320, 1:640, and 1:1,280. We assigned endpoint titers as the reciprocal of the greatest dilution in which ≥80% of the challenge virus was neutralized. According to experiments that evaluated cross-reaction between SLEV and WNV in heterologous inoculation scenarios in common quail (*Coturnix coturnix*), which indicated no cross-reaction between SLEV and WNV (A. Diaz, unpub. data), as well as evidence provided by Patiris et al. (*22*) and Ledermann et al. (*23*), we considered all serum samples with antibody titers >20 to be positive. Therefore, we considered samples with titers >20 for both viruses to indicate multiple heterologous infections.

Environmental and Biological Data

To determine the influence of different environmental and biological variables on SLEV and WNV seroprevalence, we built a buffer area with a radius of 1.5 km around the sampling sites, within which we calculated the area occupied by various classes of land cover and other variables of interest. We based our buffer of 1.5 km on the dispersal patterns of several mosquitoes of the genus *Culex*, particularly *Cx. quinquefasciatus* (*24*), and some species of territorial birds, such as house sparrows (*Passer domesticus*), rufous-collared sparrows (*Zonotrichia capensis*), and rufous horneros (*Furnarius rufus*). We used SPOT 6 images granted by the National Commission for Space Activities (https://www.argentina.gob/ar/ciencia/conae). On these images we created a shape or layer file on which polygons corresponding to the different classes of land cover were digitized. Within the buffer area, we estimated the area and distances to variables relevant for arbovirus transmission (Table 1). We used the free open software QGIS version 3.4.10 (https://www.qgis.org) for all GIS procedures and analyzed the following environmental variables: agricultural area (which included crops and pasture lands) expressed in square kilometers; tree coverage (which included native forest patches and non-native tree woodlots) expressed in square kilometers; distance to the nearest water body (expressed in kilometers); and distance to the closest urban settlement (expressed in kilometers) (Tables 1, 2). On the basis of previous host competence studies (*7*), we considered as biological variables the abundance of doves (eared doves, Picui ground doves, and spot-winged pigeons), cowbirds (grayish baywings [*Agelaioides badius*] and shiny cowbirds [*Molothrus bonariensis*]),

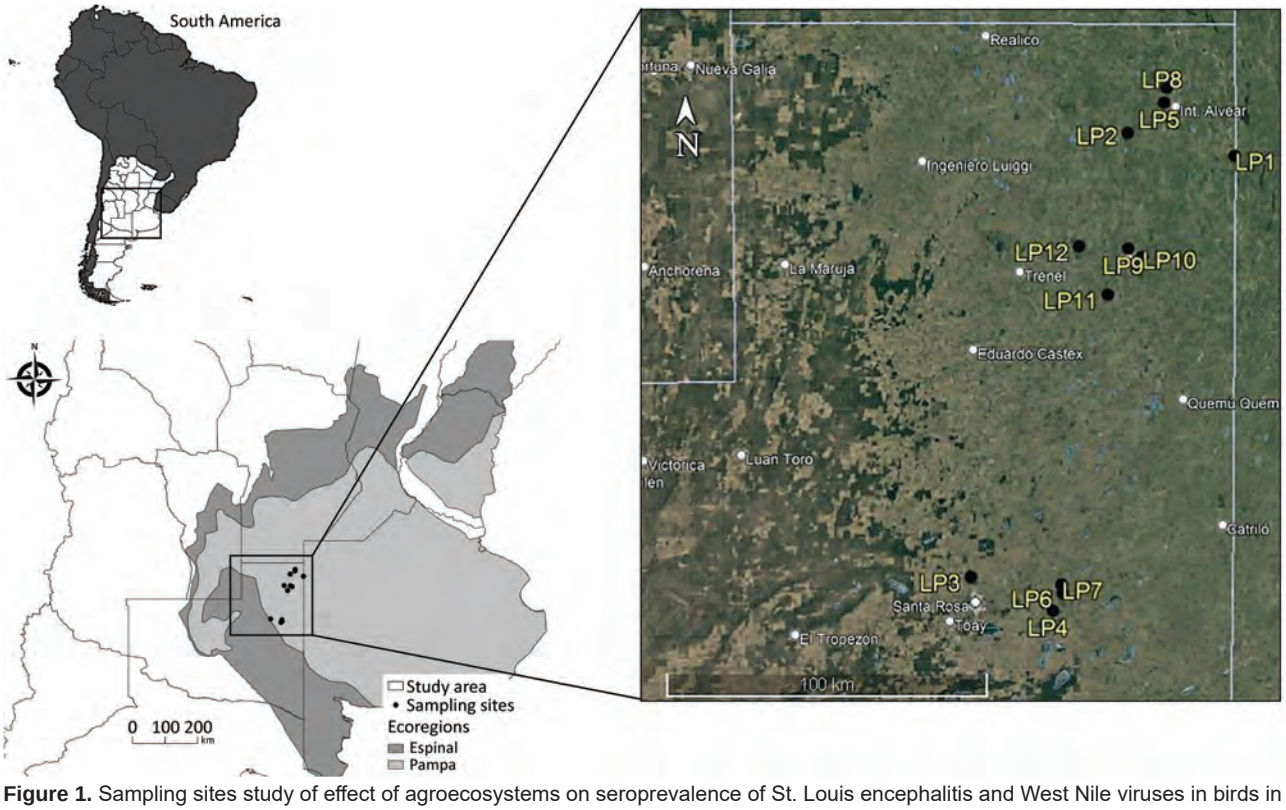

Figure 1. Sampling sites study of effect of agroecosystems on seroprevalence of St. Louis encephalitis and West Nile viruses in birds in the Pampean Grasslands, northeastern La Pampa Province, Argentina. Inset map at top left shows location of sites in South America. LP, La Pampa.

and house sparrows, considering the abundance as the total number of individuals of each species counted on each sampling site. Dove, cowbird, and sparrow abundance was estimated according to observational and acoustic bird counts on each site, for which we used the fixed width transect method of 50 × 200 m and performed 6 transects in each site according to a rarefaction analysis. The 6 transects were randomly distributed to cover as much of the site as possible and were ≥200 m apart to minimize possible biases by double counting of birds (*25*). All linear transects were surveyed once by the same single observer. Bird surveys took place during March and April 2018 and 2019, from 6:00 to 10:00 A.M.

Table 1. Models proposed to analyze the association between environmental and biological variables and SLEV/WNV seroprevalence in birds*

Model no.†	Variables	Biological justification
1/9	Null model	The environmental and biological variables considered in this study do not explain the SLEV/WNV seroprevalence.
2/10	Distance to water body	The water bodies are favorable habitats for the development of immature mosquitoes, especially of the genus *Culex*, for which a greater abundance of potential mosquito vectors will be generated in these sites. Also, birds use these sites for drinking, facilitating the encounter between hosts and vectors.
3/11	Agricultural area	Places with a homogeneous agricultural matrix will have impoverished biological communities dominated by birds of a few species, such as eared doves (*Zenaida auriculata*) and Picui ground doves (*Columbina picui*) with the potential to amplify viruses.
4/12	Distance to urban site	Peri-urban areas present better conditions for the establishment of different *Culex* mosquito species, generating a greater abundance of potential vectors.
5/13	Dove abundance	Host competence assays identified columbiform species as the main amplifying hosts for SLEV and WNV in Argentina, so a greater abundance of these species will produce greater virus circulation in those sites.
6/14	Sparrow abundance	House sparrow populations in Córdoba Province were not very efficient at amplifying SLEV, so a higher abundance of birds of this species would generate a viral dilution effect at the sites.
7/15	Agricultural area + dove abundance	Doves have a high capacity to amplify SLEV and WNV and are very abundant in disturbed environments occupied by crops and pastures, providing greater virus circulation in those places.
8/16	Distance to water body + agricultural area	Places that have larger agricultural areas and are closer to water bodies will have impoverished biological communities dominated by eared doves and Picui ground doves and high mosquito abundance.

*SLEV, St. Louis encephalitis virus; WNV, West Nile virus.
†Models 1–8 correspond to those proposed for SLEV and 9–16 correspond to those proposed for WNV.

Statistical Analyses

We estimated SLEV and WNV activities by means of neutralizing antibody prevalence. We calculated seroprevalence and 95% CIs by using the package binom (*26*) and the Pearson-Klopper method within R software (https://www.r-project.org). We analyzed associations between sampling sites, bird species, and exposure to SLEV/WNV through generalized linear mixed models (GLMM) with binomial distribution, in which the sampling year was considered as a random factor. We compared seroprevalence values for each virus evaluated in seropositive birds of each species by using the Pearson χ^2 test. We considered p values to be significant at a threshold of $\alpha = 0.05$. We investigated the association between environmental and biological variables and the SLEV/WNV seroprevalence at each sampling site by using GLMM with binomial error distribution and logit link function, considering the sampling year as a random variable in all models. We evaluated collinearity between explanatory variables by using Pearson correlation with $r > 0.60$ as a limit (Table 1). Because the environmental variables "agricultural area" and "tree coverage" were strongly correlated ($r = -0.99$), we removed the second variable from the set of models proposed, and because we found the same correlation for the variables "dove abundance" and "cowbird abundance" ($r = 0.85$), we eliminated "cowbird abundance" from the analyses. The model was selected by using the Akaike information criterion (AIC) and its corrected calculation for small sample sizes (AICc) (*27*). We compared models by using ΔAICc, which is the difference between the lowest AICc value (as the best of suitable models) and the AICc from all other models. Competing models were those differing by ΔAICc ≤2 from the top model, and Akaike weights (w) were an indication of support for each model. We evaluated the support for the performance of individual predictor variables by summing the AICc weight of a model (w_i) across all models that contained the parameter being considered (*27*). To evaluate the support for parameter estimates, we calculated 95% CIs by using unconditional variances and assumed the considered variable assumed to be significantly associated with the SLEV/WNV seroprevalence when the 95% CI excluded zero (*27*).

Table 2. Number of positive/total SLEV/WNV samples collected per site, seroprevalence in birds, and environmental and biological variables in study of effect of agroecosystems on seroprevalence of SLEV and WNV in birds, La Pampa, Argentina, 2017–2019*

Site	SLEV	%, (95% CI)	WNV	% (95% CI)	TC, km^2	AA, km^2,	UD, km	WD, km	DA†	SA‡	CA§
LP1	18/63	28.57 (17.8–41.3)	4/63	6.35 (1.7–15.4)	0.17	6.89	8.95	2.13	56	0	15
LP2	17/100	17 (10.2–25.8)	6/100	6 (2.2–12.6)	0.22	6.83	2.04	2.06	109	50	40
LP3	6/78	7.69 (2.8–15.9)	2/78	2.56 (0.3–8.9)	0.51	6.55	3.25	7.17	115	0	18
LP4	5/107	4.67 (1.5–10.5)	0/107	0 (0–3.4)	0.89	6.17	12.98	3.22	196	0	46
LP5	0/104	0 (0–3.5)	0/104	0 (0–3.5)	0.11	6.95	2.45	0.59	22	120	150
LP6	0/101	0 (0–3.5)	1/101	0.99 (0.02–5.4)	0.47	6.59	7.95	6.31	926	53	520
LP7	1/85	1.17 (0.6.3)	2/85	2.35 (0.2–8.2)	0.36	6.7	5.28	3.45	186	0	255
LP8	0/71	0 (0–5)	0/71	0 (0–5)	0.04	7.02	5.2	0.62	37	5	30
LP9	1/73	1.37 (0.03–7.3)	0/73	0 (0–4.9)	0.48	6.57	0.36	1.34	120	50	27
LP10	1/89	1.12 (0.02–6.1)	0/89	0 (0–4)	0.1	6.96	1.16	0.83	73	20	32
LP11	4/60	6.66 (1.8–16.1)	3/60	5 (1–13.9)	0.03	7.03	9.3	0.05	82	40	27
LP12	7/88	7.95 (3.2–15.7)	3/88	3.41 (0.7–9.6)	0.004	7.06	12.56	0.32	47	30	37

*AA, agricultural area; CA, cowbird abundance; DA, dove abundance; SA, sparrow abundance; SLEV, St. Louis encephalitis virus; TC, tree coverage; UD, distance to the closest urban settlement; WD, distance to the nearest water body; WNV, West Nile virus,
†No. eared doves (*Zenaida auriculata*) + Picui ground doves (*Columbina picui*) + spot-winged pigeons (*Patagioenas maculosa*).
‡No. house sparrows (*Passer domesticus*).
§No. grayish baywings (*Agelaioides badius*) + shiny cowbirds (*Molothrus bonariensis*).

Results

Of the 1,019 free-ranging birds belonging to 44 species collected and sampled, seroprevalence rates were 5.8% (60/1,019) for SLEV and 2.1% (21/1,019) for WNV. Neutralizing antibody titers were >20 for both viruses for 12 birds, which were thus considered to have multiple heterologous infections. Of the 12 sites sampled, birds were seropositive for SLEV at 9 sites, for WNV at 7, and for both viruses at 6 (Table 2, Figure 2).

The GLMM performed to analyze the associations between the sampling sites, avian species, and exposure to SLEV/WNV, showed that sampling site was a significant variable affecting seroprevalence of SLEV ($p = 5.87 \times 10^{-16}$ and WNV ($p = 0.0012$); seroprevalence for both viruses was highest at sites in the northern area (Figures 1, 2). However, bird species did not significantly influence seroprevalence of SLEV ($p = 0.50$) or WNV ($p = 0.72$).

Birds of 17 species were seropositive for SLEV and of 8 species for WNV. Species most exposed to SLEV were house wrens (*Troglodytes aedon*), chalk-browed mockingbirds (*Mimus saturninus*), monk parakeets (*Myiopsitta monachus*), eared doves, and house sparrows (Table 3), whereas those most exposed to WNV were monk parakeets, rufous horneros, and grayish baywings. We found no significant statistical difference between the viruses among seropositive birds of different species, except for house sparrows ($p = 0.0004$).

The best model explaining the variation in SLEV seroprevalence included the agricultural area as an explanatory variable ($w_i = 0.44$; Table 4). SLEV

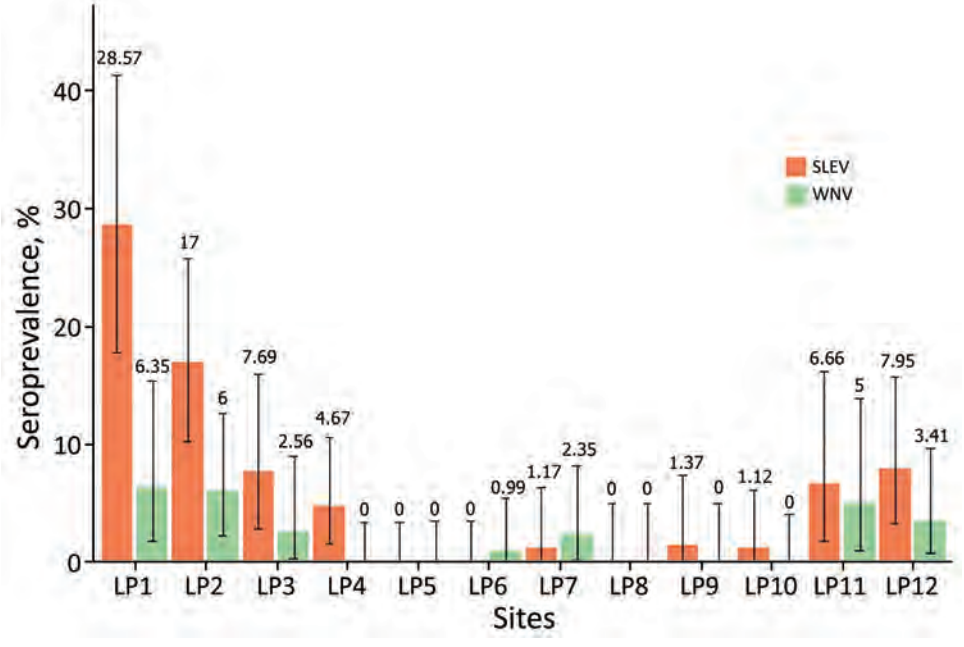

Figure 2. Spatial distribution of the seroprevalence of neutralizing antibodies for St. Louis encephalitis virus (SLEV) and West Nile (WNV) virus in free-ranging birds collected in 12 sampling sites in La Pampa province, Argentina (see Figure 1). Numbers above bars indicate specific seroprevalence for each site; error bars indicate 95% CIs. LP, La Pampa; SLEV, Saint Louis encephalitis virus; WNV, West Nile virus.

seroprevalence increased with agricultural area (Table 5). Odds ratio for this model was 1.97, which means that for each unit of increase in agricultural area size, SLEV seroprevalence increased an average of 1.97 times. The model that best explained the variation in WNV seroprevalence included the distance to the nearest water body and agricultural area as explanatory variables (w_i = 0.37; Table 6), but neither of the 2 variables was statistically significant to explain the variation in WNV seroprevalence because both 95% CIs included zero (Table 7).

Discussion

Our estimations of 6% SLEV and 2% WNV seroprevalence in avian hosts in agroecosystems of La Pampa Province are similar to those detected in and around Córdoba city, Argentina (SLEV 7.73%; WNV 1.47%) (*21*). Composition of biological communities in Córdoba are similar to those in this study.

The species of birds that were infected in the agroecosystems differed according to viruses studied and differed from those found infected by other research conducted in Argentina (*21*,*28*). In our

Table 3. SLEV/WNV species-specific seroprevalence in birds collected in different agroecosystems in study of effect of agroecosystems on seroprevalence of SLEV and WNV in birds, La Pampa Province, Argentina, 2017–2019*

Species	SLEV		WNV	
	No. pos./no. tested	% Positive (95% CI)†	No. pos./no. tested	% Positive (95% CI)†
House sparrow (*Passer domesticus*)	17/237	7.17 (4.23–11.23)	2/237	0.84 (0.10–3.01)
Rufous-collared sparrow (*Zonotrichia capensis*)	9/181	4.97 (2.29–9.23)	0/181	0 (0–2.02)
Rufous hornero (*Furnarius rufus*)	6/93	6.45 (2.40–13.51)	7/930	7.52 (3.08–14.89)
Picui ground dove (*Columbina picui*)	5/100	5 (1.64–11.28)	4/100	4 (1.10–9.92)
Grayish baywing (*Agelaioides badius*)	2/63	3.17 (0.38–11)	3/63	4.76 (0.99–13.29)
Monk parakeet (*Myiopsitta monachus*)	2/25	8 (0.98–26.03)	2/25	8 (0.98–26.03)
Eared dove (*Zenaida auriculata*)	2/26	7.69 (0.94–25.13)	1/26	3.84 (0.09–19.63)
Shiny cowbird (*Molothrus bonariensis*)	0/72	0 (0–4.99)	1/72	1.38 (0.03–7.49)
House wren (*Troglodytes aedon*)	6/63	9.52 (3.57–19.58)	0/63	0 (0–5.68)
Double-collared seedeater (*Sporophila caerulescens*)	1/19	5.26 (0.13–26.02)	0/19	0 (0–17.64)
Grassland yellow finch (*Sicalis luteola*)	1/20	5 (0.12–24.87)	0/20	0 (0–16.84)
Chalk-browed mockingbird (*Mimus saturninus*)	1/12	8.33 (0.21–38.47)	0/12	0 (0–26.46)
Tropical kingbird (*Tyrannus melancholicus*)‡	2/4	–	0/4	–
American kestrel (*Falco sparverius*)‡	2/4	–	0/4	–
Saffron finch (*Sicalis flaveola*)‡	1/6	–	0/6	–
Pale-breasted spinetail (*Synallaxis albescens*)‡	1/1	–	0/1	–
White-winged black tyrant (*Knipolegus aterrimus*)‡	1/1	–	1/1	–
Hudson´s black tyrant (*Knipolegus hudsoni*)‡	1/1	–	0/1	–
Grassland sparrow (*Ammodramus humeralis*)	0/5	–	0/5	–
Firewood-gatherer (*Anumbius annumbi*)	0/4	–	0/4	–
Sharp-billed canastero (*Asthenes pyrrholeuca*)	0/1	–	0/1	–
Hooded siskin (*Spinus magellanicus*)	0/1	–	0/1	–
Buff-winged cinclodes (*Cinclodes fuscus*)	0/1	–	0/1	–
Dark-billed cuckoo (*Coccyzus melacoryphus*)	0/3	–	0/3	–
Green-barred woodpecker (*Colaptes melanochloros*)	0/4	–	0/4	–
Rufous-browed peppershrike (*Cyclarhis gujanensis*)	0/1	–	0/1	–
White-crested elaenia (*Elaenia albiceps*)	0/1	–	0/1	–
Guira cuckoo (*Guira guira*)	0/1	–	0/1	–
Narrow-billed woodcreeper (*Lepidocolaptes angustirostris*)	0/3	–	0/3	–
Cattle tyrant (*Machetornis rixosa*)	0/4	–	0/4	–
Patagonian mockingbird (*Mimus patagonicus*)	0/1	–	0/1	–
White-banded mockingbird (*Mimus triurus*)	0/1	–	0/1	–
Screaming cowbird (*Molothrus rufoaxillaris*)	0/12	–	0/12	–
Spot-winged pigeon (*Patagioenas maculosa*)	0/2	–	0/2	–
Great kiskadee (*Pitangus sulphuratus*)	0/27	–	0/27	–
Brown cacholote (*Pseudoseisura lophotes*)	0/1	–	0/1	–
Vermilion flycatcher (*Pyrocephalus rubinus*)	0/8	–	0/8	–
Roadside hawk (*Rupornis magnirostris*)	0/1	–	0/1	–
Golden-billed saltator (*Saltator aurantiirostris*)	0/1	–	0/1	–
Greater wagtail-tyrant (*Stigmatura budytoides*)	0/1	–	0/1	–
Southern scrub-flycatcher (*Sublegatus modestus*)	0/3	–	0/3	–
Sooty-fronted spinetail (*Synallaxis frontalis*)	0/2	–	0/2	–
Chaco earthcreeper (*Tarphonomus certhioides*)	0/1	–	0/1	–
Blue-crowned parakeet (*Thectocercus acuticaudatus*)	0/1	–	0/1	–

*Dashes indicate that seroprevalence was not estimated because of the small number of serum samples tested for birds of that species. SLEV, St. Louis encephalitis virus; WNV, West Nile virus.
†Prevalence (%) defined as the no. positives divided by total samples multiplied by 100.
‡For seropositive species with <10 birds, seroprevalence was not calculated.

Table 4. Models for SLEV seroprevalence based on the generated hypotheses ranked by their AIC scores in study of effect of agroecosystems on seroprevalence of SLEV and WNV in birds, La Pampa, Argentina, 2017–2019*

Model	Variables of the model	*k*	AICc	ΔAICc	w_i
GLMM3	Agricultural area	3	388.819	0.000	0.441
GLMM8	Distance to water body + agricultural area	4	390.198	1.379	0.221
GLMM7	Agricultural area + dove abundance	4	390.244	1.425	0.216
GLMM5	Dove abundance	3	391.421	2.602	0.120
GLMM2	Distance to water body	3	401.845	13.026	0.001
GLMM1	Null model	2	408.710	19.892	0.000
GLMM6	Sparrow abundance	3	410.216	21.397	0.000
GLMM4	Distance to urban site	3	410.465	21.647	0.000

*AICc, Akaike information criterion corrected for small samples; ΔAICc, difference between AICc and the AICc from all other models; *k*, number of estimated parameters; SLEV, St. Louis encephalitis virus; w_i, relative likelihood that the specific model is the best of the suite of all models; WNV, West Nile virus.

study, the species of birds most infected with SLEV belonged to the families Troglodytidae (house wrens), Mimidae (chalk-browed mockingbirds), and Passeridae (house sparrows), although in other studies of similar characteristics and conducted in temperate and subtropical regions of Argentina, the species most infected with this virus belonged to the families Columbidae, Furnariidae, Icteridae, and Tyrannidae (*21*,*28*). For WNV, the most infected birds in our study were rufous horneros, which had already been highlighted as maintenance hosts for WNV in central Argentina (*21*), and monk parakeets, for which WNV infection had not been detected in other studies. One of the main amplifying hosts for SLEV in the United States and for WNV in Europe is the house sparrow (*29*,*30*). In previous studies conducted in the northeastern region of Argentina, SLEV seropositivity was not detected in >200 serum samples collected from house sparrows (*28*). Moreover, in urbanized temperate areas of the central region of Argentina, such as Córdoba, seroprevalence rates for house sparrows have been low for both viruses (3.92% for SLEV, 1.96% for WNV) (*21*). Furthermore, although the host competence index value for house sparrows is low (*7*), their high abundance and high exposure to SLEV observed in our study would indicate an efficient role as amplifying hosts for SLEV in agricultural areas of La Pampa Province. A possible explanation for the differences observed among the exposed bird species of and between disturbed environments (agricultural and urban) could be the presence of different vector mosquito species for the viruses evaluated with different host-feeding preferences. Changes in land use could also modify the host-seeking behavior of mosquitoes affecting avian host exposure to vectored viruses (*31*).

Although seroprevalence values in our study were low, seropositive bird species are resident and seropositive birds were detected during the 3 years sampled. This finding probably indicates endemic circulation for both viruses in this region of Argentina. Previous study of SLEV and WNV activities recorded in Pampean agricultural systems also showed low levels of exposure but in a particular group of birds, the birds of prey (*32*).

In our study, SLEV seroprevalence was positively associated with the agricultural area, and thus, inversely correlated by tree cover. In other studies, contrary to our results, SLEV infection in humans has been positively associated with proximity to areas with highly productive vegetation cover estimated by the Normalized Difference Vegetation Index (*33*,*34*), low density urban construction, and the distance to agricultural fields (*34*). These differences could be explained because the variables of interest differ (SLEV infections in humans vs. seroprevalence among birds) and the explanatory variables were also considered differently. In our study, we considered the area occupied by agricultural activities and tree coverage within a buffer of interest; in the other studies, researchers considered the distances between cases of SLEV infection in humans and the environmental variables. In turn, the differences found could also result from the fact that the tree coverage in our study area is mostly characterized by planted nonnative tree

Table 5. Parameter data for explanatory variables describing variation in SLEV seroprevalence with ΔAICc <2 in study of effect of agroecosystems on seroprevalence of SLEV and WNV in birds, La Pampa, Argentina, 2017–2019*

Explanatory variable	Parameter likelihood	Parameter estimate ± SE	95% CI
Intercept		**–3.79 ± 1.10**	**–5.96 to 1.61**
Agricultural area	**1.00**	**0.68 ± 0.22**	**0.23 to 1.13**
Distance to water body	0.25	−0.18 ± 0.22	−0.63 to 0.27
Dove abundance	0.25	−0.87 ± 1.43	−3.68 to 1.94

*Boldface indicates explanatory variables with 95% CIs excluding zero. ΔAICc, difference between the lowest Akaike information criterion corrected for small samples (AICc) and the AICc from all other models; SLEV, St. Louis encephalitis virus; WNV, West Nile virus..

Table 6. Models for WNV seroprevalence based on the generated hypotheses ranked by their Akaike information criterion scores in study of effect of agroecosystems on seroprevalence of SLEV and WNV in birds, La Pampa, Argentina, 2017–2019*

Model	Variables of the model	*k*	AICc	ΔAICc	w_i
GLMM16	Distance to water body + agricultural area	4	202.760	0.000	0.3762
GLMM11	Agricultural area	3	202.903	0.143	0.34637
GLMM15	Agricultural area + dove abundance	4	204.134	1.374	0.1872
GLMM9	Null model	2	207.459	4.699	0.035
GLMM13	Dove abundance	3	209.011	6.252	0.0156
GLMM10	Distance to water body	3	209.227	6.468	0.014
GLMM12	Distance to urban site	3	209.237	6.478	0.0154
GLMM14	Sparrow abundance	3	209.367	6.607	0.0143

*ΔAICc, difference between the lowest Akaike information criterion corrected for small samples (AICc) and the AICc from all other models; SLEV, St. Louis encephalitis virus; WNV, West Nile virus.

woodlots, which are inherently different from the green spaces or patches of native forest that characterized the vegetation in other studies.

The model that best explained the variation in WNV seroprevalence included the distance to the nearest water body and agricultural area as explanatory variables, but neither of the 2 variables explained the variation in WNV seroprevalence with statistical significance. Land use effect on WNV activity has been extensively studied, at least in the United States (*35*–*41*). Studies have shown that the abundance and distribution patterns of the mosquito vector are key factors in determining virus activity; and these, in turn, are greatly affected by land use. For example, in the northeastern United States, where the main vectors are *Cx. pipiens* and *Cx. quinquefasciatus* mosquitoes, urbanization positively affects the incidence of WNV disease in humans (*35*), whereas on the west coast of the United States, where the most efficient vectors are *Cx. tarsalis* mosquitoes, the main land cover types associated with increased WNV activity are agricultural irrigated areas, such as rice fields and orchards (*40*).

Anthropogenic activities are among the most influential factors affecting emergence of infectious diseases, particularly viral vectorborne zoonoses. Viruses carried by *Aedes* mosquitoes (e.g., chikungunya, dengue, and Zika viruses) are positively affected by urbanization as the main breeding substrates of *Ae. aegypti* and *Ae. albopictus* mosquito vectors, which become highly abundant in those anthropogenic and urban habits (*42*,*43*). However, for viruses carried by *Culex* mosquitoes (e.g., Japanese encephalitis virus, WNV, SLEV, and Usutu virus), how anthropogenic changes affect virus activity is not well known. The generalist host-feeding and host-seeking behavior and wide tolerance for rearing sites of the *Culex* mosquito vectors make it difficult to determine the effect of land use on the activity of *Culex* mosquitoborne viruses.

Our findings suggest that modified ecosystems, such as agroecosystems in La Pampa Province, have the environmental and biological factors necessary for maintaining and amplifying re-emerging viruses such as SLEV and WNV. However, our study did not analyze the change in land use but rather focused on how the current elements of the already modified landscape influence biological communities and, consequently, SLEV and WNV activity. The sites considered in this study were limited, and the environmental characterization was conducted extensively without taking into account, for example, the identity of the crops or pastures within the agricultural areas. Furthermore, because the seroprevalence data for birds do not necessarily reflect the place or the time in which they were infected, this information should be used with caution and complemented with studies on viral activity in the mosquito communities that ensures circulation of the virus at a certain time and place. Although further research on the ecology and biology of these viruses is needed to determine how crop production, monoculture areas, and associated landscapes affect vector transmission dynamics of these viruses, we conclude that the Pampean agroecosystems in Argentina affect SLEV seroprevalence among avian hosts, providing evidence of the effect of land use on the activity of arboviruses.

Table 7. Parameter data for explanatory variables describing variation in WNV seroprevalence with ΔAICc <2 in study of effect of agroecosystems on seroprevalence of SLEV and WNV in birds, La Pampa, Argentina, 2017–2019*

Explanatory variable	Parameter likelihood	Parameter estimate ± SE	95% CI
Intercept		**−4.23 ± 0.53**	**−5.28 to −3.17**
Agricultural area	1.00	1.07 ± 0.61	−0.19 to 2.34
Distance to water body	0.41	0.65 ± 0.50	−0.32 to 1.64
Dove abundance	0.21	0.35 ± 0.36	−0.36 to1.07

*Boldface indicates explanatory variables with 95% CIs excluding zero. ΔAICc, difference between the lowest Akaike information criterion corrected for small samples (AICc) and the AICc from all other models. SLEV, St. Louis encephalitis virus; WNV, West Nile virus.

Acknowledgments

We thank Luis Alberto Mansilla, Lucas Gelid, Giovana Peralta, Diego Gallego, Aitué Farana, Milagros Mansilla, Iara Mansilla, Ana Lia Arias, Mikel Larrea, Amaia Frade, Haizea Otaola, and Ibai Alcelay for their invaluable assistance in the field work as well as the private properties owners who allowed us access to their lands. We thank Brenda Konigheim, Javier Aguilar, and Romina Gallardo for their technical support with cell cultures. We also thank Cindy Kemper who kindly reviewed the manuscript.

This research received funding from Ministerio Nacional de Ciencia y Tecnología de Argentina (PICT 2016-3283, PICT 2018-1172), Consejo Nacional de Investigaciones Científicas y Técnicas (CONICET-PUE IIBYT 2017), and Secretaría de Ciencia y Tecnología–Universidad Nacional de Córdoba (SECyT-UNC). A.P.M. holds a doctoral scholarship from Consejo Nacional de Investigaciones Científicas y Técnicas.

About the Author

Ms. Mansilla is a PhD student at Colaboratorio de Biodiversidad, Ecología y Conservación), INCITAP-CONICET/FCEyN-UNLPam, La Pampa, Argentina. Her research interests include ecology of viral zoonoses and biological interactions among vectors, hosts, and viruses.

References

1. Morens DM, Folkers GK, Fauci AS. The challenge of emerging and re-emerging infectious diseases. Nature. 2004;430:242–9. https://doi.org/10.1038/nature02759
2. Gould E, Pettersson J, Higgs S, Charrel R, de Lamballerie X. Emerging arboviruses: Why today? One Health. 2017;4:1–13. https://doi.org/10.1016/j.onehlt.2017.06.001
3. Venkat H, Krow-Lucal E, Hennessey M, Jones J, Adams L, Fischer M, et al. Concurrent outbreaks of St. Louis encephalitis virus and West Nile virus disease—Arizona, 2015. MMWR Morb Mortal Wkly Rep. 2015;64:1349–50.
4. White GS, Symmes K, Sun P, Fang Y, Garcia S, Steiner C, et al. Reemergence of St. Louis encephalitis virus, California, 2015. Emerg Infect Dis. 2016;22:2185–8. https://doi.org/10.3201/eid2212.160805
5. Diaz A, Coffey LL, Burkett-Cadena N, Day JF. Reemergence of St. Louis encephalitis virus in the Americas. Emerg Infect Dis. 2018;24:2150–7. https://doi.org/10.3201/eid2412.180372
6. Beranek MD, Quaglia AI, Peralta GC, Flores FS, Stein M, Diaz LA, et al. *Culex interfor* and *Culex saltanensis* (Diptera: Culicidae) are susceptible and competent to transmit St. Louis encephalitis virus (*Flavivirus*: Flaviviridae) in central Argentina. Trans R Soc Trop Med Hyg. 2020;114:725–9. https://doi.org/10.1093/trstmh/traa058
7. Díaz A, Flores FS, Quaglia AI, Contigiani MS. Evaluation of Argentinean bird species as amplifying hosts for St. Louis encephalitis virus (Flavivirus, Flaviviridae). Am J Trop Med Hyg. 2018;99:216–21. https://doi.org/10.4269/ajtmh.17-0856
8. Hayes EB, Komar N, Nasci RS, Montgomery SP, O'Leary DR, Campbell GL. Epidemiology and transmission dynamics of West Nile virus disease. Emerg Infect Dis. 2005;11:1167–73. https://doi.org/10.3201/eid1108.050289a
9. Morales MA, Barrandeguy M, Fabbri C, Garcia JB, Vissani A, Trono K, et al. West Nile virus isolation from equines in Argentina, 2006. Emerg Infect Dis. 2006;12:1559–61. https://doi.org/10.3201/eid1210.060852
10. Adrián Diaz L, Komar N, Visintin A, Dantur Juri MJ, Stein M, Lobo Allende R, et al. West Nile virus in birds, Argentina. Emerg Infect Dis. 2008;14:689–91. https://doi.org/10.3201/eid1404.071257
11. Giayetto O, Beranek MD, Nazar FN, Diaz A. Dose dependence of susceptibility and transmission for an Argentinean West Nile virus strain in local *Culex pipiens quinquefasciatus* (Diptera: Culicidae). Trans R Soc Trop Med Hyg. 2021;115:1066–9. https://doi.org/10.1093/trstmh/traa185
12. Diaz A, Flores FS, Contigiani MS. Viremia profiles and host competence index for West Nile virus (*Flavivirus*, Flaviviridae) in three autochthonous birds species from Argentina. J Ornithol. 2011;152:21–5. https://doi.org/10.1007/s10336-010-0538-4
13. Gottdenker NL, Streicker DG, Faust CL, Carroll CR. Anthropogenic land use change and infectious diseases: a review of the evidence. EcoHealth. 2014;11:619–32. https://doi.org/10.1007/s10393-014-0941-z
14. Bilenca D, Codesido M, González Fischer C. Change in the Pampean Fauna [in Spanish]. Ciencia Hoy. 2008;18:8–17.
15. Codesido M, Zufiaurre E, Bilenca D. Relationship between pest birds and landscape elements in the Pampas of Central Argentina. Emu. 2015;115:80–4. https://doi.org/10.1071/MU13110
16. Oyarzabal M, Clavijo J, Oakley L, Biganzoli F, Tognetti P, Barberis I, et al. Unidades de vegetación de la Argentina. Ecol Austral. 2018;28:40–63. https://doi.org/10.25260/EA.18.28.1.0.399
17. Stella CA, Pall JL, Bernardos J. True bugs (Hemiptera: Heteroptera) associated with soybean (*Glycine max* (L.) Merr.) in southern cone. Munis Entomol Zool. 2017;12:380–8.
18. Cano E, Casagrande G, Conti H, Salazar Lea Plaza J, Peña Zubiarte C, Maldonado Pinedo D, et al. Integrated inventory of the natural resources of the province of La Pampa. Climate, geomorphology, soil and vegetation [in Spanish]. Buenos Aires, Argentina: National University of La Pampa, National Institute of Agricultural Technology; 1980.
19. Narosky T, Yzurieta D. Birds of Argentina & Uruguay: a field guide total edition [in Spanish]. 16th ed. Buenos Aires, Argentina: Vazquez Mazzini Editors; 2010.
20. Diaz A, Ré V, Almirón WR, Farías A, Vázquez A, Sanchez-seco MP, et al. Genotype III SLEV outbreak, Argentina, 2005. Emerg Infect Dis. 2006;12:2005–7. https://doi.org/10.3201/eid1211.060486
21. Diaz LA, Quaglia AI, Konigheim BS, Boris AS, Aguilar JJ, Komar N, et al. Activity patterns of St. Louis encephalitis and West Nile viruses in free ranging birds during a human encephalitis outbreak in Argentina. PLoS One. 2016;11:e0161871. https://doi.org/10.1371/journal.pone.0161871
22. Patiris PJ, Oceguera LF III, Peck GW, Chiles RE, Reisen WK, Hanson CV. Serologic diagnosis of West Nile and St. Louis encephalitis virus infections in domestic chickens. Am J Trop Med Hyg. 2008;78:434–41. https://doi.org/10.4269/ajtmh.2008.78.434
23. Ledermann JP, Lorono-Pino MA, Ellis C, Saxton-Shaw KD, Blitvich BJ, Beaty BJ, et al. Evaluation of widely used diagnostic tests to detect West Nile virus infections in horses previously infected with St. Louis encephalitis virus or

dengue virus type 2. Clin Vaccine Immunol. 2011;18:580–7. https://doi.org/10.1128/CVI.00201-10
24. Medeiros MCI, Boothe EC, Roark EB, Hamer GL. Dispersal of male and female *Culex quinquefasciatus* and *Aedes albopictus* mosquitoes using stable isotope enrichment. PLoS Negl Trop Dis. 2017;11:e0005347. https://doi.org/10.1371/journal.pntd.0005347
25. Bibby C, Jones M, Marsden S. Expedition field techniques: bird surveys. London: Royal Geographical Society; 1998.
26. Dorai-Raj S. binom: Binomial confidence intervals for several parameterizations. R package version 1.1–1 [cited 2021 Nov 3]. https://cran.r-project.org/web/packages/binom/binom.pdf
27. Burnham KP, Anderson DR. Model selection and multimodel inference: a practical information-theoretic approach. 2nd ed. Ecological Modelling. New York: Springer; 2002.
28. Monath TP, Sabattini MS, Pauli R, Daffner JF, Mitchell CJ, Bowen GS, et al. Arbovirus investigations in Argentina, 1977-1980. IV. Serologic surveys and sentinel equine program. Am J Trop Med Hyg. 1985;34:966–75. https://doi.org/10.4269/ajtmh.1985.34.966
29. Reisen WK. Epidemiology of St. Louis encephalitis virus. Adv Virus Res. 2003;61:139–83. https://doi.org/10.1016/S0065-3527(03)61004-3
30. Del Amo J, Llorente F, Figuerola J, Soriguer RC, Moreno AM, Cordioli P, et al. Experimental infection of house sparrows (*Passer domesticus*) with West Nile virus isolates of Euro-Mediterranean and North American origins. Vet Res (Faisalabad). 2014;45:33. https://doi.org/10.1186/1297-9716-45-33
31. Zahouli JBZ, Koudou BG, Müller P, Malone D, Tano Y, Utzinger J. Effect of land-use changes on the abundance, distribution, and host-seeking behavior of *Aedes* arbovirus vectors in oil palm-dominated landscapes, southeastern Côte d'Ivoire. PLoS One. 2017;12:e0189082. https://doi.org/10.1371/journal.pone.0189082
32. Mansilla AP, Solaro C, Orozco-Valor PM, Grande JM, Sarasola JH, Diaz A. Exposure of raptors in central Argentina to St. Louis encephalitis and West Nile viruses. J Raptor Res. 2020;54:279–86. https://doi.org/10.3356/0892-1016-54.3.279
33. Rotela CH, Spinsanti LI, Lamfri MA, Contigiani MS, Almirón WR, Scavuzzo CM. Mapping environmental susceptibility to Saint Louis encephalitis virus, based on a decision tree model of remotely-sensed data. Geospat Health. 2011;6:85–94. https://doi.org/10.4081/gh.2011.160
34. Vergara Cid C, Estallo EL, Almirón WR, Contigiani MS, Spinsanti LI. Landscape determinants of Saint Louis encephalitis human infections in Córdoba city, Argentina during 2010. Acta Trop. 2013;125:303–8. https://doi.org/10.1016/j.actatropica.2012.12.005
35. Bowden SE, Magori K, Drake JM. Regional differences in the association between land cover and West Nile virus disease incidence in humans in the United States. Am J Trop Med Hyg. 2011;84:234–8. https://doi.org/10.4269/ajtmh.2011.10-0134
36. Bradley CA, Gibbs SEJ, Altizer S. Urban land use predicts West Nile virus exposure in songbirds. Ecol Appl. 2008;18:1083–92. https://doi.org/10.1890/07-0822.1
37. Brown HE, Childs JE, Diuk-Wasser MA, Fish D. Ecological factors associated with West Nile virus transmission, northeastern United States. Emerg Infect Dis. 2008;14:1539–45. https://doi.org/10.3201/eid1410.071396
38. Chuang TW, Hockett CW, Kightlinger L, Wimberly MC. Landscape-level spatial patterns of West Nile virus risk in the northern Great Plains. Am J Trop Med Hyg. 2012;86:724–31. https://doi.org/10.4269/ajtmh.2012.11-0515
39. Ezenwa VO, Milheim LE, Coffey MF, Godsey MS, King RJ, Guptill SC. Land cover variation and West Nile virus prevalence: patterns, processes, and implications for disease control. Vector Borne Zoonotic Dis. 2007;7:173–80. https://doi.org/10.1089/vbz.2006.0584
40. Kovach TJ, Kilpatrick AM. Increased human incidence of West Nile virus disease near rice fields in California but not in southern United States. Am J Trop Med Hyg. 2018;99:222–8. https://doi.org/10.4269/ajtmh.18-0120
41. Miramontes R Jr, Lafferty WE, Lind BK, Oberle MW. Is agricultural activity linked to the incidence of human West Nile virus? Am J Prev Med. 2006;30:160–3. https://doi.org/10.1016/j.amepre.2005.10.008
42. Wilke ABB, Chase C, Vasquez C, Carvajal A, Medina J, Petrie WD, et al. Urbanization creates diverse aquatic habitats for immature mosquitoes in urban areas. Sci Rep. 2019;9:15335. https://doi.org/10.1038/s41598-019-51787-5
43. Zahouli JBZ, Koudou BG, Müller P, Malone D, Tano Y, Utzinger J. Urbanization is a main driver for the larval ecology of *Aedes* mosquitoes in arbovirus-endemic settings in south-eastern Côte d'Ivoire. PLoS Negl Trop Dis. 2017;11:e0005751. https://doi.org/10.1371/journal.pntd.0005751

Address for correspondence: Adrián Diaz, Instituto de Virología "Dr. J. M. Vanella," Laboratorio de Arbovirus, Facultad de Ciencias Médicas, Universidad Nacional de Córdoba, Enfermera Gordillo Gómez s/n, CPX5016GCA, Córdoba, Argentina; email: adrian.diaz@conicet.gov.ar, adrian.diaz@fcm.unc.edu.ar

Targeted Screening for Chronic Q Fever, the Netherlands

Daphne F.M. Reukers, Pieter T. de Boer, Alfons O. Loohuis, Peter C. Wever, Chantal P. Bleeker-Rovers, Arianne B. van Gageldonk-Lafeber, Wim van der Hoek, Aura Timen

Early detection of and treatment for chronic Q fever might prevent potentially life-threatening complications. We performed a chronic Q fever screening program in general practitioner practices in the Netherlands 10 years after a large Q fever outbreak. Thirteen general practitioner practices located in outbreak areas selected 3,419 patients who had specific underlying medical conditions, of whom 1,642 (48%) participated. Immunofluorescence assay of serum showed that 289 (18%) of 1,642 participants had a previous *Coxiella burnetii* infection (IgG II titer ≥1:64), and 9 patients were suspected of having chronic Q fever (IgG I y titer ≥1:512). After medical evaluation, 4 of those patients received a chronic Q fever diagnosis. The cost of screening was higher than estimated earlier, but the program was still cost-effective in certain high risk groups. Years after a large Q fever outbreak, targeted screening still detected patients with chronic Q fever and is estimated to be cost-effective.

Approximately 2% of patients with symptomatic or asymptomatic *Coxiella burnetii* infections show development of chronic Q fever (*1*). Chronic Q fever can manifest itself even years after the initial infection, mainly as endocarditis or vascular infection. The main risk factors for development of chronic Q fever are heart valve disorders, aortic aneurysms, vascular prosthesis, or an immunocompromised state. Chronic Q fever can cause potentially life-threatening complications and has a high mortality rate (*2*). Therefore, timely detection and treatment for patients who have chronic infections are essential.

Author affiliations: National Institute for Public Health and the Environment, Bilthoven, the Netherlands (D.F.M. Reukers, P.T. de Boer, A.B. van Gageldonk-Lafeber, W. van der Hoek, A. Timen); Q-Support Foundation, 's-Hertogenbosch, the Netherlands (A.O. Loohuis); Radboud University Medical Center, Nijmegen, the Netherlands (A.O. Loohuis, C.P. Bleeker-Rovers); Jeroen Bosch Hospital, 's-Hertogenbosch (P.C. Wever); Vrije Universiteit, Amsterdam (A. Timen)

DOI: https://doi.org/10.3201/eid2807.212273

A large Q fever outbreak that occurred in the Netherlands during 2007–2010 had >4,000 reported acute Q fever cases in humans and an estimated total number of 50,000 *C. burnetii* infections, mostly originating from dairy goat farms that experienced Q fever–induced abortion waves (*3*). In the years after the outbreak, several hospitals in the most affected regions undertook small screening studies in specific risk groups for early detection of chronic Q fever (*4*–*7*). These studies showed that there were still undiagnosed chronic Q fever patients in these risk groups. Identifying these undiagnosed patients can provide major health benefits by reducing complications and deaths. A recent model-based study from the Netherlands estimated that targeted screening of patients who had risk factors in regions that had previous outbreaks, was cost-effective (*8*). After a strong appeal from Q fever patients and the involved physicians, a screening program was launched in the Netherlands 10 years after the Q fever outbreak.

This one-time targeted chronic Q fever screening program was implemented in general practitioner practices because of 3 factors. First, because these practices have smaller catchment areas, regions with previous outbreaks can be demarcated in more detail. Second, because these practices in the Netherlands have complete and up-to-date electronic files of their patients, all target groups can directly be selected without the need for patient files from different hospitals and medical specialists. Third, patients in the Netherlands have their regular check-ups often with their general practitioner after receiving specialist care. We report results from the early phase of this screening program and provide an update of the previously conducted cost-effectiveness analysis.

Methods

Patient Selection

A chronic Q fever screening program began during 2019 in general practitioner practices located in various high-risk areas (incidence >50 acute Q

fever cases/100,000 persons or near a farm that had Q fever–induced abortion waves during the outbreak of 2007–2010) across the Netherlands. Medical risk factors for chronic Q fever after acute infection are well described (*9*), and a list of International Classification of Primary Care (ICPC) codes was compiled with consensus from different experts (Table 1). Furthermore, although studies have shown that male patients have a higher risk for *C. burnetii* cardiovascular infection, we undertook the screening in both male and female patients because of ethics considerations (*10*,*11*).

A standard general practice that had 1 general practitioner in the Netherlands had on average 2,095 patients, and it was estimated that applying the selection list of ICPC codes would yield ≈80 high-risk patients/standard practice. Participating general practitioner practices (1 practice might have several general practitioners) selected patients eligible for screening with the selected ICPC codes (Table 1). These patients received information about chronic Q fever screening and were invited to visit a nearby center to provide a blood serum sample, either at the general practitioner practice or at a local blood drawing location in the residential area. A trusted third party was hired to support the general practitioners with sending out the invitations.

Diagnostics

All samples were tested by laboratory technicians at Jeroen Bosch Hospital ('s Hertogenbosch, the Netherlands), who used an immunofluorescence assay (IFA) to detect antibodies against *C. burnetii*. An IgG II titer ≥1:64 was considered evidence of a past *C. burnetii* infection, and an IgG I titer ≥1:512 was considered a positive screening test result for suspected chronic Q fever. We sent serologic results to the general practitioner, who would refer patients to a clinical center that had expertise in chronic Q fever in case of a positive screening test result. In these centers, a definite diagnosis was based on follow-up testing, medical examination, and radiologic imaging findings (transthoracic echocardiography or a positron emission tomography scan) according to the Netherlands consensus guidelines on chronic Q fever diagnostics (*9*). This guideline classifies the probability of having chronic Q fever as proven, probable, and possible. One of the criteria in these guidelines is an IFA titer ≥1:1,024 for IgG against *C. burnetii* phase I.

Statistical and Cost-Effectiveness Analysis

We compiled patient characteristics and antibody test results with descriptive statistics. We calculated seroprevalence per general practitioner, as well as the number and percentage of suspected chronic Q fever patients per general practitioner. Previously, a health-economic decision model was developed to estimate the cost-effectiveness of the screening program (*8*). Results collected in our study were used to update the cost-effectiveness analysis. This use concerned the seroprevalence rate (i.e., prevalence of past *C. burnetii* infections), the proportion of seropositive patients receiving a definite diagnosis of chronic Q fever by risk group (cardiovascular or immune-related), and the screening costs per patient. The previous cost-effectiveness analysis envisaged a hospital-based screening program implemented in routine care by using a 2-step testing scheme, first with the ELISA, followed by the IFA test if the test result was positive. The rationale behind analysis was that the ELISA is an automated test available in any hospital, but the IFA is only conducted in a few specialized hospital laboratories. However, as mentioned, the actual screening program was implemented in general practitioner practices, and patients were directly tested by using the IFA because this test is considered to be the reference test, given its higher sensitivity.

Results

Participants

A total of 13 general practitioner practices located in regions that had a high incidence of Q fever during the outbreak or a location near an infected goat farm participated in the study (Figure 1) during

Table 1. ICPC codes used for the selection of patients to be invited for participation in the chronic Q fever screening program, the Netherlands*

ICPC code	Description
K99.01	Aortic aneurysm
K83	Nonrheumatic valve disease
K73	Congenital malformation(s) of the cardiovascular system
K71	Acute rheumatism/rheumatic heart disease
B73	Leukemia
B74	Other malignancy of the blood/lymphatic system
B90	HIV infection
D94	Ulcerative colitis/chronic enteritis (regionalis)
L04A	Use immunosuppressants (excluding corticosteroids) in the past 12 months

*ICPC, International Classification of Primary Care.

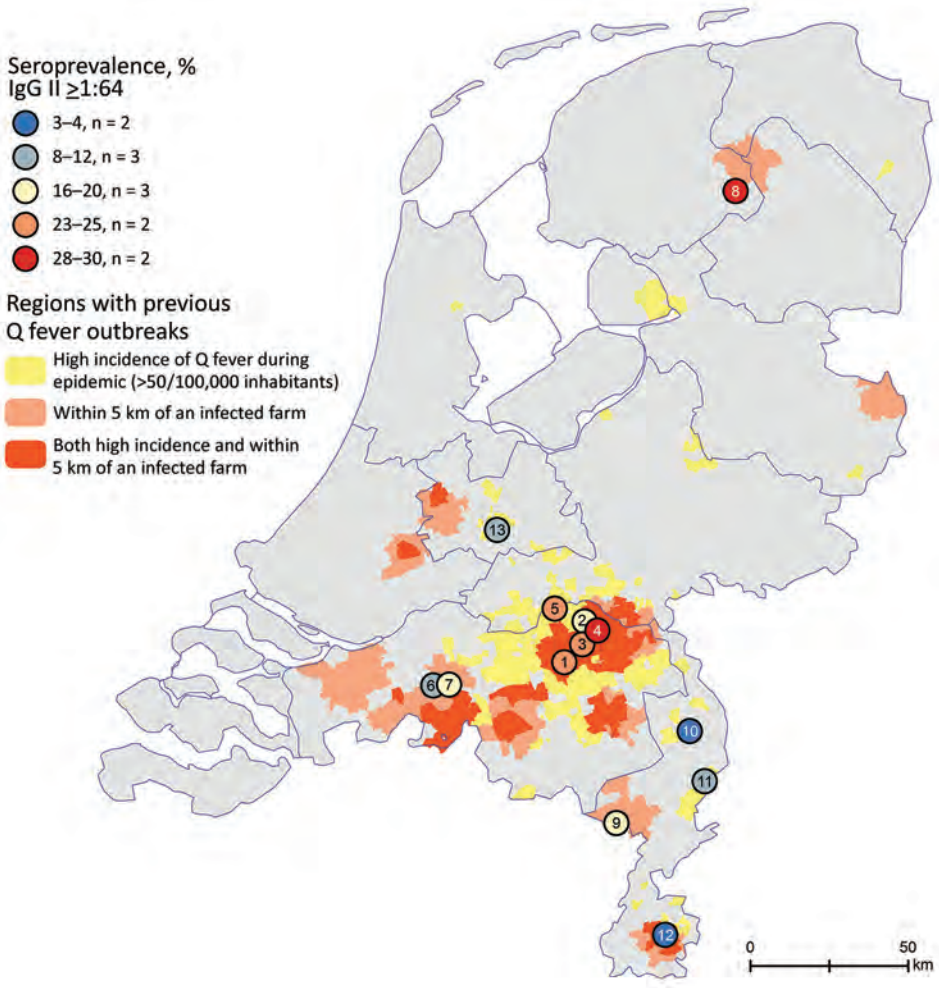

Figure 1. Locations of participating general practices (numbers in circles) in the Netherlands and seroprevalence rates for chronic Q fever measured in study of targeted screening program to detect chronic Q fever. Colors indicate areas with high incidence of acute Q fever patients or areas near an infected farm that had abortion waves during the outbreak of 2007–2010.

May 2019–December 2020. All general practitioner practices except 1 were located in the southern part of the Netherlands, where most Q fever cases were reported during the outbreak. The general practitioners invited 3,419 eligible patients, of whom 1,642 (48%) participated (Table 2). The largest practice invited 477 eligible patients, and the smallest practice invited 108 patients.

Seroprevalence

The average seroprevalence of IgG against phase II of *C. burnetii* was 18%. Seroprevalence between general practitioner practices ranged from 30% (48/160) at practice no. 4 in the Province of North-Brabant to 3% (4/147) in practice no. 10 in the province of Limburg (Table 1; Figure 1). A total of 4 general practitioner practices in the province of North-Brabant (nos. 1, 3–5), 1 general practitioner practice in the province of Friesland (no. 8), and 1 general practitioner practice in Limburg (no. 9) showed a seroprevalence rate ≥20%.

Suspected Chronic Q Fever

A total of 9 patients (0.6% of participating patients, 3.2% of patients with a past *C. burnetii* infection) showed an IgG I titer ≥1:512 and were suspected of having chronic Q fever. Six practices had ≥1 patient suspected of having chronic Q fever (46%), and 3 of these practices had 2 patients suspected of having chronic Q fever. One practice in the Province of Limburg (no. 9) (Table 2; Figure 1) had 2 patients suspected of having chronic Q fever, which was 7.1% of seropositive patients in that practice. Another practice in Limburg (no. 12) had only 2 patients who had a past infection with *C. burnetii*, of whom 1 patient was suspected of having chronic Q fever.

Patient Characteristics

We compiled patient characteristics for 3 groups: all participants, seropositive patients, and patients suspected of having chronic Q fever (Table 3). Patients suspected of having chronic Q fever were on average older and more often male than female. The most

Table 2. Results of a targeted screening program to detect chronic Q fever, the Netherlands*

GP practice†	Province	No. eligible patients‡	Study participants, no. (%)	Seroprevalence (IgG II titer ≥1:64), no. (%)	No. suspected of having chronic Q fever (IgG I titer ≥1:512)
1	NB	358	216 (60)	51 (24)	0
2	NB	250	108 (43)	18 (17)	0
3	NB	477	255 (53)	58 (23)	2
4	NB	267	160 (60)	48 (30)	2
5	NB	144	84 (58)	21 (25)	1
6	NB	381	183 (48)	22 (12)	1
7	NB	108	58 (54)	9 (16)	0
8	FR	124	40 (32)	11 (28)	0
9	LI	308	143 (46)	28 (20)	2
10	LI	376	147 (46)	4 (3)	0
11	LI	239	110 (46)	9 (8)	0
12	LI	134	53 (40)	2 (4)	1
13	UT	253	85 (34)	8 (9)	0
Total	NA	3,419	1,642 (48)	289 (18)	9

*GP, general practitioner; FR, Friesland; LI, Limburg; NA, not applicable; NB, North-Brabant; UT, Utrecht.
†Corresponding to numbers in Figure 1.
‡Eligible patients are patients who had increased risk for development of chronic Q fever after infection with *Coxiella burnetii* (see Table 1 for specified inclusion criteria).

common risk factor among the participants was heart valve disorder (28%); this group also had a relatively high percentage of seropositive patients (22%), but no patients who had this risk factor were found to be suspected of having chronic Q fever. Within the risk factor groups, vascular disorders (ICPC code K99.01) (Table 1) had the highest percentage of seropositive patients (25%) and also the highest number (n = 4) suspected of having chronic Q fever. Among patients with an immunocompromised state caused by medication (ICPC code L04A) (Table 1), 13% were seropositive, and 3 patients were suspected of having chronic Q fever.

Diagnosis

Of the 9 participants suspected of having chronic Q fever, 8 went to a Q fever expert center for further medical examination. Chronic Q fever was ruled out in 4 patients, and 4 received a diagnosis of chronic Q fever (3 with probable chronic Q fever and 1 with proven chronic Q fever). One of the patients who had probable chronic Q fever did not receive treatment. The proven chronic Q fever patient had a vascular prosthesis, and the 3 probable chronic Q fever patients had a valve disorder, a vascular prosthesis, and an immunocompromised state caused by medication.

Cost-effectiveness Analysis

We determined the relationship between prevalence of chronic Q fever and the incremental cost-effectiveness ratio (ICER) and how the use of new data on screening costs and prevalence of chronic Q fever affected the model results (Figure 2). Because of the implementation costs of a stand-alone program in general practitioner practices and higher laboratory costs (the IFA is considerably more expensive than the ELISA), the actual screening costs per patient was 8 times higher (from €7 to €56; Table 4) than in the initial cost-effectiveness analysis. The 8-fold higher screening costs per person shifts the ICER considerably upwards, implying that the screening program becomes less cost-effective. The prevalence of chronic Q fever in our study, which is based on the 4 diagnosed chronic Q fever patients, was approximately in

Table 3. Characteristics of all study participants, patients with a previous *Coxiella burnetii* infection, and patients suspected of having chronic Q fever, the Netherlands*

Characteristic	All participants, n = 1,642	Previous infection, IgG II titer ≥1:64, n = 289	Suspected of having chronic Q fever, IgG I titer ≥1:512, n = 9
Mean age, y	63	64	63
Age ≥60 y, % of total	66	65	78
Male sex, % of total	49	59	67
Risk factor, no.†			
Heart valve	460	103	0
Vascular	202	50	4
Other cardiovascular	105	20	1
Immunocompromised by illness	419	57	1
Immunocompromised by medication	445	59	3
Missing	135	18	0

*Corresponding International Classification of Primary Care codes for risk factor: heart valve, K83; vascular, K99.01; other cardiovascular, K73 and K71; immunocompromised by illness; B73, B74, B90, and D94; immunocompromised by medication, L04A.
†Some participants had multiple risk factors.

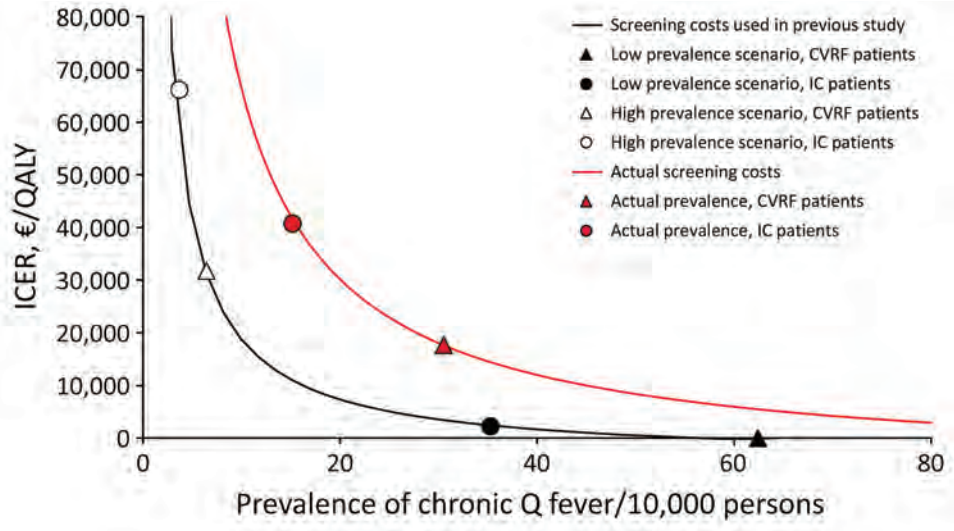

Figure 2. Relationship between the prevalence of chronic Q fever and incremental cost-effectiveness ratio of a screening program to detect chronic Q fever, the Netherlands, and screening costs for the program compared with a previously published analysis (*7*). Symbols on the line are based on a high-prevalence and low prevalence rate scenario as used in the previously published analysis and are based on actual prevalence rates found in this study. CVRF, cardiovascular risk factor; IC, immunocompromised; ICER, incremental cost-effectiveness ratio; QALY, quality-adjusted life year.

the middle of a low prevalence scenario and a high prevalence scenario considered in the previous cost-effectiveness analysis.

If one takes into account the actual screening costs and the prevalence rates, the ICER was estimated to be €17,643/quality-adjusted life year (QALY) gained for patients with a cardiovascular risk factor and €40,726/QALY gained for immunocompromised patients. Given that all detected chronic Q fever patients who had a cardiovascular risk factor were invited into the study because of a vascular or other cardiovascular disorder, the prevalence for this specific risk group was higher compared with that for all cardiovascular risk groups combined. When the analysis was stratified to vascular patients or other cardiovascular patients, screening became more cost-effective (ICER of €4,416/QALY gained).

Discussion

This study shows that, even a decade after a large Q fever outbreak, targeted screening in high-risk groups living in previously highly affected regions still detects undiagnosed chronic Q fever patients. The cost-effectiveness analysis before the screening program considered a low-prevalence and high-prevalence scenario, given the high uncertainty around this parameter at that time (*8*). The prevalence of chronic Q fever in our study was within this range. However, the screening costs per patient were considerably higher than earlier anticipated. Nevertheless, screening remained cost-effective in certain high-risk groups, when an often-used cost-effectiveness threshold for preventive measures in the Netherlands of €20,000/QALY gained is applied.

The implementation of this targeted screening program was more labor intensive than expected, thereby increasing the costs. Although all general practitioner practices have a complete and up-to-date electronic file and use the same ICPC classification system, the computer-generated list of high-risk patients still needs manual checking. Eventually, we decided to provide active support for the general practitioners from a trusted third party, which increased costs.

In half of the general practitioner practices, we found a seroprevalence of antibodies against phase II of *C. burnetii* ≥20%, and 1 practice reported a seroprevalence of 30%. Although participants are not randomly selected (most invited persons were elderly and the willingness to participate in the screening program might have been influenced by the considered risk for exposure), such a high prevalence of

Table 4. Screening cost per patient in targeted screening program to detect chronic Q fever, the Netherlands, compared with previous cost-effectiveness analysis*

Item	Previous analysis	Actual
Diagnostic test	€7.26 (ELISA/IFA)	€25.00 (IFA)
Fee for trusted third party and general practitioner	NA	€24.36†
Logistics/coordination	NA	€4.30†
Start-up costs	NA	€2.69‡
Total	€7.26	€56.35

*Previous study in (*7*). IFA, immunofluorescence assay; NA, not applicable.
†With a participation rate of 50%.
‡Total start-up costs of €135,000 divided by a previously estimated 71,000 eligible high-risk patients living in areas that had a high incidence of Q fever during the outbreak.

person with evidence of a past infection is remarkable. Previous population-based studies from the southern region of the Netherlands found seroprevalences of 2%–14% (*12*). Particularly of interest was the high seroprevalence of 28% in a general practitioner practice located in the northern region of the Netherlands, where hardly any acute Q fever cases were reported during the outbreak in 2007–2010. These figures show the complex spatial–temporal dynamics in exposure, infection, and disease.

Our study's first limitation is that, of the 9 participants suspected of having chronic Q fever, only 4 received a definite diagnosis. Antibody titers might vary for patients (*13*), and the IFA is known to have a high measurement uncertainty. Also, half of the invited persons did not participate in the screening program, and it is unknown whether this factor led to missed chronic Q fever patients. The COVID-19 pandemic, which was ongoing at the time, might have played a role because attending health services for nonacute problems were discouraged.

Of the 4 chronic Q fever patients, 3 (75%) received a probable and 1 (25%) a proven diagnosis. In the previous cost-effectiveness analysis, we based the ratio of probable and proven chronic Q fever patients on the national chronic Q fever database (31% probable and 69% proven) (*14*). Because patients who have probable chronic Q fever have a lower risk for complications and death than patients who have proven chronic Q fever (*2*), using the ratio from our study would make the screening program less cost-effective than the ratio from the database. Other hospital-based screening studies among high-risk patients also found a relatively higher proportion of probable chronic Q fever patients than in the database (*5*,*7*). A potential explanation might be that some probable patients eventually progress into proven patients before they are given a diagnosis during regular care. Therefore, we maintained the use of the ratio from the database in the updated cost-effectiveness analysis because the number of patients detected in this first phase of the screening program is still limited and might be coincidental.

In a continuation of this screenings program, some suggestions for modification to improve its (cost-)effectiveness can be made. First, the ICPC code K83 (nonrheumatic valve disease) could potentially be omitted because this disease was the largest risk group in the program, but without any suspected chronic Q fever patient. This particular ICPC code comprises a heterogeneous group of heart valve disorders, and perhaps this code is not representative for those heart valve patients that are at increased risk for chronic Q fever, as found in a previous screening study (*7*). Another explanation could be that heart valve patients at increased risk for chronic Q fever might already be represented in the category of other cardiovascular disorders (K73 and K71) (Table 1) or have a combined vascular and heart valve disorder. Second, the high-risk regions could be tailored to smaller areas near goat farms that were affected by Q fever–induced abortion waves and where airborne transmission is likely to have occurred. In our study, seroprevalence and the number of suspected chronic Q fever patients differed considerably between regions, and general practitioner practices that had the highest seroprevalence and with ≥1 suspected chronic Q fever patient were near an infected farm (≤5 km). A previous study from the Netherlands also indicated that the seroprevalence of antibodies against *C. burnetii* is strongly correlated with proximity to a goat farm, but not with Q fever incidence during the outbreak (*12*).

Results of the present screening program were communicated to the Ministry of Health, which subsequently submitted a report on the state of affairs regarding Q fever to the Parliament of the Netherlands on September 29, 2021 (*15*). If the screening program would be continued, it should be better embedded in the regular general practitioner care by creating more awareness among general practitioners and their patients of the risks of chronic Q fever and the possibilities of selecting and screening high-risk patients through the general practitioner electronic records. The active support of a third party should not be necessary and general practitioners should be able to integrate this into their daily practice with a clear and concise instruction, which needs to include the lessons learned during the early phase of this program.

Acknowledgments

We thank the general practitioners for providing assistance in the participating practices, Ben Bom for compiling the map in Figure 1, and Ton Oomen and Jente Lange for providing coordination and communication with the Ministry of Health.

This study was supported by the Ministry of Health, Welfare and Sport of the Netherlands..

About the Author

Dr. Reukers is an epidemiologist at the National Institute for Public Health and the Environment, Bilthoven, the Netherlands. Her primary research interest is respiratory infectious diseases.

References

1. Maurin M, Raoult D. Q fever. Clin Microbiol Rev. 1999;12:518–53. https://doi.org/10.1128/CMR.12.4.518
2. van Roeden SE, Wever PC, Kampschreur LM, Gruteke P, van der Hoek W, Hoepelman AI, et al. Chronic Q fever-related complications and mortality: data from a nationwide cohort. Clin Microbiol Infect. 2019;25:1390–8. https://doi.org/10.1016/j.cmi.2018.11.023
3. van der Hoek W, Hogema BM, Dijkstra F, Rietveld A, Wijkmans CJ, Schneeberger PM, et al. Relation between Q fever notifications and *Coxiella burnetii* infections during the 2009 outbreak in The Netherlands. Euro Surveill. 2012;17:20058. https://doi.org/10.2807/ese.17.03.20058-en
4. Wever PC, Arts CH, Groot CA, Lestrade PJ, Koning OH, Renders NH. Screening for chronic Q fever in symptomatic patients with an aortic aneurysm or prosthesis [in Dutch]. Ned Tijdschr Geneeskd. 2010;154:A2122.
5. Kampschreur LM, Oosterheert JJ, Hoepelman AI, Lestrade PJ, Renders NH, Elsman P, et al. Prevalence of chronic Q fever in patients with a history of cardiac valve surgery in an area where *Coxiella burnetii* is epidemic. Clin Vaccine Immunol. 2012;19:1165–9. https://doi.org/10.1128/CVI.00185-12
6. Hagenaars JC, Wever PC, van Petersen AS, Lestrade PJ, de Jager-Leclercq MG, Hermans MH, et al. Estimated prevalence of chronic Q fever among *Coxiella burnetii* seropositive patients with an abdominal aortic/iliac aneurysm or aorto-iliac reconstruction after a large Dutch Q fever outbreak. J Infect. 2014;69:154–60. https://doi.org/10.1016/j.jinf.2014.03.009
7. de Lange MM, Scheepmaker A, van der Hoek W, Leclercq M, Schneeberger PM. Risk of chronic Q fever in patients with cardiac valvulopathy, seven years after a large epidemic in the Netherlands. PLoS One. 2019;14:e0221247. https://doi.org/10.1371/journal.pone.0221247
8. de Boer PT, de Lange MM, Wielders CC, Dijkstra F, van Roeden SE, Bleeker-Rovers CP, et al. Cost-effectiveness of screening program for chronic Q fever, the Netherlands. Emerg Infect Dis. 2020;26:238–46. https://doi.org/10.3201/eid2602.181772
9. Wegdam-Blans MC, Kampschreur LM, Delsing CE, Bleeker-Rovers CP, Sprong T, van Kasteren ME, et al.; Dutch Q fever Consensus Group. Chronic Q fever: review of the literature and a proposal of new diagnostic criteria. J Infect. 2012;64:247–59. https://doi.org/10.1016/j.jinf.2011.12.014
10. Melenotte C, Gay L, Mezouar S, Bardin N, Raoult D, Mège JL. The sexual dimorphism of anticardiolipin autoantibodies in acute Q fever patients. Clin Microbiol Infect. 2019;25:763.e1–3. https://doi.org/10.1016/j.cmi.2019.02.030
11. Melenotte C, Protopopescu C, Million M, Edouard S, Carrieri MP, Eldin C, et al. Clinical features and complications of *Coxiella burnetii* infections from the French National Reference Center for Q fever. JAMA Netw Open. 2018;1:e181580. https://doi.org/10.1001/jamanetworkopen.2018.1580
12. Pijnacker R, Reimerink J, Smit LA, van Gageldonk-Lafeber AB, Zock J-P, Borlée F, et al. Remarkable spatial variation in the seroprevalence of *Coxiella burnetii* after a large Q fever epidemic. BMC Infect Dis. 2017;17:725. https://doi.org/10.1186/s12879-017-2813-y
13. Buijs SB, van Roeden SE, van Werkhoven CH, Hoepelman AI, Wever PC, Bleeker-Rovers CP, et al. The prognostic value of serological titres for clinical outcomes during treatment and follow-up of patients with chronic Q fever. Clin Microbiol Infect. 2021;27:1273–8. https://doi.org/10.1016/j.cmi.2021.03.016
14. Buijs SB, Bleeker-Rovers CP, van Roeden SE, Kampschreur LM, Hoepelman AI, Wever PC, et al. Still new chronic Q fever cases diagnosed eight years after a large Q fever outbreak. Clin Infect Dis. 2021;73:1476–83. https://doi.org/10.1093/cid/ciab476
15. National Institute for Public Health and the Environment. Advisory letter for detection of chronic Q fever patients, 2021 [in Dutch] [cited 2021 Oct 1]. https://www.rijksoverheid.nl/documenten/publicaties/2021/09/15/adviesbrief-opsporing-chronische-q-koortspatienten

Address for correspondence: Daphne F.M. Reukers, National Institute for Public Health and the Environment, Antonie van Leeuwenhoeklaan 9, 3721 MA Bilthoven, the Netherlands; email:daphne.reukers@rivm.nl

One Health Genomic Analysis of Extended-Spectrum β-Lactamase–Producing *Salmonella enterica*, Canada, 2012–2016

Amrita Bharat, Laura Mataseje, E. Jane Parmley, Brent P. Avery, Graham Cox, Carolee A. Carson, Rebecca J. Irwin, Anne E. Deckert, Danielle Daignault, David C. Alexander, Vanessa Allen, Sameh El Bailey, Sadjia Bekal, Greg J. German, David Haldane, Linda Hoang, Linda Chui, Jessica Minion, George Zahariadis, Richard J. Reid-Smith, Michael R. Mulvey

Extended-spectrum β-lactamases (ESBLs) confer resistance to extended-spectrum cephalosporins, a major class of clinical antimicrobial drugs. We used genomic analysis to investigate whether domestic food animals, retail meat, and pets were reservoirs of ESBL-producing *Salmonella* for human infection in Canada. Of 30,303 *Salmonella* isolates tested during 2012–2016, we detected 95 ESBL producers. ESBL serotypes and alleles were mostly different between humans (n = 54) and animals/meat (n = 41). Two exceptions were bla_{SHV-2} and $bla_{CTX-M-1}$ IncI1 plasmids which were found in both sources. A subclade of *S. enterica* serovar Heidelberg isolates carrying the same IncI1-bla_{SHV-2} plasmid differed by only 1–7 single nucleotide variants. The most common ESBL producer in humans was *Salmonella* Infantis carrying $bla_{CTX-M-65}$, which has since emerged in poultry in other countries. There were few instances of similar isolates and plasmids, suggesting that domestic animals and retail meat might have been minor reservoirs of ESBL-producing *Salmonella* for human infection.

Nontyphoidal *Salmonella* is a leading cause of foodborne diarrheal illness. There were an estimated 535,000 human cases of invasive infection with nontyphoidal *Salmonella* and 59,100 deaths in 2017 globally (*1*,*2*). Gastroenteritis is usually self-limiting, but antimicrobial treatment, including ceftriaxone, ciprofloxacin, trimethoprim/sulfamethoxazole, or amoxicillin, might be recommended for severe disease and invasive infections (*3*).

Extended-spectrum cephalosporins are a major class of broad-spectrum antimicrobial drugs and can be hydrolyzed by β-lactamases belonging to molecular class C (AmpC type, such as bla_{CMY-2}) and molecular class A (ESBLs, such as bla_{CTX-M}, bla_{SHV}, and some alleles of bla_{TEM}) (*4*). ESBLs are a special concern because they sometimes cause reduced susceptibility to fourth-generation cephalosporins, such as cefepime, and they tend to be carried on mobile genetic elements (*5*). ESBLs are susceptible to β-lactamase inhibitors (e.g., clavulanic acid) and cephamycin-type cephalosporins (e.g., cefoxitin). Potential reservoirs of antimicrobial drug resistance are the food chain, the community, hospitals, and the environment (*6*). Ceftiofur was used systematically in the poultry industry in Canada. However, as of 2014, the industry voluntarily eliminated

Author affiliations: Public Health Agency of Canada, Winnipeg, Manitoba, Canada (A. Bharat, L. Mataseje, G. Cox, M.R. Mulvey); University of Manitoba, Winnipeg (A. Bharat, G. Cox, M.R. Mulvey); Public Health Agency of Canada, Guelph, Ontario, Canada (E.J. Parmley, B.P. Avery, C.A. Carson, R.J. Irwin, A.E. Deckert, R.J. Reid-Smith); University of Guelph, Guelph (E.J. Parmley); Public Health Agency of Canada, St. Hyacinthe, Quebec, Canada (D. Daignault); Cadham Provincial Laboratory, Winnipeg (D.C. Alexander); Public Health Ontario Laboratories, Toronto, Ontario, Canada (V. Allen); Horizon Health Network, Saint John, New Brunswick, Canada (S. El Bailey); Laboratoire de Santé Publique du Quebec, Sainte-Anne-de-Bellevue, Quebec, Canada (S. Bekal); Queen Elizabeth Hospital, Charlottetown, Prince Edward Island, Canada (G.J. German); Queen Elizabeth II Health Sciences Centre, Halifax, Nova Scotia, Canada (D. Haldane); British Columbia Center for Disease Control, Vancouver, British Columbia, Canada (L. Hoang); Public Health Laboratory, Edmonton, Alberta, Canada (L. Chiu); University of Alberta, Edmonton (L. Chui); Roy Romanow Provincial Laboratory, Regina, Saskatchewan, Canada (J. Minion); Newfoundland and Labrador Public Health and Microbiology Laboratory, St. John's, Newfoundland, Canada (G. Zahariadis)

DOI: https://doi.org/10.3201/eid2897.211528

preventive use of antimicrobial drugs that were highly essential, including ceftiofur (*7*). As of December 1, 2018, medically essential antimicrobial drugs are available only by veterinary prescription for use in animals in Canada (*8*).

The most common ESBL-producing *Enterobacterales* are *Escherichia coli* and *Klebsiella pneumoniae* carrying CTX-M enzymes, but ESBL *Salmonella* are observed infrequently (*9*–*11*). Approximately 10% of human clinical isolates of *E. coli* and *K. pneumoniae* were ESBL producing in Canada during 2016 (*9*). Three previous studies of a combined total of >11,000 *Salmonella* isolates from humans and animals/meat in North America identified only 7 ESBL isolates during 2005–2008 (*12*–*14*).

We conducted a genomic study of surveillance isolates collected by the Canadian Integrated Program for Antimicrobial Resistance Surveillance (CIPARS) to evaluate the contribution of food animals, retail meat, and pets toward human infections of ESBL-producing *Salmonella* in Canada during 2012–2016. We also characterized ESBL plasmids by short-read and long-read whole-genome sequencing (WGS).

Methods

ESBL Detection

ESBL-producing typhoidal and nontyphoidal *Salmonella* collected from 2012–2016 were identified by CIPARS, which collects human clinical samples from all 10 provincial public health laboratories in Canada. CIPARS also collects animals/meat isolates from farms, abattoirs, and retail stores, and veterinary diagnostic samples from animal health laboratories (*15*). We conducted antimicrobial drug susceptibility testing by using broth microdilution, the Sensititer Automated Microbiology System (Trek Diagnostic Systems Ltd., https://www.trekds.com), and breakpoints established by the Clinical Laboratory Standards Institute (*16*). CIPARS carries out susceptibility testing on all *Salmonella* serotypes from animals/meat sources and 11 serotypes from human samples that are either frequently isolated or frequently multidrug-resistant (4,[5],12,i:-, Dublin, Enteritidis, Heidelberg, Infantis, Kentucky, Newport, Paratyphi A, Paratyphi B, Typhi, and Typhimurium). We performed the combination ESBL disk test (cefotaxime or ceftazidime alone or in combination with clavulanic acid) on human isolates belonging to serotypes that were identified as ESBL producing in animals/meat that were not initially tested by broth microdilution (Anatum, Worthington Agona, Albany, Bredeney, Brandenburg, California, Derby, Ohio, and Ouakam).

We subjected isolates that had a ceftriaxone MIC >0.5 mg/L to the ESBL disk test and a β-lactam PCR to detect $bla_{\text{CMY-2}}$, bla_{TEM}, $bla_{\text{CTX-M}}$, bla_{SHV}, and bla_{OXA} as described (*17*). Isolates were selected for WGS if they showed positive results in the ESBL disk test or if they contained $bla_{\text{CTX-M}}$, bla_{SHV}, or bla_{OXA}. To capture ESBL variants of bla_{TEM}, we also sequenced isolates that were positive for bla_{TEM} by PCR but lacked CMY-2 or another ESBL-hydrolyzing enzyme.

Short-Read WGS

We subjected potential ESBL-producing *Salmonella* to short-read sequencing. We extracted DNA by using the Epicenter Complete DNA and RNA Extraction Kit (Illumina, https://www.illumina.com). We prepared libraries by using the Nextera XT Kit and sequenced them on the Miseq Platform with the Miseq Reagent v3 600 Cycle Kit (both from Illumina) The average genome coverage was 95× (range 68×–147×), and the average N50 (length of the shortest contig in the group of longest contigs that together represent ≥50% of genome assembly) of assemblies was 411,319 bp (range 79,379–740,528 bp), indicating high quality of sequencing and assemblies.

Long-Read WGS

We conducted long-read WGS on a subset of isolates by using the MinION Platform (Oxford Nanopore Technologies, https://nanoporetech.com). We prepared libraries by using the Rapid Barcoding SQK-RBK004 Kit and sequenced them by using R9.4 Flowcells (both from Oxford Nanopore Technologies). All $bla_{\text{SHV-2}}$ isolates were selected for long-read sequencing because this gene was commonly detected in humans (n = 12) and animals/meat (n = 15). If an ESBL variant was observed >5 times in 1 source (humans or animals/meat), we selected a convenience sample of 3 isolates from that source for long-read sequencing ($bla_{\text{CTX-M-55}}$ and $bla_{\text{CTX-M-65}}$ in humans and $\text{bla}_{\text{CTX-M-1}}$ in animals/meat). If the ESBL enzyme was observed <5 times in 1 source, we selected 1 isolate for long-read sequencing ($bla_{\text{SHV-2}}$, $bla_{\text{CTX-M-1}}$, $bla_{\text{CTX-M-3}}$, $bla_{\text{CTX-M-9}}$, $bla_{\text{CTX-M-14}}$, and $bla_{\text{CTX-M-15}}$ in humans and $bla_{\text{CTX-M-55}}$ in animals/meat).

Assembly and Alignment

We assembled short reads by using SPAdes Galaxy version 3.11.1 (*18*). We conducted plasmid assembly by using Unicycler version 0.4.7, which combines the accuracy of short reads with the scaffolding of long reads (*19*). Determinants of antimicrobial drug resistance and plasmids were detected by using the Public Health Agency of Canada StarAMR Tool (*20*), which incorporates the

ResFinder, PointFinder, and PlasmidFinder databases (*21*,*22*). We created plasmid alignments by using the web-based GView server (https://www.server.gview.ca) parameters: minimum length 150 and minimum nucleotide identity 98%. If an alignment included only plasmids that were closed by long-read sequencing, we used the pangenome feature of GView, which displays all content for all plasmids. If an alignment included any samples that were subjected only to short-read sequencing (fragmented assemblies), we used the BLAST atlas feature of GView, which displays only homology to a closed reference plasmid. We described plasmids as being similar if they displayed >95% nucleotide identity over >90% of the length of the plasmid.

Phylogenetic Trees

We used the single-nucleotide variant (SNV) phylogenomics (SNVPhyl) pipeline (https://snvphyl.readthedocs.io/en/latest) to build genomic dendrograms based on SNVs in the core genome (*23*). In brief, we mapped reads to a reference genome by using SMALT (https://bio.tools/smalt). We called variants by using mpileup (http://comailab.genomecenter.ucdavis.edu/index.php/mpileup) and Freebayes (https://www.geneious.com/plugins/freebayes), and used consensus SNVs to build the dendrogram by using PhyML (*24*) and the generalized time reversible model. Parameters used were minimum coverage 10, minimum mapping quality 30, and SNV density filtering > 2 SNVs/20 base window. SH-like branch support values >0.95 were considered to be strong support for internal branches (*24*).

Accession Identifiers

We deposited read data for all isolates in this study to the National Center for Biotechnology Information Short Read Archive under BioProject PRJNA740259. We provided the BioSample identification for the isolates (Appendix Table, https://wwwnc.cdc.gov/EID/article/28/7/21-1528-App1.xlsx).

Results

WGS of ESBL-Producing *Salmonella*

During 2012–2016, the prevalence of class A ESBL enzymes in Canada was 0.35% in humans (54 ESBL-positive/15,401 screened) and 0.31% in the animals/meat and pet samples (41 ESBL-positive/14,923 screened) within CIPARS. The animals/meat-source *Salmonella* were from turkey/turkeys (refers to meat/animal; 5 from meat, 17 from animals), pigs (n = 11, all animals), cattle (n = 4, all animals), chicken/chickens (1 from meat, 2 from animals), and domestic cat (n = 1) (Table 1). Thus, only 6 samples were from meat, and the remaining 36 samples were from animals, including healthy animals on farms (n = 11, 26.8%), and veterinary clinical samples from sick animals (n = 24, 68.5%). The human-source *Salmonella* were from stool (n = 48), blood (n = 2), urine (n = 2), and unknown sources (n = 2). We provided detailed information on all isolates (Appendix Table).

ESBL Serotypes and Alleles

ESBLs were detected in a variety of *Salmonella* serotypes from human sources (54 isolates belonging to 11 serotypes) (Table 2) and animals/meat sources (41 isolates belonging to 14 serotypes) (Table 3). In humans, the most common ESBL-producing serotypes were Heidelberg (n = 16; 29.6%), Infantis (n = 15; 27.8%), Typhimurium (n = 7; 13.0%) and 4,[5],12,i:- (n = 5; 9.3%) (Table 2). In the animals/meat sources, the most common ESBL-producing serotypes were Albany (n = 15; 36.6%), Heidelberg (n = 6; 14.6%), and Agona (n = 4; 9.8%) (Table 3). Overall, *Salmonella* Heidelberg was the most commonly detected ESBL-producing serotype (n = 22; 23.2%) in the study.

A wider diversity of ESBL enzymes were found in human sources (9 alleles) than in animals/meat sources (4 alleles). In human-source *Salmonella*, the most common ESBLs were $bla_{\text{CTX-M-65}}$ (n = 18, 33.3%), $bla_{\text{SHV-2}}$ (n = 12, 22.2%), and $bla_{\text{CTX-M-55}}$ (n = 6, 11.1%) (Table 2). Human-source *Salmonella* also carried $bla_{\text{CTX-M-1}}$, $bla_{\text{CTX-M-3}}$, $bla_{\text{CTX-M-9}}$, $bla_{\text{CTX-M-14}}$, and $bla_{\text{CTX-M-15}}$ and $bla_{\text{SHV-5}}$ at lower frequencies. Most animals/meat-source isolates contained either $bla_{\text{CTX-M-1}}$ (n = 19, 46.3%) or $bla_{\text{SHV-2}}$ (n = 15, 36.6%); the remaining isolates contained either $bla_{\text{SHV-12}}$ (n = 6) or $bla_{\text{CTX-M-55}}$ (n = 1) (Table 3). Thus, the $bla_{\text{SHV-2}}$ gene was detected in 20% of ESBL *Salmonella* from human sources and in 33.3% of ESBL *Salmonella* from animals/meat sources. Except for isolate 12-0820, all $bla_{\text{SHV-2}}$ isolates carried

Table 1. Animals/meat hosts carrying ESBL-producing *Salmonella* sp., Canada*

Source	ESBL recovery, no. positive/no. tested (%)	Meat	Farm	Veterinary
Total	41/13,120 (0.31)	6	11	24
Chicken/chickens	3/7,239 (0.04)	1	1	1
Cat (domestic)	1/22 (4.5)	NA	NA	1
Cattle	4/981 (0.4)	0	0	4
Pigs	11/3,312 (0.33)	0	4	7
Turkey/turkeys	22/1,416 (1.55)	5	6	11

*ESBL, extended-spectrum β-lactamase; NA, not applicable.

Table 2. Distribution of ESBL-producing *Salmonella* serotypes from human sources, Canada*

Serotype	Serotype subtotal, no. (%)	*bla*$_{CTX-M-1}$	*bla*$_{CTX-M-3}$	*bla*$_{CTX-M-9}$	*bla*$_{CTX-M-14}$	*bla*$_{CTX-M-15}$	*bla*$_{CTX-M-55}$	*bla*$_{CTX-M-65}$	*bla*$_{SHV-2}$	*bla*$_{SHV-5}$
Allele subtotal	54	4 (7.4)	2 (3.7)	3 (5.6)	3 (5.6)	5 (9.3)	**6 (11.1)**	**18 (33.3)**	**12 (22.2)**	1 (1.9)
4,[5],12:i:-	5 (9.3)	0	0	0	1	1	3	0	0	0
Enteritidis	2 (3.7)	0	1	0	0	0	1	0	0	0
Heidelberg	**16 (29.6)**	3	0	0	1	0	0	0	**12**	0
Infantis	**15 (27.7)**	0	1	0	0	0	0	**14**	0	0
Newport	2 (3.7)	0	0	0	0	1	0	0	0	1
Typhimurium	**7 (1)**	1	0	2	0	0	0	4	0	0
Typhimurium O:5-	2 (3.7)	0	0	1	0	0	1	0	0	0
Other serotypes†	5 (9.3)	0	0	0	1	3	1	0	0	0

*Bold indicates >5 occurrences. ESBL, extended-spectrum β-lactamase.
†Other serotypes include 1 each of Agona, Chester, Concord, Minnesota, and Poona.

a known L31Q substitution, which is sometimes referred to as *bla*$_{SHV-2a}$.

Drug Resistance Profiles

Resistance to ampicillin, streptomycin, sulfisoxazole, and tetracycline (ASSuT) was commonly observed in ESBL-producing *Salmonella* isolates from both sources (Table 4). For human source isolates, 25 (46.2%) demonstrated the ASSuT and chloramphenicol resistance pattern. For animals/meat sources, 12 (29.3%) isolates displayed the ASSuT and gentamicin resistance pattern. Although *bla*$_{SHV}$ and *bla*$_{CTX-M}$ alleles conferred ceftriaxone resistance (MIC resistance breakpoint ≥4 mg/L), isolates that had *bla*$_{SHV}$ showed MICs of 4–8 mg/L, and isolates that had *bla*$_{CTX-M}$ showed 8-fold higher MICs of 32–64 mg/L. Intermediate or outright resistance to ciprofloxacin was frequently observed in human-source ESBL-producing *Salmonella* (n = 31, 57.4%) but not in animals/meat sources.

There was general agreement between resistance phenotypes and genotypes (Table 4). CMY-2, but not ESBLs, confer resistance to clavulanic acid; 6 animals/meat isolates had resistance to amoxicillin/clavulanic acid and all contained *bla*$_{CMY-2}$. One human-derived isolate of *Salmonella* 4,[5],12:i:- had the mobile colistin resistance gene *mcr-3.2*, along with *bla*$_{CTX-M-55}$ and other resistance genes conferring resistance to 8 classes of antimicrobial drugs; the isolate had been described (*25*). Agreement between phenotype and genotype for gentamicin was lower; 12/25 isolates that had predicted gentamicin resistance contained the *aac (3)-IVa* gene conferring MICs of 4–8 mg/L, which is 1 or 2 dilutions below the resistance breakpoint of MIC >16 mg/L and accounted for most of the discrepancy. In general, disagreements between susceptibility phenotype and genotype might be caused by resistance genes or mutations that are currently unknown.

Phylogenomic Relatedness of Strains

We created maximum-likelihood phylogenetic trees based on SNVs in the core genome for each serotype. The *Salmonella* Heidelberg phylogenetic tree showed that ESBL-producing isolates from human and animals/meat sources were genetically distinct, with some exceptions (Figure 1). Closely related *Salmonella* Heidelberg (defined as ≤20 SNVs) carrying *bla*$_{SHV-2}$ were identified from chicken thighs (N17-03250 isolated in western Canada during 2013) and humans (15-7951 and 15-4041 isolated in western Canada during 2015); these isolates differed by only 1–7 SNVs. The branch support for these 3 isolates was not strong (SH-like value 0.76). However, the isolates carried similar type A IncI1-*bla*$_{SHV-2}$ plasmids (described in the ESBL Plasmids Section). The 3 isolates carrying

Table 3. Distribution of ESBL-producing *Salmonella* serotypes from animals/meat sources, Canada*

Serotype	Serotype subtotal, no. (%)	*bla*$_{CTX-M-1}$	*bla*$_{CTX-M-55}$	*bla*$_{SHV-2}$	*bla*$_{SHV-12}$
Allele subtotal	41	**19 (46.3)**	1 (2.4)	**15 (36.6)**	**6 (14.6)**
4,[5],12:i:-	1 (2.4)	0	1	0	0
4,12:-:-	1 (2.4)	0	0	0	1
Agona	4 (9.8)	0	0	4	0
Albany	**15 (36.6)**	**15**	0	0	0
Brandenburg	2 (4.9)	0	0	1	1
California	2 (4.9)	0	0	2	0
Derby	2 (4.9)	0	0	2	0
Heidelberg	**6 (14.6)**	0	0	2	4
Ohio	2 (4.9)	0	0	2	0
Ouakam	2 (4.9)	2	0	0	0
Other serotypes†	4 (9.8)	2	0	2	0

*Bold indicates >5 occurrences. ESBL, extended-spectrum β-lactamase.
.†Other serotypes include 1 each of Anatum, Bredeney, Infantis, and Worthington.

Table 4. Phenotypic susceptibility and genetic resistance determinants for 13 antimicrobial drugs in *Salmonella* sp. Canada

	Human source, n = 54		Animals/meat source, n = 41	
Antimicrobial drug	No. resistant (%)*	Genetic determinants†	No. resistant (%)*	Genetic determinants†
Amoxicillin/clavulanic acid	0	None	6 (14.6)	bla_{CMY-2} (n = 6)
Ampicillin	54 (100)	$bla_{CTX-M-1}$, $bla_{CTX-M-3}$, $bla_{CTX-M-9}$, $bla_{CTX-M-14}$, $bla_{CTX-M-15}$, $bla_{CTX-M-55}$, $bla_{CTX-M-65}$, bla_{SHV-2}, bla_{SHV-5} (n = 54)	41 (100)	$bla_{CTX-M-1}$, $bla_{CTX-M-55}$, bla_{SHV-2}, bla_{SHV-12} (n = 41)
Azithromycin	0	None	1 (2.4)	*mphA* (n = 1)
Chloramphenicol	29 (53.7)	*floR*, *catA*, *catB*, *cmlA* (n = 27)	7 (17.1)	*floR* (n = 5)
Iprofloxacin	31 (57.4)	GyrA D87Y or D87G, *qnrA1*, *qnrB1*, *qnrS1*, *aac(6')-Ib-cr* (n = 31)	3 (7.3)	*qnrB2, qnrS1* (n = 3)
Ceftriaxone	54 (100)	$bla_{CTX-M-1}$, $bla_{CTX-M-3}$, $bla_{CTX-M-9}$, $bla_{CTX-M-14}$, $bla_{CTX-M-15}$, $bla_{CTX-M-55}$, $bla_{CTX-M-65}$, bla_{SHV-2}, bla_{SHV-5} (n = 54)	41 (100)	$bla_{CTX-M-1}$, $bla_{CTX-M-55}$, bla_{SHV-2}, bla_{SHV-12} (n = 41)
Cefoxitin	1 (1.9)	None	7 (17.1)	bla_{CMY-2} (n = 6)
Gentamicin	13 (24)	*aac(3)-IIa*, *aac-(3)-IId*, *aac(3)-IVa*, *aac(3)-Via*, and *rmtB* (n = 25)	24 (58.5)	*aac(3)-IId, aac(3)-Via, aac(6')-Iy, and aac(6')-IIc* (n = 23)
Nalidixic acid	20 (37)	GyrA D87Y or D87G, *qnrS1* (n = 20)	0	
Sulfisoxazole	35 (64.8)	*sul1*, *sul2*, *sul3* (n = 35)	26 (63.4)	*sul1*, *sul2*, *sul3* (n = 26)
Streptomycin	28 (51.9)	*aadA1*, *aadA2*, *ant(3")-Ia*, *ant(3")-Ib*, *aph(3")-Ib*, and *strA* (n = 31)	23 (56.1)	*aadA1*, *aadA2*, *ant(3")-Ia*, *ant(3")-Ib*, and *strA* (n = 29)
Sulfamethoxazole/trimethoprim	26 (48.1)	*dfrA1*, *dfrA12*, *dfrA14*, *dfrA16*, *dfrA18*, *dfrA23* (n = 26)	12 (29.3)	*dfrA1*, *dfrA14*, *drfA18* (n = 12)
Tetracycline	43 (79.6)	*tetA* and *tetB* (n = 40)	21 (51.2)	*tetA*, *tetB*, and *tetD* (n = 21)

*Where available, resistance was interpreted according to Clinical Laboratory Standards Institute breakpoints; for azithromycin, the *National Antimicrobial Resistance Monitoring System* NARMs breakpoint of 32 mg/L was used; for ciprofloxacin, both intermediate and full resistance were included.
†n value in parentheses indicates number of isolates that contained ≥1 genetic determinant of resistance.

bla_{SHV-2} were also genetically similar to 4 isolates carrying bla_{SHV-12}, differing by only 9–14 SNVs.

The phylogenetic tree for *Salmonella* Typhimurium and closely related serovars Salmonella 4,5,12,i:- and *Salmonella* Typhimurium var. O:5 showed that isolates from human and animals/meat sources were genetically distinct with 1 potential exception (Figure 2). Among *Salmonella* 4,[5],12,i:- carrying $bla_{CTX-M-55}$, 1 clinical isolate from a sick pig (N17-03254 isolated in central Canada during 2015) differed by 55–80 SNVs from 3 human isolates (13-1681, 13-4743, and 16-6914, isolated in central and western Canada during 2013 and 2016) (Figure 2). More epidemiologic studies are needed to interpret whether 55–80 SNVs indicate genetic relatedness. However, the clustering of isolates from human and pig was strongly supported (SH-like value 0.99).

Salmonella Agona and *Salmonella* Infantis were the only other serotypes in which ESBL-producing isolates were detected in both sources. Phylogenetic trees of *Salmonella* Agona did not show evidence of transmission between animals/meat and humans because isolates from the 2 sources differed by ≥77 SNVs. The United States and other countries have noted the emergence of *Salmonella* Infantis carrying CTX-M-65 on the plasmid of emerging *Salmonella* Infantis in humans and food animals, especially in poultry (*26*). For comparison, we included genome sequences of *Salmonella* Infantis from human, food animals, and retail chicken from the study by Tate et al. in our phylogenetic tree (*26*). The major clade of the tree comprised CTX-M-65–containing isolates from both studies whereby isolates differed by 1–53 SNVs. Three isolates from human sources in Canada collected during 2016 were closely related to isolates from retail chicken, chicken at slaughter, and dairy cow at slaughter collected in the United States during 2014–2015, differing by only 4–13 SNVs and clustering on a strongly supported branch (SH-like value 1.0) (Figure 3). One isolate each from Canada from a cat (N17-03255) carrying SHV-2 and a human (15-8465) carrying CTX-M-3 did not cluster with the CTX-M-65-containing isolates.

ESBL Plasmids

Although the ESBL serotypes were mostly different between humans and animals/meat isolates, it is possible that ESBL plasmids were similar because plasmids can be transmissible between serotypes. We produced complete plasmid sequences for a subset of isolates.

The bla_{SHV-2} genes from human sources were all from *Salmonella* Heidelberg, and the animals/meat isolates were from a variety of serotypes, including Agona, Anatum, Brandenburg, California, Derby, Heidelberg, Infantis, and Ohio (Table 2). All bla_{SHV-2} genes were carried on IncI plasmids, which we categorized into 3 types (types A, B, and C) on the basis of their resistance gene profiles and overall genetic content (Figure 4). Similar bla_{SHV-2} plasmids were found in isolates from humans and animals/meat (>95% nucleotide identity over >90% plasmid length).

The type A plasmids carried bla_{SHV-2} and *tetA* resistance genes and were found in humans (n = 10), chicken(s) (n = 2, one each from meat and animal), and pig (n = 1 from animal) (Figure 4). Three of the type A plasmids were from *Salmonella* Heidelberg isolates that differed by only 1–7 SNVs (N17-03250 isolated from chicken thighs during 2013; and 15-7951 and 15-4041 isolated from humans during 2015). Thus, these 3 isolates were genetically closely related and contained similar plasmids (99.9% nucleotide identity over 91% of the length of the plasmid). The type B plasmids carried *aac (3)-VIa*, *ant(3'')-Ia*, bla_{SHV-2}, and *sul1* and were found in a human (n = 1), a domestic cat (n = 1), and turkey/turkeys (n = 5). The type B plasmid from a human (12-0820 in *Salmonella* Heidelberg) was most similar to the plasmid from the domestic cat (N17-03255 in *Salmonella* Infantis) with 99.9% nucleotide identity over 93% of the length of the plasmid. Finally, the type C plasmids carried *aadA1*, bla_{SHV-2}, *dfrA1*, and *sul1*. The type C plasmids were isolated from pigs on farms and from sick pigs.

The $bla_{CTX-M-1}$–containing plasmid was the most common ESBL in animals/meat isolates and was occasionally observed in human isolates. One $bla_{CTX-M-1}$ plasmid from serotype *Salmonella* Worthington identified from a pig (N16-01063 isolated in western Canada during 2013) and all $bla_{CTX-M-1}$ plasmids from *Salmonella* Heidelberg (n = 3) and *Salmonella* Typhimurium (n = 1) from human sources in various years were carried on similar IncI plasmids (Figure 5, panel A). Of 119 coding sequences on the $bla_{CTX-M-1}$ IncI plasmid from pig (N16-01063), all but 1 coding DNA sequence was present on the human plasmids. The plasmid had only 75% nucleotide identity to the previously reported R64 reference plasmid (*27*). However, in the National Center for Biotechnology Information database (https://www.ncbi.nlm.nih.gov), there were matches to *E. coli* plasmids (e.g., accession no. CP007651.1).

In the remainder of animals/meat isolates harboring $bla_{CTX-M-1}$, the gene was carried on an IncN plasmid (Figure 5, panel B). IncN $bla_{CTX-M-1}$ plasmids were similar between isolates except for N16-01061, which was missing ≈20 kb. A representative $bla_{CTX-M-1}$ IncN plasmid from isolate N17-03257 had >99.5% nucleotide identity to plasmids from *E. coli* O16:H48 (accession no. CPO34186.1) and *Salmonella* Bredeney (accession no. CPO43184.1). The $bla_{CTX-M-55}$ was found on IncN plasmids in *Salmonella* 4,[5],12:i:- in 1 isolate each from human and animals/meat source. However, of 291 coding DNA sequences on the plasmid from a pig isolate (N17-03254), only 242 (83%) were present on the plasmid from the human isolate (13-1681) (Figure 5, panel C).

The most common combination of ESBL *Salmonella* serotype and allele in humans in this study was *Salmonella* Infantis carrying $bla_{CTX-M-65}$ (n = 14). The $bla_{CTX-M-65}$ IncFIB plasmid was almost identical to a plasmid that the National Antimicrobial Resistance Monitoring System (NARMS) has reported to be emerging in the United States in humans and

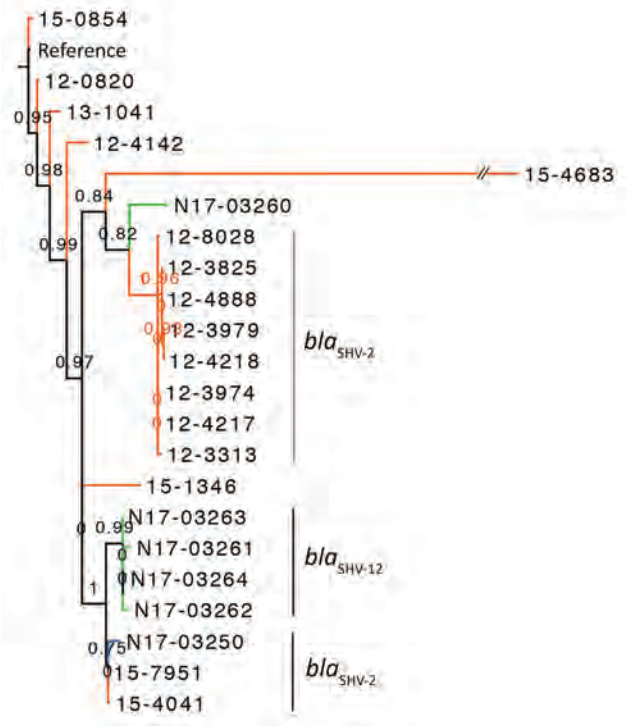

Figure 1. Phylogenetic dendrogram of *Salmonella enterica* serovar Heidelberg containing extended-spectrum β-lactamase genes, Canada. The maximum-likelihood dendrogram was created by using the single-nucleotide variant (SNV) phylogenomics (SNVPhyl) pipeline (https://snvphyl.readthedocs.io/en/latest) based on SNVs in the core genome. The reference genome is *Salmonella* Heidelberg strain 12-4374 (GenBank accession no. CP012924.1). The tree is based on a core genome that represents 94% of the reference genome. Numbers along branches indicate branch support values. *Salmonella* Heidelberg containing extended-spectrum β-lactamases were from animals (green, n = 5), food (blue, n = 1), and humans (orange, n = 16). Extended-spectrum β-lactamase genes are indicated to the right of the 3 largest clusters. The dataset comprises 394 SNVs, and SH-like branch support values are displayed.

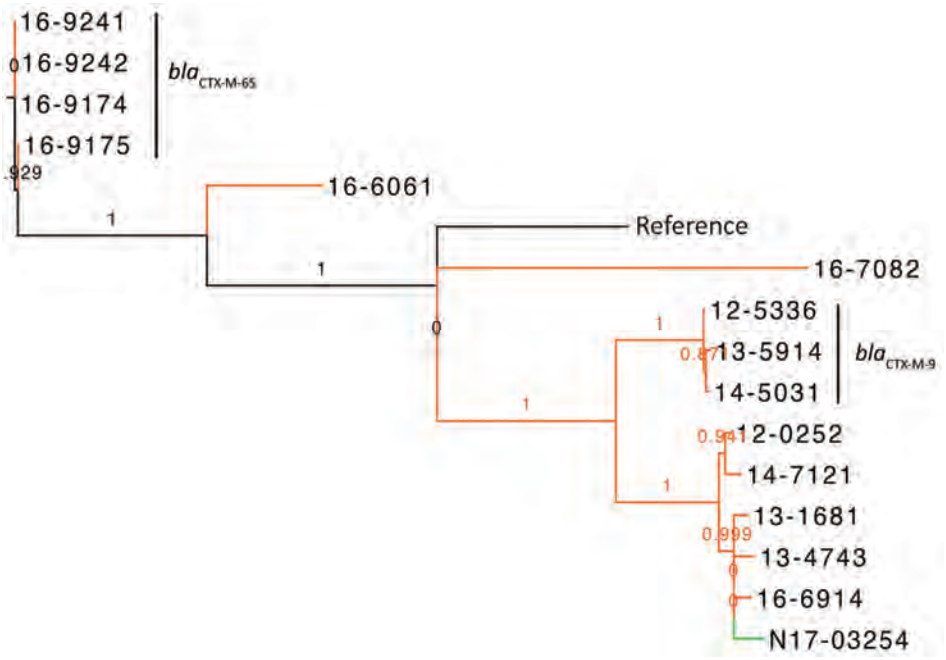

Figure 2. Phylogenetic dendrogram of extended-spectrum β-lactamase–producing *Salmonella enterica* serovars Typhimurium and 4,5,12,i:-, Canada. The maximum likelihood dendrogram was created by using the single-nucleotide variant (SNV) phylogenomics (SNVPhyl) pipeline (https://snvphyl.readthedocs.io/en/latest) based on SNVs in the core genome. The reference genome is *Salmonella* Typhimurium strain LT2 (GenBank accession no. NC_003197.2). The tree is based on a core genome that represents 96% of the reference genome. Numbers along branches indicate branch support values. Sample N17-03254 was a clinical isolate from a sick pig (green), and all other samples were from human sources (orange, n = 14). Extended-spectrum β-lactamase genes are indicated to the right of the 3 largest clusters. The dataset comprises 1,599 SNVs, and SH-like branch support values are displayed.

chickens (*26*,*28*). A representative closed plasmid from isolate 15-4113 in this study had 99.1% nucleotide identity with the reported NARMS plasmid (accession no. NZ_CP016407). Of 14 isolates of *Salmonella* Infantis carrying CTX-M-65 detected in Canada, 9 isolates contained 11 antimicrobial resistance determinants: *aac (3)-IVa*, *ant(3'')-Ia*, *aph(3'')-Ia*, *aph (4)-Ia*, $bla_{CTX-M-65}$, *dfrA14*, *floR*, *fosA3*, *gyrA* (D87Y), *sul1*, and

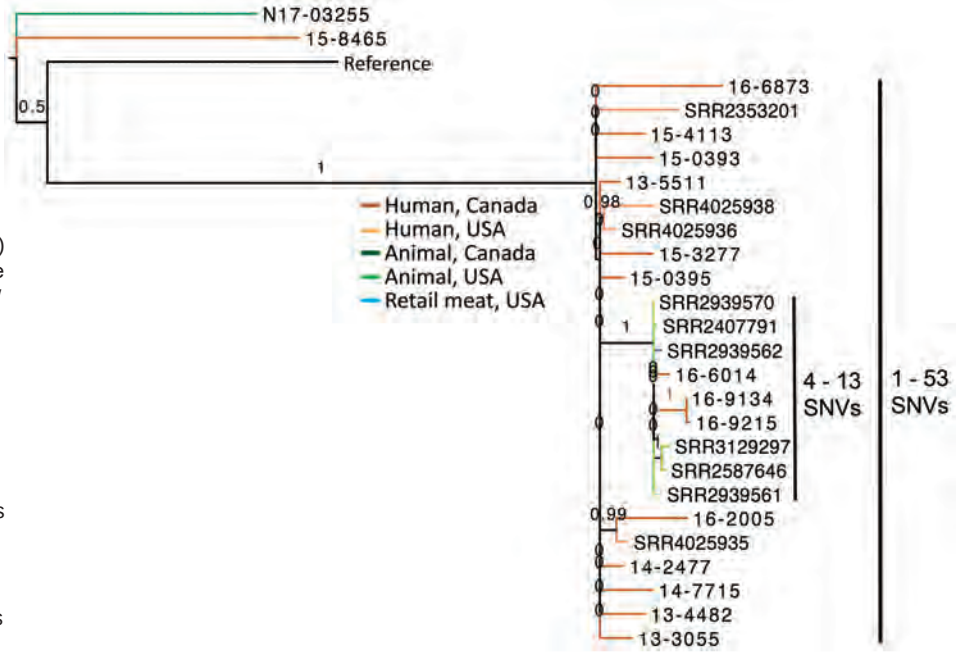

Figure 3. Phylogenetic dendrogram of extended-spectrum β-lactamase–producing *Salmonella enterica* serovars Infantis from Canada and the United States. Isolates from the United States are from Tate et al. (*26*). The maximum-likelihood dendrogram was created by using the single-nucleotide variant (SNV) phylogenomics (SNVPhyl) pipeline (https://snvphyl.readthedocs.io/en/latest) based on SNVs in the core genome. The reference genome was *Salmonella* Infantis strain 15-SA01028 (GenBank accession no. CP026660.1). The tree is based on a core genome that represents 97% of the reference genome. Numbers along branches indicate branch support values. *Salmonella* Infantis containing extended-spectrum β-lactamases were isolated from human sources in Canada (dark orange), human sources from the United States (light orange), a cat from Canada (dark green), poultry or dairy at slaughter from the United States (light green) or retail meat from the United States. Isolate N17-03255 from a cat contained SHV-2, isolate 15-8465 from a human contained CTX-M-3, and all other isolates contained CTX-M-65. The dataset comprises 491 SNVs, and SH-like branch support values are displayed.

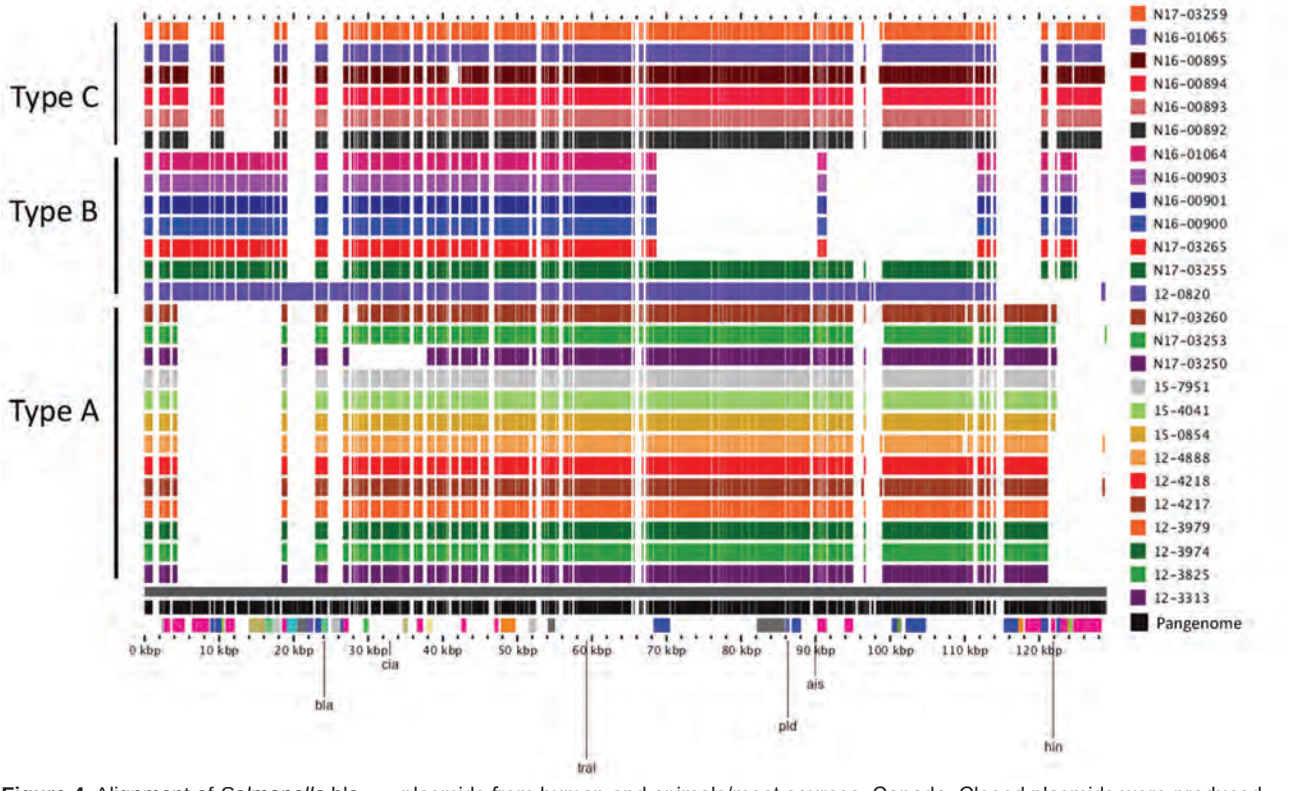

Figure 4. Alignment of *Salmonella* bla_{SHV-2} plasmids from human and animals/meat sources, Canada. Closed plasmids were produced by hybrid assembly of short and long read sequencing by using Unicycler (https://bio.tools/unicycler). Plasmids were aligned by using the pangenome feature of the GView server (https://server.gview.ca). Animals/meat sample identifications start with the letter N, and human sample identifications start with a 2-digit number. Plasmids were classified as Type A, B, or C based on their resistance gene profiles and overall similarity. All plasmids belong to the IncI1 incompatibility group.

tet(A) conferring reduced susceptibility or resistance to gentamicin, streptomycin, ampicillin, ceftriaxone, trimethoprim, chloramphenicol, ciprofloxacin, nalidixic acid, sulfisoxazole, and tetracycline. Gene *fosA3* probably confers reduced susceptibility to fosfomycin, but this antimicrobial drug was not tested. All resistance determinants except for *gyrA* (D87Y) were carried on the representative closed plasmid. Two isolates lacked *fosA3*, 2 lacked *fosA3* and *aph (4)-Ia*, and 1 lacked *fosA3*, *ant(3'')-Ia* and *aph(3')-Ia*.

Discussion

Health Canada has classified third-generation and fourth-generation cephalosporins as Category I (high importance) antimicrobial drugs based on their role in human medicine. However, Category I antimicrobial drugs are still used in food animals with a veterinary prescription with some restrictions (*8*,*29*). The frequency of ESBL-producing Enterobacterales continues to increase in humans, especially in *E. coli* and *K. pneumoniae* (*30*). In this study, the frequency of recovery of ESBL-producing *Salmonella* (i.e., no. ESBL-producing isolates/total no. isolates) during 2012–2016 was low (0.35% from humans and 0.31% from animals/meat). Recent studies in China have reported a much higher frequency of recovery of ESBL-producing *Salmonella* from food (9.7%) and food animals (17.7%) (*31*,*32*).

In our study, 76% of ESBL-producing *Salmonella* causing human infections and 49% from animals/meat isolates harbored CTX-M, and the remainder harbored SHV. During the 1990s, global outbreaks of ESBL-producing *Enterobacterales* were mainly caused by *K. pneumoniae* carrying SHV and TEM enzymes; since then, CTX-M enzymes have increased rapidly and are now the most common ESBL enzymes (*33*).

For ESBL-related infections in humans, CTX-M-14 and CTX-M-15 are the most common ESBLs in *E. coli* (*10*,*33*). However, in our study, these 2 alleles were infrequently observed in *Salmonella*. In our study, *Salmonella* Infantis carrying $bla_{CTX-M-65}$ was the most common ESBL-producer detected from human infections in Canada. In the United States, although ESBL-producing *Salmonella* are rare, *Salmonella* Infantis carrying $bla_{CTX-M-65}$ is emerging in human infections and in poultry (*26*,*28*). *Salmonella* Infantis containing $bla_{CTX-M-65}$ is also emerging in humans and poultry in

other countries, including Italy, England and Wales, Israel, Peru, and Ecuador (*34*–*38*).

The $bla_{CTX\text{-}M\text{-}65}$ is carried on a large IncFIB plasmid termed plasmid of emerging *Salmonella* Infantis along with other resistance determinants. The $bla_{CTX\text{-}M\text{-}65}$ plasmid detected in Canada was almost identical to the IncFIB $bla_{CTX\text{-}M\text{-}65}$ plasmid that was reported in the United States (*25*,*27*). This plasmid is especially concerning because it is transferrable and it carries ≤10 genes encoding resistance to ampicillin, ceftriaxone, chloramphenicol, gentamicin, nalidixic acid, streptomycin, sulfisoxazole, tetracycline, and trimethoprim. *Salmonella* Infantis containing $bla_{CTX\text{-}M\text{-}65}$ was found exclusively from human infections in our study, but human isolates from Canada collected during 2016 were closely related to isolates from humans, chicken, and dairy cow from the United States that were collected during 2014. The human cases in Canada might have been imported through retail sources, or travel, or might have been acquired from domestic food commodities that were not sampled by CIPARS during the study. Continued surveillance is needed to detect potential emergence of ESBLs in food animals, meat, and other food commodities in Canada.

In animals/meat isolates, $bla_{CTX\text{-}M\text{-}1}$ was the most common allele detected and is the most common allele in animals/meat sources from western Europe (*33*,*39*). The allele $bla_{CTX\text{-}M\text{-}27}$ is emerging in China and Vietnam and was detected in the United States, but this allele was not observed in Canada during this study (*40*,*41*).

The *Salmonella* ESBL alleles and serotypes were mostly different between humans and domestic animals/meat sources during the study period. A meta-analysis of risk factors for fecal ESBL colonization identified recent antimicrobial drug use and international travel as the 2 major risk factors (*42*). CIPARS does not collect information on human travel or imported foods, but these factors might contribute to ESBLs in humans in Canada. Although ESBLs were not detected in typhoidal *Salmonella* during the study period, several cases of extensively drug resistant *Salmnella* Typhi containing $bla_{CTX\text{-}M\text{-}15}$ were imported into Canada during 2018 and 2019 by patients who had traveled to Pakistan, where a large outbreak

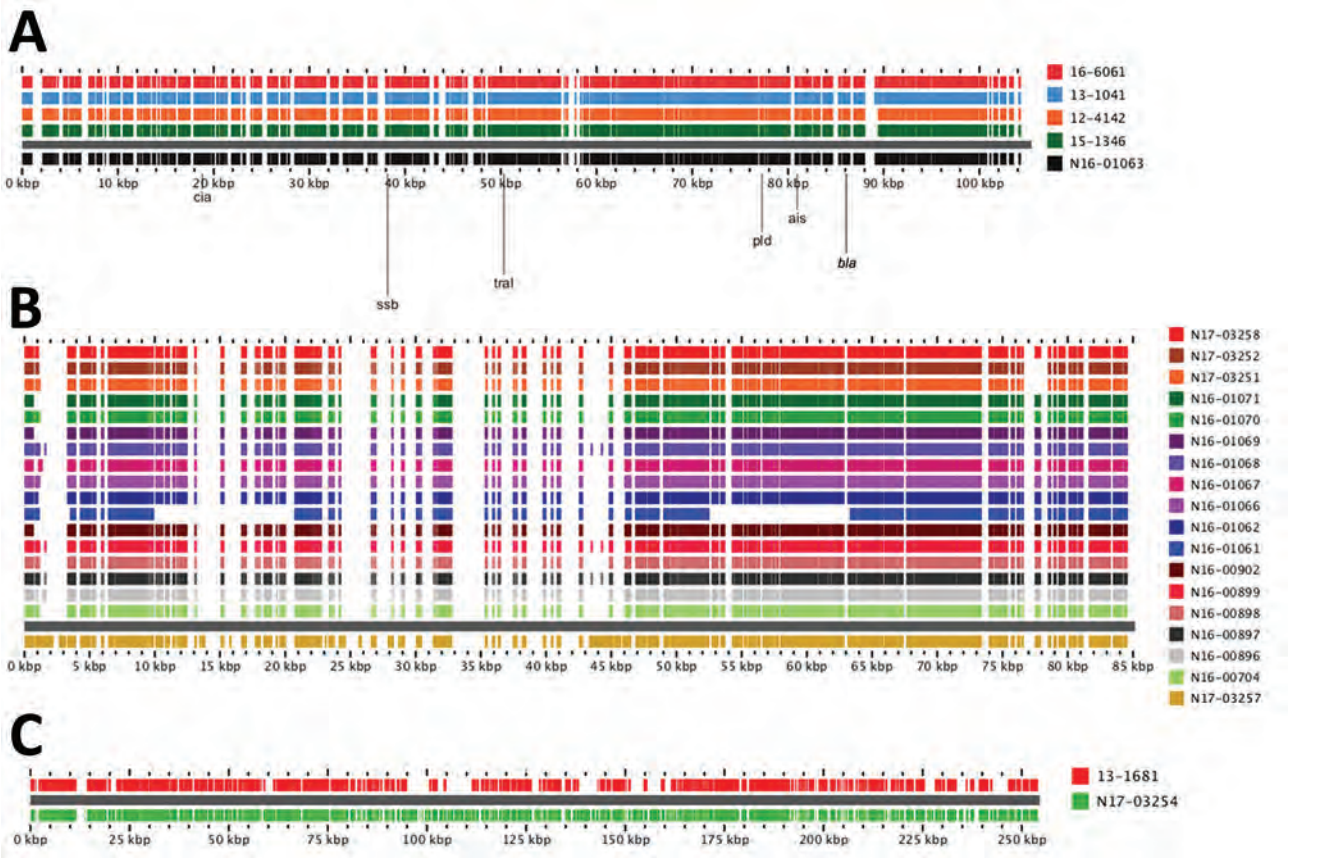

Figure 5. Alignment of *Salmonella* $bla_{CTX\text{-}M}$ plasmids from human and animals/meat sources, Canada. Alignments of $bla_{CTX\text{-}M\text{-}1}$ IncI1 (A), $bla_{CTX\text{-}M\text{-}1}$ IncN (B), and $bla_{CTX\text{-}M\text{-}55}$ IncN (C) plasmids are shown. Plasmids were aligned by using the BLAST feature of the GView server (https://server.gview.ca) and representative closed plasmids (bottom-most plasmid in each alignment) from this study. Animals/meat sample identifications start with the letter N, and human sample identifications start with a 2-digit number.

is ongoing (*43*). Pets might be another reservoir of ESBL-producing bacteria. Although CIPARS examined only 22 pet samples in this study, we detected a bla_{SHV-2} plasmid in a cat that was almost identical to a plasmid from a human isolate.

In summary, ESBL-producing *E. coli* and *K. pneumoniae* are a healthcare challenge because treatment options are limited (*30*). Although the frequency of recovery of ESBL-producing *Salmonella* was low in this study, it is essential to continue surveillance because extended-spectrum cephalosporins are a major treatment option for serious or invasive *Salmonella* infections.

Acknowledgments

We thank the Genomics Core Facility and the Bioinformatics Core Facility at the National Microbiology Laboratory for providing support with WGS and bioinformatics.

This study was supported by internal funds from the Public Health Agency of Canada.

About the Author

Dr. Bharat is the Head of Mycology and Molecular Enteric Antimicrobial Resistance at the National Microbiology Laboratory within the Public Health Agency of Canada, Winnipeg, Manitoba, Canada. Her primary research interests are antimicrobial drug resistance in *Salmonella* sp. and *E. coli*, and antifungal drug resistance in *Candida* spp.

References

1. GBD 2017 Non-typhoidal Salmonella invasive disease collaborators. The global burden of non-typhoidal *Salmonella* invasive disease: a systematic analysis for the Global Burden of Disease Study 2017. Lancet Infect Dis. 2019;19:1312–24. https://doi.org/10.1016/S1473-3099(19)30418-9 PMID: 31562022
2. Roth GA, Abate D, Abate KH, Abay SM, Abbafati C, Abbasi N, et al.; GBD 2017 Causes of Death Collaborators. Global, regional, and national age-sex-specific mortality for 282 causes of death in 195 countries and territories, 1980–2017: a systematic analysis for the Global Burden of Disease Study 2017. Lancet. 2018;392:1736–88. https://doi.org/10.1016/S0140-6736(18)32203-7
3. Shane AL, Mody RK, Crump JA, Tarr PI, Steiner TS, Kotloff K, et al. 2017 Infectious Diseases Society of America Clinical Practice Guidelines for the Diagnosis and Management of Infectious Diarrhea. Clin Infect Dis. 2017;65:1963–73. https://doi.org/10.1093/cid/cix959
4. Bush K. Past and present perspectives on β-lactamases. Antimicrob Agents Chemother. 2018;62:e01076–18. https://doi.org/10.1128/AAC.01076-18
5. Karaiskos I, Giamarellou H. Carbapenem-sparing strategies for ESBL producers: when and how. Antibiotics (Basel). 2020;9:61. https://doi.org/10.3390/antibiotics9020061
6. Hernando-Amado S, Coque TM, Baquero F, Martínez JL. Defining and combating antibiotic resistance from One Health and Global Health perspectives. Nat Microbiol. 2019;4:1432–42. https://doi.org/10.1038/s41564-019-0503-9
7. Chicken Farms of Canada. Preventative use of category I antibiotics in the poultry and egg sectors, 2013 [cited 2020 Dec 19]. https://www.chickenfarmers.ca/antibiotics
8. Health Canada. Responsible use of medically important antimicrobials in animals. 2020. p. 1–15 [cited 2020 Dec 18]. https://www.canada.ca/en/public-health/services/antibiotic-antimicrobial-resistance/animals/actions/responsible-use-antimicrobials.html
9. Denisuik AJ, Karlowsky JA, Adam HJ, Baxter MR, Lagacé-Wiens PRS, Mulvey MR, et al.; Canadian Antimicrobial Resistance Alliance (CARA) and CANWARD. Dramatic rise in the proportion of ESBL-producing *Escherichia coli* and *Klebsiella pneumoniae* among clinical isolates identified in Canadian hospital laboratories from 2007 to 2016. J Antimicrob Chemother. 2019;74(Suppl 4):iv64–71. https://doi.org/10.1093/jac/dkz289
10. Kazmierczak KM, de Jonge BLM, Stone GG, Sahm DF. Longitudinal analysis of ESBL and carbapenemase carriage among *Enterobacterales* and *Pseudomonas aeruginosa* isolates collected in Europe as part of the International Network for Optimal Resistance Monitoring (INFORM) global surveillance programme, 2013-17. J Antimicrob Chemother. 2020;75:1165–73. https://doi.org/10.1093/jac/dkz571
11. Toy T, Pak GD, Duc TP, Campbell JI, El Tayeb MA, Von Kalckreuth V, et al. Multicountry distribution and characterization of extended-spectrum β-lactamase-associated Gram-negative bacteria from bloodstream infections in Sub-Saharan Africa. Clin Infect Dis. 2019; 69(Suppl 6):S449–58. https://doi.org/10.1093/cid/ciz450
12. Sjölund-Karlsson M, Howie RL, Blickenstaff K, Boerlin P, Ball T, Chalmers G, et al. Occurrence of β-lactamase genes among non-Typhi *Salmonella enterica* isolated from humans, food animals, and retail meats in the United States and Canada. Microb Drug Resist. 2013;19:191–7. https://doi.org/10.1089/mdr.2012.0178
13. Sjölund-Karlsson M, Rickert R, Matar C, Pecic G, Howie RL, Joyce K, et al. *Salmonella* isolates with decreased susceptibility to extended-spectrum cephalosporins in the United States. Foodborne Pathog Dis. 2010;7:1503–9. https://doi.org/10.1089/fpd.2010.0607
14. Sjölund-Karlsson M, Howie R, Krueger A, Rickert R, Pecic G, Lupoli K, et al. CTX-M–producing non-Typhi *Salmonella* spp. isolated from humans, United States. Emerg Infect Dis. 2011;17:97–9. https://doi.org/10.3201/eid1701.100511
15. CIPARS. Canadian Integrated Program for Antimicrobial Resistance Surveillance (CIPARS), 2018: design and methods. 2020. p. 1–57 [cited 2022 May 3]. https://www.canada.ca/en/public-health/services/surveillance/canadian-integrated-program-antimicrobial-resistance-surveillance-cipars/cipars-reports/2018-annual-report-design-methods.html
16. Clinical and Laboratory Standards Institute. Performance standards for antimicrobial susceptibility testing (M100–ED29). Wayne (PA); The Institute; 2019. p. 1–321 [cited 2022 May 3]. https://clsi.org/media/2663/m100ed29_sample.pdf
17. Mulvey MR, Grant JM, Plewes K, Roscoe D, Boyd DA. New Delhi metallo-β-lactamase in *Klebsiella pneumoniae* and *Escherichia coli*, Canada. Emerg Infect Dis. 2011;17:103–6. https://doi.org/10.3201/eid1701.101358
18. Bankevich A, Nurk S, Antipov D, Gurevich AA, Dvorkin M, Kulikov AS, et al. SPAdes: a new genome assembly algorithm and its applications to single-cell sequencing. J Comput Biol. 2012;19:455–77. https://doi.org/10.1089/cmb.2012.0021
19. Wick RR, Judd LM, Gorrie CL, Holt KE. Unicycler: Resolving bacterial genome assemblies from short and long sequencing reads. PLOS Comput Biol. 2017;13:e1005595. https://doi.org/10.1371/journal.pcbi.1005595

20. Bharat A, Petkau A, Avery BP, Chen JC, Folster JP, Carson CA, et al. Correlation between phenotypic and in silico detection of antimicrobial resistance in *Salmonella enterica* in Canada using Staramr. Microorganisms. 2022; 10:292. https://doi.org/10.3390/microorganisms10020292
21. Zankari E, Hasman H, Cosentino S, Vestergaard M, Rasmussen S, Lund O, et al. Identification of acquired antimicrobial resistance genes. J Antimicrob Chemother. 2012;67:2640–4. https://doi.org/10.1093/jac/dks261
22. Zankari E, Allesøe R, Joensen KG, Cavaco LM, Lund O, Aarestrup FM. PointFinder: a novel web tool for WGS-based detection of antimicrobial resistance associated with chromosomal point mutations in bacterial pathogens. J Antimicrob Chemother. 2017;72:2764–8. https://doi.org/10.1093/jac/dkx217
23. Petkau A, Mabon P, Sieffert C, Knox NC, Cabral J, Iskander M, et al. SNVPhyl: a single nucleotide variant phylogenomics pipeline for microbial genomic epidemiology. Microb Genom. 2017;3:e000116. https://doi.org/10.1099/mgen.0.000116
24. Guindon S, Dufayard J-F, Lefort V, Anisimova M, Hordijk W, Gascuel O. New algorithms and methods to estimate maximum-likelihood phylogenies: assessing the performance of PhyML 3.0. Syst Biol. 2010;59:307–21. https://doi.org/10.1093/sysbio/syq010
25. Mulvey MR, Bharat A, Boyd DA, Irwin RJ, Wylie J. Characterization of a colistin-resistant *Salmonella enterica* 4,[5],12:i:- harbouring mcr-3.2 on a variant IncHI-2 plasmid identified in Canada. J Med Microbiol. 2018;67:1673–5. https://doi.org/10.1099/jmm.0.000854
26. Tate H, Folster JP, Hsu C-H, Chen J, Hoffmann M, Li C, et al. Comparative analysis of extended-spectrum-β-lactamase CTX-M-65–producing *Salmonella enterica* serovar Infantis isolates from humans, food animals, and retail chickens in the United States. Antimicrob Agents Chemother. 2017;61:e00488–17. https://doi.org/10.1128/AAC.00488-17
27. Sampei G, Furuya N, Tachibana K, Saitou Y, Suzuki T, Mizobuchi K, et al. Complete genome sequence of the incompatibility group I1 plasmid R64. Plasmid. 2010;64:92–103. https://doi.org/10.1016/j.plasmid.2010.05.005
28. Brown AC, Chen JC, Watkins LKF, Campbell D, Folster JP, Tate H, et al. CTX-M-65 Extended-spectrum β-lactamase–producing *Salmonella enterica* serotype Infantis, United States. Emerg Infect Dis. 2018;24:2284–91. https://doi.org/10.3201/eid2412.180500
29. Health Canada. Categorization of antimicrobial drugs based on importance in human medicine. 2020. p. 1–9 [cited 2020 Dec 22]. https://www.canada.ca/en/health-canada/services/drugs-health-products/veterinary-drugs/antimicrobial-resistance/categorization-antimicrobial-drugs-based-importance-human-medicine.html
30. Peirano G, Pitout JD. Extended-spectrum β-lactamase–producing Enterobacteriaceae: update on molecular epidemiology and treatment options. Drugs. 2019;79:1529–41. https://doi.org/10.1007/s40265-019-01180-3
31. Zhang C-Z, Ding X-M, Lin X-L, Sun R-Y, Lu Y-W, Cai R-M, et al. The emergence of chromosomally located $bla_{CTX-M-55}$ in *Salmonella* from foodborne animals in China. Front Microbiol. 2019;10:1268. https://doi.org/10.3389/fmicb.2019.01268
32. Wang W, Zhao L, Hu Y, Dottorini T, Fanning S, Xu J, et al. Epidemiological study on prevalence, serovar diversity, multidrug resistance, and CTX-M-type extended-spectrum β-lactamases of *Salmonella* spp. from patients with diarrhea, food of animal origin, and pets in several provinces of China. Antimicrob Agents Chemother. 2020;64:10. https://doi.org/10.1128/AAC.00092-20
33. Bevan ER, Jones AM, Hawkey PM. Global epidemiology of CTX-M β-lactamases: temporal and geographical shifts in genotype. J Antimicrob Chemother. 2017;72:2145–55. https://doi.org/10.1093/jac/dkx146
34. Franco A, Leekitcharoenphon P, Feltrin F, Alba P, Cordaro G, Iurescia M, et al. Emergence of a clonal lineage of multidrug-resistant ESBL-producing *Salmonella* Infantis transmitted from broilers and broiler meat to humans in Italy between 2011 and 2014. PLoS One. 2015;10:e0144802. https://doi.org/10.1371/journal.pone.0144802
35. Alba P, Leekitcharoenphon P, Carfora V, Amoruso R, Cordaro G, Di Matteo P, et al. Molecular epidemiology of *Salmonella* Infantis in Europe: insights into the success of the bacterial host and its parasitic pESI-like megaplasmid. Microb Genom. 2020;6:e000365. https://doi.org/10.1099/mgen.0.000365
36. Lee WWY, Mattock J, Greig DR, Langridge GC, Baker D, Bloomfield S, et al. Characterization of a pESI-like plasmid and analysis of multidrug-resistant *Salmonella enterica* Infantis isolates in England and Wales. Microb Genom. 2021;7:000658. https://doi.org/10.1099/mgen.0.000658
37. Cartelle Gestal M, Zurita J, Paz Y Mino A, Ortega-Paredes D, Alcocer I, Alcocer I. Characterization of a small outbreak of *Salmonella enterica* serovar Infantis that harbour CTX-M-65 in Ecuador. Braz J Infect Dis. 2016;20:406–7. https://doi.org/10.1016/j.bjid.2016.03.007
38. Martínez-Puchol S, Riveros M, Ruidias K, Granda A, Ruiz-Roldán L, Zapata-Cachay C, et al. Dissemination of a multidrug resistant CTX-M-65 producer *Salmonella enterica* serovar Infantis clone between marketed chicken meat and children. Int J Food Microbiol. 2021;344:109109. https://doi.org/10.1016/j.ijfoodmicro.2021.109109
39. de Been M, Lanza VF, de Toro M, Scharringa J, Dohmen W, Du Y, et al. Dissemination of cephalosporin resistance genes between *Escherichia coli* strains from farm animals and humans by specific plasmid lineages. PLoS Genet. 2014;10:e1004776. https://doi.org/10.1371/journal.pgen.1004776
40. Zhang W-H, Lin X-Y, Xu L, Gu X-X, Yang L, Li W, et al. CTX-M-27 producing *Salmonella enterica* serotypes Typhimurium and Indiana are prevalent among food-producing animals in China. Front Microbiol. 2016;7:436. https://doi.org/10.3389/fcimb.2017.00436
41. Elnekave E, Hong SL, Lim S, Hayer SS, Boxrud D, Taylor AJ, et al. Circulation of plasmids harboring resistance genes to quinolones and/or extended-spectrum cephalosporins in multiple *Salmonella enterica* serotypes from swine in the United States. Antimicrob Agents Chemother. 2019;63:901. https://doi.org/10.1128/AAC.02602-18
42. Karanika S, Karantanos T, Arvanitis M, Grigoras C, Mylonakis E. Fecal colonization with extended-spectrum beta-lactamase-producing *Enterobacteriaceae* and risk factors among healthy individuals: a systematic review and metaanalysis. Clin Infect Dis. 2016;63:310–8. https://doi.org/10.1093/cid/ciw283
43. Eshaghi A, Zittermann S, Bharat A, Mulvey MR, Allen VG, Patel SN. Importation of extensively drug-resistant *Salmonella enterica* serovar Typhi cases in Ontario, Canada. Antimicrob Agents Chemother. 2020;64:e570. https://doi.org/10.1128/AAC.02581-19

Address for correspondence: Amrita Bharat, Public Health Agency of Canada, National Microbiology Laboratory, H5050, 1015 Arlington St, Winnipeg, MB R3E 3R2, Canada, email: amrita.bharat@phac-aspc.gc.ca

Outbreak of IncX8 Plasmid–Mediated KPC-3–Producing Enterobacterales Infection, China

Lan Chen,[1] Wenxiu Ai,[1] Ying Zhou,[1] Chunyang Wu, Yinjuan Guo, Xiaocui Wu, Bingjie Wang, Lulin Rao, Yanlei Xu, Jiao Zhang, Liang Chen, Fangyou Yu

Carbapenem-resistant Enterobacterales (CRE) infection is highly endemic in China; *Klebsiella pneumoniae* carbapenemase (KPC) 2–producing CRE is the most common, whereas KPC-3–producing CRE is rare. We report an outbreak of KPC-3–producing Enterobacterales infection in China. During August 2020–June 2021, 25 bla_{KPC-3}–positive Enterobacteriale isolates were detected from 24 patients in China. Whole-genome sequencing analysis revealed that the bla_{KPC-3} genes were harbored by IncX8 plasmids. The outbreak involved clonal expansion of KPC-3–producing *Serratia marcescens* and transmission of bla_{KPC-3} plasmids across different species. The bla_{KPC-3} plasmids demonstrated high conjugation frequencies (10^{-3} to 10^{-4}). A *Galleria mellonella* infection model showed that 2 sequence type 65 K2 *K. pneumoniae* strains containing bla_{KPC-3} plasmids were highly virulent. A ceftazidime/avibactam in vitro selection assay indicated that the KPC-3–producing strains can readily develop resistance. The spread of bla_{KPC-3}–harboring IncX8 plasmids and these KPC-3 strains should be closely monitored in China and globally.

Carbapenemase-producing Enterobacterales (CPE) have emerged as important nosocomial pathogens and are a global public health concern because of the high prevalence of CRE infection and its associated mortality rate. Currently, *Klebsiella pneumoniae* carbapenemase (KPC) is the most clinically important carbapenemase globally (*1*,*2*). Since its first discovery in 1996 (*3*), more than 90 KPC variants have been documented, of which KPC-2 and KPC-3 are the most common clinical variants (*4*). bla_{KPC} genes are frequently harbored by Tn*4401* or non-Tn*4401* mobile elements (NTM_{KPC}) (*5*), and the spread of bla_{KPC} has been primarily associated with transmissible plasmids, belonging to different incompatibility groups (e.g., IncFII, IncI2, IncX, IncA/C, IncR, IncN, and ColE) (*5*).

China is regarded as a CRE-endemic region where *K. pneumoniae*, *Escherichia coli,* and *Enterobacter cloacae* complex are the most common CRE species (*6*,*7*). Among the CREs, ≈80%–90% were carbapenemase-producers, including >90% carbapenem-resistant *K. pneumoniae* and *E. coli* and ≈80% of carbapenem-resistant *E. cloacae* strains. For carbapenemase genes, the bla_{KPC-2} was the most dominant type (≈60%), followed by bla_{NDMs} and bla_{IMPs}. Interestingly, other KPC variants, especially KPC-3, are rarely detected in China. Compared with KPC-2, KPC-3 differs by a single amino acid substitution (H272Y) and shows higher hydrolysis efficiency against oxyimino-cephalosporins and carbapenems (*8*). In most KPC-endemic regions, including United States and countries in Europe, KPC-3 showed similar prevalence as that of KPC-2 enzyme, and both KPC variants were frequently detected in clinical CRE isolates. Despite China being KPC-endemic, KPC-3 has only been sporadically reported in China (*9*–*13*).

In this study, we describe a hospital outbreak of KPC-3–producing *Enterobacterales* involved with multiple species, including *Serratia marcescens*, *K. pneumoniae*, *Escherichia coli*, *Enterobacter hormaechei*, and *Proteus mirabilis* in mainland China. We obtained approval for the study from Ningbo First Hospital Ethics Committee (approval no. 2021RS095).

Author affiliations: Ningbo First Hospital, Ningbo, China (L. Chen); First Affiliated Hospital of Wenzhou Medical University, Wenzhou, China (W. Ai, C. Wu, L. Rao, J. Zhang, F. Yu); Shanghai Pulmonary Hospital, Tongji University School of Medicine, Shanghai, China (Y. Zhou, Y. Guo, X. Wu, B. Wang, Y. Xu, F. Yu); Hackensack Meridian Health Center for Discovery and Innovation, Nutley, New Jersey, USA (L. Chen); Hackensack Meridian School of Medicine, Nutley (L. Chen)

DOI: https://doi.org/10.3201/eid2807.212181

[1]These first authors contributed equally to this article.

Materials and Methods

During August 1, 2020–June 30, 2021, we collected from a tertiary hospital in Ningbo, Zhejiang Province, China, 25 nonrepeated KPC-3–producing Enterobacterales isolates showing reduced susceptibility to carbapenems. None of the patients from whom the isolates were taken had international travel history in the preceding 3 months. We detected the presence of carbapenemase genes, including bla_{KPC}, bla_{NDM}, $bla_{OXA\text{-}48\text{-}like}$, bla_{VIM}, and bla_{IMP}, by using PCR, followed by Sanger sequencing (*14*,*15*). We initially determined speciation by using matrix-assisted laser desorption/ionization time-of-flight mass spectrometry and analyzed results by using the Vitek MS database (bioMérieux, https://www.biomerieux.com); we later confirmed the results by using whole-genome sequencing (WGS) analysis.

We performed antimicrobial susceptibility testing and modified carbapenem inactivation and applied WGS to explore the molecular features of the isolates (Appendix 1, https://wwwnc.cdc.gov/EID/article/28/7/21-2181-App1.pdf). We also conducted conjugation and electroporation experiments (and performed pulsed-field gel electrophoresis (PFGE) and S1-nuclease PFGE (Appendix 1). We applied string test to examine the Hypermucoviscous phenotypes of *K. pneumoniae* strains and *Galleria mellonella* infection model to evaluate the virulence potential of sequence type (ST) 65 K2 *K. pneumoniae* strains (Appendix 1). We applied a ceftazidime/avibactam in vitro selection assay to evaluate whether the KPC-3-producing strains were easily selected to be resistant to ceftazidime/avibactam (Appendix 1).

We submitted the complete nucleotide sequences of the plasmids pFK3112-KPC-3 and pCG2111-KPC-3 to GenBank (accession nos. CP081509 [pFK3112-KPC-3] and CP081510 [pCG2111-KPC-3]). We also deposited the raw reads of the genomes we sequenced in GenBank (Bioproject accession no. PRJNA354234).

Results

Outbreak Description of bla_{KPC-3}–harboring Enterobacterales

During August 1, 2020–June 30, 2021, we detected 25 KPC-3–producing Enterobacterales isolates in patients of a tertiary hospital in eastern China, including 18 *Serratia marcescens*, 3 *K. pneumoniae*, 1 *E. coli*, 2 *E. hormaechei*, and 1 *Proteus mirabilis*. The 25 isolates were from 24 patients; 1 patient had 2 isolates from sputum (FK3015) and blood (FK3018). The strains were recovered from sputum (n = 19), blood (n = 3), urine (n = 1), puncture fluid (n = 1), and bile (n = 1).

The first KPC-3 strain (*S. marcescens* CG2008) was isolated in August 2020, and the patient was admitted to the intensive care unit (ICU) 1 (building 3) with unconsciousness attributable to a head injury sustained in an accident. After 20 days of the patient's hospitalization, we detected a carbapenem-resistant *S. marcescens* in the patient's sputum. After that, we detected 4 additional carbapenem-resistant *S. marcescens* strains in the same ICU ward during August 2020–May 2021 (Appendix 2 Table 1, https://wwwnc.cdc.gov/EID/article/28/7/21-2181-App2.xlsx). Starting in January 2021, we also found carbapenem-resistant *S. marcescens* strains (n = 6) in another ICU (building 2, ICU-2) and the wards of cardiology (building 2) (n = 2), emergency (building 3) (n = 1), and hepatobiliary and pancreatic surgery (building 3) (n = 1). In addition, starting in September 2020, we identified these KPC-3–producing strains in other *Enterobacterales* species in ICU-2 (*K. pneumoniae*), the coronary heart disease care unit (*K. pneumoniae*), ICU-1 (*P. mirabilis* and *E. coli*), the infectious disease ward (building 6) (*E. hormaechei*), and the hepatobiliary and pancreatic surgery ward (*E. hormaechei*) (Appendix 2 Table 1).

Of the patients, 23/24 were admitted into wards in medical buildings 2 and 3, including the 2 ICUs, in our hospital (Figure 1, panel A); 18 of them were infected with the *S. marcescens* (bla_{KPC-3}). Most patients shared the same ward during the same time, especially the patients from ICU-1 and ICU-2. The 2 buildings were connected by a pedestrian bridge, and frequent movement of persons (medical workers, patients, and visitors) and portable medical devices occurred between the 2 buildings, providing many opportunities for the intrahospital transmission of bacterial pathogens between buildings and wards.

Average age of these patients was 72 years (range 39–94 years), and most (79%) were men. All but 1 KPC-3 isolates were detected >2 days after admission (range 4–328 days). KPC-3 *E. coli* isolate CG2126 (from patient 22) was detected from the blood sample of a patient on the same day of admission in April 2021; however, this patient had cholangiocarcinoma and had been hospitalized in the hepatobiliary and pancreatic surgery ward 2 weeks earlier. Most patients had serious underlying diseases, including type 2 diabetes mellitus (n = 8), hypertension (n = 4), hypoproteinemia (n = 4), and cerebral infarction (n = 2). Most patients had received β-lactam antimicrobial treatments, such as piperacillin/tazobactam (n = 17), meropenem (n = 12), tigecycline (n = 12), and cefoperazone/sulbactam (n = 9). Most patients (95.8%) underwent invasive procedures that involved medical devices, including attachment of a ventilator

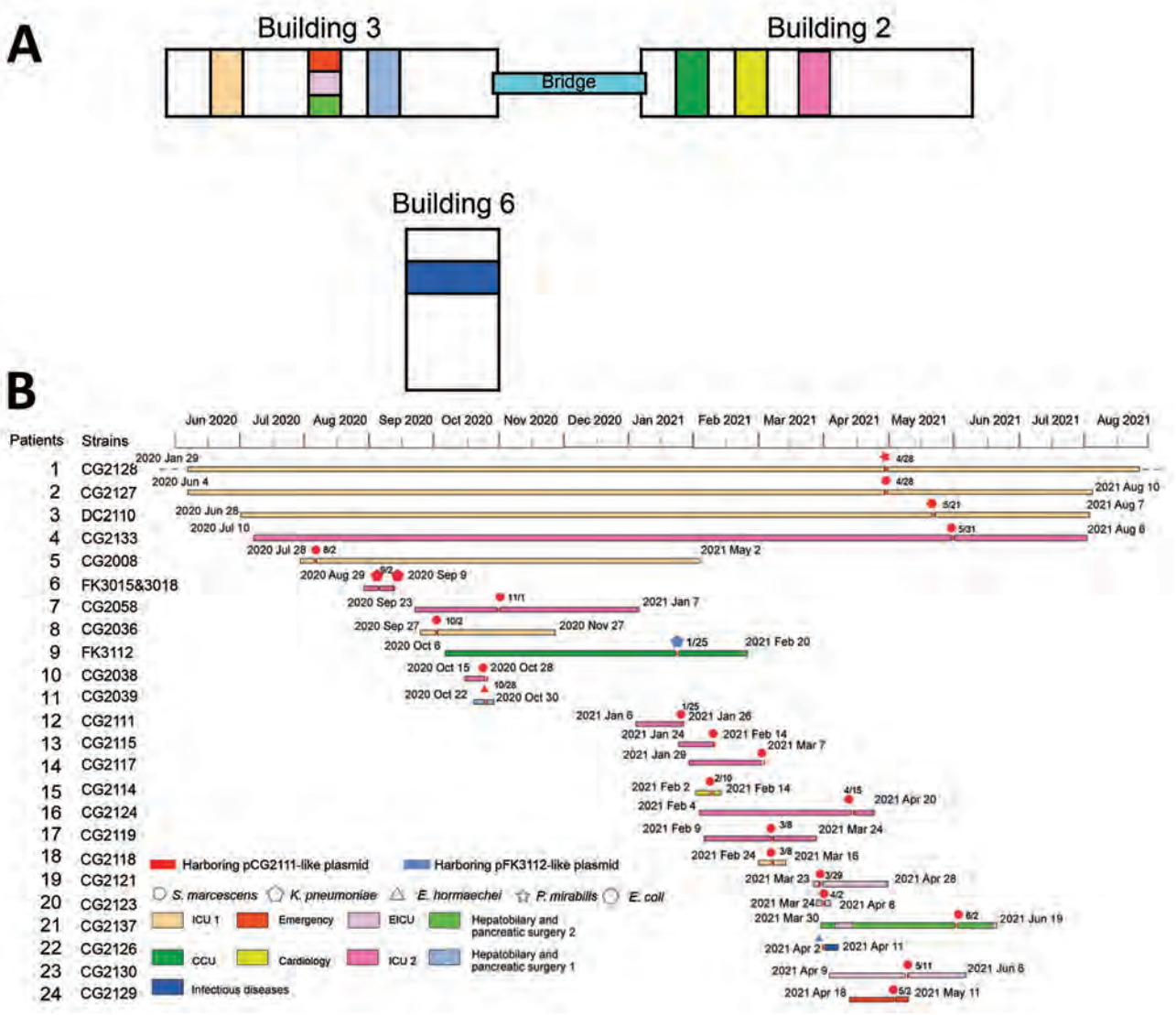

Figure 1. Characteristics of outbreak of *Klebsiella pneumoniae* carbapenemase 3–producing *Enterobacterales* infection at a tertiary hospital in Ningbo, Zhejiang Province, China, August 1, 2020–June 30, 2021. A) Spatial location features of the hospital. B) Timeline of events during the outbreak. CCU, cardiac care unit; EICU, emergency intensive care unit; ICU, intensive care unit.

(23/24), deep vein intubation (9/24), and attachment of a urinary catheter (4/24) (Appendix 2 Table 1). In addition, most patients had prolonged hospital stays (range 8–462 days), including 6 patients who were hospitalized for >6 months (Figure 1, panel B). The prognosis of some patients was poor. Half of the patients (n = 12) had deteriorating health conditions during discharge, and 3 patients died during their hospital stay (Appendix 2 Table 1).

Starting in mid-2021 (and coinciding with the COVID-19 epidemic), the hospital enacted enhanced infection control measures, including chlorhexidine skin cleaning for ICU patients, improved hand hygiene compliance in healthcare workers, easy access to hand-hygiene supplies, restriction of hospital visitors, decontamination of the patients' environment, and enhanced disinfection of medical equipment. Those measures also help to control the KPC-3 CRE outbreak, and only 1 carbapenem-resistant *S. marcescens* (attributable to NDM) was detected from August 2021 (data not shown).

Antimicrobial Susceptibility and Carbapenem Inactivation Assay

We then examined the susceptibility of the 25 isolates against 18 antibiotics (Appendix 2 Table 2). Our results indicated these isolates were all multidrug-resistant, exhibiting high-level resistance to all β-lactam

antibiotics, including carbapenems, but remained susceptible to amikacin, gentamicin, and ceftazidime/avibactam (except CG2126). The *E. hormaechei* isolate CG2126 was resistant to ceftazidime/avibactam because of the co-existence of bla_{NDM-1} (Appendix 2 Table 1). Modified carbapenem inactivation method results confirmed that all 25 isolates were carbapenemase producers, consistent with the presence of bla_{KPC-3} (or bla_{NDM-1}) genes among these isolates.

Genomic Phylogeny of KPC-3–producing Enterobacterales

We first conducted a core-genome phylogenetic analysis by using Parsnp (*16*) and compared our KPC-3–producing *S. marcescens* genomes with 748 *S. marcescens* genome assemblies from the National Center for Biotechnology Information RefSeq database (https://www.ncbi.nlm.nih.gov/refseq [accessed October 1, 2021]). A total of 73 strains were from China. The core-genome tree showed that the 18 KPC-3 *S. marcescens* strains formed a single cluster and were phylogenetically close to another cluster of 44 strains, which mostly harbored KPC-2 and were from China (named KPC-2 cluster) (Figure 2). Further core single-nucleotide polymorphism (SNP) distance analysis showed that the 18 outbreak strains differed by an average of 7 core SNPs (range 0–18), indicating clonal expansion. They differed from the China KPC-2 cluster strains by an average of 7,400 core SNPs (range 7,388–7,428) and differed from the remaining strains

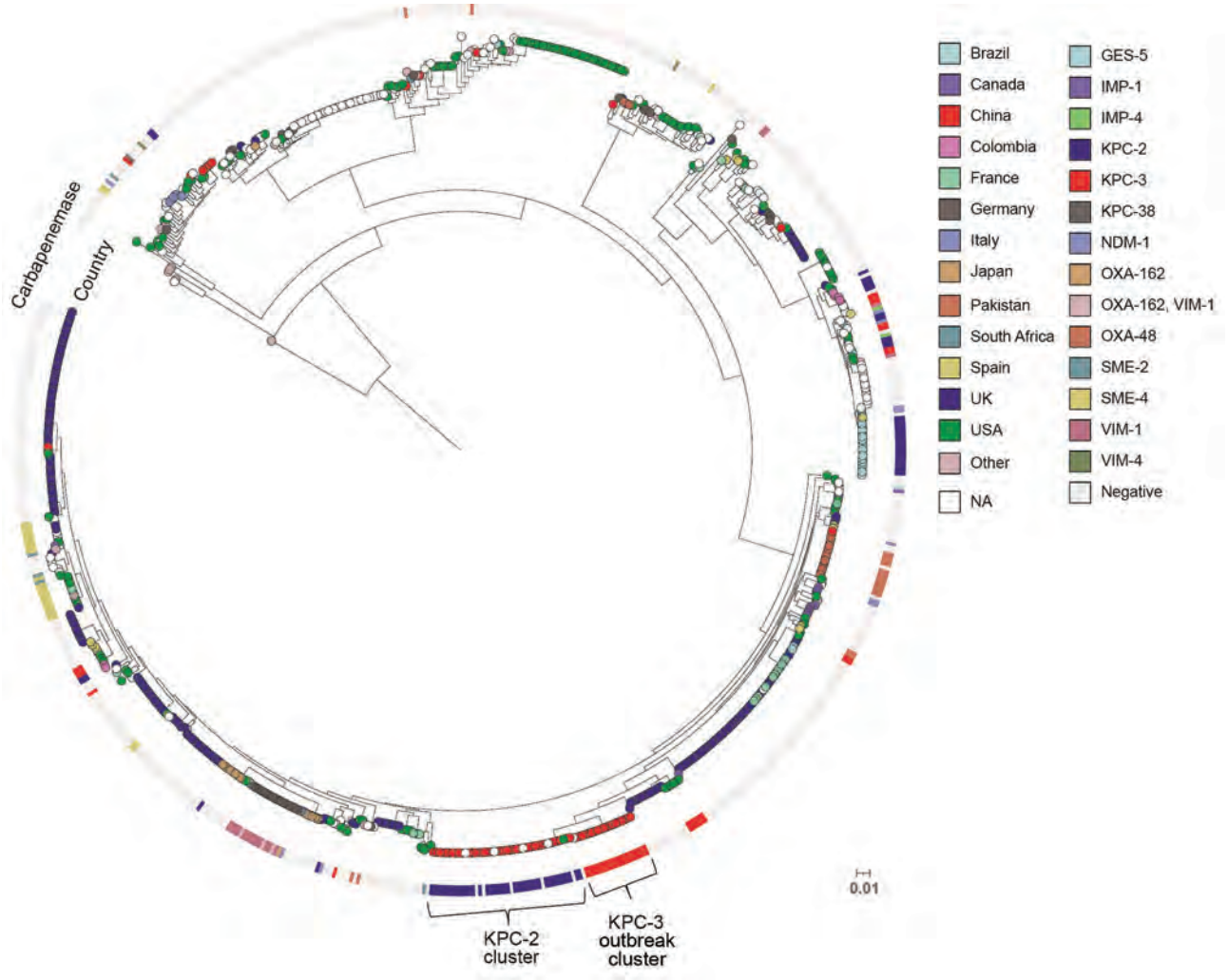

Figure 2. Core-genome phylogenetic tree of 748 *Serratia marcescens* genomes from the National Center for Biotechnology Information RefSeq database (https://www.ncbi.nlm.nih.gov/refseq) and 18 KPC 3–producing strains from an outbreak of KPC 3–producing Enterobacterales infection at a tertiary hospital in Ningbo, Zhejiang Province, China, August 1, 2020–June 30, 2021. The isolation country is color-coded and illustrated at the tips. Carbapenemases are presented as a color-coded outer circle. The tree was rooted in the midpoint. Scale bar represents 0.01 mutations per nucleotide position. KPC, *K. pneumoniae* carbapenemase; NA, not available; UK, United Kingdom; USA, United States.

from China by an average of 45,082 core SNPs (range 11,173–58,247), suggesting that the KPC-3 strains belonged to a unique clone, which is consistent with the core-genome phylogeny (Figure 2).

Three *K. pneumoniae* strains carried bla_{KPC-3}, and they belonged to 2 STs (ST65 and ST967), containing KL2 and KL18 type capsules. The 2 K2 ST65 strains were isolated from the same patient. ST65 K2 strains belonged to prototypical hypervirulent *K. pneumoniae* clone, harboring a battery of virulence genes, encoding yersiniabactin (*ybt*), colibactin (*clb*), aerobactin (*iuc*), and Salmochelin (*iro*). The 2 K2 strains also contained an IncHIB-FIB virulence plasmid, harboring the regulator of mucoid phenotype A genes *rmpA* and *rmpA2*. The 2 ST65 strains only differed by 2 core SNPs. The *E. hormaechei* strain CG2126 belonged ST127, and the *E. coli* strain was from a novel ST.

bla_{KPC-3}–harboring IncX8 Plasmids

Two representative bla_{KPC-3}-plasmids (pCG2111-KPC-3 and pFK3112-KPC-3) were completely sequenced. De novo assembly of the plasmid sequences generated a single head-to-tail contig for each plasmid. PlasmidFinder 2.1 assigned the 2 plasmids as the IncX5_2 (GenBank accession no. MF062700), whereas a recent study has reassigned IncX5_2 plasmids as a novel IncX8 group (*17*).

The pCG2111-KPC-3 was 41,852 bp in length, with an average G+C content of 46%, and harbored 57 predicted open reading frames, with bla_{KPC-3} the only intact antimicrobial resistance gene. A BLAST search (https://blast.ncbi.nlm.nih.gov/Blast.cgi) showed that pCG2111-KPC-3 was almost identical to plasmids p13190–3 (bla_{KPC-2}–harboring; GenBank accession no. MF344555) (*17*), isolated from ST392 *K. pneumoniae* in 2013, and p15WZ-82_KPC (bla_{KPC-2}–harboring; GenBank accession no. CP032355) (*18*), isolated from ST595 *K. variicola* in 2015 in China. In addition, both bla_{KPC-3} (in pCG2111-KPC-3) and bla_{KPC-2} (in p13190–3 and p15WZ-82_KPC) genes were carried by a conserved Tn*3* transposon, with the structure of *tnpA*-*npR*-IS*kpn27*-Δbla_{TEM}-$bla_{KPC-2/3}$-IS*kpn6*. We observed 2 major differences between pCG2111-KPC-3 and the other 2 *Klebsiella* IncX8 plasmids: first, pCG2111-KPC-3 harbors bla_{KPC-3}, whereas the other 2 carry bla_{KPC-2}; second, the 2 *Klebsiella* IncX8 plasmids have 8 22-bp iterons located upstream from the replication gene, whereas pCG2111-KPC-3 only has 7 copies of iteron, and 1 iteron (AAACATGATGATAAATGCGAAT) was deleted (Figure 3, 4).

The pFK3112-KPC-3 plasmid was smaller (21,888 bp in length) and had an average G+C content of 48%, carrying the same IncX8 replicon, and harbored 36 predicted

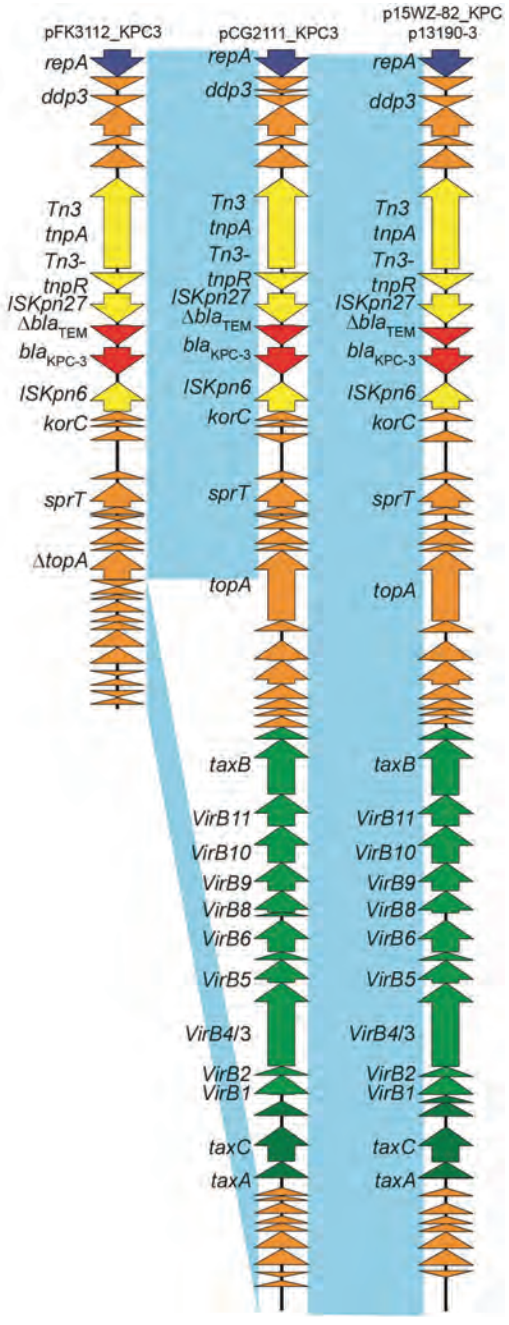

Figure 3. Comparative analysis of the bla_{KPC-3}–harboring plasmid pCG2111_KPC3 (GenBank accession no. CP081510), pFK3112_KPC3 (GenBank accession no. CP081509), p15WZ-82-KPC, and *Klebsiella pneumoniae* p13190 in isolates from an outbreak of KPC 3–producing Enterobacterales infection at a tertiary hospital in Ningbo, Zhejiang Province, China, August 1, 2020–June 30, 2021. Open reading frames are portrayed by arrows and are depicted in different colors on the basis of their predicted gene functions. Red arrows indicate resistance genes, and green arrows indicate genes associated with the type IV secretion system. Orange arrows represent the backbone genes of the plasmid, and yellow arrows denote the mobile elements. Light blue shading denotes shared regions of homology among different plasmids. KPC, *K. pneumoniae* carbapenemase.

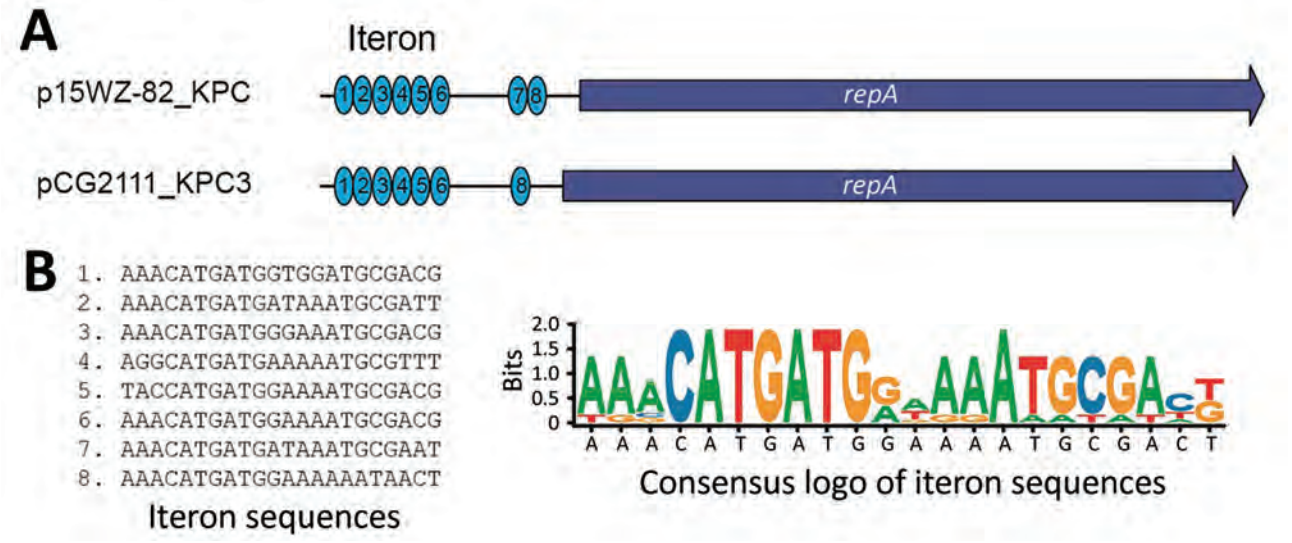

Figure 4. The iteron difference between pCG2111-KPC-3 and p15WZ-82_KPC. A) p15WZ-82_KPC IncX8 plasmids have eight 22-bp iteron copies located upstream from the replication gene, whereas pCG2111-KPC-3 only has 7 copies of iteron and the seventh iteron (in comparison to p15WZ-82_KPC) was deleted. B) The sequences of the 8 iterons are listed and a SeqLog (https://pypi.org/project/seqlog) presentation of the conserved motif is shown. KPC, *K. pneumoniae* carbapenemase.

open reading frames. In comparison to pCG2111-KPC-3, the only difference is that pFK3112-KPC-3 has a 19,964-bp deletion flanked by 5-bp repeat sequences of GCATC, encompassing the entire transfer operon from the type IA DNA topoisomerase gene *top* to the DNA distortion polypeptide gene *taxA* (Figure 3, 4).

We then used pCG2111-KPC-3 and pFK3112-KPC-3 as the reference sequences, and we used the reference mapping and mauve contig mover (*19*) functions in Geneious Prime 2020 (https://www.geneious.com) to reconstruct the IncX8 plasmids from the remaining 23 bla_{KPC-3}–haroboring strains. The analysis showed that the *S. marcescens* (n = 18), *E. coli* (n = 1), *E. hormaechei* (n = 1) (CG2039), *P. mirabilis* (n = 1), and ST65 K2 *K. pneumoniae* strains (n = 2) carried pCG2111-KPC-3–like plasmids. One *E. hormaechei* isolate (CG2126) had the pFK3112-KPC-3–like plasmid, with a ≈20-kb deletion in comparison to pCG2111-KPC-3.

We then used conjugation assay to evaluate the transconjugation ability and frequency of bla_{KPC-3}–harboring IncX8 plasmids. We selected 7 strains, 5 *S. marcescens* and 2 ST65 K2 *K. pneumoniae*, as the donors and the *E. coli* EC600 as the recipient strain. The bla_{KPC-3} plasmids from these isolates were all successfully transferred to the recipient strain. The S1-nuclease PFGE pattern showed that all the 7 transconjugants had only 1 plasmid, at a size of ≈42 kb (Figure 5). The transfer frequencies of the 7 strains ranged from 1.57×10^{-3} to 7.8×10^{-4}. The antimicrobial susceptibility testing results further confirmed the carbapenem resistance had been transferred to recipient strains. In addition, we tested the transconjugation ability of pFK3112-KPC-3 in *K. pneumoniae* FK3112, and the result showed that pFK3112-KPC-3 failed to conjugate, which is consistent with the sequence analysis showing the lack of *tra* operon.

Ceftazidime/avibactam in vitro Selection Assays

Ceftazidime/avibactam has been increasingly used in China to treat CRE infections, especially those attributable to KPC producers (*20*,*21*). We conducted a subinhibitory concentration antimicrobial selection experiment in 24 KPC-3 strains (except CG2126) to examine their potential to develop ceftazidime/avibactam resistance. After induced selection by 1/2 MIC concentration of ceftazidime/avibactam, 22 isolates (all except 2 *S. marcescens*) developed resistance (MIC ≥16/4 μg/mL), and the resistant rate was as high as 91.7%. By contrast, we conducted the same in vitro selection in 24 bla_{KPC-2}–harboirng *K. pneumoniae* strains. Only 1 strain developed ceftazidime/avibactam resistance (MIC ≥16/4 μg/mL) after 1/2 MIC induction, and the resistant rate was as low as 4.2%, which is significantly lower that of the induced resistance rate of KPC-3 strains ($p<0.05$). These results further suggested that these KPC-3-producing strains can be easily selected for resistance to ceftazidime/avibactam.

G. mellonella Infection Model of KPC-3–Producing Hypervirulent K2 *K. pneumoniae* Strains

K. pneumoniae K2 ST65 strains belong to the prototypical hypervirulent clone. A string test of the ST65

strains FK3015 and FK3018 showed positive results, consistent with their genotypes. To assess the potential virulence of these 2 isolates, we conducted the *G. mellonella* larvae infection experiment (Figure 6). After 20 hours of infection, bla_{KPC-3}–harboring ST65 strains and the hypervirulent reference K2 *K. pneumoniae* strain ATCC 43816 showed a 100% mortality rate, which was significantly higher than that observed in larvae infected with nontoxic reference classical *K. pneumoniae* strains ($p<0.05$). These results indicate that the KPC-3 K2 ST65 *K. pneumoniae* are highly virulent and the acquisition of bla_{KPC-3}–harboring IncX8 plasmids does not comprise the virulence potential in these strains.

Discussion

In this study, we report a KPC-3–producing Enterobacterales outbreak in China. In China, the spread of bla_{KPC-2} was primarily associated with IncFII(pHN7A8)-R plasmids and with epidemic *K. pneumoniae* ST11 strains (*22*–*24*), whereas this KPC-3 outbreak was primarily associated with the clonal expansion of *S. marcescens* and was mediated by an uncommon IncX8 plasmid. We also detected horizontal transmission of bla_{KPC-3}–harboring IncX8 plasmids in different Enterobacterales species. The *S. marcescens*, *E. coli*, *P. mirabilis*, *E. hormaechei* (CG2126), and the *K. pneumoniae* ST65 strains harbored the same plasmid as pCG2111-KPC-3, indicating horizontal transmission of bla_{KPC-3} plasmids in these strains. However, the origin of pCG2111-KPC-3 remains unclear. Although KPC-3 was initially detected in an *S. marcescens* isolate (CG2008), the possibility that CG2008 acquired this plasmid from other strains cannot be ruled out. bla_{KPC-2} IncX8 plasmids have been reported in *Klebsiella* isolates in China, and in our study 2 KPC-3–producing *K. pneumoniae* strains were recovered nearly at the same time as CG2008 (Appendix 2 Table 1). In addition, *S. marcescens* strains might have obtained pCG2111-KPC-3–like plasmids from other strains (e.g., *K. pneumoniae*), which was then followed by clonal expansion.

The *E. hormaechei* strain (CG2039) in patient 24 and the *K. pneumoniae* ST967 strain (FK3112) from patient 20 harbored the same truncated plasmid (pFK3112-KPC-3), which may arise by recombination after the acquisition of intact plasmid. However, our conjugation experiment showed that pFK3112-KPC-3 cannot self-conjugate, and thus a possible explanation of the presence of pFK3112-KPC-3 in *E. hormaechei* and *K. pneumoniae* strain was that the same recombination happened independently in both species or pFK3112-KPC-3 was transferred with the assistance of helper plasmids. Our analysis demonstrated that plasmid-mediated horizontal and vertical transmission have played important roles in the KPC-3 Enterobacterales outbreak.

The bla_{KPC-3}–harboring InX8 plasmid pCG2111-KPC-3 was almost identical to the bla_{KPC-2}–harboring plasmids p13190–3 and p15WZ-82_KPC from *K. pneumoniae* and *K. variicola* strains in China, suggesting that KPC-3 probably originated through a single

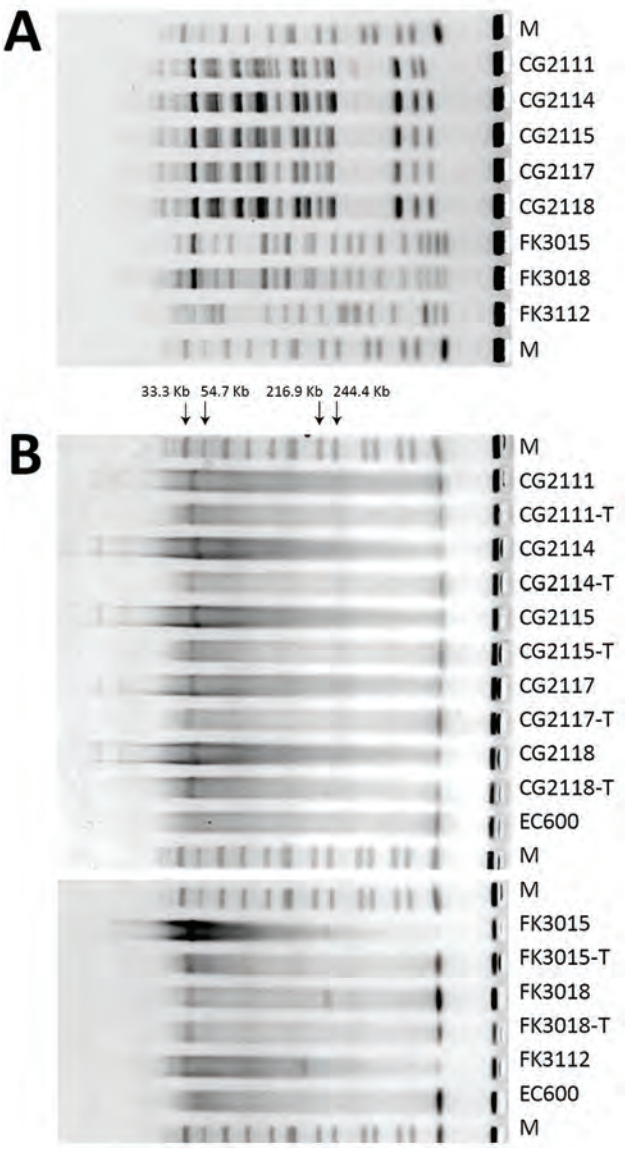

Figure 5. Pulsed-field gel electrophoresis (PFGE) profiles of selected *Klebsiella pneumoniae* carbapenemase 3–producing Enterobacterales strains isolated from patients at a tertiary hospital in Ningbo, Zhejiang Province, China, August 1, 2020–June 30, 2021. A) PFGE profiles. B) S1-nuclease PFGE profiles. EC, *Escherichia coli* EC; M, *Salmonella enterica* serotype Braenderup strain H9812; -T, the transconjugants of the corresponding strain.

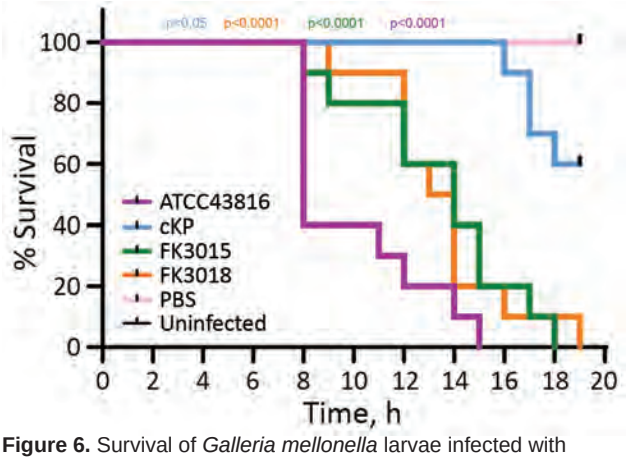

Figure 6. Survival of *Galleria mellonella* larvae infected with *Klebsiella pneumoniae* strains isolated from patients at a tertiary hospital in Ningbo, Zhejiang Province, China, August 1, 2020–June 30, 2021. A hypervirulent *K. pneumoniae* K2 strain ATCC 43816 was used as the positive control. A phosphate-buffered saline–injected and a pricking larval group (empty needle injection, uninfected) served as negative control groups. Data are pooled from ≥3 independent experiments with 10 larvae per group per run. The representative results are displayed. cKP, classical *K. pneumoniae*; PBS, phosphate-buffered saline.

amino acid substitution on the same IncX8 plasmid. A similar KPC-2 to KPC-3 change has also been described in other bla_{KPC}–harboring plasmids, including the epidemic pKpQIL-like plasmids (*25*). However, plasmids p13190–3 and p15WZ-82_KPC were identified in 7 (2013) and 5 (2015) years before the KPC-3 outbreak (2020), indicating that the bla_{KPC-2}–harboring IncX8 plasmids have already existed and possibly circulated in China previously.

Compared with the predominant bla_{KPC-2}–harboring IncFII (pHN7A8)-R plasmids (>100 kb) in China, the bla_{KPC-3}–harboring IncX8 plasmid has a smaller genome size (≈42 kb). Our results showed the conjugation frequencies of bla_{KPC-3}–harboring IncX8 ranged from 1.57×10^{-3} to 7.8×10^{-4} per donor cell, which is similar to that of the bla_{KPC-2}–harboring plasmids (6.3×10^{-3} to 1×10^{-4}) (*26*–*28*) and the epidemic bla_{NDM}–harboring IncX3 plasmids (*29*,*30*), which have spread widely across different sectors of the human population, the animal population, and the environment (*29*–*31*). Compared with the previously reported bla_{KPC-2}–harboring plasmids (p13190-3 and p15WZ-82_KPC), our KPC-3 IncX8 plasmids have 1 less copy of iterons in the replication origin. The iterons are essential for plasmid replication and inhibition of plasmid overreplication (*32*). Whether the deletion of an iteron copy could affect the plasmid replication or copy numbers, leading to increase plasmid transfer, is unclear, which warrants further studies. Nevertheless, our study clearly demonstrates that IncX8 plasmids can transfer across different clinical Enterobacterales species. Our *G. mellonella* infection model results also indicated that the acquisition of bla_{KPC-3}–harboring IncX8 in clinical hypervirulent ST65 K2 *K. pneumoniae* strains does not lead to reduced virulence. This observation could be another example of the emergence of carbapenem-resistant and hypervirulent *K. pneumoniae* strains attributable to the horizontal transfer of bla_{KPC-3}–harboring IncX8 plasmids into prototypically hypervirulent K2 strains.

Although most KPC-3 producing strains were multidrug-resistant, most of them remained sensitive to ceftazidime/avibactam. In China, ceftazidime/avibactam has been approved for clinical treatment since 2019. However, resistance emerged soon after the clinical use of ceftazidime/avibactam in different regions, including China; this resistance usually was associated with mutations in the omega loop of KPC enzymes (*33*–*35*). Ceftazidime/avibactam resistance appeared to occur more frequently in a KPC-3 than a KPC-2 background, presumably because of the higher hydrolysis activity of KPC-3 against ceftazidime (*8*,*36*). Our subinhibitory concentrations ceftazidime/avibactam selection experiment results showed that most of our KPC-3–producing strains developed resistance, and the resistance rate was as high as 91.7%. By contrast, the KPC-2-producing strains showed a <4.2% rate for developing ceftazidime/avibactam resistance. However, PCR and Sanger sequencing of subinhibitory concentrations ceftazidime/avibactam–selected KPC-3 strains (3 colonies of each stain) failed to identify amino acid mutation in KPC-3 (data not shown). We suspected alternative mechanism, such as the increased gene copy numbers, expressions, or both (*37*,*38*), might contribute to ceftazidime/avibactam resistance. Nevertheless, our results suggested that the IncX8 bla_{KPC-3} strains may readily develop ceftazidime/avibactam resistance during treatment, despite being susceptible in vitro, which poses a major challenge for the clinical application of ceftazidime/avibactam as a last resort for treating CRE infections.

In this study, most patients had underlying diseases, had lengthy hospital stays, and underwent invasive medical device treatments (e.g., treatments involving a ventilator). Mechanical ventilation is a known risk factor of nosocomial infections, including CRE-attributable infections. The close proximity of these medical wards and movement of persons between the 2 buildings probably promoted the spread of KPC-3 strains between different wards. However, this outbreak went unrecognized and unconfirmed during routine surveillance, until our genomic study commenced in later

2021. Nevertheless, the COVID-19–related enhanced infection control measures already in place effectively controlled the KPC-3 outbreak. Unfortunately, this outbreak was not recognized and confirmed during routine surveillance, which should have detected the high numbers of multidrug-resistant *Serratia* infections as an unusual, and possibly epidemic, occurrence. Our results further emphasize that genomic surveillance and improved infection control practice are essential to tackle hospital outbreaks.

In summary, we report a KPC-3 *Enterobacterales* outbreak in China, which involved both clonal and horizontal transmissions of carbapenem resistance. The further spread of the bla_{KPC-3}–harboring IncX8 plasmids and these KPC-3 strains in China and other global regions should be closely monitored.

This study was supported by grants from Shanghai Pulmonary Hospital's Department of Clinical Laboratory Medicine and the Shanghai Sailing Program (grant no. 22YF1437500).

About the Author

Ms. Chen is a researcher at Ningbo First Hospital Department of Clinical Laboratory Medicine whose research interests include antibiotic-resistance mechanisms. Ms. Ai is a researcher at First Affiliated Hospital of Wenzhou Medical University Department of Respiratory Medicine whose research interests include antibiotic-resistance mechanisms. Dr. Zhou is a researcher at Shanghai Pulmonary Hospital Department of Clinical Laboratory Medicine, Tongji University School of Medicine whose research interests include antibiotic-resistance mechanisms.

References

1. Kitchel B, Rasheed JK, Patel JB, Srinivasan A, Navon-Venezia S, Carmeli Y, et al. Molecular epidemiology of KPC-producing *Klebsiella pneumoniae* isolates in the United States: clonal expansion of multilocus sequence type 258. Antimicrob Agents Chemother. 2009;53:3365–70. https://doi.org/10.1128/AAC.00126-09
2. Piazza A, Principe L, Comandatore F, Perini M, Meroni E, Mattioni Marchetti V, et al. Whole-genome sequencing investigation of a large nosocomial outbreak caused by ST131 H30Rx KPC-producing *Escherichia coli* in Italy. Antibiotics (Basel). 2021;10:718. https://doi.org/10.3390/antibiotics10060718
3. Yigit H, Queenan AM, Anderson GJ, Domenech-Sanchez A, Biddle JW, Steward CD, et al. Novel carbapenem-hydrolyzing beta-lactamase, KPC-1, from a carbapenem-resistant strain of *Klebsiella pneumoniae.* Antimicrob Agents Chemother. 2001;45:1151–61. https://doi.org/10.1128/AAC.45.4.1151-1161.2001
4. Hirsch EB, Tam VH. Detection and treatment options for *Klebsiella pneumoniae* carbapenemases (KPCs): an emerging cause of multidrug-resistant infection. J Antimicrob Chemother. 2010;65:1119–25. https://doi.org/10.1093/jac/dkq108
5. Chen L, Mathema B, Chavda KD, DeLeo FR, Bonomo RA, Kreiswirth BN. Carbapenemase-producing *Klebsiella pneumoniae*: molecular and genetic decoding. Trends Microbiol. 2014;22:686–96. https://doi.org/10.1016/j.tim.2014.09.003
6. Zhang Y, Wang Q, Yin Y, Chen H, Jin L, Gu B, et al. Epidemiology of carbapenem-resistant *Enterobacteriaceae* infections: report from the China CRE Network. Antimicrob Agents Chemother. 2018;62:e01882–17. https://doi.org/10.1128/AAC.01882-17
7. Zhang R, Liu L, Zhou H, Chan EW, Li J, Fang Y, et al. Nationwide surveillance of clinical carbapenem-resistant *Enterobacteriaceae* (CRE) strains in China. EBioMedicine. 2017;19:98–106. https://doi.org/10.1016/j.ebiom.2017.04.032
8. Alba J, Ishii Y, Thomson K, Moland ES, Yamaguchi K. Kinetics study of KPC-3, a plasmid-encoded class A carbapenem-hydrolyzing beta-lactamase. Antimicrob Agents Chemother. 2005;49:4760–2. https://doi.org/10.1128/AAC.49.11.4760-4762.2005
9. Li G, Wei Q, Wang Y, Du X, Zhao Y, Jiang X. Novel genetic environment of the plasmid-mediated KPC-3 gene detected in *Escherichia coli* and *Citrobacter freundii* isolates from China. Eur J Clin Microbiol Infect Dis. 2011;30:575–80. https://doi.org/10.1007/s10096-010-1124-7
10. Du H, Chen L, Chavda KD, Pandey R, Zhang H, Xie X, et al. Genomic characterization of *Enterobacter cloacae* isolates from China that coproduce KPC-3 and NDM-1 carbapenemases. Antimicrob Agents Chemother. 2016;60:2519–23. https://doi.org/10.1128/AAC.03053-15
11. Miao M, Wen H, Xu P, Niu S, Lv J, Xie X, et al. Genetic diversity of carbapenem-resistant (CRE) clinical isolates from a tertiary hospital in eastern China. Front Microbiol. 2018;9:3341. https://doi.org/10.3389/fmicb.2018.03341
12. Wei J, Zou C, Wang D, Huang A, Niu S. Genetic diversity and in vitro activity of ceftazidime/avibactam and aztreonam/avibactam against imipenem-resistant *Enterobacteriaceae* isolates in southwest China: a single-centre study. J Glob Antimicrob Resist. 2020;22:448–51. https://doi.org/10.1016/j.jgar.2020.04.023
13. Tang H-J, Chen Y-T, Chiang T, Fung C-P, Chuang Y-C, Kristopher Siu L. Identification of the first imported KPC-3 *Klebsiella pneumoniae* from the USA to Taiwan. Int J Antimicrob Agents. 2014;44:431–5. https://doi.org/10.1016/j.ijantimicag.2014.07.009
14. Queenan AM, Bush K. Carbapenemases: the versatile beta-lactamases. Clin Microbiol Rev. 2007;20:440–58. https://doi.org/10.1128/CMR.00001-07
15. Nordmann P, Poirel L, Carrër A, Toleman MA, Walsh TR. How to detect NDM-1 producers. J Clin Microbiol. 2011;49:718–21. https://doi.org/10.1128/JCM.01773-10
16. Treangen TJ, Ondov BD, Koren S, Phillippy AM. The Harvest suite for rapid core-genome alignment and visualization of thousands of intraspecific microbial genomes. Genome Biol. 2014;15:524. https://doi.org/10.1186/s13059-014-0524-x
17. Fang H, Feng J, Xu Y, Zhang Y, Zhan Z, Yin Z, et al. Sequencing of pT5282-CTXM, p13190-KPC and p30860-NR, and comparative genomics analysis of IncX8 plasmids. Int J Antimicrob Agents. 2018;52:210–7. https://doi.org/10.1016/j.ijantimicag.2018.04.012
18. Yang X, Wai-Chi Chan E, Zhang R, Chen S. A conjugative plasmid that augments virulence in *Klebsiella pneumoniae.* Nat Microbiol. 2019;4:2039–43. https://doi.org/10.1038/s41564-019-0566-7

19. Rissman AI, Mau B, Biehl BS, Darling AE, Glasner JD, Perna NT. Reordering contigs of draft genomes using the Mauve aligner. Bioinformatics. 2009;25:2071–3. https://doi.org/10.1093/bioinformatics/btp356
20. Tumbarello M, Trecarichi EM, Corona A, De Rosa FG, Bassetti M, Mussini C, et al. Efficacy of ceftazidime-avibactam salvage therapy in patients with infections caused by *Klebsiella pneumoniae* carbapenemase–producing *K. pneumoniae*. Clin Infect Dis. 2019;68:355–64. https://doi.org/10.1093/cid/ciy492
21. van Duin D, Bonomo RA. Ceftazidime/avibactam and ceftolozane/tazobactam: second-generation β-lactam/β-lactamase inhibitor combinations. Clin Infect Dis. 2016;63:234–41. https://doi.org/10.1093/cid/ciw243
22. Shen P, Zhang Y, Li G, Jiang X. Characterization of the genetic environment of the bla_{KPC-2} gene among *Klebsiella pneumoniae* isolates from a Chinese hospital. Braz J Infect Dis. 2016;20:384–8. https://doi.org/10.1016/j.bjid.2016.04.003
23. Xu J, Zhao Z, Ge Y, He F. Rapid emergence of a pandrug-resistant ST11 isolate in an inpatient in a teaching hospital in China after treatment with multiple broad-spectrum antibiotics. Infect Drug Resist. 2020;13:799–804. https://doi.org/10.2147/IDR.S243334
24. Zhou H, Zhang K, Chen W, Chen J, Zheng J, Liu C, et al. Epidemiological characteristics of carbapenem-resistant collected from 17 hospitals in Nanjing district of China. Antimicrob Resist Infect Control. 2020;9:15. https://doi.org/10.1186/s13756-019-0674-4
25. Chen L, Chavda KD, Melano RG, Jacobs MR, Koll B, Hong T, et al. Comparative genomic analysis of KPC-encoding pKpQIL-like plasmids and their distribution in New Jersey and New York hospitals. Antimicrob Agents Chemother. 2014;58:2871–7. https://doi.org/10.1128/AAC.00120-14
26. Li JJ, Lee CS, Sheng JF, Doi Y. Complete sequence of a conjugative IncN plasmid harboring bla_{KPC-2}, bla_{SHV-12}, and *qnrS1* from an *Escherichia coli* sequence type 648 strain. Antimicrob Agents Chemother. 2014;58:6974–7. https://doi.org/10.1128/AAC.03632-14
27. Liu X, Chan EW-C, Chen S. Transmission and stable i nheritance of carbapenemase gene (bla_{KPC-2} or bla_{NDM-1})-encoding and *mcr-1*-encoding plasmids in clinical *Enterobacteriaceae* strains. J Glob Antimicrob Resist. 2021;26:255–61. https://doi.org/10.1016/j.jgar.2021.05.022
28. Papagiannitsis CC, Bitar I, Malli E, Tsilipounidaki K, Hrabak J, Petinaki E. IncC bla_{KPC-2}-positive plasmid characterised from ST648 *Escherichia coli*. J Glob Antimicrob Resist. 2019;19:73–7. https://doi.org/10.1016/j.jgar.2019.05.001
29. Zhao J, Zhang Y, Fan Y, Han J, Xiong Z, Liu X, et al. Characterization of an NDM-5-producing hypervirulent sequence type 65 clone from a lung transplant recipient. Emerg Microbes Infect. 2021;10:396–9. https://doi.org/10.1080/22221751.2021.1889932
30. Kong LH, Lei CW, Ma SZ, Jiang W, Liu BH, Wang YX, et al. Various sequence types of *Escherichia coli* isolates coharboring bla_{NDM-5} and *mcr-1* genes from a commercial swine farm in China. Antimicrob Agents Chemother. 2017;61:e02167–16. https://doi.org/10.1128/AAC.02167-16
31. Sugawara Y, Akeda Y, Hagiya H, Sakamoto N, Takeuchi D, Shanmugakani RK, et al. Spreading patterns of NDM-producing in clinical and environmental settings in Yangon, Myanmar. Antimicrob Agents Chemother. 2019;3:63. https://doi.org/10.1128/AAC.01924-18
32. Konieczny I, Bury K, Wawrzycka A, Wegrzyn K. Iteron plasmids. Microbiol Spectr. 2014;2(6). https://doi.org/10.1128/microbiolspec.PLAS-0026-2014
33. Winkler ML, Papp-Wallace KM, Bonomo RA. Activity of ceftazidime/avibactam against isogenic strains of *Escherichia coli* containing KPC and SHV β-lactamases with single amino acid substitutions in the Ω-loop. J Antimicrob Chemother. 2015;70:2279–86. https://doi.org/10.1093/jac/dkv094
34. Hemarajata P, Humphries RM. Ceftazidime/avibactam resistance associated with L169P mutation in the omega loop of KPC-2. J Antimicrob Chemother. 2019;74:1241–3. https://doi.org/10.1093/jac/dkz026
35. Haidar G, Clancy CJ, Shields RK, Hao B, Cheng S, Nguyen MH. Mutations in bla_{KPC-3} that confer ceftazidime-avibactam resistance encode novel KPC-3 variants that function as extended-spectrum β-lactamases. Antimicrob Agents Chemother. 2017;61:e02534–16. https://doi.org/10.1128/AAC.02534-16
36. Mehta SC, Rice K, Palzkill T. Natural variants of the KPC-2 carbapenemase have evolved increased catalytic efficiency for ceftazidime hydrolysis at the cost of enzyme stability. PLoS Pathog. 2015;11:e1004949. https://doi.org/10.1371/journal.ppat.1004949
37. Coppi M, Di Pilato V, Monaco F, Giani T, Conaldi PG, Rossolini GM. Ceftazidime-avibactam resistance associated with increased bla_{KPC-3} gene copy number mediated by pKpQIL plasmid derivatives in sequence type 258 *Klebsiella pneumoniae*. Antimicrob Agents Chemother. 2020;64:e01816–9. https://doi.org/10.1128/AAC.01816-19
38. Nelson K, Hemarajata P, Sun D, Rubio-Aparicio D, Tsivkovski R, Yang S, et al. Resistance to ceftazidime-avibactam is due to transposition of KPC in a porin-deficient strain of *Klebsiella pneumoniae* with increased efflux activity. Antimicrob Agents Chemother. 2017;61:e00989–17. https://doi.org/10.1128/AAC.00989-17

Address for correspondence: Fangyou Yu, Shanghai Pulmonary Hospital Department of Clinical Laboratory Medicine, Tongji University School of Medicine, No. 507, Zhengmin Rd, Yangpu District, Shanghai, China; e-mail: wzjxyfy@163.com; Liang Chen, Hackensack Meridian Health Center for Discovery and Innovation, Center for Discovery and Innovation, 111 Ideation Way, Nutley, NJ 07110, USA; email: liang.chen@hmh-cdi.org

Novel *Mycobacterium tuberculosis* Complex Genotype Related to *M. caprae*

Joseph Shea, Carol Smith, Tanya A. Halse, Donna Kohlerschmidt, Amy K. Rourke, Kimberlee A. Musser, Vincent Escuyer, Pascal Lapierre

We report the unusual genotypic characterization of a bacterium isolated from a clinical sample of a patient who grew up in Bangladesh and lives in the United States. Using whole-genome sequencing, we identified the bacterium as a member of the *Mycobacterium tuberculosis* complex (MTBC). Phylogenetic placement of this strain suggests a new MTBC genotype. Even though it had the same spoligotype as *M. caprae* strains, single-nucleotide polymorphism–based phylogenetic analysis placed the isolate as a sister lineage distinct from *M. caprae*, most closely related to 5 previously sequenced genomes isolated from primates and elephants in Asia. We propose a new animal-associated lineage, La4, within MTBC.

The *Mycobacterium tuberculosis* complex (MTBC) comprises multiple species, divided into human-adapted (*M. tuberculosis* and *M. africanum*) and animal-adapted (*M. bovis*, *M. orygis*, *M. caprae*, and others) tuberculosis (TB) lineages (*1*); L8, one of the most recently described, is most likely human-adapted (*2*). Human-adapted TB has been found to cause disease in certain nonhuman animals and vice versa, but some animal-adapted MTBC species (e.g., *M. suricattae*, dassie bacillus, chimpanzee bacillus) have not yet been reported to cause disease in humans (*3*). Several MTBC species and lineages have been newly reported in recent years, in part because of increased global use of highly discriminatory genotyping methods (*2*,*4*,*5*). Whole-genome sequencing (WGS) has helped classify previously misclassified or undetected rare strains, thus helping to fill gaps in the evolutionary history of TB.

In 2020, the Wadsworth Center at the New York State Department of Health (Albany, New York, USA) received an MTBC isolate from the New York City Public Health Laboratory for routine genotyping and antimicrobial resistance profiling. This isolate was cultured from a sputum sample collected from a 70-year-old patient who grew up in Bangladesh and immigrated to the United States in 2002. The patient was diagnosed with tuberculosis in 2019, 17 years after immigrating to the United States. Unpasteurized milk is a route of infection known for some TB lineages, of note *M. bovis,* and suspected for other MTBC species (*6*,*7*). The patient self-reported a childhood history of drinking raw milk but did not specify the animal source of the milk. PCR screening of the regions of difference (RD) of this isolate revealed a pattern atypical of any known species (*8*).

As part of our diagnostic workflow, we used WGS to identify the bacterium from the sample and determine its antimicrobial resistance profile and genotype, including in silico spoligotype. Our analysis revealed that this isolate was not closely related to any of >4,000 previously sequenced clinical strains in the Wadsworth Center collection. We compared results of phylogenetic analyses of this strain, designated 20-2359 by our laboratory information management system, with phylogenic characteristics from a diverse group of representative strains of *M. caprae*, *M. bovis*, and other *Mycobacterium* spp. gathered from publicly available databases.

Methods

PCR-Based Identification

We assessed strain 20-2359 using an in-house developed IS6110-targeted real-time PCR to confirm the identity to the MTBC level and to check for inhibition (*9*). We also ran PCR to differentiate *M. tuberculosis*, *M. bovis*, *M. bovis* bacillus Calmette-Guérin, *M. africanum*, *M. microti*, and *M. canettii*, based on the presence or absence of RD1, RD4, RD9, RD12, and a region exterior to RD9, according to protocols described elsewhere (*8*).

Author affiliation: Wadsworth Center, New York State Department of Health, Albany, New York, USA

DOI: https://doi.org/10.3201/eid2807.212353

WGS

We extracted DNA from 1 mL of heat-treated culture material (7H9 broth) using the InstaGene and FastPrep methods described elsewhere (*10*) and prepared sequencing libraries for the Illumina MiSeq platform using Nextera XT (https://www.illumina.com) paired-end 250 bp with 15 PCR cycles for the indexing step, as described elsewhere (*11*). We also performed nanopore sequencing on the Oxford Nanopore MinION platform using the SQK-LSK109 ligation sequencing kit (https://nanoporetech.com), as described elsewhere (*12*).

Bioinformatics Analyses

We retrieved complete genome sequences of diverse *Mycobacterium* spp. lineages from the National Center for Biotechnology Information (NCBI; https://www.ncbi.nlm.nih.gov) and generated synthetic 250 bp paired-end read sets for pipeline analyses using ArtificialFastqGenerator version 1.0.0 (https://sourceforge.net/projects/old-software-collection/files) (*13*). In addition, for analyses, we downloaded from NCBI Sequence Read Archive (SRA; https://www.ncbi.nlm.nih.gov/sra) reads for animal-associated *M. caprae* and other close MTBC relatives, lineages La2 and La1.1, as described in the recently revised nomenclature (*14*). We analyzed the sequence reads as described elsewhere (*10*) using the Wadsworth Center TB WGS bioinformatics pipeline, which includes a combination read classifications, using Kraken (*15*) and the presence or absence of specific genomic markers to determine the species and lineages of the bacteria from the sample. We screened for the presence or absence of 43 CRISPR spacers in the read sets to determine in silico spoligotyping. We mapped reads to a reference sequence, *M. tuberculosis* H37Rv, to construct consensus sequences, SNP alignments, and phylogenetic reconstructions. After completing mapping, we masked all repeated genomic regions and phage-associated loci to avoid erroneous SNP calling. We generated the SNP matrix using snp-dists (https://github.com/tseemann/snp-dists) and used Unicycler version 0.4.8-β (https://github.com/rrwick/Unicycler) with default parameters, as described elsewhere (*16*), for hybrid de novo assembly and polishing of 20-2359 using the MiSeq and MinION reads. We annotated the 20-2359 genome with pgap build5508 (https://github.com/ncbi/pgap/releases) (*17*) after trimming Illumina adaptors with bbuk from the package BBMap version 38.18 (sourceforge.net/projects/bbmap). We assembled a total of 19 contigs (N50: 476,048 bp) with a length of 4,286,739 bp and 4,015 predicted genes.

We generated phylogenetic trees from the SNP alignments using IQ-TREE version 1.6.12, with automatic best model selection transversion plus empirical base frequencies plus ascertainment bias correction plus FreeRate model with 2 categories base substitution model, and with 1,000 bootstrap support calculations (*18*). RD were bioinformatically determined using RD-Analyzer version 1.01 (*19*). The tree was rooted using the branch leading to the *M. tuberculosis, M. africanum*, *M. microti*, and *M. orygis* clusters.

Sequencing Reads, Genome Assembly, and Culture Availability

The raw sequencing reads and final genome assembly of strain 20-2359 are available at NCBI under Bioproject PRJNA771604 and nucleotide assembly JAJEJL000000000. Culture of strain 20-2359 will be available from our collection on request to the corresponding author.

Results

Initial PCR screening of 20-2359 for RD pattern yielded atypical results. Of note, RD1 was present but RD9 did not show any amplification. RD4 and RD12 had late amplification, suggesting possible mutations in the primer or probe sites of this assay, or insertions and deletions impacting the amplicon size of the targets. WGS analysis returned atypical results for identification as well. Species identification with Kraken using a local *Mycobacterium* spp. database, reported 20-2359 as *M. bovis,* although with a low percentage of specific reads. In silico–derived spoligotype listed this strain in the most up-to-date databases as most likely *M. caprae*. This rare spoligotype, 00000000000000000111111111101111111111100000, had previously been reported as *M. bovis* or *M. bovis* subspecies *caprae*–type before *M. caprae* was reported as a unique species. Three other samples in our dataset isolated from primates in China (NCBI SRA nos. SRR1792164, SRR1792165, and SRR7617662) also shared this spoligotype with 20-2359 (Appendix Table 1, https://wwwnc.cdc.gov/EID/article/28/7/21-2353-App1.pdf).

An in-house lineage identification scheme using specific SNPs also failed to positively identify the isolate (Table). We found that 20-2359 lacked 1 of 2 specific mutations required to be classified as either *M. bovis* or *M. caprae* and detected none of the known lineage-specific markers. The same markers were also missing from the monkey and elephant isolates. Genomic analyses of RD confirmed that RD1 was present, but RD4 and RD9 regions were deleted in 20-2359. A more comprehensive analysis of RD in 20-2359 using RD-Analyzer (https://rdanalyzer.com)

Table. List of markers used for species and lineage determination in investigation of novel *Mycobacterium tuberculosis* complex genotype related to *M. caprae**

Species and lineage	Specific markers	Strain 20-2359 genotype
Mycobacterium tuberculosis	gyrB403 GCG + katG203 ACC	gyrB403 TCG + katG203 ACT
M. africanum	ethA124 GAC + nt1673338 A or inhA78 GCG + atpE69 GCT	ethA124 GGC + nt1673338 C inhA78 GTG + atpE69 GCG
M. pinnipedii	inhA107 TCG + nt1473094 C	inhA107 CCG + nt1473094 G
M. microti	gyrB144 TAT + nt1473079 A	gyrB144 TAC + nt1473079 C
M. caprae	gyrB171 GTA + gyrB356 GCG	**gyrB171 GTA** + gyrB356 GCT
M. bovis bacillus Calmette-Guérin	pncA57 GAC + furA43 GTC	pncA57 CAC + furA43 GCC
M. bovis	pncA57 GAC + furA43 GCC	pncA57 CAC + **furA43 GCC**
Lineage		
1 (Indo-Oceanic)	gidB110 GTT	gidB110 GTG
2 (Beijing)	gidB92 GAC	gidB92 GAA
3 (Central-Asian)	nt2726105 A	nt2726105 G
4 (Euro-American)	katG463 CGG	katG463 CTG
5 (West African 1)	ethA124 GAC	ethA124 GGC
6 (West African 2)	inhA78 GCG	inhA78 GTG

*The codons or individual nucleotide positions were based on the sequence of the reference genome H37Rv. None of the complete marker set are present in strain 20-2359; 2 partial matches are in bold. Three primate (SRR1792164, SRR1792165, SRR7617662) and 2 elephant (DRR120408, DRR120409) isolates shared the same genotypes with 20-2359 for these markers.

revealed a presence-absence RD pattern identical to other *M. bovis*–related strains and 1 *M. caprae* strain, NCBI SRA no. ERR1462578 (Appendix Table 2). A closer look at the RD4 sequences for the specific region Rv1496–Rv1518 in *M. tuberculosis* H37Rv in 20-2359 revealed a genomic deletion in 20-2359 different from all other sequences in our dataset, resulting in a unique gene cluster when compared with the other lineages (results not shown). RD4 was deleted in 20-2359, but present in the 5 closely related strains belonging to the proposed La4 lineage, which had complete RD4 and RD patterns identical to *M. caprae*.

SNP-based phylogeny with 100% bootstrap support using *M. tuberculosis* H37Rv as a reference placed 20-2359 close to isolates from 3 primates (NCBI SRA nos. SRR1792164, SRR1792165, SRR7617662) and 2 elephants kept in captivity in Japan (NCBI SRA nos. DRR120408, DRR120409) (Figure). These 6 sequences form a distinct group that branches halfway between the *M. bovis* La1.1 and *M. caprae* La2 clades. SNP distances between members of the same clade (*M. caprae*, *M. bovis*, or La1.1) all differed by ≤802 SNPs, whereas SNP difference across clades averaged 1,369 (range: 985–1,374 SNPs) (Figure). Within the 20-2359 cluster, the maximum SNP distance between any 2 isolates was 776. The number of SNPs between the 20-2359 cluster and any *M. caprae,* La1.1, or *M. bovis* bacillus Calmette-Guérin strain averaged 1,161; the minimum was *M. caprae* SRR13888754 with 1,047.

Discussion

We identified *Mycobacterium* strains through WGS based on a combination of results from genomic database comparisons, spoligotype analysis, and detection of lineage-specific markers; each method has unique limitations. Although results generated by these methods usually agree, rare or unknown genotypes, not represented or improperly labeled in databases, can result in discordance and require a more in-depth analysis for final identification. When we first received sample 20-2359, initial presentation and culture testing did not indicate an atypical bacterium. However, when we first screened RD to confirm the strain identity, we noticed weaker amplification of some targets and the absence of RD9, indicating that the strain might belong to a less-common species or lineage within MTBC. Our attempts at identifying the strain through WGS analysis using results from Kraken, in-house lineage-specific markers, and in-silico spoligotyping all indicated it was somewhat related to *M. bovis* or *M. caprae*, but not which species or lineage.

SNP-based phylogenetic analyses using our local database, which contains >4000 clinical and nonclinical strains (data not shown), placed 20-2359 in a distinct lineage, a sister to *M. caprae* and more distantly related to *M. bovis*. A more focused phylogenetic analysis of publicly available sequences of animal-associated *M. caprae*, *M. bovis*, and other *Mycobacterium* spp. revealed that 20-2359 formed a well-supported cluster with 3 primate and 2 elephant isolates, distinct from *M. caprae*, *M. bovis*, and La1.1 (Figure). La1.1 is a newly classified animal-associated sublineage of *M. bovis* that is pyrazinamide susceptible, having branched off before acquisition of the pncA H57D mutation found in nearly all *M. bovis* strains worldwide, as described elsewhere (*14*). By comparing SNP counts between the 20-2359 cluster and the other isolates (Figure), we confirmed the distinctive nature of this cluster. The range of SNP distances (1,047–1,405) between isolates forming the 20-2359 cluster (proposed lineage La4) and isolates from other clades was lower than

that between *M. caprae* and *M. bovis* and La1.1 isolates (1,203–1,463) but higher than that between *M. bovis* and La1.1 subclade isolates (985–1,077). Phylogenetic placement of proposed lineage La4 strains, along with the SNP distances to other clades, strongly suggests that isolates from this cluster belong to a new MTBC

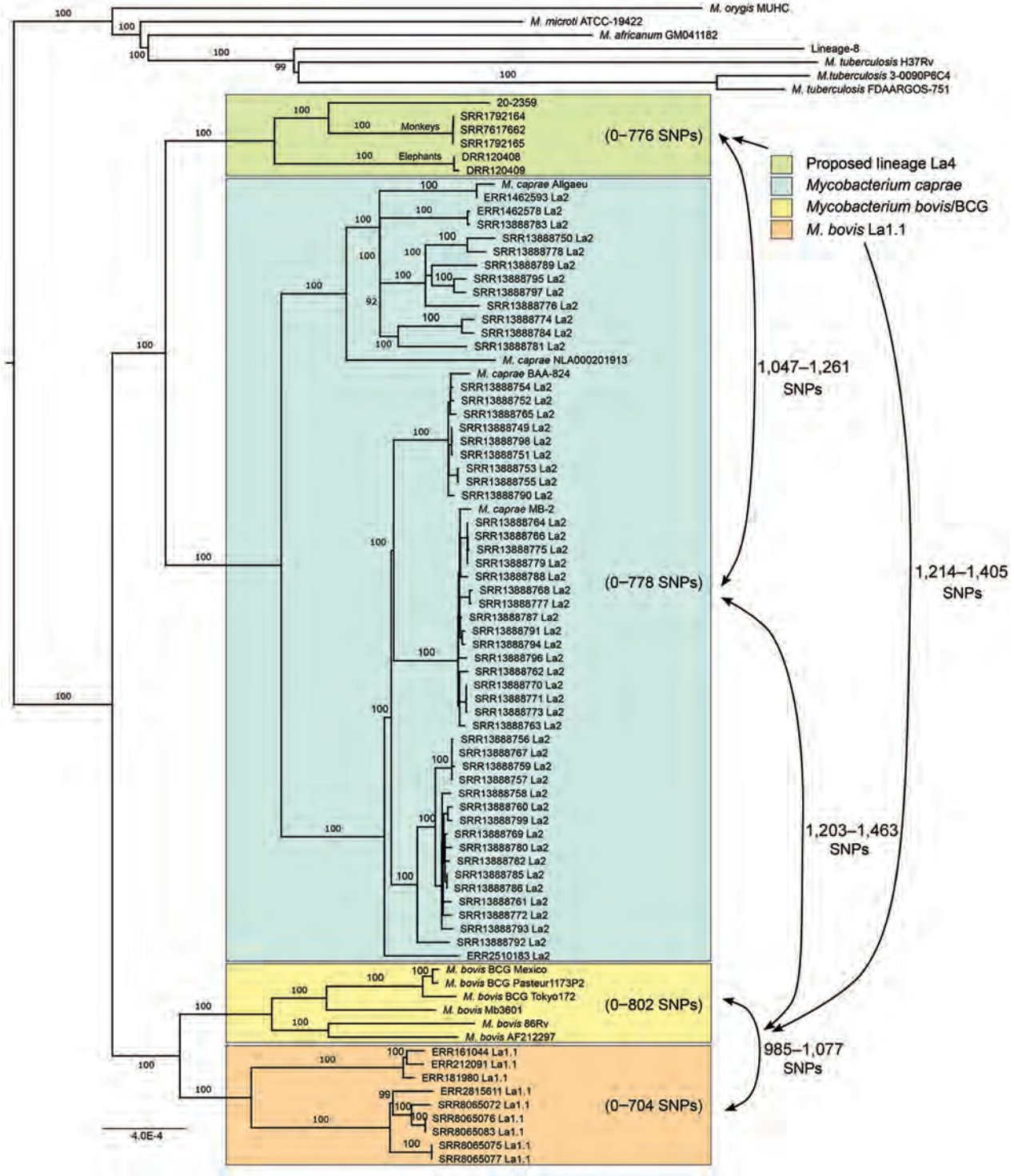

Figure. Phylogenetic SNP tree of strain 20-2359 and diverse group of representative *Mycobacterium caprae*, *M. bovis*, and other species and strains gathered from publicly available databases. Phylogenetic tree was calculated from the SNP alignment using IQ-TREE 1.6.12, with automatic best model selection (TVM+F+ASC+R2 model), and with 1,000 bootstrap support calculations (*18*). We used 14,688 variable genomic sites for this analysis. BCG, bacillus Calmette-Guérin; SNP, single-nucleotide polymorphism.

lineage associated with mammals from eastern and southeastern Asia.

We found the arrangement of RD4 in our clinical strain, 20-2359, unique from closely related primate and elephant isolates, which had complete RD4 gene clustering identical to *M. caprae* variant Allgaeu and other strains. Similarly, 20-2359 shared a spoligotype only with the 3 strains from primates, whereas the 2 strains from elephants had a spoligotype sequence with 1 extra spacer at spacer 2, identical to a spoligotype from the *M. caprae* clade. These differences within members of the 20-2359 cluster might reflect geographic diversity or differences in animal reservoirs. Limited information was available regarding the 3 MTBC samples from primates except that they were isolated in China. NCBI SRA nos. DRR120408 and DRR120409 samples were isolated at 2 time points from an elephant originally from the island of Borneo living in captivity in a zoo in Japan (*20*).

We could not establish the exact origin of clinical isolate 20-2359 based on available patient information; however, the patient grew up in Bangladesh and had potentially contracted TB through consuming raw milk. Results from a 2016 study reporting detection of *M. caprae* in 44 swamp buffalos from 4 farms in Thailand suggest that this strain type might have been encountered in the past (*21*). However, in that report, identification was based solely on spoligotype, which we have shown is conserved between some *M. caprae* strains and the new proposed lineage. The geographic location in that report is particularly intriguing given it is not typical for *M. caprae*. Although not possible to confirm with the available data, one possibility is that the swamp buffalo were infected not with *M. caprae* but with this newly described sister lineage. Given the distinct phylogenetic placement of this cluster, relatively long SNP distances to all *M. bovis*, La1.1, and *M. caprae* isolates in our dataset, and the case-patient's geographic origin, which was atypical for the presence of *M. caprae*, we propose cluster 20-2359 belongs to a new MTBC lineage, La4, based on new nomenclature for animal-adapted MTBC lineages (*14*).

Acknowledgments

We thank the Wadsworth Center Mycobacteriology and Bacteriology laboratories, Applied Genomic Technologies Center, and Media, Glassware, and Tissue Culture Core facilities for their support. We also extend our gratitude to Herns Modestil from New York City Bureau of Tuberculosis Control and to the New York City Public Health Laboratory, Department of Health and Mental Hygiene, for providing information on the clinical history of the patient.

About the Author

Mr. Shea is a microbiologist working at the Wadsworth Center, New York State Department of Health. His research interests include antimicrobial resistance and molecular epidemiology of *M. tuberculosis* complex and zoonotic tuberculosis.

References

1. Velayati AA, Farnia P. The species concept. In: Velayati AA, Farnia P, editors. Atlas of *Mycobacterium tuberculosis*. Boston: Academic Press; 2017. p. 1–16.
2. Ngabonziza JCS, Loiseau C, Marceau M, Jouet A, Menardo F, Tzfadia O, et al. A sister lineage of the *Mycobacterium tuberculosis* complex discovered in the African Great Lakes region. Nat Commun. 2020;11:2917. https://doi.org/10.1038/s41467-020-16626-6
3. Clarke C, Van Helden P, Miller M, Parsons S. Animal-adapted members of the *Mycobacterium tuberculosis* complex endemic to the southern African subregion. J S Afr Vet Assoc. 2016;87:1322. https://doi.org/10.4102/jsava.v87i1.1322
4. Coscolla M, Lewin A, Metzger S, Maetz-Rennsing K, Calvignac-Spencer S, Nitsche A, et al. Novel *Mycobacterium tuberculosis* complex isolate from a wild chimpanzee. Emerg Infect Dis. 2013;19:969–76 PubMed. https://doi.org/10.3201/eid1906.121012
5. Senghore M, Diarra B, Gehre F, Otu J, Worwui A, Muhammad AK, et al. Evolution of *Mycobacterium tuberculosis* complex lineages and their role in an emerging threat of multidrug resistant tuberculosis in Bamako, Mali. Sci Rep. 2020;10:327. https://doi.org/10.1038/s41598-019-56001-0
6. Cvetnic Z, Katalinic-Jankovic V, Sostaric B, Spicic S, Obrovac M, Marjanovic S, et al. *Mycobacterium caprae* in cattle and humans in Croatia. Int J Tuberc Lung Dis. 2007;11:652–8.
7. Doran P, Carson J, Costello E, More S. An outbreak of tuberculosis affecting cattle and people on an Irish dairy farm, following the consumption of raw milk. Ir Vet J. 2009;62:390–7. https://doi.org/10.1186/2046-0481-62-6-390
8. Halse TA, Escuyer VE, Musser KA. Evaluation of a single-tube multiplex real-time PCR for differentiation of members of the *Mycobacterium tuberculosis* complex in clinical specimens. J Clin Microbiol. 2011;49:2562–7. https://doi.org/10.1128/JCM.00467-11
9. Halse TA, Edwards J, Cunningham PL, Wolfgang WJ, Dumas NB, Escuyer VE, et al. Combined real-time PCR and rpoB gene pyrosequencing for rapid identification of *Mycobacterium tuberculosis* and determination of rifampin resistance directly in clinical specimens. J Clin Microbiol. 2010;48:1182–8. https://doi.org/10.1128/JCM.02149-09
10. Shea J, Halse TA, Lapierre P, Shudt M, Kohlerschmidt D, Van Roey P, et al. Comprehensive whole-genome sequencing and reporting of drug resistance profiles on clinical cases of *Mycobacterium tuberculosis* in New York State. J Clin Microbiol. 2017;55:1871–82. https://doi.org/10.1128/JCM.00298-17
11. Votintseva AA, Pankhurst LJ, Anson LW, Morgan MR, Gascoyne-Binzi D, Walker TM, et al. Mycobacterial DNA extraction for whole-genome sequencing from early positive liquid (MGIT) cultures. J Clin Microbiol. 2015;53:1137–43. https://doi.org/10.1128/JCM.03073-14
12. Smith C, Halse TA, Shea J, Modestil H, Fowler RC, Musser KA, et al. Assessing nanopore sequencing for clinical diagnostics: a comparison of next-generation sequencing

(NGS) methods for *Mycobacterium tuberculosis*. J Clin Microbiol. 2020;59:e00583–20. https://doi.org/10.1128/JCM.00583-20
13. Frampton M, Houlston R. Generation of artificial FASTQ files to evaluate the performance of next-generation sequencing pipelines. PLoS One. 2012;7:e49110. https://doi.org/10.1371/journal.pone.0049110
14. Zwyer M, Çavusoglu C, Ghielmetti G, Pacciarini ML, Scaltriti E, Van Soolingen D, et al. A new nomenclature for the livestock-associated *Mycobacterium tuberculosis* complex based on phylogenomics. Open Res Europe. 2021;1:100. https://doi.org/10.12688/openreseurope.14029.2
15. Wood DE, Salzberg SL. Kraken: ultrafast metagenomic sequence classification using exact alignments. Genome Biol. 2014;15:R46. https://doi.org/10.1186/gb-2014-15-3-r46
16. Wick RR, Judd LM, Gorrie CL, Holt KE. Unicycler: Resolving bacterial genome assemblies from short and long sequencing reads. PLOS Comput Biol. 2017;13:e1005595. https://doi.org/10.1371/journal.pcbi.1005595
17. Tatusova T, DiCuccio M, Badretdin A, Chetvernin V, Nawrocki EP, Zaslavsky L, et al. NCBI prokaryotic genome annotation pipeline. Nucleic Acids Res. 2016;44:6614–24. https://doi.org/10.1093/nar/gkw569
18. Nguyen L-T, Schmidt HA, von Haeseler A, Minh BQ. IQ-TREE: a fast and effective stochastic algorithm for estimating maximum-likelihood phylogenies. Mol Biol Evol. 2015;32:268–74. https://doi.org/10.1093/molbev/msu300
19. Faksri K, Xia E, Tan JH, Teo Y-Y, Ong RT-H. *In silico* region of difference (RD) analysis of *Mycobacterium tuberculosis* complex from sequence reads using RD-Analyzer. BMC Genomics. 2016;17:847. https://doi.org/10.1186/s12864-016-3213-1
20. Yoshida S, Suga S, Ishikawa S, Mukai Y, Tsuyuguchi K, Inoue Y, et al. *Mycobacterium caprae* infection in captive Borneo elephant, Japan. Emerg Infect Dis. 2018;24:1937–40. https://doi.org/10.3201/eid2410.180018
21. Chuachan U, Kanistanon K, Kampa J, Chaiprasert A. Molecular epidemiology of bovine tuberculosis in swamp buffalos in lower northeastern Thailand using spoligotyping. Khon Kaen University Veterinary Journal. 2016;26:61–76.

Address for correspondence: Pascal Lapierre, Wadsworth Center, New York State Department of Health, 150 New Scotland Ave, Albany, NY 12208, USA; email: pascal.lapierre@health.ny.gov

etymologia revisited

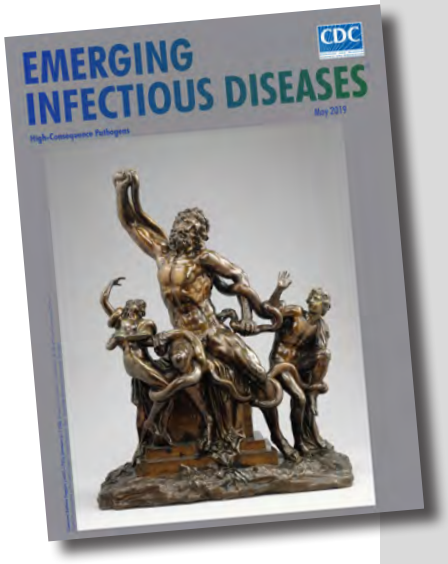

Originally published in May 2019

Nipah Virus

[ne´-pə vī´-rəs]

In 1994, a newly described virus, initially called equine morbillivirus, killed 13 horses and a trainer in Hendra, a suburb of Brisbane, Australia. The reservoir was subsequently identified as flying foxes, bats of the genus *Pteropus* (Greek pteron ["wing"] + *pous* ["foot"]). In 1999, scientists investigated reports of febrile encephalitis and respiratory illness among workers exposed to pigs in Malaysia and Singapore. (The pigs were believed to have consumed partially eaten fruit discarded by bats.)

The causative agent was determined to be closely related to Hendra virus and was later named for the Malaysian village of Kampung Sungai Nipah. The 2 viruses were combined into the genus *Henipavirus*, in the family *Paramyxoviridae*. Three additional species of *Henipavirus*—Cedar virus, Ghanaian bat virus, and Mojiang virus—have since been described, but none is known to cause human disease. Outbreaks of Nipah virus occur almost annually in India and Bangladesh, but *Pteropus* bats can be found throughout the tropics and subtropics, and henipaviruses have been isolated from them in Central and South America, Asia, Oceania, and East Africa.

Sources:

1. Centers for Disease Control and Prevention. Outbreak of Hendra-like virus—Malaysia and Singapore, 1998–1999. MMWR Morb Mortal Wkly Rep. 1999;48:265–9.
2. Selvey LA, Wells RM, McCormack JG, Ansford AJ, Murray K, Rogers RJ, et al. Infection of humans and horses by a newly described morbillivirus. Med J Aust. 1995;162:642–5.

https://wwwnc.cdc.gov/eid/article/25/5/et-2505_article

Chronic Pulmonary Disease Caused by *Tsukamurella toyonakaense*

Tomoki Kuge, Kiyoharu Fukushima, Yuki Matsumoto, Haruko Saito, Yuko Abe, Eri Akiba, Kako Haduki, Tadayoshi Nitta, Akira Kawano, Michio Tanaka, Yumi Hattori, Takahiro Kawasaki, Takanori Matsuki, Takayuki Shiroyama, Daisuke Motooka, Kazuyuki Tsujino, Keisuke Miki, Masahide Mori, Seigo Kitada, Shota Nakamura, Tetsuya Iida, Atsushi Kumanogoh, Hiroshi Kida

Unidentified *Mycobacterium* species are sometimes detected in respiratory specimens. We identified a novel *Tsukamurella* species (*Tsukamurella* sp. TY48, RIMD 2001001, CIP 111916^T), *Tsukamurella toyonakaense*, from a patient given a misdiagnosis of nontuberculous mycobacterial pulmonary disease caused by unidentified mycobacteria. Genomic identification of this *Tsukamurella* species helped clarify its clinical characteristics and epidemiology.

In clinical practice, unidentified *Mycobacterium* species are sometimes detected in respiratory specimens. Few *Mycobacterium* species can be identified by using methods available in clinical practice, although there are ≈200 species of nontuberculous mycobacteria (NTM) (*1*). We reported a case of pulmonary disease caused by a novel *Tsukamurella* species identified by using multilocus sequence typing (MLST) and whole-genome sequencing (WGS) (*2*).

The Study

We investigated the epidemiology of unidentified pathogenic mycobacteria by using TRCReady MTB and MAC (Tosoh Bioscience, https://www.tosohbioscience.com), AccuProbe (Gen-Probe Inc., https://www.gen-probe.com), COBAS AMPLICOR (Roche Diagnostics, https://www.roche.com), and a DNA–DNA hybridization assay (Kyokuto Pharmaceutical Industrial, https://www.kyokutoseiyaku.co.jp). WGS analysis of preserved unidentified mycobacteria culture isolates was approved by the institutional research ethics board (TNH2019063–2). The requirement for informed consent was waived because of the retrospective nature of the analysis. The opt-out recruitment method was applied to provide an opportunity for all patients to decline participation. Results of WGS analysis of TY48 were deposited in BioProject (accession no. PRJDB10620) and BioSample (accession no. SAMD00250050).

We performed MLST and WGS of culture isolates from 8 patients given diagnoses of NTM pulmonary disease caused by unidentified mycobacteria. We identified *Mycobacterium shimoidei*, *M. shinjukuense*, *M. paragordonae*, *M. heckeshornense*, *M. lentiflavum* (3 isolates), and a novel *Tsukamurella* species (*Tsukamurella* sp. TY48, RIMD 2001001, CIP 111916^T).

The patient with *Tsukamurella* infection was an 82-year-old woman who had received a diagnosis of NTM pulmonary disease 23 years earlier. Then a 59-year-old previously healthy woman, she was referred to our hospital because of abnormal chest radiographic findings. Although she had no symptoms, chest computed tomography findings showed centrilobular nodules and bronchiectasis. During follow-up, a cough and occasional hemoptysis developed. *M. chelonae* was repeatedly identified from her sputum. We started airway clearance therapy with erythromycin and expectorants. After 2 years of treatment, the *M. chelonae* disappeared from her sputum. However, her symptoms and radiologic findings slowly but steadily progressed (Figure 1), and rapidly growing acid-fast bacilli were repeatedly detected in her sputum for 8 years. The culture isolates were Ziehl-Neelsen stain positive. However, the species/subspecies could not be identified by using conventional methods. Therefore, she was given a diagnosis of NTM pulmonary disease caused by unidentified mycobacteria.

Author affiliations: Osaka University, Osaka, Japan (T. Kuge, K. Fukushima, Y. Matsumoto, Y. Abe, M. Tanaka, Y. Hattori, T. Shiroyama, D. Motooka, S. Nakamura, T. Iida, A. Kumanogoh); Toneyama Medical Center, Osaka (K. Fukushima, H. Saito, E. Akiba, K. Haduki, T. Nitta, A. Kawano, T. Kawasaki, T. Matsuki, K. Tsujino, K. Miki, M. Mori, H. Kida); Kitada Respiratory Clinic, Osaka (S. Kitada)

DOI: https://doi.org/10.3201/eid2807.212320

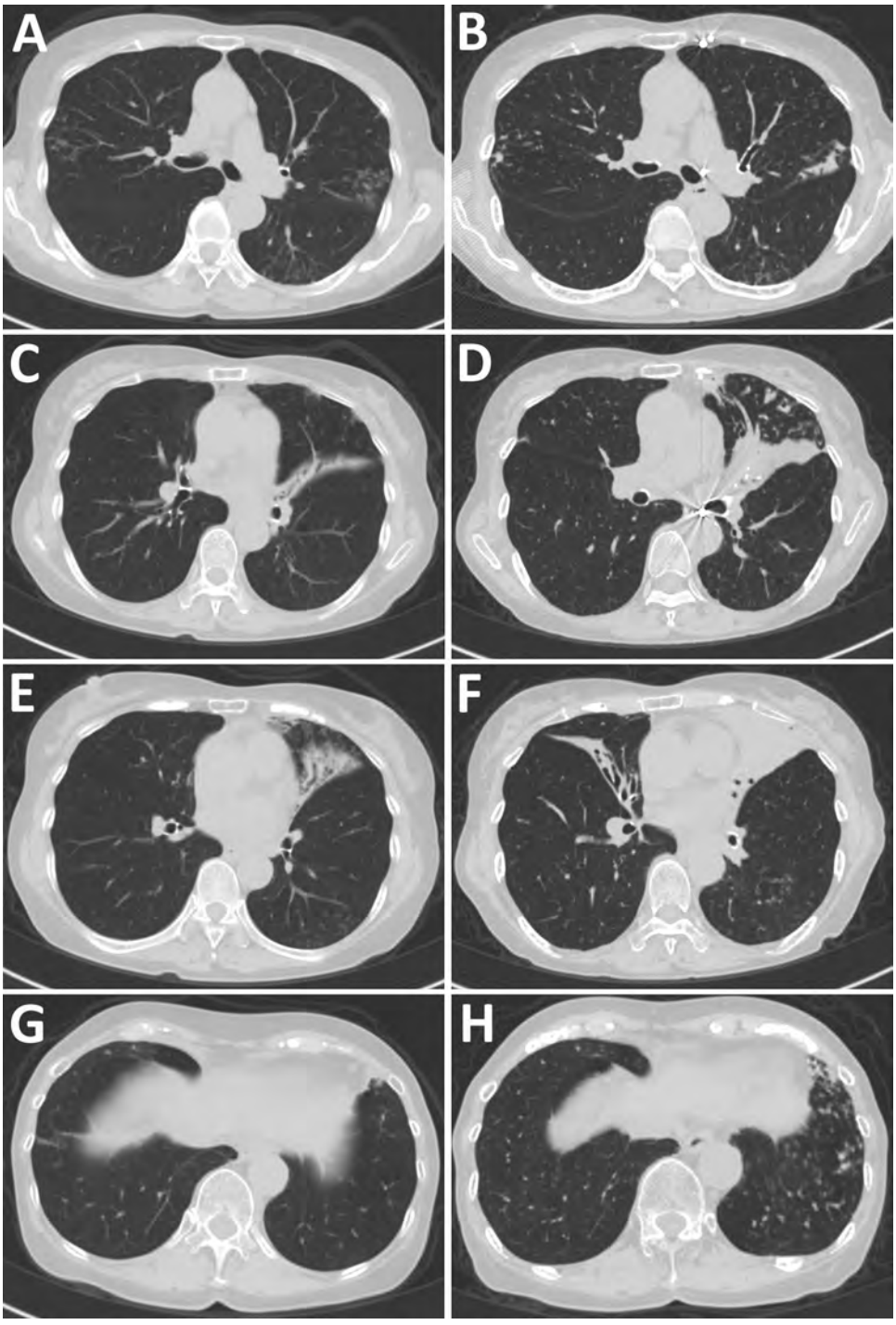

Figure 1. Comparison of chest computed tomography findings over time for patient who had chronic pulmonary disease caused by *Tsukamurella toyonakaense*. Findings are shown from before *Tsukamurella* species was detected (A, C, E, and G) and 6 years later (B, D, F, and H). A and B show that nodules in right segment 2 and left segment 6 were unchanged. C and D show that bronchiectasis in lingula had progressed. E and F show that bronchiectasis newly appeared in the middle lobe. G and H show that nodules newly appeared in left segments 8–10.

We continued erythromycin treatment for >20 years on the basis of evidence regarding successful treatment of NTM pulmonary disease with erythromycin (3). However, her symptoms and radiologic findings of lung destruction and structural alterations slowly but steadily progressed.

Because of this progression, we performed WGS by using a MinION Sequencer and Flow Cell R94 (Oxford Nanopore Technologies, https://nanoporetech.com). We extracted genomic DNA from cultured isolates by using a NucleoSpin Microbial DNA Kit (Takara Bio, https://www.takarabio.com) and prepared a library by using the Rapid Barcoding Kit (Oxford Nanopore Technologies). Using MinION raw sequencing reads, we performed MLST analysis on the 184-gene accessory genome with mlstverse

software (https://www.multiverse.io) as reported (*1*). The unidentified mycobacterium was presumed to be *M. fallax* (MLST score 0.083). However, the low MLST score prompted a deeper analysis of the bacterial genome.

We conducted a 16S rRNA analysis by performing a homology search using blastn (https://blast.ncbi.nlm.nih.gov) and compared our data with that in the SILVA rRNA database (*4*). The phylogenetic tree constructed using full-length 16S rRNA genes showed that strain TY48 was closely related to other *Tsukamurella* species (>98.7%), whereas its homology to 2 type species belonging to the related bacteria *Gordonia bronchialis* and *Williamsia muralis* was only 94.0% (Figure 2). We next determined the complete genome sequence of TY48 as reported (*1*) and performed WGS by using MinION and HiSeq 2500 instruments (Illumina, https://www.illumina.com). We performed genome assembly for strain TY48 by using flye (https://www.flye.com) for long reads obtained from MinION and corrected sequencing error by using pilon (https://bio.tools/pilon).

A comparison of the TY48 genome sequence with those of other *Tsukamurella* species indicated that the nearest related species was *T. paurometabola* (average nucleotide identity of 86.2%) (Table 1). This finding suggested that *Tsukamurella* sp. TY48 (RIMD 2001001; CIP 111916^T) was a novel *Tsukamurella* species.

We performed antimicrobial drug susceptibility tests for rapidly growing mycobacteria by using the broth microdilution method in accordance with Clinical and Laboratory Standards Institute M24-A2 guidelines (*5*). We transferred the culture to Middlebrook 7H9 broth and vortexed. We adjusted the culture medium to a 0.5 McFarland standard with sterile distilled water; we then added 60 μL of the 0.5 McFarland suspension to a Cation-Adjusted Mueller-Hinton Broth (Kyokuto Pharmaceutical Industrial Co. Ltd., https://www.kyokutoseiyaku.co.jp) and dispensed 100 μL of this solution into each well of the panel. After confirming adequate growth of the control over a 3-day incubation in a standard atmosphere at 30°C, we determined the MICs (μg/mL) for 15 drugs: clarithromycin, 0.25; azithromycin, ≤0.25; cefoxitin, ≤8; imipenem, ≤0.5; meropenem, ≤0.5; faropenem, ≤1; amikacin, ≤1; tobramycin, 2; minocycline, ≤0.25; doxycycline, ≤1; linezolid, ≤4; moxifloxacin, ≤0.25; ciprofloxacin ≤0.5; levofloxacin, ≤0.5; and trimethoprim/sulfamethoxazole, ≤2/38. *Tsukamurella* sp. TY48 was sensitive to all 15 drugs.

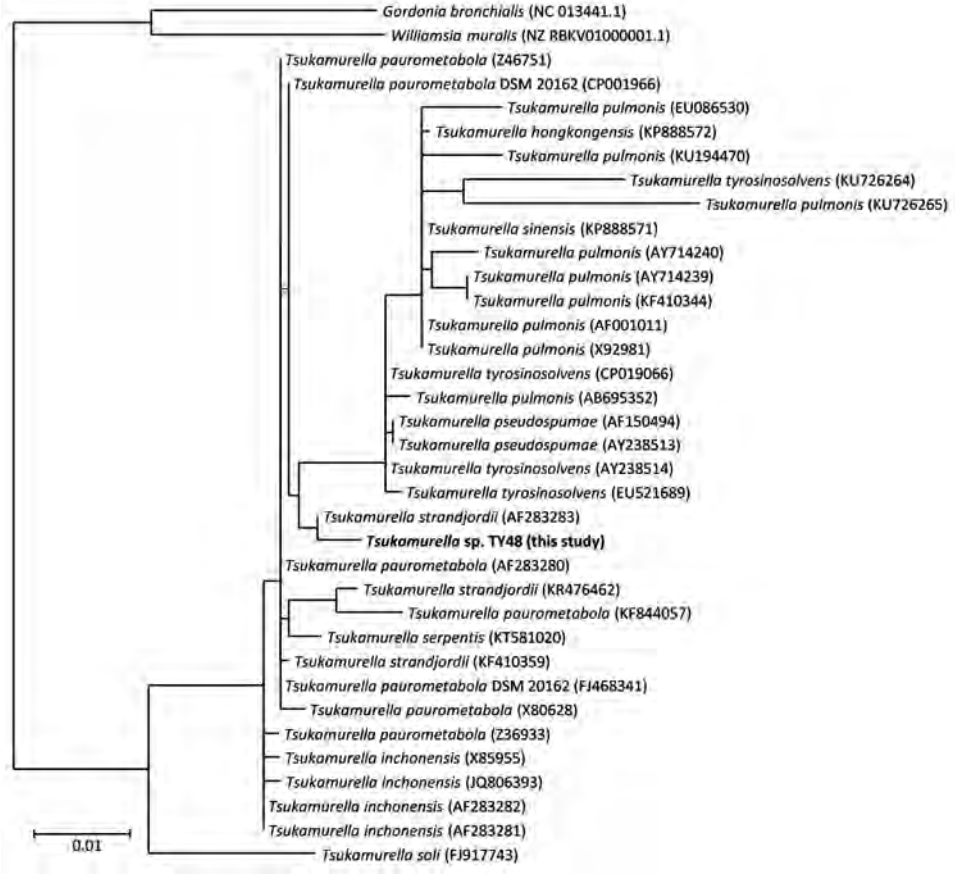

Figure 2. Maximum-likelihood phylogenetic tree constructed by using 16S rRNA sequences of *Tsukamurella* spp. and other bacterial species. Bold indicates strain isolated in this study. Reference sequences were obtained from SILVA database (*4*) release 138 as small subunit reference nonredundant 99 sequences, which showed >98.7% identity with strain TY48. GenBank accession numbers are provided for reference sequences. Scale bar indicates nucleotide substitutions per site.

Table 1. Eight species of *Tsukamurella* used for calculation of average nucleotide identity*

Species	Strain	Reference sequence accession no.	Reference sequence category
T. paurometabola	DSM20162^T	GCF_000092225.1	Representative genome
T. tyrosinosolvens	NCTC13231^T	GCF_900637875.1	Representative genome
T. pulmonis	CCUG3572^T	GCF_001575165.1	Representative genome
T. sputi	HKU70^T	GCF_007858445.1	Representative genome
T. conjunctivitidis	HKU72^T	GCF_007858475.1	Representative genome
T. asaccharolytica	HKU71^T	GCF_007858435.1	Representative genome
T. spumae	DSM44113^T	GCF_012396015.1	NA
T. pseudospumae	JCM15929	GCF_001575195.1	Representative genome

*NA, not available.

We renamed TY48 as *T. toyonakaense* after the location of its discovery, Toyonaka, Japan. *T. toyonakaense* is an aerobic, nonmotile, gram-positive rod that grows at 30°C and 37°C, but not at 42°C, and produces catalase. After a 72-h incubation at 30°C on 7H11 agar, it forms white and creamy, rough, nonpigmented colonies (10 mm in diameter). According to the API 50 CH system (bioMérieux, https://www.biomerieux.com), this bacterium can assimilate fructose, glucose, starch, sucrose, and trehalose but not arabinose, mannitol, mannose, or xylose.

After diagnosis, we attempted combination drug therapy with clarithromycin (200 mg/d) and ethambutol (250 mg/d). The patient refused continuation of treatment after 2 weeks because of antimicrobial drug–induced fatigue. We then resumed treatment with erythromycin. Her symptoms and radiologic findings are slowly improving (Table 2, https://wwwnc.cdc.gov/EID/article/28/7/21-2320-T2.htm; Appendix, https://wwwnc.cdc.gov/EID/article/28/7/21-2320-App1.pdf).

Conclusions

Tsukamurella species are aerobic, gram-positive, partially acid-fast, and nonmotile bacilli that can cause opportunistic infections, including pulmonary disease (*6*). Sixteen species of *Tsukamurella* have been classified (*7*). Only 9 pulmonary disease cases have been reported (*8*,*9*) (Table 2).

The prevalence of *Tsukamurella* pulmonary disease is probably underestimated. The genus *Tsukamurella* is often misidentified as related genera because it is difficult to identify in most clinical microbiology laboratories (*10*). Because of its partially acid-fast bacilli and cavitary shadow in radiologic examination, *Tsukamurella* pulmonary disease is often confused with *Mycobacterium* infection and often treated with antituberculous drugs (*9*). Yu et al. genotyped specimens from 101 NTM pulmonary disease patients by using 16S rRNA and 16S–23S rRNA internal transcribed spacer sequences and detected *Tsukamurella* species in ≈1% of the specimens (*11*). If one considers the prevalence of NTM pulmonary disease, the actual prevalence of *Tsukamurella* pulmonary disease is probably much higher than the 9 reported cases.

Tsukamurella commonly causes acute onset pneumonia with cavity and consolidation (Table 2) and fever, coughing, sputum, fatigue, and hemoptysis. Although appropriate drugs and treatment durations are unknown, combination medications of ≥2 drugs, including rifampin or quinolone, are widely used and presumed effective on the basis of case reports (*6*,*8*,*12*–*14*). These reports also indicated a good prognosis for *Tsukamurella* pulmonary disease (*8*,*12*,*13*). No relapses were reported, in contrast to NTM pulmonary disease. Although the Clinical and Laboratory Standards Institute has proposed breakpoints for aerobic actinomycetes (*5*), no definitive drug breakpoints for *Tsukamurella* spp. have been established. However, the strain we identified showed extensive antimicrobial drug susceptibility.

Because a clinically applicable identification technique is not available, *Tsukamurella* infections are probably underestimated and more prevalent than has been recognized. Misidentification as related genera, especially *Mycobacterium*, results in missed opportunities to properly treat *Tsukamurella* infections. Use of genomic sequencing to identify *Tsukamurella* species and more cases of *Tsukamurella* infections will help identify clinical characteristics and clarify epidemiology of *Tsukamurella* pulmonary disease.

Acknowledgments

We thank the patient for granting permission to publish her information and Traci Raley and Katie Oakley for editing drafts of this manuscript.

This study was supported in part by the Japan Agency for Medical Research and Development (grants JP20fk0108129, JP21fk0108129h0702, and JP21lm0203007), GlaxoSmithKline (grant A-32), the Japan Society for the Promotion of Science Grants-in-Aid for Scientific Research (grants JP21K16118 and JP21K08194), the Smoking Research Foundation, the Takeda Science Foundation, and the Japan Intractable Diseases (Nanbyo) Research Foundation (grant 2020B02).

K.F. designed the study; K.H., H.S., T.N., and A.K. performed mycobacterial culture and analysis of culture isolates; K.F. and T.K. performed clinical and laboratory data extraction and analysis; Y.A., T.S., E.A., Takahiro Kawasaki, T.M., K.T., M.M., K.M., and H.K. assisted with data extraction and analysis; Y.M., D.M., and S.N. performed multilocus typing analysis and whole-genome analysis; M.T., Y.H., and T.I. analyzed biochemical profiles of the strain; K.F. and S.K. wrote the manuscript; and A.K. and H.K. supervised the study. All authors read and approved the manuscript.

About the Author

Dr. Kuge is a clinical fellow in respiratory medicine in the respiratory medicine department of Osaka University Medical Hospital, Osaka, Japan. His primary research interest is respiratory infections.

References

1. Matsumoto Y, Kinjo T, Motooka D, Nabeya D, Jung N, Uechi K, et al. Comprehensive subspecies identification of 175 nontuberculous mycobacteria species based on 7,547 genomic profiles. Emerg Microbes Infect. 2019;8:1043–53. https://doi.org/10.1080/22221751.2019.1637702
2. Kuge T, Fukushima K, Matsumoto Y, Abe Y, Akiba E, Haduki K, et al. Pulmonary disease caused by a newly identified mycobacterium: *Mycolicibacterium toneyamachuris*: a case report. BMC Infect Dis. 2020;20:888. https://doi.org/10.1186/s12879-020-05626-y
3. Komiya K, Kurashima A, Ihi T, Nagai H, Matsumoto N, Mizunoe S, et al. Long-term, low-dose erythromycin monotherapy for *Mycobacterium avium* complex lung disease: a propensity score analysis. Int J Antimicrob Agents. 2014;44:131–5. https://doi.org/10.1016/j.ijantimicag.2014.03.017
4. Quast C, Pruesse E, Yilmaz P, Gerken J, Schweer T, Yarza P, et al. The SILVA ribosomal RNA gene database project: improved data processing and web-based tools. Nucleic Acids Res. 2013;41(D1):D590–6. https://doi.org/10.1093/nar/gks1219
5. Woods GL, Brown-Elliott BA, Conville PS, Desmond EP, Hall GS, Lin G, et al. Susceptibility testing of Mycobacteria, Nocardiae, and other aerobic Actinomycetes. 2nd ed. Wayne (PA): Clinical and Laboratory Standards Institute; 2011.
6. Mehta YB, Goswami R, Bhanot N, Mehta Z, Simonelli P. *Tsukamurella* infection: a rare cause of community-acquired pneumonia. Am J Med Sci. 2011;341:500–3. https://doi.org/10.1097/MAJ.0b013e3182129d02
7. Teng JL, Fong JY, Fok KM, Lee HH, Chiu TH, Tang Y, et al. *Tsukamurella asaccharolytica* sp. nov., *Tsukamurella conjunctivitidis* sp. nov. and *Tsukamurella sputi* sp. nov., isolated from patients with bacteraemia, conjunctivitis and respiratory infection in Hong Kong. Int J Syst Evol Microbiol. 2020;70:995–1006. https://doi.org/10.1099/ijsem.0.003861
8. Inchingolo R, Nardi I, Chiappini F, Macis G, Ardito F, Sali M, et al. First case of *Tsukamurella pulmonis* infection in an immunocompetent patient. Respir Med CME. 2010;3:23–5. https://doi.org/10.1016/j.rmedc.2009.02.004
9. Yang L, Cao Y, Dan Z, Wang Z, Wang X. Community-acquired *Tsukamurella pneumonia* in a young immunocompetent adult: a case misdiagnosed as pulmonary tuberculosis and literature review. Postgrad Med. 2017;129:563–6. https://doi.org/10.1080/00325481.2017.1344513
10. Teng JL, Tang Y, Wong SS, Fong JY, Zhao Z, Wong CP, et al. MALDI-TOF MS for identification of *Tsukamurella* species: *Tsukamurella tyrosinosolvens* as the predominant species associated with ocular infections. Emerg Microbes Infect. 2018;7:80. https://doi.org/10.1038/s41426-018-0083-4
11. Yu XL, Lu L, Chen GZ, Liu ZG, Lei H, Song YZ, et al. Identification and characterization of non-tuberculous mycobacteria isolated from tuberculosis suspects in southern-central China. PLoS One. 2014;9:e114353. https://doi.org/10.1371/journal.pone.0114353
12. Alcaide ML, Espinoza L, Abbo L. Cavitary pneumonia secondary to *Tsukamurella* in an AIDS patient. First case and a review of the literature. J Infect. 2004;49:17–9. https://doi.org/10.1016/S0163-4453(03)00139-7
13. Perez VA, Swigris J, Ruoss SJ. Coexistence of primary adenocarcinoma of the lung and *Tsukamurella* infection: a case report and review of the literature. J Med Case Reports. 2008;2:207. https://doi.org/10.1186/1752-1947-2-207
14. Maalouf R, Mierau SB, Moore TA, Kaul A. First case report of community-acquired pneumonia due to *Tsukamurella pulmonis*. Ann Intern Med. 2009;150:147–8. https://doi.org/10.7326/0003-4819-150-2-200901200-00022

Address for correspondence: Kiyoharu Fukushima, Department of Respiratory Medicine and Clinical Immunology, Osaka University Graduate School of Medicine, 2-2 Yamadaoka, Suita, Osaka, Japan; e-mail: fukushima@imed3.med.osaka-u.ac.jp

SARS-CoV-2 Delta–Omicron Recombinant Viruses, United States

Kristine A. Lacek, Benjamin L. Rambo-Martin, Dhwani Batra, Xiao-yu Zheng, Norman Hassell, Hitoshi Sakaguchi, Thomas Peacock, Natalie Groves, Matthew Keller, Malania M. Wilson, Mili Sheth, Morgan L. Davis, Mark Borroughs, Jonathan Gerhart, Samuel S. Shepard, Peter W. Cook, Justin Lee, David E. Wentworth, John R. Barnes, Rebecca Kondor, Clinton R. Paden

To detect new and changing SARS-CoV-2 variants, we investigated candidate Delta–Omicron recombinant genomes from Centers for Disease Control and Prevention national genomic surveillance. Laboratory and bioinformatic investigations identified and validated 9 genetically related SARS-CoV-2 viruses with a hybrid Delta–Omicron spike protein.

Emerging variants of SARS-CoV-2 are characterized and monitored closely by national genomic surveillance. In addition to sequencing efforts from US public health, academic, and commercial laboratories, the Centers for Disease Control and Prevention (CDC) collects and sequences SARS-CoV-2 specimens from 64 partners across state, tribal, local, and territorial public health agencies through the National SARS-CoV-2 Strain Surveillance program (https://www.cdc.gov/coronavirus/2019-ncov/variants/cdc-role-surveillance.html) and funds SARS-CoV-2 sequencing through a nationwide network of commercial laboratory testing companies. To date, these efforts have contributed 1.8 million SARS-CoV-2 genomes from the United States to public repositories. The purpose of this genomic surveillance system is to detect and respond dynamically to new and changing SARS-CoV-2 variants (*1*).

Author affiliations: Centers for Disease Control and Prevention, Atlanta, Georgia, USA (K.A. Lacek, B.L. Rambo-Martin, D. Batra, X. Zheng, N. Hassell, M. Keller, M.M. Wilson, M. Sheth, M.L. Davis, M. Burroughs, J. Gerhart, S.S. Shepard, P.W. Cook, J. Lee, D.E. Wentworth, J.R. Barnes, R. Kondor, C.R. Paden); General Dynamics Information Technology, Inc., Atlanta (X. Zheng); Retired, Yotsukaido City, Japan (H. Sakaguchi); UK Health Security Agency, London, UK (T. Peacock, N. Groves); Imperial College London, London (T. Peacock); ASRT Incorporated, Smyrna, Georgia, USA (M.L. Davis, J. Gerhart)

DOI: https://doi.org/10.3201/eid2807.220526

Recombination is an evolutionary mechanism frequently observed in coronaviruses (*2*,*3*), and it can lead to rapid accumulation of mutations and heightened transmissibility (*4*). SARS-CoV-2 recombination events have also been found to arise disproportionately in the spike gene (Y. Turkahia et al., unpub. data, https://www.biorxiv.org/content/10.1101/2021.08.04.455157V1). Recombination between Alpha and Delta SARS-CoV-2 variants has been documented (*5*–*7*).

Given the divergence of the Delta and Omicron variant genomes, as well as the known immune-escape properties of Omicron (*8*,*9*), a Delta–Omicron recombinant strain could alter the landscape of vaccine and therapeutic effectiveness. In early 2022, viruses resulting from recombination between Delta and Omicron were reported, but further inspection indicated that these claims seemed to have resulted from laboratory artifact or co-infections (*10*). With this study, we identified candidate Delta–Omicron recombinant genomes from the CDC national genomic surveillance and attempted to rule out laboratory contamination or sequencing error.

The Study

We identified 9 candidate recombinant sequences (Table) from CDC national genomic surveillance dataset made publicly available in GenBank and GISAID EpiCoV (https://www.gisaid.org). Using Bolotie, a rapid interclade recombination detection method (*3*), we identified these sequences as candidate recombinant genomes, having 1 parent in Delta (clade 21J) and 1 in Omicron (clade 21K). Bolotie describes a single breakpoint between nucleotide positions 22035 and 22577 (referenced to GenBank accession no. NC_045512.2); there are no differentiating mutations between clades 21J and 21K within this range. These sequences (EPI_ISL_8720194, EPI_

Table. Candidate recombinant samples, states, collection dates, and Bolotie outputs for the SARS-CoV-2 AY.119.2:BA.1.1 recombinant cluster, United States*

GISAID accession no.	State	GISAID virus name	Collection date	Bolotie results
EPI_ISL_8720194	TN	hCoV-19/USA/TN-CDC-ASC210559252/2021	2021 Dec 31	21J (Delta): 1-22032; 21K (Omicron): 22033-29903
EPI_ISL_9147438	NJ	hCoV-19/USA/NJ-CDC-IBX952397337138/2022	2022 Jan 4	21J (Delta): 1-22032; 21K (Omicron): 22033-29903
EPI_ISL_8981712	PA	hCoV-19/USA/PA-CDC-LC0473996/2022	2022 Jan 4	21J (Delta): 1-22032; 21K (Omicron): 22033-29903
EPI_ISL_8981824	PA	hCoV-19/USA/PA-CDC-LC0474055/2022	2022 Jan 4	21J (Delta): 1-22032; 21K (Omicron): 22033-29903
EPI_ISL_8981459	PA	hCoV-19/USA/PA-CDC-LC0474301/2022	2022 Jan 4	21J (Delta): 1-22032; 21K (Omicron): 22033-29903
EPI_ISL_9088187	MA	hCoV-19/USA/MA-CDC-STM-HZEBR92XC/2022	2022 Jan 12	21J (Delta): 1-22032; 21K (Omicron): 22033-29903
EPI_ISL_9147935	NJ	hCoV-19/USA/NJ-CDC-IBX640654818289/2022	2022 Jan 12	21J (Delta): 1-22032; 21K (Omicron): 22033-29903
EPI_ISL_10389336	NJ	hCoV-19/USA/NJ-CDC-ASC210553977/2022	2022 Feb 12	21J (Delta): 1-22032; 21K (Omicron): 22033-29903
EPI_ISL_10389339	NJ	hCoV-19/USA/NJ-CDC-ASC210553978/2022	2022 Feb 12	21J (Delta): 1-22032; 21K (Omicron): 22033-29903

*These 9 candidate recombinant viruses were identified by an exhaustive search of publicly available SARS-CoV-2 viral genomes with orf1ab:2855V,4176N,6248S and S:95I,142D,157-,346K,501Y mutations. hCoV-19/USA/PA-CDC-LC0474055/2022 and hCoV-19/USA/PA-CDC-LC0474301/2022 underwent resequencing at the Centers for Disease Control and Prevention. Bolotie (*3*) identified all 9 as recombinant genomes between Delta (clade 21J) and Omicron (clade 21K). Bolotie cannot determine the true breakpoint because of high sequence homology, but the same region is identified for all 9 sequences (nt position 22032 as referenced to GenBank accession no. NC_045512.2).

ISL_9147438, EPI_ISL_9147935, EPI_ISL_8981459, EPI_ISL_8981824, EPI_ISL_9088187 [A. Bolze et al., unpub .data, https://www.medrxiv.org/content/medrxiv/early/2022/03/12/2022.03.09.22272113.full.pdf], EPI_ISL_8981712, EPI_ISL_10389339, EPI_ISL_10389336) contain hallmark mutation sets from both Omicron and Delta SARS-CoV-2 lineages, changing from Delta-associated substitutions to Omicron-associated substitutions between spike protein amino acids 158 and 339 (Appendix Figure 1, panel A, https://wwwnc.cdc.gov/EID/article/28/7/22-0526-App1.pdf). This breakpoint is distinct from the 2 clusters of apparent Delta–Omicron recombinants identified in the United Kingdom (https://github.com/cov-lineages/pango-designation/issues/422 and https://github.com/cov-lineages/pango-designation/issues/441), which have a breakpoint upstream of spike in the *ORF1ab* gene (Appendix Figure 1, panel A), and these samples show a singular breakpoint, unlike concurrently observed Delta–Omicron recombinants in France (P. Colson et al., unpub. data, https://www.medrxiv.org/content/10.1101/2022.03.03.22271812V1).

To rule out Delta and Omicron co-infection, laboratory contamination, and bioinformatic error, we examined the raw read data from the 9 candidate recombinants created from molecular loop and amplicon-based sequencing strategies. Two of these specimens were readily available from the original diagnostic laboratory, and extracted RNA was shipped to CDC for confirmatory sequencing. We used Illumina (https://www.illumina.com) and PacBio (https://www.pacb.com) sequencing of 2 whole-genome amplicon strategies, as well as spike-gene amplification followed by Oxford Nanopore (https://nanoporetech.com) sequencing (Appendix). All sequencing strategies yielded functionally identical consensus sequences compared with the corresponding original sequencing strategies.

Nextclade (*11*) classified the 9 whole genomes as 21K (Omicron/BA.1). We then split the genomes at position 22150 (within the predicted recombination site range). Nextclade classified the first 22150 base fragment as clade 21J (Delta) and the remainder as clade 21K (Omicron/BA.1). Pangolin version 3.1.20 (pangoLEARN 1.2.123, Scorpio 0.3.16, https://cov-lineages.org) assigned a lineage of none to the full-genome sequences. Pangolin classified the first 22150 base fragment of each recombinant as AY.43 (Delta), although the call was not supported by Scorpio. Inspection of this region revealed closer homology to AY.119.2 (Delta) sequences because of mutations orf1ab:A2855V and orf1ab:A6248S, which are common to AY.119 lineages, and orf1ab:K4176N, which is found in a subset of AY.119.2 (Delta) sequences. The remaining sequence fragment from nt 22151 to the 3′ end was classified by pangolin as BA.1.1 (Omicron). This observation has been documented in the PANGO-designations repository (https://github.com/cov-lineages/pango-designation/issues/439) and is under review for potential lineage assignment.

Detailed sequence analysis confirmed the 2 resequenced specimens as true recombinants and indicated no evidence of co-infection or contamination.

Comparison with a representative AY.119.2 (Delta) specimen indicated characteristic Delta mutations (C21618G, C21846T, G21987A, and deletion 22029–22034) at >99% frequency (>600× coverage for Oxford Nanopore, >1,800× coverage for PacBio, >1000× coverage for Illumina) in the 5′ end of the recombinant (Appendix Figure 1, panel B). The 2 BA.1.1 (Omicron) deletions at the beginning of the spike gene (21765–21770 and 21987–21995) and the characteristic Omicron 9-base insertion after nt 22205 were not present in read data, consistent with a Delta origin for the 5′ end of the spike gene. After position 22577, the mutation profiles mirrored that of a representative BA.1.1 (Omicron) specimen (Appendix Figure 1, panel B). Analysis of individual Oxford Nanopore reads showed characteristic Delta mutations co-occurring with Omicron single-nucleotide variants on the same reads (sharing Delta 22029–22034 deletion and Omicron 22673 T>C; Appendix Figure 2). The translated spike protein is a hybrid, containing characteristic amino acids from both Delta and Omicron parents with a breakpoint between the N terminal domain and receptor-binding domain of spike S1 protein (Appendix Figure 1, panel A).

To visualize the parents of the recombinant genomes, we split all candidate recombinant genomes at position 22150, within the predicted breakpoint, and used Nextclade (*11*) to place each genome fragment (1–22150 and 22151 through the 3′ end) onto a reference tree. We visualized the 2 trees as a tanglegram tree with Auspice (*12*). Nucleotides 1–22150 clustered with clade 21J (Delta) sequences, and the remaining fragment of the genome clustered with 21K (Omicron/BA.1) (Appendix Figure 3).

Conclusions

Our results provide evidence of a recombinant SARS-CoV-2 genome containing a hybrid spike protein derived from a Delta (AY.119.2)–Omicron (BA.1.1) recombination event. However, the ability to effectively identify and confirm additional recombinant viruses remains challenging because of the range of sequence quality available in the public domain. These limitations are a result of amplification inefficiency and consensus-calling algorithmic error, as well as cases of co-infection or potential sample contamination.

Comparative phenotypic characterization of virus isolates from the recombinant cluster was not possible because all specimens were chemically inactivated. In the spike protein, there are no additional amino acid substitutions within the receptor-binding domain compared with BA.1.1 (Omicron) lineage viruses. Recombinant viruses with this hybrid spike protein were detected over the course of 6 weeks, but the number of cases resulting from those viruses remains low. Most cases were identified within the mid-Atlantic region of the United States. However, epidemiologic linkage cannot be determined because CDC does not collect identifying information for these samples.

Systematic virus surveillance is essential for long-term monitoring of SARS-CoV-2 evolution. Given the potential public health consequences of new variants emerging from recombination, investigations involving laboratory and bioinformatic components, such as the one presented here, are critical for correctly identifying and tracking these viruses.

Acknowledgments

We thank the public health program and laboratory staff members who contribute to National SARS-CoV-2 Strain Surveillance, including the Association of Public Health Laboratories, commercial laboratory staff members, laboratories submitting tagged baseline SARS-CoV-2 sequences via GISAID EpiCov and GenBank, CDC COVID-19 Pandemic Response Laboratory Task Force, Strain Surveillance and Emerging Variants Bioinformatics Working Group, Natalie Thornburg, and colleagues in the UK Health Security Agency. Furthermore, we gratefully acknowledge the authors from the originating laboratories responsible for obtaining the specimens and the submitting laboratories where genetic sequence data were generated and shared via GISAID. A full acknowledgment table can be found with the EPI_SET ID EPI_SET_20220412tv, in the Data Acknowledgement Locator under GISAID resources (https://www.gisaid.org/epi-search).

All authors have completed and submitted the International Committee of Medical Journal Editors form for disclosure of potential conflicts of interest. No potential conflicts of interest were disclosed.

About the Author

Ms. Lacek is an informatics health scientist with the Influenza Division, National Center for Immunization and Respiratory Diseases, Centers for Disease Control and Prevention, Atlanta, Georgia. Her primary research interests include viral genomics, next-generation sequencing, and genome assembly.

References

1. National Center for Immunization and Respiratory Diseases (NCIRD) DoVD. Science brief: emerging SARS-CoV-2 variants [cited 2022 Feb 17]. https://www.cdc.gov/coronavirus/2019-ncov/science/science-briefs/scientific-brief-emerging-variants.html

2. Lai MM, Baric RS, Makino S, Keck JG, Egbert J, Leibowitz JL, et al. Recombination between nonsegmented RNA genomes of murine coronaviruses. J Virol. 1985;56:449–56. https://doi.org/10.1128/jvi.56.2.449-456.1985
3. Varabyou A, Pockrandt C, Salzberg SL, Pertea M. Rapid detection of inter-clade recombination in SARS-CoV-2 with Bolotie. Genetics. 2021;218:iyab074.
4. Li X, Giorgi EE, Marichannegowda MH, Foley B, Xiao C, Kong X-P, et al. Emergence of SARS-CoV-2 through recombination and strong purifying selection. Sci Adv. 2020;6:eabb9153. https://doi.org/10.1126/sciadv.abb9153
5. Sekizuka T, Itokawa K, Saito M, Shimatani M, Matsuyama S, Hasegawa H, et al. Genome recombination between Delta and Alpha variants of severe acute respiratory syndrome coronavirus 2 (SARS-CoV-2). Jpn J Infect Dis. 2022 Feb 28 [Epub ahead of print].
6. Escalera-Zamudio M, Sánchez HGC, Arredondo LJD, Gutiérrez BRE. Proposal to redesignate B.1.631 as recombinant lineage XB [cited 2022 Feb 18]. https://virological.org/t/re-proposal-to-redesignate-b-1-631-as-recombinant-lineage-xb/746
7. Jackson B, Rambaut A, Pybus OG, Robertson DL, Connor T, Loman NJ, et al. Recombinant SARS-CoV-2 genomes involving lineage B.1.1.7 in the UK [cited 2022 Feb 18]. https://virological.org/t/recombinant-sars-cov-2-genomes-involving-lineage-b-1-1-7-in-the-uk/658.
8. Liu L, Iketani S, Guo Y, Chan JF, Wang M, Liu L, et al. Striking antibody evasion manifested by the Omicron variant of SARS-CoV-2. Nature. 2022;602:676–81. https://doi.org/10.1038/s41586-021-04388-0
9. Chakraborty C, Bhattacharya M, Sharma AR. Emerging mutations in the SARS-CoV-2 variants and their role in antibody escape to small molecule-based therapeutic resistance. Curr Opin Pharmacol. 2022;62:64–73. https://doi.org/10.1016/j.coph.2021.11.006
10. Kreier F. Deltacron: the story of the variant that wasn't. Nature. 2022;602:19. https://doi.org/10.1038/d41586-022-00149-9
11. Aksamentov I, Roemer C, Hodcroft EB, Neher RA. Nextclade: clade assignment, mutation calling and quality control for viral genomes. J Open Source Softw. 2021;6:3773. https://doi.org/10.21105/joss.03773
12. Hadfield J, Megill C, Bell SM, Huddleston J, Potter B, Callender C, et al. Nextstrain: real-time tracking of pathogen evolution. Bioinformatics. 2018;34:4121–3. https://doi.org/10.1093/bioinformatics/bty407

Address for correspondence: Clinton R. Paden, Centers for Disease Control and Prevention, 1600 Clifton Rd NE, Mailstop H18-6, Atlanta, GA 30329-4027, USA; email: cpaden@cdc.gov

etymologia revisited

Petri Dish
[pe'tre 'dish]

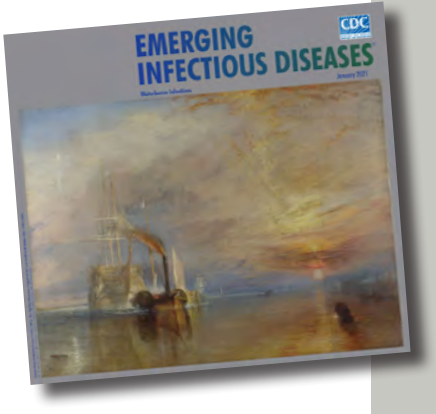

The Petri dish is named after the German inventor and bacteriologist Julius Richard Petri (1852–1921). In 1887, as an assistant to fellow German physician and pioneering microbiologist Robert Koch (1843–1910), Petri published a paper titled "A minor modification of the plating technique of Koch." This seemingly modest improvement (a slightly larger glass lid), Petri explained, reduced contamination from airborne germs in comparison with Koch's bell jar.

Sources:

1 Central Sheet for Bacteriology and Parasite Science [in German]. Biodiversity Heritage Library. Volume 1, 1887 [cited 2020 Aug 25]. https://www.biodiversitylibrary.org/item/210666#page/313/mode/1up
2. Petri JR. A minor modification of the plating technique of Koch [in German]. Cent für Bacteriol und Parasitenkd. 1887;1:279–80.
3. Shama G. The "Petri" dish: a case of simultaneous invention in bacteriology. Endeavour. 2019;43:11–6. DOIExternal
4. The big story: the Petri dish. The Biomedical Scientist. Institute of Biomedical Science [cited 2020 Aug 25]. https://thebiomedicalscientist.net/science/big-story-petri-dish

Originally published in January 2021

https//wwwnc.cdc.gov/eid/article/27/1/et-2701_article

Highly Pathogenic Avian Influenza A(H5N8) Clade 2.3.4.4b Virus in Dust Samples from Poultry Farms, France, 2021

Fabien Filaire, Laetitia Lebre, Charlotte Foret-Lucas, Timothée Vergne, Patrick Daniel, Aurélie Lelièvre, Antoine de Barros, Adam Jbenyeni, Pierrick Bolon, Mathilde Paul, Guillaume Croville, Jean-Luc Guérin

Avian influenza A(H5N8) virus has caused major epizootics in Europe since 2016. We conducted virologic analysis of aerosol and dust collected on poultry farms in France during 2020–2021. Our results suggest dust contributes to viral dispersal, even early in an outbreak, and could be a valuable surveillance tool.

Avian influenza is a viral disease caused by influenza A viruses, segmented, negative, single-stranded RNA viruses belonging to the *Orthomyxoviridae* family. Wild aquatic birds are the virus reservoir and generate occasional worldwide panzootic outbreaks during seasonal migrations (*1*). Highly pathogenic avian influenza (HPAI) virus subtypes can cause panzootic outbreaks associated with high mortality in wild and domestic birds, as well as substantial economic losses for the poultry industry, and are a major threat to public health because of their zoonotic potential.

During winter 2020–21, the HPAI H5N8 virus belonging to the A/goose/Guangdong/1/1996 clade 2.3.4.4b lineage caused hundreds of outbreaks among wild and domestic flocks across Europe (*2*,*3*). France was severely affected; 492 poultry farms, primarily duck farms, were infected during December 5, 2020–May 3, 2021. Despite reinforced surveillance activities, the virus spread rapidly, posing major challenges for surveillance and control. Officially recognized surveillance methods involve tracheal or cloacal swab-based sampling (*4*,*5*). However, these methods are laborious and have technical requirements that make application on such a massive scale difficult; thus, newer surveillance methods are needed.

Epidemiologic modeling of this outbreak suggested within-farm viral transmission was extremely fast, and the environment was a major source of contamination for neighboring farms (*6*). HPAI viruses disperse in aerosols, in fomites carried by human and animal vectors, and via feathers, fecal particles, and to a great extent, dust (*7*–*9*). Poultry farms are known to heavily generate dust particles that spread from feed, litter, feces, and animal skin and feathers (*9*,*10*). These particles can act as vehicles for bacteria and viruses and are classified, depending on their size, as inhalable (<100 μm), thoracic (<10 μm), or respirable (<4 μm) (*10*). In poultry houses, most dust consists of nonrespirable particles >4 μm (*10*). We evaluated the role of dust as a vehicle of H5N8 clade 2.3.4.4b virus and assessed whether dust or aerosol sampling is a viable alternative to bird swab sampling for HPAI virus surveillance.

The Study

During December 2020–April 2021, we conducted a study in 63 poultry houses located in 4 departments (administrative units) in France highly affected by HPAI H5N8 virus outbreaks. On the basis of daily official outbreak reports, we identified HPAI-infected poultry houses and poultry houses in close vicinity or with epidemiologic links to infected houses. The study included a total of 48 duck houses, 12 chicken houses, 2 quail houses, and 1 goose house. We selected farms identified as being near an HPAI outbreak to reflect a range of sanitary statuses and infection stages (i.e., no, mild, or severe clinical signs; high mortality rates). We specifically included houses without

Author affiliations: THESEO France, Laval, France (F. Filaire); Université de Toulouse, Toulouse, France (F. Filaire, L. Lebre, C. Foret-Lucas, T. Vergne, A. De Barros, A. Jbenyeni, P. Bolon, M. Paul, G. Croville, J.-L. Guérin); Laboratoires des Pyrénées et des Landes, Mont-de-Marsan, France (P. Daniel); SOCSA 40, Amou, France (A. Lelièvre)

DOI: https://doi.org/10.3201/eid2807.212247

clinical signs among animals to evaluate virus dispersal and dust testing for HPAI surveillance in the early stages of infection.

In each selected poultry house, we collected surface dust with 2 wipes on the building's walls and feeders (*9*,*11*) (Appendix, https://wwwnc.cdc.gov/EID/article/28/7/21-2247-App1.pdf). In 19 houses, we also collected aerosol samples by using 2 devices, Coriolis Compact (Bertin Instruments, https://www.bertin-instruments.com) and the NIOSH BC 251 developed by the National Institute for Occupational Safety and Health (NIOSH; https://www.cdc.gov/niosh) (Appendix). Furthermore, we collected tracheal swab samples from 20 randomly selected birds in each house (Appendix Table 1). We chose tracheal over cloacal swab samples because the typical respiratory shedding and tropism of HPAI H5N8 clade 2.3.4.4 viruses enables earlier detection in the respiratory tract than cloacae (*12*,*13*).

We performed real-time quantitative reverse transcription PCR on all samples to detect HPAI virus at the molecular level by targeting the matrix protein and H5 genes (Appendix). We compared cycle threshold (Ct) distributions of each sample by using raincloud plots and a boxplot model (Figure 1). In general, Ct values for tracheal swabs (≈25.2) and dust (≈28.6) were similar (Figure 1; Appendix). Between the 2 aerosol collectors, the Coriolis device showed more positive results (Ct <40) than the NIOSH BC 251 sampler. Furthermore, we noted HPAI H5N8

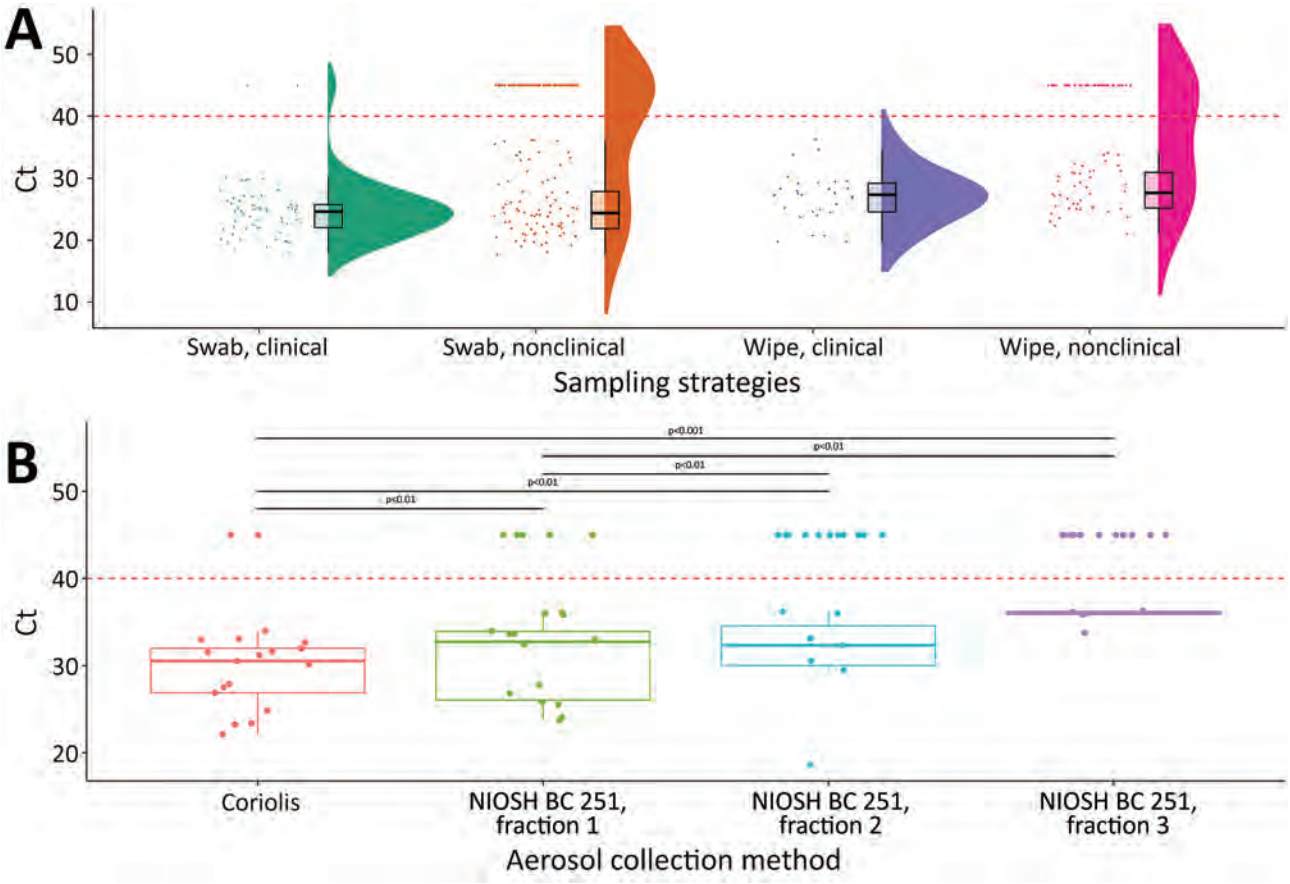

Figure 1. Ct values of highly pathogenic avian influenza A(H5N8) clade 2.3.4.4b virus detected by real-time quantitative reverse transcription PCR from tracheal swab and environmental samples collected on poultry farms, France, December 2020–April 2021. We used a Wilcoxon test for statistical analysis and considered samples with Ct ≤40 negative. Each dot indicates a Ct value from 1 wipe sample or 1 pool of 5 tracheal swab samples. Box plots show 95% CI for Ct values; horizontal lines in boxes indicate means and error bars SDs. Red dashed horizontal lines indicate Ct of 40, the cutoff value for negative results. A) Half-violin, scatter, and box plots of Ct values for samples collected by using tracheal swab samples or surface wipe samples from 63 poultry houses with and without clinical signs among animals. Half-violins show distribution of Ct values for each sample type. B) C_t values for aerosol samples collected in 19 poultry houses. Aerosol samples were collected by using the Coriolis Compact (Bertin Instruments, https://www.bertin-instruments.com) and the NIOSH BC 251 (https://www.cdc.gov/niosh). The NIOSH BC 251 sampling device has 3 fractions for different particle sizes; fraction 1 for >4 μm, fraction 2 for 1–4 μm, and fraction 3 for <1 μm. Ct, cycle threshold; NIOSH, National Institute for Occupational Safety and Health.

Table 1. Estimated sensitivity of sampling methods and sampling strategies by latent class analysis for detection of highly pathogenic avian influenza A(H5N8) virus on poultry farms, France, December 2020–April 2021

Clinical signs	Samples*	Estimated sensitivity of sampling method (95% credible interval)†	Estimated sensitivity of sampling strategy (95% credible interval)‡
Clinical signs in flock	Tracheal swab	0.77 (0.44–0.99)	1.00 (0.90–1.00)
	Wipe	0.89 (0.64–1.00)	0.99 (0.87–1.00)
	Coriolis	0.93 (0.69–1.00)	0.93 (0.69–1.00)
	NIOSH BC 251	0.93 (0.69–1.00)	0.93 (0.69–1.00)
No clinical signs in flock	Tracheal swab	0.46 (0.15–0.97)	0.92 (0.48–1.00)
	Wipe	0.90 (0.67–1.00)	0.99 (0.89–1.00)
	Coriolis	0.92 (0.63–1.00)	0.92 (0.63–1.00)
	NIOSH BC 251	0.67 (0.34–0.91)	0.67(0.34–0.91)

*Each farm or building was sampled by using 20 tracheal swab samples (pooled in sets of 5 for RT-PCR) and 2 wipe samples from surfaces; on 19 farms we also collected 1 air sample from each of the 2 aerosol collection devices, the Coriolis Compact (Bertin Instruments, https://www.bertin-instruments.com) and the NIOSH BC 251 developed by the National Institute for Occupational Safety and Health (https://www.cdc.gov/niosh).
†Sampling method relates to the simple analysis of individual samples; individual tracheal swab samples are those analyzed in pools of 5 samples; thus, the sensitivity of the sampling method corresponds to the probability that a single sample, or a pooled sample for the tracheal swabs, tests positive in an infected poultry house.
‡Sampling strategy relates to the combined analysis of the different individual samples at the farm or building level, assuming that the farm or building is positive when ≥1 individual sample tests positive; thus, the sensitivity of the sampling strategy corresponds to the probability that ≥1 sample, or ≥1 pool of 5 tracheal swab samples, tests positive in an infected poultry house.

virus was more easily detected in the largest particles, those ≥1 μm (Figure 1). These results suggest that the HPAI H5N8 virus dispersion is associated with large dust particles, which could be a major vehicle for viral spread.

To estimate the sensitivity of the 4 different sampling methods (tracheal swab samples, surface wipes, and Coriolis and NIOSH aerosol samplers) in houses with or without poultry showing clinical signs, we used a latent class modeling approach, necessary when no standard has been established (*14*). We adjusted the model to cross-detect each farm by the 4 different sampling methods and estimated model parameters in a Bayesian framework (Appendix). Model outputs suggested that the different sampling methods had equivalent sensitivity in HPAI-infected flocks showing clinical signs. Surface dust and aerosol sampling showed substantially higher sensitivity in HPAI-infected flocks without clinical signs, but the difference was not statistically significant despite overlap of 95% credible intervals (Table 1; Figure 2).

Finally, to assess the infectiousness of environmental samples, we processed 25 surface dust or aerosol samples taken from 5 animal houses and used these for virus isolation in embryonated eggs (Appendix). Among 25 samples, 12 (48%) tested positive,

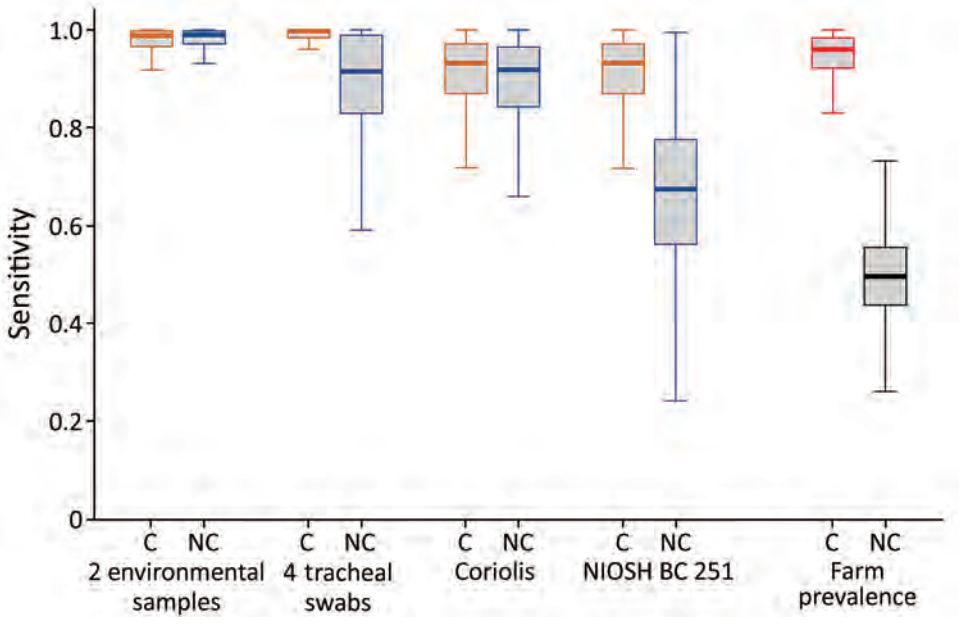

Figure 2. Sensitivity comparison of 4 sampling techniques used to detect highly pathogenic avian influenza A(H5N8) clade 2.3.4.4b virus from 63 poultry farms, France, December 2020–April 2021. Sampling was conducted in poultry houses with and without clinical signs among flocks. Box plots show 95% CIs; horizontal lines in boxes indicate means, error bars SDs. The 2 environmental samples refer to 2 wipes collected in the animal houses, 1 on feeders and 1 on walls. Tracheal swab samples refer to 4 pools of 5 swab samples collected per house. Aerosol samples were collected from 19 poultry houses by using the Coriolis Compact (Bertin Instruments, https://www.bertin-instruments.com) and the NIOSH BC 251 (https://www.cdc.gov/niosh). The NIOSH BC 251 sampling device has 3 fractions for different particle sizes; fraction 1 for >4 μm, fraction 2 for 1–4 μm, and fraction 3 for <1 μm. Farm-level disease prevalence was 0.96 for houses in which animals had clinical signs and 0.5 in houses in which animals did not have clinical signs. C, clinical signs; NC, no clinical signs; NIOSH, National Institute for Occupational Safety and Health.

Table 2. Viral isolation assays on chicken embryonated eggs performed on 5 of the 63 poultry houses in a study to detect highly pathogenic avian influenza A(H5N8) virus on poultry farms, France, December 2020–April 2021*

	House 11		House 26		House 29		House 30		House 34	
Sample type†	Ct	VI	Ct	VI	Ct	VI	Ct	VI	Ct	VI
Tracheal swab	25	+	20.7	+	21.9	+	18.9	+	20	+
Dust wipe, feeders	25.8	–	25.1	–	27.4	+	29.5	+	24.2	+
Dust wipe, walls	27.5	+	25.5	–	30.1	+	28.3	+	23	+
Coriolis	32	–	33.6	–	27.8	–	25.8	+	26.9	+
NIOSH BC251										
Fraction 1	34	–	33.6	–	27.8	–	25.8	+	23.7	+
Fraction 2	–	ND	36	–	32.4	–	33.1	–	18.6	+
Fraction 3	–	ND	–	ND	36.3	–	–	ND	–	ND

*Ct, cycle threshold; ND, not done; VI, virus isolation; +, positive; –, negative.
†Each farm or building was sampled by using 4 pools of 5 tracheal swab samples, 2 wipe samples (1 from feeders, 1 from walls), and on 19 farms, 1 air sample from each of the 2 aerosol collection devices, the Coriolis Compact (Bertin Instruments, https://www.bertin-instruments.com) and the NIOSH BC 251, developed by the National Institute for Occupational Safety and Health (https://www.cdc.gov/niosh). NIOSH BC 251 sampling device has 3 fractions for different particle sizes; fraction 1 for >4 µm, fraction 2 for 1–4 µm, and fraction 3 for <1 µm.

confirming that viral isolation is possible from these sampling methods (Table 2).

Conclusions

We used field conditions to evaluate whether dust from poultry farms contained HPAI viruses and to compare surface dust and aerosol testing for HPAI virus against official swab-based methods. We used wipe tests to collect surface dust and 2 bioaerosol devices to collect aerosol samples during the 2020–21 HPAI H5N8 virus epizootic outbreak in France. Standard molecular analysis detected high viral RNA loads in the early phase of flock infection, before clinical signs appeared. In addition, size fractioning of aerosol samples revealed that high RNA viral loads and infectious viral particles were associated with the largest particles (>1 µm), which are easy to collect and use for molecular analysis. However, the field conditions we used cannot be reproduced in experimental animal trials because of ethical and biosecurity requirements, which result in dramatically lower dust loads than those found in the field.

Recent research on influenza transmission routes revealed that nonrespiratory airborne particles are more likely to cause infection than are droplets or fomites (*7*). Infectious aerosols generated from inert objects handled by humans or dispersed through animal movements can lead to further infection. Dust can carry infectious particles and is omnipresent in poultry houses (*10*) and so could be a major means of viral transmission and dispersal in the environment. These findings suggest that biosecurity protocols should strongly emphasize limiting the amount of dust dispersed via farm equipment to reduce the spread of HPAI viruses.

Of note, for early detection, before flock animals show clinical signs of illness, we found that surface dust sampling using wipe tests and aerosol sampling using a high flow rate collection device are more sensitive than tracheal swab samples. The higher sensitivity of environmental sampling methods for early detection is likely because of infection dynamics at the flock level. During the early phases of infection, only a few animals are infectious, making the probability of detecting virus during individual swab-based sampling low (*6*). Swab sampling also is time consuming, labor-intensive, and expensive, whereas dust wiping is inexpensive, fast, easy to perform, and noninvasive.

In conclusion, we detected HPAI H5N8 clade 2.3.4.4b virus in dust samples from poultry farms during a large epizootic in France. Our findings suggest dust wipe samples are an efficient surveillance tool and could enable more rapid virus detection and implementation of measures to curb virus spread.

Acknowledgments

We thank Bertin Instruments, France, and the National Institute for Occupational Safety & Health (NIOSH), United States, for the loan of aerosol collectors.

This study was performed in the framework of the Chair for Avian Biosecurity, hosted by the National Veterinary College of Toulouse and funded by the Direction Générale de l'Alimentation, Ministère de l'Agriculture et de l'Alimentation, France. F.F. is funded by Theseo, a company of the LanXess Group, France. This work also received financial support from the FEDER/Région Occitanie Recherche et Sociétés 2018-AI-TRACK.

About the Author

Mr. Filaire is an engineer in biosciences and a PhD candidate in a collaborative project between the Host-Pathogen Interactions Joint Research Unit, National Veterinary School and INRAe, Toulouse, France; EIP Purpan, Toulouse; and Theseo, Lanxess Group, Laval, France. His research focus is on innovative methods for detection and characterization of emerging viruses.

References

1. Munster VJ, Baas C, Lexmond P, Waldenström J, Wallensten A, Fransson T, et al. Spatial, temporal, and species variation in prevalence of influenza A viruses in wild migratory birds. PLoS Pathog. 2007;3:e61. https://doi.org/10.1371/journal.ppat.0030061
2. Lewis NS, Banyard AC, Whittard E, Karibayev T, Al Kafagi T, Chvala I, et al. Emergence and spread of novel H5N8, H5N5 and H5N1 clade 2.3.4.4 highly pathogenic avian influenza in 2020. Emerg Microbes Infect. 2021;10:148–51. https://doi.org/10.1080/22221751.2021.1872355
3. European Food Safety Authority; European Centre for Disease Prevention and Control and European Union Reference Laboratory for Avian Influenza; Adlhoch C, Fusaro A, Kuiken T, Niqueux É, Staubach C, Terregino C, et al. Avian influenza overview May–August 2020. EFSA J. 2020;18:e06270. PubMed https://doi.org/10.2903/j.efsa.2020.6270
4. World Organisation for Animal Health (OIE). Avian influenza (including infection with high pathogenicity avian influenza viruses). In OIE terrestrial manual 2021. Geneva: The Organisation; 2021.
5. Nielsen SS, Alvarez J, Bicout DJ, Calistri P, Depner K, Drewe JA, et al.; EFSA Panel on Animal Health and Welfare (EFSA AHAW Panel). Scientific opinion on the assessment of the control measures of the category A diseases of Animal Health Law: Highly Pathogenic Avian Influenza. EFSA J. 2021;19:e06372. https://doi.org/10.2903/j.efsa.2021.6372
6. Vergne T, Gubbins S, Guinat C, Bauzile B, Delpont M, Chakraborty D, et al. Inferring within-flock transmission dynamics of highly pathogenic avian influenza H5N8 virus in France, 2020. Transbound Emerg Dis. 2021;68:3151–5. https://doi.org/10.1111/tbed.14202
7. Asadi S, Gaaloul ben Hnia N, Barre RS, Wexler AS, Ristenpart WD, Bouvier NM, et al. Influenza A virus is transmissible via aerosolized fomites. Nat Commun. 2020; 11:4062. https://doi.org/10.1038/s41467-020-17888-w
8. Spekreijse D, Bouma A, Koch G, Stegeman A. Quantification of dust-borne transmission of highly pathogenic avian influenza virus between chickens. Influenza Other Respir Viruses. 2013;7:132–8. https://doi.org/10.1111/j.1750-2659.2012.00362.x
9. Lopez KM, Nezworski J, Rendahl A, Culhane M, Flores-Figueroa C, Muñoz-Aguayo J, et al. Environmental sampling survey of H5N2 highly pathogenic avian influenza–infected layer chicken farms in Minnesota and Iowa. Avian Dis. 2018;62:373–80. https://doi.org/10.1637/11891-050418-Reg.1
10. Zhao Y, Aarnink AJA, De Jong MCM, Groot Koerkamp PWG. Airborne microorganisms from livestock production systems and their relation to dust. Crit Rev Environ Sci Technol. 2014; 44:1071–128. https://doi.org/10.1080/10643389.2012.746064
11. Carrique-Mas JJ, Breslin M, Sayers AR, McLaren I, Arnold M, Davies R. Comparison of environmental sampling methods for detecting *Salmonella* in commercial laying flocks in the UK. Lett Appl Microbiol. 2008;47:514–9. https://doi.org/10.1111/j.1472-765X.2008.02450.x
12. Gaide N, Foret-Lucas C, Figueroa T, Vergne T, Lucas MN, Robertet L, et al. Viral tropism and detection of clade 2.3.4.4b H5N8 highly pathogenic avian influenza viruses in feathers of ducks and geese. Sci Rep. 2021;11:5928. https://doi.org/10.1038/s41598-021-85109-5
13. Beerens N, Germeraad EA, Venema S, Verheij E, Pritz-Verschuren SBE, Gonzales JL. Comparative pathogenicity and environmental transmission of recent highly pathogenic avian influenza H5 viruses. Emerg Microbes Infect. 2021;10:97–108. https://doi.org/10.1080/22221751.2020.1868274
14. van Smeden M, Naaktgeboren CA, Reitsma JB, Moons KG, de Groot JA. Latent class models in diagnostic studies when there is no reference standard—a systematic review. Am J Epidemiol. 2014;179:423–31. https://doi.org/10.1093/aje/kwt286
15. Raynor PC, Adesina A, Aboubakr HA, Yang M, Torremorell M, Goyal SM. Comparison of samplers collecting airborne influenza viruses: 1. primarily impingers and cyclones. PLoS One. 2021;16:e0244977. https://doi.org/10.1371/journal.pone.0244977

Address for correspondence: Jean-Luc Guerin, UMR IHAP 1225, École Nationale Vétérinaire de Toulouse, 23 chemin des capelles, 31076 Toulouse CEDEX 3, France; email: jean-luc.guerin@envt.fr

Genetically Diverse Highly Pathogenic Avian Influenza A(H5N1/H5N8) Viruses among Wild Waterfowl and Domestic Poultry, Japan, 2021

Kosuke Okuya, Junki Mine, Kaori Tokorozaki, Isshu Kojima, Mana Esaki, Kohtaro Miyazawa, Ryota Tsunekuni, Saki Sakuma, Asuka Kumagai, Yoshihiro Takadate, Yuto Kikutani, Tsutomu Matsui, Yuko Uchida, Makoto Ozawa

Genetic analyses of highly pathogenic avian influenza H5 subtype viruses isolated from the Izumi Plain, Japan, revealed cocirculation of 2 genetic groups of clade 2.3.4.4b viruses among migratory waterfowl. Our findings demonstrate that both continuous surveillance and timely information sharing of avian influenza viruses are valuable for rapid risk assessment.

Highly pathogenic avian influenza (HPAI) viruses are known to have zoonotic potential (*1*). Therefore, global surveillance for HPAI virus in in domestic poultry and wild waterfowl is essential for assessing potential risk for both public and animal health.

During winter 2020–21, an emerging HPAI A(H5N8) virus caused outbreaks in wild birds and domestic poultry in East Asia (*2*–*5*). Genetic and phylogenetic analyses revealed that the H5 hemagglutinin (HA) genes of H5N8 virus belonged to clade 2.3.4.4b and were divided into 2 genetic groups, G1 and G2 (*6*). The G1 viruses showed high genetic similarity with the HPAI H5N8 viruses circulating in Europe during winter 2019–20 (*7*), but the G2 viruses concurrently caused HPAI outbreaks in Europe and Asia during winter 2020–21 (*8*). We report the genetic characteristics of 4 HPAI viruses isolated from the Izumi Plain, Japan, in November 2021.

Author affiliations: Kagoshima University, Kagoshima, Japan (K. Okuya, I. Kojima, M. Esaki, M. Ozawa); National Agriculture and Food Research Organization, Tsukuba, Japan (J. Mine, K. Miyazawa, R. Tsunekuni, S. Sakuma, A. Kumagai, Y. Takadate, Y. Uchida); Kagoshima Crane Conservation Committee, Izumi, Japan (K. Tokorozaki, T. Matsui, M. Ozawa); Ministry of Agriculture, Forestry and Fisheries, Tokyo, Japan (Y. Kikutani)

DOI: https://doi.org/10.3201/eid2807.212586

The Study

During routine winter 2021–22 avian influenza virus (AIV) surveillance, we detected HPAI virus in environmental water samples collected from a crane roosting site in the Arasaki area of the Izumi Plain on November 8, 2021 (Figure 1). We inoculated embryonated chicken eggs (*9*) with those water samples and isolated AIVs of mixed subtypes, most likely due to co-inoculation with multiple AIVs. We could not determine the neuraminidase (NA) subtype due to the mixed virus populations. However, using the MinION Mk1B nanopore sequencer (Oxford Nanopore Technologies, https://nanoporetech.com), as described previously (*10*), we confirmed that 1 virus isolate, A/environment/Kagoshima/KU-ngrB4/2021 (mixed), was an HPAI H5 subtype (Table). In addition to the H5 HA gene, we detected HA genes of H3 and H4 subtypes and NA genes of N6 and N8 subtypes from A/environment/Kagoshima/KU-ngrB4/2021 (mixed). Based on our BLAST analysis (https://blast.ncbi.nlm.nih.gov), HA gene segments of the detected H3 virus showed the highest similarity to those from H3N8 virus A/duck/Mongolia/MN18-14/2018 (97.65%) and the H4 virus showed the highest similarity to HA genes from H4N2 virus A/duck/Bangladesh/41653/2019 (98.85%). The NA gene segment of H3N6 virus showed the highest similarity to those from H3N6 virus A/duck/Mongolia/MN18-1/2018 (98.8%) and the NA gene segment of H3N8 virus showed highest similarity to H5N8 virus A/water/Tottori/NK1201-2/2021 (99.36%). In contrast to the HA and NA gene segments, we detected only single nucleotide sequences in the remaining 6 gene segments. The closest relatives of these 6 gene segments all were derived from recent HPAI H5N8 viruses. In

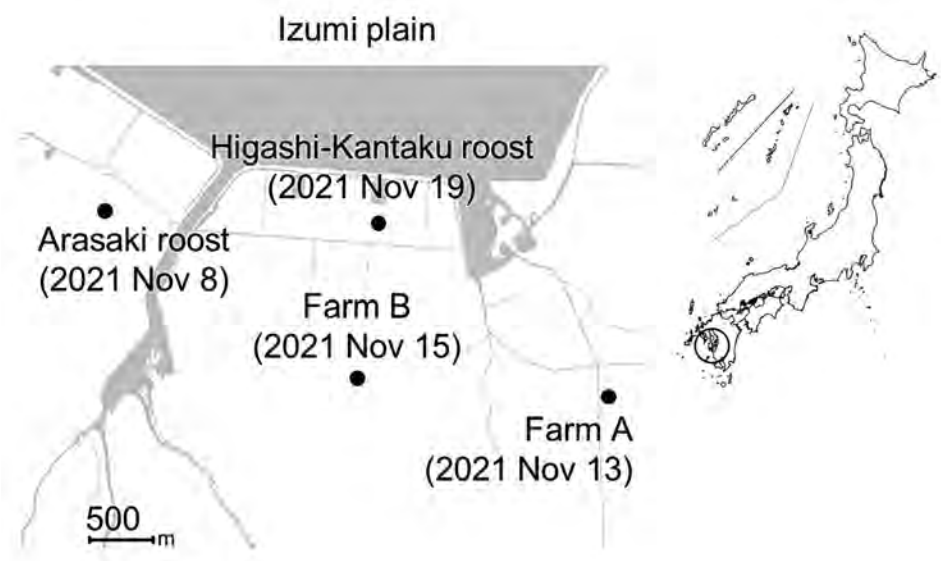

Figure 1. Locations on the Izumi Plain, Japan, where highly pathogenic avian influenza A(H5N1/H5N8) viruses were detected among wild waterfowl roosts and domestic poultry farms, 2021. Dots indicate location and date of avian influenza A detection. Inset map shows location of Izumi Plain in Japan.

addition, the H5 HA gene, N8 NA gene, and remaining gene segments from 2 virus isolates, A/environment/Kagoshima/KU-ngrB4/2021 (mixed) and A/hooded crane/Kagoshima/KU-5T/2021 (H5N8), were nearly identical (>99.8%).

A layer chicken farm, farm A, reported unusual mortality among chickens on November 13, 2021 (Figure 1). We used the Miseq platform (Illumina, https://www.illumina.com) to perform viral genome sequencing on isolates from farm A and found an H5N1 virus isolate, A/chicken/Kagoshima/21A6T/2021, possessed the high pathogenicity H5 HA gene (Table). After HPAI virus outbreak notification from farm A, local authorities conducted legally mandated urgent investigations at 25 chicken farms located within 3 km of the farm. Subsequent investigations discovered another HPAI virus outbreak at a layer chicken farm, farm B (Figure 1), before increased poultry mortality occurred there on November 15, 2021. Of note, Miseq viral genome sequencing revealed that the farm B virus was an HPAI H5N8 virus, A/chicken/Kagoshima/B3T/2021 (Table).

On November 19, 2021, a hooded crane (*Grus monacha*) was found dead at a second roosting area in Higashi-Kantaku (Figure 1). Using a tracheal swab sample from the dead crane, we isolated another HPAI H5N8 virus, A/hooded crane/Kagoshima/KU-5T/2021, and sequenced its genome by using the MinION Mk1B (Table). Thus, we detected 4 HPAI H5 viruses from different sources within a 5-km radius in only 12 days.

Using BLAST, we analyzed the nucleotide sequences of all 8 gene segments from each virus isolate (Table). The sequences sharing the highest nucleotide identity with the polymerase basic 2, nucleoprotein, and nonstructural protein gene segments from 1 isolate, A/chicken/Kagoshima/21A6T/2021 (H5N1), were sequences from low pathogenicity avian influenza (LPAI) viruses isolated from wild ducks (Table). These findings indicate that the HPAI H5N1 virus we detected is a genetic reassortant recently generated between HPAI and LPAI viruses.

In contrast, each gene segment from isolates A/chicken/Kagoshima/B3T/2021 (H5N8) and A/hooded crane/Kagoshima/KU-5T/2021 (H5N8) shared relatively high similarity (>99%) with those from HPAI H5N8 viruses isolated from a tundra swan (*Cygnus columbianus*) or environmental samples collected in China during the 2019–20 and 2020–21 winter seasons (Table). In addition, nucleotide sequences of all 8 gene segments from both isolates were almost identical to each other (Appendix Figure 1, https://wwwnc.cdc.gov/EID/article/28/7/21-2586-App1.pdf). These results suggest that the HPAI outbreak on farm B was caused by HPAI H5N8 virus progenies that have been detected in migratory waterfowl in East Asia since 2019. Of note, the HPAI viruses we detected did not demonstrate any amino acid substitutions related to mammalian adaptation, such as a single amino acid substitution of glutamine to lysine at position 591 (Q591K), E627K, or D701N in the polymerase basic 2 protein (*11*–*13*); nor Q226L, N224K, or G228S in the H5 HA protein (*14*,*15*).

The phylogenetic tree of the H5 HA gene revealed that all 4 HPAI viruses we detected belong to genetic group G2 of clade 2.3.4.4b (Figure 2; Appendix Figure 2). The H5 HA gene from A/chicken/Kagoshima/21A6T/2021 (H5N1) comprises a cluster with HA genes from HPAI H5N8 viruses detected

Table. Collection date, GISAID accession numbers, closest genetic relatives, and percentage genetic identity compared with other viruses among highly pathogenic avian influenza A(H5N1/H5N8) viruses detected in the Izumi Plain, Japan, 2021*

Isolated virus	Collection date	Gene	Accession no.	Closest relative†	% Identity
A/environment/Kagoshima/KU-ngrB4/2021 (mixed)	2021 Nov 8	HA	EPI1933367	A/environment sample/China/TZ001/2021 (H5N8)	99.47
A/chicken/Kagoshima/21A6T/2021 (H5N1)	2021 Nov 13	PB2	EPI1940236	A/duck/Bangladesh/37630/2019 (H10N4)	97.72
		PB1	EPI1940237	A/layer hen/Slovakia/A-chicken-Slovakia-Pah_14–2020/2020 (H5N8)	98.20
		PA	EPI1940238	A/chicken/Nigeria/VRD21–98_21VIR2288–6/2021 (H5N1)	98.05
		HA	EPI1933663	A/chicken/Nigeria/VRD21–43_21VIR2288–4/2021 (H5N8)	98.71
		NP	EPI1940239	A/teal/Egypt/MB-D-487OP/2016 (H7N3)	98.20
		NA	EPI1940240	A/chicken/Nigeria/VRD21–109_21VIR2370–425/2021 (H5N1)	97.83
		M	EPI1940241	A/*Cygnus columbianus*/Hubei/56/2020 (H5N8)	99.29
		NSP	EPI1940242	A/environment/Bangladesh/42635/2020 (H10N7)	99.28
A/chicken/Kagoshima/B3T/2021 (H5N8)	2021 Nov 15	PB2	EPI1933684	A/environment sample/China/TZ001/2021 (H5N8)	99.61
		PB1	EPI1933685	A/environment sample/China/TZ001/2021 (H5N8)	99.30
		PA	EPI1933683	A/*Cygnus columbianus*/Hubei/116/2020 (H5N8)	99.40
		HA	EPI1933687	A/environment sample/China/TZ001/2021 (H5N8)	99.53
		NP	EPI1933680	A/environment sample/China/TZ001/2021 (H5N8)	99.67
		NA	EPI1933686	A/*Cygnus columbianus*/Hubei/51/2020 (H5N8)	99.15
		M	EPI1933682	A/*Cygnus columbianus*/Hubei/56/2020 (H5N8)	99.59
		NSP	EPI1933681	A/environment sample/China/TZ001/2021 (H5N8)	99.64
A/hooded crane/Kagoshima/KU-5T/2021 (H5N8)	2021 Nov 19	PB2	EPI1933368	A/environment sample/China/TZ001/2021 (H5N8)	99.56
		PB1	EPI1933369	A/environment sample/China/TZ001/2021 (H5N8)	99.30
		PA	EPI1933370	A/*Cygnus columbianus*/Hubei/116/2020 (H5N8)	99.49
		HA	EPI1933371	A/environment sample/China/TZ001/2021 (H5N8)	99.47
		NP	EPI1933372	A/environment sample/China/TZ001/2021 (H5N8)	99.67
		NA	EPI1933373	A/*Cygnus columbianus*/Hubei/51/2020 (H5N8)	99.09
		M	EPI1933374	A/*Cygnus columbianus*/Hubei/56/2020 (H5N8)	99.39
		NSP	EPI1933375	A/environment sample/China/TZ001/2021 (H5N8)	99.76

*GISAID, https://www.gisaid.org. HA, hemagglutinin; M, matrix; NA, neuraminidase; NP, nucleoprotein; NSP, nonstructural protein; PA, polymerase; PB1, polymerase basic 1; PB2, polymerase basic 2.
†Representative viruses with the highest nucleotide identity retrieved from the NCBI GenBank (https://www.ncbi.nlm.nih.gov/genbank) database on December 3, 2021.

during the 2021–22 winter season in Europe, and we tentatively designated this cluster as subgroup G2b (Figure 2). These results suggest that genetically similar HPAI H5 viruses simultaneously invaded Europe and East Asia during the 2021–22 winter season, possibly because the migratory waterfowl populations flying to each region shared the same breeding areas during summer 2021. The H5N1 NA gene tree indicated that the closest ancestors might be LPAI viruses (Appendix Figure 1, panel A), but genetic similarity to recent HPAI viruses detected in Africa and Europe was also evident (Table). Phylogenetic trees of the remaining 6 H5N1 genes also attested that A/chicken/Kagoshima/21A6T/2021 (H5N1) is a likely genetic reassortant recently generated between HPAI and LPAI viruses (Appendix Figure 1, panels B–G).

Unlike A/chicken/Kagoshima/21A6T/2021 (H5N1), the gene constellations of A/chicken/Kagoshima/B3T/2021 (H5N8) and A/hooded crane/Kagoshima/KU-5T/2021 (H5N8) were the same as HPAI H5N8 viruses detected during the 2020–21 winter season in East Asia, as we noted in subgroup G2a (Figure 2; Appendix Figure 1, panels B–H). These results suggest that A/chicken/Kagoshima/21A6T/2021 (H5N1) and the 3 other HPAI viruses we detected evolved individually among migratory waterfowl.

Conclusions

The results of this study, together with the contemporary HPAI outbreaks in other regions, including neighboring countries and in Europe, suggest that the HPAI H5N8 viruses isolated at farm B were introduced from migratory waterfowl overwintering on the same plain. Genetic analyses also revealed that 2 genetic subgroups of HPAI H5N1/H5N8 viruses, G2a and G2b, cocirculated among the

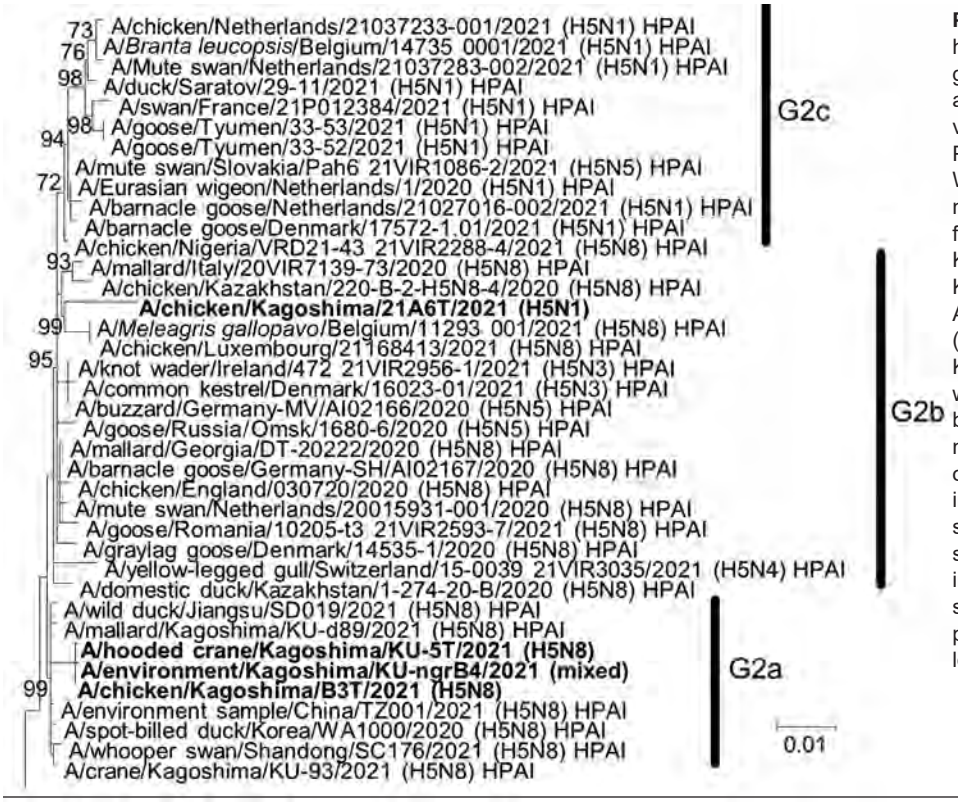

Figure 2. Phylogenetic tree of hemagglutinin genes of genetic group 2 (G2) of highly pathogenic avian influenza A(H5N1/H5N8) viruses isolated on the Izumi Plain, Japan, in November 2021. We phylogenetically analyzed the nucleotide sequences of the genes from A/environment/Kagoshima/KU-ngrB4/2021 (mixed), A/chicken/Kagoshima/21A6T/2021 (H5N1), A/chicken/Kagoshima/B3T/2021 (H5N8), and A/hooded crane/Kagoshima/KU-5T/2021 (H5N8) with representative counterparts by using the maximum-likelihood method with a bootstrapping set of 1,000 replicates. Bold text indicates viruses isolated in this study. Bootstrap values >70% are shown at the nodes. Scale bar indicates the number of nucleotide substitutions per site. HPAI, highly pathogenic avian influenza; LPAI, low pathogenicity avian influenza.

migratory waterfowl on the Izumi Plain. The HA genes from the HPAI H5 viruses isolated in Europe during the 2021–22 winter season formed a single cluster that was distinct from G2a and G2b; because HPAI viruses belonging to this cluster have not yet been isolated in Asia, we tentatively designated this genetic subgroup as G2c (Figure 2). This subgroup, which has been causing HPAI outbreaks in Europe since October 2021, could be introduced into East Asia.

In conclusion, we isolated and analyzed 4 HPAI H5N1/H5N8 viruses of clade 2.3.4.4b from the Izumi Plain, Japan, and found potential reassortment between HPAI and LPAI viruses. Our findings support the need for continuous surveillance and timely information sharing for rapid assessment of the potential risks to public and animal health.

Acknowledgments

We thank Satoru Taura, Naoko Maruta, Natsuko Nishi, and Donna Koyamada for their technical assistance. We thank the authors and originating and submitting laboratories for their sequences in GISAID's EpiFlu Database (https://www.gisaid.org) on which this research is based. We thank the Ministry of Agriculture, Forestry and Fisheries, the Ministry of the Environment, the Prefecture of Kagoshima, and the City of Izumi for their kind cooperation.

This research was commissioned by the Kagoshima Crane Conservation Committee and was supported by Grant-in-Aid for Research Activity Start-up from the Japan Society for the Promotion of Science (JSPS) (JSPS KAKENHI grant no. 21K20610); by Regulatory Research Projects for Food Safety, Animal Health and Plant Protection project no. JPJ008617.18065101 (FY2018–2022) from the Ministry of Agriculture, Forestry, and Fisheries of Japan; and by the contracted research activity for crane conservation with the City of Izumi, Japan.

About the Author

Dr. Okuya is an assistant professor at the Joint Faculty of Veterinary Medicine, Kagoshima University, Kagoshima, Japan. His primary research interest is the ecology of wildlifeborne viruses, including influenza viruses.

References

1. Li KS, Guan Y, Wang J, Smith GJ, Xu KM, Duan L, et al. Genesis of a highly pathogenic and potentially pandemic H5N1 influenza virus in eastern Asia. Nature. 2004;430:209–13. https://doi.org/10.1038/nature02746
2. Jeong S, Lee DH, Kwon JH, Kim YJ, Lee SH, Cho AY, et al. Highly pathogenic avian influenza clade 2.3.4.4b subtype H5N8 virus isolated from Mandarin duck in South Korea, 2020. Viruses. 2020;12:1389. https://doi.org/10.3390/v12121389
3. Isoda N, Twabela AT, Bazarragchaa E, Ogasawara K, Hayashi H, Wang ZJ, et al. Re-invasion of H5N8 high

pathogenicity avian influenza virus clade 2.3.4.4b in Hokkaido, Japan, 2020. Viruses. 2020;12:1439. https://doi.org/10.3390/v12121439
4. Khalil AM, Fujimoto Y, Kojima I, Esaki M, Ri K, Masatani T, et al. Genetic characterization of H5N8 highly pathogenic avian influenza viruses isolated from falcated ducks and environmental water in Japan in November 2020. Pathogens. 2021;10:171. https://doi.org/10.3390/pathogens10020171
5. Sakuma S, Uchida Y, Kajita M, Tanikawa T, Mine J, Tsunekuni R, et al. First outbreak of an H5N8 highly pathogenic avian influenza virus on a chicken farm in Japan in 2020. Viruses. 2021;13:489. https://doi.org/10.3390/v13030489
6. Baek YG, Lee YN, Lee DH, Shin JI, Lee JH, Chung DH, et al. Multiple reassortants of H5N8 clade 2.3.4.4b highly pathogenic avian influenza viruses detected in South Korea during the winter of 2020–2021. Viruses. 2021;13:490. https://doi.org/10.3390/v13030490
7. Świętoń E, Fusaro A, Shittu I, Niemczuk K, Zecchin B, Joannis T, et al. Sub-Saharan Africa and Eurasia ancestry of reassortant highly pathogenic avian influenza A(H5N8) virus, Europe, December 2019. Emerg Infect Dis. 2020;26:1557–61. https://doi.org/10.3201/eid2607.200165
8. Zecchin B, Goujgoulova G, Monne I, Salviato A, Schivo A, Slavcheva I, et al. Evolutionary dynamics of H5 highly pathogenic avian influenza viruses (clade 2.3.4.4B) circulating in Bulgaria in 2019–2021. Viruses. 2021;13:2086. https://doi.org/10.3390/v13102086
9. Okuya K, Kawabata T, Nagano K, Tsukiyama-Kohara K, Kusumoto I, Takase K, et al. Isolation and characterization of influenza A viruses from environmental water at an overwintering site of migratory birds in Japan. Arch Virol. 2015;160:3037–52. https://doi.org/10.1007/s00705-015-2610-0
10. Khalil AM, Hatai H, Fujimoto Y, Kojima I, Okajima M, Esaki M, et al. A lethal case of natural infection with the H5N8 highly pathogenic avian influenza virus of clade 2.3.4.4 in a Mandarin duck. Zoonotic Dis. 2022;2:32–6. https://doi.org/10.3390/zoonoticdis2010004
11. Gabriel G, Dauber B, Wolff T, Planz O, Klenk HD, Stech J. The viral polymerase mediates adaptation of an avian influenza virus to a mammalian host. Proc Natl Acad Sci U S A. 2005;102:18590–5. https://doi.org/10.1073/pnas.0507415102
12. Hatta M, Gao P, Halfmann P, Kawaoka Y. Molecular basis for high virulence of Hong Kong H5N1 influenza A viruses. Science. 2001;293:1840–2. https://doi.org/10.1126/science.1062882
13. Yamada S, Hatta M, Staker BL, Watanabe S, Imai M, Shinya K, et al. Biological and structural characterization of a host-adapting amino acid in influenza virus. PLoS Pathog. 2010;6:e1001034. https://doi.org/10.1371/journal.ppat.1001034
14. Imai M, Watanabe T, Hatta M, Das SC, Ozawa M, Shinya K, et al. Experimental adaptation of an influenza H5 HA confers respiratory droplet transmission to a reassortant H5 HA/H1N1 virus in ferrets. Nature. 2012;486:420–8. https://doi.org/10.1038/nature10831
15. Herfst S, Schrauwen EJ, Linster M, Chutinimitkul S, de Wit E, Munster VJ, et al. Airborne transmission of influenza A/H5N1 virus between ferrets. Science. 2012;336:1534–41. https://doi.org/10.1126/science.1213362

Address for correspondence: Makoto Ozawa, Department of Pathogenetic and Preventive Veterinary Science, Joint Faculty of Veterinary Medicine, Kagoshima University, 1-21-24 Korimoto, Kagoshima 890-0065, Japan; email: mozawa@vet.kagoshima-u.ac.jp

Multisystem Inflammatory Syndrome after Breakthrough SARS-CoV-2 Infection in 2 Immunized Adolescents, United States

Lyndsey D. Cole, Molly Slate, Samantha Minneman, Michael J. Bozzella

Eight weeks after having laboratory-confirmed SARS-CoV-2 breakthrough infections, 2 otherwise healthy, fully immunized adolescent patients in the United States who were experiencing related signs and symptoms were diagnosed with multisystem inflammatory syndrome in children. Our findings indicate that COVID-19 vaccination does not completely protect adolescents against multisystem inflammatory syndrome.

Multisystem inflammatory syndrome in children (MIS-C) is a hyperinflammatory illness occurring after SARS-CoV-2 infection; ≈30% of case-patients are adolescents (*1*). The United States reported 7,880 MIS-C cases and 66 deaths as of March 28, 2022 (*1*). MIS-C is an exception to the lower incidence and death from SARS-CoV-2–associated health conditions in children than adults (*2*). In April–June 2020, estimated MIS-C incidence across 7 US jurisdictions was 316 (95% CI 278–357) cases per 1 million SARS-CoV-2 infections in persons <21 years of age (*3*). The small but serious risk of MIS-C has been cited in support of pediatric SARS-CoV-2 immunization (*4*,*5*).

The BNT162b2 Pfizer-BioNTech mRNA COVID-19 vaccine (https://www.pfizer.com) was approved in December 2020 for children ≥16 years of age and in May 2021 for children 12–15 years of age (*6*). As of April 20, 2022, a total of 68% of US children 12–17 years of age had been fully immunized (*6*). Data about the effects of SARS-CoV-2 immunization on MIS-C are limited, although some evidence suggests the vaccine offers protection against MIS-C in adolescents (*7*,*8*). We describe 2 cases of MIS-C after breakthrough SARS-CoV-2 infection in fully immunized adolescents.

Author affiliation: University of Colorado, Aurora, Colorado, USA

DOI: https://doi.org/10.3201/eid2807.220560

The Study

In the first case, headache and myalgia developed in a healthy 14-year-old boy (day 1 of illness); by day 7, fever, abdominal pain, diarrhea, emesis, bloodshot eyes, red cracked lips, and rash had also developed. On day 10, he was brought for treatment to the emergency department and admitted to a quaternary-care pediatric hospital.

Three months earlier, he completed the Pfizer-BioNTech 2-dose COVID-19 vaccine series (Figure). One month later, he experienced 3 days of coughing and congestion and tested positive by PCR for SARS-CoV-2 infection, from which he recovered.

At hospital admission, examination noted sickly appearance, fever (39.1°C), tachycardia, rash, conjunctivitis, cracked lips, and abdominal tenderness. Laboratory testing revealed hyponatremia; thrombocytopenia; lymphopenia; and elevated C-reactive protein (CRP), N-terminal pro-brain natriuretic peptide (NT-proBNP), and liver function test levels (Table 1). Echocardiogram revealed trivial pericardial effusion. Abdominal ultrasound and chest radiograph results were unremarkable. SARS-CoV-2 spike and nucleocapsid IgG results were positive. Other infectious condition test results were negative (Table 2).

On the patient's first day of hospitalization, the infectious diseases section was consulted, and we determined that the patient's illness met Centers for Disease Control and Prevention MIS-C criteria (*1*). The next day, he received infliximab (10 mg/kg), followed by intravenous immunoglobulin. Rash, headache, conjunctivitis, and CRP improved; however, fever, malaise, and nausea persisted, and cardiac markers rose, prompting a second infliximab dose on hospitalization day 3. His fever subsided, and signs, symptoms, and laboratory results improved (Table 1).

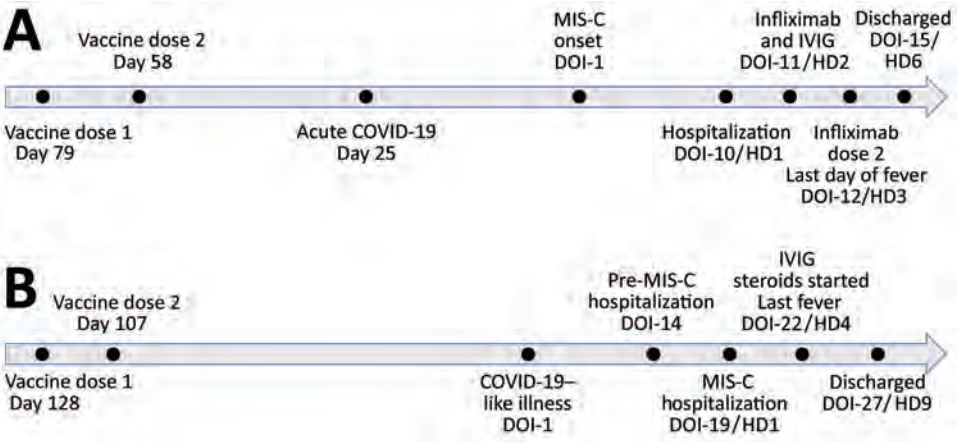

Figure. Time courses for vaccination, illness, diagnosis, and treatment for 2 adolescent MIS-C case-patients, United States. A) Case-patient 1; B) case-patient 2. DOI, day of illness (since onset); HD, hospital day; IVIG, intravenous immunoglobulin; MIS-C, multisystem inflammatory syndrome in children.

On hospitalization day 5, echocardiogram showed no effusion; he was discharged the next day.

Infectious diseases follow-up 3 weeks after hospital discharge revealed fatigue and occasional mild abdominal pain but normalized laboratory results. Cardiology follow-up 6 weeks after hospital discharge revealed ongoing fatigue. An echocardiogram showed new mild left main coronary artery enlargement (Z-score +2.7). We planned no interventions beyond interval outpatient monitoring.

In the second case, fever and fatigue, followed by congestion, cough, myalgias, headache, nausea, and vomiting, developed in an otherwise healthy 14-year-old girl (day 1 of illness). On day 3, rapid SARS-CoV-2 and influenza test results were negative. On day 12, she was brought to the emergency department for

Table 1. Laboratory results for 2 adolescent MIS-C case-patients, by day in hospital, United States*

	Case-patient 1, hospitalization for MIS-C						Case-patient 2‡						
							Pre–MIS-C hospitalization		Hospitalization for MIS-C				
Result†	HD1	HD2	HD3	HD4	HD5	HD6	HD1	HD4	HD1	HD3	HD5	HD7	HD9
Leukocytes, × 10^9 cells/L	↓3.6	↓4.1	↓2.3	↓2.6	↓3.1	↓2.7	11.9	NA	7.8	5.8	↓2.9	5.4	9.0
Hemoglobin, g/dL	12.5	13.1	12.4	12.2	12.4	↓10.5	13.5	NA	13.8	↓10.8	↓10.4	↓10.3	↓10.5
Platelets, 10^9/L	↓98	↓109	188	237	321	362	290	NA	373	265	NA	305	331
Absolute neutrophil count, × 10^9 cells/L	2.4	3.3	↓1	↓0.9	↓1	↓0.6	NA	NA	↓1.4	1.8	2.0	3.6	4.7
Absolute lymphocyte count, × 10^9 cells/L	1	↓0.6	1.1	1.3	1.7	1.8	NA	NA	5.8	2.3	↓0.6	1.2	2.8
ESR, mm/h	NA	6	7	↑23	↑24	↑25	↑18	NA	↑22	↑96	NA	NA	NA
Sodium, mmol/L	↓130	↓136	↓134	↓133	↓132	137	↓135	NA	↓136	137	↓127	↓136	139
Creatinine, mg/dL	↑1.2	↑1.0	↑0.9	0.7	↑0.8	0.6	0.7	NA	↑1.0	↑2.2	↑3.9	↑2.3	↑1.3
AST, U/L	↑165	↑207	↑131	↑114	↑200	↑164	↑297	↑164	↑102	↑169	↑53	28	33
ALT, U/L	↑221	↑243	↑196	↑167	↑195	↑162	↑249	↑269	↑188	↑177	↑123	↑57	45
GGT, U/L	↑126	↑137	↑129	↑128	↑136	NA	NA	NA	↑342	↑209	NA	NA	NA
LDH, U/L	↑1,484	NA	↑1,155	↑928	↑863	NA	↑1,313	NA	↑982	NA	NA	NA	NA
C-reactive protein, mg/L	↑135	↑86	↑64	↑36	↑19	↑11	↑23	NA	↑17	↑47	↑56	↑19	10
Ferritin, ng/mL	↑750	NA	↑576	↑626	↑754	↑578	↑593	NA	191	284	NA	NA	NA
Albumin, g/dL	NA	↓2.9	↓2.8	↓2.8	↓3.1	↓3.1	↓3.1	↓3.2	3.6	↓2.6	3.0	↓3.1	↓3.1
aPTT, s	↑42.9	36.5	↑38.9	↑39.4	NA	NA	↓20.5	NA	28.9	31.3	NA	NA	NA
PT, s	14	12.6	13.5	13.7	14.1	13.5	13.4	NA	13.5	14.7	NA	NA	NA
Fibrinogen, mg/dL	328	354	302	269	317	NA	258	NA	413	NA	NA	NA	NA
D-dimer, μg/mL	NA	↑>4	↑>4	↑>4	↑3.1	NA	NA	NA	↑2.8	NA	NA	NA	NA
Troponin-I, ng/mL	0.03	↑0.04	↑0.05	0.03	0.02	NA	<0.02	NA	<0.02	NA	NA	NA	NA
NT-proBNP, pg/mL	↑365	↑477	↑601	↑1,020	↑212	NA	66	NA	85	↑3,190	↑3,360	↑1,300	↑1,590

*ALT, alanine aminotransferase; aPTT, activated partial thromboplastin time; AST, aspartate aminotransferase; ESR, erythrocyte sedimentation rate; GGT, gamma-glutamyl transpeptidase; HD, hospital day; LDH, lactate dehydrogenase; MIS-C, multisystem inflammatory syndrome in children; NT-proBNP, N-type pro-brain natriuretic peptide; PT, prothrombin time; ↑, increased outside of reference range; ↓, decreased outside of reference range.
†Reference ranges: leukocytes, 5.2–9.7 × 10^9 cells/L; hemoglobin, 11.8–15.8 g/dL; platelets, 150–500 × 10^9/L; absolute neutrophil count, 1.8–6.6 × 10^9 cells/L; absolute lymphocyte count, 1.0–4.8 × 10^9/L; ESR, <15 mm/h; sodium, 137–145 mmol/L; creatinine, 0.2–0.7 mg/dL; AST, 15–40 U/L; ALT, <50 U/L; GGT, 10–28 U/L; LDH, 360–730 U/L; C-reactive protein, 0–10 mg/L; ferritin, 6–464 ng/mL; albumin 3.5–5 g/dL; aPTT, 23.5–37.5 s; PT, 11.5–15.0 s; fibrinogen, 200–450 mg/dL; D-dimer, <0.5 μg/mL; troponin-I, <0.03 ng/mL; NT-proBNP, <125 pg/mL
‡Omitted data for case-patient 2 from HD2 and HD3 of pre–MIS-C hospitalization and data from HD4, HD6, and HD8 of hospitalization for MIS-C were unnecessary for demonstrating clinical trends

Table 2. Infectious laboratory results for 2 adolescents after multisystem inflammatory syndrome in children symptom onset and throughout hospitalization, United States*

Laboratory test	Case-patient 1	Case-patient 2
SARS-CoV-2 spike IgG	Positive	NA
SARS-CoV-2 nucleocapsid IgG	Positive	Positive
SARS-CoV-2 PCR	Negative	Positive†
Other respiratory pathogen panel PCR	Negative	Negative
Blood culture, peripheral, 2 sets	Negative	Negative
Urine culture	Negative	Negative
Epstein Barr virus ab panel	Consistent with prior infection	Negative
Gastrointestinal pathogen panel PCR	Negative	NA
Group A *Streptococcus* throat PCR	Negative	NA
Quantiferon tuberculosis gold	Negative	NA
HIV Ag/Ab, 4th-generation	NA	Nonreactive
Rapid plasma regain	NA	Nonreactive
Parvovirus IgM and IgG	NA	Negative
Anti-streptolysin-O	NA	Negative
Anti-deoxyribonuclease B	NA	Negative

*Ag, antigen; Ab, antibody.
†Case-patient 2 had a positive SARS-CoV-2 PCR result on day-of-illness 11, followed by a negative result on day-of-illness 19.

persistent fever, headache, cough, and vomiting. Three months before her illness, she had completed the 2-dose Pfizer-BioNTech COVID-19 vaccine series (Figure).

Results from computed tomography of her head and chest radiograph were unremarkable. SARS-CoV-2 PCR was positive. She was prescribed amoxicillin for possible sinusitis and discharged. On day 14, she returned to the hospital for dyspnea and required low-flow oxygen for hypoxemia. Electrocardiogram, troponin, and NT-proBNP test results were normal. She was admitted and received 1 dose of remdesivir, which we discontinued because of elevated liver function test results (Table 1), and 2 doses of dexamethasone; we also discontinued amoxicillin. She improved and was discharged on day 18. However, she returned the next day with recrudescent fever, emesis, and new diffuse rash, including on her palms and soles. Laboratory testing demonstrated elevated CRP, D-dimer, liver function, NT-proBNP, and creatinine levels (Table 1). Abdominal ultrasound and computed tomography showed incidentally enlarged kidneys. We empirically started clindamycin and ceftriaxone treatment and readmitted her.

At readmission on day 19, differential diagnoses included MIS-C, acute COVID-19 with hyperinflammation, sepsis, toxic shock syndrome, drug reaction, and vasculitis or other autoimmune disease. Echocardiogram results were unremarkable. A SARS-CoV-2 nucleocapsid IgG test was positive. Additional infectious and rheumatologic test results were negative (Table 2). After discussion among multidisciplinary specialists, we considered MIS-C most likely, with a suspicion that her earlier symptoms might have resulted from acute COVID-19, which evolved over 3 weeks into MIS-C. We discontinued antibiotics.

On day 4 of her second hospitalization, she received intravenous immunoglobulin and methylprednisolone. Her fever quickly subsided, signs and symptoms resolved, and laboratory results improved (Table 1). On hospitalization day 9, she was discharged with an oral prednisone taper. Infectious disease follow-up 3 weeks after discharge revealed mild fatigue and headaches but normalized laboratory results. Cardiology follow-up through 12 weeks after discharge indicated fatigue, but echocardiogram and exercise stress testing results were unremarkable.

Conclusions

We report 2 cases in which fully vaccinated, otherwise healthy adolescent patients were diagnosed with MIS-C after laboratory-confirmed SARS-CoV-2 breakthrough infections. Diagnoses were based on CDC criteria, and clinical findings were similar to descriptions from cohort studies published elsewhere (*9*–*11*). Based on Brighton Collaboration MIS-C case definitions (https://brightoncollaboration.us), we considered MIS-C diagnosis definitive in case-patient 1 and probable in case-patient 2, although her condition had some features more suggestive of acute COVID-19 with hyperinflammation (*12*). Neither case met SARS-CoV-2 vaccine-associated MIS-C criteria (*12*).

As adolescent SARS-CoV-2 immunization rates have increased, so has interest in the effects of vaccination on adolescent MIS-C. In a fall 2021 study in France, 0/33 adolescents with MIS-C were fully vaccinated against COVID-19 (*7*). Seven (21%) had received 1 shot of a 2-dose vaccine; hazard ratio for MIS-C was 0.09 (95% CI 0.04–0.21) among the partially vaccinated compared with unvaccinated patients (p<0.001) (*7*). A January 2022 report estimated 91% (95% CI 78%–97%) vaccine effectiveness against MIS-C based on 102 case-patients and 181 hospitalized controls at 24 US pediatric hospitals during July–December 2021 (*8*). Only 5% of MIS-C

case-patients were fully vaccinated, compared with 36% of controls. None of the 5 fully COVID-19–vaccinated MIS-C patients, compared with 39% of unvaccinated patients, required invasive mechanical ventilation, vasoactive medications, or extracorporeal membrane oxygenation (*8*), suggesting decreased MIS-C severity in vaccinated patients, similar to our 2 case-patients. Another US review reported mechanical ventilation use in 14% and vasopressor use in 38% of 21 patients with MIS-C after SARS-CoV-2 vaccination; 52% had received only 1 of 2 vaccine doses, and median time from second dose to MIS-C onset was 5 days, shorter than expected to reach full vaccine efficacy (*13*). Although those findings could suggest vaccine-associated MIS, 71% of patients showed evidence of SARS-CoV-2 breakthrough infection (*13*). Our case-patients demonstrated clear breakthrough infections, ruling out vaccine-associated MIS based on Brighton criteria (*12*).

Although COVID-19 vaccines appear to be effective against MIS-C (*7*,*8*), whether effectiveness results from decreased risk of acquiring SARS-CoV-2 or reduced likelihood of developing MIS-C after a breakthrough infection remains unclear. Because vaccine effectiveness against older versus newer variants might differ, potential vaccine effect on MIS-C rates after breakthrough infections becomes more important (*14*). Additional research is needed, particularly among age groups younger than those in our study, which account for most MIS-C cases. However, our findings indicate that even full COVID-19 vaccination in adolescents is not 100% effective against MIS-C.

About the Author

Dr. Cole is completing a dual fellowship in pediatric infectious diseases and rheumatology at Children's Hospital Colorado, affiliated with the University of Colorado School of Medicine. Her primary research interests are periodic fever/autoinflammatory syndromes, immune dysregulation, and infectious triggers of rheumatologic or inflammatory conditions.

References

1. Centers for Disease Control and Prevention. Health department-reported cases of multisystem inflammatory syndrome in children (MIS-C) in the United States. 2021 [cited 2022 Apr 28]. https://www.cdc.gov/mis-c/cases/index.html
2. Mehta NS, Mytton OT, Mullins EWS, Fowler TA, Falconer CL, Murphy OB, et al. SARS-CoV-2 (COVID-19): what do we know about children? A systematic review. Clin Infect Dis. 2020;71:2469–79. https://doi.org/10.1093/cid/ciaa556
3. Payne AB, Gilani Z, Godfred-Cato S, Belay ED, Feldstein LR, Patel MM, et al.; MIS-C Incidence Authorship Group. Incidence of multisystem inflammatory syndrome in children among US persons infected with SARS-CoV-2. JAMA Netw Open. 2021;4:e2116420. https://doi.org/10.1001/jamanetworkopen.2021.16420
4. Klass P, Ratner AJ. Vaccinating children against Covid-19—the lessons of measles. N Engl J Med. 2021;384:589–91. https://doi.org/10.1056/NEJMp2034765
5. Castagnola E, Mariani M, Sticchi C, Sticchi L, Spiazzi R, Caorsi R, et al. Incidence rate of MIS-C in paediatrics: a good reason to vaccinate children against SARS-CoV-2. Acta Paediatr. 2022;111:123–4. https://doi.org/10.1111/apa.16081
6. American Academy of Pediatrics. Children and COVID-19 vaccination trends. Summary of data publicly reported by the Centers for Disease Control and Prevention [cited 2022 Apr 28]. https://www.aap.org/en/pages/2019-novel-coronavirus-covid-19-infections/children-and-covid-19-vaccination-trends
7. Levy M, Recher M, Hubert H, Javouhey E, Fléchelles O, Leteurtre S, et al. Multisystem inflammatory syndrome in children by COVID-19 vaccination status of adolescents in France. JAMA. 2022;327:281–3. https://doi.org/10.1001/jama.2021.23262
8. Zambrano LD, Newhams MM, Olson SM, Halasa NB, Price AM, Boom JA, et al.; Overcoming COVID-19 Investigators. Effectiveness of BNT162b2 (Pfizer-BioNTech) mRNA vaccination against multisystem inflammatory syndrome in children among persons aged 12–18 years—United States, July–December 2021. MMWR Morb Mortal Wkly Rep. 2022;71:52–8.
9. Centers for Disease Control and Prevention. Multisystem inflammatory syndrome in children (MIS-C) associated with coronavirus disease 2019 (COVID-19). 2020 [cited 2022 Jan 9]. https://emergency.cdc.gov/han/2020/han00432.asp
10. Feldstein LR, Tenforde MW, Friedman KG, Newhams M, Rose EB, Dapul H, et al.; Overcoming COVID-19 Investigators. Characteristics and outcomes of US children and adolescents with multisystem inflammatory syndrome in children (MIS-C) compared with severe acute COVID-19. JAMA. 2021;325:1074–87. https://doi.org/10.1001/jama.2021.2091
11. Godfred-Cato S, Bryant B, Leung J, Oster ME, Conklin L, Abrams J, et al.; California MIS-C Response Team. COVID-19–associated multisystem inflammatory syndrome in children—United States, March–July 2020. MMWR Morb Mortal Wkly Rep. 2020;69:1074–80. https://doi.org/10.15585/mmwr.mm6932e2
12. Vogel TP, Top KA, Karatzios C, Hilmers DC, Tapia LI, Moceri P, et al. Multisystem inflammatory syndrome in children and adults (MIS-C/A): case definition & guidelines for data collection, analysis, and presentation of immunization safety data. Vaccine. 2021;39:3037–49. https://doi.org/10.1016/j.vaccine.2021.01.054
13. Yousaf AR, Cortese MM, Taylor AW, Broder KR, Oster ME, Wong JM, et al.; MIS-C Investigation Authorship Group. Reported cases of multisystem inflammatory syndrome in children aged 12-20 years in the USA who received a COVID-19 vaccine, December, 2020, through August, 2021: a surveillance investigation. Lancet Child Adolesc Health. 2022;6:303–12. https://doi.org/10.1016/S2352-4642(22)00028-1
14. Cele S, Jackson L, Khoury DS, Khan K, Moyo-Gwete T, Tegally H, et al.; NGS-SA; COMMIT-KZN Team. Omicron extensively but incompletely escapes Pfizer BNT162b2 neutralization. Nature. 2022;602:654–6. https://doi.org/10.1038/s41586-021-04387-1

Address for correspondence: Michael Bozzella, Children's Hospital Colorado, 4090 Briargate Pkwy, Colorado Springs, CO 80920, USA; email: michael.bozzella@childrenscolorado.org

Natural History of and Dynamic Changes in Clinical Manifestation, Serology, and Treatment of Brucellosis, China

Hongyu Wang,[1] Hongyan Liu,[1] Qiran Zhang,[1] Xiaobo Lu,[1] Dan Li,[1] Haocheng Zhang,[1] Yan A. Wang, Rongjiong Zheng, Yi Zhang, Zhangfan Fu, Ke Lin, Chao Qiu, Yan O. Wang, Ye Gu, Jingwen Ai, Wenhong Zhang

Medscape EDUCATION ACTIVITY

In support of improving patient care, this activity has been planned and implemented by Medscape, LLC and Emerging Infectious Diseases. Medscape, LLC is jointly accredited by the Accreditation Council for Continuing Medical Education (ACCME), the Accreditation Council for Pharmacy Education (ACPE), and the American Nurses Credentialing Center (ANCC), to provide continuing education for the healthcare team.

Medscape, LLC designates this Journal-based CME activity for a maximum of 1.00 ***AMA PRA Category 1 Credit(s)™***. Physicians should claim only the credit commensurate with the extent of their participation in the activity.

Successful completion of this CME activity, which includes participation in the evaluation component, enables the participant to earn up to 1.0 MOC points in the American Board of Internal Medicine's (ABIM) Maintenance of Certification (MOC) program. Participants will earn MOC points equivalent to the amount of CME credits claimed for the activity. It is the CME activity provider's responsibility to submit participant completion information to ACCME for the purpose of granting ABIM MOC credit.

All other clinicians completing this activity will be issued a certificate of participation. To participate in this journal CME activity: (1) review the learning objectives and author disclosures; (2) study the education content; (3) take the post-test with a 75% minimum passing score and complete the evaluation at http://www.medscape.org/journal/eid; and (4) view/print certificate. For CME questions, see page 1542.

Release date: June 21, 2022; Expiration date: June 21, 2023

Learning Objectives

Upon completion of this activity, participants will be able to:

- Describe diagnosis and epidemiologic features of human brucellosis, according to a large, retrospective cohort study in China
- Determine clinical characteristics of human brucellosis during the disease course and after treatment, according to a large, retrospective cohort study in China
- Identify serologic surveillance of human brucellosis during the disease course and after treatment, and long-term treatment outcomes, according to a large, retrospective cohort study in China

CME Editor

Jill Russell, BA, Technical Writer/Editor, Emerging Infectious Diseases. *Disclosure: Jill Russell, BA, has disclosed no relevant financial relationships.*

CME Author

Laurie Barclay, MD, freelance writer and reviewer, Medscape, LLC. *Disclosure: Laurie Barclay, MD, has disclosed the following relevant financial relationships: stocks, stock options, or bonds from AbbVie Inc. (former).*

Authors

Hongyu Wang, MD; Hongyan Liu, MD; Qiran Zhang, MD; Xiaobo Lu, MD; Dan Li, MD; Haocheng Zhang, MD; Yan A. Wang, MD; Yi Zhang, MD; Zhangfan Fu, MS; Ke Lin, MS; Chao Qiu, PhD; Yan O. Wang, MD; Ye Gu, MD; Jingwen Ai, MD; *and* ***Wenhong Zhang, MD.***

Author affiliations: National Medical Center for Infectious Disease, National Clinical Research Center for Aging and Medicine, Shanghai Key Laboratory of Infectious Diseases and Biosafety Emergency Response, Huashan Hospital, Fudan University, Shanghai, China (H. Wang, Q. Zhang, H. Zhang, Y. Zhang, Z. Fu, K. Lin, C. Qiu, J. Ai, W. Zhang); The Sixth People's Hospital of Shenyang, Shenyang, China (H. Liu, D. Li, Y.A. Wang, Y.O. Wang, Y. Gu); Emergency Treatment and Innovation Center of Public Health Emergencies, Shenyang (H. Liu, D. Li, Y.A. Wang, Y.O. Wang, Y. Gu); Center for Infectious Diseases, the First Affiliated Hospital of Xinjiang Medical University, Wulumuqi, China (X. Lu, R. Zheng); Key Laboratory of Medical Molecular Virology (MOE/MOH), Shanghai Medical College, Fudan University, Shanghai (W. Zhang)

DOI: https://doi.org/10.3201/eid2807.211766

[1]These authors contributed equally to this article.

Serum agglutination test plus exposure history were used to diagnose most cases of human brucellosis in 2 China provinces. After appropriate treatment, 13.3% of acute brucellosis cases progressed to chronic disease; arthritis was an early predictor. Seropositivity can persist after symptoms disappear, which might cause physicians to subjectively extend therapeutic regimens.

Brucellosis is a zoonosis caused by the bacterium *Brucella* that typically manifests in insidious onset of fever, malaise, arthralgias, and nonspecific physical findings, including hepatomegaly, splenomegaly, or lymphadenopathy (*1*). Accurate diagnosis and proper management of human brucellosis continues to challenge clinicians. Several studies have described the clinical characteristics of human brucellosis and evaluated diagnostic methods, but most of these studies are cross-sectional and focused on baseline manifestations or diagnostic accuracy (*2*–*6*). Much remains unclear about the dynamic changes of clinical manifestations, serology, and the tendency of brucellosis to persist and become chronic during development and treatment.

The Study

We conducted a retrospective, real-world cohort study at 8 hospitals in Liaoning and Xinjiang Provinces, 2 of the most brucellosis-endemic areas in China, to investigate the characteristics of brucellosis during natural history and treatment. We enrolled patients confirmed to have brucellosis during 2014–2020. We collected information on contact history, clinical manifestations, laboratory parameters, and antibiotic therapy from the hospital information system and treatment outcome by telephone (Appendix, https://wwwnc.cdc.gov/EID/article/28/7/21-1766-App1.pdf). This research was carried out according to the principles of the Declaration of Helsinki. The study protocol was approved by the Ethics Committees of Huashan Hospital of Fudan University (KY2019–412). Informed consent was obtained from all patients before diagnosis, and patient data were anonymized.

We included 5,270 patients confirmed to have brucellosis during September 2014–December 2020. Three persons were excluded for positive HIV detection, 668 were excluded because they lacked positive culture or serologic results, and 1,191 were excluded for incomplete clinical information. We ultimately enrolled 3,411 persons; we performed follow-up for 1,676 persons at periods of 14, 28, 42, 90, 180, 360, or 720 days after diagnosis and treatment initiation (Appendix Figure 1).

Median participant age was 48 years (interquartile range 35.8–57.0 years). Most participants were men (2,452; 73.9%) and worked as farmers or herdsmen (2,776; 82.4%). A total of 2,066 (60.6%) had exposure history with suspicious animals, 1,686 (49.4%) had contact history with brucellosis patients, and 1,129 (33.1%) resided in a brucellosis-endemic area (Table 1).

Blood cultures were collected from 1,827 participants for diagnostic purposes; results were positive in 424 (23.2%) persons. Serum agglutination tests (SAT) were collected from 3,381 persons, and 3,351 (99.1%) reported positive results. A total of 1,797 persons received both tests; 394 (21.9%) tested positive on both, 28 (1.6%) tested positive by culture only, and 1,375 (76.5%) tested positive by SAT only. Among 2,264 patients with positive titers on SAT, titers were >1:400 in 36.0%, 1:200 in 28.4%, 1:100 in 35.2%, and 1:50 in 0.4% (Table 1). Seasonal epidemics were observed during March–July each year, whereas total diagnosed cases decreased annually during 2015–2019 (Appendix Figure 2).

We observed the natural history of brucellosis with symptom duration <180 days (early stage) or >180 days (late stage) before patients received antibiotic therapy. The 3 most common symptoms in early-stage disease were fatigue (72.3%), fever (64.0%), and sweating (34.6%). The most common symptoms in late-stage disease were fatigue (71.6%), fever (61.1%), and arthritis (36.6%) (Figure 1, panel A). Arthritis was more common in the late stage than the early stage (20.7%; p<0.0001). We observed neurobrucellosis in 9.9% of patients in the early stage and in 4.1% of patients in the late stage (p = 0.0020). After adjusting for confounding factors through propensity score-matching (PSM) (*7*), culture-diagnosed patients (compared with patients with SAT-diagnosed brucellosis) had higher incidence of fever (311 [81.8%] vs. 244 [58.9%]; p<0.0001), sweating (177 [46.6%] vs. 95 [25.0%]; p<0.0001), poor appetite (271 [71.3%] vs. 195 [51.3%]; p<0.0001), and hepatosplenomegaly (67 [17.6%] vs. 45 [11.8%]; p<0.0001). These patients also exhibited higher C-reactive protein (34.5 $\pm$ 1.8 vs. 24.7 $\pm$ 1.7; p = 0.0002) and erythrocyte sedimentation rate (45.6 $\pm$ 1.7 vs. 29.3 $\pm$ 1.4; p = 0.0290), which could be caused by active bloodstream infection (Appendix Table 1).

Among 1,676 participants with whom we conducted follow-up, we observed further clinical characteristics after treatment initiation. Most newly developed manifestations were reported within the first 2 weeks, but most patients recovered with persistent treatment (Appendix Figure 3). Two weeks after treatment initiation, 107 patients had newly developed cardiac inflammation, 112 neurobrucellosis, 140 urogenital inflammation, and 146 arthritis. Overall, 1,453 (86.7%) persons with acute brucellosis

symptomatically recovered within 180 days after appropriate treatment, whereas 223 (13.3%) were still symptomatic after 180 days and chronic brucellosis developed (Figure 1, panel B) (*8*). In the chronic phase, arthritis (89 [25.6%]), fatigue (60 [17.3%]), and fever (57 [16.4%]) became the 3 most common manifestations (Appendix Figure 4).

After conducting PSM for age, sex, nationality, and year of enrollment, we performed multivariate logistic regression to identify risk factors for chronic brucellosis in 148 acute cases and 148 chronic cases (Table 2). Fever, sweating, myalgia, arthritis, and C-reactive protein and erythrocyte sedimentation rates at baseline were possible predictors for chronic brucellosis in univariate analysis ($p<0.10$). Arthritis was the only risk factor after multivariate analysis (odds ratio 4.11 [95% CI 1.22–16.92]; $p = 0.0318$).

Dynamic SAT surveillance among 1,676 participants suggested that 53.8% (902/1,676) remained seropositive 42 days after treatment and 33.9% (518/1,676) remained seropositive 180 days after treatment (Figure 2, panel A). In acute cases, 413 remained seropositive and 1,040 seroconverted after 180 days. In chronic cases, 105 remained seropositive and 118 seroconverted ($p<0.0001$). The overall SAT titers decreased at the chronic phase; fewer patients had a titer of >1:400 (Figure 2, panel B).

We observed treatment outcomes in 432 patients without systemic involvement, of whom 307 (71.1%) received doxycycline and rifampin, 29 (6.7%) received doxycycline and levofloxacin, and 96 (22.2%) received triad therapy. In comparison with the standard 6-week treatment course (*8*–*10*), 75.2% (325/432) patients received antibiotic therapy for >42 days; median course of treatment was 90 (interquartile range 43–193) days (Figure 2, panel C). Further analysis in treatment elongation found that 26/325 (8.0%) were still symptomatic; the most common manifestations were sweating (61.5%), fatigue (50.0%), and fever (26.9%). A total of 174/325 (53.5%) participants were asymptomatic but seropositive, which could lead clinicians to subjectively extend antibiotic treatment; 125/325 (38.5%) participants were asymptomatic and

Table 1. Demographic characteristics of brucellosis case-patients at enrollment in study of natural history and dynamic changes in clinical signs, serology, and treatment of brucellosis, China, 2014–2020*

Characteristic	Case-patients, n = 3,411
Median age, y (IQR)†	48.0 (35.8–57.0)
<20	143 (4.4)
20–40	933 (29.0)
40–60	1,629 (50.6)
>60	515 (16.0)
Sex‡	
M	2,452 (73.9)
F	867 (26.1%)
Nationality§	
Han	1,818 (53.6)
Others	1,572 (46.4)
Occupation¶	
Farmer	2,591 (76.9)
Herdsman	185 (5.5)
Veterinarian	33 (1.0)
Other	560 (16.6)
Contact history	
Exposure to suspicious animals	2,066 (60.6)
Contact with brucellosis patients	1,686 (49.4)
Residence in endemic area	1,129 (33.1)
Exposure to Brucella	58 (1.7)
Diagnostic test#	
Brucella culture	424 (23.2)
Antibody (SAT)	3,351 (99.1)
Titers**	
1:50	9 (0.4)
1:100	797 (35.2)
1:200	643 (28.4)
>1:400	815 (36.0)

*Values are no. (%) except as indicated. IQR, interquartile range; SAT, serum agglutination test.
†Information on age was available for 3,220 participants.
‡Information on sex was available for 3,319 participants.
§Information on nationality was available for 3,390 participants.
¶Information on occupation was available for 3,369 participants.
#A total of 1,827 participants received Brucella culture, and 3,381 received SAT.
**Among 3,381 participants tested by SAT, 2,264 had detailed positive titer information.

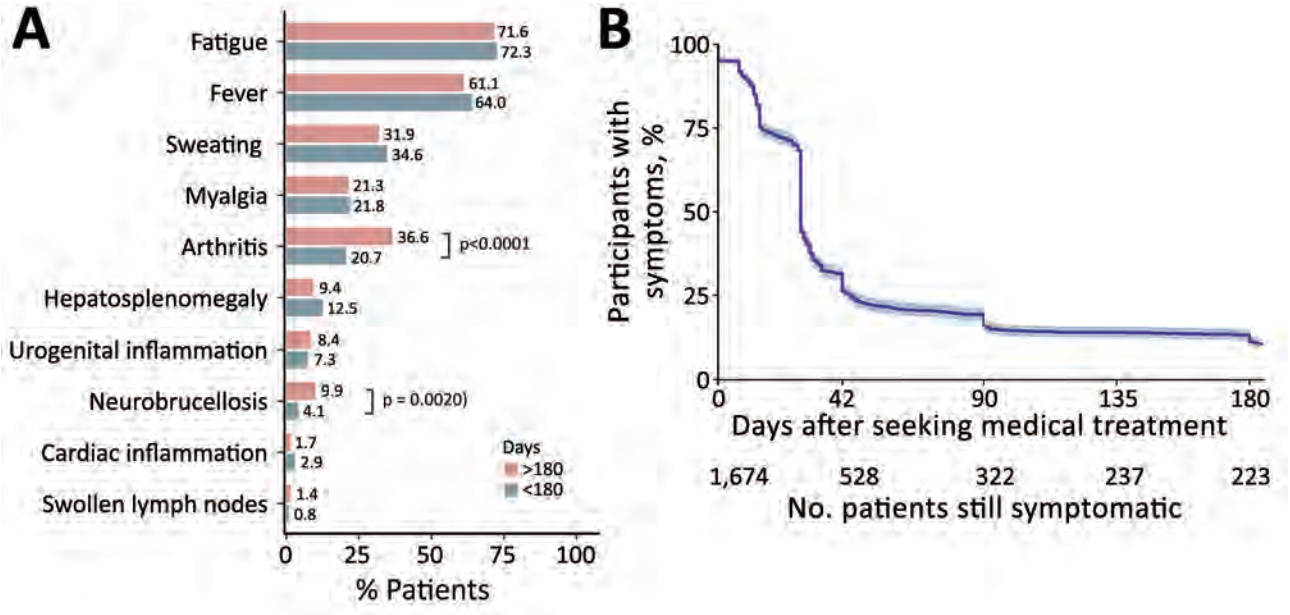

Figure 1. Dynamic characteristics of clinical manifestations in case-patients with acute and chronic brucellosis, China, 2014–2020. A) Natural symptom development with symptom duration <180 days (early stage) or >180 days (late stage) before patients received antibiotic therapy. B) Kaplan-Meier curve of symptomatic case-patients after treatment initiation.

seronegative (Figure 2, panel D). We further analyzed 107 participants who completed treatment within 42 days to determine whether standard treatment led to persistent symptoms or recurrence. Of those participants, 48/107 (44.9%) remained seropositive, 2/107 (1.9%) reported persistent symptoms, and 1/107 (0.9%) participant's illness was considered a recurrence 2 years later.

The first limitation of our study is that we failed to follow up culture results during treatment. Second, we failed to distinguish transient and persistent exposure history, which might play a role in persistent symptoms or serologic results. Finally, infection was diagnosed by heterogenous methods, including culture and a series of serologic tests, which might introduce bias in baseline and prognosis analysis.

Conclusions

Our study gives a thorough, dynamic description of clinical characteristics and serologic surveillance during the natural history and treatment of human brucellosis in a large population. Culture was 23.2% positive but SAT 99.1% positive in confirmed brucellosis. SAT plus exposure history remained the most effective diagnostic tool. Human brucellosis had variable manifestations at different disease

Table 2. Comparison of acute and chronic brucellosis at enrollment in study of natural history and dynamic changes in clinical signs, serologic testing, and treatment of brucellosis, China, 2014–2020*

Characteristic	Acute brucellosis, n = 148	Chronic brucellosis, n = 148	Univariate analysis OR (95% CI)	Univariate analysis p value	Multivariate analysis OR (95% CI)	Multivariate analysis p value
Symptom, no. (%)						
Fever	108 (73.0)	97 (65.5)	0.74 (0.53–1.04)	0.0753	1.28 (0.35–5.42)	0.7159
Sweating	52 (35.1)	65 (43.9)	1.38 (1.00–1.90)	0.0471	2.33 (0.69–7.55)	0.1578
Myalgia	30 (20.3)	45 (30.4)	1.75 (1.23–2.45)	0.0014	2.48 (0.68–8.34)	0.1466
Poor appetite	89 (60.1)	92 (62.2)	1.06 (0.77–1.47)	0.7427		
Hepatosplenomegaly	23 (15.5)	21 (14.2)	0.82 (0.50–1.28)	0.3971		
Arthritis	63 (42.6)	74 (50.0)	1.68 (1.22–2.31)	0.0013	4.11 (1.22–16.92)	0.0318
Urogenital inflammation	18 (12.2)	13 (8.8)	0.75 (0.43–1.24)	0.2883		
Neurobrucellosis	5 (3.4)	8 (5.4)	1.60 (0.76–3.06)	0.1805		
Laboratory test result, ± SD						
Leukocytes, 10^9 cells/L	6.4 ± 0.2	5.9 ± 0.2	0.96 (0.89–1.03)	0.2480		
Lymphocytes, 10^9 cells/L	1.9 ± 0.1	2.0 ± 0.1	0.92 (0.75–1.12)	0.4038		
Monocytes, 10^9 cells/L	0.5 ± 0.1	0.5 ± 0.0	0.68 (0.35–1.13)	0.2227		
CRP, mg/dL	33.7 ± 3.6	23.8 ± 3.3	0.99 (0.99–1.00)	0.0522	0.99 (0.97–1.02)	0.6948
Procalcitonin, ng/mL	0.1 ± 0.0	0.2 ± 0.1	1.02 (0.64–1.29)	0.8930		
ESR, mm/h	42.8 ± 6.9	20.9 ± 6.4	0.97 (0.95–1.00)	0.0481	0.98 (0.94–1.00)	0.1371

*CRP, C-reactive protein; ESR, erythrocyte sedimentation rate; OR, odds ratio.

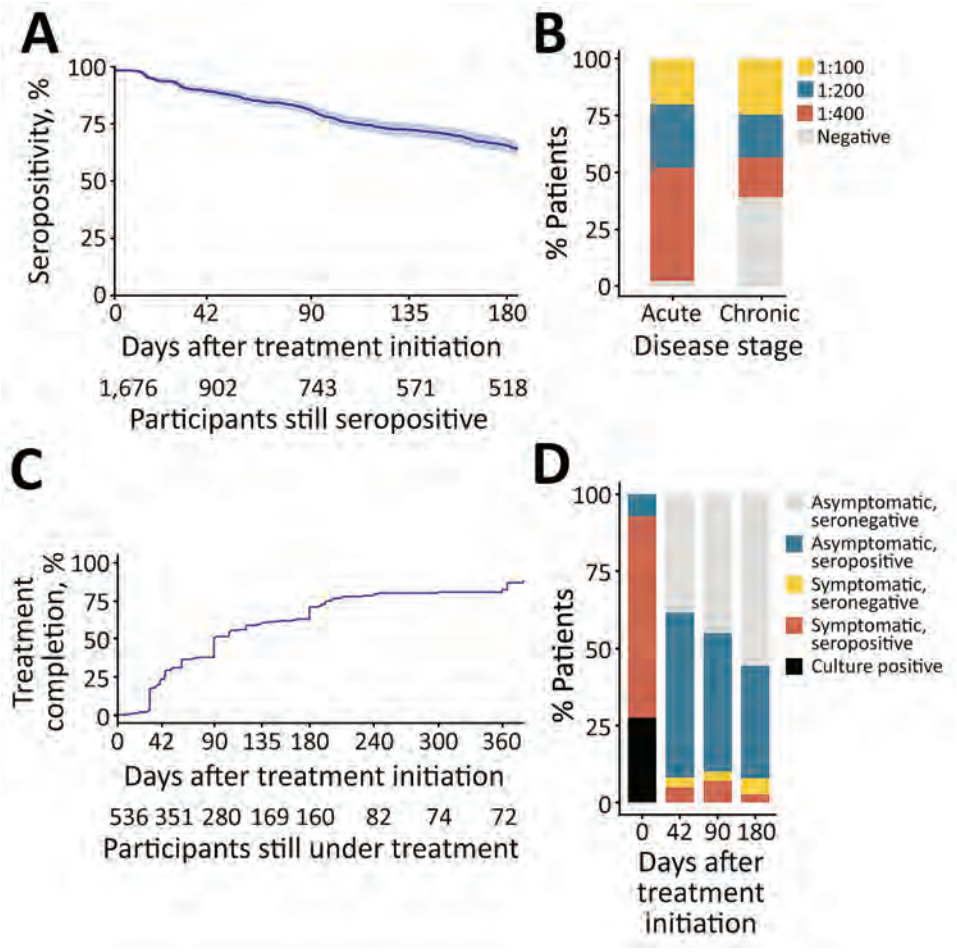

Figure 2. Dynamic characteristics of serum agglutination test and treatment courses in case-patients with brucellosis, China, 2014–2020. A) Seroconversion after treatment initiation; B) serum agglutination test titer distribution at baseline and 180 days after treatment initiation; C) treatment length of case-patients without systemic involvement; D) possible reasons for lengthened treatment in brucellosis case-patients without systemic involvement.

stages. Untreated cases mainly manifested as fatigue, fever, or sweating in the early stage, whereas fatigue, fever, and arthritis were the most common symptoms at the late stage. After appropriate treatment, 13.3% of acute brucellosis cases progressed to chronic disease. Arthritis can serve as an early predictor of chronic brucellosis. Seropositivity can persist after symptoms disappear, which might cause physicians to subjectively and unnecessarily extend therapeutic regimens.

Acknowledgments

We thank all the physicians that participated in this study for patient enrollment and follow-up and give our greatest appreciation to all health workers for their valuable input to the control of diseases.

This study was funded by Shanghai Municipal Science and Technology Major Project, Shanghai Key Laboratory of Infectious Diseases and Biosafety Emergency Response, Huashan Hospital, Fudan University (No. 20dz2260100, 21NL2600100, 20dz2210400), National Natural Science Foundation of China (no. 82002141), Shanghai Youth Science and Technology Talents Sailing Project (20YF1404300) and Key Discipline Construction Plan from Shanghai Municipal Health Commission (GWV-10.1-XK01, GWV-3.1, GWV-2).

The data that support the findings of this study are available from the corresponding author on reasonable request.

About the Author

Dr. H. Wang is a medical doctor in the Department of Infectious Diseases, Fudan University–affiliated Huashan Hospital, Shanghai, China. Her primary research interests are human brucellosis, severe pneumonia, and COVID-19.

References

1. Franco MP, Mulder M, Gilman RH, Smits HL. Human brucellosis. Lancet Infect Dis. 2007;7:775–86. https://doi.org/10.1016/S1473-3099(07)70286-4
2. Hasanjani Roushan MR, Mohrez M, Smailnejad Gangi SM, Soleimani Amiri MJ, Hajiahmadi M. Epidemiological features and clinical manifestations in 469 adult patients with brucellosis in Babol, Northern Iran. Epidemiol

Infect. 2004;132:1109–14. https://doi.org/10.1017/S0950268804002833
3. Kokoglu OF, Hosoglu S, Geyik MF, Ayaz C, Akalin S, Buyukbese MA, et al. Clinical and laboratory features of brucellosis in two university hospitals in Southeast Turkey. Trop Doct. 2006;36:49–51. https://doi.org/10.1258/004947506775598752
4. Memish Z, Mah MW, Al Mahmoud S, Al Shaalan M, Khan MY. Brucella bacteraemia: clinical and laboratory observations in 160 patients. J Infect. 2000;40:59–63. https://doi.org/10.1053/jinf.1999.0586
5. Osoba AO, Balkhy H, Memish Z, Khan MY, Al-Thagafi A, Al Shareef B, et al. Diagnostic value of Brucella ELISA IgG and IgM in bacteremic and non-bacteremic patients with brucellosis. J Chemother. 2001;13(Suppl 1):54–9. https://doi.org/10.1080/1120009X.2001.11782330
6. Ruiz-Mesa JD, Sánchez-Gonzalez J, Reguera JM, Martín L, Lopez-Palmero S, Colmenero JD. Rose Bengal test: diagnostic yield and use for the rapid diagnosis of human brucellosis in emergency departments in endemic areas. Clin Microbiol Infect. 2005;11:221–5. https://doi.org/10.1111/j.1469-0691.2004.01063.x
7. Benedetto U, Head SJ, Angelini GD, Blackstone EH. Statistical primer: propensity score matching and its alternatives. Eur J Cardiothorac Surg. 2018;53:1112–7. https://doi.org/10.1093/ejcts/ezy167
8. Zhang W, Zhang Y; Editorial Board of Chinese Journal of I nfectious Diseases. Chinese consensus guidelines for diagnosis and management of Brucellosis. 2017 [cited 2020 Oct 24]. https://kns.cnki.net/kcms/detail/detail.aspx?dbcode=CJFD&dbname=CJFDZHYX&filename=ZHCR201712001&v=sN5G45eVI%25mmd2Fat9QoWJOcHw1HZ2lAhahab4JxrG07mQPVlruZm7rIQrBZkc1821u9p
9. Bossi P, Tegnell A, Baka A, van Loock F, Hendriks J, Werner A, et al. Bichat guidelines for the clinical manage-ment of brucellosis and bioterrorism-related brucellosis. Euro Surveill. 2004;9:E15–6. https://doi.org/ 10.2807/esm.09.12.00506-en
10. Tuon FF, Cerchiari N, Cequinel JC, Droppa EEH, Moreira SDR, Costa TP, et al.; Brucellosis Workgroup. Guidelines for the management of human brucellosis in the State of Paraná, Brazil. Rev Soc Bras Med Trop. 2017;50:458–64. https://doi.org/10.1590/0037-8682-0319-2016

Address for correspondence: Jingwen Ai or Wenhong Zhang, Department of Infectious Disease, Huashan Hospital, Fudan University, No. 12, Wulumuqi Rd, Jingan District, Shanghai, 200040, China; email: jingwenai1990@126.com or zhangwenhong@fudan.edu.cn; Ye Gu, The Sixth People's Hospital of Shenyang, Shenyang, 110013, China; email: GUYE2020@126.com

etymologia revisited

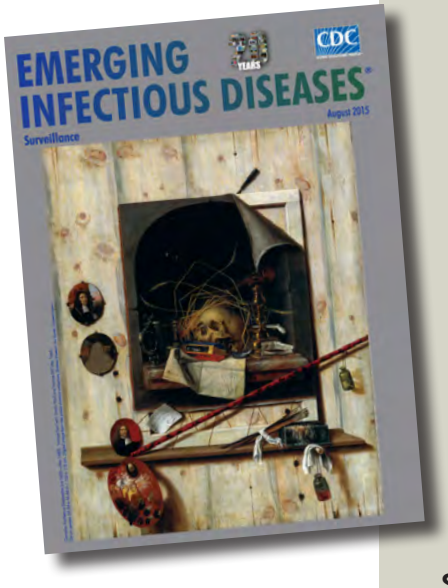

Originally published in August 2015

Escherichia coli

[esh"ə-rik'e-ə co'lī]

A gram-negative, facultatively anaerobic rod, *Escherichia coli* was named for Theodor Escherich, a German-Austrian pediatrician. Escherich isolated a variety of bacteria from infant fecal samples by using his own anaerobic culture methods and Hans Christian Gram's new staining technique. Escherich originally named the common colon bacillus *Bacterium coli commune*. Castellani and Chalmers proposed the name *E. coli* in 1919, but it was not officially recognized until 1958.

Sources:

1. Oberbauer BA. Theodor Escherich—Leben und Werk. Munich: Futuramed-Verlag; 1992.
2. Shulman ST, Friedmann HC, Sims RH. Theodor Escherich: the first pediatric infectious diseases physician? Clin Infect Dis. 2007;45:1025–9 .

https://wwwnc.cdc.gov/eid/article/21/8/et-2108_article

Anncaliia algerae Microsporidiosis Diagnosed by Metagenomic Next-Generation Sequencing, China

Chen Liu,[1] Qin Chen,[1] Ping Fu, Yun-Ying Shi

We report a case of *Anncaliia algerae* microsporidia infection in an immunosuppressed kidney transplant recipient in China. Light microscopy and transmission electron microscopy initially failed to identify *A. algerae*, which eventually was detected by metagenomic next-generation sequencing. Our case highlights the supporting role of metagenomic sequencing in early identification of uncommon pathogens.

Anncaliia algerae is an uncommon, yet emerging microsporidian parasitic pathogen that can affect immunocompromised patients and cause fatal myositis (*1*,*2*). We report a case of *A. algerae* microsporidiosis, which was initially missed by conventional light microscopy (LM) and subsequent transmission electron microscopy (TEM) of biopsied muscle but eventually identified by metagenomic next-generation sequencing (mNGS).

The Study

In March 2021, a 45-year-old male kidney transplant recipient in China was admitted to the hospital for a 2-month history of muscle pain. He was receiving prednisone, tacrolimus, and mycophenolate mofetil for maintenance immunosuppression. The patient did not have respiratory symptoms at admission. Physical examination showed low fever and tenderness and generalized weakness in all 4 limbs. Laboratory investigations revealed serum creatine kinase level within reference range but low CD4+ T lymphocyte count (45 cells/μL; reference range 471–1,220 cells/μL). Serum cytomegalovirus DNA was 1.64×10^2 copies/mL. Results of tests for heavy metals, parasites, and myositis-specific autoantibodies were negative.

Author affiliations: West China Hospital of Sichuan University, Chengdu, China (C. Liu, Q. Chen, P. Fu, Y.-Y. Shi); Chengdu 363 Hospital of Southwest Medical University, Chengdu (Q. Chen)

DOI: https://doi.org/10.3201/eid2807.212315

The patient was febrile (37.3°C) at admission. Although immunosuppressant drugs were tapered dramatically, and broad-spectrum antimicrobial drugs and ganciclovir were added, the patient remained febrile (Figure 1). Chest computed tomography (CT) imaging showed patchy irregular ground-glass opacity in the left upper lung lobe. Electromyography testing showed myogenic damage in the biceps brachii muscle. Magnetic resonance imaging of lower extremities revealed swollen soft tissue. Bronchoalveolar lavage (BAL) testing was negative for bacteria, fungi, and *Pneumocystis jirovecii* DNA.

The patient's myalgia and weakness worsened, his serum creatine kinase level increased (Appendix Figure 1, https://wwwnc.cdc.gov/EID/article/28/7/21-2315-App1.pdf), and watery diarrhea developed. Stool microscopy, gastroduodenoscopy, and colonoscopy revealed no specific abnormalities; repeated chest CT scans showed increased inflammatory exudation and bilateral pleural effusion.

No specific findings were reported from the initial LM of the left biceps brachii biopsy specimen except for degradation and necrosis of myofibers. We performed a second fiberoptic bronchoscopy and sent BAL fluid for untargeted mNGS via NextSeq 550 (Illumina, https://www.illumina.com), which revealed *P. jirovecii* (142 sequence reads) and *A. algerae* (127 sequence reads) within 48 hours of receiving the specimen (Appendix Table 1; Appendix Figure 2, panel A).

Because the previous biopsy results were negative and we were unfamiliar with *A. algerae* microsporidia, we performed a literature review and then reviewed the initial muscle biopsy again. We considered the possibility of a combined infection of *P. jirovecii* and *A. algerae*, and we consulted an infectious disease specialist who suggested adding oral sulfamethoxazole/trimethoprim (SMZ/TMP; 1,600/

[1]These first authors contributed equally to this article.

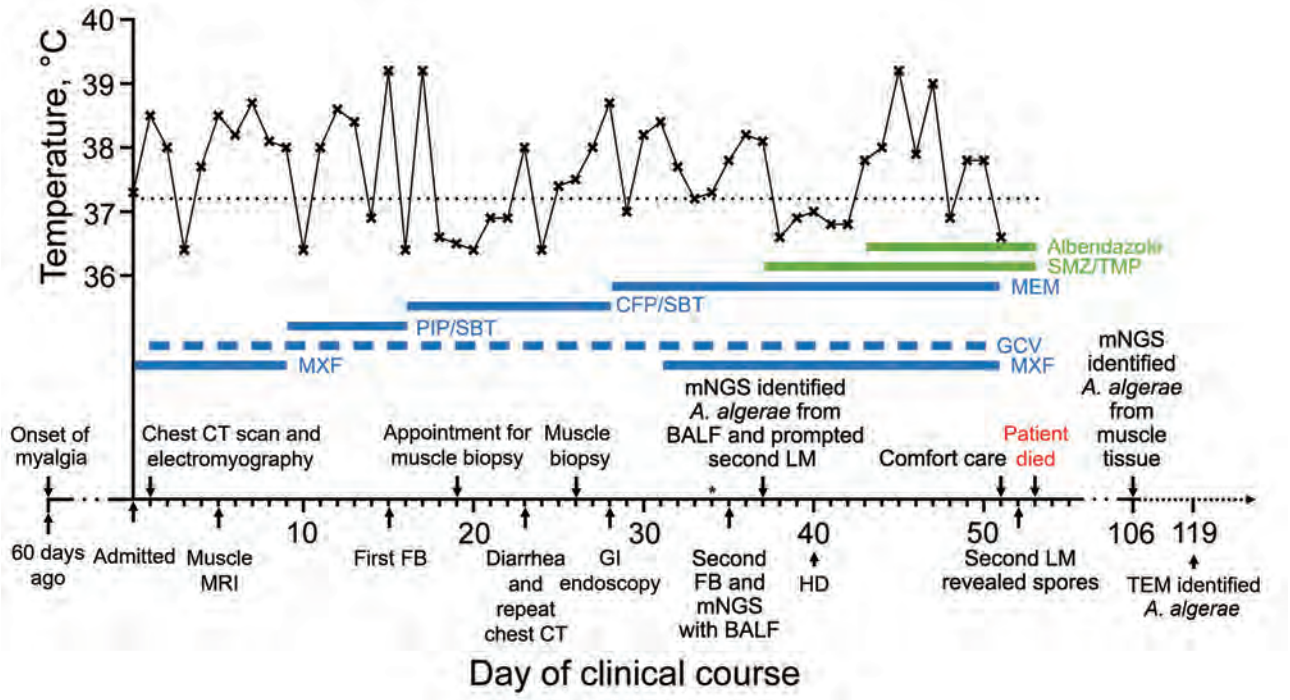

Figure 1. Clinical course of a 45-year-old patient with *Anncaliia algerae* microsporidia infection, China. The upper section of the graph shows the body-temperature curve (black line); dotted black line indicates 37.2°, the upper limit of normal body temperature. Thick blue and green lines indicate medications administered; dashed thick blue line indicates a dosing frequency of every other day. Major events during the patient's course are indicated by arrows on the x-axis. Asterisk on day 34 denotes the initial light microscopy, which failed to detect *A. algerae* spores. BALF, bronchoalveolar lavage fluid; CFP/SBT, cefoperazone/sulbactum; CT, computed tomography; FB, fiberoptic bronchoscopy; GCV, ganciclovir; GI, gastrointestinal; HD, hemodialysis; LM, light microscopy; MEM, meropenem; mNGS, metagenomic next-generation sequencing; MRI, magnetic resonance imaging; MXF, moxifloxacin; PIP/SBT, piperacillin/sulbactum; SMZ/TMP, sulfamethoxazole/trimethoprim; TEM, transmission electron microscopy.

320 mg 3×/d), which might be effective against both pathogens. After SMZ/TMP treatment, the patient's temperature returned to normal for 5 successive days before climbing to 37.8°C on day 43 of admission; we added oral albendazole (400 mg 2×/d) (Figure 1), according to published cases (*1*,*3*,*4*).

However, the patient's condition continued to deteriorate. On day 51, he decided on comfort care and died 2 days later (Figure 1). On day 52, one day before the patient died, we discovered multiple oval organisms measuring 2–3 μm in scattered clusters under LM in the muscle biopsy sample (Figure 2, panels A–D). After the patient died, we performed mNGS using muscle tissue from the previous biopsy, which yielded 65,311 sequence reads mapped to *A. algerae* (Appendix Table 2; Appendix Figure 2, panel B). *A. algerae* was confirmed by subsequent PCR testing on muscle tissue, but PCR testing of the remaining BAL specimen yielded no findings because not enough fluid was available in the sample after previous examinations. Eventually, we identified *A. algerae* via TEM in the third sample section (Figure 1; Figure 2, panels E, F). We deposited the *A. algerae* sequences into the National Center for Biotechnology Information Sequence Read Archive (accession nos. SRR18339014 for the BAL sample, SRR18339013 for the muscle sample).

Conclusions

A. algerae is a microsporidial species that has been reported to cause human infections since 1999 (*5*). Of 12 reported cases of human *A. algerae* infection (*1*–*11*), 11 were among immunocompromised patients (Table). Thus, immunodeficiency, as in this patient, appears to be a critical risk factor for *A. algerae* infection. Although the modes of *A. algerae* transmission to humans remain uncertain, waterborne transmission, either through ingestion of or exposure to spore-contaminated water, has been postulated as the most likely route (*2*,*4*,*6*). This patient lived near ditches in a rural area of the warm and humid Sichuan Basin and was readily exposed to waters possibly contaminated by *A. algerae* spores.

A. algerae infection in humans primarily manifests as myositis (*1*–*11*), and in reports we reviewed, 5 (62.5%) of 8 case-patients who had *A. algerae* myositis

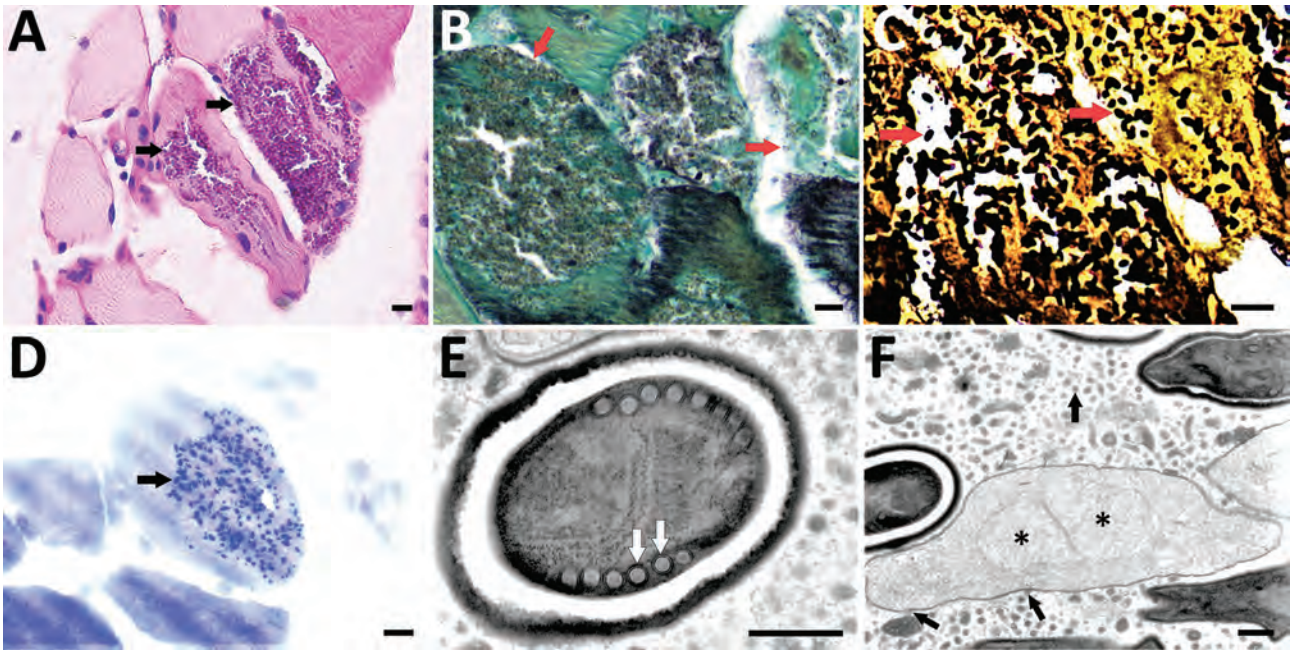

Figure 2. Light microscopy and transmission electron microscopy of left biceps branchii muscle biopsy tissue from a 45-year-old man with microsporidiosis caused by *Anncaliia algerae*, China. A–D) Light microscopy using different stains. A) Periodic acid-Schiff stain. Scale bar indicates 10 μm. Original magnification ×50. B) Gomori methenamine silver stain. Scale bar indicates 10 μm. Original magnification ×63. C) Warthin-Starry stain. Scale bar indicates 10 μm. Original magnification ×63. D) Toluidine blue stain. Scale bar indicates 10 μm. Arrows indicate myocytes replaced by aggregates of 2–3 μm ovoid organisms. Original magnification ×63. E, F) Transmission electron microscopy showing *Anncaliia*-like microsporidia. Scale bars indicate 500 nm. E) A mature spore with electron-dense exospore, electron-lucent endospore, and a single row of 6 to 8 polar tubule coils (arrows). Original magnification ×8,000. F) Proliferating form of microsporidia showing diplokaryotic nuclei (stars) with vesiculotubular structures extending from the meront cell membrane and aggregating in the host cell cytoplasm (arrows). Original magnification ×3,000.

died (Table). Because of fatality risk, early diagnosis and prompt interventions are crucial. To date, biopsy and microscopy remain the standard approaches in microsporidia identification (*12*), and the role of mNGS has yet to be confirmed.

Although LM is the fastest diagnostic tool for microsporidiosis, it has several limitations. First, LM is unable to identify the genus and species of microsporidia. Second, the actual turnaround time (5–7 days in our hospital) for LM varies among institutions,

Table. Clinical characteristics of 12 previously reported cases of human *Anncaliia algerae* microsporidia infection*

Case reports	Age, y/sex	Immunocompromised/ underlying conditions	Related symptoms	Positive biopsy sample sites	Treatment	Outcome
Watts et al. 2014 (*1*)	67/M	Y/RA	Myalgias	Vastus lateralis	Albendazole	Survived
	66/M	Y/RA	Myalgias	Vastus lateralis	NG	Died
Coyle et al. 2004 (*2*)	57/F	Y/RA	Myalgias	Quadriceps femoris	Albendazole	Died
Boileau et al. 2016 (*3*)	49/M	Y/CLL	Myalgias	Vastus lateralis	Albendazole and fumagillin	Survived
Sutrave et al. 2018 (*4*)	66/M	Y/GVHD	Myalgias	Vastus lateralis	Albendazole	Survived
Visvesvara et al. 1999 (*5*)	67/M	N/N	Eye discomfort	Cornea	Albendazole and fumagillin	Survived
Ziad et al. 2021 (*6*)	55/M	Y/psoriatic arthritis	Myalgias	Vastus lateralis, intercostal muscle, and tongue	Albendazole	Died
Visvesvara et al. 2005 (*7*)	11/M	Y/ALL	Skin lesions	Skin	NA	NA
Cali et al. 2010 (*8*)	69/M	Y/CLL	Hoarseness	False vocal cord	Albendazole	Died
Field et al. 2012 (*9*)	49/F	Y/lung transplant	Myalgias	Deltoid and tongue	NG	Died
Chacko et al. 2013 (*10*)	56/M	Y/kidney transplant	Myalgias	Deltoid	Albendazole	Died
Anderson et al. 2019 (*11*)	60/M	Y/kidney and pancreas transplant	Skin lesions	Lower extremity, finger, tongue, urine, and sputum	Albendazole	Died

*ALL, acute lymphoblastic leukemia; CLL, chronic lymphocytic leukemia; GVHD, graft-versus-host disease; NA, data not available; NG, treatment for *A. algerae* was not given because the patient was undiagnosed before death; RA, rheumatoid arthritis.

which could cause diagnostic delays. Third, the accuracy of LM diagnosis relies on laboratory conditions and microscopist experience. In addition, morphologic features of *A. algerae* spores overlap with those of other organisms, such as small yeasts, which has led to misdiagnosis under LM (*1*,*11*). Thus, familiarity with *A. algerae* spores and their appearance on histopathology preparations are crucial for rapid diagnosis. In this case, *A. algerae* spores initially were missed by the microscopist and were detected 2 weeks later during retrospective review because of the relatively long turnaround time.

TEM remains the standard technique for determining the specific microsporidia genus by identifying the ultrastructural characteristics (*12*). TEM examines a smaller area of tissue at one time but usually has a longer turnaround time than routine LM. TEM results are available in 1–2 days in some institutions, but turnaround time in our hospital takes ≈10–14 days.

As an unbiased, culture-free method capable of detecting all potential pathogens, untargeted mNGS enables identification of unexpected or unknown organisms (*13*). Compared with hypothesis-driven methods, such as PCR, shotgun mNGS is hypothesis-free, enables survey of all DNA and RNA in multiple samples en masse (*13*), and generally takes 24–48 hours to produce results. However, mNGS is unlikely to replace conventional diagnostic testing because of its limitations, such as high cost (US $522 for DNA detection and $894 for both DNA and RNA in our hospital), lack of a unified workflow, and no standard methods for interpreting results (*13*). Instead, mNGS can serve as a valuable adjunct tool in diagnosing uncommon or unexplained infections when conventional methods such as LM fail.

Albendazole and fumagillin have been used to treat *A. algerae* infections in previously reported cases (Table). We have easy access to albendazole, but no access to fumagillin. SMZ/TMP was reported to have no effect against *Enterocytozoon bieneusi* microsporidiosis (*14*), but data regarding effectiveness against *A. algerae* microsporidia were limited. Treatment was greatly delayed in this patient because of our lack of clinical experience with *A. algerae* microsporidia and the late microscopy findings. Early treatment, along with minimized immunosuppression, might be crucial for the successful management of *A. algerae* infection (*1*,*3*,*4*).

In conclusion, *A. algerae* microsporidia infection requires early diagnosis and prompt intervention. LM alone cannot identify microsporidia genus and species; thus, TEM or genomic sequencing are needed for correct diagnosis. As a sensitive, culture-independent approach, mNGS could be a promising adjunct tool for the early identification of uncommon pathogens, such as *A. algerae* and other microsporidia.

Acknowledgments

We thank Song Lei for providing professional help in the transmission electron microscopy of *A. algerae* spores in muscle tissue. We also thank Teng Xu and Huan Xu for providing the mNGS methods, interpreting the mNGS results, and performing PCR tests.

This work was supported by the National Natural Science Foundation of China (grant no. 81771714) and 1.3.5 Project for Disciplines of Excellence, West China Hospital, Sichuan University (grant no. ZYJC18004).

About the Author

Mr. Liu is a doctoral student at the Department of Nephrology and Kidney Research Institute, West China Hospital of Sichuan University, Chengdu, China. His research interest is infections in renal transplant patients.

References

1. Watts MR, Chan RCF, Cheong EYL, Brammah S, Clezy KR, Tong C, et al. *Anncaliia algerae* microsporidial myositis. Emerg Infect Dis. 2014;20:185–91. https://doi.org/10.3201/eid2002.131126
2. Coyle CM, Weiss LM, Rhodes LV III, Cali A, Takvorian PM, Brown DF, et al. Fatal myositis due to the microsporidian *Brachiola algerae*, a mosquito pathogen. N Engl J Med. 2004;351:42–7. https://doi.org/10.1056/NEJMoa032655
3. Boileau M, Ferreira J, Ahmad I, Lavallée C, Qvarnstrom Y, Dufresne SF. Successful treatment of disseminated *Anncaliia algerae* microsporidial infection with combination fumagillin and albendazole. Open Forum Infect Dis. 2016;3:ofw158. https://doi.org/10.1093/ofid/ofw158
4. Sutrave G, Maundrell A, Keighley C, Jennings Z, Brammah S, Wang M-X, et al. *Anncaliia algerae* microsporidial myositis, New South Wales, Australia. Emerg Infect Dis. 2018;24:1528–31. https://doi.org/10.3201/eid2408.172002
5. Visvesvara GS, Belloso M, Moura H, Da Silva AJ, Moura IN, Leitch GJ, et al. Isolation of *Nosema algerae* from the cornea of an immunocompetent patient. J Eukaryot Microbiol. 1999;46:10S. PubMed
6. Ziad F, Robertson T, Watts MR, Copeland J, Chiu G, Wang D, et al. Fatal disseminated *Anncaliia algerae* myositis mimicking polymyositis in an immunocompromised patient. Neuromuscl Disord. 2021;31:877–80. https://doi.org/10.1016/j.nmd.2021.06.007
7. Visvesvara GS, Moura H, Leitch GJ, Schwartz DA, Xiao LX. Public health importance of *Brachiola algerae* (Microsporidia)—an emerging pathogen of humans. Folia Parasitol (Praha). 2005;52:83–94. https://doi.org/10.14411/fp.2005.011
8. Cali A, Neafie R, Weiss LM, Ghosh K, Vergara RB, Gupta R, et al. Human vocal cord infection with the microsporidium *Anncaliia algerae*. J Eukaryot

Microbiol. 2010;57:562–7. https://doi.org/10.1111/j.1550-7408.2010.00510.x
9. Field AS, Paik JY, Stark D, Qiu MR, Morey A, Plit ML, et al. Myositis due to the microsporidian *Anncaliia* (Brachiola) *algerae* in a lung transplant recipient. Transpl Infect Dis. 2012;14:169–76. https://doi.org/10.1111/j.1399-3062.2012.00724.x
10. Chacko B, Trevillian P. Microsporidial myositis in a kidney transplant recipient [abstract 82]. In: Program and abstracts of Annual Scientific Meeting Transplantation Society of Australia and New Zealand. Canberra (ACT, Australia): Transplantation Society of Australia and New Zealand; 2013. p. 96.
11. Anderson NW, Muehlenbachs A, Arif S, Bruminhent J, Deziel PJ, Razonable RR, et al. A fatal case of disseminated microsporidiosis due to *Anncaliia algerae* in a renal and pancreas allograft recipient. Open Forum Infect Dis. 2019;6:ofz285. https://doi.org/10.1093/ofid/ofz285
12. Franzen C, Müller A. Microsporidiosis: human diseases and diagnosis. Microbes Infect. 2001;3:389–400. https://doi.org/10.1016/S1286-4579(01)01395-8
13. Chiu CY, Miller SA. Clinical metagenomics. Nat Rev Genet. 2019;20:341–55. https://doi.org/10.1038/s41576-019-0113-7
14. Costa SF, Weiss LM. Drug treatment of microsporidiosis. Drug Resist Updat. 2000;3:384–99. https://doi.org/10.1054/drup.2000.0174

Address for correspondence: Yun-Ying Shi, Department of Nephrology, West China Hospital of Sichuan University, No. 37 Guoxue Alley Wuhou District, Chengdu 610041, China; email: yyshi0130@163.com

Deaths from Tick-Borne Encephalitis, Sweden

Renata Varnaitė, Sara Gredmark-Russ, Jonas Klingström

We assessed standardized mortality ratio in tick-borne encephalitis (TBE) in Sweden, 2004–2017. Standardized mortality ratio for TBE was 3.96 (95% CI 2.55–5.90); no cases in patients <40 years of age were fatal. These results underscore the need for further vaccination efforts in populations at risk for TBE.

Tick-borne encephalitis (TBE) is caused by the TBE virus (TBEV), which is transmitted to humans via infected ticks or, on rare occasions, via ingestion of contaminated milk from an infected animal (*1*). TBE is endemic in parts of Asia and Europe, including Sweden. TBEV has 3 subtypes: European, Siberian, and Far Eastern (*2*). The European subtype of TBEV is the only known subtype in Sweden (*1*,*3*). TBE is typically a biphasic disease manifesting with febrile influenza-like illness during the first phase, followed by a second phase of neurologic symptoms of different severity, ranging from meningitis to severe meningoencephalitis (*4*). Long-term sequelae are common and a case-fatality rate (CFR) of 0.5% has previously been reported in Europe (*5*–*7*).

TBE became a notifiable disease in Sweden in 2004, and from then on, all cases of TBE are reported to the Public Health Agency of Sweden. Advanced age is a risk factor for severe TBE, and CFRs increase with age (*5*,*7*–*9*). However, CFRs do not account for baseline mortality, a particularly important consideration for the elderly population. To investigate the relative contribution of TBE to overall mortality rates in Sweden, we performed a case–control study and calculated standardized mortality ratio (SMR) for TBE-diagnosed patients during 2004–2017.

The Study

Cases of patients with notifiable infectious disease diagnoses in Sweden are reported to the Public Health Agency of Sweden. This case–control study relies on 3 data sources: TBE cases reported to the Public Health Agency of Sweden during 2004–2017; Swedish population register from Statistics Sweden; and the Swedish National Board of Health and Welfare's Cause of Death Register. The Regional Ethical Review Board in Stockholm, Sweden, approved the study.

We included all 2,941 TBE cases that were reported to the Public Health Agency of Sweden during July 1, 2004–December 31, 2017 (Table). The number of annual TBE cases has gradually increased during 2004–2017; TBE incidence followed a typical seasonal pattern of 90% of all cases reported during June–October (Figure 1, panels A, B). TBE was reported in all age groups; 53% of the cases were in the age group of 40–69 years (Table; Figure 2, panel A). Sixty percent of all reported TBE patients were male (n = 1,777) and 40% female (n = 1,164) (Table; Figure 2, panel A). The median age at diagnosis was 48 (IQR 33–63) years for male patients, 49 (33–61) years for female patients, and 48 (33–62) years for all TBE patients.

To assess deaths from TBE in Sweden, we measured CFRs and SMR. We matched each reported TBE case (n = 2,941) with 20 control persons from the population register of Sweden on the basis of age, sex, and county of residence (n = 58,820). We then linked TBE cases and matched controls to the Swedish National Cause of Death Register. We identified fatal TBE cases, those in which the patient died ≤90 days after the reporting date, as well as deaths within the matched control population during the same time period (Appendix Figure, https://wwwnc.cdc.gov/EID/article/28/7/22-0010-App1.pdf).

We found that the overall CFR in TBE during 2004–2017 was 0.75%; in male patients, CFR was 0.56%, and in female patients, 1.03% (Table). CFR increased with age, reaching 3.45% in the 80–89-year age group. Although TBE was reported in all age groups, we noted no fatal cases within 90 days of reporting date in patients <40 years of age (Table).

To account for the baseline mortality rate in the Swedish population, we next measured SMR by

Author affiliations: Karolinska Institutet, Stockholm, Sweden (R. Varnaitė, S. Gredmark-Russ, J. Klingström); Karolinska University Hospital, Stockholm (S. Gredmark-Russ); Umeå University, Umeå, Sweden (S. Gredmark-Russ)

DOI: https://doi.org/10.3201/eid2807.220010

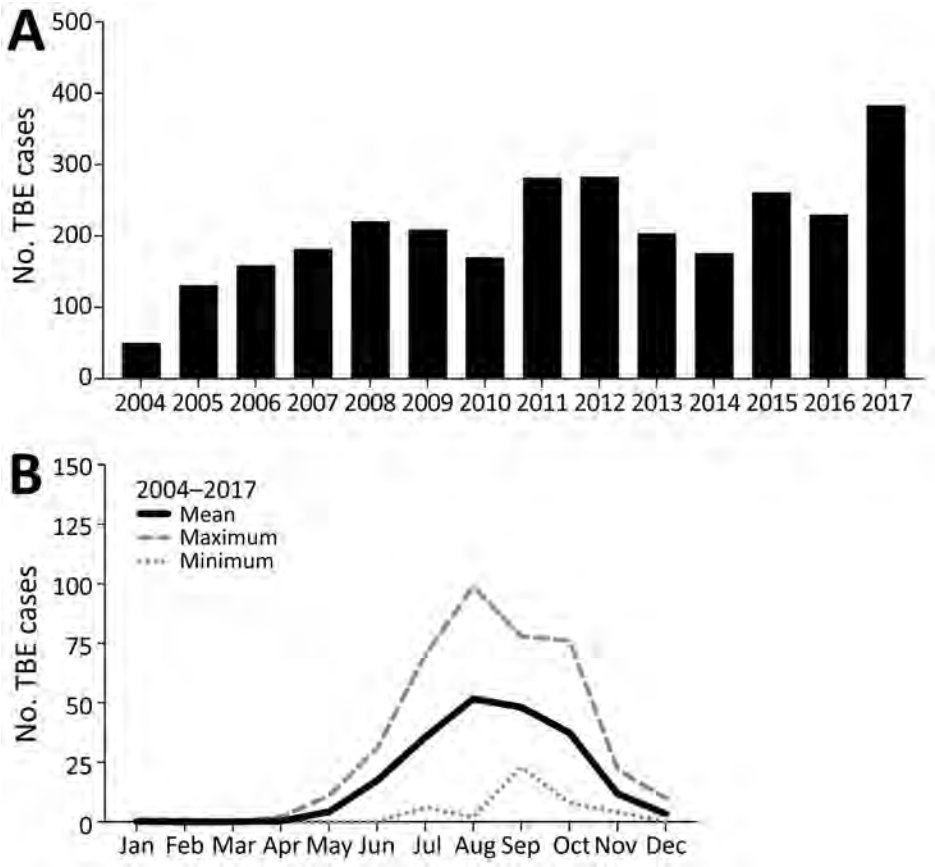

Figure 1. TBE cases reported to the Public Health Agency of Sweden, 2004–2017. A) All cases. B) Mean number of cases reported by month, with minimum (dotted line) and maximum (dashed line) numbers shown. TBE, tick-borne encephalitis.

dividing the number of deaths in TBE-diagnosed persons by the expected number of deaths estimated from the matched controls (Appendix Figure). We calculated 95% CI for SMRs using mid-P exact test at the Open Source Epidemiologic Statistics for Public Health (*10*). The overall SMR for TBE was 3.96 (95% CI 2.55–5.9; p<0.001) (Table; Figure 2, panel B). We observed higher SMR in female patients (SMR 6.32, 95% CI 3.42–10.74; p<0.001) than male patients (SMR 2.74, 95% CI 1.39–4.88; p = 0.006), which suggested a potential sex-related difference in deaths due to TBE (Table; Figure 2, panel B). When we stratified patients by age, we observed statistically significant SMRs of 5.71 (95% CI 2.32–11.89; p<0.001) in TBE patients 60–69 years of age and 5.00 (95% CI 2.54–8.91; p<0.001) in TBE patients 70–79 years of age (Table).

Table. Characteristics of TBE cases reported to the Public Health Agency of Sweden during 2004–2017*

Group	No. (%)	Case-fatality rate, %	Mortality rate in controls, %	No. observed deaths, total, M/F	Expected deaths	SMR (95% CI)	p value
Total cases	2,941 (100)	0.75	0.19	22	5.55	**3.96 (2.55–5.9)**	**<0.001**
Sex							
M	1,777 (60)	0.56	0.21	10	3.65	**2.74 (1.39–4.88)**	**0.006**
F	1,164 (40)	1.03	0.16	12	1.90	**6.32 (3.42–10.74)**	**<0.001**
Age group							
0–9	143 (5)	0	0	0	0	NA	NA
10–19	212 (7)	0	0	0	0	NA	NA
20–29	256 (9)	0	0	0	0	NA	NA
30–39	379 (13)	0	0.01	0	0.05	NA	NA
40–49	532 (18)	0.19	0.02	1, 0/1	0.10	10.00 (0.5–49.32)	0.100
50–59	546 (19)	0.37	0.16	2, 0/2	0.85	2.35 (0.39–7.77)	0.264
60–69	480 (16)	1.25	0.22	6, 4/2	1.05	**5.71 (2.32–11.89)**	**<0.001**
70–79	301 (10)	3.32	0.66	10, 3/7	2.00	**5.00 (2.54–8.91)**	**<0.001**
80–89	87 (3)	3.45	1.50	3, 3/0	1.30	2.31 (0.59–6.28)	0.186
90–99	5 (0.2)	0	4.00	0	0.20	NA	NA

*Bold text indicates statistically significant values. NA, not applicable; SMR, standardized mortality ratio (SMR) within 90 d after the reporting date of TBE; TBE, tick-borne encephalitis.

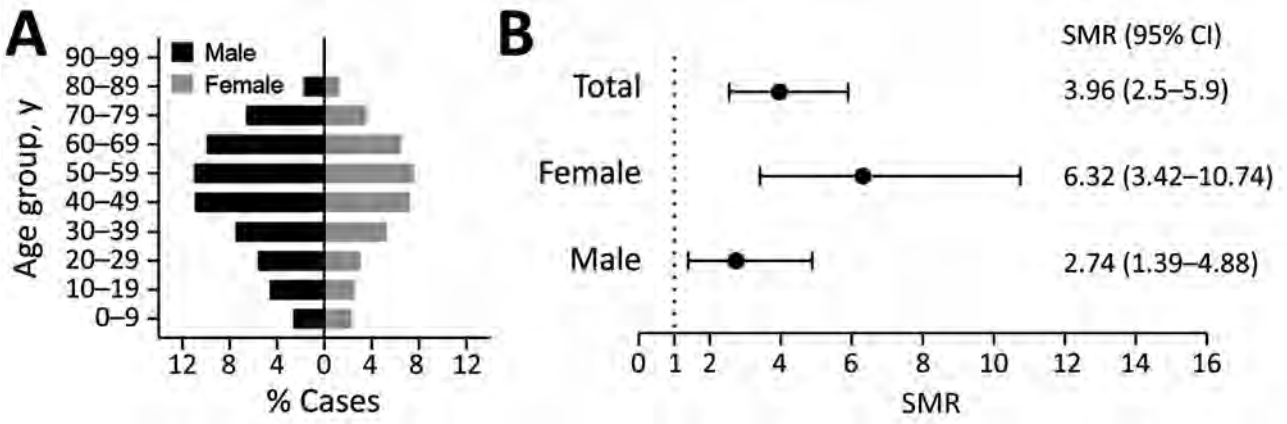

Figure 2. Age and distribution of TBE cases reported to the Public Health Agency of Sweden, 2004–2017. A) Percentages of all cases by sex and age group. B) SMRs of cases by sex. Bars indicate 95% CI within 90 days after the reporting date. SMR, standardized mortality ratio.

Conclusions

In this case–control study, we found the mortality rate in TBE patients in Sweden to be ≈4-fold higher than that of the matched control population. CFR of 0.75% for TBE in this study is comparable with previously reported CFR of 0.5% in Europe (*5*). Although TBEV infection has been reported for all age groups, including children, we found no fatal cases within 90 days after the reporting date in persons <40 years of age. However, in TBE patients >60 years of age, we observed a significantly higher SMR, highlighting the need for further vaccination efforts against TBE, particularly within this age group. This finding is consistent with other studies that reported TBE to be more severe in older patients (*5*,*7*,*11*).

TBE incidence is typically higher in male than female patients; we observed the same pattern over a 14-year period in Sweden (*5*), where 60% of all TBE patients were male. However, despite higher incidence in male patients, we found higher CFRs and SMR in female TBE patients. In several infectious diseases, male patients show higher incidence and have more severe outcomes than female patients (*12*). Our results indicate that there may also be a sex-dependent difference in the outcome of TBE, but because we had a relatively low number of fatal TBE cases in our study, this sex-dependent difference in deaths should be investigated in a larger TBE patient cohort.

A strength of this study is the use of national registers that enabled us to estimate baseline mortality rates in the national population matched to TBE cases by sex, age, and county of residence. SMR, as opposed to CFR, accounts for the baseline mortality rate within a given population subgroup, which is a particularly important consideration when estimating deaths in the elderly population. A limitation of this study is that the controls were matched to TBE cases without taking into consideration lifestyle, socioeconomic status, or comorbidities. Because this disease requires an active lifestyle for exposure, it is possible that TBE patients in Sweden are healthier than the control populations, which could result in the underestimation of SMR in our study. On the other hand, the total deaths from TBE may be overestimated considering that TBEV-infected persons can follow a subclinical course of infection and may not be reported in the healthcare system (*13*).

In summary, we saw a substantially increased SMR for TBE patients in Sweden during 2004–2017 compared with the general population. Our findings highlight the need for further vaccination efforts against this disease, particularly for older persons.

This study was supported by grants from the Swedish Research Council (Dnr 2020-06249 and 2021-06602), Marianne and Marcus Wallenberg Foundation, by grants provided by Region Stockholm (ALF project), by Region Stockholm (clinical research appointment) and by Center for Innovative Medicine, Region Stockholm, and Karolinska Institutet for S.G.R., and by Center for Innovative Medicine, Region Stockholm, for J.K.

About the Author

Dr. Varnaitė is a researcher at the Center for Infectious Medicine, Karolinska Institutet, Sweden. Her research interests include acute viral infections and human immunology with a focus on emerging viral infections.

References

1. Süss J. Tick-borne encephalitis 2010: epidemiology, risk areas, and virus strains in Europe and Asia—an overview. Ticks Tick Borne Dis. 2011;2:2–15. https://doi.org/10.1016/j.ttbdis.2010.10.007

2. Ecker M, Allison SL, Meixner T, Heinz FX. Sequence analysis and genetic classification of tick-borne encephalitis viruses from Europe and Asia. J Gen Virol. 1999;80:179–85. https://doi.org/10.1099/0022-1317-80-1-179
3. Pettersson JH-O, Golovljova I, Vene S, Jaenson TGT. Prevalence of tick-borne encephalitis virus in *Ixodes ricinus* ticks in northern Europe with particular reference to southern Sweden. Parasit Vectors. 2014;7:102–11. https://doi.org/10.1186/1756-3305-7-102
4. Kaiser R. Tick-borne encephalitis. Infect Dis Clin North Am. 2008;22:561–75, x. https://doi.org/10.1016/j.idc.2008.03.013
5. Beauté J, Spiteri G, Warns-Petit E, Zeller H. Tick-borne encephalitis in Europe, 2012 to 2016. Euro Surveill. 2018;23:1800201. https://doi.org/10.2807/1560-7917.ES.2018.23.45.1800201
6. Günther G, Haglund M, Lindquist L, Forsgren M, Sköldenberg B. Tick-bone encephalitis in Sweden in relation to aseptic meningo-encephalitis of other etiology: a prospective study of clinical course and outcome. J Neurol. 1997;244:230–8. https://doi.org/10.1007/s004150050077
7. Mickienė A, Laiskonis A, Günther G, Vene S, Lundkvist A, Lindquist L. Tickborne encephalitis in an area of high endemicity in Lithuania: disease severity and long-term prognosis. Clin Infect Dis. 2002;35:650–8. https://doi.org/10.1086/342059
8. Kaiser R. The clinical and epidemiological profile of tick-borne encephalitis in southern Germany 1994–98: a prospective study of 656 patients. Brain. 1999;122:2067–78. https://doi.org/10.1093/brain/122.11.2067
9. Lenhard T, Ott D, Jakob NJ, Pham M, Bäumer P, Martinez-Torres F, et al. Predictors, neuroimaging characteristics and long-term outcome of severe European tick-borne encephalitis: a prospective cohort study. PLoS One. 2016;11:e0154143. https://doi.org/10.1371/journal.pone.0154143
10. Dean A, Sullivan K, Soe M. OpenEpi: open source epidemiologic statistics for public health [cited 2021 Jul 21]. https://www.openepi.com
11. Kaiser R. Tick-borne encephalitis: clinical findings and prognosis in adults. Wien Med Wochenschr. 2012;162:239–43. https://doi.org/10.1007/s10354-012-0105-0
12. Fish EN. The X-files in immunity: sex-based differences predispose immune responses. Nat Rev Immunol. 2008;8:737–44. https://doi.org/10.1038/nri2394
13. Gustafson R, Svenungsson B, Gardulf A, Stiernstedt G, Forsgren M. Prevalence of tick-borne encephalitis and Lyme borreliosis in a defined Swedish population. Scand J Infect Dis. 1990;22:297–306. https://doi.org/10.3109/00365549009027051

Address for correspondence: Jonas Klingström, Center for Infectious Medicine, Department of Medicine Huddinge, Karolinska Institutet, 141 86 Stockholm, Sweden; email: jonas.klingstrom@ki.se

etymologia revisited

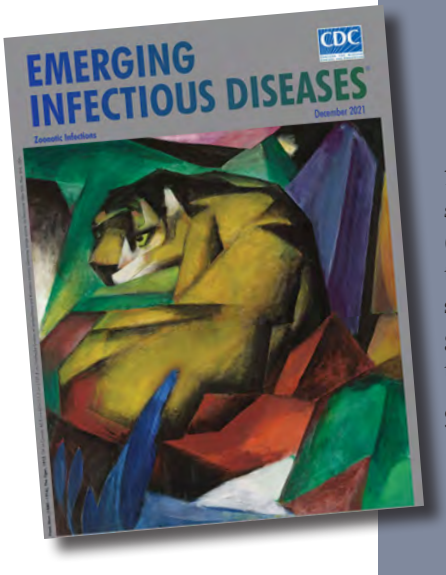

Originally published in December 2021

Trichinella spiralis

[tri kuh neh′ luh spr a′ luhs]

Trichinella is derived from the Greek words *trichos* (hair) and *ella* (diminutive); *spiralis* means spiral. In 1835, Richard Owen (1804–1892) and James Paget (1814–1899) described a spiral worm (*Trichina spiralis*)–lined sandy diaphragm of a cadaver. In 1895, Alcide Raillet (1852–1930) renamed it as *Trichinella spiralis* because *Trichina* was attributed to an insect in 1830. In 1859, Rudolf Virchow (1821–1902) described the life cycle. The genus includes many distinct species, several genotypes, and encapsulated and nonencapsulated clades based on the presence/absence of a collagen capsule.

Sources

1. Campbell WC. History of trichinosis: Paget, Owens and the discovery of *Trichinella spiralis*. Bull Hist Med. 1979;53:520–52.
2. Centers for Disease Control and Prevention. Trichinellosis: general information [cited 2021 May 11]. https://www.cdc.gov/parasites/trichinellosis/gen_info/faqs.html
3. Gottstein B, Pozio E, Nöckler K. Epidemiology, diagnosis, treatment, and control of trichinellosis. Clin Microbiol Rev. 2009;22:127–45. https://doi.org/10.1128/CMR.00026-08
4. Observations on *Trichina spiralis*. Boston Med Surg J. 1860; 63:294–8. https://doi.org/10.1056/NEJM186011080631504
5. Zarlenga D, Thompson P, Pozio E. *Trichinella* species and genotypes. Res Vet Sci. 2020;133:289–96. https://doi.org/10.1016/j.rvsc.2020.08.012

https//wwwnc.cdc.gov/eid/article/27/12/et-2712_article

Use of Human Intestinal Enteroids to Evaluate Persistence of Infectious Human Norovirus in Seawater

Marion Desdouits,[1] David Polo,[1,2] Cecile Le Mennec, Sofia Strubbia,[3] Xi-Lei Zeng, Khalil Ettayebi, Robert L. Atmar, Mary K. Estes, Françoise S. Le Guyader

Little data on the persistence of human norovirus infectivity are available to predict its transmissibility. Using human intestinal enteroids, we demonstrate that 2 human norovirus strains can remain infectious for several weeks in seawater. Such experiments can improve understanding of factors associated with norovirus survival in coastal waters and shellfish.

Human noroviruses are the major cause of viral gastroenteritis worldwide (*1*) and the most common cause of foodborne or waterborne outbreaks in Europe (*2*). Noroviruses spread through fecal–oral transmission, mainly person to person, but also spread through environmental contamination (*1*). Food and drinks can be contaminated by infected food handlers and, during production, by human sewage spillover (*3*). When grown in contaminated seawater, filter-feeding shellfish bioaccumulate human noroviruses in their tissues (*2*,*4*). Shellfish, especially those eaten raw, are among the main foods involved in foodborne epidemics (*2*,*5*).

Noroviruses are diverse, positive-stranded RNA viruses, classified into ≥10 genogroups (G) and many genotypes; most noroviruses that infect humans belong to genogroups GI and GII (*6*). Since 1995, the epidemiology of human noroviruses has been dominated by the GII.4 genotype (*1*). Of note, GII.4 appears to be predominantly transmitted person to person, whereas other genotypes, such as GII.6, GII.3, and some from GI, are more often implicated in foodborne or waterborne outbreaks (*1*–*5*). This difference might reflect variations in particle resistance to environmental conditions (*1*,*7*), but empirical data are lacking.

The small, nonenveloped human norovirus particles are considered very stable outside their host, especially in aquatic environments (*1*,*7*,*8*). Particles are also highly infectious, leading to human infection even when very low amounts of virus are present in shellfish (*9*). Yet, for almost 50 years, the lack of a reproducible cell culture system impaired the direct assessment of human norovirus infectivity in environmental conditions. Hence, data used for risk assessment rely on molecular assays or surrogate viruses (*2*). Previously, we used a surrogate calicivirus, Tulane virus (TuV), to estimate the persistence of infectious human norovirus in shellfish (*10*). However, because surrogates might underestimate the actual stability of human norovirus (*11*) and do not enable comparisons between different norovirus strains, direct assessments of infectivity in the environment and foods are needed to learn more about foodborne transmission and design optimal sanitary regulations (*2*).

Since 2016, human intestinal enteroids (HIEs) have enabled the in vitro cultivation of many human norovirus strains and represent a physiologically relevant model to assess whether the virus is infectious (*12*–*15*). In this study, we used HIEs to evaluate the

Author affiliations: Institut Français de Recherche pour l'Exploitation de la Mer, Nantes, France (M. Desdouits, D. Polo, C. Le Mennec, S. Strubbia, F.S. Le Guyader); Baylor College of Medicine, Houston, Texas, USA (X.-L. Zeng, K. Ettayebi, R.L. Atmar, M.K. Estes)

DOI: https://doi.org/10.3201/eid2807.220219

[1]These first authors contributed equally to this article.

[2]Current affiliation: Centro de Investigaciones Biologicas–Facultade de Bioloxía & CRETUS, Universidade de Santiago de Compostela, Santiago de Compostela, Spain.

[3]Current affiliation: SECALIM UMR 104 Oniris/Inrae, Nantes, France.

Table 1. Characteristics of seawater samples used for 3 experiments using human intestinal enteroids to evaluate persistence of infectious human norovirus

Experiment	1	2	3
Collection date*	2018 Sep 5	2018 Oct 16	2019 Apr 30
Physio-chemistry			
Salinity, %	36.5 (35†)	35	33.3
Turbidity, NTU	0.67	7.50	1.14
pH	7.8	7.9	7.9
Total suspended solids, mg/L	4.0	3.0	1.0
Dissolved organic carbon, mg/L	2.3	1.6	2.1
Phosphate, mg/L	0.079	0.082	0.192
Nitrate, mg/L	0.4	0.3	0.8
Microbiology			
Total nonmarine bacteria/100 mL	100	>300	37
Total marine bacteria/100 mL	>300	>300	>300
Escherichia coli/100 mL	0	0	0

*Coastal seawater samples were collected and sand-filtered at the same experimental shellfish farm at different dates, kept at 4°C, and used within 1 week of collection. NTU, Nephelometric Turbidity Units.
†Salinity of seawater was adjusted to 35% using distilled water for experiment 1.

persistence of infectious human norovirus in natural seawater, the last matrix before bioaccumulation by shellfish, in comparison with TuV.

The Study

We compared the stability in seawater of 2 human norovirus strains, GII.4 (TCH11-64) and GII.3 (TCH04-577), obtained from human stool filtrates as described previously (*12*), and 1 TuV strain (M33) produced in simian LLC-MK2 cells (*10*). Ethics approval for collection of virus-containing fecal samples and human intestinal cells was obtained from the Baylor College of Medicine Institutional Review Board. We conducted 3 experiments with fresh samples of natural seawater (Table 1). We used viral stocks to spike 120 mL of seawater, which we then split into 10 mL-aliquots and incubated at 12°C in a thermostatic cabinet (Memmert, https://www.memmert.com) (Figure 1). Once or twice a week, we randomly sampled an aliquot, extracted nucleic acids from 100 µL by using the NucliSens kit on a MiniMag (bioMérieux, https://www.biomerieux.com), and assessed the viral genome concentration by quantitative reverse transcription PCR (*10*).

During experiments 1 and 2, the genomic concentration of human norovirus GII.3 remained highly stable; 0.8 $\log_{10}$ losses in experiment 1 and 1.2 $\log_{10}$ losses in experiment 2 occurred over 5 weeks (Figure 2, panels A, B). We did not assess GII.4 virus in experiment 1, but we observed similar stability at the genomic level in experiment 2, a 0.5 $\log_{10}$ decrease (Figure 2, panel B). During experiment 3, GII.3 and GII.4 genomic concentrations were ≥1 $\log_{10}$ lower than the other experiments at day 0 and reached a total loss of 1.8 and 2.7 $\log_{10}$ over 4 weeks (Figure 2, panel C). For the 3 experiments, TuV genomic levels were higher than human norovirus at day 0 but decreased more quickly; total losses of 2.7 (experiment 1), 3.2 (experiment 2) and 3.4 (experiment 3) $\log_{10}$ occurred over 5 weeks (Figure 2, panels A–C),

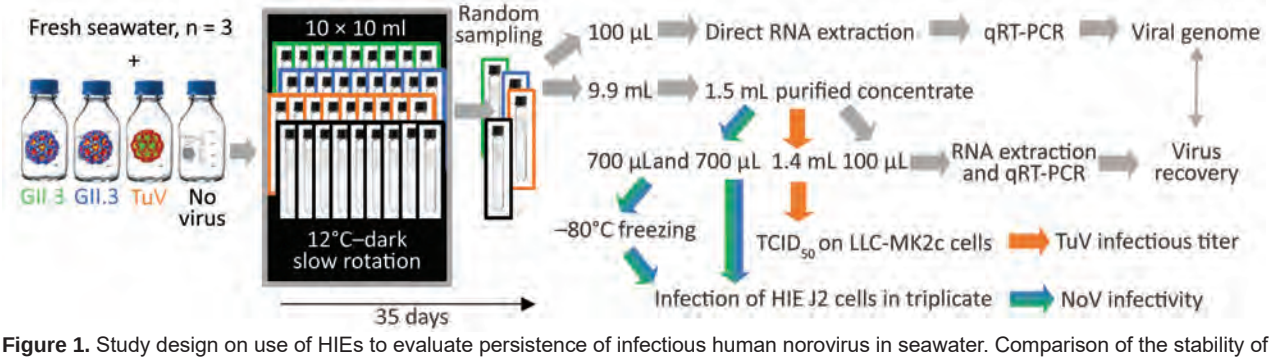

Figure 1. Study design on use of HIEs to evaluate persistence of infectious human norovirus in seawater. Comparison of the stability of 2 human norovirus strains (GII.3 indicated by green, GII.4 indicated by blue) and TuV (orange) in seawater. We conducted 3 independent experiments with different fresh seawater samples. Spiked seawater (120 mL) was split in 10 mL aliquots in glass tubes, incubated at 12°C in the dark under constant rotation (10 rpm), and randomly sampled once or twice per week for 5 weeks (35 days). Grey arrows indicate steps or treatments applied to all samples; blue-green arrows indicate steps or treatments applied to human norovirus and control without virus; orange arrows indicate steps or treatments applied to TuV only. HIE, human intestinal enteroid, NoV, norovirus; qRT-PCR, one-step quantitative reverse transcription PCR; $TCID_{50}$, 50% median tissue culture infectious dose; TuV, Tulane virus.

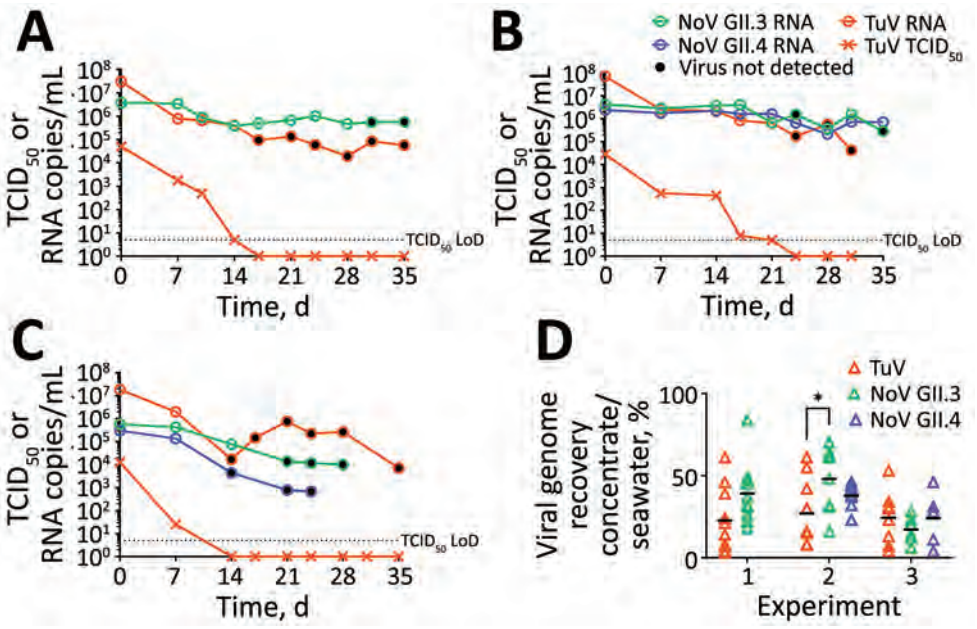

Figure 2. Persistence of viral RNA and infectious norovirus and Tulane virus in seawater. Concentration of viral RNA measured by quantitative reverse transcription PCR (qRT-PCR) in seawater (circles, RNA copies/mL), and of infectious TuV measured by $TCID_{50}$ (cross, $TCID_{50}$/mL), during experiments 1 (A), 2 (B), and 3 (C). Open circles mark the detection of infectious virus on HIE cells (human norovirus) or through $TCID_{50}$ on LLC-MK2 cells (TuV). Black circles indicate the absence of infectious virus detection. Dotted lines indicate the theoretical LoD of the $TCID_{50}$ assay (5 $TCID_{50}$/mL). D) Recovery of the viral genome after purification and concentration steps, defined as the ratio (%) of viral genome in the concentrate to that in the seawater, as measured by qRT-PCR, for each virus and time point during the 3 experiments. Black lines indicate the mean per experiment and virus. Recovery was not statistically different between experiments and viruses except for TuV and norovirus GII.3 during experiment 2 (analysis of variance, Sidak's multiple comparisons test; *p = 0.0318) (GraphPad Prism version 9.2.0, https://www.graphpad.com/scientific-software/prism). LoD, limit of detection; NoV, norovirus; $TCID_{50}$, 50% median tissue culture infectious dose; TuV, Tulane virus.

consistent with the decay rate observed previously in contaminated oysters (*10*).

For the remainder (9.9 mL) of the seawater aliquots, we filter-sterilized, concentrated by centrifugal ultrafiltration, and desalted, adapting a method used to purify infectious TuV from oysters (*10*). To verify efficacy, we used 100 µL of purified concentrate for RNA extraction to quantify the viral genome and to calculate the proportion of virus recovered in the concentrate compared with the proportion of virus in seawater (Figure 1). For all experiments combined, viral recovery ranged from 4% to 61% for TuV, 6% to 70% for GII.3, and 4% to 37% for GII.4 (Figure 2, panel D). The recovery of human norovirus tended to be even higher than for TuV, especially in the case of GII.3 in experiment 2 (Figure 2, panel D).

We used purified concentrates of TuV to assess its infectious titer through 50% tissue culture infectious

Table 2. Detection of infectious human norovirus GII.3 or GII.4 in 3 experiments using HIEs to assess persistence of infectivity*

	Experiment 1		Experiment 2				Experiment 3			
	GII.3		GII.3		GII.4		GII.3		GII.4	
Time	Inf	GMFI†	Inf	GMFI†	Inf	GMFI†	Inf	GMFI†	Inf	GMFI†
0	+	267, 1,082,‡ 103§	+	496	+	1,290	+	639, 600§	+	429, 845§
7	+	248, 787‡	+	293	+	476	+	486, 205§	+	3.2, 50§
10	+	31, 2.0‡		ND		ND		ND		ND
14	+	366, 10,‡ 8.2§	+	31§	+	151§	+	3.2, 0.4§	–	No Ct
17	+	6.7, 1,‡ 12§	+	53§	+	139§	–	No Ct	–	No Ct
21	+	12, 13,‡ 4.2§	+	70§	+	102§	–	No Ct	–	No Ct
24	+	3.1, 15.7,‡ 3.1§	+	3.1§	+	46§	–	No Ct	–	No Ct
28	+	0.5, 83,‡ no Ct§	+	213	+	3.7	–	No Ct	–	No Ct
31	–	0.7, no Ct‡	+	6.1§	+	16§	–	No Ct	–	No Ct
35	–	0.9, 1.0‡	–	0.8§	+	25§	–	No Ct	–	No Ct

*No ct indicates GMFI could not be calculated because norovirus genome could not be detected by quantitative reverse transcription PCR at 1h or 72h postinfection or both. Ct, cycle threshold; G, genotype; GMFI, geometric mean fold increase; HIE, human intestinal enteroids; Inf, infectious; ND, not done: +, positive (detected); –, negative (not detected).
†Each value represents the GMFI in human norovirus genome copies, between 1h and 72h post-infection, in triplicate wells of HIE cultures (n = 3). Evidence of replication was defined as a GMFI >3.0. Freshly prepared and undiluted viral concentrates were used to infect HIE in most experiments and time points, expect for experiment 2 where HIE cultures died after day 7.
‡Fresh viral concentrates diluted 1/10 in culture medium were also used in experiment 1.
¶To assess the possibility to freeze viral concentrates before the HIE infectivity assay, pure viral concentrate stored frozen at −80°C for several weeks and thawed once for culture on HIE were also used in some assays and showed results similar to those with fresh concentrates in 10 out of 11 tests.

dose on LLC-MK2 cells (*10*) (Figure 1). Infectious TuV was detected for 14 days during experiment 1 and for 21 days during experiment 2 (Figure 2, panels A, B), similar to the length of detection in contaminated oysters (*10*). Experiment 3 also showed a faster loss of infectious TuV, which was not detected after 7 days (Figure 2, panel C).

We used the purified concentrates of human norovirus to infect differentiated jejunal J2 HIE monolayers in triplicate (*12*), either upon collection or after storage at −80°C (Figure 1). The geometric mean fold increase (GMFI) in viral genome was measured between 1 hour and 72 hours after infection; the virus was considered infectious when GMFI >3.0 (Table 2). We detected infectious human norovirus GII.3 at up to 28 days (experiment 1), 31 days (experiment 2), and 14 days (experiment 3); infectious norovirus GII.4 was recovered throughout the 35 days in experiment 2 and through day 7 in experiment 3 (Table 2). Progressive loss in human norovirus infectivity is suggested by the GMFI decrease during all experiments for both viruses (Table 2). Of note, for all experiments, infectious GII.3 and GII.4 were detected for longer periods of time than infectious TuV (Figure 2, panels A–C), suggesting that human norovirus is more stable than TuV in seawater, especially because the initial concentrations of TuV were higher (Figure 2, panels A–C). Our results also suggest that the persistence of GII.3 and GII.4 is similar in these settings, but this finding needs further validation with a quantitative assay, because J2 HIE monolayers are more susceptible to GII.4 than GII.3 (*12*). Indeed, we observed the absence of infectious human norovirus when input genome levels were close to the sensitivity threshold of the assay (2×10^4 for GII.3, 1.2×10^3 for GII.4) (*12*), which suggests that infectious human norovirus particles might still have been present but were undetected. Finally, all virus data show that experiment 3 differs from the 2 others, which could have been caused by uncharacterized variables of the different seawater samples.

Conclusions

This study demonstrates that HIEs can be used to study infectious human norovirus persistence in seawater, an environmental matrix, and confirms the virus's high stability. Using 3 natural seawater samples, we observed persistent yet variable viability of human norovirus, showing that the nature of the seawater affects viral infectivity. This model will enable further research assessing possible factors at play, such as the bacterial flora or the physio-chemical parameters of the water. Together with data on foodborne outbreaks, this model will help determine the behavior of human norovirus in the environment and thus protect human health by enabling sanitary regulations to be adapted for actual infectious risks.

Acknowledgments

We are thankful to Jacques Le Pendu for helpful discussions, sharing reagents, and technical help with norovirus and enteroids.

This work was funded by the Direction Générale de l'Alimentation (DGAl) and the Agence Nationale de la Recherche (project GOyAVE, n°19-CE35-0014-01).

About the Author

Dr. Desdouits is an environmental virology researcher at the Health, Environment and Microbiology Laboratory at Institut Français de Recherche pour l'Exploitation de la Mer (Ifremer), Nantes, France. Her main interests lie in understanding the contamination of coastal waters and shellfish with human enteric pathogens such as norovirus, and how virus diversity and persistence contribute to the foodborne transmission of these pathogens.

References

1. de Graaf M, van Beek J, Koopmans MPG. Human norovirus transmission and evolution in a changing world. Nat Rev Microbiol. 2016;14:421–33. https://doi.org/10.1038/nrmicro.2016.48
2. Savini F, Giacometti F, Tomasello F, Pollesel M, Piva S, Serraino A, et al. Assessment of the impact on human health of the presence of norovirus in bivalve molluscs: what data do we miss? Foods. 2021;10:2444. https://doi.org/10.3390/foods10102444
3. Mathijs E, Stals A, Baert L, Botteldoorn N, Denayer S, Mauroy A, et al. A review of known and hypothetical transmission routes for noroviruses. Food Environ Virol. 2012;4:131–52. https://doi.org/10.1007/s12560-012-9091-z
4. Le Guyader FS, Atmar RL, Le Pendu J. Transmission of viruses through shellfish: when specific ligands come into play. Curr Opin Virol. 2012;2:103–10. https://doi.org/10.1016/j.coviro.2011.10.029
5. Marsh Z, Shah MP, Wikswo ME, Barclay L, Kisselburgh H, Kambhampati A, et al. Epidemiology of foodborne norovirus outbreaks—United States, 2009–2015. Food Saf (Tokyo). 2018;6:58–66. https://doi.org/10.14252/foodsafetyfscj.2017028
6. Chhabra P, de Graaf M, Parra GI, Chan MC-W, Green K, Martella V, et al. Updated classification of norovirus genogroups and genotypes. J Gen Virol. 2019;100:1393–406. https://doi.org/10.1099/jgv.0.001318
7. Pogan R, Dülfer J, Uetrecht C. Norovirus assembly and stability. Curr Opin Virol. 2018;31:59–65. https://doi.org/10.1016/j.coviro.2018.05.003
8. Boehm AB, Silverman AI, Schriewer A, Goodwin K. Systematic review and meta-analysis of decay rates of waterborne mammalian viruses and coliphages in surface waters. Water Res. 2019;164:114898. https://doi.org/10.1016/j.watres.2019.114898

9. Teunis PFM, Le Guyader FS, Liu P, Ollivier J, Moe CL. Noroviruses are highly infectious but there is strong variation in host susceptibility and virus pathogenicity. Epidemics. 2020;32:100401. https://doi.org/10.1016/j.epidem.2020.100401
10. Polo D, Schaeffer J, Teunis P, Buchet V, Le Guyader FS. Infectivity and RNA persistence of a norovirus surrogate, the Tulane virus, in oysters. Front Microbiol. 2018;9:716. https://doi.org/10.3389/fmicb.2018.00716
11. Manuel CS, Moore MD, Jaykus LA. Predicting human norovirus infectivity—recent advances and continued challenges. Food Microbiol. 2018;76:337–45. https://doi.org/10.1016/j.fm.2018.06.015
12. Ettayebi K, Crawford SE, Murakami K, Broughman JR, Karandikar U, Tenge VR, et al. Replication of human noroviruses in stem cell–derived human enteroids. Science. 2016;353:1387–93. https://doi.org/10.1126/science.aaf5211
13. Costantini V, Morantz EK, Browne H, Ettayebi K, Zeng XL, Atmar RL, et al. Human norovirus replication in human intestinal enteroids as model to evaluate virus inactivation. Emerg Infect Dis. 2018;24:1453–64. https://doi.org/10.3201/eid2408.180126
14. Chan MC, Cheung SKC, Mohammad KN, Chan JCM, Estes MK, Chan PKS. Use of human intestinal enteroids to detect human norovirus infectivity. Emerg Infect Dis. 2019;25:1730–5. https://doi.org/10.3201/eid2509.190205
15. Overbey KN, Zachos NC, Coulter C, Jacangelo J, Schwab KJ Recovery of infectious human norovirus GII.4 Sydney from fomites via replication in human intestinal enteroids. Front Cell Infect Microbiol. 2021;11:693090. https://doi.org/10.3389/fcimb.2021.693090

Address for correspondence: Marion Desdouits, Ifremer, rue de l'Ile d'Yeu, 44311 Nantes CEDEX 03, France; email: marion.desdouits@ifremer.fr

Isolation and Characterization of Novel Reassortant Influenza A(H10N7) Virus in a Harbor Seal, British Columbia, Canada

Yohannes Berhane, Tomy Joseph, Oliver Lung,
Carissa Embury-Hyatt, Wanhong Xu, Paul Cottrell, Stephen Raverty

We isolated a novel reassortant influenza A(H10N7) virus from a harbor seal in British Columbia, Canada, that died from bronchointerstitial pneumonia. The virus had unique genome constellations involving lineages from North America and Eurasia and polymerase basic 2 segment D701N mutation, associated with adaptation to mammals.

Influenza A viruses (IAVs) are one of the most consequential pathogens of birds and terrestrial mammals. IAVs (family *Orthomyxoviridae*) are enveloped, segmented, negative-sense, single-stranded RNA viruses, subtyped based on the surface glycoproteins hemagglutinin (H) and neuraminidase (N) embedded in the virus envelope. With the exceptions of H17N10 and H18N11 IAVs in bats, all other existing combinations of H (n = 16) and N (n = 9) subtypes are found in wild aquatic and shore birds, their natural reservoir hosts (*1*).

Phylogenetically, IAVs can be separated into 2 genetically distinct lineages, Eurasia (EA) and North America (NA), because of the fidelity of migratory waterfowl to distinct flyways (*2*). However, in areas where migratory flyways overlap, there are, although rare, IAVs with gene segments from both NA and EA lineages. Surveillance studies in Alaska (United States) and Newfoundland (Canada) documented a preponderance of IAVs with whole-genome segments from EA lineage viruses and only rarely, reassortant IAVs with EA and NA gene segment constellations (*3*,*4*). In 2014, along the Pacific flyway corridor in Canada and the United States, goose/Guangdong/1/96 (Gs/GD) lineage H5N8 virus was detected in wild waterfowl (*5*). The Gs/GD virus reassorted with NA lineage IAVs, subsequently resulting in devastating losses among commercial poultry flocks in Canada and the United States.

Wild bird–origin IAVs can breach the host species barrier and cause outbreaks involving several terrestrial mammals. After crossing the species barrier, some IAVs can become established in new hosts and circulate independently of their reservoir hosts. Different species of marine mammals are susceptible to IAV infection through exposure at haul-out sites, where they might comingle with wild birds, infected sympatric marine mammal species, terrestrial wildlife, including mink and river otters, and through direct exposure to infected humans or waterfowl in rehabilitation facilities (*6*). Previous outbreaks and individual case reports have shown that seals are susceptible to and have died as a result of infection with H10N7, H3N8, H7N7, H4N6, and other IAVs (*6*).

The Study

A live adult male harbor seal weighing 49 kg washed ashore at Combers Beach near Tofino, British Columbia (BC), Canada, but died before he could be captured alive. On June 1, 2021, the seal was brought to the Animal Health Center Laboratory (Abbotsford, BC, Canada) for necropsy. The seal was in moderate body and fair postmortem condition. The most

Author affiliations: University of Manitoba Department of Animal Science, Winnipeg, Manitoba, Canada (Y. Berhane); Canadian Food Inspection Agency, Winnipeg (Y. Berhane, O. Lung, C. Embury-Hyatt, W. Xu); Western College of Veterinary Medicine, Saskatoon, Saskatchewan, Canada (Y. Berhane, S. Raverty); Ministry of Agriculture, Food and Fisheries, Abbotsford, British Columbia, Canada (T. Joseph, S. Raverty); University of Manitoba Department of Biological Sciences, Winnipeg (O. Lung); Fisheries and Aquaculture Management, Vancouver, British Columbia, Canada (P. Cottrell); University of British Columbia Institute for Oceans and Fisheries, Vancouver (S. Raverty)

DOI: https://doi.org/10.3201/eid2807.212302

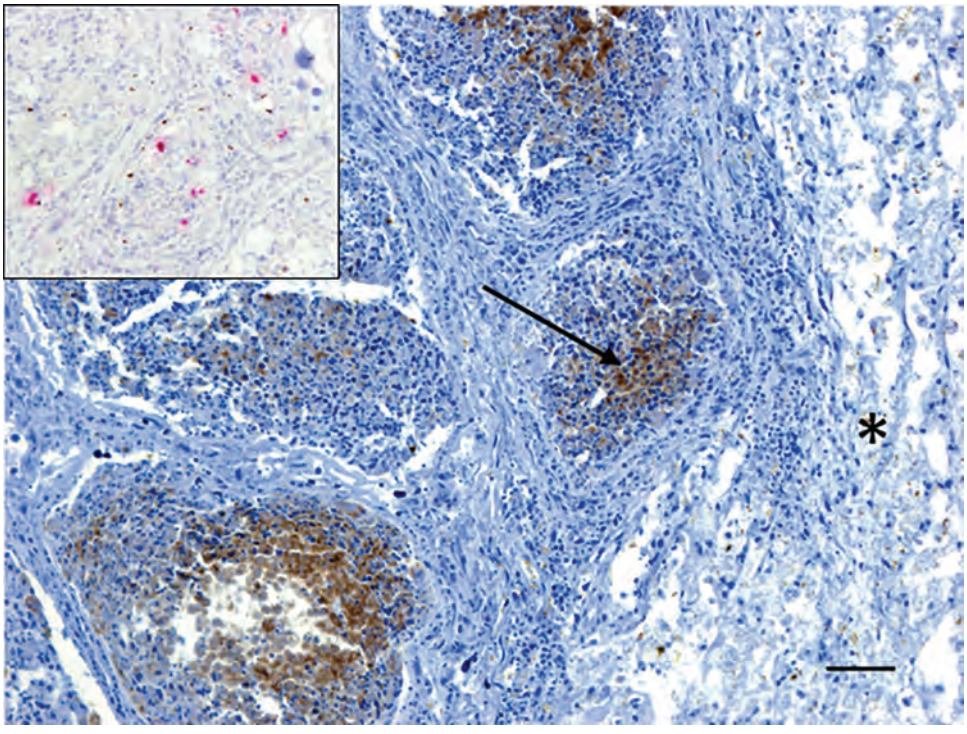

Figure 1. Immunohistochemistry testing for influenza A virus antigen in lung tissue of an adult male harbor seal, British Columbia, Canada. Viral antigen (arrow) was detected by immunohistochemistry within the bronchiolar-associated lymphoid tissue but not in adjacent lung parenchyma (*). Viral RNA could also be detected in bronchiolar-associated lymphoid tissue by in situ hybridization (inset, pink areas). Scale bar = 50 μm.

notable findings from gross examination were serosanguinous fluid within the thoracic cavity and focally extensive hemorrhage and edema from the skin to the visceral pleura along the right midlateral aspect of the thorax, with focal visceral to parietal pleural adhesion. Histopathology revealed necrotizing bronchitis and bronchiolitis, peribronchiolar lymphoid hyperplasia, alveolar histiocytosis, and perivascular lymphoplasmacytic cuffing. Immunohistochemistry testing identified IAV viral antigen within the bronchiolar-associated lymphoid tissue of 2 bronchioles in more severely affected areas of the lungs and in situ hybridization confirmed IAV RNA (Figure 1). Aerobic cultures of the lungs, hilar lymph node, brain, intercostal skeletal muscle, and small intestine yielded variable mixed growth of *Streptococcus phocae* and *Serratia liquefaciens* with no fungal growth from the lung. PCR testing of pooled tissues proved positive for consensus influenza virus and mollicutes (we confirmed *Mycoplasma* spp., but were unable to speciate) and negative for canine distemper virus.

We extracted RNA samples from the hilar lymph node, thymus, spleen, and lungs, and thoracic fluid tested positive on a real-time reverse transcription PCR assay based on IAV matrix (M) genes, as described elsewhere (*7*). We isolated all IAV PCR-positive samples in embryonated specific pathogen–free chicken eggs from lung tissue samples only. We amplified all 8 viral gene segments from original lung specimens and isolates as described elsewhere (*8*), then purified amplified reverse transcription PCR products using a QIAGEN QIAquick PCR purification kit (https://www.qiagen.com) and determined the concentration of the amplicons used for sequencing using an

Table. Similarity of all 8 gene segments and their associated proteins for influenza A(H10N7) virus from a harbor seal in British Columbia, Canada, to closest matches in GenBank*

Segment	Similarity† (%)	Closest match	GenBank accession no.	Lineage
PB2	2,225/2,280 (97.59)	A/ruddy turnstone/New Jersey/AI13-2822/2013	MH500897	North America
PB1	2,240/2,274 (98.50)	A/Mallard/WA/AH0042257S.2.A/2015(H6N8)	MN254524	North America
PA	2,117/2,151 (98.42)	A/blue-winged teal/Texas/AI11-3220/2011(H3N8)	CY205900	North America
H	1,613/1,686 (95.67)	A/duck/Bangladesh/24035/2014 (H10N1)	KY616787	Eurasia
NP	1,467/1,497 (98.00)	A/duck/Hokkaido/W90/2007(H10N7)	LC121485	Eurasia
N	1,372/1,416 (96.89)	A/duck/Mongolia/742/2015(H10N7)	LC121446	Eurasia
M	973/982 (99.08)	A/Mallard duck/Alberta/486/2019(H1N1)	MT624434	North America
NS1/NEP	821/844 (97.27)	A/duck/Hokkaido/56/2017(H12N2)	MK592497	Eurasia

*H, hemagglutinin; M, matrix; N, neuraminidase; NP, nucleoprotein; NS1/NEP, nonstructural protein 1/nuclear export protein; PA, acidic polymerase; PB, basic polymerase.
†Nucleotide matches at identical sites.

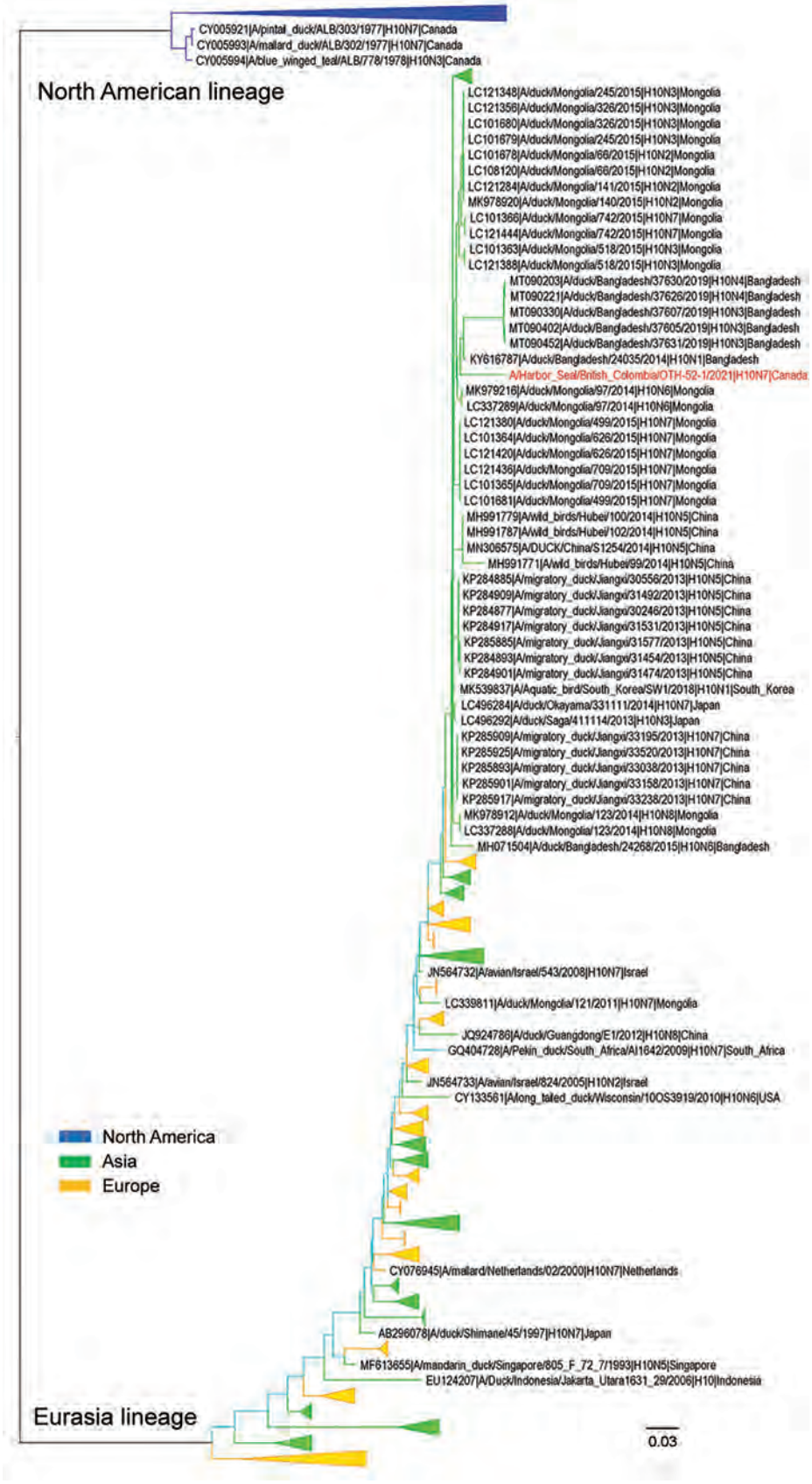

Figure 2. Maximum-likelihood phylogenetic tree of influenza A virus subtype H10 hemagglutinin gene from an adult male harbor seal, British Columbia, Canada (red text), and reference sequences. Phylogenetic analyses were based on the full-length nucleotide sequence of the hemagglutinin gene of strains representing the H10 subtype (n = 1,512). The evolutionary relationship was inferred using RAxML (https://github.com/stamatak/standard-RAxML) based on the general time-reversible model with 1,000 bootstrap replicates. For purposes of clarity, some clades are collapsed, and colors are assigned to indicate the origin of the gene: blue for North America, green for Asia, and yellow for Europe. The tree was drawn to scale; branch lengths are measured in number of substitutions per site.

Invitrogen Qubit dsDNA BR assay kit (https://www.thermofisher.com) on the Qubit Fluorometer. We performed library prep using Illumina Nextera XT Library preparation kit (https://www.illumina.com) and sequencing using Illumina MiSeq, as described elsewhere (*9*). We assembled IAV full genome segments using DNASTAR SeqMan NGen software version 15.3.0 (https://www.dnastar.com).

Full genome sequences of the virus obtained from the original lung tissue samples and isolates from lungs were 100% identical. Further analysis demonstrated that 4 gene segments, polymerase basic (PB) 1 and 2, polymerase acidic (PA), and M segments, originated from unknown NA lineage IAVs of wild bird origin. The remaining 4 gene segments, H, N, nucleoprotein (NP), and nonstructural (NS) were derived from EA lineage IAVs. We designated the virus A/harbor seal/British Colombia/OTH-52-1/2021(H10N7) and deposited sequences from the original sample and isolates into the National Center for Biotechnology Information genome database (https://www.ncbi.nlm.nih.gov/genome) under accession nos. OL336415 (PB2), OL336416 (PB1), OL336417 (PA), OL336418 (H), OL336419 (NP), OL336420 (N), OL336421 (M), and OL336422 (NS). We compared percentage similarity between all 8 gene segments and their associated proteins and closest matches in GenBank (Table). Phylogenetic analysis demonstrated that the H gene of the virus clades with EA lineage IAVs was circulating in wild birds (Figure 2).

Further analysis of the virus genome revealed that the H10N7 virus carries a glutamic acid (E) residue at the aa 627 site of PB2 determined to be associated with decreased replication in mammal cells using growth kinetics and with decreased virulence in mice using lethal dose challenge (*10*,*11*). We also observed an aspartic acid substitution at site aa 701, which has been associated with systemic replication and mortality in mice (*11*,*12*). In addition, this residue substitution in guinea pigs conferred efficient replication of the virus in the nose, trachea, and lungs (*11*). Key amino acid changes were also observed in NP and M segments. The presence of lysine at the aa 319 site in the NP gene segment has been implicated in species adaptation (*12*) and substitution in the A/seal/Mass/1/1980(H7N7) backbone conferred increased binding to importin alpha1. In the M protein, aspartate at aa 30 and alanine at aa 215 sites also increased virulence as indicated by the decreased postexposure survival rate in mice (*13*).

Conclusions

In our study of a harbor seal infected with a novel reassortment H10N7 IAV containing a unique constellation of NA and EA lineage gene segments, we found no conclusive evidence of where and when the reassortment occurred. However, the seal was recovered at a location within the Pacific avian flyway, where Gs/GD lineage H5N8 virus was detected in 2014 and later reassorted with NA lineage viruses to create novel reassortant H5N2 and H5N1 IAVs that were responsible for large outbreaks in domestic poultry in Canada and the United States (*5*). Harbor seals share habitat with seabirds and shorebirds, and the seal in our study may have been infected through spillover directly from infected birds as happened in cases reported elsewhere (*6*,*8*). In previous outbreaks in seals, the proximate cause of death was attributed to secondary or opportunistic *Mycoplasma* spp. (*14*), which were also detected in this case, or bacterial infection. Finally, because novel IAVs in marine mammals have been shown to be potentially zoonotic (*15*), IAV circulation among seals could have important public health implications for humans and other mammals.

Acknowledgments

The authors thank Tamiko Hisanaga, Matt Suderman, Estella Moffat, and Katherine Handel for their technical assistance. The authors also thank staff from the necropsy, bacteriology, virology, and molecular diagnostics sections of the British Columbia Animal Health Centre for their technical assistance.

This study was supported by the Public Health Agency of Canada and Canadian Food Inspection Agency to support genetic and antigenic monitoring of influenza A virus in animals.

About the Author

Dr. Berhane is a virologist with the National Centre for Foreign Animal Disease, Canadian Food Inspection Agency in Winnipeg, Manitoba, Canada, and has appointments with the Department of Animal Science, University of Manitoba, Winnipeg, and Department of Veterinary Pathology, Western College of Veterinary Medicine, University of Saskatchewan, Saskatoon, Saskatchewan, Canada.

References

1. Wu Y, Wu Y, Tefsen B, Shi Y, Gao GF. Bat-derived influenza-like viruses H17N10 and H18N11. Trends Microbiol. 2014;22:183–91. https://doi.org/10.1016/j.tim.2014.01.010
2. Webster RG, Bean WJ, Gorman OT, Chambers TM, Kawaoka Y. Evolution and ecology of influenza A viruses. Microbiol Rev. 1992;56:152–79. https://doi.org/10.1128/mr.56.1.152-179.1992
3. Huang Y, Wille M, Benkaroun J, Munro H, Bond AL, Fifield DA, et al. Perpetuation and reassortment of gull

influenza A viruses in Atlantic North America. Virology. 2014; 456-457:353–63. https://doi.org/10.1016/j.virol.2014.04.009
4. Ramey AM, Reeves AB, Sonsthagen SA, TeSlaa JL, Nashold S, Donnelly T, et al. Dispersal of H9N2 influenza A viruses between East Asia and North America by wild birds. Virology. 2015;482:79–83. https://doi.org/10.1016/j.virol.2015.03.028
5. Ramey AM, DeLiberto TJ, Berhane Y, Swayne DE, Stallknecht DE. Lessons learned from research and surveillance directed at highly pathogenic influenza A viruses in wild birds inhabiting North America. Virology. 2018;518:55–63. https://doi.org/10.1016/j.virol.2018.02.002
6. Venkatesh D, Bianco C, Núñez A, Collins R, Thorpe D, Reid SM, et al. Detection of H3N8 influenza A virus with multiple mammalian-adaptive mutations in a rescued Grey seal (*Halichoerus grypus*) pup. Virus Evol. 2020;6:veaa 016. https://doi.org/10.1093/ve/veaa016
7. Weingartl HM, Berhane Y, Hisanaga T, Neufeld J, Kehler H, Emburry-Hyatt C, et al. Genetic and pathobiologic characterization of pandemic H1N1 2009 influenza viruses from a naturally infected swine herd. J Virol. 2010;84:2245–56. https://doi.org/10.1128/JVI.02118-09
8. Zhou B, Donnelly ME, Scholes DT, St George K, Hatta M, Kawaoka Y, et al. Single-reaction genomic amplification accelerates sequencing and vaccine production for classical and Swine origin human influenza a viruses. J Virol. 2009;83:10309–13. https://doi.org/10.1128/JVI.01109-09
9. Xu W, Weese JS, Ojkic D, Lung O, Handel K, Berhane Y. Phylogenetic inference of H3N2 canine influenza A outbreak in Ontario, Canada in 2018. Sci Rep. 2020;10:6309. https://doi.org/10.1038/s41598-020-63278-z
10. Bogs J, Kalthoff D, Veits J, Pavlova S, Schwemmle M, Mänz B, et al. Reversion of PB2-627E to -627K during replication of an H5N1 Clade 2.2 virus in mammalian hosts depends on the origin of the nucleoprotein. J Virol. 2011;85:10691–8. https://doi.org/10.1128/JVI.00786-11
11. Li J, Ishaq M, Prudence M, Xi X, Hu T, Liu Q, et al. Single mutation at the amino acid position 627 of PB2 that leads to increased virulence of an H5N1 avian influenza virus during adaptation in mice can be compensated by multiple mutations at other sites of PB2. Virus Res. 2009;144:123–9. https://doi.org/10.1016/j.virusres.2009.04.008
12. Gabriel G, Dauber B, Wolff T, Planz O, Klenk HD, Stech J. The viral polymerase mediates adaptation of an avian influenza virus to a mammalian host. Proc Natl Acad Sci U S A. 2005; 102:18590–5. https://doi.org/10.1073/pnas.0507415102
13. Fan S, Deng G, Song J, Tian G, Suo Y, Jiang Y, et al. Two amino acid residues in the matrix protein M1 contribute to the virulence difference of H5N1 avian influenza viruses in mice. Virology. 2009;384:28–32. https://doi.org/10.1016/j.virol.2008.11.044
14. van Kuppeveld FJ, van der Logt JT, Angulo AF, van Zoest MJ, Quint WG, Niesters HG, et al. Genus- and species-specific identification of mycoplasmas by 16S rRNA amplification. Appl Environ Microbiol. 1992;58:2606–15. https://doi.org/10.1128/aem.58.8.2606-2615.1992
15. van den Brand JMA, Wohlsein P, Herfst S, Bodewes R, Pfankuche VM, van de Bildt MWG, et al. Influenza A (H10N7) virus causes respiratory tract disease in harbor seals and ferrets. PLoS One. 2016;11:e0159625. https://doi.org/10.1371/journal.pone.0159625

Address for correspondence: Stephen Raverty, Animal Health Center–Pathology, 1767 Angus Campbell Rd, Abbotsford, Vancouver, BC V3G 2M3, Canada; email: stephen.raverty@gov.bc.ca

Suspected Cat-to-Human Transmission of SARS-CoV-2, Thailand, July–September 2021

Thanit Sila, Jutapoln Sunghan, Wison Laochareonsuk, Smonrapat Surasombatpattana, Chanon Kongkamol, Thammasin Ingviya, Pisud Siripaitoon, Narongdet Kositpantawong, Siripen Kanchanasuwan, Thanaporn Hortiwakul, Boonsri Charernmak, Ozioma Forstinus Nwabor, Kachornsakdi Silpapojakul, Sarunyou Chusri

A veterinarian in Thailand was diagnosed with COVID-19 after being sneezed on by an infected cat owned by an infected patient. Genetic study supported the hypothesis of SARS-CoV-2 transmission from the owner to the cat, and then from the cat to the veterinarian.

COVID-19, caused by SARS-CoV-2, has been suspected to be a zoonosis because of its link to a live animal market in Wuhan, China (*1*). In addition, several countries in the Americas, Africa, Europe, and Asia have reported the occurrence of COVID-19 in various animal species, including minks, cats, dogs, lions, and tigers (*2*). However, most of these infections primarily originated from humans and were transmitted to the animal (i.e., reverse zoonosis), with numerous reports in domestic cats (*2*,*3*). A recent report describes a possible animal-to-human transmission of SARS-CoV-2 from infected farm minks to farmworkers in the Netherlands (*4*). We describe a suspected zoonotic SARS-CoV-2 transmission from a cat to a human.

Case Report

During July–September 2021, the COVID-19 pandemic was shifting from the Alpha variant to the Delta variant. On August 15, 2021, in Songkhla, a business province in southern Thailand, patient A, a 32-year-old previously healthy female veterinarian who lived alone in a dormitory on campus visited the hospital of Prince of Songkla University, located in Hatyai District, Songkhla Province, with a history of fever, clear nasal discharge, and productive cough of 2 days' duration. Results of a physical examination, including a chest radiograph, were otherwise unremarkable. When questioned about her history, she said that 5 days earlier, she and 2 other veterinarians (patients E and F) had examined a cat belonging to 2 men (patients B and C).

Patients B and C, a 32- and 64-year-old son and father, were from Bangkok, the capital city of Thailand. They were confirmed positive for SARS-CoV-2 infection by reverse transcription PCR (RT-PCR) a day earlier and were transferred to Prince of Songkla University hospital because of the unavailability of hospital beds in Bangkok. Together with their cat, patients B and C were transported by an ambulance in a 20-hour, 900-km trip on August 8, 2021 (Figure 1). On arrival, the patients were immediately admitted to an isolation ward. The cat that had been sleeping on the same beds as the patients was sent to the university veterinarian hospital for an examination by patient A on August 10, 2021, and found to be clinically normal. Patient A retrieved nasal and rectal swab specimens from the cat while patients E and F restrained it. During the nasal swabbing, the sedated cat sneezed in the face of patient A. All 3 veterinarians were wearing disposable gloves and N95 respirator masks without face shields or eye goggles at the time. The entire veterinarian–cat encounter lasted ≈10 minutes.

Three days after exposure to the cat, patient A became symptomatic but did not seek medical consultation until August 15, when the RT-PCR

Author affiliations: Prince of Songkla University Faculty of Medicine, Songkhla, Thailand (T. Sila, W. Laochareonsuk, S. Surasombatpattana, C. Kongkamol, T. Ingviya, P. Siripaitoon, N. Kositpantawong, S. Kanchanasuwan, T. Hortiwakul, B. Charernmak, O.F. Nwabor, K. Silpapojakul, S. Chusri); Prince of Songkla University Faculty of Veterinary Science, Songkhla (J. Sunghan)

DOI: https://doi.org/10.3201/eid2807.212605

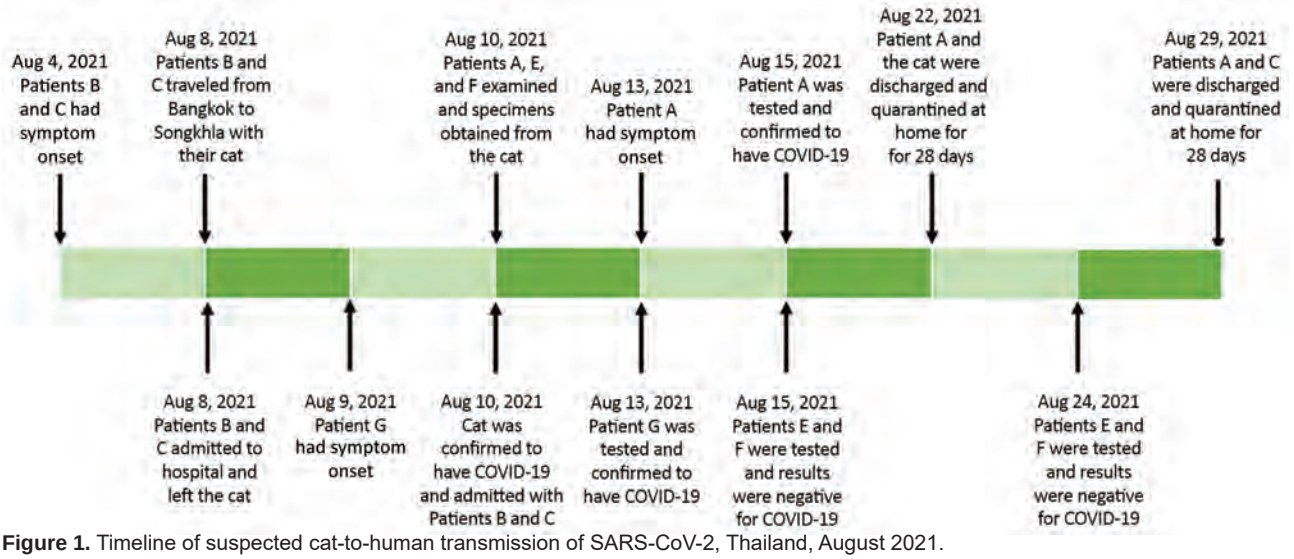

Figure 1. Timeline of suspected cat-to-human transmission of SARS-CoV-2, Thailand, August 2021.

test results of the cat returned COVID-19–positive (Table). On investigation, nasopharyngeal swab specimens from patient A showed detectable SARS-CoV-2 (Table). Patients A, B and C and the cat were admitted for isolation in the hospital. Test results for the swab specimens from patients E and F were negative.

No close contacts of patient A were diagnosed with COVID-19. Contact tracing investigations of all the 30 personnel working at the Veterinary Hospital identified 1 additional contact with COVID-19, a veterinarian who worked in the Department of Large Animals (patient G). Patient G had fever onset 1 day before the cat's arrival and had tested positive for COVID-19 on August 13, 2021. He reported no direct or indirect contact with the cat or patients A, E, or F.

Before genotyping, we tested viral RNA from the cat, patients A, B, C, and G, and other patients in Songkhla Province for SARS-CoV-2 by using RT-PCR. Primer sets were designed to target the nucleoprotein and open reading frame 1ab genes (Table). For viral whole-genome sequencing, we performed library preparation for the SARS-CoV-2 genome by using QIAseq DIRECT SARS-CoV-2 kits (QIAGEN, https://www.qiagen.com) on an Illumina NextSeq 550 (Illumina, https://www.illumina.com) at the Translational Medicine Research Center at Prince of Songkla University. We identified the PANGO lineages by using Pangolin and Pangolearn (https://cov-lineages.org/resources/pangolin/pangolearn.html) (Table). We generated maximum-likelihood phylogenetic trees of the representative cases and others from aligned consensus sequences by using an IQ-TREE (http://www.iqtree.org) with 1,000 bootstraps. We visualized the phylogenetic tree by using FigTree (http://tree.bio.ed.ac.uk/software/figtree). The genomes of patients B and C and the cat were identical to that obtained from patient A, but they were distinct from those of other patients in the same province (Figure 2). The pairwise distance between patient A and the cat was shown to be similar (5) by MEGA 11 (https://www.megasoftware.net) with 1,000 bootstraps (Table).

Conclusions

The identical SARS-CoV-2 genome sequences obtained from patient A and the sequences derived from the cat

Table. Sample metadata of SARS-CoV-2 genome derived from feline and human patients after suspected cat-to-human transmission of SARS-CoV-2, Thailand, July–September 2021*

Patient	Sequence ID	Type of sample	Cycle threshold		PANGO lineage	Pairwise distance, bp
			ORF1ab gene	N gene		
A	Patient_A	Nasopharyngeal swab	20	16	B.1.167.2	0.00
B	Patient_B	Nasopharyngeal swab	19	22	B.1.167.2	0.00
C	Patient_C	Nasopharyngeal swab	15	20	B.1.167.2	0.00
G	Patient_G	Nasopharyngeal swab	24	26	B.1.167.2.30	40.00
Cat	Throat_cat	Throat swab	17	16	B.1.167.2	0.00
Cat	Rectal_cat	Rectal swab	21	15	B.1.167.2	0.00

*PANGO lineages identified by using Pangolin and Pangolearn (https://cov-lineages.org/resources/pangolin/pangolearn.html). N, nucleoprotein; ORF, open reading frame.

and its 2 owners, together with the temporal overlapping of the animal and human infections, indicated that their infections were epidemiologically related. Because patient A had no prior meetings with patients B or C, she probably acquired SARS-CoV-2 from the cat when it sneezed in her face. The genome sequences were distinct from that of patient G and other sequences circulating in the same province, and by using the pairwise distance formula, we were able to rule out external transmission (*5*). The Alpha variant was widely spread until the end of July 2021 in Songkhla Province; on the other hand, in Bangkok, the Delta variant has been widespread since the beginning of July 2021 (*6*).

The transmission chain of SARS-CoV-2 infections in this cluster probably began in Bangkok. Cats are known to be susceptible to SARS-CoV-2 infection (*8*–*10*), especially during close interactions with humans with symptomatic SARS-CoV-2 infections (*7*). Because infected cats have relatively short incubation and contagious periods (*8*–*10*), this cat probably had acquired its SARS-CoV-2 infection no longer than a week before possibly transmitting the disease to patient A.

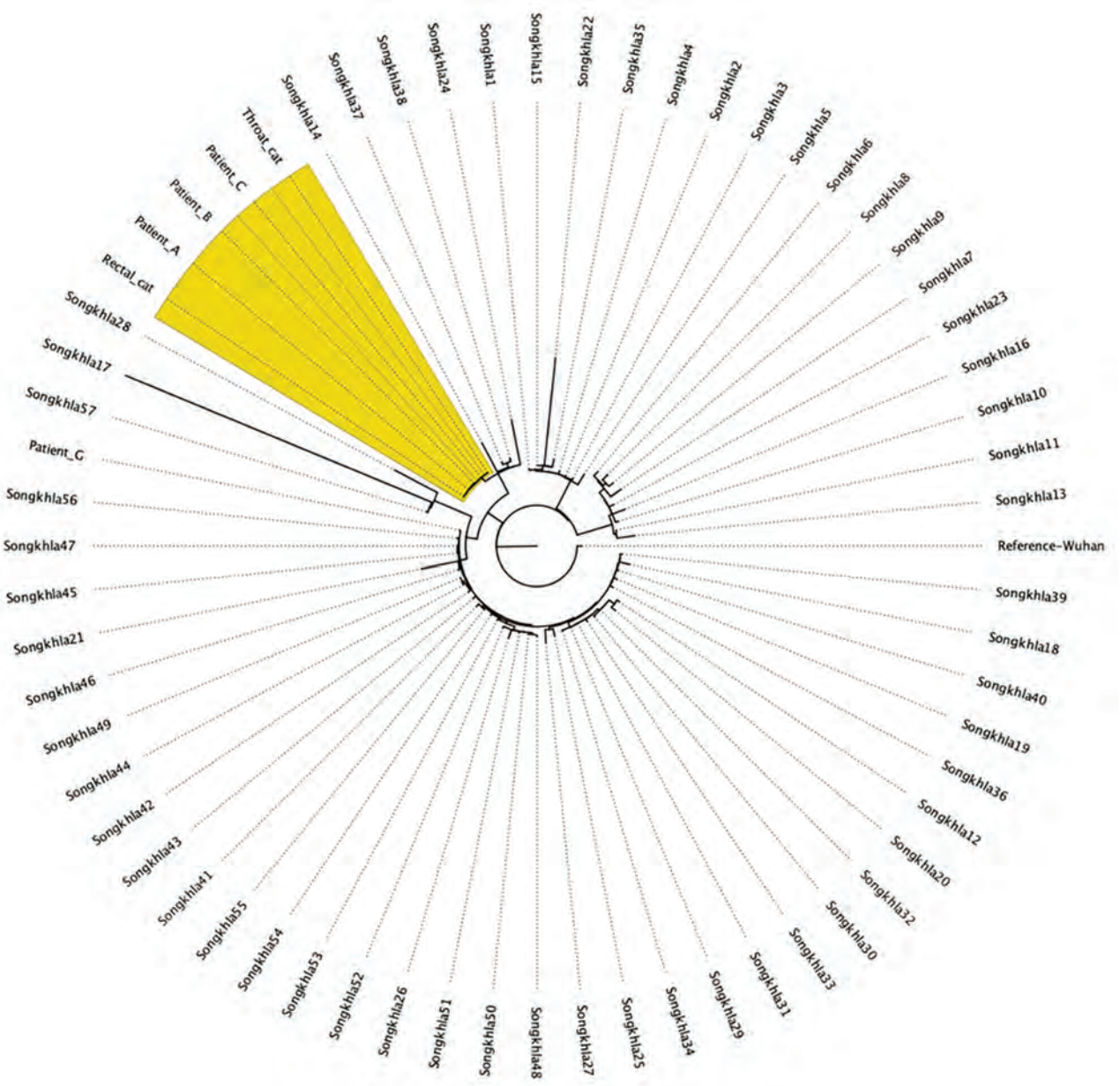

Figure 2. Phylogenetic tree of SARS-CoV-2 genome sequences retrieved from patients A, B, and C and the cat belonging to patients B and C (yellow shading) compared with reference sequences from COVID-19 patients from Songkhla Province, Thailand, July–September 2021. Tree constructed with IQ-TREE (http://www.iqtree.org) by using the maximum-likelihood method and 1,000 bootstrap replicates.

Although direct or indirect (fomites) contacts are also potential routes of transmission to patient A, these possibilities are less likely because she wore gloves and washed her hands before and after examining the cat. Transmission from the cat sneeze is hypothesized because of this brief but very close encounter. The relatively low RT-PCR cycle thresholds (*11*) in the nasal swab obtained from the cat suggest that the viral load was high and infectious (*12*,*13*). Because patient A wore an N95 mask without a face shield or goggles, her exposed ocular surface was vulnerable to infection by droplets expelled from the cat. Her infection signifies the possibility of ocular transmission and the importance of wearing protective goggles or face shields in addition to a mask during close-range interactions with high-risk humans or animals.

In summary, we have provided evidence that cats can transmit the SARS-CoV-2 infection to humans. However, the incidence of this transmission method is relatively uncommon because of the short (median 5 days) duration of cats shedding viable viruses (*8*–*10*). Nevertheless, to prevent transmission of SARS-CoV-2 from humans to cat, persons with suspected or confirmed COVID-19 should refrain from contact with their cat. Eye protection as part of the standard personal protection is advisable for caregivers during close interactions with cats suspected to be infected.

Acknowledgments

The authors thank David Patterson for manuscript revision.

T.S., W.L., J.S., and S.S. performed experiments and data interpretation. C.K. and T.I. contributed to epidemiologic data collection, analysis, and manuscript editing. T.S., W.L., and S.S. provided access to the crucial experimental components. P.S., N.K., S.K., T.H., B.C., and S.C. contributed to clinical data collection and interpretation. S.C. drafted the manuscript and provided scientific content of the manuscript. O.F.N. provided grammatical revision of the manuscript. S.C. conceived the idea and experimental design of the study. All authors read and approved the final manuscript.

About the Author

Mr. Sila is a graduate student at Prince of Songkla University's Department of Health Science and Medical Research in the Faculty of Medicine. His primary research interests include genomics, evolutionary microbiology, bioinformatics, sequence and genome analysis, and viral culture.

References

1. Zhu N, Zhang D, Wang W, Li X, Yang B, Song J, et al.; China Novel Coronavirus Investigating and Research Team. A novel coronavirus from patients with pneumonia in China, 2019. N Engl J Med. 2020;382:727–33. https://doi.org/10.1056/NEJMoa2001017
2. World Organisation for Animal Health. COVID-19 portal [cited 2021 October 13]. https://www.oie.int/app/uploads/2021/09/sars-cov-2-situation-report-4.pdf
3. Hobbs EC, Reid TJ. Animals and SARS-CoV-2: species susceptibility and viral transmission in experimental and natural conditions, and the potential implications for community transmission. Transbound Emerg Dis. 2021;68:1850–67. https://doi.org/10.1111/tbed.13885
4. Oude Munnink BB, Sikkema RS, Nieuwenhuijse DF, Molenaar RJ, Munger E, Molenkamp R, et al. Transmission of SARS-CoV-2 on mink farms between humans and mink and back to humans. Science. 2021;371:172–7. https://doi.org/10.1126/science.abe5901
5. Worby CJ, Chang HH, Hanage WP, Lipsitch M. The distribution of pairwise genetic distances: a tool for investigating disease transmission. Genetics. 2014;198:1395–404. https://doi.org/10.1534/genetics.114.171538
6. World Health Organization. Classification of Omicron (B1.1.529): SARS-CoV-2 variant of concern [cited 2022 Mar 26]. https://reliefweb.int/sites/reliefweb.int/files/resources/2022_01_19_tha-sitrep-219-covid-19_th_r02.pdf
7. Goryoka GW, Cossaboom CM, Gharpure R, Dawson P, Tansey C, Rossow J, et al. One Health investigation of SARS-CoV-2 infection and seropositivity among pets in households with confirmed human COVID-19 cases—Utah and Wisconsin, 2020. Viruses. 2021;13:1813. https://doi.org/10.3390/v13091813
8. Bosco-Lauth AM, Hartwig AE, Porter SM, Gordy PW, Nehring M, Byas AD, et al. Experimental infection of domestic dogs and cats with SARS-CoV-2: pathogenesis, transmission, and response to reexposure in cats. Proc Natl Acad Sci U S A. 2020;117:26382–8. https://doi.org/10.1073/pnas.2013102117
9. Halfmann PJ, Hatta M, Chiba S, Maemura T, Fan S, Takeda M, et al. Transmission of SARS-CoV-2 in domestic cats. N Engl J Med. 2020;383:592–4. https://doi.org/10.1056/NEJMc2013400
10. Shi J, Wen Z, Zhong G, Yang H, Wang C, Huang B, et al. Susceptibility of ferrets, cats, dogs, and other domesticated animals to SARS-coronavirus 2. Science. 2020;368:1016–20. https://doi.org/10.1126/science.abb7015
11. Segalés J, Puig M, Rodon J, Avila-Nieto C, Carrillo J, Cantero G, et al. Detection of SARS-CoV-2 in a cat owned by a COVID-19-affected patient in Spain. Proc Natl Acad Sci U S A. 2020;117:24790–3. https://doi.org/10.1073/pnas.2010817117
12. Bullard J, Dust K, Funk D, Strong JE, Alexander D, Garnett L, et al. Predicting infectious severe acute respiratory syndrome coronavirus 2 from diagnostic samples. Clin Infect Dis. 2020;71:2663–6. https://doi.org/10.1093/cid/ciaa638
13. Singanayagam A, Patel M, Charlett A, Lopez Bernal J, Saliba V, Ellis J, et al. Duration of infectiousness and correlation with RT-PCR cycle threshold values in cases of COVID-19, England, January to May 2020. Euro Surveill. 2020;25:2001483. https://doi.org/10.2807/1560-7917.ES.2020.25.32.2001483

Address for correspondence: Sarunyou Chusri, Division of Infectious Diseases, Department of Internal Medicine, Faculty of Medicine, Prince of Songkla University, 15 Kanchanavanich Rd, Hatyai District, Songkhla, 90110, Thailand; email: sarunyouchusri@hotmail.com

Potential Threats to Human Health from Eurasian Avian-Like Swine Influenza A(H1N1) Virus and Its Reassortants

Shuai-Yong Wang,[1] Feng Wen,[1] Ling-Xue Yu, Juan Wang, Man-Zhu Wang, Jie-Cong Yan, Yan-Jun Zhou, Wu Tong, Tong-Ling Shan, Guo-Xin Li, Hao Zheng, Chang-Long Liu, Ning Kong, Guang-Zhi Tong, Hai Yu

During 2018–2020, we isolated 32 Eurasian avian-like swine influenza A(H1N1) viruses and their reassortant viruses from pigs in China. Genomic testing identified a novel reassortant H3N1 virus, which emerged in late 2020. Derived from G4 Eurasian H1N1 and H3N2 swine influenza viruses. This virus poses a risk for zoonotic infection.

Since emerging in 2001, Eurasian avian-like (EA) swine influenza A(H1N1) virus has gradually become the predominant lineage and continues to circulate among pigs in China (*1*–*3*). Introduction of the 2009 pandemic H1N1 virus (pH1Na) among pigs has increased its reassortment with EA H1N1 swine influenza A viruses (IAVs), and several reassortant variants with the potential to infect humans have been detected in China (*4*–*8*).

Multiple genotypes have been identified in EA H1N1 swine IAVs from pigs in China, and recent data suggest that the potentially pandemic genotype 4 (G4) reassortant has predominated among swine populations in China since 2016 (*4*,*8*). To clarify their prevalence and genotype characterizations, we isolated 32 swine IAVs in China during 2018–2020, including 6 novel reassortant H3N1 viruses that carry the hemagglutinin (HA) gene derived from human H3N2 lineage, and conducted phylogenic analysis of 8 gene segments from these viruses.

Author affiliations: Chinese Academy of Agricultural Sciences, Shanghai, China (S.-Y. Wang, L.-X. Yu, J. Wang, M.-Z. Wang, J.-C. Yan, Y.-J. Zhou, W. Tong, T.-L. Shan, G.-X. Li, H. Zheng, C.-L. Liu, N. Kong, G.-Z. Tong, H. Yu); Foshan University, Foshan, Guangdong, China (F. Wen).

DOI: https://doi.org/10.3201/eid2807.211822

The Study

During January 2018–December 2020, we collected 1,006 swab samples from pigs with symptoms typical of swine influenza, such as fever and cough, on pig farms across 6 provinces (Shanghai, Jiangsu, Zhejiang, Tianjin, Hebei, and Shandong) in China. We isolated viruses using MDCK cells and determined viral whole-genome sequences by Sanger sequencing. We isolated a total of 32 swine IAVs from the 1,006 swab samples, an isolation rate of 3.18% (Table). To determine the phylogenetic evolution of the 32 isolates, we performed genetic analyses using available sequences of related viruses from the GenBank and GISAID (https://www.gisaid.org) databases.

Phylogenetic analysis revealed that the HA genes of 26 viruses isolated in the study were grouped within clade 1C.2.3 of EA H1N1 lineage (Figure 1). However, the HA genes of the 6 novel reassortant H3N1 viruses were located in the recently circulating human-like H3N2 lineage and shared the highest genetic identity (99.7%–99.9%) with a swine H3N2 virus (A/Swine/Guangdong/NS2701/2012) in China (Figure 2). The neuraminidase (NA) genes of all 32 isolates were grouped within the EA H1N1 lineage (Appendix Figure, https://wwwnc.cdc.gov/EID/article/28/7/21-1822-App1.pdf). On the basis of sequence analysis of the HA and NA genes, we identified the 32 swine IAVs isolated in this study as EA H1N1 (n = 26; isolation rate: 2.58%) and H3N1 (n = 6; isolation rate: 0.6%), indicating that EA H1N1 was the predominant virus subtype circulating among the sampled pig population in China.

Origins of the 6 internal gene segments, polymerase basic (PB) 1 and 2, polymerase acidic (PA),

[1]These first authors contributed equally to this article.

Table. Detailed information of 32 viruses isolated in study of Eurasian avian-like swine influenza A(H1N1) virus and its reassortant viruses, China*

Strain name	Date collected	Place collected	Gene segment								G
			PB2	PB1	PA	HA	NP	NA	M	NS	
A/swine/Shanghai/37/2018	1/2018	Shanghai	EA	EA	EA	EA	EA	EA	EA	EA	1
A/swine/Shanghai/56/2018	1/2018	Shanghai	EA	EA	EA	EA	EA	EA	EA	EA	1
A/swine/Shanghai/72/2018	1/2018	Shanghai	EA	EA	EA	EA	EA	EA	EA	EA	1
A/swine/Shanghai/136/2018	3/2018	Shanghai	EA	EA	EA	EA	EA	EA	EA	EA	1
A/swine/Hebei/11/2018	3/2018	Hebei	EA	EA	EA	EA	EA	EA	EA	EA	1
A/swine/Hebei/47/2018	3/2018	Hebei	EA	EA	EA	EA	EA	EA	EA	EA	1
A/swine/Shandong/8/2018	3/2018	Shandong	pH1N1	pH1N1	pH1N1	EA	pH1N1	EA	pH1N1	pH1N1	2
A/swine/Zhejiang/5/2018	12/2018	Zhejiang	pH1N1	pH1N1	pH1N1	EA	pH1N1	EA	pH1N1	TRIG	4
A/swine/Shandong/20/2018	12/2018	Shandong	pH1N1	pH1N1	pH1N1	EA	pH1N1	EA	EA	TRIG	5
A/swine/Jiangsu/16/2018	12/2018	Jiangsu	pH1N1	pH1N1	pH1N1	EA	pH1N1	EA	EA	TRIG	5
A/swine/Jiangsu/28/2018	12/2018	Jiangsu	pH1N1	pH1N1	pH1N1	EA	pH1N1	EA	EA	TRIG	5
A/swine/Hebei/16/2019	1/2019	Tianjin	pH1N1	pH1N1	pH1N1	EA	pH1N1	EA	pH1N1	pH1N1	2
A/swine/Zhejiang/19/2019	1/2019	Zhejiang	pH1N1	pH1N1	pH1N1	EA	pH1N1	EA	pH1N1	TRIG	4
A/swine/Shandong/66/2019	1/2019	Shandong	pH1N1	pH1N1	pH1N1	EA	pH1N1	EA	pH1N1	TRIG	4
A/swine/Shandong/73/2019	1/2019	Shandong	pH1N1	pH1N1	pH1N1	EA	pH1N1	EA	pH1N1	TRIG	4
A/swine/Jiangsu/91/2019	11/2019	Jiangsu	pH1N1	pH1N1	pH1N1	EA	pH1N1	EA	pH1N1	TRIG	4
A/swine/Zhejiang/22/2019	12/2019	Zhejiang	pH1N1	pH1N1	pH1N1	EA	pH1N1	EA	EA	TRIG	5
A/swine/Heibei/66/2019	12/2019	Hebei	pH1N1	pH1N1	pH1N1	EA	pH1N1	EA	EA	TRIG	5
A/swine/Tianjin/27/2019	12/2019	Tianjin	pH1N1	pH1N1	pH1N1	EA	pH1N1	EA	EA	TRIG	5
A/swine/Tianjin/50/2020	10/2020	Tianjin	pH1N1	pH1N1	pH1N1	EA	pH1N1	EA	pH1N1	TRIG	4
A/swine/Tianjin/82/2020	10/2020	Tianjin	pH1N1	pH1N1	pH1N1	EA	pH1N1	EA	pH1N1	TRIG	4
A/swine/Zhejiang/25/2020	10/2020	Zhejiang	pH1N1	pH1N1	pH1N1	EA	pH1N1	EA	pH1N1	TRIG	4
A/swine/Jiangsu/93/2020	10/2020	Jiangsu	pH1N1	pH1N1	pH1N1	EA	pH1N1	EA	pH1N1	TRIG	4
A/swine/Shandong/88/2020	10/2020	Shandong	pH1N1	pH1N1	pH1N1	EA	pH1N1	EA	pH1N1	TRIG	4
A/swine/Tianjin/121/2020	11/2020	Tianjin	pH1N1	pH1N1	pH1N1	EA	pH1N1	EA	EA	TRIG	5
A/swine/Jiangsu/100/2020	11/2020	Jiangsu	pH1N1	pH1N1	pH1N1	EA	pH1N1	EA	EA	TRIG	5
A/swine/Zhejiang/76/2020	12/2020	Zhejiang	pH1N1	pH1N1	pH1N1	H3	pH1N1	EA	pH1N1	TRIG	nH3N1
A/swine/Zhejiang/83/2020	12/2020	Zhejiang	pH1N1	pH1N1	pH1N1	H3	pH1N1	EA	pH1N1	TRIG	nH3N1
A/swine/Zhejiang/109/2020	12/2020	Zhejiang	pH1N1	pH1N1	pH1N1	H3	pH1N1	EA	pH1N1	TRIG	nH3N1
A/swine/Zhejiang/211/2020	12/2020	Zhejiang	pH1N1	pH1N1	pH1N1	H3	pH1N1	EA	pH1N1	TRIG	nH3N1
A/swine/Zhejiang/269/2020	12/2020	Zhejiang	pH1N1	pH1N1	pH1N1	H3	pH1N1	EA	pH1N1	TRIG	nH3N1
A/swine/Zhejiang/360/2020	12/2020	Zhejiang	pH1N1	pH1N1	pH1N1	H3	pH1N1	EA	pH1N1	TRIG	nH3N1

*EA, Eurasian; G, genotype; HA, hemagglutinin; M, matrix; NA, neuraminidase; NP, nucleoprotein; NS, nonstructural; pH1N1, 2009 pandemic influenza (H1N1); PA, polymerase acidic protein; PB1, polymerase basic protein 1; PB2, polymerase basic protein 2; TRIG, triple reassortant internal gene.

nucleoprotein (NP), matrix (M), and nonstructural (NS) genes, were remarkably diverse: EA H1N1, pH1N1, and TRIG (triple-reassortant internal gene) lineages (Appendix Figure). Among 6 EA H1N1 swine viruses, all internal gene segments were of EA H1N1 lineage. Among 26 reassortant EA H1N1 and H3N1 viruses, the PB2, PB1, PA, and NP genes all originated from the pH1N1 lineage; the M genes were mainly from both the pH1N1 and EA H1N1 lineages. Almost all NS genes originated from the TRIG lineage, but 2 originated from the pH1N1 lineage. On the basis of phylogenetic analyses of the 8 gene segments, including from HA and NA genes, we identified the viruses isolated in our study as G1 (n = 6), G2 (n = 2), G4 (n = 10), G5 (n = 8), and novel H3N1 (n = 6) viruses, according to the genotype classification existing at that time (*7*,*8*). We isolated viruses year-round to capture seasonal strains. Over the 36-month survey period, G1 viruses disappeared after 2018, G2 viruses were sporadically detected in 2018–2019, and G4 viruses, with an isolation rate of 1.0%, became a predominant genotype beginning in 2018. In our annual surveillance, we found another predominant virus genotype, G5, that had an isolation rate of 0.8%. These results suggest that the internal genes of the pH1N1 lineage had become predominant in contemporary swine IAVs among the pigs in the survey region.

Of note, in late 2020, we detected the H3N1 swine IAVs in 6 isolates (all from Zhejiang Province), indicating that this is a novel emerging recombinant genotype. Phylogenetic analyses demonstrated that the 6 novel H3N1 reassortant swine IAVs contained NA genes from the EA H1N1; PB2, PB1, PA, NP, and M genes from pH1N1; and NS genes from TRIG swine lineages. This combination is similar to the potentially pandemic G4 viruses except for the HA genes, suggesting that the emergence of novel H3N1 reassortant swine IAVs was a natural reassortant event that derived from G4 and H3N2 swine IAVs.

Conclusions

Because of their susceptibility to avian, swine, and human IAVs, pigs are regarded as a mixing vessel for generating novel reassortant influenza viruses capable of replicating and spreading among humans (*9*,*10*). Implications for human health reinforce the

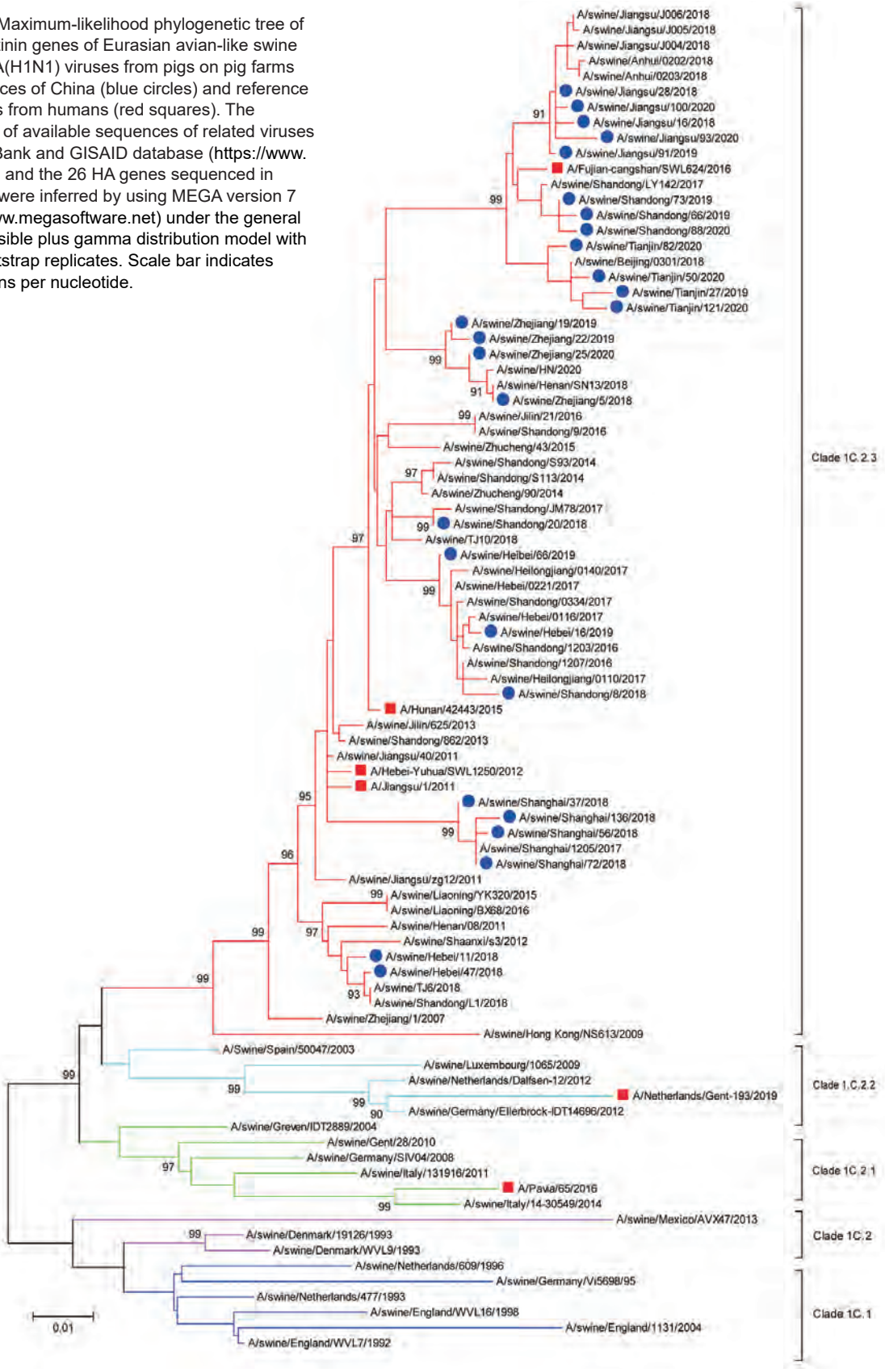

Figure 1. Maximum-likelihood phylogenetic tree of hemagglutinin genes of Eurasian avian-like swine influenza A(H1N1) viruses from pigs on pig farms in 6 provinces of China (blue circles) and reference sequences from humans (red squares). The phylogeny of available sequences of related viruses from GenBank and GISAID database (https://www.gisaid.org) and the 26 HA genes sequenced in this study were inferred by using MEGA version 7 (https://www.megasoftware.net) under the general time-reversible plus gamma distribution model with 1,000 bootstrap replicates. Scale bar indicates substitutions per nucleotide.

Figure 2. Maximum-likelihood phylogenetic tree of hemagglutinin genes of novel swine influenza A(H3N1) viruses from pigs on pig farms in 6 provinces of China (blue circles) and reference sequences from humans (red squares). The phylogeny of available sequences of related viruses from GenBank and GISAID database (https://www.gisaid.org) and the 6 HA genes sequenced in this study were inferred by using MEGA version 7 (https://www.megasoftware.net) under the general time-reversible plus gamma distribution model with 1,000 bootstrap replicates. Scale bar indicates substitutions per nucleotide.

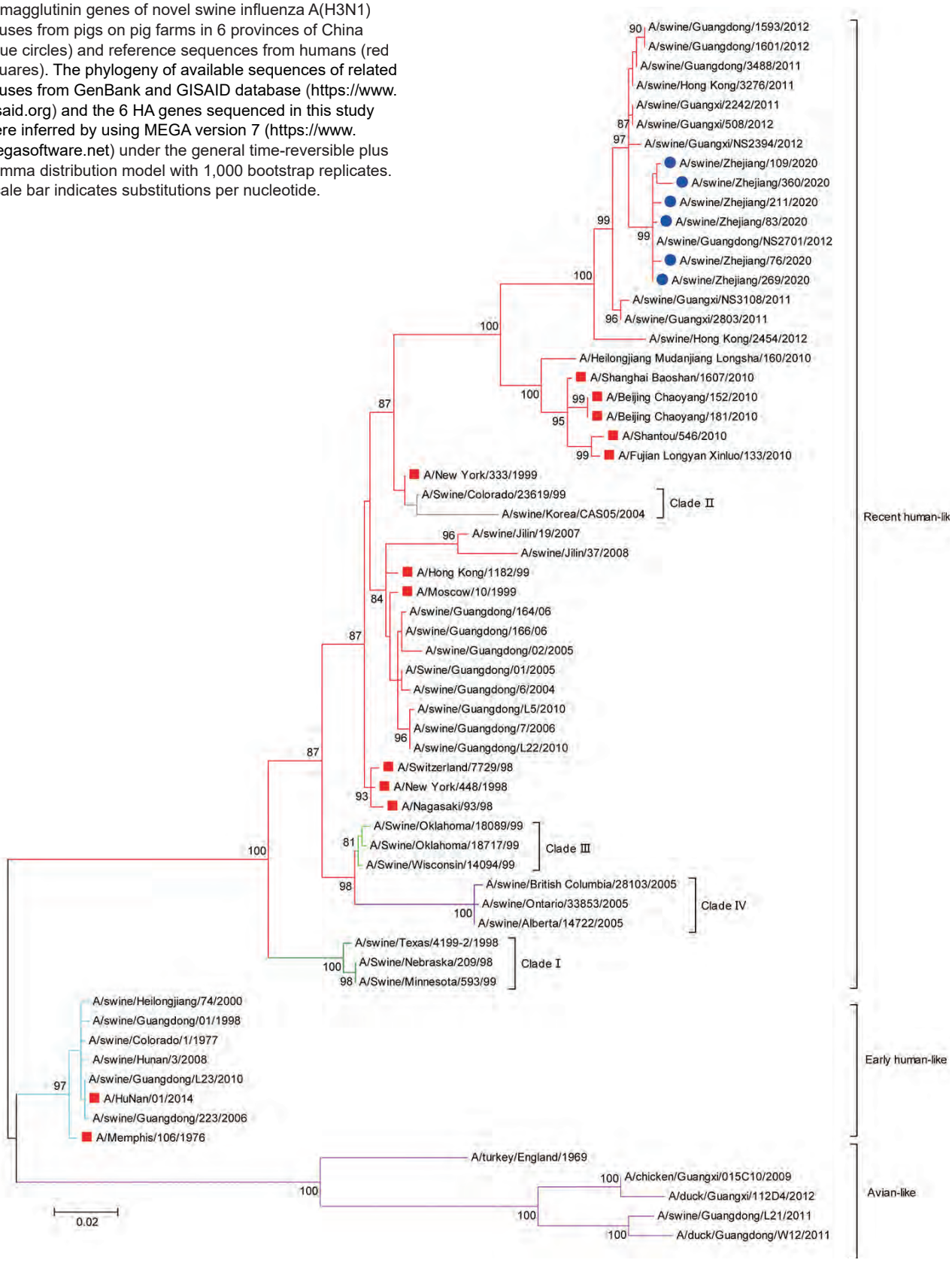

importance of continuous surveillance of swine IAVs in the pig population. China has the most varied swine influenza virus ecosystem in the world and different subtypes simultaneously circulate among pigs (*11*,*12*). The emergence of potentially pandemic G4 EA H1N1 virus has increased the chances of reassortment with enzootic swine IAVs and the subsequential emergence of novel reassortant swine IAVs.

We isolated 6 EA H1N1 swine viruses and 26 reassortant EA H1N1 and H3N1 swine viruses in this study. Analysis results indicated that the reassortment of gene segments between EA H1N1 swine viruses and other enzootic swine viruses occurred frequently, and the reassortant swine viruses became established among the sampled pig population. Previous studies have reported several cases of human disease from EA H1N1 swine IAV or its reassortant viruses in Europe and China (*13*–*15*).

Our study, based on swine epidemiologic data from China, demonstrates that EA H1N1 swine influenza virus and its reassortant viruses circulate in swine populations and pose potential threats to human health. Furthermore, we isolated and documented the genetic evolution of novel reassortant H3N1 viruses between potentially pandemic G4 EA H1N1 and H3N2 swine IAVs. These findings highlight the need for surveillance for novel H3N1 viruses in swine and human populations to enable early interventions to avert outbreaks and protect animal and human health.

This work was supported by grants from National Natural Science Foundation of China (31970175) and China Agriculture Research System of MOF and MARA (NYCYTX-009).

About the Author

Dr. Wang is a PhD student at the Shanghai Veterinary Research Institute, Chinese Academy of Agricultural Sciences, China. His primary research interests include the epidemiology and pathogenic mechanisms of influenza viruses.

References

1. Vijaykrishna D, Smith GJ, Pybus OG, Zhu H, Bhatt S, Poon LL, et al. Long-term evolution and transmission dynamics of swine influenza A virus. Nature. 2011;473:519–22. https://doi.org/10.1038/nature10004
2. Liu J, Bi Y, Qin K, Fu G, Yang J, Peng J, et al. Emergence of European avian influenza virus-like H1N1 swine influenza A viruses in China. J Clin Microbiol. 2009;47:2643–6. https://doi.org/10.1128/JCM.00262-09
3. Yang H, Chen Y, Qiao C, He X, Zhou H, Sun Y, et al. Prevalence, genetics, and transmissibility in ferrets of Eurasian avian-like H1N1 swine influenza viruses. Proc Natl Acad Sci U S A. 2016;113:392–7. https://doi.org/10.1073/pnas.1522643113
4. Liang H, Lam TT, Fan X, Chen X, Zeng Y, Zhou J, et al. Expansion of genotypic diversity and establishment of 2009 H1N1 pandemic-origin internal genes in pigs in China. J Virol. 2014;88:10864–74. https://doi.org/10.1128/JVI.01327-14
5. He P, Wang G, Mo Y, Yu Q, Xiao X, Yang W, et al. Novel triple-reassortant influenza viruses in pigs, Guangxi, China. Emerg Microbes Infect. 2018;7:85. https://doi.org/10.1038/s41426-018-0088-z
6. Zhu H, Zhou B, Fan X, Lam TT, Wang J, Chen A, et al. Novel reassortment of Eurasian avian-like and pandemic/2009 influenza viruses in swine: infectious potential for humans. J Virol. 2011;85:10432–9. https://doi.org/10.1128/JVI.05352-11
7. Sun YF, Wang XH, Li XL, Zhang L, Li HH, Lu C, et al. Novel triple-reassortant H1N1 swine influenza viruses in pigs in Tianjin, northern China. Vet Microbiol. 2016;183:85–91. https://doi.org/10.1016/j.vetmic.2015.12.006
8. Sun H, Xiao Y, Liu J, Wang D, Li F, Wang C, et al. Prevalent Eurasian avian-like H1N1 swine influenza virus with 2009 pandemic viral genes facilitating human infection. Proc Natl Acad Sci U S A. 2020;117:17204–10. [Erratum in Proc Natl Acad Sci U S A. 2020;117:23194] https://doi.org/10.1073/pnas.1921186117
9. Ito T, Couceiro JN, Kelm S, Baum LG, Krauss S, Castrucci MR, et al. Molecular basis for the generation in pigs of influenza A viruses with pandemic potential. J Virol. 1998;72:7367–73. PubMed https://doi.org/10.1128/JVI.72.9.7367-7373.1998
10. Ma W, Kahn RE, Richt JA. The pig as a mixing vessel for influenza viruses: human and veterinary implications. J Mol Genet Med. 2008;3:158–66.
11. Yu Y, Wu M, Cui X, Xu F, Wen F, Pan L, et al. Pathogenicity and transmissibility of current H3N2 swine influenza virus in southern China: a zoonotic potential. Transbound Emerg Dis. 2021:1–13. https://doi.org/10.1111/tbed.14190
12. Lam TT, Zhu H, Wang J, Smith DK, Holmes EC, Webster RG, et al. Reassortment events among swine influenza A viruses in China: implications for the origin of the 2009 influenza pandemic. J Virol. 2011;85:10279–85. https://doi.org/10.1128/JVI.05262-11
13. Parys A, Vandoorn E, King J, Graaf A, Pohlmann A, Beer M, et al. Human infection with Eurasian avian-like swine influenza A(H1N1) virus, the Netherlands, September 2019. Emerg Infect Dis. 2021;27:939–43. https://doi.org/10.3201/eid2703.201863
14. Li X, Guo L, Liu C, Cheng Y, Kong M, Yang L, et al. Human infection with a novel reassortant Eurasian-avian lineage swine H1N1 virus in northern China. Emerg Microbes Infect. 2019;8:1535–45. https://doi.org/10.1080/22221751.2019.1679611
15. Zhu W, Zhang H, Xiang X, Zhong L, Yang L, Guo J, et al. Reassortant Eurasian avian-like influenza A(H1N1) virus from a severely ill child, Hunan Province, China, 2015. Emerg Infect Dis. 2016;22:1930–6. https://doi.org/10.3201/eid2211.160181

Address for correspondence: Hai Yu, Shanghai Veterinary Research Institute, Chinese Academy of Agricultural Sciences, No.518, Ziyue Road, Minhang District, Shanghai 200241, China; email: haiyu_008@126.com

Determining Infected Aortic Aneurysm Treatment Using Focused Detection of *Helicobacter cinaedi*

Jien Saito, Emiko Rimbara, Shingo Inaguma, Chihiro Hasegawa, Shinji Kamiya, Akihiro Mizuno, Yoshiaki Sone, Tatsuhito Ogawa, Yukihide Numata, Satoru Takahashi, Miki Asano

We detected *Helicobacter cinaedi* in 4 of 10 patients with infected aortic aneurysms diagnosed using blood or tissue culture in Aichi, Japan, during September 2017–January 2021. Infected aortic aneurysms caused by *H. cinaedi* had a higher detection rate and better results after treatment than previously reported, without recurrent infection.

Infected aortic aneurysms account for 0.7%–3% of all aortic aneurysms and are associated with a 26%–44% mortality rate (*1*). No consensus exists about appropriate antimicrobial therapy and treatment duration for infected aneurysms. Moreover, determining surgical treatment in each case requires carefully considering the causative bacterium and the patient's medical background (*2*). Recently, several cases of infected aortic aneurysms caused by *Helicobacter cinaedi*, a rare, difficult-to-detect causative bacterium have been reported (*3*).

First identified in 1984, *H. cinaedi*, a gram-negative rod with spiral morphology and bipolar flagella, is indigenous to the intestinal tract of humans and other animals (*4*,*5*). This bacterium produces a cytolethal distending toxin that invades epithelial cells (*6*) and is associated with bacteremia in compromised hosts and infected aortic aneurysms, mediated by bacterial translocation from the intestinal mucosa (*7*,*8*). Because of the high recurrence rate for *H. cinaedi* bacteremia, it is recommended that patients receive prolonged treatment of at least 3 months with appropriate antimicrobial drugs (*9*). We sought to determine the efficacy of treatment for infected aortic aneurysms through the focused detection of *H. cinaedi*.

Author affiliation: Nagoya City University East Medical Center, Aichi, Japan (J. Saito, S. Inaguma, C. Hasegawa, S. Kamiya, A. Mizuno, Y. Sone, T. Ogawa, Y. Numata, M. Asano); National Institute of Infectious Diseases, Tokyo, Japan (E. Rimbara); Nagoya City University, Aichi (S. Takahashi)

DOI: https://doi.org/10.3201/eid2807.212505

The Study

During September 2017–January 2021, we treated 10 patients with infected aortic aneurysms from a single center in Aichi, Japan. Diagnosis, including for recurrent aneurysms, was based on either positive culture or PCR of aortic tissue resected at the time of surgery or positive blood or puncture culture of an abscess caused by a hematogenous infection in patients who did not undergo open surgery and had clinical findings localized to the aortic aneurysm.

We started patients on antimicrobial therapy with meropenem when *H. cinaedi* was suspected or gram-negative rods were identified, then changed to sulbactam/ampicillin after confirming drug sensitivity. After 4 weeks of treatment or a negative inflammatory reaction, the antimicrobial treatment was switched to minocycline or amoxicillin/clavulanate for 3–6 months. If other causative bacteria were identified, antimicrobial drugs were changed based on drug sensitivity results and continued for 3–6 months. Rifampin-soaked graft replacement was the first-choice surgical treatment, irrespective of causative bacterium.

Among the 10 patients with infected aortic aneurysms, *H. cinaedi* was the causative bacterium in 4, *Staphylococcus aureus* in 3, *Salmonella enterica* serovar Enteritidis in 1, and *Enterobacter cloacae* in 1. Treatment included vascular replacement in 7 patients (2 with *H. cinaedi*), endovascular stent grafting in 1 (with *H. cinaedi*), and medical treatment in 2 patients (1 with *H. cinaedi*). One patient with aortic rupture and *Salmonella* Enteritidis infection died postoperatively from multiorgan failure; the other 9 patients had good courses of recovery without recurrence (Table 1).

Table 1. Demographic and clinical variables of 10 patients with infected aortic aneurysms with or without *Helicobacter cinaedi*, Aichi, Japan, September 2017–January 2021*

Variables	Total, n = 10	*H. cinaedi*, n = 4	Non–*H. cinaedi*, n = 6
Age, median (IQR)	77 (70.5–83.0)	77.5 (70.0–84.3)	77 (71.0–82.3)
Sex			
M	8	3	5
F	2	1	1
Comorbidity			
Diabetes mellitus	3	2	1
Chronic kidney disease	1	1	0
Cancer	2	1	1
Steroid use	1	0	1
Sign or symptom			
Pain	8	3	5
Fever	7	3	4
Shock	1	0	1
Laboratory findings, median (IQR)			
Leukocytes, $\times 10^3$ cells/μL	9.6 (8.8–11.0)	8.4 (7.4–9.5)	1.1 (9.5–17.2)
C-reactive protein, mg/dL	7.6 (5.1–22.1)	4.3 (3.8–5.1)	21.6 (11.0–23.6)
Procalcitonin, ng/dL	0.19 (0.05–0.76)	0.14 (0.04–0.38)	0.38 (0.08–1.53)
Aneurysm diameter, mm, median (IQR)	40.5 (32.8–44.8)	32.5 (25.5–39.8)	44.5 (37.3–55.5)
Aneurysm location			
Thoracic aorta	1	1	0
Thoracoabdominal aorta	1	0	1
Abdominal aorta	8	3	5
Aneurysm form			
Saccular	7	4	3
Fusiform	3	0	3
Rupture	3	0	3
Aortoduodenal fistula	2	0	2
Surgery			
Emergency	3	0	3
Urgent	2	1	1
Elective	5	3	2
Endovascular	1	1	0
Nonsurgical treatment only	2	1	1
Death	1	0	1

*IQR, interquartile range.

All 4 of the *H. cinaedi*–infected case-patients were immunocompromised (diabetes mellitus, chronic kidney disease, cancer). However, their clinical findings were mild, and C-reactive protein levels tended to be low (*H. cinaedi*/non–*H. cinaedi* median 4.3/21.6 mg/dL) at hospital admission. All patients had saccular aneurysms and severely calcified aortas. Surgical findings showed highly adherent areas around the aneurysms with intimal defects but without abscess formation. Pathological examination revealed severe lymphocytic infiltration in the aneurysmal wall with loss of elastic fibers. In contrast, 3 of 5 patients in the non–*H. cinaedi* group showed abscesses and hematomas around the infections (Figure 1).

We performed blood cultures using the BacT/Alert system (bioMérieux, https://www.biomerieux.com) and grew microaerobic cultures in the presence of hydrogen using a commercial hydrogen generator (SUGIYAMA-GEN Co., Ltd., http://sugiyama-gen.com). In the *H. cinaedi* group, we used multilocus sequence typing (MLST) to identify the subtype, and we immunostained aortic tissues with antiserum against the whole-cell lysate of *H. cinaedi* raised in rabbits (Figure 2) (*10*).

Among the *H. cinaedi* patients, we were able to subculture isolates from 3; the range of blood culture growth times, 75.3–160.8 h (median 90.6 h), was longer than that among the non–*H. cinaedi* patients, 12.3–28.3 h (median 12.3 h). Drug susceptibility testing demonstrated levofloxacin-resistant *H. cinaedi*, although the sequence type on MLST was different in each case (Tables 1, 2).

Conclusions

Infected aortic aneurysms caused by *H. cinaedi* are increasingly being recognized, especially in Japan, although the detection rate remains low (*3*). One study reported 734 cases of infected aortic aneurysms caused by various organisms, including *Salmonella*, *Staphylococcus*, *Streptococcus*, and *Escherichia coli*, but not *H. cinaedi* (*1*). Infected aortic aneurysms are a critical disease with high mortality, and whereas identifying the causative bacteria is effective in determining treatment, 23.3%–25% of cases are caused by

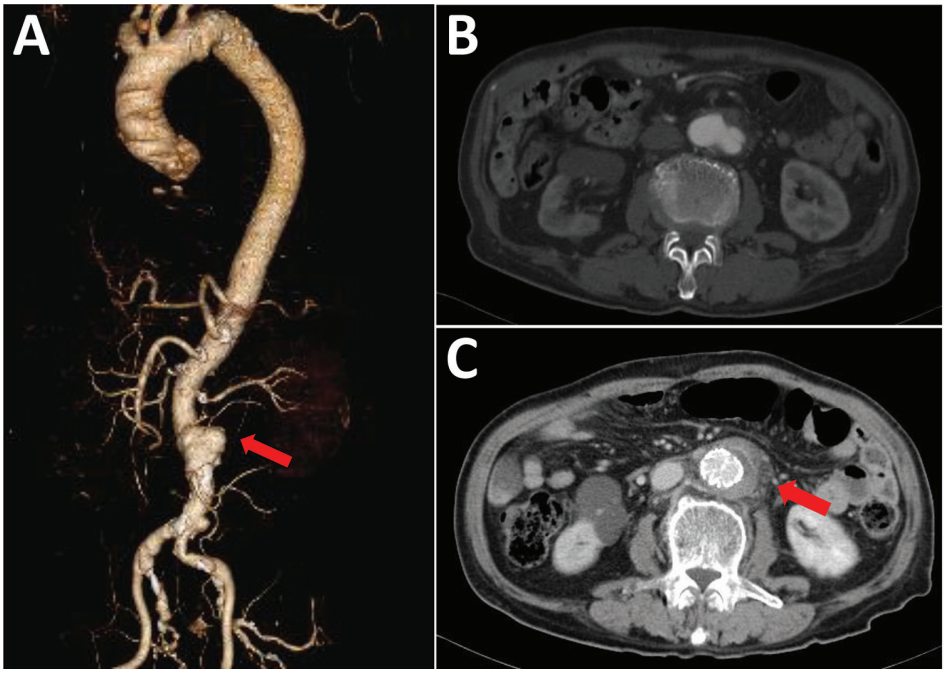

Figure 1. Contrast-enhanced computed tomography imaging for Case-patient 3 in the *Helicobacter cinaedi* group of 10 patients with infected aortic aneurysms with or without *H. cinaedi*, Aichi, Japan, September 2017–January 2021. A, B) The infrarenal aortic aneurysm had a maximum short diameter of 39 mm and a cystic protrusion of 19 mm (arrow in panel A) before the operation. C) After the operation, the adipose tissue concentration increased around the aneurysm (arrow).

unidentified bacteria (*1*). In our study, the detection rate for *H. cinaedi* in infected aortic aneurysms was high, 40%, although the absolute number of cases was small. Of note, infections caused by *H. cinaedi* all showed good clinical courses. *H. cinaedi* is known to cause nosocomial infections; however, nosocomial

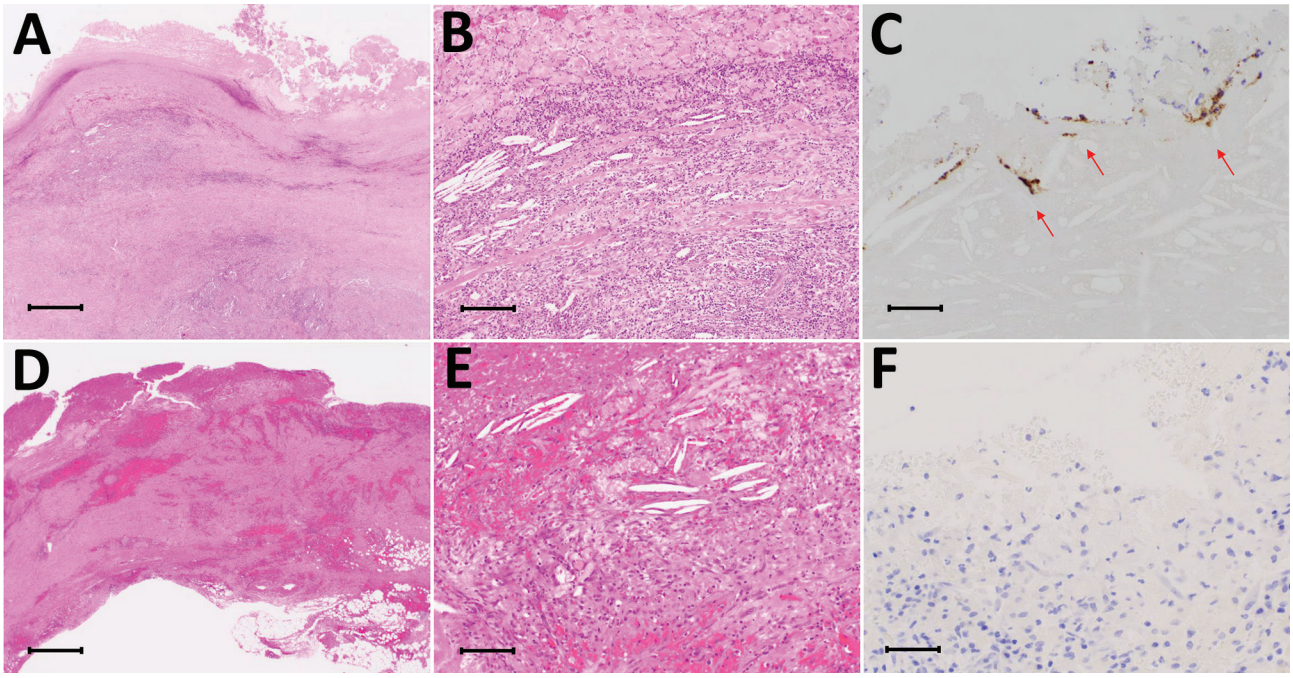

Figure 2. Comparison of images from patients in the *Helicobacter cinaedi* group with patients from the non–*H. cinaedi* group among 10 patients with infected aortic aneurysms with or without *H. cinaedi*, Aichi, Japan, September 2017–January 2021. Immunohistochemistry was performed on the whole cell lysates of *H. cinaedi* strain MRY08-1234 isolated from immunocompromised patients in Japan by raising anti–rabbit *H. cinaedi* IgG. One of 2 case-patients with resected tissue in the *H. cinaedi* group had positive immunostaining (patient 1). A–C) Case-patient 1 in the *H. cinaedi* group. D–F) Case-patient 4 in the non–*H. cinaedi* group. In images from both patients, lymphocyte and neutrophil infiltrates, cholesterol clefts, foam cells, plasma cells, foreign body giant cells, and hemosiderin deposition are visible (A, B, D, E; hematoxylin & eosin). Immunohistochemistry stain shows of *H. cinaedi* organisms in the aortic intima (arrow in C) and negative results (F). Scale bars: 1,000 μm in A, D; 100 μm in B, E; 50 μm in C, F.

Table 2. Bacteriological examination, method of treatment, and outcomes for 10 patients with infected aortic aneurysms with or without *Helicobacter cinaedi*, Aichi, Japan, September 2017–January 2021*

Patient no.	Age, y/sex	Location	Blood cultures	ID	Comorbidity	Procedure‡	Antimicrobial use period	Outcome
H. cinaedi group, n = 4†								
1	72/M	Aortic arch	75.3/negative	ST6	DM	TAR (positive)	6 mo	Survival at 4 y
2	64/F	Right common iliac	Negative	Unknown	DM	Y graft (negative)	6 mo	Survival at 3 y
3	83/M	Infrarenal aorta	86.5/160.8	ST18	Malignant lymphoma	EVAR (NA)	6 mo	Survival at 2 y
4	88/M	Infrarenal aorta	90.6/93.0	ST21	CKD	Medical treatment only (NA)	3 mo	Survival at 1 y
Non–*H. cinaedi* group, n = 6§								
1	70/M	Infrarenal aorta	Negative	MSSA	None	Y graft	6 mo	Survival at 4 y
2	74/M	Infrarenal aorta	Negative	*Listeria monocytogenes*	None	Y graft	6 mo	Survival at 4 y
3	67/M	Infrarenal aorta	12.6/12.6	*Enterobacter cloacae*	AEF	Y graft	6 mo	Survival at 3 y
4	83/M	Infrarenal aorta	12.3/12.3	MSSA	DM	Y graft	3 mo	Survival at 3 y
5	86/F	Thoracoabdominal aorta	Negative	MSSA	None	Medical treatment only	3 mo	Survival at 1 y
6	80/M	Infrarenal aorta	28.3/28.3	*Salmonella enteritidis*	None	Y graft	Until death	Death at POD 5

*DM, diabetes mellitus; CKD, chronic kidney disease; TAR, total arch replacement; EVAR, endovascular aortic repair; NA, not applicable; MSSA, methicillin-susceptible *Staphylococcus aureus*; AEF, aorto-enteric fistula; POD, postoperative day; ST, sequence type.
†16S RNA results were positive for all patients.
‡Y graft replacement for abdominal aortic aneurysm.
§Tissue culture results for all patients returned in 1 d; patient 5 had an abscess.

infections were ruled out as mode of infection here because the 3 isolates that underwent MLST had different sequence types (*11*).

The Bactec FX system (https://www.bd.com), widely used for blood culturing of *H. cinaedi*, is generally considered to be more sensitive than the bioMérieux BacT/Alert system (*8*). Nevertheless, by assuming *H. cinaedi* was the causative bacterium of the infected aortic aneurysms for our patients and simply allowing a longer incubation period of 10 days versus the usual 5 days, the BacT/Alert system detected the bacterium in 3/4 cases, comparable to the Bactec FX system (*12*). It is sometimes difficult to grow bacterial subcultures in microaerophilic conditions; however, adding 5%–10% hydrogen effectively helps form characteristic thin-spread colonies (*4*). PCR reliably detects and identifies species, but matrix-assisted laser desorption/ionization time-of-flight mass spectrometry is also useful (*13*), although unfortunately this testing method results in a time lag between initiating treatment on and identifying bacteria.

H. cinaedi infects atherosclerotic sites, leading to the progression of atherosclerosis through lipid accumulation (*5*,*14*). Progression is slow, often taking months, and leads to no clinical findings even if a local infection is established (*7*,*15*). Considering the slow, localized progression and difficulty of detection of atherosclerosis associated with *H. cinaedi* infection, aortic aneurysms thought to be noninfectious might actually be infected by *H. cinaedi*. Clarifying the relationship between this bacterium and atherosclerotic diseases might lead to additional treatments.

No infected aortic aneurysms caused by *H. cinaedi* have resulted in rupture, and cases usually pass without recurrence following an appropriate period of antibiotic treatment. Because nonsurgical treatment has been shown to be effective, open surgery during the acute phase of infection might be overindicated. Endovascular stent grafting, a less invasive treatment than the standard vascular replacement procedure, followed by use of appropriate antimicrobial agents might successfully complete treatment (*3*). This treatment is beneficial among aging patients, and it is hoped that the presence of these bacteria in infected aortic aneurysms will be widely recognized, with treatment and diagnosis proceeding simultaneously.

In summary, although *H. cinaedi* is a relatively rare cause of infected aortic aneurysms, it might be overlooked because of its low initial detection rate. Detection during treatment initiation can improve patient life expectancy by enabling effective antimicrobial therapy and expanding treatment options.

Acknowledgments

We thank M. Asano for the useful discussions and careful proofreading of the manuscript and Tuge Kaori, Okaniwa Izumi, and Tsukamoto Haruka for helping us cultivate the bacteria. We also thank Editage for English language editing.

This work was supported by Japan Society for the Promotion of Science Grants-in-Aid for Scientific Research (KAKENHI) grant no. JP16K18928 and Japan Agency for Medical Research and Development (AMED) under grant no. JP20fk0108148j0001.

About the Author

Dr. Saito is a researcher in the Department of Cardiovascular Surgery at Nagoya City University. His main research interests include *Helicobacter cinaedi* infections and arteriosclerosis.

References

1. Sörelius K, Budtz-Lilly J, Mani K, Wanhainen A. Systematic review of the management of mycotic aortic aneurysms. Eur J Vasc Endovasc Surg. 2019;58:426–35. https://doi.org/10.1016/j.ejvs.2019.05.004
2. Lee CH, Hsieh HC, Ko PJ, Li HJ, Kao TC, Yu SY. In situ versus extra-anatomic reconstruction for primary infected infrarenal abdominal aortic aneurysms. J Vasc Surg. 2011;54:64–70. https://doi.org/10.1016/j.jvs.2010.12.032
3. Matsuo T, Mori N, Mizuno A, Sakurai A, Kawai F, Starkey J, et al. Infected aortic aneurysm caused by *Helicobacter cinaedi*: case series and systematic review of the literature. BMC Infect Dis. 2020;20:854. https://doi.org/10.1186/s12879-020-05582-7
4. Fennell CL, Totten PA, Quinn TC, Patton DL, Holmes KK, Stamm WE. Characterization of *Campylobacter*-like organisms isolated from homosexual men. J Infect Dis. 1984;149:58–66. https://doi.org/10.1093/infdis/149.1.58
5. Kawamura Y, Tomida J, Morita Y, Fujii S, Okamoto T, Akaike T. Clinical and bacteriological characteristics of *Helicobacter cinaedi* infection. J Infect Chemother. 2014;20:517–26. https://doi.org/10.1016/j.jiac.2014.06.007
6. Taylor NS, Ge Z, Shen Z, Dewhirst FE, Fox JG. Cytolethal distending toxin: a potential virulence factor for *Helicobacter cinaedi*. J Infect Dis. 2003;188:1892–7. https://doi.org/10.1086/379837
7. Kushimoto K, Yonekura R, Umesue M, Oshiro Y, Yamasaki H, Yoshida K, et al. Infected thoracic aortic aneurysm caused by *Helicobacter cinaedi*. Ann Vasc Dis. 2017;10:139–42. https://doi.org/10.3400/avd.cr.16-00126
8. Araoka H, Baba M, Okada C, Kimura M, Sato T, Yatomi Y, et al. First evidence of bacterial translocation from the intestinal tract as a route of *Helicobacter cinaedi* bacteremia. Helicobacter. 2018;23:e12458. https://doi.org/10.1111/hel.12458
9. Araoka H, Baba M, Kimura M, Abe M, Inagawa H, Yoneyama A. Clinical characteristics of bacteremia caused by *Helicobacter cinaedi* and time required for blood cultures to become positive. J Clin Microbiol. 2014;52:1519–22. https://doi.org/10.1128/JCM.00265-14
10. Rimbara E, Mori S, Matsui M, Suzuki S, Wachino J, Kawamura Y, et al. Molecular epidemiologic analysis and antimicrobial resistance of *Helicobacter cinaedi* isolated from seven hospitals in Japan. J Clin Microbiol. 2012;50:2553–60. https://doi.org/10.1128/JCM.06810-11
11. Rimbara E, Mori S, Kim H, Matsui M, Suzuki S, Takahashi S, et al. *Helicobacter cinaedi* and *Helicobacter fennelliae* transmission in a hospital from 2008 to 2012. J Clin Microbiol. 2013;51:2439–42. https://doi.org/10.1128/JCM.01035-13
12. Miyake N, Chong Y, Nishida R, Nagasaki Y, Kibe Y, Kiyosuke M, et al. A dramatic increase in the positive blood culture rates of *Helicobacter cinaedi*: the evidence of differential detection abilities between the Bactec and BacT/Alert systems. Diagn Microbiol Infect Dis. 2015;83:232–3. https://doi.org/10.1016/j.diagmicrobio.2015.07.017
13. Taniguchi T, Sekiya A, Higa M, Saeki Y, Umeki K, Okayama A, et al. Rapid identification and subtyping of *Helicobacter cinaedi* strains by intact-cell mass spectrometry profiling with the use of matrix-assisted laser desorption ionization-time of flight mass spectrometry. J Clin Microbiol. 2014;52:95–102. https://doi.org/10.1128/JCM.01798-13
14. Khan S, Okamoto T, Enomoto K, Sakashita N, Oyama K, Fujii S, et al. Potential association of *Helicobacter cinaedi* with atrial arrhythmias and atherosclerosis. Microbiol Immunol. 2012;56:145–54. https://doi.org/10.1111/j.1348-0421.2012.00421.x
15. Oyama K, Khan S, Okamoto T, Fujii S, Ono K, Matsunaga T, et al. Identification of and screening for human *Helicobacter cinaedi* infections and carriers via nested PCR. J Clin Microbiol. 2012;50:3893–900. https://doi.org/10.1128/JCM.01622-12

Address for correspondence: Jien Saito, Department of Cardiovascular Surgery, Nagoya City University East Medical Center, 1-2-23 Wakamizu, Chikusa-ku, Nagoya, Aichi, 464-8547, Japan; email: jien36@icloud.com

Who is this person?

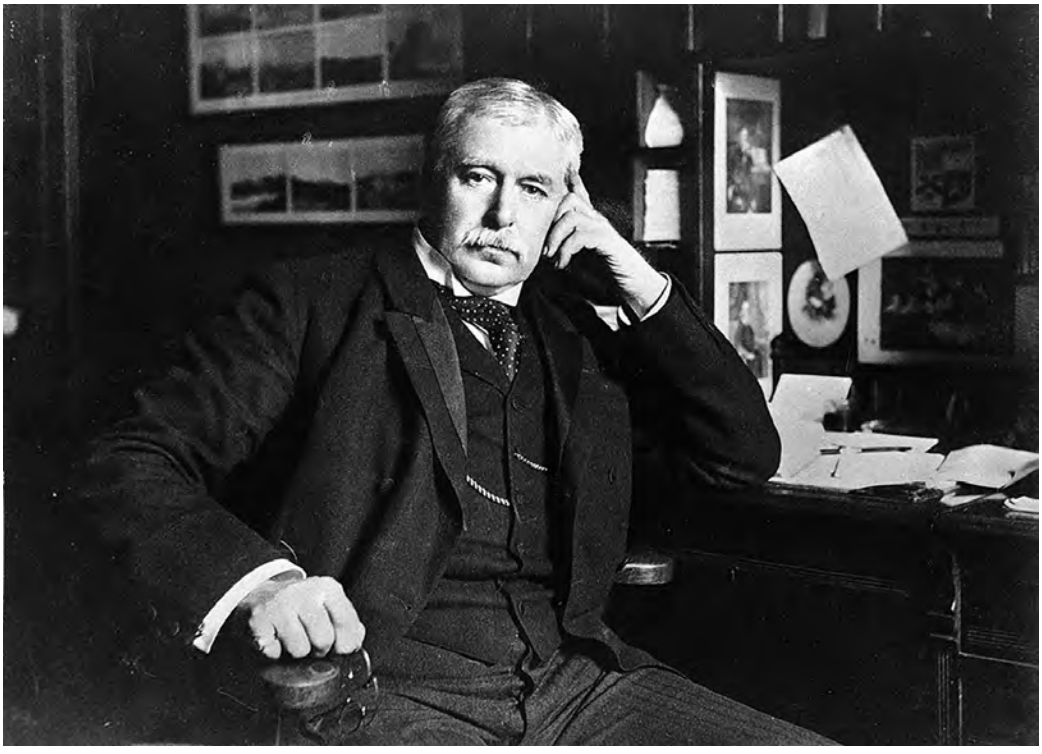

Here is a clue: He first described the filarial parasite *Mansonella ozzardi* in 1897.

A) Sir Patrick Manson
B) George Carmichael Low
C) Albert Tronson Ozzard
D) Joseph Bancroft
E) Thomas Lane Bancroft

See next page for the answer.

Sir Patrick Manson

James Lee Crainey, Uziel Ferreira Suwa, Sérgio Luiz Bessa Luz

Working in the port of Amoy (now known as the port of Xiamen), China (*1*–*5*), Sir Patrick Manson noted that *Wuchereria bancrofti* microfilariae appeared with marked periodicity in the blood of infected persons and that they developed inside blood-fed mosquitoes (*1*–*4*) (https://era.ed.ac.uk/bitstream/handle/1842/28457/LowGC_1910redux.pdf). Although Manson did not initially think that mosquito bites were the mode by which these parasites were transmitted, his study was revolutionary because it was the first to show that insects play a role in infectious disease transmission (*1*–*4*) (https://era.ed.ac.uk/bitstream/handle/1842/28457/LowGC_1910redux.pdf). In the ≈150 years since Manson's observation, millions of lives and disability-adjusted life-years have been saved by interventions developed to control vectorborne diseases, nearly all of which can in some way or another trace their provenance to his discovery (*5*). Manson's effect on the field of global health research is, however, by no means limited to the legacy of his research discoveries and by no means entirely uncontroversial (*1*–*3*,*6*).

At the International Congress of Medicine, held in London in August 1913, Sir Patrick Manson was awarded a gold medal and commemorative plaque in recognition of his contributions to the field of tropical medicine (*1*). As French Professor Raphaël Blanchard, who had the medal designed and struck, presented the awards, he described Manson as the "father of tropical medicine" (*1*). Although global health researchers today increasingly recognize that Manson was deeply complicit in the colonization of global health, there are still many good reasons why Blanchard's "father of tropical medicine" sobriquet has managed to stick (*1*–*3*,*6*).

In addition to his role in creating medical schools and societies in Hong Kong, where he lived and worked early in his professional career, Manson successfully persuaded his own national government of its need to invest in tropical disease research and training infrastructure within Britain for the health and prosperity of its wider empire (*1*–*3*,*6*). As a medical adviser to the colonial office, Manson successfully advocated for creating the Royal Society of Tropical Medicine (RSTM) and the foundation of the London School of Hygiene and Tropical Medicine (LSHTM) and the Liverpool School of Tropical Medicine (LSTM), which both remain in operation to this day (*1*–*3*,*6*). In fact, the LSTM and LSTHM are now widely regarded as being among the world's most prestigious tropical medicine research institutes. Although the RSTM does not command the same level of authority it once did, it still exerts influence over the field of tropical disease research through its various house journals, grant schemes, prizes, and prominent presidents (https://rstmh.org) (*1*–*3*,*6*).

Through teaching and mentoring staff and students inside and outside of these institutes, Manson also effected the direction of scientific inquiry that followed his own (*1*–*3*). By showing that mosquitoes can inoculate people with malaria and filarial parasites, Sir Ronald Ross, George Carmichael Low, and Thomas Lane Bancroft played critical roles in advancing Manson's vector research (*1*–*3*,*6*). Although these men are now all regarded as accomplished scientists in their own right, there is no doubt that all 3 benefited greatly from Manson's mentorship and support (*1*–*3*,*6*). Manson's guide to tropical medicine, which he wrote and updated 6 times during his lifetime, is arguably, however, a more valuable and lasting contribution to research training than was his mentoring. First published in 1897, and then for over a century edited by some of the field's most eminent research scientists, *Manson's Tropical Disease* is now in its 23rd edition and continues to be among the most authoritative tropical medicine reference textbooks for students, researchers, and practitioners (*7*).

This book title is, however, not the only surviving tribute to Manson's name; several parasites, disease vectors, and diseases are named after him (*7*–*9*). In homage to Manson, when Ernest Carroll Faust

Author affiliation: Fundação Oswaldo Cruz Amazônia, Manaus, Brazil

DOI: https://doi.org/10.3201/eid2807.210818

created the *Mansonella* genus in 1929 and classified *M. ozzardi* within it, he also proposed that the human disease it causes should be named mansonelliasis (*8*). After a series of taxonomic revisions in the 1980s, 2 more filarial parasites of humans (*M. perstans* and *M. streptocerca*) were placed within the *Mansonella* genus; thus, today the terms mansonelliasis and mansonellosis are both commonly used to describe the microfilaremic disease caused by any of these 3 filarial parasites (*9*).

At Blachard's suggestion, when Manson first described *M. ozzardi*, he decided to name it after the French surgeon Jean Nicolas Demarquay (*10*). This naming seemed a fitting tribute for Manson to make to the man who first discovered the parasite he had used to make his name (*Wuchereria bancrofti*) but whose discovery was not initially recognized by the international research community (*1*,*2*) (https://era.ed.ac.uk/bitstream/handle/1842/28457/LowGC_1910redux.pdf). Manson's homage would, however, not endure because when he first described *M. ozzardi*, he used the name *Filaria demarquayi* to describe parasites from the Caribbean and the name *Filaria ozzardi* to describe parasites from Guyana (*10*). Although the question of whether parasites from the Caribbean and *M. ozzardi* parasites from mainland South America should be regarded as separate species remained controversial until their DNA was comparted more than a century later (*11*), Manson would eventually conclude (correctly) that both were of the same species and that *F. demarquayi* should be treated as a synonym for *F. ozzardi* (*12*).

Manson's decision to synonymize *F. demarquayi* was surprising because he had made clear in his original description of the species that he had found Caribbean *F. demarquayi* parasites several years before he had seen the Guyana parasites and because a report of Manson's discovery of *F. demarquayi* parasites had also been published in the Proceedings of the Academy of Natural Sciences of Philadelphia before his British Medical Journal publication (*12*,*13*). The name *F. demarquayi* thus seemed to have primacy by most standard nomenclature protocols. However, when erecting the *Mansonella* genus, Faust followed Manson's synonymization proposal, arguing that the *F. demarquayi* species name had already been used to describe a dubious filarial parasite species in 1892 and was thus unavailable as a name for Manson's parasites (*8*).

The contemporary name for the parasite species, *Mansonella ozzardi*, thus pays homage to Manson and to an industrious colonial medical officer from present-day Guyana, Albert Tronson Ozzard, who had only a limited role in the parasite's description (*8*,*10*,*14*). With modern researchers and research institutions, including those that Manson founded, increasingly recognizing the need for the decolonization of global health, it is thus tempting to suggest that changing the name of a New World parasite species, whose contemporary name pays homage to 2 British colonial servants and does not obey conventional nomenclature protocols, could contribute to such a process (*6*,*8*,*14*). The distribution of mansonellosis seems to be restricted to poor regions of Latin America, the Caribbean, and Africa, where Manson never set foot (*3*,*9*). Given all this and the fact that *M. perstans*, like onchocerciasis, most likely arrived in Latin America because of slavery, an argument can thus be made that changing the name of mansonellosis could also contribute to the decolonization process (*15*).

Presently, there are no specific disease burden estimates for mansonellosis, and only mild symptoms (e.g., joint pains, chills, headaches, corneal lesions) have been robustly linked to it (*9*). Perhaps after more is known about mansonellosis, it will be time for it to have a name that reflects its public health burden rather than a name that pays tribute to the colonial father of tropical disease, Sir Patrick Manson.

About the Author

Dr. Crainey is a productivity research fellow at the Brazilian National Council for Scientific and Technological Development and a public servant for the Brazilian Ministry of Health, working as a "Pesquisador em Saúde Pública" (public health researcher) at the Fundação Oswaldo Cruz "Instituto Leônidas e Maria Deane" in Manaus, Brazil. His research is focused on the public health significance of filarial parasites and vectors in the Amazon region.

References

1. McGregor IA. Royal Society of Tropical Medicine and Hygiene Meeting at Manson House, London, 3 October 1994. The third Manson oration. Patrick Manson 1844–1922: the birth of the science of tropical medicine. Trans R Soc Trop Med Hyg. 1995;89:1–8. https://doi.org/10.1016/0035-9203(95)90636-3
2. To KKW, Yuen KY. In memory of Patrick Manson, founding father of tropical medicine and the discovery of vector-borne infections. Emerg Microbes Infect. 2012;1:e31. https://doi.org/10.1038/emi.2012.32
3. Haynes DM. Framing tropical disease in London: Patrick Manson, *Filaria perstans*, and the Uganda sleeping sickness epidemic, 1891–1902. Soc Hist Med. 2000;13:467–93. https://doi.org/10.1093/shm/13.3.467
4. Manson P. On the development of *Filaria sanguis hominis* and on the mosquito considered as a nurse. [zoology]. The Linnean Society Journal. 1878;14:304–11.

5. Wilson AL, Courtenay O, Kelly-Hope LA, Scott TW, Takken W, Torr SJ, et al. The importance of vector control for the control and elimination of vector-borne diseases. PLoS Negl Trop Dis. 2020;14:e0007831. https://doi.org/10.1371/journal.pntd.0007831
6. Cranna V, Hirsch L. Decolonising the London School of Hygiene & Tropical Medicine's Archives Service. Archit Rec. 2021;42:248–65. https://doi.org/10.1080/23257962.2021.1993806
7. Farrar J, Hotez P, Junghanss T, Kang G, Lalloo D, White N. Manson's tropical diseases. 23rd ed. London: Saunders Ltd.; 2013. p. 1360.
8. Faust EC. Human helminthology; a manual for clinicians, sanitarians and medical zoologists. Philadelphia: Lea and Febiger; 1929. p. 616.
9. Ta-Tang TH, Crainey JL, Post RJ, Luz SL, Rubio JM. Mansonellosis: current perspectives. Res Rep Trop Med. 2018;18;9:9–24. https://doi.org/10.2147/RRTM.S125750
10. Manson P. On certain new species of nematode haematozoa occurring in America. BMJ. 1897;2:1837–8.
11. Crainey JL, Marín MA, Silva TRRD, de Medeiros JF, Pessoa FAC, Santos YV, et al. *Mansonella ozzardi* mitogenome and pseudogene characterisation provides new perspectives on filarial parasite systematics and CO-1 barcoding. Sci Rep. 2018;8:6158. https://doi.org/10.1038/s41598-018-24382-3
12. Manson P. Tropical disease: a manual of diseases of warm climates. 6th ed. London: Cassell and Company Limited; 1917. p. 968.
13. Henry FP. Remarks on filaria. Proc Acad Nat Sci Philadelphia. 1896:271–5.
14. Anonymous. Dr. Albert Tronson Ozzard. BMJ. 1929;1:483–4. https://doi.org/10.1136/bmj.1.3557.483-a
15. Tavares da Silva L, Crainey J, Ribeiro da Silva T, Suwa U, Vicente A, Fernandes de Medeiros J, et al. Molecular verification of New World *Mansonella perstans* parasitemias. Emerg Infect Dis. 2017;23:545–7. https://doi.org/10.3201/eid2303.161159

Address for correspondence: James Lee Crainey, Instituto Leônidas e Maria Deane, Fundação Oswaldo Cruz (Fiocruz), 476 Rua Terezina, Adrianópolis, Manaus, Amazonas, Brazil; email: james.lee@fiocruz.br, lee.crainey@gmail.com

Emerging from an Isolation Cocoon, 2022

Ron Louie

"The caterpillar does all the work but the butterfly gets all the publicity."
—Attributed to George Carlin

The security layers started peeling away, seemingly too soon.
Once constricting, every movement and moment a struggle,
who would guess that the loosening would be so worrying?

Preposterous miracles had manifested themselves, albeit
imperfectly; so one emerges, reviving afresh in the sunlight, imbibing
the unmasked scents, even as the serial-killing fiend remains free.

A *kaleidoscope* of butterflies is what one calls a mass fluttering;
that term could well apply to humans here, self-identifying their
unique variants and varieties of existence, behaviors, and beliefs.

The excess of loss has been unthinkable, and not to be forgotten.
Preventive interventions were knowingly imprecise; lacking their own
protections, from denials, was another hazard for the republic's health.

Poets have long lyricized ideal truth, but the pandemic taught
how fragile truth can be, the fragile beauty of a glistening bubble,
buffeted almost to bursting by a cacophony of ravenous twittering.

Yet one can now stretch out shimmering wings, so to speak,
with the brash confidence befitting a monarch, fully expecting
to start a new cycle in life, despite the circling shadows overhead.

About the Author

Dr. Louie is a clinical professor of Pediatrics, Hematology-Oncology, at the University of Washington, Seattle. He is interested in medical epistemology and blogs about dementia and caregiving with that perspective. He previously published the poem Isolation Cocoon, May 2020—After Zhuangzi's Butterfly Dream (https://wwwnc.cdc.gov/eid/article/26/11/20-2993_article).

Address for correspondence: Ron Louie, UW Department of Pediatrics, 4800 Sand Point Way NE, Seattle, WA 98199, USA; email: ronlouie@uw.edu

Author affiliation: University of Washington, Seattle, Washington, USA

DOI: https://doi.org/10.3201/eid2807.220488

Bagaza Virus in Wild Birds, Portugal, 2021

João Queirós, Sílvia C. Barros, Alberto Sánchez-Cano, Ana Margarida Henriques, Teresa Fagulha, Fábio Abade dos Santos, Margarida D. Duarte, Catarina Fontoura-Gonçalves, David Gonçalves, Marisa Rodrigues, Teresa Cardona Cabrera, Isabel G. Fernández de Mera, Christian Gortazar, Ursula Höfle, Paulo Célio Alves

Author affiliations: Universidade do Porto Centro de Investigação em Biodiversidade e Recursos Genéticos, Vairão, Portugal (J. Queirós, C. Fontoura-Gonçalves, D. Gonçalves, M. Rodrigues, P.C. Alves); Estação Biológica de Mértola, Mértola, Portugal (J. Queirós, D. Gonçalves, M. Rodrigues, P.C. Alves); Universidade do Porto, Porto, Portugal (J. Queirós, D. Gonçalves, P.C. Alves); Instituto Nacional de Investigação Agrária e Veterinária, Oeiras, Portugal (S.C. Barros, A.M. Henriques, T. Fagulha, F.A. Abade dos Santos, M.D. Duarte); Instituto de Investigación en Recursos Cinegéticos, Ciudad Real, Spain (A. Sánchez-Cano, T.C. Cabrera, I.G. Fernández de Mera, C. Gortazar, U. Höfle)

DOI: http://doi.org/10.3201/eid2807.212408

Bagaza virus emerged in Spain in 2010 and was not reported in other countries in Europe until 2021, when the virus was detected by molecular methods in a corn bunting and several red-legged partridges in Portugal. Sequencing revealed high similarity between the 2021 strains from Portugal and the 2010 strains from Spain.

Bagaza virus (BAGV) is a single-stranded, positive-sense RNA virus. The virus belongs to the mosquitoborne cluster of the genus *Flavivirus,* family *Flaviviridae,* which includes such other emerging pathogens as West Nile, Japanese encephalitis, dengue, Zika, and yellow fever viruses, all of which are associated with neurologic disease in animals and humans and have zoonotic potential (*1*). BAGV was first isolated in 1966 from a pool of *Culex* species mosquitoes in the Bagaza District of Central African Republic and was detected subsequently in several species of mosquitoes. The first BAGV-associated deaths in vertebrates were detected in Spain, in 2010, in red-legged partridges (*Alectoris rufa*) and ring-necked pheasants (*Phasianus colchicus*) (*2*) and then, in 2016, in Himalayan monal pheasants (*Lophophorus impejanus*) in South Africa (*3*).

BAGV infection causes neurologic disease in red-legged partridges, gray partridges (*Perdix perdix*), ring-necked pheasants, and, to a lesser degree, in common wood pigeons (*Columba palumbus*) (*1*–*6*). Estimated mortality rates range from 23% to 30% in naturally and experimentally infected red-legged partridges (*5*,*7*); rates are higher (up to 40%) in experimentally infected gray partridges (*6*) and lower rates in pheasants and columbiformes (*4*,*7*). We describe a BAGV outbreak in Portugal in autumn 2021, associated with abnormal fatalities in red-legged partridges and 1 corn bunting (*Emberiza calandra*).

On September 1, 2021, three red-legged partridges were found dead in Serpa, southern Portugal. From September through mid-October, 9 partridges and 1 corn bunting were found dead in the same area (Appendix Table, https://wwwnc.cdc.gov/EID/article/28/7/21-2408-App1.pdf). Local reports emerged of partridges displaying neurologic signs compatible with potential viral infection, such as disorientation and motor incoordination. Twelve of the 13 birds were necropsied. Laboratory examinations and preliminary diagnoses were conducted at the Research Institute in Hunting Resources (Ciudad Real, Spain) and at the Center for Research on Biodiversity and Genetic Resources (*InBIO* Laboratório Associado, Vairão, Portugal). Official diagnosis was determined at the National Institute of Agrarian and Veterinary Research, I.P. (Lisbon, Portugal). Growing feathers were collected from 30 partridges live-trapped in the same area on October 3.

Researchers conducted molecular detection by using RNA extracted from various sampling points (feather pulp, brain, heart, kidney, spleen, and intestine) and followed 2 strategies targeting different regions of the BAGV genome (nonstructural 2b, nonstructural 5 [NS5], and 3′ nontranslated region) (Appendix Table); first, a duplex quantitative reverse transcription PCR (RT-PCR) for the simultaneous and differential detection of Japanese encephalitis and Ntaya flavivirus serocomplexes (*8*), and second, a uniplex quantitative RT-PCR specific for the NS5 coding region of BAGV (*9*). The researchers used conventional nested RT-PCR for sequencing to target part of the NS5 gene (*10*) and an in-house RT-PCR (developed at the National Institute of Agrarian and Veterinary Research) to target part of the NS2b gene (Appendix Table).

Out of the 12 necropsied birds, 8 red-legged partridges and 1 corn bunting (75%) tested positive for BAGV, as did 4 of 30 live-captured red-legged partridges (13.3%) (Appendix Table). The 108 bp sequences obtained from duplex quantitative RT-PCR from partridge 9 and the corn bunting showed 100% similarity with the 3′ nontranslated region of the BAGV reference strain (GenBank accession no. HQ644143) detected in the 2010 outbreak in Spain (Appendix

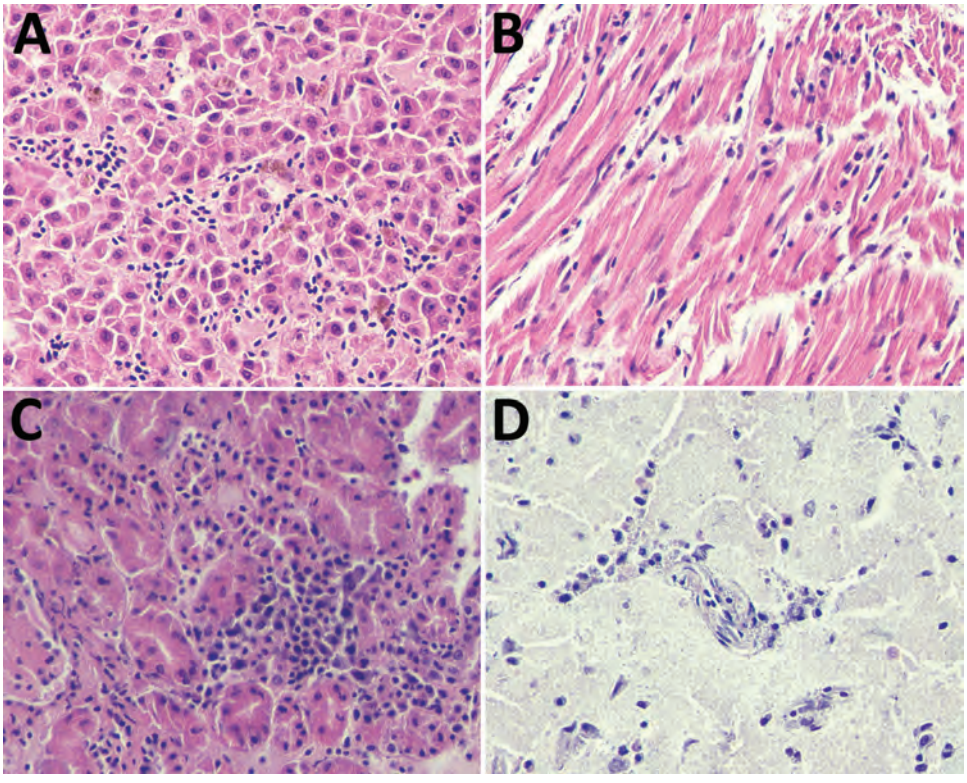

Figure. Microscopic lesions caused by Bagaza virus infection in liver, heart, kidney, and brain tissue of red-legged partridges (*Alectoris rufa*), Portugal, 2021. A) In liver, congestion, hemozoin presence in Kupffer cells, focal hepatocyte necrosis, and a moderate mononuclear infiltrate are visible despite some freezing artifacts. B) In heart, congestion, hemorrhage, edema, degeneration of myofibers of the myocardium, and endothelial swelling and moderate to abundant diffuse mononuclear infiltrates are visible. C) In kidney, tubulointerstitial nephritis characterized by congestion, hemorrhage necrosis of proximal convoluted tubular epithelium, and diffuse moderate to abundant mononuclear inflammatory infiltrate are visible. D) In brain, mild nonpurulent encephalitis with congestion, mononuclear cell extravasation, and endothelial cell swelling are visible. Hematoxilin eosin staining; original magnification ×400.

Table). In comparing the NS5 regions, researchers found very high similarities with HQ644143 in the 110 base pair sequences obtained from 6 partridges by nested RT-PCR (99.1%) and in the 171 base pair sequences taken from 2 partridges by RT-PCR (98.8%).

Upon necropsy, all birds were in good body condition, suggesting an acute disease course. Histopathology, albeit hampered by autolysis and freezing artifacts, revealed lymphoid depletion in the spleen and severe congestion, moderate to abundant diffuse mononuclear inflammatory infiltrates, and focal necrosis in all tissues. The heart, brain, kidney, and liver were the most affected organs (Figure).

This work confirms BAGV emergence in Portugal, in autumn 2021, associated with abnormal fatalities in red-legged partridges. Active circulation of BAGV was also evidenced in the studied region, where 13.3% of live-captured red-legged partridges testing positive for BAGV, even though ecologic and demographic studies are required to determine the extent and magnitude of the outbreak. Substantial population decline in the red-legged partridge can be anticipated in this region of Portugal on the basis of the mortality rate previously estimated for this species (*4*,*7*). The fatal case in a songbird, the corn bunting, suggests that BAGV might have a broader spectrum and effect in wild bird species. This finding, combined with the small size of the analyzed sequences, suggests the need for further research to identify the vectors for BAGV in Portugal and their role in the epidemiology of the disease, and elucidate the phylogenetic relationships between the 2021 strains in Portugal and 2010 strains in Spain against known BAGV strains.

No conclusions can be made from this research regarding the origin of this infection. However, the introduction of the virus in Portugal might be linked to persistence of the disease and migration of infected wild birds from North Africa or Spain.

Acknowledgments

We thank the personnel from the hunting sector for their help during field work (sampling and capturing) and Fernanda Simões for the sex determination of partridges 7 and 8 by molecular methods.

About the Author

Mr. Queirós is a junior researcher at CIBIO, Centro de Investigação em Biodiversidade e Recursos Genéticos, *InBIO* Laboratório Associado, BIOPOLIS Program in Genomics, Biodiversity and Land Planning, University of Porto. His research interests include the epidemiology of emerging infectious diseases in wildlife species and their interface with livestock and humans, as well as population genetics and phylogeography.

References

1. Benzarti E, Linden A, Desmecht D, Garigliany M. Mosquito-borne epornitic flaviviruses: an update and review. J Gen Virol. 2019;100:119–32. https://doi.org/10.1099/jgv.0.001203
2. Agüero M, Fernández-Pinero J, Buitrago D, Sánchez A, Elizalde M, San Miguel E, et al. Bagaza virus in partridges and pheasants, Spain, 2010. Emerg Infect Dis. 2011;17:1498–501. https://doi.org/10.3201/eid1708.110077
3. Steyn J, Botha EM, Lourens C, Coetzer JAW, Venter M. Bagaza virus in Himalayan monal pheasants, South Africa, 2016–2017. Emerg Infect Dis. 2019;25:2299–302. https://doi.org/10.3201/eid2512.190756
4. Gamino V, Gutiérrez-Guzmán AV, Fernández-de-Mera IG, Ortíz JA, Durán-Martín M, de la Fuente J, et al. Natural Bagaza virus infection in game birds in southern Spain. Vet Res (Faisalabad). 2012;43:65. https://doi.org/10.1186/1297-9716-43-65
5. Llorente F, Pérez-Ramírez E, Fernández-Pinero J, Elizalde M, Figuerola J, Soriguer RC, et al. Bagaza virus is pathogenic and transmitted by direct contact in experimentally infected partridges, but is not infectious in house sparrows and adult mice. Vet Res (Faisalabad). 2015;46:93. https://doi.org/10.1186/s13567-015-0233-9
6. Cano-Gómez C, Llorente F, Pérez-Ramírez E, Soriguer RC, Sarasa M, Jiménez-Clavero MÁ. Experimental infection of grey partridges with Bagaza virus: pathogenicity evaluation and potential role as a competent host. Vet Res (Faisalabad). 2018;49:44. https://doi.org/10.1186/s13567-018-0536-8
7. García-Bocanegra I, Zorrilla I, Rodríguez E, Rayas E, Camacho L, Redondo I, et al. Monitoring of the Bagaza virus epidemic in wild bird species in Spain, 2010. Transbound Emerg Dis. 2013;60:120–6. https://doi.org/10.1111/j.1865-1682.2012.01324.x
8. Elizalde M, Cano-Gómez C, Llorente F, Pérez-Ramírez E, Casades-Martí L, Aguilera-Sepúlveda P, et al. A duplex quantitative real-time reverse transcription-PCR for simultaneous detection and differentiation of flaviviruses of the Japanese encephalitis and Ntaya serocomplexes in birds. Front Vet Sci. 2020;7:203. https://doi.org/10.3389/fvets.2020.00203
9. Buitrago D, Rocha A, Tena-Tomás C, Vigo M, Agüero M, Jiménez-Clavero MA. Real-time fluorogenic reverse transcription polymerase chain reaction assay for the specific detection of Bagaza virus. J Vet Diagn Invest. 2012;24:959–63. https://doi.org/10.1177/1040638712452723
10. Sánchez-Seco MP, Rosario D, Domingo C, Hernández L, Valdés K, Guzmán MG, et al. Generic RT-nested-PCR for detection of flaviviruses using degenerated primers and internal control followed by sequencing for specific identification. J Virol Methods. 2005;126:101–9. https://doi.org/10.1016/j.jviromet.2005.01.025

Address for correspondence: João Queirós, CIBIO, Centro de Investigação em Biodiversidade e Recursos Genéticos, InBIO Laboratório Associado, BIOPOLIS Program in Genomics, Biodiversity and Land Planning, Campus de Vairão, Universidade do Porto, 4485-661 Vairão, Portugal; email: joao.queiros@cibio.up.pt

Hodgkin Lymphoma after Disseminated *Mycobacterium genavense* Infection, Germany

Janina Trauth, Thomas Discher, Moritz Fritzenwanker, Can Imirzalioglu, Tobias Arnold, Dagmar Steiner, Elvira Richter, Laura Crisponi, Bodo Grimbacher, Susanne Herold

Author affiliations: Justus Liebig University, Giessen, Germany (J. Trauth, T. Discher, M. Frizenwanker, C. Imirzalioglu, S. Herold); University Hospital Gießen, Gießen (T. Arnold, D. Steiner); MVZ Labor Doctor Limbach and Kollegen, Heidelberg, Germany (E. Richter); Istituto di Ricerca Genetica e Biomedica, Consiglio Nazionale delle Ricerche (CNR), Monserrato, Cagliari, Italy (L. Crisponi); Medical Center–University of Freiburg, Freiburg, Germany (L. Crisponi, B. Grimbacher)

DOI: http://doi.org/10.3201/eid2807.220425

Mycobacterium genavense infection, a rare nontuberculous mycobacteria infection, occurs in heavily immunocompromised patients (i.e., those with advanced HIV disease, genetic disorders, or acquired immunologic disorders and those undergoing immunosuppressive therapy). We report a case of disseminated *M. genavense* infection preceding Hodgkin lymphoma in a patient without obvious risk factors for this infection.

Mycobacterium genavense was first described in 1992 in HIV-positive patients with low CD4 counts and disseminated mycobacterial disease (*1*). Since the 2000s, additional risk factors for this bacterial infection became known (e.g., solid organ transplantation, hematopoietic stem cell transplantation, Epstein-Barr virus–associated lymphoproliferative disorder, neutralizing anti–interferon γ autoantibodies, adenosine deaminase deficiency, nuclear factor κB1 deficiency) (*2*,*3*). Clinical manifestations of *M. genavense* commonly involve blood and lymph nodes but can include the gastrointestinal tract, spleen, liver, and bone marrow; pneumonia, prosthetic joint infection, endobronchial mass, and brain mass have also been described.

A previously healthy 23-year-old woman sought medical treatment at University Hospital Gießen (Gießen, Germany) for progressive cervical lymphadenopathy (Figure, panel A) and fever originating 4 months prior. A professional animal keeper, she had no history of previous infections or autoimmune disease, an unremarkable family history, and no travel outside of Europe; her tattoos showed no signs of irritation. She experienced gender dysphoria and used masculinizing hormone therapy (testosterone). We

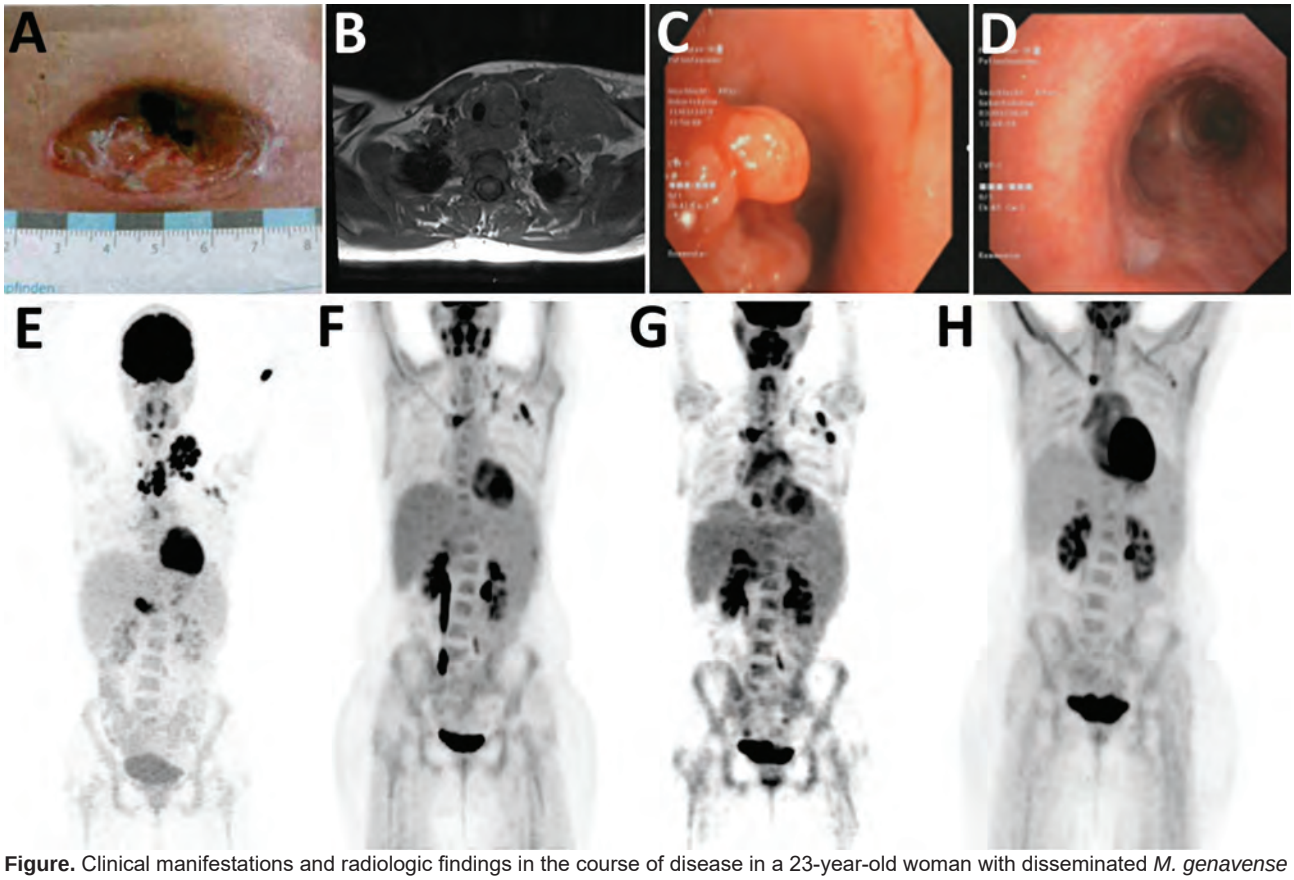

Figure. Clinical manifestations and radiologic findings in the course of disease in a 23-year-old woman with disseminated *M. genavense* infection preceding Hodgkin lymphoma, Germany. A) Cervical wound after initial lymph node extirpation. B) Magnetic resonance imaging at the time of initial evaluation. C) Endobronchial view of tracheo-esophageal fistula before positioning of a stent. D) Endobronchial view of the prior tracheo-esophageal fistula after treatment. Whitish scar tissue is seen at the bottom left. E) ^{18}F-FDG-PET scan at initial evaluation (maximum intensity projection). Cervical lymph node mass is seen, with no pathologic uptake in the abdomen. F) ^{18}F-FDG-PET scan after 6 months of antibiotic treatment showing reduced uptake. G) ^{18}F-FDG-PET scan shortly before Hodgkin lymphoma was diagnosed showing new hepatosplenomegaly and lymphadenopathy. H) ^{18}F-FDG-PET scan after antibiotic and chemotherapy without pathologic enhancement

excluded common causes of cervical lymphadenopathy (e.g., HIV, tuberculosis, bacterial abscess, Epstein-Barr virus, lymphoma, toxoplasmosis, bartonellosis, and syphilis), but the extensive lymphadenopathy pointed to a severe disease (Figure, panel B, E). Multiple conglomerate, necrotizing mediastinal lymph nodes resulted in a tracheo-esophageal fistula (Figure, panel C), which required esophageal stenting.

Cervical lymph nodes showed a necrotizing, giant cell–containing inflammatory reaction. We detected acid-fast bacteria on microscopic examination and subsequently identified it as *M. genavense* by using broad-range 16S-rDNA PCR and Sanger sequencing of the resulting amplicon (Appendix, https://wwwnc.cdc.gov/EID/article/28/7/22-0425-App1.pdf). In blood and bone marrow, we detected no mycobacteria. From culture on solid medium and mycobacteria growth indicator tube, we were unable to recover outgrowth. *M. genavense* cannot be cultivated in routine liquid and solid media (Löwenstein–Jensen and Stonebrink) but requires special supplementation for recovery on culture (Middlebrook 7H11 agar [ThermoFisher, https://www.thermofisher.com] supplemented with mycobactin J) and an incubation period >100 days. Standardized susceptibility testing is not available (*4*).

For this nontuberculous mycobacteria (NTM) disease, diagnostic criteria are ill defined and no treatment guidelines are established. Reported case-patients are treated with a 2- to 4-drug regimen, including mostly macrolides, rifampin, ethambutol, and amikacin or fluroquinolones. The regimen for this patient consisted of clarithromycin, rifabutin, ethambutol, and temporary add-on doses of levofloxacin, amikacin, clofazimine, or bedaquiline. During the ensuing months, the wounds and tracheo-esophageal fistula slowly healed (Figure, panel D), and imaging showed decreased uptake (Figure, panel F).

As a professional pet keeper, the patient had close contact with domestic animals, including birds. Zoonotic transmission of *M. genavense* has not been well described (*5*), but it does pose a potential risk for susceptible hosts. Because a predisposing risk factor for the patient's NTM disease had not been identified, we ruled out several conditions: acquired immunodeficiency, idiopathic CD4 lymphocytopenia, Mendelian susceptibility to mycobacterial disease, and neutralizing anti–interferon γ autoantibodies or a defect in the (proximal) interferon γ receptor signaling pathway (data not shown). A targeted gene panel with a focused analysis on 810 genes associated with immune and blood disorders did not identify a genetic variant that could alone explain the phenotype; however, we detected several rare variants (Appendix).

After 11 months of antibiotic therapy, an ^{18}F-FDG-PET scan revealed new lymphadenopathy and splenomegaly (Figure, panel G). CD4-to-CD8 ratio dropped from 1.7 to 1.0, and we found new low-level EBV viremia (350 copies/mL). On the basis of new tissue samples from mediastinal lymph nodes, we diagnosed classical Hodgkin lymphoma (HL [mixed type]) stage IV. Mycobacterial PCR was negative in all these samples and, retrospectively, all previous samples were tumor-free. Six cycles of chemotherapy (brentuximab combined with doxorubicin, vinblastine, dacarbazine) were followed by 4 doses of nivolumab because of histologically confirmed mixed response. One year after treatment completion and cessation of antimycobacterial therapy, liquid biopsy and an ^{18}F-FDG-PET scan showed complete remission and no signs of NTM infection (Figure, panel H).

In other reports of *M. genavense* infections related to lymphomas, patients acquired the infection during immunosuppressive therapy; however, in this patient, infection preceded HL. Genetic and environmental factors are relevant in the pathogenesis of HL (*6*) and in pathogenic pathways triggered by virus infections (e.g., HIV and Epstein-Barr virus) (*7*); bacterial antigen triggering has been implicated recently in early developmental stages of the disease (*8*). Other reports have discussed an increased risk for HL after tuberculosis infection (*9*) and HL associated with concomitant tuberculosis, leprosy, and *Mycobacterium avium* complex disease (*10*).

M. genavense remains a diagnostic challenge because standard media and incubation times do not yield bacterial growth, which can result in missed diagnoses. Research is needed to gain a clear understanding of the interplay of NTM and HL, specifically in regard to how mycobacterial antigens trigger pathogenic pathways during HL development and the role of HL in causing local immune escape mechanisms and immunologic imbalance resulting in susceptibility to infections.

In conclusion, we report a patient with disseminated *M. genavense* infection preceding HL who recovered after antimycobacterial therapy and first- and second-line chemotherapy. A zoonotic source of *M. genavense* infection is likely. Furthermore, because sex hormones affect immunity and testosterone is a susceptibility factor for mycobacterial disease, masculinizing hormone therapy could have contributed to susceptibility.

About the Author

Dr. Trauth is attending physician at University Hospital Gießen, Germany. Her primary interests include pulmonary infections and antibiotic stewardship.

References

1. Böttger EC, Teske A, Kirschner P, Bost S, Chang HR, Beer V, et al. Disseminated "*Mycobacterium genavense*" infection in patients with AIDS. Lancet. 1992;340:76–80. https://doi.org/10.1016/0140-6736(92)90397-L
2. Bustamante J, Boisson-Dupuis S, Abel L, Casanova J-L. Mendelian susceptibility to mycobacterial disease: genetic, immunological, and clinical features of inborn errors of IFN-γ immunity. Semin Immunol. 2014;26:454–70. https://doi.org/10.1016/j.smim.2014.09.008
3. Mahmood M, Ajmal S, Abu Saleh OM, Bryson A, Marcelin JR, Wilson JW. *Mycobacterium genavense* infections in non-HIV immunocompromised hosts: a systematic review. Infect Dis (Lond). 2018;50:329–39. https://doi.org/10.1080/23744235.2017.1404630
4. Griffith DE, Aksamit T, Brown-Elliott BA, Catanzaro A, Daley C, Gordin F, et al.; ATS Mycobacterial Diseases Subcommittee; American Thoracic Society; Infectious Disease Society of America. An official ATS/IDSA statement: diagnosis, treatment, and prevention of nontuberculous mycobacterial diseases. Am J Respir Crit Care Med. 2007;175:367–416. https://doi.org/10.1164/rccm.200604-571ST
5. Schmitz A, Korbel R, Thiel S, Wörle B, Gohl C, Rinder M. High prevalence of *Mycobacterium genavense* within flocks of pet birds. Vet Microbiol. 2018;218:40–4. https://doi.org/10.1016/j.vetmic.2018.03.026
6. Cartwright RA, Watkins G. Epidemiology of Hodgkin's disease: a review. Hematol Oncol. 2004;22:11–26. https://doi.org/10.1002/hon.723
7. Carbone A, Gloghini A, Caruso A, De Paoli P, Dolcetti R. The impact of EBV and HIV infection on the microenvironmental niche underlying Hodgkin lymphoma pathogenesis. Int J Cancer. 2017;140:1233–45. https://doi.org/10.1002/ijc.30473
8. Weniger MA, Küppers R. Molecular biology of Hodgkin lymphoma. Leukemia. 2021;35:968–81. https://doi.org/10.1038/s41375-021-01204-6
9. Li G, Chen G-L, Zhou Y, Yao G-Q, Yang S, Ji D-M. Increased risk of lymphoma in men or the elderly infected with tuberculosis. Mediterr J Hematol Infect Dis. 2021;13:e2021053. https://doi.org/10.4084/MJHID.2021.053

10. Varkey MR, Ali J, Lapinel NC. The chicken and the egg dilemma: a case of disseminated MAC with Hodgkin's lymphoma. Respir Med Case Rep. 2020;31:101253. https://doi.org/10.1016/j.rmcr.2020.101253

Address for correspondence: Janina Trauth, University Hospital Gießen and Marburg GmbH, Section of Infectious Diseases, Klinikstr 33, 35392 Gießen, Germany; email: janina.trauth@innere.med.uni-giessen.de

Natural Reassortment of Eurasian Avian-Like Swine H1N1 and Avian H9N2 Influenza Viruses in Pigs, China

Wanying Sun,[1] Samuel S.M. Cheng,[1] Kristy N.T. Lam, Tsz C. Kwan, Ricky W.K. Wong, Leo H.K. Lau, Gigi Y.Z. Liu, Leo L.H. Luk, John K.C. Li, Haogao Gu, Malik Peiris, Leo L.M. Poon

Author affiliations: School of Public Health, The University of Hong Kong, Hong Kong, China (W. Sun, S.S.M. Cheng, K.N.T. Lam, T.C. Kwan, R.W.K. Wong, L.H.K. Lau. G.Y.Z. Liu, L.L.H. Luk, J.K.C. Li, H. Gu, M. Peiris, L.L.M. Poon); Centre for Immunology and Infection, Hong Kong (M. Peiris, L.L.M. Poon); HKU-Pasteur Research Pole, The University of Hong Kong, Hong Kong (M. Peiris, L.L.M. Poon)

DOI: http://doi.org/10.3201/eid2807.220642

Several zoonotic influenza A viruses detected in humans contain genes derived from avian H9N2 subtypes. We uncovered a Eurasian avian-like H1N1 swine influenza virus with polymerase basic 1 and matrix gene segments derived from the H9N2 subtype, suggesting that H9N2 viruses are infecting pigs and reassorting with swine influenza viruses in China.

Swine are regarded as a mixing vessel for influenza A viruses (IAVs) (*1*). Avian, swine, and human IAVs can co-infect pigs and generate novel reassortants of zoonotic or pandemic potential. The emergence of pandemic H1N1 IAV (pH1N1), containing viral segments from avian, swine, and human viruses, highlighted the key role of pigs in contributing to IAV reassortment and evolution (*2*). Research in China also showed evidence of avian H5, H7, H9, and H10 influenza infections in pigs (*3*). Avian IAVs linked to human infection in this region contained internal genes derived from avian H9N2 viruses, indicating that the internal genes of the H9N2 virus might aid zoonotic transmission (*4*). We report detection of a swine IAV with polymerase basic (PB) 1 and matrix (M) gene segments of avian H9N2 origin.

In April 2021, we resumed monthly influenza surveillance program of imported pigs in a local slaughterhouse, which had been interrupted by COVID-19 outbreaks (*5*). We collected individual nasal swab samples (≈75 samples per visit), which we kept chilled in virus transport medium until they reached the laboratory. We then subjected swab samples to IAV isolation by using MDCK cells, as previously described (*2*). We identified cultures with cytopathic effect and tested them using a standard hemagglutination assay with turkey red blood cells. We tested hemagglutination-positive cultures with a universal influenza reverse transcription PCR assay specific for M segments (*6*). We studied samples that were positive for this reaction by using next-generation sequencing to deduce the full virus genomes (*6*).

During April 2021–February 2022, we collected a total of 829 porcine nasal swab samples (Table). We isolated 8 IAVs: 7 from August 2021 and 1 from September 2021. Virus sequences deduced from this study are available from GISAID (isolate nos. EPI_ISL_12471293–300). We compared those sequences with reference sequences (Appendix Table, https://wwwnc.cdc.gov/EID/article/28/7/22-0642-App1.pdf). IAVs detected in August 2021 were H3N2 viruses. The hemagglutinin (HA) and neuraminidase (NA) segments of those viruses were associated with human-like H3N2 swine influenza A virus; however, their internal gene segments all were derived from the pH1N1 lineage (Figure; Appendix Figures 1–6). These viruses were genetically not identical but highly similar. The influenza-positive pigs came from farms located in 2 provinces across southern China. Because this slaughterhouse followed a daily clearance policy requiring that all imported live pigs be slaughtered within 24 hours of admittance, our results suggest influenza transmission between pigs in the preslaughter transport chain outside Hong Kong. This

[1]These authors contributed equally to this article.

Table. Swine influenza viruses detected in imported pigs, China, April 2021–February 2022

Year and month	No. nasal swabs	No. virus isolates	Isolation rate, %
2021			
Apr	60	0	0
May	75	0	0
Jun	75	0	0
Jul	75	0	0
Aug	75	7*	9.3
Sep	75	1†	1.3
Oct	79	0	0
Nov	85	0	0
Dec	80	0	0
2022			
Jan	75	0	0
Feb	75	0	0
Total	829	8	0.97

*All H3N2; pigs were imported from 2 provinces in southern China.
†H1N1, pig was from imported from a province in southern China.

H3N2 genotype was previously detected in pigs from Guangxi, China (*7*).

The swine H1N1 IAV that we isolated in September 2021, A/swine/HK/NS419/2021, a reassortant between multiple swine influenza lineages (Figure; Appendix Figures 1–6). The PB1 and M gene segments of this virus are of avian H9N2 virus subtype. This virus contains PB2, polymerase acidic, and NP gene segments derived from the pH1N1 lineage. Its HA and NA gene segments are of Eurasian avian-like H1N1 lineage, and its nonstructural gene segment is of a triple reassortant lineage. We further purified the isolated virus by using plaque assays to exclude the possibility of a mixed infection. We confirmed that all plaque-purified viral clones had an identical genotype.

The A/swine/HK/NS419/2021 isolate featured a PB1 gene segment of SH/F/98–like lineage and an M gene segment of G1-like H9N2 lineage (Figure). Similar PB1 and M sequences have been detected in zoonotic viruses in humans (Figure), PB1 in H10N8 and M in H7N9, but we did not find mutations known for mammalian host adaptation in these 2 segments. The encoded proteins of the PB1 and M gene segments that we isolated featured amino acid sequences rarely observed in mammalian and avian IAVs, including H9 (PB1, 97K, 156N, 397V, 535V, 688I, and 704T; M1, 31I and 46V; and M2, 25S). We could not determine whether these were random or adaptive mutations. The PB1 segment of avian H9N2 is highly compatible to other polymerase genes from mammalian IAVs (*8*). Such results suggest the need for further characterization of these mutations, particularly those in the PB1 gene.

A recent report in China discussed multiple Eurasian avian-like H1N1 swine influenza reassortants with internal genes derived from pH1N1 and triple reassortant lineages (*9*). One group of these reassortants (genotype 4) displayed a genotype similar to A/swine/HK/NS419/2021, the only exception being that the virus's PB1 and M gene segments were of pH1N1 lineage. That report showed that genotype 4 Eurasian avian-like swine IAVs can bind to human sialic acid receptors (i.e., α2,3), enabling efficient virus replication in human airway epithelial cells, and achieve efficient aerosol transmission in ferrets (*9*). Serologic surveillance further showed that 10% of studied swine workers were positive for the genotype 4 reassortant (*9*). Our own sequence analyses suggest that some of the genotype 4 viruses and our Eurasian avian-like H1N1 viruses might share a common ancestry (e.g., A/swine/Shandong/1207/2016; Appendix Figures 1–6). Further risk assessment on the pandemic potential of this genotype and its reassortants is needed (*10*).

In summary, many zoonotic IAVs in humans have genes derived from H9N2 subtypes. Our results suggest that avian H9N2 IAVs are infecting swine and reassorting with swine IAVs, which indicates the need for continued monitoring of swine IAVs in both China and outlying regions.

This project has been funded in whole or in part with federal funds from the National Institute of Allergy and Infectious Diseases, National Institutes of Health, US Department of Health and Human Services, under contract no. 75N93021C00016 by grants from the National Institute of Allergy and Infectious Diseases and from the Research Grants Council of Hong Kong theme-based research schemes (T11-712/19-N) and Research Grants Council of Hong Kong (GRF 17110920) grants from Hong Kong.

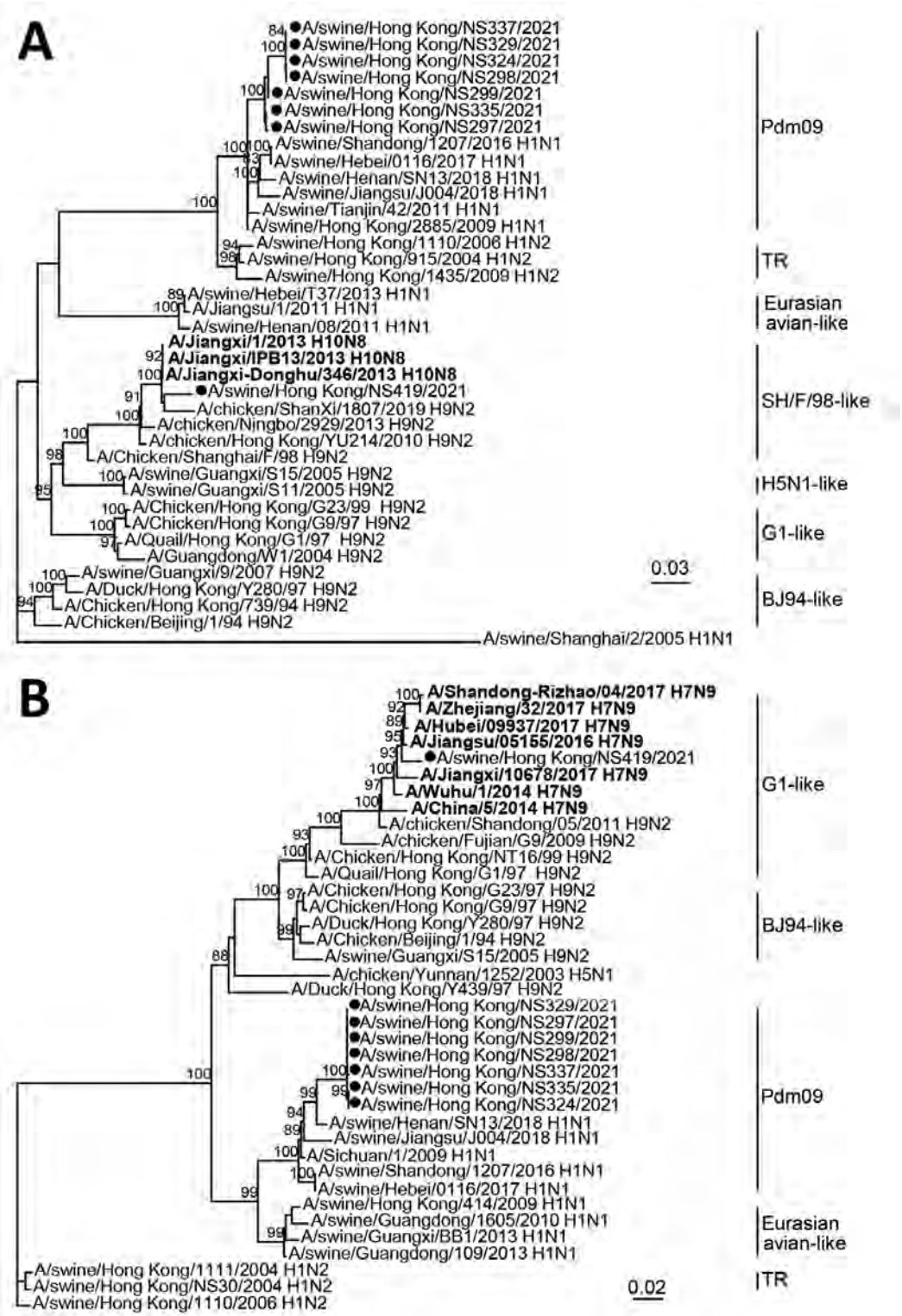

Figure. Phylogenetic tree of polymerase basic 1 (A) and matrix (B) gene sequences of swine influenza viruses from China and reference sequences. Bold indicates human H7N9 and H10N8 sequences. Viral sequences generated in this study (black circles) and those downloaded from public domains (Appendix Table, https://wwwnc.cdc.gov/EID/article/28/7/22-0642-App1.pdf) were aligned by using Muscle version 3.8 (http://www.drive5.com/muscle). Phylogenetic trees were constructed by IQ-TREE 1.6.12 (http://www.iqtree.org) by using the generalized time reversible plus gamma model. Major animal viral lineages are as shown. Bootstrap values ≥80% are shown. Scale bar indicates estimated genetic distance.

About the Author

Miss Sun is a postgraduate student at The University of Hong Kong, Hong Kong, China. Her primary research interest is bioinformatics.

References

1. Webby R, Richt J. Influenza in swine. In: Webster RG, Monto AS, Braciale TJ, Lamb RA, editors. Textbook of influenza, 2nd edition. Chichester: Wiley Blackwell; 2013. p. 190–202.
2. Smith GJ, Vijaykrishna D, Bahl J, Lycett SJ, Worobey M, Pybus OG, et al. Origins and evolutionary genomics of the 2009 swine-origin H1N1 influenza A epidemic. Nature. 2009;459:1122–5. https://doi.org/10.1038/nature08182
3. Chauhan RP, Gordon ML. A systematic review analyzing the prevalence and circulation of influenza viruses in swine population worldwide. Pathogens. 2020;9:E355. https://doi.org/10.3390/pathogens9050355
4. Shi W, Li W, Li X, Haywood J, Ma J, Gao GF, et al. Phylogenetics of varied subtypes of avian influenza viruses in China: potential threat to humans. Protein Cell. 2014;5:253–7. https://doi.org/10.1007/s13238-014-0036-1
5. Gu H, Xie R, Adam DC, Tsui JL, Chu DK, Chang LDJ, et al. Genomic epidemiology of SARS-CoV-2 under an elimination strategy in Hong Kong. Nat Commun. 2022;13:736. https://doi.org/10.1038/s41467-022-28420-7
6. Al-Ghadeer H, Chu DKW, Rihan EMA, Abd-Allah EA, Gu H, Chin AWH, et al. Circulation of influenza A(H5N8) virus, Saudi Arabia. Emerg Infect Dis. 2018;24:1961–4. https://doi.org/10.3201/eid2410.180846
7. He P, Wang G, Mo Y, Yu Q, Xiao X, Yang W, et al. Novel triple-reassortant influenza viruses in pigs, Guangxi, China. Emerg Microbes Infect. 2018;7:85. https://doi.org/10.1038/s41426-018-0088-z
8. Cui H, Che G, de Jong MCM, Li X, Liu Q, Yang J, et al. The PB1 gene from H9N2 avian influenza virus showed high compatibility and increased mutation rate after reassorting with a human H1N1 influenza virus. Virol J. 2022;19:20. https://doi.org/10.1186/s12985-022-01745-x
9. Sun H, Xiao Y, Liu J, Wang D, Li F, Wang C, et al. Prevalent Eurasian avian-like H1N1 swine influenza virus with 2009 pandemic viral genes facilitating human infection. Proc Natl Acad Sci U S A. 2020;117:17204–10. https://doi.org/10.1073/pnas.1921186117
10. Cheung JTL, Tsang TK, Yen HL, Perera RAPM, Mok CKP, Lin YP, et al. Determining existing human population immunity as part of assessing influenza pandemic risk. Emerg Infect Dis. 2022;28:977–85. https://doi.org/10.3201/eid2805.211965

Address for correspondence: Malik Peiris or Leo Poon, School of Public Health, The University of Hong Kong, 7 Sassoon Road, Hong Kong, China; email: malik@hku.hk or llmpoon@hku.hk

Persistent SARS-CoV-2 Alpha Variant Infection in Immunosuppressed Patient, France, February 2022

Slim Fourati, Guillaume Gautier, Myriam Chovelon, Alexandre Soulier, Melissa N'Debi, Vanessa Demontant, Céline Kennel, Christophe Rodriguez, Jean-Michel Pawlotsky

Author affiliations: Hôpital Henri Mondor (AP-HP), Université Paris-Est, Créteil, France (S. Fourati, A. Soulier, M. N'Debi, V. Demontant, C. Rodriguez, J.-M. Pawlotsky); William Morey General Hospital, Chalon-sur-Saône, France (G. Gautier, M. Chovelon, C. Kennel)

DOI: https://doi.org/10.3201/eid2807.220467

We describe persistent circulation of SARS-CoV-2 Alpha variant in an immunosuppressed patient in France during February 2022. The virus had a new pattern of mutation accumulation. The ongoing circulation of previous variants of concern could lead to reemergence of variants with the potential to propagate future waves of infection.

Immunosuppressed patients can have prolonged SARS-CoV-2 infection (*1*). Studies have reported the occurrence and selection of multiple mutations in the spike glycoprotein sequence in immunosuppressed patients with persistent SARS-CoV-2 infections (*2*–*6*). To date, intrahost mutations have been described essentially in the ancestral wild-type SARS-CoV-2 virus (*3*,*5*–*8*), especially during prolonged infection with variants of concern (VOCs) (*9*). Additional SARS-CoV-2 mutations in immunocompromised persons could enable increased virus transmissibility and immune evasion, shaping the emergence of new VOCs. We describe a new mutation accumulation pattern in SARS-CoV-2 Alpha virus in an immunosuppressed patient.

An 84-year-old woman with evolutive mantle cell lymphoma who was receiving maintenance rituximab and lenalidomide treatment was admitted to the hospital on May 17, 2021. She had asthenia, fever, and hypoxia (93% oxygen saturation). At admission (day 0), she tested positive for SARS-CoV-2 RNA (Figure). She had received 2 vaccine doses 84 and 66 days before admission. She did not have respiratory symptoms, but a chest computed tomography scan showed ground-glass opacities in her lungs. The patient was hospitalized and treated with corticosteroids for 10 days. She tested SARS-CoV-2–positive again on August 26, day 101 after her initial

positive test. On September 27 (day 133), she tested SARS-CoV-2–negative and was considered virologically cured. She received a vaccine booster (third) dose at day 164 and a fourth dose on day 201, but we did not detect spike receptor binding domain antibodies at days 133, 201, or 210.

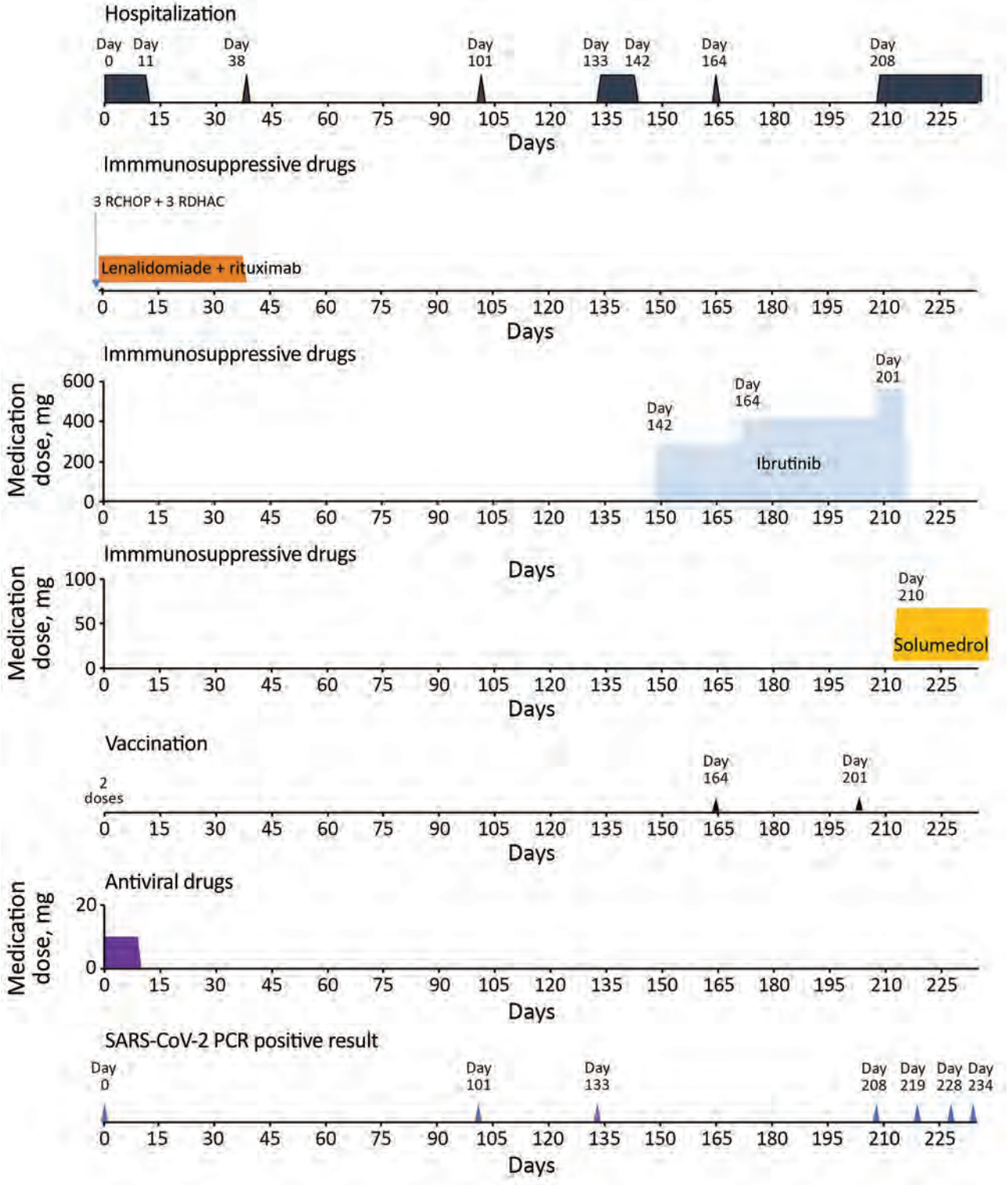

Figure. Timeline of SARS-CoV-2 diagnostic tests, hospitalizations, booster vaccination, and treatments for an immunosuppressed patient with persistent SARS-CoV-2 Alpha variant infection, France, 2022. RCHOP, combination therapy of rituximab, cyclophosphamide, doxorubicine, vincristine, and prednisone; RDHAC, combination therapy of rituximab, cytarabine, dexamethasone, and carboplatine.

Beginning in October 2021, the patient experienced intermittent fever and diarrhea because her lymphoma progressed, as shown by an abdominal computed tomography scan; she was started on a second-line treatment with ibrutinib (Figure). She was hospitalized again in early January 2022 (day 208) after clinicians discovered an evolutive lymph node mass. At admission, she tested SARS-CoV-2–positive despite the absence of COVID-19 symptoms. SARS-CoV-2 RNA levels from nasopharyngeal swab samples were high; cycle threshold values were 19 on day 208, 18 on day 228, and 22 on day 234.

At days 0, 101, 208, and 234, multiplex mutation-specific reverse transcription PCR revealed the absence of spike amino acid mutations E484Q, E484K, and L452R, and K417N was not detected on days 208 and 234, suggesting that the patient was not infected with Delta or Omicron variants, the 2 dominant variants in France at the time. These results suggested that the patient was infected with the Alpha variant, which was the dominant variant circulating when she first tested positive.

To determine whether the patient was infected with a new strain or reinfected with the same persistently replicating variant, we performed whole-genome sequencing on samples collected on days 208 (January 11, 2022) and 228 (January 31, 2022) and identified lineage B.1.1.7 (Alpha variant). Older samples were not available for sequencing. Our analysis revealed the presence of amino acid substitutions and mutations in addition to characteristics of the Alpha variant, including mutations in open reading frame (ORF) 1a (nonstructural protein 3, n = 4), spike protein (n = 6), matrix protein (n = 1), envelope protein (n = 2), ORF3a (n = 1), and ORF7 (n = 2) (Appendix Figure, https://wwwnc.cdc.gov/EID/article/28/7/22-0467-App1.pdf).

The SARS-CoV-2 mutational pattern in this immunosuppressed patient adds several new mutations to the Alpha variant characteristic. Although earlier samples were not available for sequencing, mutations in later samples align with an ongoing selection process. The mutations we observed share similarities with those observed in other VOCs and variants of interest, pointing to evolutionary convergence, such as spike del241–247, which also is found in part in the Beta variant. Several mutations that likely play a role in immune evasion were selected in the spike nucleocapsid terminal domain (e.g., K77E, S248F, and del14–18) and receptor-binding domain (L452M). These mutations have rarely been reported in isolates submitted to GISAID (https://www.gisaid.org), suggesting that, when considered individually, they could be maladaptive.

In January 2022, the Alpha variant was no longer circulating in France, according to strains submitted to GISAID. Our case highlights the potential for persistence of supposedly extinct SARS-CoV-2 variants that might cause prolonged infection in immunocompromised patients and acquire adaptive mutations that confer increased transmissibility, antigenic divergence, and reduced pathogenicity, with obvious public health implications (*1*,*3*). Similar cases likely exist in other parts of the world because SARS-CoV-2 genome sequencing and reporting to GISAID are far from exhaustive.

Omicron-infected patients not immunized against older variants appear to mount a weak or no neutralizing response against variants that preceded Omicron, including VOCs (R.K. Suryawanshi et al., unpub. data, https://doi.org/10.1101/2022.01.13.2269243). Because the next dominant variant could emerge from a variant other than Omicron, ongoing circulation of older VOCs could feed reemergence of variants that eliminate Omicron, particularly in unvaccinated populations, emphasizing the crucial role of vaccination to prevent new SARS-CoV-2 waves.

In conclusion, this report highlights the need to reinforce precautions to avert nosocomial and community transmission involving immunocompromised patients, who might shed older SARS-CoV-2 variants longer. Prospective genomic surveillance for SARS-CoV-2 variants is needed in persons with prolonged infection, particularly in countries with many immunocompromised persons, such as countries with a high HIV prevalence and low vaccination rates.

Funding for this study was provided by the ministry of health of France as part of the surveillance program for SARS-CoV-2 genomic evolution.

S.F. has served as a speaker for GlaxoSmithKline, Abbvie, and Abbott Diagnostics. C.R. has served as an advisor and speaker for Illumina and Vela Diagnostics. J.-M.P. has served as an advisor and speaker for Abbvie, Gilead, Merck, Assembly Biosciences, and Arbutus. The remaining authors have no conflicts of interest to disclose.

About the Author

Prof. Fourati is a researcher at the University of East Paris, Créteil, France. He is also a clinical virologist in the Department of Microbiology, Henri Mondor Hospital, Créteil, France. His primary research interests include viral evolution and adaptation, viral hepatitis, and respiratory viruses, including SARS-CoV-2.

References

1. Corey L, Beyrer C, Cohen MS, Michael NL, Bedford T, Rolland M. SARS-CoV-2 variants in patients with immunosuppression. N Engl J Med. 2021;385:562–6. https://doi.org/10.1056/NEJMsb2104756
2. Wang Y, Wang D, Zhang L, Sun W, Zhang Z, Chen W, et al. Intra-host variation and evolutionary dynamics of SARS-CoV-2 populations in COVID-19 patients. Genome Med. 2021;13:30. https://doi.org/10.1186/s13073-021-00847-5
3. Khateeb D, Gabrieli T, Sofer B, Hattar A, Cordela S, Chaouat A, et al. SARS-CoV-2 variants with reduced infectivity and varied sensitivity to the BNT162b2 vaccine are developed during the course of infection. PLoS Pathog. 2022;18:e1010242. https://doi.org/10.1371/journal.ppat.1010242
4. Weigang S, Fuchs J, Zimmer G, Schnepf D, Kern L, Beer J, et al. Within-host evolution of SARS-CoV-2 in an immunosuppressed COVID-19 patient as a source of immune escape variants. Nat Commun. 2021;12:6405. https://doi.org/10.1038/s41467-021-26602-3
5. Cele S, Karim F, Lustig G, San JE, Hermanus T, Tegally H, et al.; COMMIT-KZN Team. SARS-CoV-2 prolonged infection during advanced HIV disease evolves extensive immune escape. Cell Host Microbe. 2022;30:154–162.e5. https://doi.org/10.1016/j.chom.2022.01.005
6. Choi B, Choudhary MC, Regan J, Sparks JA, Padera RF, Qiu X, et al. Persistence and evolution of SARS-CoV-2 in an immunocompromised host. N Engl J Med. 2020;383:2291–3. https://doi.org/10.1056/NEJMc2031364
7. Pérez-Lago L, Aldámiz-Echevarría T, García-Martínez R, Pérez-Latorre L, Herranz M, Sola-Campoy PJ, et al.; on behalf of Gregorio Marañón Microbiology-Id Covid Study Group. Different within-host viral evolution dynamics in severely immunosuppressed cases with persistent SARS-CoV-2. Biomedicines. 2021;9:808. https://doi.org/10.3390/biomedicines9070808
8. Avanzato VA, Matson MJ, Seifert SN, Pryce R, Williamson BN, Anzick SL, et al. Case study: prolonged infectious SARS-CoV-2 shedding from an asymptomatic immunocompromised individual with cancer. Cell. 2020;183:1901–12.e9. https://doi.org/10.1016/j.cell.2020.10.049
9. Truffot A, Andréani J, Le Maréchal M, Caporossi A, Epaulard O, Germi R, et al. SARS-CoV-2 variants in immunocompromised patient given antibody monotherapy. Emerg Infect Dis. 2021;27:2725–8. https://doi.org/10.3201/eid2710.211509

Address for correspondence: Slim Fourati, Henri Mondor Hospital, 51 av du Marechal de Lattre de Tassigny, Créteil 94010, France; email: slim.fourati@aphp.fr

Increased Stability of SARS-CoV-2 Omicron Variant over Ancestral Strain

Alex Wing Hong Chin, Alison Man Yuk Lai, Malik Peiris, Leo Lit Man Poon

Author affiliations: The University of Hong Kong, Hong Kong, China (A.W.H. Chin, A.M.Y. Lai, M. Peiris, L.L.M. Poon); Centre for Immunology & Infection, Hong Kong (A.W.H. Chin, M. Peiris, L.L.M. Poon)

DOI: https://doi.org/10.3201/eid2807.220428

As of April 2022, the Omicron BA.1 variant of concern of SARS-CoV-2 was spreading quickly around the world and outcompeting other circulating strains. We examined its stability on various surfaces and found that this Omicron variant is more stable than its ancestral strain on smooth and porous surfaces.

The Omicron SARS-CoV-2 variant of concern (VOC) is highly transmissible in humans. As of April 2022, it has outcompeted other known variants and dominated in different regions (*1*). Its spike protein has >30 mutations compared with the ancestral strain (*2*). A 2022 structural study indicates the Omicron spike protein is more stable than that of the ancestral strain (*3*); this finding prompted us to hypothesize that Omicron VOC is also more stable on different surfaces. We previously showed that the ancestral SARS-CoV-2 strain can still be infectious at room temperature for several days on smooth surfaces and several hours on porous surfaces (*4*).

We used previously described ancestral SARS-CoV-2 (PANGO lineage A) and Omicron VOC (PANGO lineage BA.1) in this study (*5*,*6*). We tested their stability on different surfaces using our previously described protocol (*4*,*7*). In brief, we applied a 5-μL droplet of each virus (10^7 50% tissue culture infectious dose [$TCID_{50}$]/mL) on different surfaces in triplicate. We incubated the treated surfaces at room temperature (21°C–22°C) for different time points as indicated and then immersed them in viral transport medium for 30 min to recover the residual infectious virus. We titrated the recovered virus by $TCID_{50}$ assays using Vero E6 cells, as described (*4*,*7*).

Compared with the ancestral SARS-CoV-2, the Omicron BA.1 variant was more stable on all surfaces we studied (Table). On day 4 postinoculation, we recovered no infectious ancestral SARS-CoV-2 from stainless steel, polypropylene sheet, or 2 of 3 glass

Table. Stability of ancestral SARS-CoV-2 and of Omicron variant on different surfaces*

Material	Incubation time†	Ancestral SARS-CoV-2		Omicron variant	
		Mean $\log_{10}$($TCID_{50}$/mL) ±SD‡	% Reduction in viral titer	Mean $\log_{10}$($TCID_{50}$/mL) ±SD‡	% Reduction in viral titer
Stainless steel	0	5.02 ±0.39	NA	5.35 ±0.18	NA
	3 h	4.21 ±0.36	85.15	4.82 ±0.23	69.78
	6 h	3.73 ±0.10	95.80	4.62 ±0.31	79.86
	1 d	2.99 ±0.17	99.21	4.65 ±0.17	80.28
	2 d	2.08 ±0.11	99.91	4.51 ±0.15	85.82
	4 d	§	>99.93	3.72 ±0.12	97.72
	7 d	§	>99.93	3.58 ±0.30	98.19
Polypropylene	0	4.85 ±0.23	NA	5.43 ±0.16	NA
	3 h	4.12 ±0.19	81.72	4.65 ±0.34	81.27
	6 h	3.53 ±0.15	95.43	4.33 ±0.14	92.34
	1 d	3.13 ±0.34	97.86	4.45 ±0.23	89.25
	2 d	2.01 ±0.10¶	>99.86	4.34 ±0.25	91.53
	4 d	§	>99.88	3.97 ±0.19	96.48
	7 d	§	>99.88	2.95 ±0.27	99.65
Glass	0	5.10±0.24	NA	5.65 ±0.28	NA
	3 h	4.26 ±0.05	86.79	4.90 ±0.15	83.62
	6 h	3.69 ±0.11	96.42	4.52 ±0.13	93.20
	1 d	2.83 ±0.13	99.49	4.20 ±0.01	96.84
	2 d	2.14 ±0.13	99.90	4.43 ±0.29	93.87
	4 d	1.96 ±0.00¶	>99.93	4.06 ±0.16	97.64
	7 d	§	>99.93	3.76 ±0.10	98.83
Tissue paper	0	4.70 ±0.22	NA	5.21 ±0.14	NA
	5 min	3.85 ±0.28	84.98	4.64 ±0.70	53.94
	15 min	2.12 ±0.14	99.75	3.72 ±1.22	72.99
	30 min	§	>99.84	2.92 ±0.40	99.34
	60 min	§	>99.84	§	>99.95
Printing paper	0	5.21 ±0.00	NA	5.34 ±0.13	NA
	5 min	2.69 ±0.16	99.68	3.26 ±0.42	98.91
	15 min	§	>99.94	2.20 ±0.33¶	>99.91
	30 min	§	>99.94	2.16 ±0.36¶	>99.92
	60 min	§	>99.94	§	>99.96

*Tests were performed in triplicate. NA, not applicable; $TCID_{50}$, 50% tissue culture infectious dose.
†The samples were incubated at room temperature (21°C–22°C).
‡Vero E6 cells were used for titration of viable viruses.
§All the triplicates were below detection limit of the $TCID_{50}$ assay.
¶One or two out of three replicates were below detection limit of the $TCID_{50}$ assay.

samples. We did not recover infectious virus from glass on day 7. In contrast, infectious Omicron variant was still recoverable from all treated surfaces on day 7 postincubation.

The stability of the Omicron variant was also higher than ancestral SARS-CoV-2 on porous surfaces, such as tissue paper and printing paper. On tissue paper, viable ancestral SARS-CoV-2 was no longer recoverable after a 30-minute incubation. However, we detected viable Omicron variant after a 30-minute incubation. On printing paper, we detected no infectious virus after a 15-minute incubation. In contrast, viable Omicron variant was recovered from 2 of 3 replicates after a 30-minute incubation.

To confirm our observations, we used transmembrane serine protease 2 (TMPRSS2)–expressing Vero E6 cells to titrate infectious virus particles recovered from treated stainless steel and printing paper (Appendix Table, https://wwwnc.cdc.gov/EID/article/28/7/22-0428-App1.pdf). On stainless steel, infectious ancestral virus was undetectable on day 10 postincubation, whereas viable Omicron variant was still recoverable. Similarly, no infectious ancestral virus was detected on printing paper after a 30-minute incubation, whereas we detected viable Omicron variant in 1 out of 3 replicates. Although the virus could be trapped in the porous materials and inefficiently recovered, our findings confirm that Omicron variant is more stable than its ancestral strain on surfaces.

We noted that the cell line used for virus titration can affect our findings. It has been reported that Omicron variant is less dependent upon TMPRSS2 for cell entry (*8*); therefore, we were not surprised that different cell lines led to different viral inactivation profiles. Nonetheless, results from both cell lines suggest that the Omicron variant is more stable than the ancestral strain. This observation is consistent with other recent findings (R. Hirose et al., unpub. data, https://www.biorxiv.org/content/10.1101/2022.01.18.476607v1). More evidence is needed to account for the increased transmissibility of Omicron variant. The virus's stability on surfaces may be one factor and should be taken

into consideration when recommending control measures against infection. A recent study revealed that an infectious dose as low as 10 $TCID_{50}$ units could infect >50% of human study participants (*9*). Our findings indicate that Omicron variant has an increased likelihood for transmission by the fomite route; they may also indicate that the enhanced stability deduced from structural studies (*3*) and now demonstrated on different surfaces may be relevant for droplet or aerosol transmission of SARS-CoV-2. Of interest, stability of avian influenza A(H5N1) viruses has been shown to have an association with transmissibility of avian influenza virus between mammals by the airborne route, although the mechanisms underlying this association are not fully understood (*10*). Further studies on the stability of Omicron variant and its emerging subvariants in droplets and aerosols are warranted.

One limitation of our study is that the experiments were conducted in a well-controlled laboratory environment. Variations in environmental conditions would affect the rate of viral inactivation. Therefore, the time required for virus inactivation that we demonstrated may not reflect all real-life scenarios. In addition, the components of the viral droplet medium applied in this study were different from those of the respiratory droplets, which could also affect the stability of the virus. Nonetheless, our findings demonstrate that the Omicron variant is more stable than the ancestral SARS-CoV-2 on different surfaces, a finding that may be relevant for determining recommendations for public health measures to limit virus transmission.

Acknowledgments

This work was supported by the Hong Kong Health and Medical Research Fund (no. COVID190116) and Theme-based Research Scheme of Research Grant Council (no. T11-705/21-N), and InnoHK grants for Centre for Immunology & Infection.

About the Author

Dr. Chin is currently a research assistant professor of the University of Hong Kong. His research interests include basic virology and pathogenesis of emerging respiratory viruses.

References

1. World Health Organization. Coronavirus update 74: addressing the challenges of SARS-CoV-2 variants for public health. 2022 25 Feb [cited 2022 Apr 29]. https://www.who.int/publications/m/item/update-74-addressing-the-challenges-of-sars-cov-2-variants-for-public-health
2. Wang L, Cheng G. Sequence analysis of the emerging SARS-CoV-2 variant Omicron in South Africa. J Med Virol. 2022;94:1728–33. https://doi.org/10.1002/jmv.27516
3. Cui Z, Liu P, Wang N, Wang L, Fan K, Zhu Q, et al. Structural and functional characterizations of infectivity and immune evasion of SARS-CoV-2 Omicron. Cell. 2022;185:860–871.e13. https://doi.org/10.1016/j.cell.2022.01.019
4. Chin AWH, Chu JTS, Perera MRA, Hui KPY, Yen HL, Chan MCW, et al. Stability of SARS-CoV-2 in different environmental conditions. Lancet Microbe. 2020;1:e10. https://doi.org/10.1016/S2666-5247(20)30003-3
5. Sia SF, Yan LM, Chin AWH, Fung K, Choy KT, Wong AYL, et al. Pathogenesis and transmission of SARS-CoV-2 in golden hamsters. Nature. 2020;583:834–8. https://doi.org/10.1038/s41586-020-2342-5
6. Cheng SMS, Mok CKP, Leung YWY, Ng SS, Chan KCK, Ko FW, et al. Neutralizing antibodies against the SARS-CoV-2 Omicron variant BA.1 following homologous and heterologous CoronaVac or BNT162b2 vaccination. Nat Med. 2022;28:486–9. https://doi.org/10.1038/s41591-022-01704-7
7. Behzadinasab S, Chin A, Hosseini M, Poon L, Ducker WA. A surface coating that rapidly inactivates SARS-CoV-2. ACS Appl Mater Interfaces. 2020;12:34723–7. https://doi.org/10.1021/acsami.0c11425
8. Meng B, Abdullahi A, Ferreira IATM, Goonawardane N, Saito A, Kimura I, et al.; CITIID-NIHR BioResource COVID-19 Collaboration; Genotype to Phenotype Japan (G2P-Japan) Consortium; Ecuador-COVID19 Consortium. Altered TMPRSS2 usage by SARS-CoV-2 Omicron impacts infectivity and fusogenicity. Nature. 2022;603:706–14. https://doi.org/10.1038/s41586-022-04474-x
9. Killingley B, Mann AJ, Kalinova M, Boyers A, Goonawardane N, Zhou J, et al. Safety, tolerability and viral kinetics during SARS-CoV-2 human challenge in young adults. Nat Med. 2022. https://doi.org/10.1038/s41591-022-01780-9
10. Imai M, Herfst S, Sorrell EM, Schrauwen EJ, Linster M, De Graaf M, et al. Transmission of influenza A/H5N1 viruses in mammals. Virus Res. 2013;178:15–20. https://doi.org/10.1016/j.virusres.2013.07.017

Address for correspondence: Alex Wing Hong Chin, School of Public Health, The University of Hong Kong, Hong Kong; email: alexchin@hku.hk; Leo Lit Man Poon, School of Public Health, The University of Hong Kong, Hong Kong; email: llmpoon@hku.hk

Type 1 Diabetes Mellitus Associated with Nivolumab after Second SARS-CoV-2 Vaccination, Japan

Toshihiro Sato, Shinjiro Kodama, Keizo Kaneko, Junta Imai, Hideki Katagiri

Author affiliation: Tohoku University Hospital, Sendai, Japan

DOI: https://doi.org/10.3201/eid2807.220127

Recently, along with increasing use of immune checkpoint inhibitors such as nivolumab, the incidence of immune-related adverse events, including type 1 diabetes mellitus, has become a serious problem. We report a patient who had immune checkpoint inhibitor–associated type 1 diabetes mellitus that developed after a second mRNA-based SARS-CoV-2 vaccination.

In response to the COVID-19 pandemic, mRNA-based SARS-CoV-2 vaccination has spread rapidly worldwide. This vaccine has shown high efficacy for preventing infection and disease exacerbation. However, adverse immunologic effects, including myocarditis, have been reported (*1*,*2*). Thus, immune system disturbances induced by these vaccines are suspected.

Immune checkpoint inhibitors (ICIs), including nivolumab, target programmed cell death protein-1 and have been used to treat malignancies, including melanoma, nonsmall cell lung cancer, and renal cell carcinoma. However, immune-related adverse events, including type 1 diabetes mellitus (T1D), also develop after ICI therapies (*3*,*4*); this form of diabetes has been called immune checkpoint inhibitor–induced diabetes mellitus (*5*). We report a patient who had checkpoint inhibitor–induced diabetes mellitus develop after he received a second mRNA-based SARS-CoV-2 vaccination.

A 43-year-old man who had malignant melanoma (pT3bN1bM0 stage IIIC) received nivolumab treatment (480 mg 1× every 4 wks) 12 months before admission. Fasting plasma glucose level was 94 mg/dL and glycated hemoglobin (HbA1c) 5.6% at treatment initiation. Plasma glucose and HbA1c were tested every 4 weeks. His range of plasma glucose was 90–123 mg/dL and that of HbA1c was 5.4%–5.7% (Figure). Positron emission tomography–computed tomography showed no metastasis or recurrence of the tumor 1 month before admission.

The man received his first SARS-CoV-2 vaccination 35 days before admission. No apparent adverse reactions occurred, except for local pain. The last nivolumab dose was administered 21 days before admission and the second SARS-CoV-2 vaccination 14 days before admission. The next day, he had a slight fever (temperature 37°C), which soon subsided. Thirst, polydipsia, and polyuria appeared 2 days after the second vaccination. He started drinking 3 L of water/day, and his weight decreased by 5 kg over the next 12 days.

Twelve days after the second vaccination, his blood glucose level was 655 mg/dL and his HbA1c 8.0%. Levels of ketone bodies increased; 3-hydroxybutyric acid was 2,813 μmol/L and acetoacetate 1,936 μmol/L. He was urgently admitted to the hospital

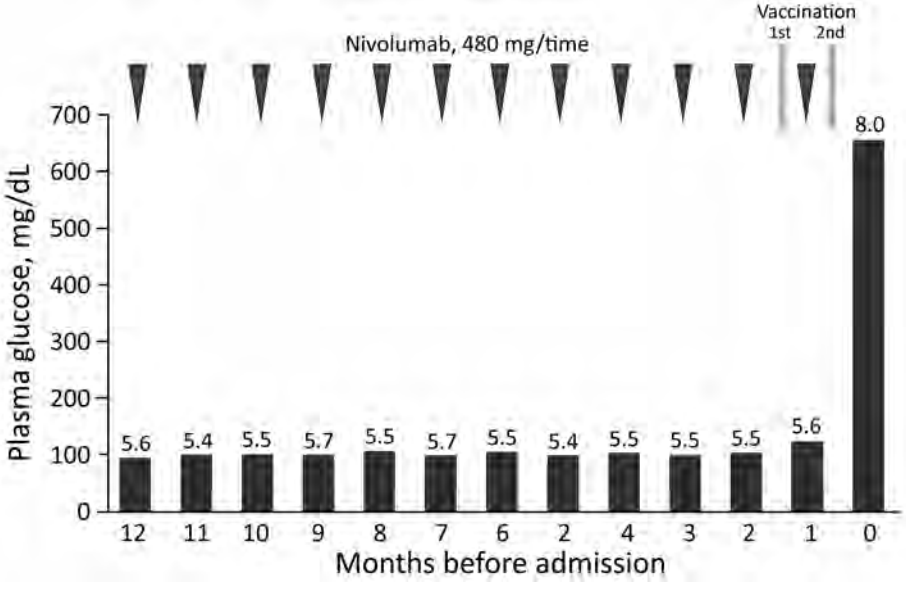

Figure. Clinical course after immune checkpoint inhibitors treatment initiation for type 1 diabetes mellitus associated with nivolumab after second SARS-CoV-2 vaccination, Japan. Numbers above bars are percentage glycated hemoglobin values.

because of a diagnosis of ICI-associated T1D and marked ketosis.

Laboratory tests at admission showed severely impaired insulin secretion capacity; fasting C-peptide immunoreactivity (CPR) was 0.33 ng/mL, 24-hour urinary CPR 5.74 μg/day and 3.82 μg/day, and ΔCPR during the glucagon load test was 0.03 ng/mL (Table). Tests results for islet-specific autoantibodies against glutamic acid decarboxylase, insulinoma-associated antigen 2, and zinc transporter 8 were negative. Human leukocyte antigen typing identified no specific alleles, including DR4, known to be related to T1D (Table). Blood glucose decreased in response to continuous intravenous administration of insulin and saline. On the second day of hospitalization, we switched from intravenous to subcutaneous injection of insulin. The patient's blood glucose level was ultimately controlled by intensive insulin therapy (degludec 9 U before dinner and lispro 24 U before breakfast, 5 U before lunch, and 15 U before dinner). Five months after discharge, the patient still requires multiple daily insulin injections for glycemic control.

Recently, along with increasing use of ICIs, the incidence of immune-related adverse events, including T1D, has become a serious problem. Our patient had been receiving nivolumab for 1 year. During treatment, his blood glucose level was tested every 4 weeks, and no increases were detected. However, 2 days after the second mRNA vaccination, he had typical symptoms of severe hyperglycemia (i.e., thirst, polydipsia and polyuria, and subsequent weight loss). Fourteen days after the second vaccination, blood glucose level was markedly increased, and the patient had nearly depleted insulin secretion, but his HbA1c was <8.5%. Test results for islet-related autoantibodies were negative. Therefore, we gave the patient a diagnosis of the fulminant form of T1D (*6*), which was associated with ICI treatment.

Most patients with nivolumab-associated T1D reportedly have this complication develop within 7 months after ICI treatment initiation (*4*). However, for this patient, 12 months, an exceptionally long time, had elapsed when T1D manifested. Therefore, some other factor might have triggered onset of ICI-associated T1D.

SARS-CoV-2 mRNA vaccination reportedly alters immune conditions (*7*). The association between SARS-CoV-2 mRNA vaccines and myocarditis has recently received attention; myocarditis frequently occurred within 1 week, often just 2–4 days, after the second vaccination, mostly affecting young men (*1*,*2*).

Table. Laboratory test results for a patient who had type 1 diabetes mellitus associated with nivolumab after a second SARS-CoV-2 vaccination, Japan*

Laboratory test	Value
Venous blood gas analysis	
pH	7.36
pCO_2, mm Hg	41.1
Bicarbonate, mmol/L	22.6
Anion gap, mmol/L	10.0
Biochemical	
Creatinine, mg/dL	0.84
Glomerular filtration rate, mL/min/1.73 m^2	79.0
Amylase, U/L	59.0
Lipase, U/L	26.0
Diabetes-related tests	
Plasma glucose, mg/dL	665
HbA1c, %	8.0
Acetoacetate, μmol/L	1,936
3-hydroxybutyric acid, μmol/L	2,813
Fasting CPR, ng/mL	0.13
24-h CPR, μg/day†	5.74/3.82
GAD antibody, U/mL	<5.0
IA-2 antibody, U/mL	<0.4
ZnT8 antibody, U/mL	<10
Glucagon load test	
Fasting CPR, ng/mL	0.09
After 6 min CPR, ng/mL	0.12
Delta CPR, ng/mL	0.03
DNA typing	
HLA-DRB1*11:01-DQB1*03:01:01	NA
HLA-DRB1*13:02:01-DQB1*06:04:01	NA

*CPR, C-peptide immunoreactivity; GAD, glutamic acid decarboxylase; HbA1c, glycated hemoglobin; HLA, human leukocyte antigen; IA-2, insulinoma-associated antigen 2; NA, not applicable; ZnT8, zinc transporter 8.
†The 24-h CPR was measured twice for this patient because values can fluctuate greatly for patients who have diabetes.

Clinical courses described were similar to that for our patient. Our patient had typical symptoms of severe hyperglycemia begin 2 days after the second SARS-CoV-2 vaccine dose. Thus, we speculate that the mRNA vaccine administered before manifestation of hyperglycemic symptoms might have triggered fulminant onset of T1D in this patient, who was at risk because of receiving ICI treatment.

Because of their high efficacy, mRNA vaccines should be applicable for inhibition of many diseases, not only viral infections but also malignancies. The clinical course of the patient we report suggests that caution should be exercised when administering mRNA vaccines, especially to persons at risk for autoimmune diseases, such as patients receiving ICI treatments, because T1D, particularly its fulminant onset, can be life-threatening if not promptly recognized and treated. However, we cannot rule out the possibility that T1D development in this patient was unrelated to the vaccination. Accumulation of similar observations would clarify the relationship between SARS-CoV-2 vaccination and development of T1D, especially that associated with ICI treatment.

About the Author

Dr. Sato is a research scientist in the Department of Diabetes and Metabolism, Tohoku University Hospital, Sendai, Japan, and a graduate student at Tohoku University Graduate School of Medicine. His primary research interest is elucidation of mechanisms developing diabetes.

References

1. Mevorach D, Anis E, Cedar N, Bromberg M, Haas EJ, Nadir E, et al. Myocarditis after BNT162b2 mRNA vaccine against COVID-19 in Israel. N Engl J Med. 2021;385:2140–9. https://doi.org/10.1056/NEJMoa2109730
2. Witberg G, Barda N, Hoss S, Richter I, Wiessman M, Aviv Y, et al. Myocarditis after COVID-19 vaccination in a large health care organization. N Engl J Med. 2021;385:2132–9. https://doi.org/10.1056/NEJMoa2110737
3. Michot JM, Bigenwald C, Champiat S, Collins M, Carbonnel F, Postel-Vinay S, et al. Immune-related adverse events with immune checkpoint blockade: a comprehensive review. Eur J Cancer. 2016;54:139–48. https://doi.org/10.1016/j.ejca.2015.11.016
4. Baden MY, Imagawa A, Abiru N, Awata T, Ikegami H, Uchigata Y, et al.; consultation of the Japan Diabetes Society Committee on Type 1 Diabetes Mellitus Research. Characteristics and clinical course of type 1 diabetes mellitus related to anti-programmed cell death-1 therapy. Diabetol Int. 2018;10:58–66. https://doi.org/10.1007/s13340-018-0362-2
5. Quandt Z, Young A, Anderson M. Immune checkpoint inhibitor diabetes mellitus: a novel form of autoimmune diabetes. Clin Exp Immunol. 2020;200:131–40. https://doi.org/10.1111/cei.13424
6. Imagawa A, Hanafusa T, Awata T, Ikegami H, Uchigata Y, Osawa H, et al. Report of the Committee of the Japan Diabetes Society on the research of fulminant and acute-onset type 1 diabetes mellitus: new diagnostic criteria of fulminant type 1 diabetes mellitus. J Diabetes Investig. 2012;3:536–9. https://doi.org/10.1111/jdi.12024
7. Sahin U, Muik A, Derhovanessian E, Vogler I, Kranz LM, Vormehr M, et al. COVID-19 vaccine BNT162b1 elicits human antibody and T_H1 T cell responses. Nature. 2020;586:594–9. https://doi.org/10.1038/s41586-020-2814-7

Address for correspondence: Hideki Katagiri, Department of Diabetes and Metabolism, Tohoku University Hospital, 1-1 Seiryo, Aoba, Miyagi, Sendai 980-8574, Japan, email: katagiri@med.tohoku.ac.jp

University-Associated SARS-CoV-2 Omicron BA.2 Infections, Maricopa County, Arizona, USA, 2022

Nicole Fowle, Brenna Garrett, O'Zandra L. Floyd, Jennifer Collins, Aaron D. Krasnow, Mario Islas, Steven C. Holland, Matthew F. Smith, Efrem S. Lim, Nicole M. Jarrett, Sarah E. Scott

Author affiliations: Maricopa County Department of Public Health, Phoenix, Arizona, USA (N. Fowle, B. Garrett, O.L. Floyd, J. Collins, N.M. Jarrett, S.E. Scott); Arizona State University, Tempe, Arizona, USA (A.D. Krasnow, M. Islas, S.C. Holland, M.F. Smith, E.S. Lim)

DOI: https://doi.org/10.3201/eid2807.220470

We investigated a university-affiliated cohort of SARS-CoV-2 Omicron BA.2 infections in Arizona, USA. Of 44 cases, 43 were among students; 26 persons were symptomatic, 8 sought medical care, but none were hospitalized. Most (55%) persons had completed a primary vaccine series; 8 received booster vaccines. BA.2 infection was mild in this young cohort.

In November 2021, cases of highly transmissible SARS-CoV-2 B.1.1.529 Omicron BA.1 variant were identified in southern Africa (*1*; F.P. Lyngse et al., unpub. data, https://doi.org/10.1101/2022.01.28.22270044). By January 2022, BA.1 was the dominant variant circulating globally, and the BA.2 variant had been detected in several countries, including the United States (*2*,*3*; F.P. Lyngse et al.). The BA.1 variant causes milder illness compared with the B.1.617.2 and AY (Delta) subvariants, especially in younger persons and vaccinated persons (*4*; J.A. Lewnard et al., unpub. data, https://doi.org/10.1101/2022.01.11.22269045), but clinical severity of BA.2 is not yet well described. We describe illness severity and clinical outcomes of a 44-person US university-affiliated cohort, comprised predominantly of students, who tested positive for BA.2.

On January 24, 2022, the Maricopa County Department of Public Health (MCDPH), Arizona, USA, was notified of a BA.2 cluster in persons at a university. Cases were identified through routine surveillance by the university-affiliated genomics laboratory (Appendix, https://wwwnc.cdc.gov/EID/article/28/7/22-0470-App1.pdf). MCDPH investigated to describe the epidemiologic and clinical outcomes of the cohort.

We defined a case as a university student or staff member with a SARS-CoV-2 PCR-positive

saliva specimen collected during January 3–23 that was tested in the university laboratory and identified as BA.2 by next-generation sequencing. MCDPH and the university distributed electronic questionnaires to all case-patients via text message, email, or both, which is county and university protocol for anyone with SARS-CoV-2 infection (Appendix). MCDPH investigators also conducted telephone interviews with case-patients to collect information on demographics, recent travel, clinical symptoms and outcomes, and vaccination history. We considered a case lost to follow-up if the person could not be contacted by telephone or refused the telephone interview and they did not respond to either electronic questionnaire. We supplemented race/ethnicity (when otherwise unknown), vaccination history, and university clinic visit data by using the Arizona State Immunization Information System and university records.

We defined illness onset as the first date a case-patient experienced any SARS-CoV-2 symptom or the specimen collection date if a person was asymptomatic or lost to follow-up. We categorized vaccination status as unknown or unvaccinated when no documentation of vaccination was available, or a case-patient reported being unvaccinated. We categorized status as completed a primary series when case-patients had documentation of receiving a Food and Drug Administration–authorized or approved vaccination series or a series listed for emergency use by the World Health Organization and considered case-patients boosted when they had documentation of an additional vaccine dose after completing a primary series. We considered a case previously infected if the patient had a SARS-CoV-2–positive PCR or antigen test collected >90 days before BA.2 illness onset in the statewide communicable disease database.

We identified 44 cases, 43 (98%) were in students, which accounted for <1% of 6,268 university-affiliated persons who tested SARS-CoV-2–positive during the study period (*5*). Case-response rate to either questionnaire was 75%. Median age among case-patients was 21 (interquartile range 19–24) years; 29 (66%) were male; 12 (27%) identified as Asian/non-Hispanic, 3 (7%) as White/non-Hispanic, and 29 (66%) as other or unknown race/ethnicity.

At least 26 (59%) case-patients experienced ≥1 symptom, most of which were consistent with a viral upper respiratory tract infection, such as sore throat, rhinorrhea and cold-like symptoms, cough, and fever (Table). Only 8 (18%) case-patients sought medical attention from the university clinic ≤7 days before or after their BA.2-positive specimen collection date, but none were hospitalized, and none died.

Of 44 cases, 24 (55%) completed only the primary vaccine series, 8 (18%) received booster vaccines, 12 (27%) had an unknown or unvaccinated status, and 1 (2%) was previously infected with SARS-CoV-2. Of 32 case-patients who completed a primary series, 16 (50%) received an mRNA vaccine, either Comirnaty (Pfizer-BioNTech, https://www.pfizer.com) or

Table. Characteristics of SARS-CoV-2 B.1.1.529 Omicron BA.2 cases among students and staff affiliated with a local university, Maricopa County, Arizona, USA, January 2022*

Characteristics	No. (%)
Median age, y (IQR)	21 (19–24)
Sex	
M	29 (66)
F	15 (34)
Race and ethnicity	
Asian, non-Hispanic	12 (27)
White, non-Hispanic	3 (7)
Other/unknown	29 (66)
University affiliation	
Student	43 (98)
Staff	1 (2)
Case interview response type	
Telephone interview and electronic survey	20 (45)
Electronic survey only	13 (30)
Lost to follow-up	11 (25)
University clinic visit ≤7 d of illness onset†	
Y	8 (18)
N	36 (82)
Symptom status	
No symptoms	8 (18)
Unknown	10 (23)
Any COVID-19 symptom	26 (59)
Sore throat	18 (41)
Cough	16 (36)
Runny nose, cold-like symptoms	16 (36)
Fever	15 (34)
Muscle aches	11 (25)
Fatigue	10 (23)
Chills	4 (9)
Headache	4 (9)
Shortness of breath	2 (5)
Difficulty breathing	2 (5)
New loss of taste or smell	2 (5)
Diarrhea	2 (5)
Vomiting	1 (2)
Outcome	
Hospitalized	0
Died	0
COVID-19 vaccination status	
Primary series completed, not boosted	24 (55)
mRNA, Pfizer or Moderna	16 (50)
Janssen/Johnson & Johnson	5 (16)
Vaxzevria, Oxford-AstraZeneca	11 (34)
Primary series and booster completed	8 (18)
Unknown or unvaccinated	12 (27)
Median days from primary vaccination series completion to illness onset (IQR)‡	216 (164–269)
Median days from booster vaccine dose to illness onset (IQR)	27 (19–42)

*Illness onset is defined as the first day of symptom onset or the day of positive specimen collection (if asymptomatic or lost to follow-up). IQR, interquartile range.
†Within 7 days before or 7 days after illness onset.
‡Excludes case-patients who received a booster dose of COVID-19 vaccine (n = 8).

Spikevax (Moderna, https://www.moderna.com), 11 (34%) received Vaxzevria (Oxford-AstraZeneca, https://www.astrazeneca.com), and 5 (16%) received Janssen/Johnson & Johnson (https://www.jnj.com).

The mild illness and outcomes we describe might have been driven by the cohort's age rather than viral characteristics. Because our study involves a univwersity-affiliated cohort, these findings might not be generalizable to more diverse populations. Also, the low telephone interview participation rate prevented collection of close contact information to assess transmission dynamics. In addition, a potential unknown bias in random specimen selection for sequencing could limit the ability to generalize outcomes to this population.

In conclusion, >50% of 44 case-patients in our cohort experienced symptomatic BA.2 infection, but <25% sought medical care, suggesting BA.2 infection in a young population might be mild. In addition, nearly 75% of case-patients completed a primary vaccination series which, in addition to their age, might have contributed to their mild illness. However, data were insufficient to compare if vaccination status affected whether case-patients experienced symptoms or sought medical care. Among persons who completed a primary vaccine series, only 25% received booster vaccines. By March 2022, in alignment with Centers for Disease Control and Prevention recommendations (*6*), >33% of Maricopa County residents ≥18 years of age had received a booster dose. However, targeted efforts might be needed to encourage booster vaccines among university students (*7*).

Acknowledgments

We thank Sushmitha Ananth, Isabel Ayala-Vargas, Serena Bailey, Sarah Battaglia, Gerardo Calderon, Allyssa Del Rosario, Samantha Fetterley, Diana Griffin, Casey Guidera, Olivia Hunziker, Kimberly Kemp, Riley Matulewic, Madison Meyer, Bianca Muñoz, Patrice Nipape, Nathalie Nunez, Kiana Perez, Katrina Reading, and Sarah Reimus for conducting case investigations; Jessica White and Rebecca Sunenshine for their subject matter expertise and review; and Regan Sullins, James Hu, Nghia Pham, and Vel Murugan for their laboratory contributions.

This work was supported by the Epidemiology and Laboratory Capacity for Prevention and Control of Emerging Infectious Diseases COVID-19 response supplemental funding between Maricopa County Department of Public Health, Arizona Department of Health Services (ADHS), and the Centers for Disease Control and Prevention (CDC) (award no. NU50CK000511), ADHS (award no. CTR053916), CDC [CDC broad agency agreement no. 75D30121C11084] and the Tohono O'Odham Nation (award no. 2020-01 ASU).

About the Author

Mrs. Fowle is an infectious disease epidemiologist who leads and supervises the COVID-19 Investigations Branch at the Maricopa County Department of Public Health, Phoenix, Arizona, USA. Her primary research interests include vaccine-preventable diseases, outbreak investigations, data analysis, and epidemiologic methods.

References

1. CDC COVID-19 Response Team. SARS-CoV-2 B.1.1.529 (Omicron) variant—United States, December 1–8, 2021. MMWR Morb Mortal Wkly Rep. 2021;70:1731–4. https://doi.org/10.15585/mmwr.mm7050e1
2. GISAID. Tracking of variants [cited 2022 Mar 21]. https://www.gisaid.org/hcov19-variants
3. UK Health Security Agency. COVID-19 variants identified in the UK [cited 2022 Feb 14]. https://www.gov.uk/government/news/covid-19-variants-identified-in-the-uk
4. Wolter N, Jassat W, Walaza S, Welch R, Moultrie H, Groome M, et al. Early assessment of the clinical severity of the SARS-CoV-2 omicron variant in South Africa: a data linkage study [cited 2022 Feb 15]. Lancet. 2022;399:437–46. https://doi.org/10.1016/S0140-6736(22)00017-4
5. Arizona State University. Weekly COVID-19 report, ASU's COVID-19 data update archive 2022 Jan [cited 2022 Mar 1]. https://eoss.asu.edu/health/announcements/coronavirus/management#archive
6. Centers for Disease Control and Prevention. COVID-19 vaccine booster shots [cited 2022 Mar 21]. https://www.cdc.gov/coronavirus/2019-ncov/vaccines/booster-shot.html
7. Maricopa County Department of Public Health. Maricopa County COVID-19 vaccine data [cited 2022 Mar 21]. https://www.maricopa.gov/5671/Public-Vaccine-Data

Address for correspondence: Nicole Fowle, Maricopa County Department of Public Health, 4041 N Central Ave, Ste 600, Phoenix, AZ 85012, USA; email: nicole.fowle@maricopa.gov2

Zoster Meningitis in an Immunocompetent Child after COVID-19 Vaccination, California, USA

Sarah K. Daouk,[1] Edwin Kamau,[1] Kristina Adachi, Grace M. Aldrovandi

Author affiliation: David Geffen School of Medicine at University of California, Los Angeles, USA

DOI: http://doi.org/10.3201/eid2807.220600

Varicella zoster virus reactivation after COVID-19 vaccination has been reported in older or immunocompromised adults. We report zoster meningitis from live-attenuated varicella vaccine reactivation in an immunocompetent child after COVID-19 vaccination. This type of case is rare; COVID-19 and varicella vaccines remain safe and effective for appropriate recipients in the pediatric population.

The COVID-19 mRNA vaccines authorized in the United States are highly effective and safe, causing few adverse events (*1*). Cases of varicella zoster virus (VZV) reactivation after COVID-19 vaccination have been reported, but most occurred in older adults with comorbid conditions and known risk factors for VZV reactivation (*2*,*3*). We report a case of zoster meningitis reactivation from live-attenuated varicella vaccine (vOka) in a healthy child, occurring in close temporal relation with Pfizer-BioNTech (https://www.pfizer.com) BNT162b2 vaccination.

We evaluated a 12-year-old boy at the UCLA Mattel Children's Hospital (Los Angeles, CA, USA) for papulovesicular rash with lumbar L1 dermatomal distribution; the rash gradually progressed to the L2 area (Figure), trunk, and scalp. The rash was preceded by a 1-week history of severe flank and thigh pain. The patient initially was seen at another hospital, where abdominal/pelvic computed tomography imaging led to a diagnosis of kidney stones and mesenteric adenitis. His pain persisted after discharge, and he then developed the vesicular rash described, along with twitching movements, headache, and photophobia. No change in mentation or focal neurologic findings were noted. The patient was otherwise healthy and taking no medications, including inhaled corticosteroids. His immunizations were up-to-date, including 2 doses of vOka, 1 at age 12 months and another at 18 months. He received his first dose of BNT162b2 vaccine 11 days before onset of the symptoms described.

Laboratory studies revealed levels of leukocytes, platelets, C-reactive protein and transaminases within reference ranges. The cerebrospinal fluid had a leukocyte level of 252 cells/mm^3 (reference range 0–5 cells/mm^3) and a protein level of 96 mg/dL (reference range 15–45 mg/dL). Results of gram stain and cultures were negative. Cerebrospinal fluid and vesicular lesions were PCR-positive for VZV and were determined to be the vOka strain by the Centers for Disease Control and Prevention using a VZV fluorescence resonance energy transfer PCR. A cerebrospinal fluid viral meningoencephalitis antibody panel with >30 targets detected only VZV antibodies (Quest Diagnostics, http://www.questdiagnostics.com). The ePlex respiratory pathogen panel PCR (GenMark Diagnostics, https://www.genmarkdx.com) was positive for only rhinovirus/enterovirus, presumably representing recent infection. Other studies, including those for HIV, herpes simplex virus, SARS-CoV-2, and QuantiFERON-TB, were negative. Immunologic (T-cell, B cell, and natural killer cell cytotoxicity) studies revealed no underlying immunodeficiency. Exome sequencing performed using the Agilent SureSelect Clinical Research Exome XT kit (Agilent Technologies, https://www.agilent.com) and an Illumina HiSeq 2500 (Illumina, https://www.illumina.com) established no clinically important variants. The patient was treated with intravenous acyclovir for 10 days and recovered uneventfully.

The incidence of uncomplicated herpes zoster (HZ) in vaccinated children is rare: an estimated 48 cases/100,000 person-years compared with 230 cases/100,000 person-years in unvaccinated children, a 79% reduction (*4*). Rarer yet are cases where vOka reactivation led to meningitis; only 14 cases have been reported in children, 3 of whom were immunocompromised and 6 of whom had received the recommended 2 doses of vOKa (*5*). The average age of these patients was 12.5 years, and the time to HZ reactivation from their first vaccine dose averaged 11.5 years. Similarly, this patient experienced HZ reactivation when he was 12 years old, 11 years after when he received his first vOka dose, which was administered in his thigh. The L1/L2 location of his rash is consistent with vaccine-associated HZ, wherein the virus travels from the site of inoculation to establish latency in the lumbosacral plexus. In contrast, rash with HZ reactivation after infection occurs in the most common sites of vesicles, including the face and lower cervical or upper thoracic dermatomes (*6*).

[1]These authors contributed equally to this article.

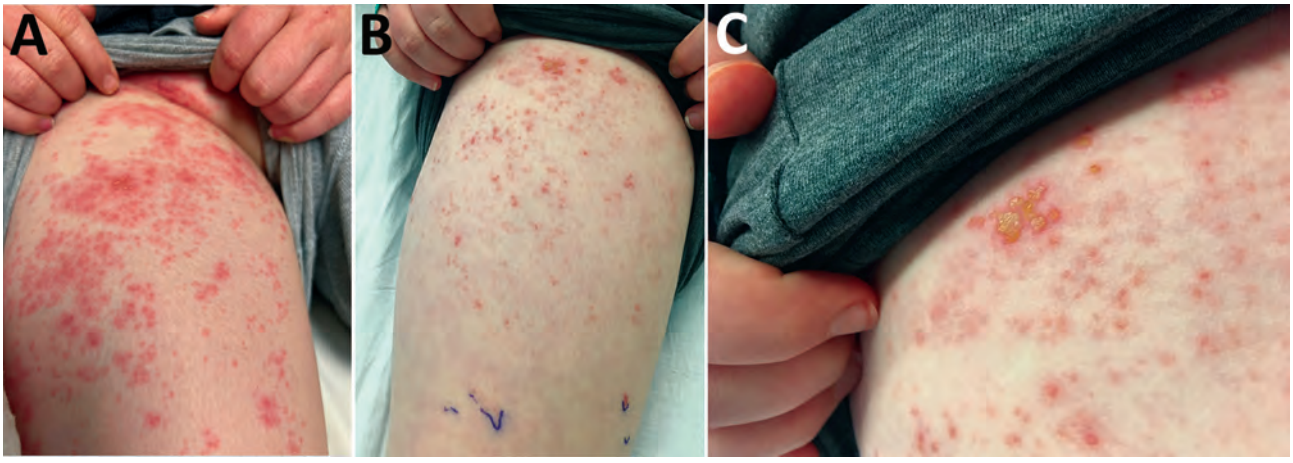

Figure. Rash in a 12-year-old boy with zoster meningitis after COVID-19 vaccination, California, USA. A) Rash on right groin and thigh at admission; B, C) improving rash after 4 days of acyclovir.

HZ reactivation is more frequent in adults, particularly in the elderly, because of waning of cellular immunity, and among immunocompromised persons. Changes in the immune status after COVID-19 vaccination has been postulated to lead to VZV reactivation (*2*,*3*). Reports have described reactivation of herpes virus infections after vaccination and after use of oral corticosteroids (*5*,*7*). HSV reactivation also has been reported following COVID-19 mRNA vaccines (*8*). In immunocompetent children, HZ has been linked to changes in cytokine profiles, similar to those seen after neurotropic viral infection, including infection with enteroviruses (*5*). At the time of HZ reactivation, this patient also was recovering from rhinovirus infection, which can suppress and dysregulate immune competence (*9*). We hypothesize that COVID-19 vaccination led to a shift in CD8 T-cell immunity, resulting in this unusual and rarely observed reactivation and dissemination. Immune dysregulation attributable to rhinovirus infection also might have exacerbated the immune shift after COVID-19 vaccination.

In conclusion, COVID-19 and varicella vaccines are extremely effective and safe in preventing disease in children. However, to ensure appropriate patient care, clinicians must be aware that rare sequelae, such as HZ reactivation, zoster meningitis, or both, might also occur.

About the Author

Dr. Daouk is a fellow in the UCLA Department of Pediatrics, Division of Infectious Diseases whose primary interests include medical education, vaccine-preventable disease and preventative medicine. Dr. Kamau is a CPEP Fellow in the Department of Pathology and Laboratory Medicine at UCLA whose primary interests include clinical microbiology and epidemiological studies.

References

1. Barda N, Dagan N, Ben-Shlomo Y, Kepten E, Waxman J, Ohana R, et al. Safety of the BNT162b2 mRNA Covid-19 vaccine in a nationwide setting. N Engl J Med. 2021;385:1078–90. https://doi.org/10.1056/NEJMoa2110475
2. Katsikas Triantafyllidis K, Giannos P, Mian IT, Kyrtsonis G, Kechagias KS. Varicella zoster virus reactivation following COVID-19 vaccination: a systematic review of case reports. Vaccines (Basel). 2021;9:1013. https://doi.org/10.3390/vaccines9091013
3. Desai HD, Sharma K, Shah A, Patoliya J, Patil A, Hooshanginezhad Z, et al. Can SARS-CoV-2 vaccine increase the risk of reactivation of varicella zoster? A systematic review. J Cosmet Dermatol. 2021;20:3350–61. https://doi.org/10.1111/jocd.14521
4. Weinmann S, Chun C, Schmid DS, Roberts M, Vandermeer M, Riedlinger K, et al. Incidence and clinical characteristics of herpes zoster among children in the varicella vaccine era, 2005–2009. J Infect Dis. 2013;208:1859–68. https://doi.org/10.1093/infdis/jit405
5. Ramachandran PS, Wilson MR, Catho G, Blanchard-Rohner G, Schiess N, Cohrs RJ, et al. Meningitis caused by the live varicella vaccine virus: metagenomic next generation sequencing, immunology exome sequencing and cytokine multiplex profiling. Viruses. 2021;13:2286. https://doi.org/10.3390/v13112286
6. Moodley A, Swanson J, Grose C, Bonthius DJ. Severe herpes zoster following varicella vaccination in immunocompetent young children. J Child Neurol. 2019;34:184–8. https://doi.org/10.1177/0883073818821498
7. Walter R, Hartmann K, Fleisch F, Reinhart WH, Kuhn M. Reactivation of herpesvirus infections after vaccinations? Lancet. 1999;353:810. https://doi.org/10.1016/S0140-6736(99)00623-6
8. Fathy RA, McMahon DE, Lee C, Chamberlin GC, Rosenbach M, Lipoff JB, et al. Varicella-zoster and herpes simplex virus reactivation post-COVID-19 vaccination: a review of 40 cases in an international dermatology registry. J Eur Acad Dermatol Venereol. 2022;36:e6–9. https://doi.org/10.1111/jdv.17646
9. Kirchberger S, Majdic O, Stockl J. Modulation of the immune system by human rhinoviruses. Int Arch Allergy Immunol. 2007;142:1–10. https://doi.org/10.1159/000095993

Address for correspondence: Grace M. Aldrovandi, David Geffen School of Medicine at University of California, 11633 San Vicente Blvd, Los Angeles, CA 90449, USA; email: galdrovandi@mednet.ucla.edu

Circulation of Enterovirus D68 during Period of Increased Influenza-Like Illness, Maryland, USA, 2021

Amary Fall, Nicholas Gallagher, C. Paul Morris, Julie M. Norton, Andrew Pekosz, Eili Klein, Heba H. Mostafa

Author affiliations: Johns Hopkins School of Medicine, Baltimore, Maryland, USA (A. Fall, N. Gallagher, C.P. Morris, J.M. Norton, A. Pekosz, E. Klein, H.H. Mostafa); National Institute of Allergy and Infectious Disease, National Institutes of Health, Bethesda, Maryland, USA (C.P. Morris); Johns Hopkins Bloomberg School of Public Health, Baltimore (A. Pekosz); Center for Disease Dynamics, Economics, and Policy, Washington, DC, USA (E. Klein)

DOI: https://doi.org/10.3201/eid2807.212603

We report enterovirus D68 circulation in Maryland, USA, during September–October 2021, which was associated with a spike in influenza-like illness. The characterized enterovirus D68 genomes clustered within the B3 subclade that circulated in 2018 in Europe and the United States.

In early July 2021, the United States began to relax COVID-19 infection control measures. As the number of COVID-19 cases began to fall, cases of influenza-like illness (Appendix Table 1, https://wwwnc.cdc.gov/EID/article/28/7/21-2603-App1.pdf) continued to be seen in the Johns Hopkins Hospital system (Baltimore, MD, USA) through October 2021 (Appendix Figure 1). Enterovirus/rhinovirus were detectable throughout the pandemic (*1*,*2*), but their positivity markedly increased to reach 20.7% (of all samples tested for enterovirus/rhinovirus) in October 2021, surpassing all other respiratory viruses (Appendix Figure 2) (*2*).

Enterovirus-D68 (EV-D68) was associated with a large outbreak of respiratory disease in children in North America in 2014 and was subsequently linked to the occurrence of acute flaccid myelitis (AFM) (*3*). After the 2014 outbreak, active surveillance of EV-D68 was implemented in many countries in Asia, Europe, Africa, and the Americas. Data obtained through surveillance during 2014–2018 suggested a biennial circulation cycle in Europe and North America (*4*,*5*). However, despite this expected biennial pattern, EV-D68 detection in 2020 was lower than anticipated, and limited cases were detected in the United States (*6*). This change in the circulation of EV-D68 in 2020 might have been secondary to the widespread mitigation measures for COVID-19. Of note, a recent study from 8 countries in Europe reported a rapid increase in EV-D68 infections during July 31–October 14, 2021, which coincided with a period of relaxed COVID-19 mitigation measures (*7*).

For this study, we collected samples positive for enterovirus/rhinovirus after the standard-of-care diagnosis at the Johns Hopkins Medical Microbiology Laboratory during September–October 2021 (Figure; Appendix). Research was conducted under Johns Hopkins Institutional Review Board protocol IRB00221396 with a waiver of consent. Remnant nasopharyngeal clinical specimens from patients that tested positive for enterovirus/rhinovirus during September–October 2021 were retrieved for the study. Genomes were made publicly available in GenBank (accession nos. OL826825–36).

We employed an optimized typing approach by using Nanopore next-generation sequencing (NGS) to characterize the enterovirus types (September–October 2021) associated with the increase in influenza-like illness. In brief, we used primers specific for enterovirus species A–D to amplify a ≈4,500-nt fragment that covers the whole P1 region (about half of the genome) (*8*) and then performed sequencing (Appendix). Of 280 enterovirus/rhinovirus-positive samples, we collected 262 for genotyping (Figure). We detected enterovirus in 28.6% of the 63 successfully sequenced samples (18/63); 94.4% (17/18) were EV-D68 and 5.6% (1/18) were coxsackievirus A6 (CV-A6). Even though the primers used for amplification were specific for enteroviruses, rhinoviruses were characterized in 45 of the 63 samples; those rhinoviruses consisted primarily of species C (26/45), followed by A (13/45) and B (6/45).

The whole cohort of patients positive for enterovirus/rhinovirus during September–October 2021 ranged in age from <1 year to >90 years; mean age was 16.7 years and median age 5 years. The male:female ratio was 1:1. On the other hand, the median age of EV-D68–positive patients was 2 years, and the male:female ratio was 1:3 (Appendix Table 2). EV-D68 was detected in 15/168 (8.9%) pediatric specimens positive for enterovirus/rhinovirus during the study time frame. Symptoms or signs of viral or respiratory illness were reported in all pediatric patients with EV-D68 (N = 15) (Appendix Table 2), and 5 patients (33.3%) were admitted and required supplemental oxygen, admission to the intensive care unit, or both. No neurologic complications including AFM

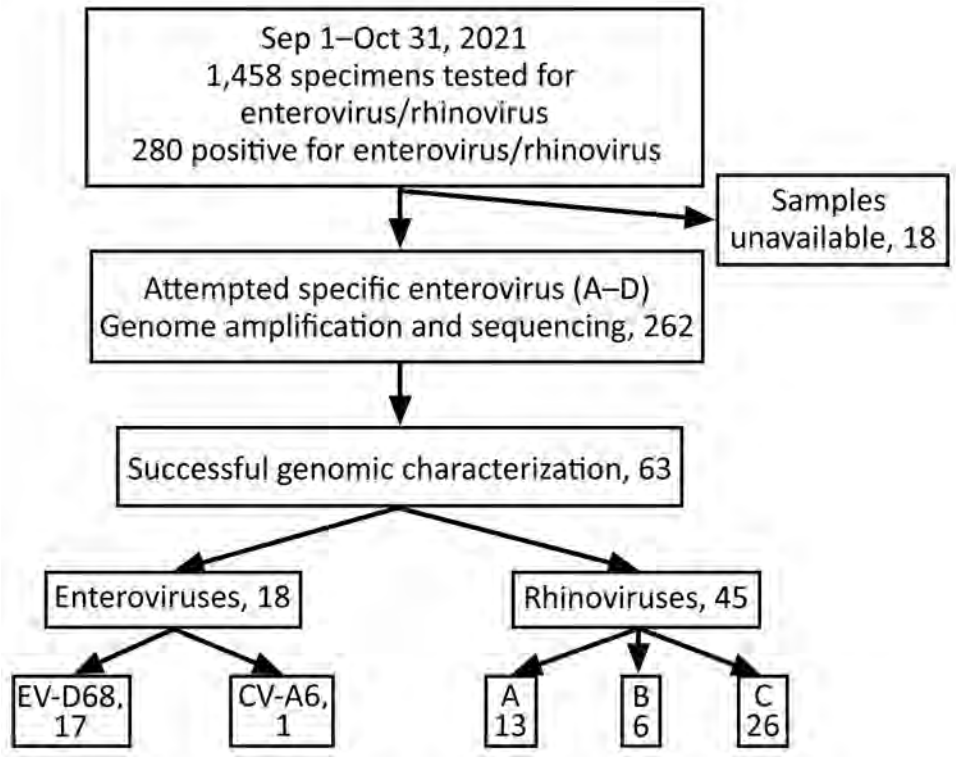

Figure. Flowchart of patients and specimens in study of circulation of EV-D68 during period of increased influenza-like illness, Maryland, USA, 2021. CV-A6, coxsackievirus A6; EV-D68, enterovirus D68.

were observed (Appendix Table 2). Of note, no AFM cases were diagnosed at Johns Hopkins Hospital during the study time frame. Most cases of enterovirus were detected in residents of the city of Baltimore (11/17). A total of 12 EV-D68 sequences, subclade B3, had a complete 5′ half of the genome (3000–4200 bp). EV-D68 genomes clustered with strains detected in 2019 from several countries in Europe (Appendix Figure 3).

We report a predominance of EV-D68 among the circulating enteroviruses during the same period in which enterovirus/rhinovirus positivity increased in this hospital system (*2*). The predominance of EV-D68 in our study (27% of total enterovirus/rhinovirus-typed genomes) was higher than the 0.4% and 3.6% observed in 2019 and 2020 in the United States (*6*) and comparable to the 24.3% reported before the COVID-19 pandemic in 2018 (*6*).

The EV-D68 strains detected belong to the B3 subclade, which had not been reported from the United States since 2018 (*6*) but was detected in Europe in 2019 (*9*). The strains we detected form a distinct cluster within the B3 subclade that circulated in 2018 in Europe and the United States but seem very close to those characterized in Europe in 2019. Nevertheless, it was reported that strains circulating in Europe in 2019 are common ancestors of strains detected in the United States in 2018 (*9*). That report might explain why the strains we identified are more closely related to subclade B3 from the United States than to those from Europe in 2018.

This publication was made possible by support from the Sherrilyn and Ken Fisher Center for Environmental Infectious Diseases, Division of Infectious Diseases, Johns Hopkins University School of Medicine. Its contents are solely the responsibility of the authors and do not necessarily represent the official view of the Fisher Center or Johns Hopkins University School of Medicine.

H.H.M. is supported by the HIV Prevention Trials Network sponsored by the National Institute of Allergy and Infectious Diseases. Funding was provided by the Johns Hopkins Center of Excellence in Influenza Research and Surveillance (HHSN272201400007C), National Institute on Drug Abuse, National Institute of Mental Health, and Office of AIDS Research, of the NIH, DHHS (UM1 AI068613), the NIH RADx-Tech program (3U54HL143541-02S2), National Institute of Health RADx-UP initiative (grant R01 DA045556-04S1), Centers for Disease Control (contract 75D30121C11061), the Johns Hopkins University President's Fund Research Response, the Johns Hopkins Department of Pathology, and the Maryland Department of Health. E.K. was supported by Centers for Disease Control and Prevention MInD-Healthcare Program (Grant no. U01CK000589).

About the Author

Dr. Fall is a postdoctoral research fellow in the Department of Pathology, Division of Medical Microbiology, Johns Hopkins School of Medicine. His primary research focus is respiratory viral surveillance, particularly enteroviruses and adenoviruses. Dr. Mostafa is an assistant professor of pathology and director of the Molecular Virology Laboratory at Johns Hopkins School of Medicine. Her research focuses on viral genomic evolution and its association with outbreaks and severe disease.

References

1. Olsen SJ, Winn AK, Budd AP, Prill MM, Steel J, Midgley CM, et al. Changes in influenza and other respiratory virus activity during the COVID-19 pandemic—United States, 2020–2021. MMWR Morb Mortal Wkly Rep. 2021;70:1013–9. https://doi.org/10.15585/ mmwr.mm7029a1
2. Uhteg K, Amadi A, Forman M, Mostafa HH. Circulation of Non-SARS-CoV-2 respiratory pathogens and coinfection with SARS-CoV-2 amid the COVID-19 pandemic. Open Forum Infect Dis. 2021;9:b618. https://doi.org/10.1093/ofid/ofab618
3. Aliabadi N, Messacar K, Pastula DM, Robinson CC, Leshem E, Sejvar JJ, et al. Enterovirus D68 infection in children with acute flaccid myelitis, Colorado, USA, 2014. Emerg Infect Dis. 2016;22:1387–94. https://doi.org/10.3201/eid2208.151949
4. Kramer R, Sabatier M, Wirth T, Pichon M, Lina B, Schuffenecker I, et al. Molecular diversity and biennial circulation of enterovirus D68: a systematic screening study in Lyon, France, 2010 to 2016. Euro Surveill. 2018;23:1700711.
5. Messacar K, Pretty K, Reno S, Dominguez SR. Continued biennial circulation of enterovirus D68 in Colorado. J Clin Virol. 2019;113:24–6.
6. Shah MM, Perez A, Lively JY, Avadhanula V, Boom JA, Chappell J, et al. Enterovirus D68-associated acute respiratory illness—new vaccine surveillance network, United States, July–November 2018–2020. MMWR Morb Mortal Wkly Rep. 2021;70:1623–8. https://doi.org/10.15585/mmwr.mm7047a1
7. Benschop KS, Albert J, Anton A, Andrés C, Aranzamendi M, Armannsdóttir B, et al. Re-emergence of enterovirus D68 in Europe after easing the COVID-19 lockdown, September 2021. Euro Surveill. 2021;26. https://doi.org/10.2807/1560-7917.ES.2021.26.45.2100998
8. Joffret ML, Polston PM, Razafindratsimandresy R, Bessaud M, Heraud JM, Delpeyroux F. Whole genome sequencing of enteroviruses species A to D by high-throughput sequencing: application for viral mixtures. Front Microbiol. 2018;9:2339. https://doi.org/10.3389/fmicb.2018.02339
9. Midgley SE, Benschop K, Dyrdak R, Mirand A, Bailly JL, Bierbaum S, et al. Co-circulation of multiple enterovirus D68 subclades, including a novel B3 cluster, across Europe in a season of expected low prevalence, 2019/20. Euro Surveill. 2020;25. https://doi.org/10.2807/1560-7917.ES.2020.25.2.1900749

Address for correspondence: Heba Mostafa, The Johns Hopkins Hospital, Meyer B-121F, 600 N. Wolfe St, Baltimore, MD 21287, USA; email: Hmostaf2@jhmi.edu

Genomic Evidence of In-Flight SARS-CoV-2 Transmission, India to Australia, April 2021

Freya Hogarth, Pasqualina Coffey, Laura Goddard, Sarah Lewis, Shereen Labib, Mathilda Wilmot, Patiyan Andersson, Norelle Sherry, Torsten Seemann, Benjamin P. Howden, Kevin Freeman, Robert Baird, Ian Hosegood, Kathleen McDermott, Nick Walsh, Ben Polkinghorne, Catherine Marshall, Jane Davies, Vicki Krause, Ella M. Meumann

Author affiliations: Australian Government Department of Health, Canberra, Australian Capital Territory, Australia (F. Hogarth); The Australian National University, Canberra (F. Hogarth, B. Polkinghorne); Centre for Disease Control, Darwin, Northern Territory, Australia (P. Coffey, L. Goddard, S. Lewis, S. Labib, V. Krause); The University of Melbourne at The Peter Doherty Institute for Infection and Immunity, Melbourne, Victoria, Australia (M. Wilmot, P. Andersson, N. Sherry, T. Seemann, B.P. Howden); Royal Darwin Hospital, Darwin (K. Freeman, R. Baird, C. Marshall, J. Davies, E.M. Meumann); Qantas Airways Limited, Mascot, New South Wales, Australia (I. Hosegood); National Critical Care and Trauma Response Centre, Darwin (K. McDermott, N. Walsh); Menzies School of Health Research and Charles Darwin University, Darwin (J. Davies, E.M. Meumann)

DOI: https://doi.org/10.3201/eid2807.212466

Epidemiologic and genomic investigation of SARS-CoV-2 infections associated with 2 repatriation flights from Australia to India in April 2021 indicated that 4 passengers transmitted SARS-CoV-2 to ≥11 other passengers. Results suggest transmission despite mandatory mask use and predeparture testing. For subsequent flights, predeparture quarantine and expanded predeparture testing were implemented.

During the first epidemic wave of SARS-CoV-2, Australia closed its borders; during March 28, 2020–November 1, 2021, international arriving passengers were required to undergo mandatory supervised quarantine (*1*). This initial response contributed to the end of the first pandemic wave in June 2020 and resulted in periods of COVID-19 control throughout the country (*2*).

Beginning October 23, 2020, a quarantine facility in Darwin, Northern Territory, Australia, received persons who arrived via government-assisted repatriation flights. On April 15 and 17, 2021, two repatriation flights (flights 1 and 2) carrying pas-

Table. Detailed information of case-patients belonging to SARS-CoV-2 genomic clusters detected after 2 flights from India to Darwin, Northern Territory, Australia, on April 15 and April 17, 2021*

Cluster and case-patient	Age group, y/sex	Family group	Virus Pango lineage	Cycle threshold	Symptom onset date	Date tested positive	Vaccinated	Seat no.
1								
A	30–39/M	None	B.1.617.2	14.3	Asymptomatic	Apr 15	N	56B
B	40–49/M	I	B.1.617.2	15.6	Asymptomatic	Apr 15	N	43D
C	20–29/F	I	B.1.617.2	11.6	Apr 20	Apr 20	N	43E
D	1–5/F	I	B.1.617.2	11.6	Asymptomatic	Apr 20	N	43F
E	<1/M	I	B.1.617.2	12.2	Asymptomatic	Apr 20	N	43D
F	30–39/M	II	B.1.617.2	22.6	Apr 20	Apr 20	N	43K
G	10–19/F	II	B.1.617.2	18	Apr 20	Apr 20	N	43H
H	1–5/M	II	B.1.617.2	26.5	Asymptomatic	Apr 20	N	43J
I	<1/F	II	B.1.617.2	19	Asymptomatic	Apr 20	N	43K
2								
J	20–29/F	None	B.1.617.1	12.4	Apr 16	Apr 15	N	42A
K	50–59/M	None	B.1.617.1	16.6	Apr 17	Apr 20	N	51H
L	1–5/M	III	B.1.617.1	22	Asymptomatic	Apr 22	N	42B
M	1–5/M	III	B.1.617.1	18.1	Apr 22	Apr 22	N	43B
N	30–39/F	III	B.1.617.1	20	Asymptomatic	Apr 22	N	43B
3								
O	50–59/F	IV	B.1.617.2	14.9	Asymptomatic	Apr 15	Y	3E
P	60–69/M	IV	B.1.617.2	14.9	Apr 15	Apr 16	Y	3F
Q	10–19/F	None	B.1.617.2	11.4	Asymptomatic	Apr 17	N	4E
4								
R	50–59/M	V	B.1.617.2	14.9	Asymptomatic	Apr 22	N	55A
S	60–69/F	V	B.1.617.2	14.9	Apr 22	Apr 23	N	55B
5								
T	10–19/M		B.1.617.2	11.7	Apr 17	Apr 18	N	48C
U	30–39/M	VI	B.1.617.2	16.1	Asymptomatic	Apr 24	N	48B
V	30–39/F	VI	B.1.617.2	12.8	Not available	Apr 24	N	48A
W	1–5/M		B.1.617.2	24.5	Asymptomatic	Apr 24	N	48J
6								
X	30–39/M	VII	B.1.1.7	10.9	Asymptomatic	Apr 17	N	43F
Y	40–49/M	VII	B.1.1.7	13.1	Asymptomatic	Apr 17	N	43E

sengers from 2 regions of India experiencing major COVID-19 outbreaks landed in Darwin. The percentages of passengers positive for COVID-19 were substantially greater for these 2 flights (24/164 [15%] and 23/181 [13%]) than for all previous repatriation flights to Darwin (225/9,651 [2%] during October 2020–April 2021).

In the 48 hours before flying, all passengers on the 2 flights had tested negative for SARS-CoV-2 by quantitative reverse transcription PCR (qRT-PCR). All passengers except infants and children were required to wear masks (*3*). COVID-19 vaccination coverage among passengers was low; 24/345 (7%) passengers had received ≥1 dose, and only 14 had received 2 doses of the same vaccine ≥14 days apart. At arrival, passengers entered quarantine, where they were tested for SARS-CoV-2 by qRT-PCR on days 0, 7, and 12, in addition to testing if symptomatic (Appendix 1, https://wwwnc.cdc.gov/EID/article/28/7/21-2466-App1.pdf).

Of the 47 passengers with positive results, 21 tested positive at arrival (arrival case-patients) and 26 tested positive ≥1 day after arriving in quarantine (quarantine case-patients) (Appendix 1 Figures 1, 2). Of the 21 arrival case-patients (Table), 18 were asymptomatic. qRT-PCR cycle threshold values were available for 18/21 (86%) arrival case-patients; median was 15.2 (range 8.4–34.1) cycles. For quarantine case-patients, median time of symptom onset was 5 (range 0–8) days after arrival, and the median number of days from arrival to a positive test result was 4 (range 1–7) days.

Among 41 (87%) of 47 SARS-CoV-2 genome sequences generated from case-patients on flights and 1 and 2, variant types were Delta (B.1.617.2) for 27 (57%), Kappa (B.1.617.1) for 10 (21%), Alpha (B.1.1.7) for 3 (6%), and A.23.1 sublineage for 1 (2%). Of 41 sequences, 25 (59%) belonged to 1 of 6 genomic clusters (Table; Figure; Appendix 1 Figure 3).

To determine whether infections were likely to have been acquired during flight, we analyzed case interviews, flight manifests, and genomic sequencing. Of the 21 arrival case-patients, 4 (19%) (identified as B, J, O, and T) on both flights were likely to have transmitted SARS-CoV-2 to ≥11 other passengers (F–I, L–N, Q, and U–W) who had sequences that belonged to the same SARS-CoV-2 genomic clusters, who did not belong to the same family group of an arrival case-patient, and who had been seated within 2 rows of an arrival case-patient. Using this

information, we calculated secondary attack rates of 6% (8/143) for flight 1 and 2% (3/168) for flight 2. Five case-patients (C–E, P, and Y) with genomically linked virus belonged to arrival case family groups for which transmission possibly occurred before, during, or after the flight. One case-patient (K) with virus belonging to a genomic cluster was seated >2 rows from an arrival case-patient with genomically linked virus. Virus from 2 quarantine case-patients (R and S) genomically linked them to each other but not to an arrival case-patient (Table; Figure; Appendix 1). Only 5 quarantine case-patients from the flights had sequences that did not belong to a SARS-CoV-2 genomic cluster (Appendix 1 Figures 1, 2). Genomics refuted transmission to 6 quarantine case-patients seated within 2 rows of an arrival case-patient, linking 3 to a different cluster.

Soon after the 2 repatriation flights reported here, other repatriation flights from India were suspended, but flights resumed on May 15, 2021, when mandatory 72-hour preflight quarantine of passengers within India was instituted and testing of passengers was expanded to include rapid antigen testing on entry to preflight quarantine, qRT-PCR testing 48 hours before departure, and rapid antigen testing on the day of departure (*4*). During May 15–October 14, 2021, SARS-CoV-2 test results were positive for 13 (0.29%) of 4,543 passengers on repatriation flights from India and 30 (0.28%) of 10,679 passengers on repatriation flights to Darwin. Probable contributors to reduced repatriation cases were increasing vaccination rates and abatement of the Delta wave in India and globally (*5*).

At the time of this study, COVID-19 vaccination rates in Australia were low, most jurisdictions had little or no community transmission of SARS-CoV-2, and quarantine was key to reducing international incursions. We could not exclude transmission in the departure lounge and during boarding; however, spatial proximity of case-patients who did not belong to the same family groups but had genomically linked virus supported in-flight transmission. Previous studies that reported in-flight transmission of SARS-CoV-2 (*6*–*10*) did not include preflight testing, whereas our study included complete preflight and postflight testing and genomic sequencing. In conclusion, our investigation revealed evidence of flight-associated SARS-CoV-2 transmission on 2 repatriation flights from India to Australia during the Delta variant wave in April 2021.

Acknowledgments

We gratefully acknowledge contact tracing staff at the Northern Territory Centre for Disease Control Public

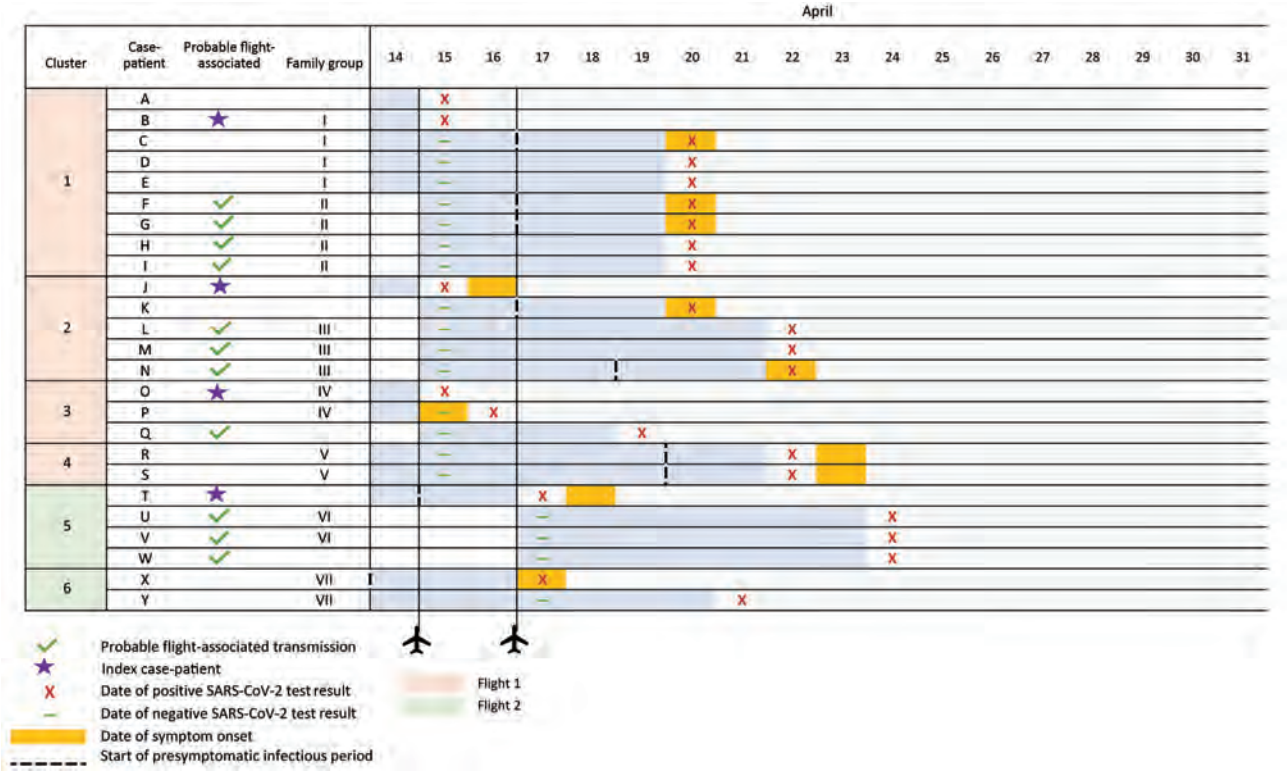

Figure. Schematic showing genomic clusters and in-flight transmission of SARS-CoV-2 on 2 flights from India to Australia, April 2021.

Health Unit for interviewing case-patients and assisting with this investigation. We acknowledge the work of various laboratory staff at the Royal Darwin Hospital, who tested specimens and provided the results that contributed to the quality of this report. We thank the Australian Medical Assistance Team managed by the National Critical Care and Trauma Centre and staff at the Howard Springs International Quarantine Centre for their collaboration and the safe management of these international arrivals during quarantine. We thank Qantas Airways for repatriating persons home to Australia and their cooperation and valuable contribution to this investigation.

This work was supported by the Medical Research Future Fund (MRF9200006).

About the Author

Ms. Hogarth is a Master of Philosophy (Applied Epidemiology) Scholar at the Australian National University. She is undertaking her field placement at the Australian Government Department of Health, where she has contributed to the national COVID-19 response.

References

1. Australian Government Department of Health. We're opening borders to the world. 2021 Nov 1 [cited 2022 Mar 12]. https://www.health.gov.au/news/were-opening-our-borders-to-the-world
2. Giles ML, Wallace EM, Alpren C, Brady N, Crouch S, Romanes F, et al. Suppression of severe acute respiratory syndrome coronavirus 2 (SARS-CoV-2) after a second wave in Victoria, Australia. Clin Infect Dis. 2021;73:e808–10. https://doi.org/10.1093/cid/ciaa1882
3. Australian Government Department of Health. Coronavirus (COVID-19) advice for international travellers [cited 2021 May 15]. https://www.health.gov.au/news/health-alerts/novel-coronavirus-2019-ncov-health-alert/coronavirus-covid-19-travel-and-restrictions/coronavirus-covid-19-advice-for-international-travellers
4. Worldometer. India: coronavirus [cited 2021 Mar 2]. https://www.worldometers.info/coronavirus/country/india
5. Qantas Airways Limited. Special flight from India to Australia [cited 2021 Jul 28]. https://www.qantas.com/in/en/travel-info/travel-updates/coronavirus/qantas-international-network-changes/flights-delhi-darwin.html
6. Speake H, Phillips A, Chong T, Sikazwe C, Levy A, Lang J, et al. Flight-associated transmission of severe acute respiratory syndrome coronavirus 2 corroborated by whole-genome sequencing. Emerg Infect Dis. 2020;26:2872–80. https://doi.org/10.3201/eid2612.203910
7. Murphy N, Boland M, Bambury N, Fitzgerald M, Comerford L, Dever N, et al. A large national outbreak of COVID-19 linked to air travel, Ireland, summer 2020. Euro Surveill. 2020;25:2001624. https://doi.org/10.2807/1560-7917.ES.2020.25.42.2001624
8. Khanh NC, Thai PQ, Quach H-L, Thi NH, Dinh PC, Duong TN, et al. Transmission of SARS-CoV-2 during long-haul flight. Emerg Infect Dis. 2020;26:2617–24. https://doi.org/10.3201/eid2611.203299
9. Swadi T, Geoghegan JL, Devine T, McElnay C, Sherwood J, Shoemack P, et al. Genomic evidence of in-flight transmission of SARS-CoV-2 despite predeparture testing. Emerg Infect Dis. 2021;27:687–93. https://doi.org/10.3201/eid2703.204714
10. Chen J, He H, Cheng W, Liu Y, Sun Z, Chai C, et al. Potential transmission of SARS-CoV-2 on a flight from Singapore to Hangzhou, China: an epidemiological investigation. Travel Med Infect Dis. 2020;36:101816. https://doi.org/10.1016/j.tmaid.2020.101816

Address for correspondence: Ella M. Meumann, Menzies School of Health Research, PO Box 41096, Casuarina, NT 0811, Australia; email: ella.meumann@menzies.edu.au

Strongyloides Hyperinfection Syndrome among COVID-19 Patients Treated with Corticosteroids

Jani M. Kim, Geetha Sivasubramanian

Author affiliation: University of California San Francisco, Fresno, California, USA

DOI: https://doi.org/10.3201/eid2807.220198

Widespread use of corticosteroids for COVID-19 treatment has led to *Strongyloides* reactivation and severe disease in patients from endemic areas. We describe a US patient with COVID-19 and *Strongyloides* hyperinfection syndrome and review other reported cases. Our findings highlight the need for *Strongyloides* screening and treatment in high-risk populations.

Strongyloidiasis is caused by the soil-transmitted helminth *Strongyloides stercoralis* and affects ≈613.8 million persons worldwide (*1*). *S. stercoralis* infections can be asymptomatic or chronic or can cause life-threatening larva dissemination, especially in immunocompromised patients (*2*).

Among COVID-19 patients, dexamethasone is the standard treatment for persons requiring supplemental oxygen, but among persons from *Strongyloides*-

endemic areas, exposure to corticosteroids can cause life-threatening *S. stercoralis* hyperinfection (*3*). We describe a case of *Strongyloides* hyperinfection syndrome in a COVID-19 patient and review other reported cases.

A 63-year-old man, who was originally from Cambodia, was admitted to a hospital in Central Valley, California, USA, for a 4-day history of fever, cough, and respiratory distress. His medical history included diabetes mellitus and alcohol use disorder. Admission laboratory testing showed a leukocyte count of 8,500 cells/μL (absolute lymphocyte count 660 cells/μL, reference range 800–4,800 cells/μL) and absolute eosinophil count of 0 cells/μL (reference range 0–800 cells/μL). A nasopharyngeal swab sample tested SARS-CoV-2–positive by PCR. Chest radiographs showed patchy bilateral airspace consolidations. By day 5 of hospitalization, the patient's respiratory failure worsened, and he required supplemental oxygen via high-flow nasal cannula. Chest computed tomography imaging showed multifocal bilateral airspace opacities. The patient received intravenous dexamethasone (6 mg/d for 10 d); during the first 5 days of treatment, he also received baricitinib (10 mg 1×/d) and remdesivir (100 mg/d). The patient's respiratory status improved, and he was discharged to a skilled nursing facility.

The patient returned to the hospital 6 days later with respiratory failure and altered mental status. He was febrile (temperature 39°C) and hypoxic and required intubation. Blood tests revealed a leukocyte of 5,300 cells/μL (absolute lymphocyte count 1,000 cells/μL) and absolute eosinophil count of 100 cells/μL. Blood and sputum cultures were positive for methicillin-sensitive *Staphylococcus aureus*, and we initiated intravenous cefazolin (2 g every 8 h for 10 d). The patient transiently improved, but then fever developed and persisted. After 10 days of broad-spectrum antimicrobial drug therapy, the patient's blood cultures were negative. Echocardiography, magnetic resonance imaging, and computed tomography scans did not identify a focus of infection.

Because of the patient's continued fever and worsening respiratory failure, we performed a diagnostic bronchoscopy on day 28 of his illness. Microscopic examination of the bronchoalveolar lavage fluid revealed parasitic worms consistent with *Strongyloides* spp. (Figure). Stool samples were negative for parasites, but *Strongyloides* serum IgG was positive. The patient's absolute eosinophil count increased to 1,500 cells/μL, and we began oral ivermectin (200 μg/kg for 14 d).

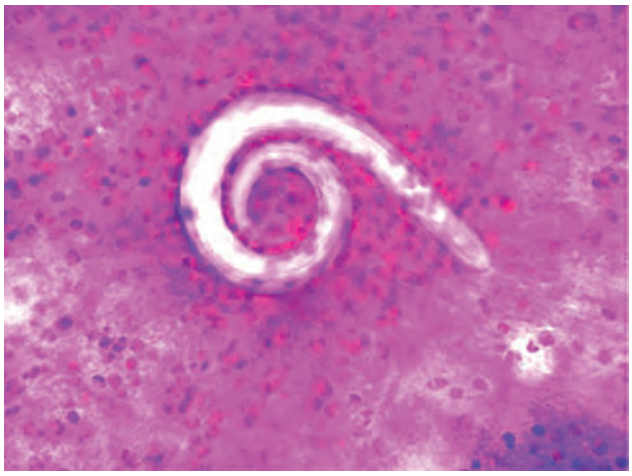

Figure. Bronchoalveolar lavage sample showing larval forms of *Strongyloides stercoralis* in a patient with COVID-19, United States. Original magnification ×200.

Subsequent respiratory culture was positive for extended spectrum β-lactamase *Escherichia coli*. The patient continued to have encephalopathy, and we recommended a lumbar puncture, but the procedure was not performed because of his hemodynamic instability. We changed the patient's therapy to intravenous meropenem (2 g every 8 h), but his condition did not improve. He was eventually transitioned to comfort care and died.

S. stercoralis parasites are endemic in tropical and subtropical regions, but data on strongyloidiasis prevalence is likely underreported, even in endemic areas (*1*). Patients can develop chronic *S. stercoralis* infection, but an immunocompetent host's immune system can regulate infection by controlling adult worm population density in the intestines. However, when a host becomes immunocompromised, larval migration to organs can increase during the autoinfection cycle, causing *Strongyloides* hyperinfection syndrome. Exposure to corticosteroids, human T-cell leukemia virus type 1 co-infection, and solid organ transplantation can increase risk for *Strongyloides* hyperinfection syndrome (*2*). Dexamethasone is the standard treatment for COVID-19 patients who require oxygen therapy; other immunosuppressive agents, including interleukin-6 inhibitors such as tocilizumab, also are commonly used.

Other strongyloidiasis cases have been reported in COVID-19 patients (*4*–*9*) (Table 1). *Strongyloides* hyperinfection syndrome can cause signs and symptoms similar to those of severe COVID-19, including fever, chills, dyspnea, gastrointestinal symptoms, and rash. These vague symptoms can cause missed or delayed strongyloidiasis diagnosis,

Table 1. Characteristics of previously reported *Strongyloides* infections in patients with SARS-CoV-2 pneumonia*

Ref no.	Patient age, y/sex	Reporting country	Country of origin	COVID-19 treatment	*Strongyloides* Diagnosis	*Strongyloides* Treatment	Eosinophil pattern
(*3*)	59/M	Belgium	Ecuador	Anakinra, methylprednisolone 80 mg tapered over 1 month	Positive serologic test; RT-PCR positive for *S. stercoralis* in fecal samples	Single dose ivermectin	Initial eosinopenia (0 cells/mL), elevated to 2,670 cells/mL after steroid exposure, decreased after ivermectin
(*4*)	68/M	United States	Ecuador	Tocilizumab ×1 d and methylprednisolone ×8 d	Sputum culture positive for larvae; positive *Strongyloides* IgG serology	Ivermectin and albendazole ×2 wk	Initial eosinopenia (0 cells/mL), elevated to 1,900 cells/mL after steroid exposure, decreased to 900 cells/mL after ivermectin
(*5*)	59/M	Italy	Southern Italy	Hydroxychloroquine, lopinavir/ritonavir, tocilizumab ×2 d, dexamethasone ×11 d	Stool microscopy positive for rhabditiform larvae; serology positive at 1:640	Oral ivermectin ×4 d	Elevated to 5,540 cells/μL after steroid exposure, rapid decrease after ivermectin
(*6*)	53/M	India	Central India	Methylprednisolone 60 mg intravenous 2×/d ×5 d	Stool microscopy positive for rhabditiform larvae of *S. stercoralis*	Ivermectin and albendazole ×2 wk	Unremarkable
(*7*)	69/M	Spain	Colombia	Methylprednisolone	Bronchoalveolar fluid positive for larvae	Oral ivermectin ×2 wk	Unremarkable
(*8*)	44/M	Spain	Bolivia	Dexamethasone	Positive ELISA IgG serology, 2.27†	Oral ivermectin ×2 d	Eosinopenia before treatment, no further report
	74/F	Spain	Honduras	Dexamethasone	Positive ELISA IgG serology, 2.47†	Oral ivermectin ×2 d	Eosinopenia before treatment, no further report

*All patients recovered. Ref, reference; RT-PCR, reverse transcription PCR.
†Normal value <1.01.

demonstrating the need for increased awareness of this condition and systematic screening of high-risk patients.

Algorithms to aid clinicians with risk assessment, screening, and treatment for *Strongyloides* infection in COVID-19 patients have been proposed (*10*). *Strongyloides* hyperinfection syndrome should be included in the differential diagnosis for patients from endemic areas who receive dexamethasone for COVID-19 and experience clinical decompensation, especially with gram-negative rod bacteremia, pneumonia, or meningitis. Serologic testing should be performed simultaneously and should not delay treatment. Presumptive oral ivermectin for 1–2 days can be considered for COVID-19 patients with higher risk for strongyloidiasis who need dexamethasone (*10*).

Chronic peripheral eosinophilia can be a marker for prompt *Strongyloides* screening. Several case studies have shown a pattern of initial eosinopenia in patients with chronic strongyloidiasis and COVID-19 suppressed with corticosteroids (*4*–*6*). Eosinophils became elevated in these patients because *Strongyloides* hyperinfection developed after corticosteroid administration. In some cases, eosinophilia improved with ivermectin treatment.

In conclusion, *Strongyloides* hyperinfection cases are rising in certain COVID-19 patients. Standardized protocols for *Strongyloides* screening and treatment are needed, especially for patients from endemic countries. To prevent this complication, clinicians should consider *Strongyloides* screening in COVID-19 patients from endemic areas who require corticosteroid treatment.

About the Author

Dr. Kim is an infectious diseases fellow at the University of California San Francisco, Fresno, California. Her primary interests are HIV/AIDS and fungal infections.

References

1. Buonfrate D, Bisanzio D, Giorli G, Odermatt P, Fürst T, Greenaway C, et al. The global prevalence of Strongyloides stercoralis infection. Pathogens. 2020;9:468. https://doi.org/10.3390/pathogens9060468
2. Nutman TB. Human infection with Strongyloides stercoralis and other related Strongyloides species. Parasitology. 2017;144:263–73. https://doi.org/10.1017/S0031182016000834
3. Pereira CVM, Mastandrea GRA, Medeiros ACCS, Gryschek RCB, Paula FM, Corral MA. COVID-19 and strongyloidiasis: what to expect from this coinfection?

Clinics (São Paulo). 2021;76:e3528. https://doi.org/10.6061/clinics/2021/e3528
4. Stylemans D, Van Cauwelaert S, D'Haenens A, Slabbynck H. COVID-19–associated eosinopenia in a patient with chronic eosinophilia due to chronic strongyloidiasis. Infect Dis Clin Pract (Baltim MD). 2021;29:e305–6. https://doi.org/10.1097/IPC.0000000000000991
5. Lier AJ, Tuan JJ, Davis MW, Paulson N, McManus D, Campbell S, et al. Case report: disseminated strongyloidiasis in a patient with COVID-19. Am J Trop Med Hyg. 2020;103:1590–2. https://doi.org/10.4269/ajtmh.20-0699
6. Marchese V, Crosato V, Gulletta M, Castelnuovo F, Cristini G, Matteelli A, et al. Strongyloides infection manifested during immunosuppressive therapy for SARS-CoV-2 pneumonia. Infection. 2021;49:539–42. https://doi.org/10.1007/s15010-020-01522-4
7. Gautam D, Gupta A, Meher A, Siddiqui F, Singhai A. Corticosteroids in Covid-19 pandemic have the potential to unearth hidden burden of strongyloidiasis. IDCases. 2021;25:e01192. https://doi.org/10.1016/j.idcr.2021.e01192
8. Norman FF, Chamorro S, Braojos F, López-Miranda E, Chamorro J, González I, et al. Strongyloides in bronchoalveolar lavage fluid: practical implications in the COVID-19 era. J Travel Med. 2022;29: taab114 . https://doi.org/10.1093/jtm/taab114
9. Feria L, Torrado M, Anton-Vazquez V. Reactivation of Strongyloides stercoralis in patients with SARS-CoV-2 pneumonia receiving dexamethasone. Med Clínica (Barc). 2022;158:242–3. PubMed https://doi.org/10.1016/j.medcle.2021.05.011
10. Stauffer WM, Alpern JD, Walker PF. COVID-19 and dexamethasone: a potential strategy to avoid steroid-related Strongyloides hyperinfection. JAMA. 2020;324:623–4. https://doi.org/10.1001/jama.2020.13170

Address for correspondence: Geetha Sivasubramanian, Division of Infectious Diseases, Department of Internal Medicine, University of California San Francisco, 155 N Fresno St, Ste 307, Fresno, CA 93701, USA; email: geetha.sivasubramanian@ucsf.edu

Mental Health Conditions and Severe COVID-19 Outcomes after Hospitalization, United States

Alain K. Koyama, Emilia H. Koumans, Kanta Sircar, Amy M. Lavery, Jean Y. Ko, Joy Hsu, Kayla N. Anderson, David A. Siegel

Author affiliation: Centers for Disease Control and Prevention, Atlanta, Georgia, USA

DOI: http://doi.org/10.3201/eid2807.212208

Among 664,956 hospitalized COVID-19 patients during March 2020–July 2021 in the United States, select mental health conditions (i.e., anxiety, depression, bipolar, schizophrenia) were associated with increased risk for same-hospital readmission and longer length of stay. Anxiety was also associated with increased risk for intensive care unit admission, invasive mechanical ventilation, and death.

Persons with mental health conditions (MHCs) might be at higher risk for severe COVID-19 outcomes after hospitalization because of poor access to care and a higher incidence of underlying conditions. Most studies have been limited by small samples or aggregation of MHCs, which can conceal differences in risk (*1*,*2*). Previous studies also have not examined length of stay (LOS) and readmission as outcomes. We examined patient records from a large, US-based electronic database to determine whether select MHCs were associated with severe COVID-19 outcomes, increased LOS, and same-hospital readmission.

The Premier Healthcare Database Special COVID-19 Release (accessed October 1, 2021) contained discharge data from >900 hospitals, representing ≈20 of annual admissions in the United States. (*3*). We identified patients hospitalized with COVID-19 and discharged during March 1, 2020–July 31, 2021, by using discharge codes from the International Classification of Diseases, 10th Revision, Clinical Modification (B97.29 for March 2020–April 2020 or U07.1 for April 2020–July 2021). MHCs of interest were anxiety, depression, bipolar disorder, and schizophrenia (identified from encounters from January 2019 through the index COVID-19 admission). Because patients could have multiple MHC diagnoses, categories were not mutually exclusive. Outcomes were intensive care unit (ICU) admission, invasive mechanical ventilation (IMV), 30-day same-hospital readmission

(all-cause), in-hospital death (all-cause), and LOS. We used mixed effects models to examine the association between each MHC and each outcome. The reference group comprised patients who did not have MHC diagnoses of any type (i.e., anxiety, depression, bipolar disorder, schizophrenia, attention-deficit/hyperactivity disorder, obsessive-compulsive disorder, severe stress and adjustment disorders, eating disorders, disruptive disorders, impulse-control disorders, and conduct disorders).

We used logistic models to estimate adjusted odds ratios (aORs) and corresponding 95% CIs for each dichotomous outcome (ICU admission, IMV, readmission, and death) and Poisson models to estimate the percentage difference and 95% CIs for LOS. A random intercept accounted for clustering by hospitals. We adjusted models for age, sex, race and ethnicity, insurance type, admission month, hospital characteristics (urbanicity and US Census Division region), and the Elixhauser Comorbidity Index (a measure of overall comorbidity based on 29 conditions) (*4*). We used SAS 9.4 (SAS Institute, https://www.sas.com) for statistical analyses.

Of our study sample of 664,956 hospitalized patients, 77.1% of patients were ≥50 years of age (Table). Male patients outnumbered female patients in having no MHC diagnoses (55.0%) or schizophrenia (53.8%); female patients outnumbered male patients in having anxiety (61.0%), depression (61.7%), or bipolar disorder (58.8%). We stratified COVID-19 outcomes among hospitalized patients by MHC diagnosis (Figure). Patients with anxiety, compared with those without any MHC, had a significantly higher odds of ICU admission (aOR 1.36, 95% CI 1.34–1.38), IMV (aOR 1.44, 95% CI 1.41–1.47), and in-hospital death (aOR 1.31, 95% CI 1.28–1.34). Patients with any of the MHCs, compared with patients without any MHC, had a significantly higher odds of readmission (anxiety, aOR 1.31 [95% CI 1.28–1.35]; depression: aOR 1.36 [95% CI 1.33–1.40]; bipolar disorder, aOR 1.50 [95% CI 1.41–1.59]; schizophrenia, aOR 1.40 [95% CI 1.31–1.49]). Similarly, each MHC was significantly associated with a longer mean LOS (anxiety, 34.8 days [95% CI 34.5–35.1]; depression, 19.5 days [95% CI 19.2–19.8]; bipolar disorder, 20.6 days [95% CI 19.9–21.2]; schizophrenia, 25.6 days [95% CI 24.9–26.3]).

Anxiety was most strongly associated with severe outcomes in this patient sample; anxiety, depression, bipolar disorder, and schizophrenia were each independently associated with a higher risk of 30-day readmission and longer LOS. Comparing these results against the heterogeneous findings of prior studies is difficult for several reasons: aggregation of MHC, use of data early in the pandemic, populations with different risk profiles, and small samples (*2*,*5*,*6*). Most prior studies did not show a significant association between anxiety and a higher risk for ICU admission, IMV, or death (*2*,*5*), and most did not examine readmission or LOS as outcomes. MHCs might exacerbate respiratory disease and result in a greater risk for readmission or longer LOS in nonpsychiatric hospitalizations (*7*–*9*). These outcomes might be attributed to increased prevalence and severity of underlying conditions, immune dysregulation, use of psychotropic

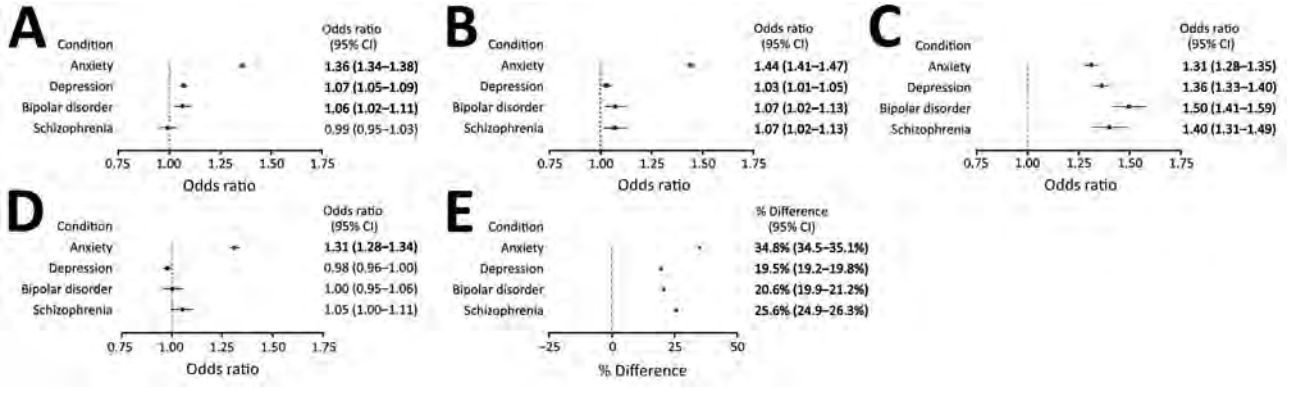

Figure. Outcomes of hospitalized COVID-19 patients (n = 664,956), by mental health condition diagnosis, compared with patients without mental health condition diagnoses in the Premier Healthcare Database Special COVID-19 Release, United States, March 2020–July 2021. For each condition, odds ratios represent the odds of the given outcome for patients with the condition compared with patients without mental health conditions. For length of stay, percentages represent the percentage difference in length of stay for patients with the condition compared with patients without mental health conditions. Covariates were selected based on factors known or plausibly associated with both the mental health condition and given outcome. Bolded values indicate statistical significance (2-sided α = 0.05), adjusted for multiple comparisons using the Bonferroni-Holm method. Descriptive statistics for each outcome, by mental health condition, and results from unadjusted models, are provided in the Appendix (https://wwwnc.cdc.gov/EID/article/28/7/21-2208-App1.pdf).

Table. Characteristics of 664,956 hospitalized COVID-19 patients, by mental health condition diagnosis, from the Premier Healthcare Database Special COVID-19 Release, United States, March 2020–July 2021*

Parameter	No. (%) patients				
	No mental health conditions	Anxiety	Depression	Bipolar disorder	Schizophrenia
Total	485,784 (73.1)	114,902 (17.3)	96,167 (14.5)	15,370 (2.3)	12,304 (1.9)
Patient characteristics					
Age group, y					
0–17	5,415 (1.1)	608 (0.5)	584 (0.6)	97 (0.6)	25 (0.2)
18–39	61,751 (12.7)	11,584 (10.1)	7,598 (7.9)	2,527 (16.4)	1,421 (11.5)
40–49	50,127 (10.3)	11,863 (10.3)	7,949 (8.3)	1,996 (13.0)	1,095 (8.9)
50–64	129,896 (26.7)	33,511 (29.2)	26,320 (27.4)	5,455 (35.5)	4,251 (34.5)
65–74	101,996 (21.0)	26,561 (23.1)	23,756 (24.7)	3,298 (21.5)	3,512 (28.5)
≥75	136,599 (28.1)	30,775 (26.8)	29,960 (31.2)	1,997 (13.0)	2,000 (16.3)
Sex					
F	218,428 (45.0)	70,105 (61.0)	59,327 (61.7)	9,032 (58.8)	5,682 (46.2)
M	267,356 (55.0)	44,797 (39.0)	36,840 (38.3)	6,338 (41.2)	6,622 (53.8)
Race/ethnicity					
Non-Hispanic White	241,534 (49.7)	78,634 (68.4)	67,015 (69.7)	10,267 (66.8)	6,409 (52.1)
Non-Hispanic Black	93,192 (19.2)	14,482 (12.6)	12,736 (13.2)	2,743 (17.8)	3,644 (29.6)
Hispanic	94,476 (19.4)	13,783 (12.0)	9,955 (10.4)	1,348 (8.8)	1,158 (9.4)
Non-Hispanic Asian	13,989 (2.9)	1,446 (1.3)	1,054 (1.1)	122 (0.8)	192 (1.6)
Other or unknown†	42,593 (8.8)	6,557 (5.7)	5,407 (5.6)	890 (5.8)	901 (7.3)
Health insurance					
Medicare	236,378 (48.7)	65,874 (57.3)	61,486 (63.9)	8,787 (57.2)	8,264 (67.2)
Medicaid	71,593 (14.7)	15,960 (13.9)	12,591 (13.1)	3,908 (25.4)	2,969 (24.1)
Private	133,735 (27.5)	26,102 (22.7)	17,015 (17.7)	1,817 (11.8)	493 (4.0)
Other†	44,078 (9.1)	6,966 (6.1)	5,075 (5.3)	858 (5.6)	578 (4.7)
Admission month					
2020 Mar or earlier	16,773 (3.5)	2,350 (2.0)	1,981 (2.1)	344 (2.2)	481 (3.9)
2020 Apr–Jun	70,536 (14.5)	12,946 (11.3)	11,968 (12.4)	2,578 (16.8)	2,959 (24.0)
2020 Jul–Sep	72,514 (14.9)	15,462 (13.5)	12,696 (13.2)	2,090 (13.6)	1,749 (14.2)
2020 Oct–Dec	149,494 (30.8)	40,166 (35.0)	34,329 (35.7)	4,830 (31.4)	3,651 (29.7)
2021 Jan–Mar	118,438 (24.4)	29,742 (25.9)	24,432 (25.4)	3,686 (24.0)	2,440 (19.8)
2021 Apr–Jun	46,674 (9.6)	11,904 (10.4)	9,076 (9.4)	1,587 (10.3)	863 (7.0)
2021 Jul	11,355 (2.3)	2,332 (2.0)	1,685 (1.8)	255 (1.7)	161 (1.3)
Elixhauser Comorbidity Index‡	4.0 (9.2)	6.2 (10.6)	6.9 (10.8)	5.7 (9.7)	6.4 (9.6)
Hospital characteristics					
Urbanicity					
Urban	585,009 (88.0)	429,073 (88.3)	99,530 (86.6)	83,505 (86.8)	13,682 (89.0)
Rural	79,947 (12.0)	56,711 (11.7)	15,372 (13.4)	12,662 (13.2)	1,688 (11.0)
Region					
East North Central	8,534 (1.8)	3,738 (3.3)	3,193 (3.3)	487 (3.2)	427 (3.5)
East South Central	79,512 (16.4)	15,288 (13.3)	13,917 (14.5)	2,567 (16.7)	2,669 (21.7)
Middle Atlantic	73,667 (15.2)	21,736 (18.9)	18,361 (19.1)	3,052 (19.9)	2,236 (18.2)
Mountain	19,812 (4.1)	6,684 (5.8)	6,544 (6.8)	747 (4.9)	520 (4.2)
New England	133,540 (27.5)	30,544 (26.6)	23,226 (24.2)	3,778 (24.6)	2,965 (24.1)
Pacific	32,915 (6.8)	9,537 (8.3)	7,610 (7.9)	957 (6.2)	608 (4.9)
South Atlantic	64,156 (13.2)	13,504 (11.8)	11,708 (12.2)	1,753 (11.4)	1,290 (10.5)
West North Central	39,377 (8.1)	8,394 (7.3)	6,840 (7.1)	1,180 (7.7)	727 (5.9)
West South Central	34,271 (7.1)	5,477 (4.8)	4,768 (5.0)	849 (5.5)	862 (7.0)

*Values are no. (%) except as indicated.
†Missing values, when present, are categorized in the other category.
‡Higher values suggest a higher degree of comorbidity. Expressed as mean (±SD).

medications, socioeconomic disadvantage, or a combination of these factors (*8*,*9*).

Limitations of our study include residual confounding by such unavailable data as socioeconomic status, smoking status, and other substance use. MHCs among patients we studied might not have captured instances of milder disease because we identified those conditions by codes from the International Classification of Diseases, Tenth Revision, Clinical Modification. For example, the greater risk for death among patients with anxiety compared with patients with other MHCs could be attributed to differentially overcapturing more severe cases of anxiety. Hospital readmissions also might have been incompletely captured because data were only available on readmissions to the same hospital as the index admission for COVID-19. In addition, 58,743 patients (8.8%) had >1 MHC, potentially leading to misclassification.

By disaggregating MHCs, we demonstrated the differences in the risks associated with each

individual condition. These findings might improve understanding of the risk for severe COVID-19 outcomes associated with MHCs and add evidence for considering MHCs as high-risk conditions for patients with COVID-19.

This study was reviewed by the Centers for Disease Control and Prevention and was deemed exempt from institutional review board oversight per 45 CFR §46.101(b)(4) and exempt from patient-informed consent based on 45 CFR §164.506(d)(2)(ii)(B). Authors did not receive financial support in the conduct of this study. Authors report no competing interests.

About the Author

Dr. Koyama is an epidemiologist at the Centers for Disease Control and Prevention, Atlanta, Georgia, USA. His research background includes epidemiology, neuropsychiatry, and health services research.

References

1. Barcella CA, Polcwiartek C, Mohr GH, Hodges G, Søndergaard K, Niels Bang C, et al. Severe mental illness is associated with increased mortality and severe course of COVID-19. Acta Psychiatr Scand. 2021;144:82–91. https://doi.org/10.1111/acps.13309
2. Fond G, Nemani K, Etchecopar-Etchart D, Loundou A, Goff DC, Lee SW, et al. Association between mental health disorders and mortality among patients with COVID-19 in 7 countries: a systematic review and meta-analysis. JAMA Psychiatry. 2021;78:1208–17. https://doi.org/10.1001/jamapsychiatry.2021.2274
3. Premier Applied Sciences. Premier Healthcare Database white paper: data that informs and performs. 2020 [cited 2021 July 14]. http://offers.premierinc.com/rs/381-NBB-525/images/PHD_COVID-19_White_Paper.pdf
4. Moore BJ, White S, Washington R, Coenen N, Elixhauser A. Identifying increased risk of readmission and in-hospital mortality using hospital administrative data: the AHRQ Elixhauser Comorbidity Index. Med Care. 2017;55:698–705. https://doi.org/10.1097/MLR.0000000000000735
5. Castro VM, Gunning FM, McCoy TH, Perlis RH. Mood disorders and outcomes of COVID-19 hospitalizations. Am J Psychiatry. 2021;178:541–7. https://doi.org/10.1176/appi.ajp.2020.20060842
6. Cummins L, Ebyarimpa I, Cheetham N, Tzortziou Brown V, Brennan K, Panovska-Griffiths J. Factors associated with COVID-19 related hospitalisation, critical care admission and mortality using linked primary and secondary care data. Influenza Other Respir Viruses. 2021;15:577–88. https://doi.org/10.1111/irv.12864
7. Coughlin SS. Anxiety and depression: linkages with viral diseases. Public Health Rev. 2012;34:7. https://doi.org/10.1007/BF03391675
8. Jansen L, van Schijndel M, van Waarde J, van Busschbach J. Health-economic outcomes in hospital patients with medical-psychiatric comorbidity: a systematic review and meta-analysis. PLoS One. 2018;13:e0194029. https://doi.org/10.1371/journal.pone.0194029
9. Ronaldson A, Elton L, Jayakumar S, Jieman A, Halvorsrud K, Bhui K. Severe mental illness and health service utilisation for nonpsychiatric medical disorders: a systematic review and meta-analysis. PLoS Med. 2020;17:e1003284. https://doi.org/10.1371/journal.pmed.1003284

Address for correspondence: Alain K. Koyama, Centers for Disease Control and Prevention, 4770 Buford Hwy NE, MS-S107-3, Atlanta, GA 30341, USA; email: akoyama@cdc.gov

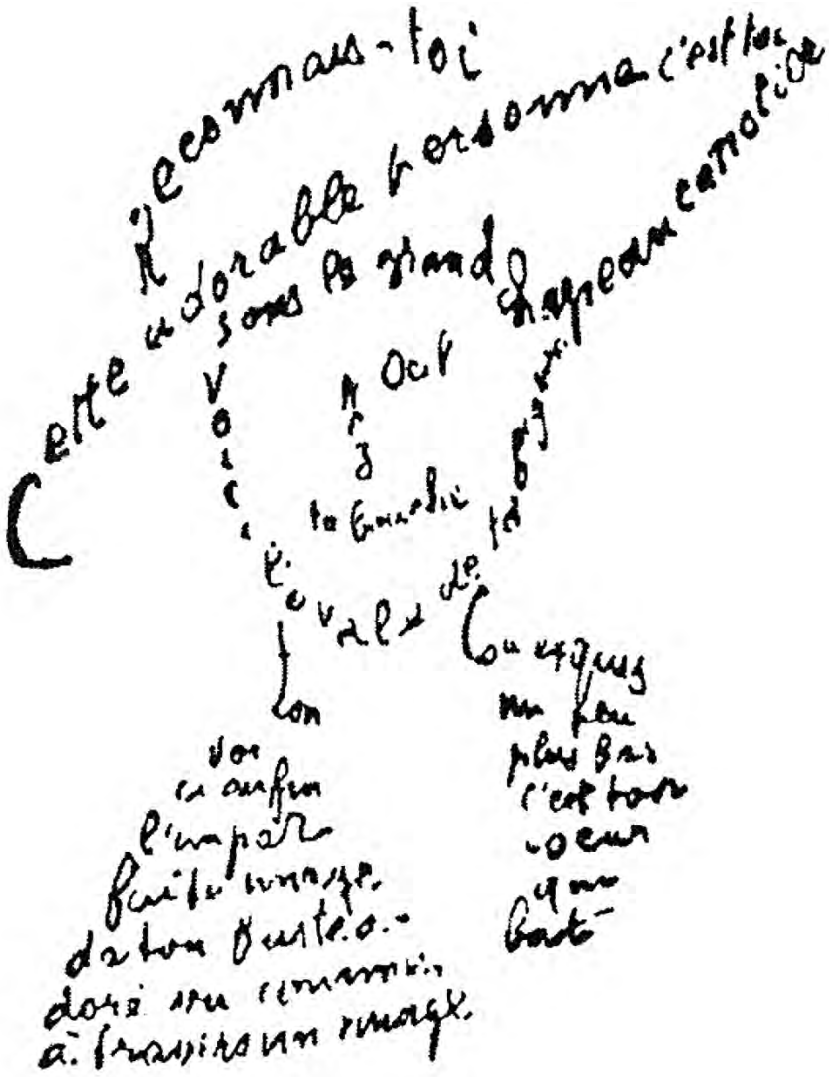

***Guillaume Apollinaire* (1880–1918), *Calligram of Guillaume Apollinaire*, entitled *Poème du 9 Février 1915* (Poem of February 9, 1915).** Printed in Calligrammes: Poèmes de la Paix et de la Guerre 1913–1916 (Calligrams: Poems of Peace and War 1913–1916). Paris, Mercure de France, 1918. Digital image available from the Online Collection of Duke University Libraries.

Of Those We Have Lost and Those Who Have Saved So Many Others

Terence Chorba

Modernism is a term ascribed to styles and transformative movements in multiple cultural spheres—philosophy, music, art, architecture, and literature. In its essence, modernism has at its core experimentation, as a term usually applied to efforts and creations of the late 19th or early 20th century, but sometimes later, characterized by intentional departures from traditional forms.

There are many well-known examples of modernist efforts in their respective spheres and periods. In biology, Charles Darwin questioned the concept of human uniqueness with the theory of evolution. In literature, the term modernist has been applied to European and American writers who created substantive

Author affiliation: Centers for Disease Control and Prevention, Atlanta, Georgia, USA

DOI: https://doi.org.10.3201/eid2807.AC2807

departures from tradition, as was seen in the works of Fyodor Dostoyevsky, Gustave Flaubert, James Joyce, and William Carlos Williams. In music, modernism is a term ascribed to the period 1890–1930, and postmodernism is a term sometimes accorded to phenomena with modernist qualities but occurring after 1930; however, some critics use modernism to describe a movement of rebellion that continues, dependent on the musician's attitude rather than the musician's moment in time. Certainly, Ella Fitzgerald, Miles Davis, Bob Dylan, John Lennon, Charles Mingus, the Rolling Stones, and Neil Young created musical forms that featured modernist iconoclasm, stepping well beyond the early 20th century. In art, modernism is used as a broader categorization of several novel stylistic departures including realism, postimpressionism, fauvism, cubism, dadaism, surrealism, abstract expressionism, and minimalism, each with elements of deliberate experimentation and innovation.

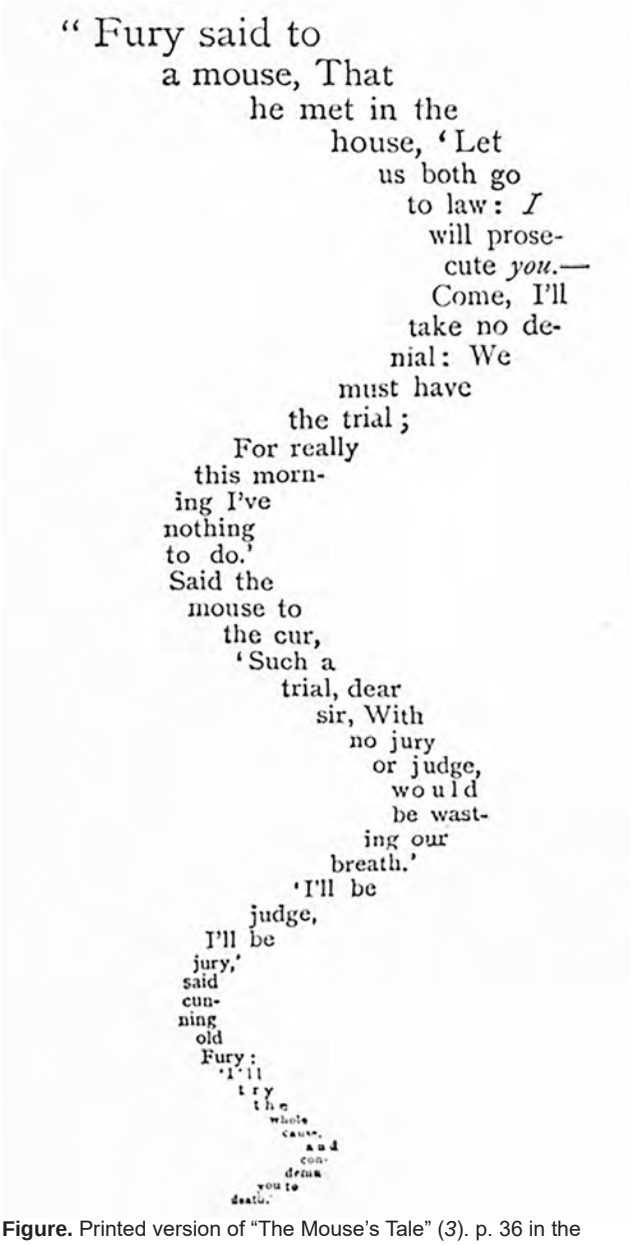
" Fury said to
a mouse, That
he met in the
house, 'Let
us both go
to law: I
will prose-
cute you.—
Come, I'll
take no de-
nial: We
must have
the trial;
For really
this morn-
ing I've
nothing
to do.'
Said the
mouse to
the cur,
'Such a
trial, dear
sir, With
no jury
or judge,
would
be wast-
ing our
breath.'
'I'll be
judge,
I'll be
jury,'
said
cun-
ning
old
Fury:
'I'll
try
the
whole
cause,
and
con-
demn
you to
death.'

Figure. Printed version of "The Mouse's Tale" (*3*). p. 36 in the 1865 edition of *Alice's Adventures in Wonderland.* Source: https://www.gutenberg.org/files/11/11-h/11-h.htm#link2HCH0003

Guillaume Apollinaire (1880–1918) was a renowned Belarus-born French poet and critic of modernist art; he created the terms "cubism" in 1911 and "surrealism" in 1917. Apollinaire was also a pioneer in his period for his collection of shape poems called calligrams, published in 1918 in *Calligrammes: Poemès de la paix et de la guerre 1913–1916* (*Calligrams: Poems of Peace and War 1913–1916*). Shape poems, also known as concrete poems, are poetic works that are shaped like their subjects or topics. Calligrams are a subset of this genre in which the text is thematically arranged such that the visual image of what is written or typed closely reflects what the words themselves express. The image on this month's cover is one such calligram that described how Apollinaire was enamored of his beloved, using a female visual image and illustrating the eye (*oeil*), nose (*nez*), mouth (*bouche*), and neck (*cou*) using those very words (in French) in the visual representation of those parts of the image: "*Reconnais-toi. Cette adorable personne c'est toi. Sous le grand chapeau canotier. Nez. Oeil. Ta bouche. Voici l'ovale de ta figure. Ton cou exquis. Voici enfin l'imparfaite image de ton buste adoré vu comme à travers un nuage. Un peu plus bas c'est ton coeur qui bat.*" ["You recognize that this lovely person, that's you, under a wide boater's hat….Nose. Eye. Your mouth. Here, the oval of your face…your exquisite neck. And finally, here is the flawed picture of your beloved bust seen as through a mist. And down a little farther is your heart that is beating."]

Although Apollinaire's calligrams are thought of as a departure from other formulaic categories of poetry (e.g., haiku or the Shakespearean sonnet), elements of such calligraphic experimentation and innovation have been found in older cultures. As an Alexandrian poet of the fourth century BCE, Simmias of Rhodes has been renowned for three shape poems written (in Greek) in the shape of a pair of wings (πτέρυγες), an egg (ὠόν), and a hatchet (πέλεκυς). During the Middle Ages, micrography in the form of Hebrew and Muslim shape poems was developed, sometimes serving as a workaround for religious restrictions on graven images, to remain devout in observation of Jewish or Islamic law. A more recent historical example is "The Mouse's Tale," a visually shaped poem in Lewis Carroll's *Alice in Wonderland*, in which the mouse begins to tell Alice his story by saying, "Mine is a long and

a sad tale!", leading Alice to think that the mouse is referring to its tail (Figure). For all these authors, the trick of the shape poem, especially the calligram, was to create a poem that depends both on form and words for meaning, with primacy given over to the visual effect, as a synthesis of visual art and lyrics.

On November 9, 1918, two days before the armistice of the First World War, Apollinaire died at age 38. He was but another casualty in the second wave of the great influenza A(H1N1) pandemic that had begun in the winter months of early 1918, and his death was characteristic of most deaths documented in that pandemic, occurring among those in their childbearing years. Persons 40–65 years of age tended to have relative immunity to this pathogen, the result of virus exposure decades earlier. That pandemic helped to end the four years of conflict in Europe in which more died of infectious disease than of combat wounds themselves. Two other great poets, both renowned in English-speaking circles, were lost in that war to infectious disease: John McCrae, who died of meningitis (*In Flanders Fields*—"In Flanders fields the poppies blow between the crosses, row on row"), and Rupert Brooke, who died of septicemia resulting from an infected mosquito bite (*The Soldier*—"If I should die, think only this of me: That there's some corner of a foreign field that is forever England"). Going beyond the war into 1919, about 500 million persons became infected with the circulating influenza virus worldwide, comparable to estimates of the number of persons who have become infected to date with SARS-CoV-2, the causative agent of COVID-19.

Pandemics and wars leave vacuums in all sectors, and the arts are no exception. In the current COVID-19 pandemic, among celebrated musicians alone, we have lost John Prine, Trini Lopez, Charley Pride, Mamu Dibango, Antoine Hodge, and many others. As the death toll from COVID-19 has exceeded 1 million in the United States and 6,250,000 worldwide, myriad preventive and therapeutic measures that have evolved over the past century, including vaccines, antivirals, antibiotics, and monoclonal antibodies, have kept this grim tally from growing even worse. During the ongoing SARS-CoV-2 pandemic, modern healthcare resources have saved millions of lives, including those of many creative souls—musicians, writers, poets, illustrators, sculptors, painters, and graphic artists—in contrast to conditions during the influenza A pandemic at the end of the First World War. The work of many heroes, including research scientists, public health responders, administrators, healthcare providers, support personnel, and advocates, should be acknowledged and celebrated.

Bibliography

1. Biographie (Guillaume Apollinaire official website). Macomb (IL): Western Illinois University [cited 2022 May 6]. http://www.wiu.edu/Apollinaire/Biographie.htm
2. Carroll L. The mouse's tale [cited 2022 May 16]. https://www.gutenberg.org/files/11/11-h/11-h.htm#link2HCH0003
3. Childs P. Modernism. Abingdon-on-Thames (UK): Routledge; 2000.
4. Latour P. Charles Mingus, jazz and modernism. Thesis submitted to McGill University, 2012. p. 15–44 [cited 2022 May 16]. https://escholarship.mcgill.ca/concern/file_sets/f7623h00f?locale=en
5. Maingon C, Tatu L. Creative minds in the aftermath of the Great War: four neurologically wounded artists. Front Neurol Neurosci. 2018;43:37–46. https://doi.org/10.1159/000490403
6. McDonald L. Calligrammes and COVID-19: The visual poetry of Guillaume Apollinaire and the pandemic. [cited 2022 May 6]. https://www.st-artmagazine.com/artsand-culture/2020/11/5/calligrammes-and-covid-19-the-visual-poetry-of-guillaume-apollinaire-and-the-pandemic
7. McHard JL. The future of modern music: a philosophical exploration of modernist music in the 20th century and beyond, 3rd ed. Livonia (MI): Iconic Press; 2008.
8. Taubenberger JK, Morens DM. 1918 influenza: the mother of all pandemics. Emerg Infect Dis. 2006;12:15–22.
9. Vitturi BK, Sanvito WL. The neurology behind three wounded French artists during the great world war. Arq Neuropsiquiatr. 2020;78:380–2. https://doi.org/10.1590/0004-282x20190157
10. Wilton P. Spanish flu outdid WWI in number of lives claimed. CMAJ. 1993;148:2036–7.
11. World Health Organization. Coronavirus (COVID-19) dashboard [cited 2022 May 6]. https://covid19.who.int

Address for correspondence: Terence Chorba, Division of Tuberculosis Elimination, Centers for Disease Control and Prevention, 1600 Clifton Rd NE, Mailstop US12-4, Atlanta, GA 30329-4027, USA; email: tlc2@cdc.gov

EMERGING INFECTIOUS DISEASES®

Upcoming Issue

- Investigation of COVID-19 Outbreak among Wildland Firefighters during Wildfire Response, Colorado, USA, 2020
- Ethnic Group Differences in Incidence of Nontuberculous Mycobacterial Pulmonary Infection, Hawaii, USA 2005–2019
- Characterization of Emerging Serotype 19A Pneumococcal Strains in Invasive Disease and Carriage, Belgium
- Association of Environmental Factors with Intensity of Seasonal Seropositivity of *Erysipelothrix rhusiopathiae* in Arctic Caribou
- Dog Ownership and Risk for Alveolar Echinococcosis, Germany
- Novel Reassortant Avian Influenza A(H5N6) Virus, China, 2021
- *Spiroplasma ixodetis* Infections in Immunocompetent and Immunosuppressed Patients after Tick Exposure, Sweden
- Toxigenic *Corynebacterium diphtheriae* Infection in a Cat in Texas
- Novel Chronic Anaplasmosis in Splenectomized Patient, Amazon Rainforest
- Robustness of SARS-CoV-2 Mu Variant against Naturally Acquired and Vaccine-Induced Immune Responses
- Serial Intervals for SARS-CoV-2 Omicron and Delta Variants, Belgium, November 19–December 31, 2021
- Estimating COVID-19 Vaccine Effectiveness for Skilled Nursing Facility Healthcare Personnel, California, USA
- *Bacillus subtilis* var. *natto* Bacteremia of Gastrointestinal Origin
- Invasive *Streptococcus oralis* Expressing Serotype 3 Pneumococcal Capsule, Japan
- Imported Monkeypox from International Traveler, Maryland, USA, 2021
- Imported Monkeypox from International Traveler, Maryland, USA, 2021
- Weighing Potential Benefits and Harms of *Mycoplasma genitalium* Testing and Treatment Approaches
- Transmissibility of SARS-CoV-2 B.1.1.214 and Alpha Variants during 4 COVID-19 Waves, Kyoto, Japan, January 2020–June 2021

Complete list of articles in the August issue at http://www.cdc.gov/eid/upcoming.htm

Earning CME Credit

To obtain credit, you should first read the journal article. After reading the article, you should be able to answer the following, related, multiple-choice questions. To complete the questions (with a minimum 75% passing score) and earn continuing medical education (CME) credit, please go to http://www.medscape.org/journal/eid. Credit cannot be obtained for tests completed on paper, although you may use the worksheet below to keep a record of your answers.

You must be a registered user on http://www.medscape.org. If you are not registered on http://www.medscape.org, please click on the "Register" link on the right hand side of the website.

Only one answer is correct for each question. Once you successfully answer all post-test questions, you will be able to view and/or print your certificate. For questions regarding this activity, contact the accredited provider, CME@medscape.net. For technical assistance, contact CME@medscape.net. American Medical Association's Physician's Recognition Award (AMA PRA) credits are accepted in the US as evidence of participation in CME activities. For further information on this award, please go to https://www.ama-assn.org. The AMA has determined that physicians not licensed in the US who participate in this CME activity are eligible for *AMA PRA Category 1 Credits*™. Through agreements that the AMA has made with agencies in some countries, AMA PRA credit may be acceptable as evidence of participation in CME activities. If you are not licensed in the US, please complete the questions online, print the AMA PRA CME credit certificate, and present it to your national medical association for review.

Article Title

Updated Estimates and Prevalence of Chagas Disease among Adults, United State

CME Questions

1. Which of the following statements regarding Chagas disease in the United States is most accurate?

A. 70% to 80% of adults eventually develop cardiac or gastrointestinal disease
B. Serology against *Trypanosoma cruzi* becomes negative about 4 weeks after treatment among adults
C. Autochthonous infections with *T. cruzi* occur in southern states from coast to coast
D. Survival rates for end-stage cardiomyopathy associated with Chagas disease are lower compared with other indications for transplant

2. What does the current study find regarding the epidemiology of Chagas' disease in the United States?

A. Nearly 29,000 US residents born in Latin America had Chagas disease from 2014 to 2018
B. Chagas disease was most prevalent among adolescents and young adults
C. There were approximately 1000 congenital *T. cruzi* infections annually
D. The estimated total number of locally acquired infections may be 10,000

3. Which metropolitan area is estimated to have the highest number of people with *T. cruzi* infection in the current study?

A. New York
B. Houston
C. Washington, DC
D. Los Angeles

4. Persons from which of the following countries of origin had the highest prevalence of Chagas disease in the current study?

A. Mexico
B. Guatemala
C. Venezuela
D. Bolivia

Earning CME Credit

To obtain credit, you should first read the journal article. After reading the article, you should be able to answer the following, related, multiple-choice questions. To complete the questions (with a minimum 75% passing score) and earn continuing medical education (CME) credit, please go to http://www.medscape.org/journal/eid. Credit cannot be obtained for tests completed on paper, although you may use the worksheet below to keep a record of your answers.

You must be a registered user on http://www.medscape.org. If you are not registered on http://www.medscape.org, please click on the "Register" link on the right hand side of the website.

Only one answer is correct for each question. Once you successfully answer all post-test questions, you will be able to view and/or print your certificate. For questions regarding this activity, contact the accredited provider, CME@medscape.net. For technical assistance, contact CME@medscape.net. American Medical Association's Physician's Recognition Award (AMA PRA) credits are accepted in the US as evidence of participation in CME activities. For further information on this award, please go to https://www.ama-assn.org. The AMA has determined that physicians not licensed in the US who participate in this CME activity are eligible for *AMA PRA Category 1 Credits*™. Through agreements that the AMA has made with agencies in some countries, AMA PRA credit may be acceptable as evidence of participation in CME activities. If you are not licensed in the US, please complete the questions online, print the AMA PRA CME credit certificate, and present it to your national medical association for review..

Article Title

Natural History of and Dynamic Changes in Clinical Manifestation, Serology, and Treatment of Brucellosis, China

CME Questions

1. Your patient is a 47-year-old male farmer with suspected brucellosis. According to the large, retrospective cohort study in China by Wang and colleagues, which of the following statements about diagnosis and epidemiologic features of human brucellosis is correct?

A. Clinical features were most useful in diagnosing human brucellosis in China
B. More than half of patients diagnosed with brucellosis had positive blood cultures
C. Approximately one-quarter of patients had positive exposure history
D. Seasonal epidemics occurred from March to July each year; total newly diagnosed cases decreased annually between 2015 and 2019

2. According to the large, retrospective cohort study in China by Wang and colleagues, which of the following statements about clinical characteristics of human brucellosis during the disease course and after treatment is correct?

A. Before receipt of antibiotics, fatigue, fever, and arthritis were the 3 most common symptoms in early-stage brucellosis (symptom duration <180 days)
B. Baseline C-reactive protein (CRP) and erythrocyte sedimentation rate (ESR) were the best predictors for chronic brucellosis
C. At 2 weeks posttreatment, some patients developed new cardiac inflammation (n = 107), neurobrucellosis (n = 112), urogenital inflammation (n = 140), or arthritis (n = 146)
D. Cases diagnosed by culture vs SAT were less likely to have hepatosplenomegaly

3. According to the large, retrospective cohort study in China by Wang and colleagues, which of the following statements about serologic surveillance of human brucellosis during the disease course and after treatment and long-term treatment outcomes is correct?

A. After appropriate treatment, 13.3% of acute brucellosis cases progressed to chronicity (still symptomatic after 180 days)
B. Treatment should be discontinued once symptoms disappear
C. In the chronic phase, loss of appetite was the most common symptom
D. 15% of brucellosis cases remained seropositive at 180 days posttreatment